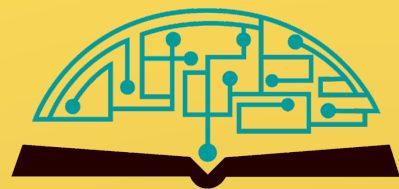


IJHSR

International
Journal of
High School
Research



December 2023 | Volume 5 | Issue 7

ijhighschoolresearch.org

ISSN (Print) 2642-1046

ISSN (Online) 2642-1054



Marine Biology Research at Bahamas

Unique and exclusive partnership with the Gerace Research Center (GRC) in San Salvador, Bahamas to offer marine biology research opportunities for high school teachers and students.

- Terra has exclusive rights to offer the program to high school teachers and students around world.
- All trips entail extensive snorkeling in Bahamian reefs as well as other scientific and cultural activities.
- Terra will schedule the program with GRC and book the flights from US to the GRC site.
- Fees include travel within the US to Island, lodging, meals, and hotels for transfers, and courses.
- For more information, please visit terraed.org/bahamas.html

Terra is a N.Y. based 501.c.3 non-profit organization dedicated for improving K-16 education

Table of Contents

December 2023 | Volume 5 | Issue 6

1	Machine Learning Augmented Histopathological Diagnosis of an Aggressive Variant of Liver Cancer <i>Vivasvat Rastogi, Shashvat Rastogi</i>
7	Applying Linear Regression to The World Happiness Report <i>Ankur A. Dabholkar</i>
11	An Examination of Stroke and Air Pollution Trends in Taiwan, 1990 to 2022 <i>Audrey Wang</i>
18	IoT - SMART Urinal cum Disinfectant Flush System <i>Bhupen Sai Bandi</i>
22	Should NBA Teams Sell the Farm for Superstars? Distribution of Player Investment and its Impact on Competitive Outcomes <i>Brent A. Dsouza</i>
28	Development of Polymer-assisted Compaction of DNA Nanoparticles for Cancer Treatment <i>Caroline Shen</i>
33	Variations in Predominant Risk Factors and Interventions for Diarrheal Diseases in Children Under Five Years of Age <i>Mai Nguyen</i>
48	Distant Supervision for Early Detection of Acute Lung Injury (ACL) <i>Eana Shab</i>
53	Accessible, AI-enabled TeleMedicine Solution for Multi-organ Dysfunction Caused by SARS Infections <i>Gatik Trivedi</i>
58	Trend and Prediction Analysis of Rainfall and Temperature in Dindigul District, Tamil Nadu, India <i>Harnishya Palanichamy</i>
71	Finding the Exact Value of $\cos(\pi/7)$ <i>Punnawit Kasean</i>
78	Performance Benefit Analysis of Linked Rainwater Harvesting Systems <i>Saewoong Ian Park</i>
83	Comparative Analysis of the Prevalence of Domestic Violence in India, Basis the NFHS 2015-16 and 2019-21 <i>Jassimmrat K. Bhatia</i>
94	Anxiety about COVID-19 and Future Expectations among High School Students <i>Justin J. Shin</i>
100	Efficacy of Si Wu-Tang on Treating Primary Dysmenorrhea: A Systematic Review and Meta-Analysis <i>Yiyi Liu</i>
105	Deep Learning-based Automatic Measures of Spinal Curvature in Idiopathic Scoliosis <i>Yubeen Lee, Seoyoung Park, Seunghoon Han</i>
109	Prediction of a City's Power Consumption by Artificial Neural Networks <i>Maxwell Y. Chen</i>
112	Nutritional Status of Sickle Cell Disease Patients: A Literature Review <i>Minjoon Hur</i>
119	The Effect of Autoinducer Analogs on the Quorum Sensing Systems of <i>E. coli</i> K12 <i>Sai Ashutosh Chellarapu, Eswar Pondugula</i>
123	Using Biomimetics to Mimic Bamboo to Create a More Robust and More Durable Material <i>Sean Jung</i>
130	Arsenic in Groundwater and Its Carcinogenicity <i>Shriya Raja</i>
136	Investigation of Functional Role of a Novel Biomarker: CCNC Gene Deletion on Human Leukemia Cancer <i>Sooah Yoo</i>
140	A new approach to Turing completeness in <i>Baba</i> is You <i>Caleb J. Su</i>
147	How Does Trust in Government Institutions Affect the Demand for Cryptocurrencies? <i>Veer Krishan Choudhari</i>
152	Evaluating Beyond Meat's Success in the Consumer Market for Plant-Based Meat <i>Victor T. Weng</i>
161	Review of the Neural Correlates of Intelligence and Convergence on a Holistic Approach <i>Quinn B. Smith</i>
181	Effects of Caffeinated Beverages on Cardiac Dynamics Monitoring Data and Physically Subjective Perceptions of Adolescents in China <i>Xue Haowen</i>

Editorial Board

International Journal of High School Research

■ EXECUTIVE PRODUCER

Dr. Fehmi Damkaci

President, Terra Science and Education

■ CHIEF EDITOR

Dr. Richard Beal

Terra Science and Education

■ COPY EDITORS

Ryan Smith, Terra Science and Education

■ ISSUE REVIEWERS

Dr. Rafaat Hussein, Associate Professor, SUNY ESF.

Dr Gayatri Ramakrishna, Delhi, India.

Dr. Neelima Bahal, Uttrakhand, India.

Max Norton, University of British Columbia, Canada. **Farooq Sabir**,

The University of Texas at Austin USA.

Dr. Kristie L. Ebi, MPH, University of Washington..

Dr. Stacey Alexeeff, Kaiser Permanente Division of Research.

Dr M.Purna Kishore, Institute of Technology & Sciences..

Prof. Dr. Ravi Sekhar Yarrabothu, Vignan's Scien, Tech & Res

Dr. Thrisul Kumar, Andhra Pradesh/India.

Fozia Anwar, Higher College of Technology Sharjah.

Rajan Khona, Cambridge International School Dubai, UAE.

Dr. John Fred Briones, Director at Tessera Therapeutics.

Dr. Weiqiang Chen, Memorial Sloan Kettering Cancer Cent.

Dr. Min Huang, Director at Pfizer.

Dr. Surya Aggarwal, New York University.

Dr. Mary Tate, Yale University.

Dr. Donald Little, University of Michigan.

Dr. Rumaira Letinson, Borough of Manhattan College.

Dr. Jim Jabir, St. John's University, USA

Dr. Anita Raja, Hunter College, USA

Dr. Zohaib Karib, University of Michigan, USA

Dr. Raga Krishnakumar, Florida Institute of Technology, USA

Dr. Vipul Kishore, Florida Tech University, USA

Dr. Seong Kyun Cheong, Virginia Tech University

Dr. Yaowu Xu, Google, Mountain View, CA, USA.

Dr. Bingzhang Lu, Weill Cornell Medical College.

Dr. Harry Lee, Un. of Hawaii at Manoa, USA.

Dr. R. Vijayakumar, St. Joseph's College

Dr. S. Selvakumar, Government Arts and Sci. College, India.

Dmitry Berdinskiy, Mahidol University Ratchathewi, Thailand.

Wasamon Jantai, Chulalongkorn University, Thailand.

Taeseo Ku, Konkuk University, Seoul, South Korea.

Sang Hwa Jung, Korea Institute of Civil Engineer., South Korea

Younghun Jung, Korea Disaster Prevention Ass. South Korea.

Srishti Kapoor, Amity University, Gurgaon (Haryana).

Ankita Dave, CSIR-CSMCRI Gujarat, Gurgaon (Haryana).

Dr. Ji- Young Choi, Ohio State University.

Joseph Svec, St. Joseph University Long Island, USA.

Kun Zhu, China Agricultural University, China

Ji Daili, Institute of Botany, Chinese academy of science, China.

Hye Jin Yoo, Seoul National University Hospital Seoul.

Dong Ik Cha, Samsung Medical Center Seoul.

Tasleem Raza, Lucknow Medical College Lucknow, India.

Emokpae, University of Benin Benin City, Nigeria.

Dr. Ying Guo, California State University, USA.

Jackie Goodrich, University of Michigan.

Dr. Laurie Svoboda, Univ. of Michigan Medical School.

Dr. Byungho Lim, Korea Research Institute of Chemical.

Dr. Yoon Kim, Korea Advc. Instit. of Science and Tech.

Dr. Hee Won Lee, Seoul National University.

Dr. Jing Chen, Virginia Tech University.

Dr. Jorge A. Peña Díaz, Finlay Lab.

Ellis Michael, Google.

Jim Purbrick, Oculus London, England.

Chaitanya Mishra, Meta London, England

Umesh Mahtani, Professor of Vidyashilp University.

Dr. Shumank Deep, Asc. prof. Inst. of Man. Stud., India.

Jonathan De Caro, Wake Forest Graduate Researcher.

Nicolas Ajzenman, Prof. McGill University.

Dr. Albert Malkin, Assistant Professor MPED

Richard Haier, University of California at Irvine, USA

Michael Cole, Rutgers University, NJ, USA

Professor Zhou Boda, Tsinghua Univ. Medicine, China.

Professor Kong Lingyun, Beijing Tsinghua Changgung China.

Professor Wang Weimin, Peking Un. Health Sci. China.

Young Kim, Northrop Grumman El Segundo, CA, USA.

Soo Kim, Seoul National University

Audrey Yoon, Stanford University Palo Alto, CA, USA

Machine Learning Augmented Histopathological Diagnosis of an Aggressive Variant of Liver Cancer

Vivasvat Rastogi, Shashvat Rastogi

Vasant Valley School, Vasant Kunj Rd, Pocket 7, Sector C, Vasant Kunj, New Delhi, Delhi 110070, India; vivasvatrastogi@gmail.com
Mentor: Dr. Archana Rastogi

ABSTRACT: Liver cancer (Hepatocellular carcinoma) is one of the most common and fatal cancers. “Macrotrabecular-massive Hepatocellular carcinoma” (MTM-HCC), a recently identified aggressive variant, is characterized by thick trabeculae in 50% of the tumor area. Histopathology is the gold standard for diagnosis; however, microscopy is labor-intensive and time-consuming.

Four thousand and four hundred anonymized digitized histopathology images of HCC were used to create three main models and were randomly allocated to training (1600), validation (400), and test (400) for each. Convolutional neural network (CNN) model was created in Python using TensorFlow and Keras to predict the occurrence of Macrotrabecular patterns. After experimenting with different architectures (Inception V3, MobileNet V2, and ConvNet, VGG), optimizers and loss functions, Inception V3, RMSProp, and Binary Cross entropy were chosen. Performances were evaluated by confusion matrix and AUROC. Data augmentation improved accuracy by 25%. ML model-based Mobile App, for real-time detection of images, was developed. Independent internal and external validation was performed.

Training, validation, and test accuracies for Macrotrabecular vs non- Macrotrabecular and other patterns ranged from 96%-98%. AUROC ranged from 0.97-0.99. Internal and external validation showed an accuracy of 96-98%.

This model showed good performance and high accuracy. This is the first study to apply ML models to assist Pathologists in detecting an aggressive variant of liver cancer.

KEYWORDS: Computational biology and bioinformatics; Computational modeling; Machine learning (ML)-based mobile app; liver cancer; macrotrabecular -massive HCC.

■ Introduction

Liver cancer is the fifth most frequent and the second most fatal cancer worldwide.¹ Hepatocellular carcinoma (HCC) accounts for 85-90% of all malignant liver cancers.² HCC is associated with poor outcomes due to a lack of methods for early detection, accurate prognostication, and personalized treatments.³

Tumor tissue analysis has a well-established role in the diagnosis, theragnostic, and prognosis of HCC. Morphologic variants and phenotypes in tumor biopsies/ surgical specimens are important surrogate markers for molecular aberrations. Identifying various subtypes is a pre-requisite for prognostication, individualizing treatment, and correct allocation to new clinical trials.³ Histopathology is the gold standard for the diagnosis of HCC subtypes.³

The macrotrabecular pattern of cancer cell arrangement (> six cells thick) represents an aggressive HCC subtype. Its presence in more than 50% of total tumors is classified as “Macrotrabecular -massive HCC (MTM-HCC)”.⁴ Hallmark features of this subtype are presentation with advanced clinical stage, large size, high tumor marker levels, vessel invasion, higher recurrence, reduced survival, and specific molecular derangements.^{1,2} MTM-HCC needs more aggressive management, including liver transplantation and specific molecular therapies; hence, prompt and correct diagnosis is crucial.

Histopathological diagnosis of MTM-HCC requires manual microscopic examination of approximately 10-30 tumor

tissue sections (with 1000s of fields/ patches).⁵ This is a highly strenuous, time-consuming, and cumbersome task. Given the high tumor burden, there is an immediate need to adapt to newer methods of computational pathology. Digitization of tumor tissue slides and artificial intelligence (AI)-based analysis can impart objectivity, increase accuracy, and reduce inter-observer variability, which is a big step toward personalized medicine.

AI-based diagnostic and predictive liver cancer models are uncommon and created using radiology imaging. Data on AI-assisted Pathology image modeling is rare. The scarce literature on AI modeling on HCC pathology images includes a model for determining HCC differentiation, a model for distinguishing HCC from another less common type of liver cancer, and a model for predicting survival.⁶⁻¹¹ Machine Learning (ML) models can help in the quantification & early diagnosis of HCC subtypes. None of the published studies has evaluated AI's role in diagnosing aggressive MTM-HCC subtypes to assist Pathologists.

We hypothesize that ML models, created using digital histopathology images and their usage through a mobile app. can assist Pathologists in detecting MTM- HCC in large volumes of digitized images with high accuracy & objectivity and in a shorter time, thus helping in prognostication & timely decision of treatments. Therefore, the present work is aimed to diagnose an aggressive variant of liver cancer (MTM-HCC) by ML-assisted digital Pathology image analysis. The main objectives were to develop CNN models after experimenting

with different architectures and to create a Mobile App that uses the ML model for real-time detection of Macrotrabecular patterns in digitized tissue slide images.

■ Methods

Data:

Digital images of hematoxylin & eosin-stained (HE) and formalin-fixed paraffin-embedded (FFPE) obtained from a pool of patients with HCC (n=105), who underwent surgical resection (partial or total hepatectomy) at a large liver dedicated tertiary care institute, were used. The images were retrieved from the study of histological patterns and their clinical relevance already published by the mentor.⁵ This study required only archived digitized images with complete anonymity of the patient details. Thus, completely de-identified digital images were used and randomly numbered.

Four thousand four hundred digital images (200x magnification) representing different histological patterns of HCC, along with adjacent non-neoplastic liver and other primary cancer (cholangiocarcinoma), were used to develop the CNN model. The main histological patterns of HCC selected for the model were defined according to the published literature.^{4,12} Macrotrabecular was defined as the trabecular thickness of more than six cancer cells; micro trabecular had a trabecular thickness of 3–5 cell thick plate; pseudoglandular pattern was characterized by trabeculae forming glandular lumina with or without bile or proteinaceous material in the lumina. (Figure 1)

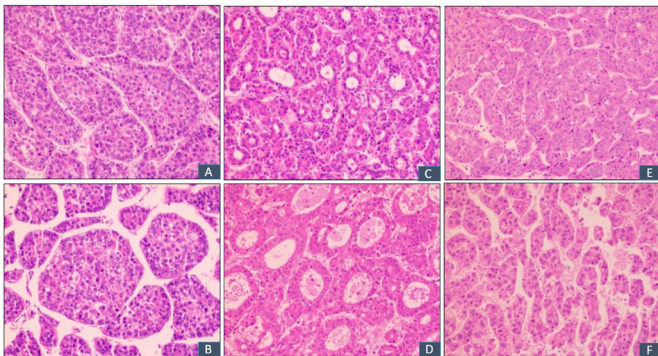


Figure 1: Histopathological images of macrotrabecular (A, B); pseudoglandular (C, D); microtrabecular (E, F) patterns. [HE stains; 200x magnification] Anonymized digital images were used for the ML model development.

Procedure:

Digital Histopathology images were scaled down to 25% of the original size, with a final size of 1024 x 822 pixels (from 40.4 MB to 3.4 MB).

CNN models were created, using supervised learning, in TensorFlow & Keras to distinguish Macrotrabecular from other patterns (Microtrabecular & Pseudoglandular). The model was programmed in Python. Details of the model development are provided later.

Accuracies of models were tested for four architectures (Inception V3, MobileNet V2, ConvNet, VGG), three optimizers, two loss functions, and with & without Data augmentation. Inception V3, RMSProp & Binary Cross entropy were chosen for the final training of models. Data augmentation improved

accuracy by ~25%. Transfer Learning was applied for Inception V3.

A total of 6 models were created (3 main + 3 pre-test): Macrotrabecular vs. Microtrabecular, Macrotrabecular vs. Pseudoglandular, and Macrotrabecular vs. Non-Macrotrabecular, and one pre-test model for each (e.g., macrotrabecular+microtrabecular vs. others (normal, cholangiocarcinoma, pseudoglandular) for the 1st main model). To improve the generalisability of models, images of tissue with pre-analytical lab-related artifacts such as tissue folds, cracks, stain deposits, and over and under-stained sections were randomly mixed while modeling. The models were exported as tflite files. (Figure 2)

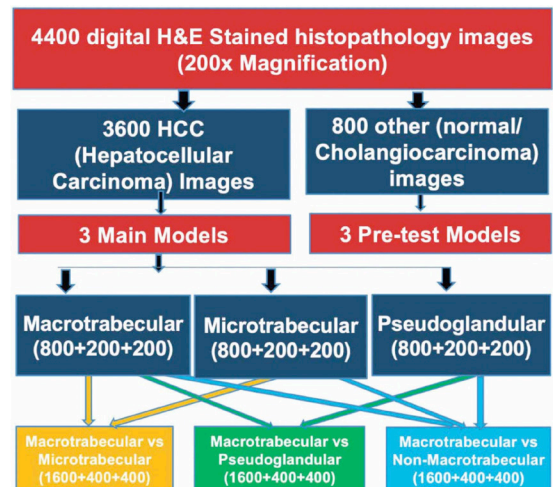


Figure 2: Data split for the creation of various models.

A mobile app was created with Flutter and Dart. The app (Livpath-AI) gives the option of 3 models to users, takes an image from the camera/gallery as input, runs the pre-test model, and provides prediction by running the main model if the pre-test was successful. (Figure 3)

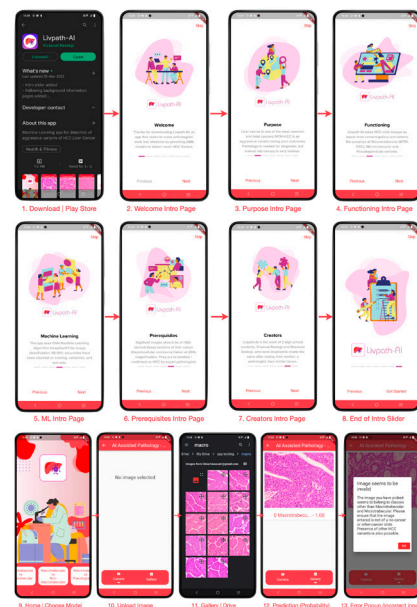


Figure 3: Livpath-AI Mobile App Workflow. Digital images acquired from the camera/gallery are analyzed by ML models, and the mobile application outputs the class probabilities.

Confusion matrices and AUROC curves were created based on test data predictions for the three main models. i.e., Macrotrabecular vs. Microtrabecular, Macrotrabecular vs. Pseudoglandular, and Macrotrabecular vs. non-Macrotrabecular.

Internal validation was performed on the independent test set 2 with HE images of FFPE cancer tissues captured at 400x magnification. External validation was performed by expert liver Pathologists of Public & Private hospitals by testing deidentified anonymized digital images of HE stained and 200x magnification using the Livpath-AI app.

Convolutional neural network (ML Model):

The model was programmed in Python using Tensorflow and Keras. Libraries used to carry out the task are shown below. The data, in the form of a zip file, was extracted from Google Drive onto Google Colaboratory (Figure 4).

```
import zipfile
import tensorflow as tf
from keras_preprocessing.image import ImageDataGenerator
from google.colab import drive

drive.mount('/content/drive')
local_zip = '/content/drive/MyDrive/Copy of train.zip'
zip_ref = zipfile.ZipFile(local_zip, 'r')
zip_ref.extractall('/tmp/train')
zip_ref.close()

local_zip = '/content/drive/MyDrive/Copy of valid.zip'
zip_ref = zipfile.ZipFile(local_zip, 'r')
zip_ref.extractall('/tmp/test')
zip_ref.close()
```

Figure 4: Data import.

The following code was written to carry out Data Augmentation, that is, reshaping the same image by rotating, zooming, shifting, etc., to increase accuracy with a relatively small dataset (Figure 5).

```
TRAINING_DIR = "tmp/train/train"
training_datagen = ImageDataGenerator(
    rescale = 1./255,
    rotation_range=40,
    width_shift_range=0.2,
    height_shift_range=0.2,
    shear_range=0.2,
    zoom_range=0.2,
    horizontal_flip=True,
    fill_mode='nearest'
)

VALIDATION_DIR = "tmp/test/valid"
validation_datagen = ImageDataGenerator(rescale = 1./255)

train_generator = training_datagen.flow_from_directory(
    TRAINING_DIR,
    target_size=(150,150),
    class_mode='categorical',
)

validation_generator = validation_datagen.flow_from_directory(
    VALIDATION_DIR,
    target_size=(150,150),
    class_mode='categorical',
)
```

Figure 5: Data augmentation.

CNN Models with the following layers/architecture were prepared: InceptionV3 using transfer learning, MobileNet V2 from Tensorflow, ConvNet with a Dense final layer for the binary prediction task, and VGG (Visual Geometry Group). These were used independently and not in the same notebook (Figures 6-9).

```
#InceptionV3
!wget --no-check-certificate \
https://storage.googleapis.com/mledu-
datasets/inception_v3_weights_tf_dim_ordering_tf_kernels_notop.h5 \
-O /tmp/inception_v3_weights_tf_dim_ordering_tf_kernels_notop.h5

from tensorflow.keras.applications.inception_v3 import InceptionV3
local_weights_file = '/tmp/inception_v3_weights_tf_dim_ordering_tf_kernels_notop.h5'
pre_trained_model = InceptionV3(input_shape = (150, 150, 3),
include_top = False,
weights = None)
pre_trained_model.load_weights(local_weights_file)

for layer in pre_trained_model.layers:
    layer.trainable = False
```

```
last_layer = pre_trained_model.get_layer('mixed7')
last_output = last_layer.output
x = layers.Flatten()(last_output)
x = layers.Dense(1024, activation='relu')(x)
x = layers.Dropout(0.2)(x)
x = layers.Dense(2, activation='softmax')(x)

model = Model(pre_trained_model.input, x)
```

Figure 6: InceptionV3.

```
#VGG
model = tf.keras.models.Sequential([
    # BLOCK-1
    tf.keras.layers.Conv2D(32, (2,2), activation = 'relu',
input_shape=(150,150,3), padding = 'same'),
    tf.keras.layers.BatchNormalization(),
    tf.keras.layers.Conv2D(32, (2,2), activation = 'relu', padding = 'same'),
    tf.keras.layers.BatchNormalization(),
    tf.keras.layers.MaxPool2D((2,2)),
    tf.keras.layers.Dropout(0.2),
    # BLOCK-2
    tf.keras.layers.Conv2D(64, (2,2), activation = 'relu', padding = 'same'),
    tf.keras.layers.BatchNormalization(),
    tf.keras.layers.Conv2D(64, (2,2), activation = 'relu', padding = 'same'),
    tf.keras.layers.BatchNormalization(),
    tf.keras.layers.MaxPool2D((2,2)),
    tf.keras.layers.Dropout(0.3),
    # BLOCK-3
    tf.keras.layers.Conv2D(128, (2,2), activation = 'relu', padding = 'same'),
    tf.keras.layers.Conv2D(128, (2,2), activation = 'relu', padding = 'same'),
    tf.keras.layers.BatchNormalization(),
    tf.keras.layers.MaxPool2D((2,2)),
    tf.keras.layers.Dropout(0.4),
    # BLOCK-4
    tf.keras.layers.Conv2D(256, (2,2), activation = 'relu', padding = 'same'),
    tf.keras.layers.BatchNormalization(),
    tf.keras.layers.Conv2D(256, (2,2), activation = 'relu', padding = 'same'),
    tf.keras.layers.BatchNormalization(),
    tf.keras.layers.MaxPool2D((2,2)),
    tf.keras.layers.Dropout(0.4),
    # End BLOCK
    tf.keras.layers.Flatten(),
    tf.keras.layers.Dense(512, activation = 'relu'),
    tf.keras.layers.BatchNormalization(),
    tf.keras.layers.Dropout(0.5),
    tf.keras.layers.Dense(256, activation = 'relu'),
    tf.keras.layers.BatchNormalization(),
    tf.keras.layers.Dropout(0.3),
    tf.keras.layers.Dense(512, activation = 'relu'),
    tf.keras.layers.BatchNormalization(),
    tf.keras.layers.Dropout(0.3),
    tf.keras.layers.Dense(2, activation='softmax')
])
```

Figure 7: VGG.

```
#ConvNet
model = tf.keras.models.Sequential([
    tf.keras.layers.Conv2D(64, (2,2), activation='relu', input_shape=(150, 150, 3)),
    tf.keras.layers.MaxPooling2D(2, 2),
    tf.keras.layers.Conv2D(64, (2,2), activation='relu'),
    tf.keras.layers.MaxPooling2D(2, 2),
    tf.keras.layers.Conv2D(128, (2,2), activation='relu'),
    tf.keras.layers.MaxPooling2D(2,2),
    tf.keras.layers.Conv2D(128, (2,2), activation='relu'),
    tf.keras.layers.MaxPooling2D(2,2),
    tf.keras.layers.Flatten(),
    tf.keras.layers.Dropout(0.5),
    tf.keras.layers.Dense(512, activation='relu'),
    tf.keras.layers.Dense(2, activation='softmax')
])
```

Figure 8: ConvNet.

```
#MobileNetV2
mobile_net_layers = tf.keras.applications.mobilenet_v2.MobileNetV2(
    input_shape=None,
    alpha=1.0,
    include_top=True,
    weights='imagenet',
    input_tensor=None,
    pooling=None,
    classes=1000,
    classifier_activation='softmax'
)
mobile_net_layers.trainable = False
model = tf.keras.Sequential([
    mobile_net_layers,
    tf.keras.layers.Dropout(0.3),
    tf.keras.layers.Dense(2, activation='softmax')
])
```

Figure 9: MobileNetV2.

The model was compiled using several optimizers and loss functions (one combination at a time) (Figure 10).

```
model.compile(loss = 'binary_crossentropy', optimizer='rmsprop',
metrics=['accuracy'])
```

Figure 10: Model compilation.

The model was trained by defining the training, validation, epochs, and call back dataset (Figure 11).

```
history = model.fit(train_generator, epochs=256, validation_data =
validation_generator, verbose = 1, callbacks=[callbacks])
```

Figure 11: Training.

The model was exported as a .tflite file. A mobile app with Flutter, based on Dart Programming language, was further created and published on Google Play Store (<https://play.google.com/store/apps/details?id=com.vivasvatrastogi.livpathai>).

A link to the GitHub repository is as follows: <https://github.com/Vivasvat-Rastogi/flutterML>

Results and Discussion

Performance Evaluation of Models:

Initial training and validation were performed with different combinations of architectures, optimizers, loss functions, and with or without data augmentation. Accuracies are shown in Table 1.

Table 1: Initial experimentation accuracies – InceptionV3, Binary crossentropy, and RMSprop showed highest accuracies.

Criteria	Divisions	Training Accuracy	Validation Accuracy
Data Augmentation	With Data Augmentation	0.82	0.95
	Without Data Augmentation	0.61	0.68
Optimisers	rmsprop	0.82	0.95
	Adam	0.83	0.90
	SGD	0.75	0.85
Loss Functions	binary_crossentropy	0.82	0.95
	Mean_squared_error	0.84	0.85
Architectures	ConvNet	0.82	0.95
	VGG	0.93	0.75
	Inception V3	0.95	0.98
	MobileNet V2	0.82	0.97

Based on the above, all the models were trained with InceptionV3 architecture using transfer learning, rmsprop optimizer, binary cross entropy loss function, and data augmentation. The final main models' accuracies were in the range of 97.5-98.5 and are shown in Table 2.

Table 2: Final models' accuracies ranged from 97.5 to 98.5.

Model	Training / Validation/ Test Accuracy		
Macro- vs Micro-trabecular	98	97.5	97.5
Macro- vs Pseudoglandular	98.5	97.5	98
Macro- vs non-macrotrabecular	98.5	98	98.5

The below confusion matrices show the actual vs. model-predicted data statistics. (Figure 12)

PREDICTED \ ACTUAL	ACTUAL		PREDICTED \ ACTUAL	ACTUAL		PREDICTED \ ACTUAL	ACTUAL	
	MACROTRABECULAR	PSEUDOGLANDULAR		MACROTRABECULAR	NON-MACROTRABECULAR		MACROTRABECULAR	MICROTRABECULAR
MACROTR.	196	4	MACROTR.	198	4	MACROTR.	196	6
PSEUDOGL.	4	196	NON-MACROTR.	2	196	MICROTR.	4	194

Figure 12: Confusion Matrices. Accuracy for different models 96-98%

Training, validation, and test accuracies ranged from 96%-98%. The area under ROC for different test groups ranged from 0.97-0.99. (Figure 13)

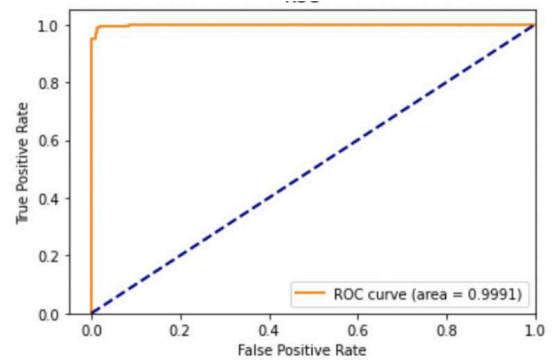


Figure 13: AUROC for Macrotrabecular versus non-Macrotrabecular was 0.99

Internal validation in an independent set of images at higher magnification (400x) displayed an accuracy of 98%. Whereas, Livpath-AI-based external validation by two different expert pathologists showed an accuracy of 96%.

Discussion

In the present study, a machine learning model and a mobile App were developed to detect an aggressive variant of liver cancer using digital histopathology images with high accuracy and objectivity in a very short time. Given the high tumor burden, scarcity of Pathologists, and concerns about the time & labor of expert Pathologists, this model has great significance. Once HCC is diagnosed by Pathologists, Machine learning (ML) based detection of Macrotrabecular patterns can assist them by reducing their workload & saving time. Even lab staff or junior pathologists can capture and test digital images with the mobile App, and expert pathologists can verify the model result remotely. Thus, in the present study, the integration of computational pathology & artificial intelligence was done to assist histopathologists.

HCC subtypes have distinct morphological characteristics and unique clinical and biological correlates. These subtypes are extremely relevant to prognosis and therapeutic decisions. Recent publications have highlighted the importance of tissue diagnosis, especially for the subtypes of HCC in the era of molecular therapies.^{1,3,5}

Ziol *et al.* identified a histologic subtype of HCC associated with specific molecular features and poor prognostic factors such as large tumor size, high serum alpha-fetoprotein (AFP) levels, satellite nodules, and vascular invasion. The authors designated this subtype as "MTM-HCC." This subtype was an independent predictor of early and overall recurrence.¹

These studies developed CNN models based on histological images and displayed high accuracy. In the study by Zeng *et al.*, areas under the receiver operating characteristic curves (AUCs) for prediction ranged from 0.78-0.91. Their different models generalized well in the validation dataset with AUCs ranging from 0.81- 0.92.¹¹ Cheng *et al.* model showed good performance with an AUC value of 93.5%.¹⁰ Lin *et al.* demonstrated over 90% accuracy of their CNN model for determining HCC differentiation.

Conclusion

Summary:

Four thousand four hundred anonymized digital images of HCC tumor tissue were randomly segregated for the train-

ing, validation, and test groups in a ratio of 4:1:1. Patch size for model development was 1024x822 pixels. CNN model was created in Python; TensorFlow and Keras were applied to distinguish macrotrabecular architecture from microtrabecular and pseudoglandular. Different architectures (ConvNet, VGG, Inception V3, Mobile Net V2), optimizers & loss functions were experimented with and finally Inception V3 (transfer learning), RMSProp, and Binary Cross entropy were chosen. Very high accuracy was achieved with InceptionV3 and MobileNet V2. Confusion Matrix and AUROC showed high accuracy (96-96%) for internal and external validation data sets. In addition, Mobile App (Android and iOS) was created using Flutter & Dart.

In conclusion:

ML (CNN) models created using digitized histopathology images of HCC showed good performance and high accuracy in detecting the MTM-HCC subtype. This model is the first to apply ML to assist Pathologists in diagnosing aggressive variants of liver cancer. ML models & Livpath-AI app quantifying the digital histopathological features can make Pathologist's tasks less labor intensive and time efficient. Early diagnosis with highly accurate ML assistance to Pathologists is a step forward toward optimizing patient care.

The way forward is testing and validating on a large cohort of HCC images from different centers and applying other CNN architectures.

Acknowledgments

The authors thank Dr. Archana Rastogi, Professor (Department of Pathology), Institute of Liver & Biliary Sciences, Delhi, India, for providing anonymized digitized histopathological images of liver cancer.

References

- Ziol, M.; Poté, N.; Amaddeo, G.; Laurent, A.; Nault, J. C.; Oberti F.; Costentin, C.; Michalak, S.; Bouattour, M.; Francoz, C.; Pageaux, G. P.; Ramos, J.; Decaens, T.; Luciani, A.; Guiu, B.; Vilgrain, V.; Aubé, C.; Derman, J.; Charpy, C.; Zucman-Rossi, J.; Barget, N.; Seror, O.; Ganne-Carrié, N.; Paradis, V.; Calderaro, J. Macrotrabecular-massive hepatocellular carcinoma: A distinctive histological subtype with clinical relevance. *Hepatology* 2018, Jul, 68 (1), 103-112. Doi: 10.1002/hep.29762. Epub 2018 May 9. PMID: 29281854.
- Li, X.; Yao, Q.; Liu, C.; Wang, J.; Zhang, H.; Li, S.; Cai, P. Macrotrabecular-Massive Hepatocellular Carcinoma: What Should We Know? *J Hepatocell Carcinoma* 2022, 5(9), 379-387. Doi: 10.2147/JHC.S364742. PMID: 35547829; PMCID: PMC9084381.
- Rastogi, A. Changing role of histopathology in the diagnosis and management of hepatocellular carcinoma. *World J Gastroenterol* 2018, 24(35), 4000-4013. Doi: 10.3748/wjg.v24.i35.4000. PMID: 30254404; PMCID: PMC6148422.
- Calderaro, J.; Couchy, G.; Imbeaud, S.; Amaddeo, G.; Letouze, E.; Blanc, J.F.; Laurent, C.; Hajji, Y.; Azoulay, D.; Bioulac-Sage, P.; Nault, J.C.; Zucman-Rossi, J. Histological subtypes of hepatocellular carcinoma are related to gene mutations and molecular tumor classification. *J. Hepatol.* 2017, 4, 727-738.
- Rastogi, A.; Maiwall, R.; Ramakrishna, G.; Modi, S.; Taneja, K.; Bihari, C.; Kumar, G.; Patil, N.; Thapar, S.; Choudhury, A.K.; Mukund, A.; Pamecha, V.; Sarin, S.K. Hepatocellular carcinoma: Clinicopathological associations amidst marked phenotypic heterogeneity. *Pathol Res Pract.* 2021, 217, 153290. Doi: 10.1016/j.prp.2020.153290. Epub 2020 Nov 24. PMID: 33307344.
- Kiani, A.; Uyumazturk, B.; Rajpurkar, P.; Wang, A.; Gao, R.; Jones, E.; Yu, Y.; Langlotz, C.P.; Ball, R.L.; Montine, T.J.; Martin, B.A.; Berry, G.J.; Ozawa, M.G.; Hazard, F.K.; Brown, R.A.; Chen, S.B.; Wood, M.; Allard, L.S.; Ylagan, L.; Ng, A.Y.; Shen, J. Impact of a deep learning assistant on the histopathologic classification of liver cancer. *NPJ Digit Med* 2020, 3 (23). PMID: 32140566 Doi: 10.1038/s41746-020-0232-8.
- Saillard, C.; Schmauch, B.; Laifa, O.; Moarii, M.; Toldo, S.; Zaslavskiy, M.; Pronier, E.; Laurent, A.; Amaddeo, G.; Regnault, H.; Sommacale, D.; Ziol, M.; Pawlotsky, J.M.; Mulé, S.; Luciani, A.; Wainrib, G.; Clozel, T.; Courtiol, P.; Calderaro, J. Predicting Survival After Hepatocellular Carcinoma Resection Using Deep Learning on Histological Slides. *Hepatology* 2020, 72 (2000-2013). PMID: 32108950 Doi: 10.1002/hep.31207.
- Lin, H.; Wei, C.; Wang, G.; Chen, H.; Lin, L.; Ni, M.; Chen, J.; Zhuo, S. Automated classification of hepatocellular carcinoma differentiation using multiphoton microscopy and deep learning. *J Biophotonics* 2019, 12(7), e201800435. PMID: 30868728 Doi: 10.1002/jbio.201800435.
- Ahn, J. C.; Qureshi, T. A.; Singal, A. G.; Li, D.; Yang, J. D. Deep learning in hepatocellular carcinoma: Current status and future perspectives. *World J Hepatol.* 2021, 13(12), 2039-2051. Doi: 10.4254/wjh.v13.i12.2039. PMID: 35070007; PMCID: PMC8727204.
- Cheng, N.; Ren, Y.; Zhou, J.; Zhang, Y.; Wang, D.; Zhang, X.; Chen, B.; Liu, F.; Lv, J.; Cao, Q.; Chen, S.; Du, H.; Hui, D.; Weng, Z.; Liang, Q.; Su, B.; Tang, L.; Han, L.; Chen, J.; Shao, C. Deep Learning-Based Classification of Hepatocellular Nodular Lesions on Whole-Slide Histopathologic Images. *Gastroenterology* 2022, 162 (7):1948-1961.e7. Doi: 10.1053/j.gastro.2022.02.025. Epub 2022 Feb 22. PMID: 35202643.
- Zeng, Q.; Klein, C.; Caruso, S.; Maille, P.; Laleh, N. G.; Sommacale, D.; Laurent, A.; Amaddeo, G.; Gentien, D.; Rapinat, A.; Regnault, H.; Charpy, C.; Nguyen, C.T.; Tournigand, C.; Brustia, R.; Pawlotsky, J.M.; Kather, J.N.; Maiuri, M.C.; Loménie, N.; Calderaro, J. Artificial intelligence predicts immune and inflammatory gene signatures directly from hepatocellular carcinoma histology. *J Hepatol.* 2022, 77(1):116-127. Doi: 10.1016/j.jhep.2022.01.018. Epub 2022 Feb 7. PMID: 35143898.
- Tan, P. S.; Nakagawa, S.; Goossens, N.; Venkatesh, A.; Huang, T.; Ward, S. C.; Sun, X.; Song, W.M.; Koh, A.; Canasto-Chibuque, C.; Deshmukh, M.; Nair, V.; Mahajan, M.; Zhang, B.; Fiel, M.L.; Kobayashi, M.; Kumada, H.; Hoshida, Y. Clinico-pathological indices to predict hepatocellular carcinoma molecular classification. *Liver Int.* 2016, 36 (1), 108-118.
- Liao, H.; Long, Y.; Han, R.; Wang, W.; Xu, L.; Liao, M.; Zhang, Z.; Wu, Z.; Shang, X.; Li, X.; Peng, J.; Yuan, K.; Zeng, Y. Deep learning-based classification and mutation prediction from histopathological images of hepatocellular carcinoma. *Clin Transl Med* 2020, 10, e102. PMID: 32536036 Doi: 10.1002/ctm2.102
- Wang, H.; Jiang, Y.; Li, B.; Cui, Y.; Li, D.; Li, R. Single-Cell Spatial Analysis of Tumor and Immune Microenvironment on Whole-Slide Image Reveals Hepatocellular Carcinoma Subtypes. *Cancers (Basel)* 2020, 12 (12), 3562. Doi: 10.3390/cancers12123562. PMID: 33260561; PMCID: PMC7761227.
- Chen, M.; Zhang, B.; Topatana, W.; Cao, J.; Zhu, H.; Juengpanich, S.; Mao, Q.; Yu, H.; Cai, X. Classification and Mutation Prediction based on Histopathology H&E images in Liver Cancer using Deep Learning. *NPJ Precis Oncol* 2020, 4, 14. PMID: 32550270 Doi: 10.1038/s41698-020-0120-3.
- Lu, L.; Daigle, B. J. Jr. Prognostic Analysis of Histopathological Images using Pre-trained Convolutional Neural Networks: Applica

- tion to Hepatocellular carcinoma. *PeerJ* **2020**, *8*, e8668. Doi: 10.7717/peerj.8668. PMID: 32201640; PMCID: PMC7073245.
17. Shi, J. Y.; Wang, X.; Ding, G. Y.; Dong, Z.; Han, J.; Guan, Z.; Ma, L. J.; Zheng, Y.; Zhang, L.; Yu, G. Z.; Wang, X. Y.; Ding, Z. B.; Ke, A. W.; Yang, H.; Wang, L.; Ai, L.; Cao, Y.; Zhou, J.; Fan, J.; Liu, X.; Gao, Q. Exploring prognostic indicators in the pathological images of hepatocellular carcinoma based on deep learning. *Gut* **2021**, *70* (5), 951-961. Doi: 10.1136/gutjnl-2020-320930. PMID: 32998878 Doi: 10.1136/gutjnl-2020-320930.
18. Yamashita, R.; Long, J.; Saleem, A.; Rubin, D. L.; Shen, J. Deep Learning Predicts Postsurgical Recurrence of Hepatocellular Carcinoma from Digital Histopathologic Images. *Sci Rep* **2021**, *11*(1), 2047. Doi: 10.1038/s41598-021-81506-y. PMID: 33479370; PMCID: PMC7820423

■ Authors

Vivasvat Rastogi and Shashvat Rastogi are brothers and seniors at Vasant Valley School, Delhi, India.

Both authors are keenly interested in technology, Computer Science, Math, Music, and Sanskrit. They have won several prestigious STEM awards at international, national, state, and school levels and play several musical instruments. They presented this research work in Regeneron ISEF 2023 under the category “Computational Biology & Bioinformatics” and won the fourth grand award in this category.

Applying Linear Regression to The World Happiness Report

Ankur A. Dabholkar

Clark High School, 523 W Spring Creek Pkwy, Plano, Texas, 75013, USA; ankur.dabholkar.1@gmail.com
Mentor: Evgeny Goncharov

ABSTRACT: In this paper, we use The World Happiness Report to illustrate the use of linear regression. We perform some linear regression using the dataset values to pinpoint the effectiveness of linear regression in data analysis. The results show that linear regression can be used to precisely define trends in the data between the output variable and the input variables.

KEYWORDS: Mathematics, Statistics; Analysis; Linear Regression; Social Science; World Happiness Report.

■ Introduction

The World Happiness Report is a measure of the general level of happiness in the world.¹ It measures happiness through a global survey, which includes questions about the demographic, economic, and emotional standpoints of the countries' population. The main question of the survey is rating the survey taker's level of happiness on a scale of 0-10, with 10 being the happiest, and 0 being the least happy. Typically, the countries that have a higher development level have a happiness rating above 7. Countries with a lower development level usually have a happiness rating below 5. For example, Iceland has a happiness rating of 7.554, whereas Kenya has a happiness rating of 4.607. This rating of happiness corresponds with certain statistics recorded by research and census surveys in its respective countries. Some aspects of a country that are included in the dataset are the country's GDP per capita and the country's healthy life expectancy. Intuitively, this means that there is some level of correlation between the aspects of a country that contribute to its development and the overall happiness of that country. With certain mathematical tools, the strength of the correlation between the happiness of a country and the statistics that define a country can be measured and quantified.² Calculus is an extremely useful mathematical concept to utilize while calculating the connection between variables and outputs.³ This type of calculation is called linear regression. It produces an equation correlating columns on a dataset (which represent data points) to the final output column in the dataset. The World Happiness Report is an excellent dataset to run a linear regression on as it contains many general trends between its variables and outputs, which can be found using linear regression. One way to execute linear regression is by writing a program in Python.⁴ Python has many tools which make data analysis and linear regression clean and concise. It also offers visual representations of the data in low dimensions.

The rest of the paper is organized as follows. In the Limits and Differentiation, One-parameter Linear Regression, and Multiple-Parameter Linear Regression sections, we introduce limits, differentiation and linear regression, as well as small examples taken from the dataset, so if the reader is familiar with

these concepts, they should feel free to skip to the Dataset section.

■ Methods

Limits and Differentiation:

To introduce linear regression, we need to be able to find the minimums of certain functions which is done via derivatives. Therefore, we remind the reader of some calculus concepts.

Informally, one can think of the limit³ of a function $f(x)$ at the point x_0 as the value that $f(x)$ approaches as x approaches x_0 . The formal definition is as follows.

Definition. The limit of a function $f(x)$ at the point x_0 is equal to L if for every $\epsilon > 0$ there is a $\delta > 0$ such that if $0 < |x - x_0| < \delta$, then $|f(x) - L| < \epsilon$. We denote this limit by $\lim_{x \rightarrow x_0} f(x) = L$ if it exists. L if it exists.

A derivative at x_0 refers to the slope of the tangent line at that point on the function's graph. The derivative's importance to our research is that derivatives can help with minimizing functions. Minimums are useful for being able to discern which function best fits the data.

~This determines a function $f'(x)$ that we call the derivative of $f(x)$ if the limit is defined.

$$f'(x_0) = \lim_{h \rightarrow 0} \frac{f(x_0 + h) - f(x_0)}{h}$$

One-parameter Linear Regression:

Linear Regression with one parameter is a statistical analysis process that predicts and measures the correlation between two variables, the single *input* variable and the output variable that we are trying to predict. It produces a line in the coordinate plane (along with the equation for the line) that correlates best with the given dataset. Linear Regression is performed by minimizing a certain loss function. Intuitively, a loss function⁷ minimizes errors of the model based on a training example or a dataset. We shall consider the case of a quadratic loss function which is known as the Least Squares Approximation method.

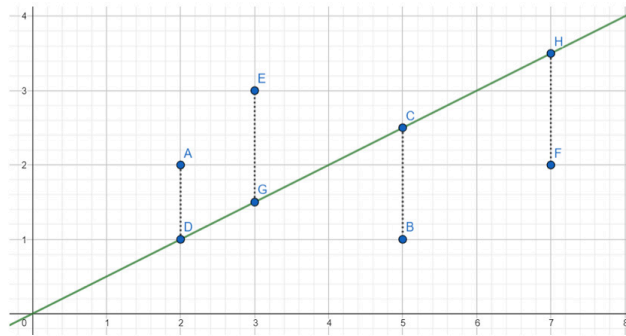


Figure 1: Example of a predicted line for a data set.

Algorithm 1. Suppose that the dataset consists of pairs $(x_i, y_i), i = 1, \dots, n$. We would like to approximate it by a line of the form $y=kx+b$, that finds the coefficients k and b that best approximate the data. Consider the loss function,

$$L(k, b) = \sum_{i=1}^n (kx_i + b - y_i)^2 = (kx_1 + b - y_1)^2 + \dots + (kx_n + b - y_n)^2.$$

This function measures how close the actual data points are to the corresponding points on the line. For example, Figure 1 entails a random dataset of 4 points A, B, E, and F. In the figure, the dotted lines are the distances corresponding to the individual terms in the loss function. This function has one local minimum⁷ (k_{min}, b_{min}) , obtained by solving the system of linear equations

$$\frac{\partial L}{\partial k} = \frac{\partial L}{\partial b} = 0$$

where the ∂ stands for the partial derivative defined as follows.

Definition. We define the partial derivative⁵ of function $L(k, b)$ with respect to k as

$$\frac{\partial L}{\partial k} = \lim_{h \rightarrow 0} \frac{L(k+h, b) - L(k, b)}{h}$$

This determines a function that is the derivative of the function $L(k, b)$ solely through the change of k , with b acting as a constant. The partial derivative of function $L(k, b)$ with respect to b is defined as

$$\frac{\partial L}{\partial b} = \lim_{h \rightarrow 0} \frac{L(k, b+h) - L(k, b)}{h}$$

This equation is like the first partial derivative, however, instead of b acting as a constant, k acts as a constant to make the derivative only depend on the change of b .

The system of equations produces the global minimum of the function corresponding to the best level of correlation between the predicted line and the dataset.

Example 1. In the following example, we are taking a sample of the dataset we are using for this research. We are comparing the GDP column with the Ladder Score column, which essentially compares the economic status of a country to the average happiness rating in that country. The single parameter is the Logged GDP per capita, and the output is the Happiness Rating at the country level. Figure 2 depicts that there is a linear correlation between the two.

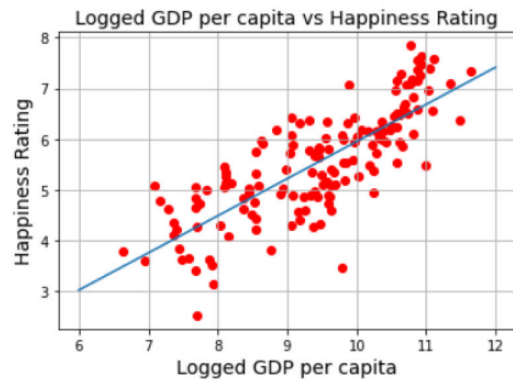


Figure 2: The line-of-best-fit depicts a correlation between GDP and Happiness.

Once linear regression is performed on the data (using Least Squares Approximation) the line-of-best-fit that is produced has

$$b=-1.3719060741319824, k=0.73203909$$

As shown in Figure 2, the line does correlate with the data well.

Multiple-parameter Linear Regression:

Linear Regression with multiple parameters k_0, \dots, k_n can calculate the strength of correlation of multiple variables. There are multiple input variables and only one output variable. It provides a linear function of the form

$$k_0x_0+k_1x_1+\dots+k_nx_n+b$$

that best approximates the data (using the least squares method to judge how good the approximation is). The method is a direct generalization to Algorithm 1 (the loss function is similar but now depends on k_0, \dots, k_n, b).

Algorithm 2. Suppose that the dataset consists of vectors $(x_{1i}, \dots, x_{ni}, y_i), i=1, \dots, m$. We would like to approximate the dataset by a hyperplane⁸ of the form $y=k_1x_1+k_2x_2+\dots+k_nx_n+b$, that finds the coefficients k_1, \dots, k_n and b that best approximate the data. Consider the loss function

$$L(k_1, \dots, k_n, b) := \sum_{i=1}^m (k_1x_{1i} + \dots + k_nx_{ni} + b - y_i)^2$$

This function has one local⁷ minimum $(k_1^{min}, \dots, k_n^{min}, b^{min})$, obtained by solving the system of linear equations

$$\frac{\partial L}{\partial k_1} = \dots = \frac{\partial L}{\partial k_n} = \frac{\partial L}{\partial b} = 0$$

where the ∂ symbol is the partial derivative of the loss function with respect to the variable that follows. The system of equations is the global minimum of the function corresponding to the best level of correlation between the predicted hyperplane and the dataset.

Example 2. In this example, we are once again taking a sample of the dataset we are using for this research. We are comparing the GDP column and the social support column to the Ladder Score column. This compares the correlation between both the economy of a country and the social situation of a country with the average happiness rating in that country. Figure 3 depicts a plane that correlates with the data for these parameters well.

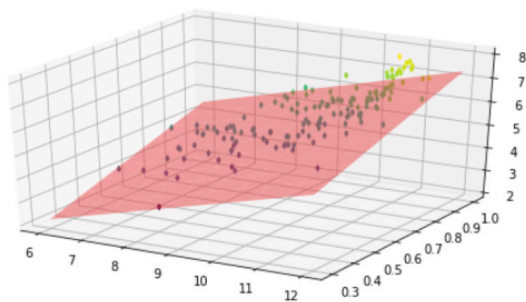


Figure 3: A plane predicted by the data points.

Once linear regression is performed on the data (using Least Squares Approximation) the plane-of-best-fit that is produced (with coefficients approximated to 3 digits) is

$$z=0.472x+3.333y-1.639$$

Dataset:

The original source used for this research contains data from about 150 countries. The dataset consists of columns of data that contain values for each country.² The Ladder score specifies the average country-level happiness rating. The dataset has the following columns of importance, which we will use as parameters¹:

- **Logged GDP per capita:** The subsequent explanation of the data references how per capita measurements are more accurate than total measurements of GDP, as such the column should be described as a per capita metric.
- **Social Support:** This column gives a scale on how much support an individual in the country feels they receive from others around them.
- **Healthy Life Expectancy:** This column provides the average number of years a person born in that country is expected to live based on previous years and interpolation and extrapolation.
- **Freedom to Make Life Choices:** This column gives a measure of how the government allows the population to make decisions.
- **Generosity:** This column is the average level of generosity throughout the population of the country.
- **Perceptions of Corruption:** This designates a relative level of corruption in a country.

The columns of the 5 happiest countries are shown in Table 1

Implementation:

Table 1: Data about the 5 happiest countries.

Country	Ladder Score	Logged GDP per capita	Social Support	Healthy Life Expectancy	Freedom to make life choices	Generosity	Perceptions of corruption
Finland	7.842	10.775	0.95	72.0	0.949	-0.098	0.186
Denmark	7.620	10.933	0.954	72.7	0.946	0.030	0.179
Switzerland	7.571	11.117	0.942	74.4	0.919	0.025	0.292
Iceland	7.554	10.878	0.983	73.0	0.955	0.160	0.673
Netherlands	7.464	10.932	0.942	72.4	0.913	0.175	0.338

For this research, all coding and linear regression will be done in Python.⁴ First, for linear regression to be possible, we will need to import the pandas library (along with other libraries), so the dataset can be read. Lines 1-4 of the code achieve this.

```
import pandas as pd
from sklearn import linear_model
import statsmodels.api as sm
data = pd.read_csv('world-happiness-report-2021.csv')
```

The pandas library is a Python, open-source package focused on data analysis and allows for multiple-parameter linear regression. Once this package is imported, we will then have to import the dataset for analysis. The “hyperplane-of-best-fit” will be found, and the correlation of the data will be measured between certain parameters and the average happiness in that country. The regression coefficients that are produced by the code will show the respective dataset columns’ effect on country-level happiness. The full code can be found on request, as the rest of the code is merely formatting and setting up the linear regression.

The main way to measure correlation is Pearson’s coefficient.⁶ We set the coefficient equal to a variable P (Which it is in the data table in Section 5). If $|P|=1$ then the dataset correlates perfectly with the predicted function. If $1>|P|>.7$, then the dataset correlates strongly with the predicted function. When $.7>|P|>.3$, then the dataset somewhat correlates with the predicted function. When $.3>|P|>0$, then the dataset weakly correlates (and does not correlate at all when $|P|=0$) with the predicted function. The resulting findings will be analyzed by the following code:

```
print(correlation.loc[['Logged GDP per capita','Social support','Healthy life expectancy','Freedom to make life choices','Generosity','Perceptions of corruption'],'Ladder score'])
model = sm.OLS(Y, X).fit()
predictions = model.predict(X)
print_model = model.summary()
print(print_model)
```

Results and Discussion

Upon running the code, we get,

Table 2: Coefficients (coef) and Pearson’s correlation coefficient (P) produced by code.

	coef	std err	P
Constant	-2.2372	0.630	
Logged GDP per capita	0.2795	0.087	0.789760
Social support	2.4762	0.668	0.756888
Healthy life expectancy	0.0303	0.013	0.768099
Freedom to make life choices	2.0105	0.495	0.607753
Generosity	0.3644	0.321	-0.017799
Perceptions of corruption	-0.6051	0.291	-0.421140

Approximating three significant digits, the hyperplane of best fit is as follows:

$$f(x_1, x_2, x_3, x_4, x_5, x_6) = 0.280x_1 + 2.476x_2 + 0.030x_3 + 2.010x_4 + 0.364x_5 - 0.605x_6 - 2.237$$

where x_1 is the input for Logged GDP per capita, x_2 is the input for social support, x_3 is the input for Healthy life expectancy, x_4 is the input for Freedom to make life choices, x_5 is the input for Generosity, and x_6 is the input for Perceptions of corruption. The regression coefficients indicate the contributions that each input makes toward the Ladder Score. Intuitively, the results mean that all the columns have a positive effect

when considering the magnitude of each column's effect on happiness, the regression coefficients' values do not accurately reflect their respective column's impact on happiness. This is because, when considering the scale of the actual data values, social support and Freedom to make life choices are measured on a 0-1 scale, whereas inputs like Logged GDP per capita and Healthy life expectancy are measured on a much larger scale, causing the regression coefficients to be larger with respect to columns with lower data values instead of their actual effect on happiness. When each column is put to the same 0-1 scale (including Ladder score), and linear regression is applied again, the regression coefficients change significantly, and the resulting equation is

$$f(x_1, x_2, x_3, x_4, x_5, x_6) = 0.415x_1 + 0.310x_2 + 0.297x_3 + 0.249x_4 + 0.025x_5 - 0.072x_6 - 0.285$$

It is important to note that following the scale changes, the Pearson correlation coefficients do not change in comparison to the P column in Table 2. Indeed, merely scaling the data does not alter the correlation of the input data with the output data but produces regression coefficients so that they more accurately reflect each column's effect on happiness. The coefficients show that Logged GDP per capita has the largest effect on happiness, followed by social support, and the Perceptions of corruption column is the only data column that has an adverse effect on happiness. This interpretation of the regression coefficients produced by linear regression illustrates the effectiveness of linear regression in showing statistical trends in datasets such as the World Happiness Report.

■ Conclusion

To use linear regression with multiple parameters effectively, one must first be able to employ derivatives on loss functions to be able to find the minimum of that function. Once this is achieved, linear regression can be used to measure the correlation that parameters have to the overall output. The regression coefficients show that the World Happiness Report contains data values that correlate strongly with country-level happiness, exemplified by the regression coefficients in the equation produced by the linear regression calculation.

■ Future Research

Some research could involve other aspects of countries that could be quantified. The economy and government system (GDP, Social Support, and Perceptions of Corruption) are emphasized in our research, but some social examples include the Crude Birth Rate (CBR), and Crude Death Rate (CDR), which measure the number of births per 1000 people, and the number of deaths per 1000 people respectively. Along with this, some historical developments, such as economic failures and social unrest, could affect happiness.⁹ These parameters could have a relatively strong correlation with the data, as these values tend to change with development. Another way to extend this research is to use an output other than the World Happiness Report. This may include the Human Development Index (HDI)¹⁰ or the Quality-of-Life measure (QoL). This will influence which parameters correlate well, as development and quality of life may depend on parameters that are not equally as important to happiness.

■ Acknowledgments

I would like to thank Evgeny Goncharov for advising me and giving me invaluable support throughout the process of writing this paper.

■ References

1. Helliwell, J.; Huang, H.; Wang, S.; Norton, M. Statistical Appendix 1 for Chapter 2 of World Happiness Report 2021. <https://happiness-report.s3.amazonaws.com/2021/Appendix1WHR2021C2.pdf> (accessed 2023-05-14).
2. Singh, A. World Happiness Report 2021, 2021. <https://www.kaggle.com/datasets/ajaypalsinghlo/world-happiness-report-2021>
3. Strang, G. Calculus, 3rd ed.; Wellesley-Cambridge Press: Wellesley, MA, 2017.
4. Real Python. Linear regression in python. <https://realpython.com/linear-regression-in-python/> (accessed Sep 10, 2022).
5. Hilton, P. J. Partial Derivatives; Routledge & Kegan Paul PLC: London, England, 1960. (Accessed 2022-09-07).
6. Sedgwick, P. Pearson's correlation coefficient. <https://doi.org/10.1136/bmj.e4483> (accessed Sep 10, 2022).
7. Mahendru, K. Understanding Loss Functions to Maximize Machine Learning Model Performance (Updated 2023). https://www.analyticsvidhya.com/blog/2019/08/detailed-guide-7-loss-functions-machine-learning-python-code/#What_Are_Regression_Loss_Functions? (accessed 2023-05-11).
8. DeepAI. Hyperplane. <https://deepai.org/machine-learning-glossary-and-terms/hyperplane> (accessed 2023-05-16).
9. Ortiz-Ospina, E.; Roser, M. Happiness and Life Satisfaction. <https://ourworldindata.org/happiness-and-life-satisfaction> (accessed 2023-05-17).
10. Hall, J.; Helliwell, J. F. <https://hdr.undp.org/system/files/documents/happinessandhdpdf.pdf> (accessed 2023-05-18).

■ Authors

Ankur Dabholkar is a 10th-grade student at Clark High School in Plano. His areas of interest include data analysis and world systems. He plans to major in computer science or social sciences.

An Examination of Stroke and Air Pollution Trends in Taiwan, 1990 to 2022

Audrey Wang

Notre Dame High School, 596 S Second St, San Jose, CA 95112, USA; audreywangaa@gmail.com
Mentor: Makenna Lenover

ABSTRACT: Air pollution has been found to correlate with rising stroke levels in Taiwan's population, but a comprehensive analysis of trends throughout the past three decades has not yet been done. While research is still ongoing into the biological mechanisms through which airborne pollutants affect the vasculature, pollution is thought to increase the risk of stroke by hardening arteries in the brain and increasing the risk of clots. Taiwan's concentration of industrial sectors and its mountainous topography— which traps airborne pollution— make the issue especially serious. In Taiwan, stroke is the most common cause of disability and the third most common cause of death. This topic has been examined before but not evaluated in a longer timeframe. To investigate this, I conducted a literature review from 1995 to 2022 and analyzed current epidemiological data to analyze trends and identify solutions. This research not only depicts Taiwanese residents' situation but that of the global community as a whole. Jet streams moving across the earth are distributing pollution from various places while simultaneously, stroke is growing as a global health risk, making this a universally relevant issue.

KEYWORDS: Translational Medical Sciences; Disease Prevention; Stroke; Air pollution; Taiwan; Cardiovascular disease; Cerebrovascular disease; East Asia.

■ Introduction

Over the last three decades, evidence has emerged linking air pollution and cardiovascular mortality and morbidity, and pollution is responsible for approximately 9 million deaths per year, about 1 in 6 deaths globally.¹ The island nation of Taiwan has both high levels of air pollution and a population more susceptible to stroke, making it an interesting avenue to examine this issue. In 2020, 16% of Taiwan's population was 65 years old and above, a share which is projected to grow to 40% by 2060.² Health conditions such as cardiovascular diseases, stroke, and diabetes are increasingly common due to the island's aging population. In addition, stroke is the leading cause of complex disability, often leaving survivors and their families with severe financial issues due to their inability to work. Increasing air pollution has influenced stroke morbidity and mortality worldwide, including in Taiwan. One form of pollution, particulate matter or PM_{2.5} (tiny particles or droplets in the air that are two and one-half microns or less in width), is capable of entering the lungs and the bloodstream, causing cardiovascular, cerebrovascular (stroke), and respiratory issues.³ Although the biological links between stroke and air pollution have been thoroughly examined, a holistic review of all research on this topic in Taiwan has not been done in the last three decades. Therefore, this review set out to evaluate the extent to which different forms of air pollution in Taiwan have affected the susceptibility to stroke of its population throughout the years.

■ Introduction to air pollution

What is Air Pollution?:

Air pollution is a general term that includes a mixture of numerous components from various sources. Currently, airborne

particulate matter (PM) and gaseous pollutants such as ozone (O₃), sulfur dioxide (SO₂), carbon monoxide (CO), and nitrogen oxides, including nitrogen dioxide (NO₂) and nitrogen oxide (NO), are considered to pose a risk to human health.⁴ PM_{2.5} is generally accepted as the most harmful to human health due to the range of health effects it is associated with, as well as its ubiquity in the environment.⁵

Human-produced air pollution typically comes from sources such as vehicle emissions, fuel oils, and natural gas used to heat homes, byproducts of commercial manufacturing, and power generation— specifically coal-powered power plants. Natural air pollution is another contributor; smoke released by wildfires, ash and gasses from volcanic eruptions, and gasses such as methane are all produced naturally, though human activities can exacerbate negative impacts.⁶

Increasing Global Concerns:

While global rates of air pollution are improving, 99% of the global population still breathes air that exceeds the World Health Organization's air quality limits.⁷ Over 6,000 cities in 117 countries are now monitoring air quality, but their residents are still being exposed to harmful levels of fine particulate matter and nitrogen dioxide. Low and middle-income countries are exposed to the highest pollution levels, with less than 1% of cities in compliance with WHO recommendations.⁷

Air pollution is especially harmful to already vulnerable populations. In 2021, an estimated 40,000 deaths under the age of five were directly linked to PM_{2.5} air pollution.⁸ Populations with different biological coping capacities— the elderly, fetuses and children, and people with pre-existing diseases are far more impacted by air pollution than average.⁹ In the United States, a meta-analysis found a strong negative association be-

tween socioeconomic status and air pollution exposure and a similar trend in other areas, including New Zealand, Asia, and Africa.¹⁰ Recent research also shows that exposure to PM_{2.5} increases both the risk of contracting COVID-19 and suffering more severe symptoms when infected, including death.¹¹

Taiwan's Vulnerability to Pollution:

Air pollution in Taiwan was the highest among the Four Asian Tigers— Hong Kong, Singapore, South Korea, and Taiwan¹² and even higher than some cities in China and Southeast Asia. Additionally, the annual PM₁₀ (particulate matter with a diameter of 10 micrometers or smaller) average in Taipei ranked 1,089 out of 1,600 cities worldwide.¹³ The yearly average of PM_{2.5} exposure in Taiwan has been at 20-30 [µg/m³]- four to six times the current WHO guidelines— for the past three decades.^{14, 55}

Taiwan's mountainous topography and robust industrial sector contribute to its high air pollution concentration. Taiwan's capital city is situated within the Taipei Basin— a "bowl" surrounded by mountains.¹⁵ This causes the formation of temperature inversions (when air temperature increases by height, trapping cooler air below), which can trap smog and other pollutants.¹⁶ Polluting industries are concentrated in specific locales; industrial centers are located along its northern and western coasts, surrounded by water and high mountains. Domestic sources of pollution, such as incineration of organic matter, combustion of fossil fuels, and automobile traffic within cities, also contribute to the pollution issue.¹⁷

How Air Pollution Spreads:

Air pollution can spread worldwide through wind patterns and jet streams, meaning that pollution originating in Asia can still affect places on the other side of the world. East Asian pollutants such as carbon monoxide (CO), nitrogen oxides (NO), particulate matter (PM), and sulfur oxides (SO_x)¹⁸ are emitted from combustion and industrial sources and are carried toward the equator by cold winds.¹⁹ These pollutants cross the North Pacific Ocean in the mid to upper troposphere (the lowest region of the atmosphere) and have even been documented to descend to the surface in North America.²⁰ Studies have recorded frequent exportation of Asian dust, sulfate aerosol, and mercury to western North America.²⁰ In 2006, export-related air pollution originating in China accounted for 12 to 24% of sulfate concentrations in the Western United States.⁵⁶ Precipitation and transportation of food can also distribute pollution.²¹ Hemispheric transport of air pollution is especially difficult to control because it would likely require international regulation.⁵⁶

Many cities in western Taiwan are affected by both local and transboundary pollutants; Taiwan's geographic location— close to the southeast of China— often receives transboundary pollution from East Asia and Indochina.²² Despite rapid progress in combating the issue, China remains the tenth most polluted country globally, with particulate pollution almost four times the WHO guideline.²³ Northeastern monsoons in the winter can transport airborne particulate matter (PM_{2.5}) from northern China, Korea, and Japan towards downwind regions such as Taiwan and the Philippines.²⁴

This type of long-range transport causes the deterioration of regional and ambient air quality in those areas.²⁵

How Air Pollution Affects the Body (Biologically):

In 2019, the Global Burden of Disease Study found that air pollution— which includes ambient particulate matter pollution (with a diameter of <2.5 µm; PM_{2.5})— contributed to 213 million DALYs (disability-adjusted life years) and 6.67 million deaths.²⁶ In Latin America, where large populations were exposed to relatively high levels of air pollution, a meta-analysis found that an increased risk of mortality was strongly associated with increased ambient concentrations of PM₁₀ and O₃ gasses— previous corroborating observations in other parts of the world. The same study also found that people with lower socioeconomic status, infants, and young children were more susceptible to both PM₁₀ and O₃.²⁷ Primary and secondary pollutants can also exacerbate the effects of climate change, affecting public health through more extreme temperatures and lessening crop yields.²⁸

Various diseases and health conditions are associated with air pollution, most commonly of the respiratory and circulatory systems. For example, in response to higher ambient PM concentrations, hospital admissions in the United Kingdom for several cardiovascular and pulmonary diseases acutely increased.²⁹ It was also found that prenatal or perinatal exposure to air pollutants could lead to the late onset of respiratory diseases in children and adults.³⁰ Particulate matter can enter the bronchopulmonary tract, passing multiple protective mechanisms depending on the size and chemical nature of the pollutants.³⁰ For example, PM_{2.5} can invade more deeply into the lungs due to its smaller size.

Additionally, air pollution also impairs human health through both development and chronic disease. Exposure to vehicular pollutants was associated with quantifiable impairment of brain development in the young and the exacerbation of cognitive decline in the elderly.³¹ PM₁₀ air pollution may also be associated with higher average blood sugar levels in newly diagnosed type 2 diabetes patients.³² Additional correlations were also found with preterm birth, reproductive health, rheumatic diseases, and neurodegenerative diseases.³³⁻³⁶

Air pollution can enter the body through the skin or the lungs when we breathe, where it can then enter the bloodstream.^{37,38} Because of its ubiquity in our environments and how easily it enters the body, it can be almost impossible to avoid the health effects of pollution. Air pollution can affect ecosystems in various ways— causing acid rain, contaminating water sources and soil, and even killing plants or animals.³⁹

Overview of Stroke:

A stroke, also known as a brain attack, occurs when the blood supply to part of the brain is blocked or a blood vessel within the brain bursts. In both cases, parts of the brain become damaged and die, which can cause lasting brain damage, long-term disability, or even death. The brain controls the body's movements and functions, stores memories, and is the source of all thoughts, emotions, and language. To work correctly, the brain needs oxygen-rich blood, which the arteries supply. However, brain cells start to die within minutes if something blocks the blood flow, causing a stroke.⁴⁰

In 2019, stroke was the second leading cause of death globally, and prevalence increases as the world population ages.⁴¹ Additionally, more and more young people are being affected; the burden of stroke in people under 65 years increased over the past few decades, with the incidence rising by 25% amongst adults between 20 to 64 years.⁴²

Quick treatment is critical for recovery, but in a survey done by the CDC, only 38% of respondents in the United States were aware of all significant symptoms and knew to call 911.⁴³ Due to its ability to cause immense damage to a person's health in the span of minutes, its growing prevalence, and the lack of life-saving awareness surrounding its treatment, stroke is an extremely critical public health issue.

Stroke in Taiwan:

Stroke is the third leading cause of death and the most common cause of disability in Taiwan.⁴⁴ Other factors such as age, gender, hypertension, diabetes, obesity, atrial fibrillation, and smoking contribute significantly to stroke morbidity. The average years of potential life lost before age 70 for stroke is 13.8 years. Stroke also significantly burdens the Taiwanese national healthcare system, costing an estimated 475 million US dollars.⁴⁴

In contrast to Western countries⁴⁵, the incidence of stroke is rising in Taiwan, according to a study presented at the ASEAN Federation of Cardiology Congress in 2018. After adjusting for the aging population, the incidence of ischemic stroke increased from 110 to 122 per 100,000 person-years, and intracerebral hemorrhage rose from 30 to 38 per 100,000 person-years.⁴⁶ Cardiovascular disease remains a significant cause of death in Asian populations, and previous reports have shown that stroke is more common in Asian than in Western populations.⁴⁶ In 2002, 60% of the world's total stroke mortality occurred in East Asia.⁴⁷ Asian populations tend to be more susceptible to stroke due to aging populations and underlying genetic predispositions.⁴⁸

Summary of Literature on Air Pollution and Stroke in Taiwan :

The link between pollution rates and cerebrovascular disease burden in Taiwan has been examined in numerous previous studies. The general consensus is that increased rates of hospital admissions for a variety of cardiovascular events are associated with short term⁵⁷⁻⁶¹ exposure to pollutants such as nitrogen dioxide (NO₂), sulfur dioxide (SO₂), ozone (O₃), and PM_{2.5} and PM₁₀ and that certain patients (such as those with advanced age and hypertension) are more susceptible to air pollution's impacts on hospitalization.⁶²

Residents of Kaohsiung— a city on the southwest coast of Taiwan and the center of the island's heavy industry— showed elevated rates of cerebrovascular disease.⁶⁰ Sources of pollution include frequent Asian dust storm (ADS) events (when dust originating in Mongolia and China is windblown to Taiwan)^{63,64}, and traffic-related pollution.^{65,66}

Methods

A comprehensive search of peer-reviewed journals, articles, and reports was completed using a set of key terms, including stroke and air pollution, stroke and Taiwan, air pollution and cardiovascular disease, pollution and cerebrovascular disorder,

air pollution and health, ischemic stroke, and air pollution in Taiwan. The main database used was the United States National Library of Medicine's PubMed database. I additionally reviewed the references section of each article to find additional information. This search covered 29 peer-reviewed articles published between 1995 and 2022, cited throughout.

Using Excel functions, I calculated the R² values and correlation coefficients from data on the mortality rate of cerebrovascular diseases and the recorded levels of different air pollutants from 2010 to 2015 in Taiwan. The data for mortality rate was obtained through the Statista database and was cross-referenced for accuracy with studies of cerebrovascular mortality rate in Taiwan from the literature examined in this review.^{49,53} The pollutant data was obtained from a cohort study conducted in Taiwan, which used data on air pollutants from air quality monitoring stations across Taiwan and evaluated the risk of stroke using stroke data from Taiwan's universal health insurance program.⁴⁹

Results and Discussion

Data Analysis:

I compiled stroke and air pollution data in Taiwan to investigate the trends and plotted them to identify potential correlations. Figure 1 shows the annual cerebrovascular disease mortality rate and year from 2010 to 2020, demonstrating the overall trend for stroke prevalence in the past few decades. Figure 2 shows the annual NO₂, SO₂, PM_{2.5}, NO_x, and O₃ pollution rates in Taiwan versus the year to illustrate pollution trends throughout the study period (annual average pollution levels are summarized across periods with varying pollution levels). Both stroke and pollution rates have been on a downward trend in Taiwan. Then, individual pollutants were plotted with annual cerebrovascular mortality rates to determine whether the two factors were correlated (Figures 3-7). PM_{2.5} and O₃ pollution seemed to be the most correlated with stroke prevalence, with correlation coefficients of 0.72 and 0.892, respectively. The other forms of pollutants had lower correlation coefficients ((Figures 3-7; Table 1).

Mortality Rate of Cerebrovascular Diseases (per 100,000 population) vs. Year

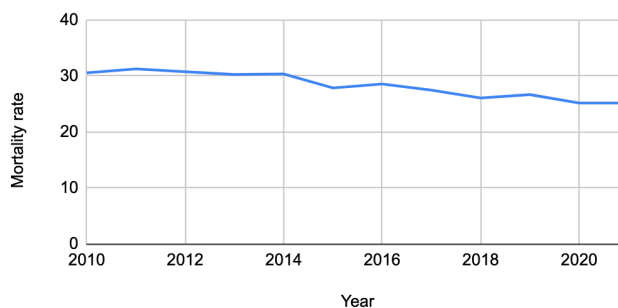


Figure 1: The annual mortality rate of Cerebrovascular diseases in the years 2010 to 2021.

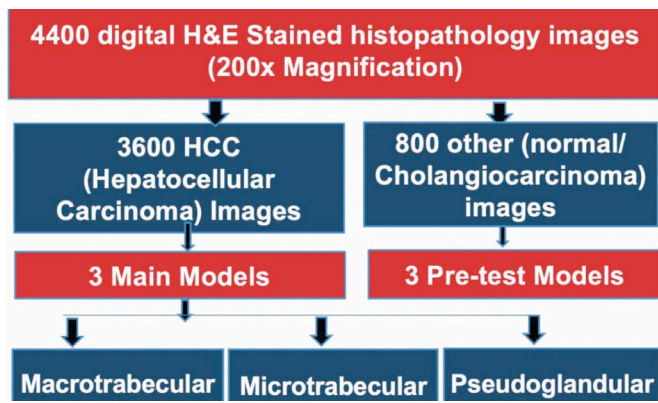


Figure 2: Years 2010 to 2015 and annual rates of pollutants NO₂, SO₂, PM_{2.5}, NO_x, and O₃.^{49, 49}

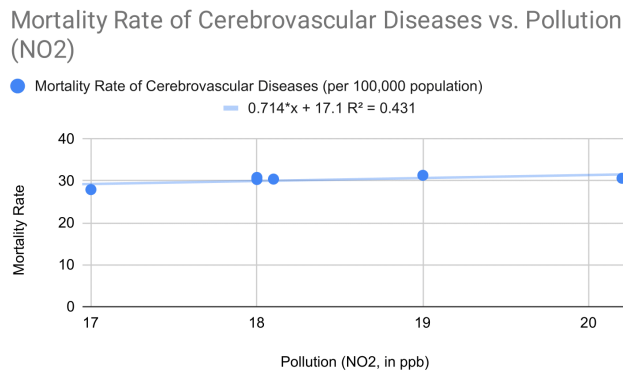


Figure 3: The annual rates of cerebrovascular disease mortality and pollution (NO₂), 2010 to 2015.⁵³

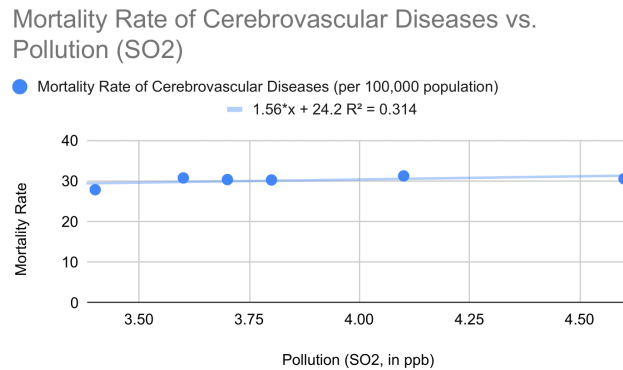


Figure 4: The annual rates of cerebrovascular disease mortality and pollution (SO₂), 2010 to 2015.^{49, 53}

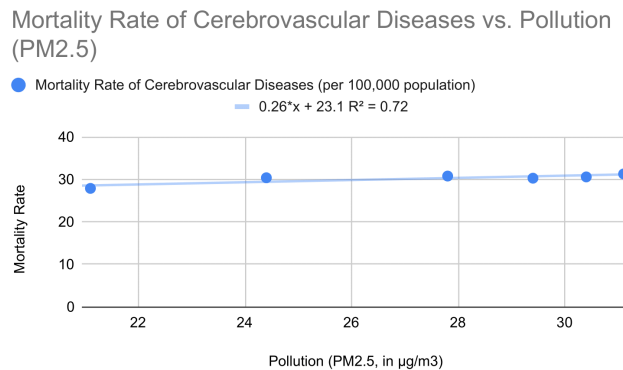


Figure 5: The annual rates of cerebrovascular disease mortality and pollution (PM_{2.5}), 2010 to 2015.^{49, 53}

Mortality Rate of Cerebrovascular Diseases vs. Pollution (NO_x)

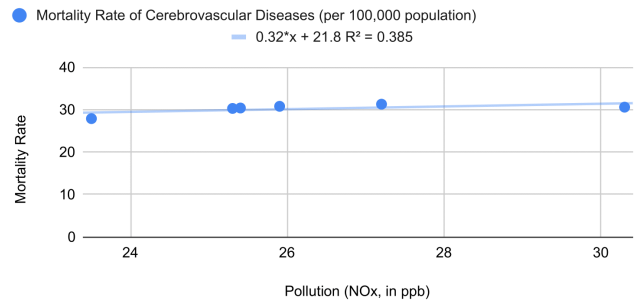


Figure 6: The annual rates of cerebrovascular disease mortality and pollution (NO_x), 2010 to 2015.^{49, 53}

Mortality Rate of Cerebrovascular Diseases vs. Pollution (O3)

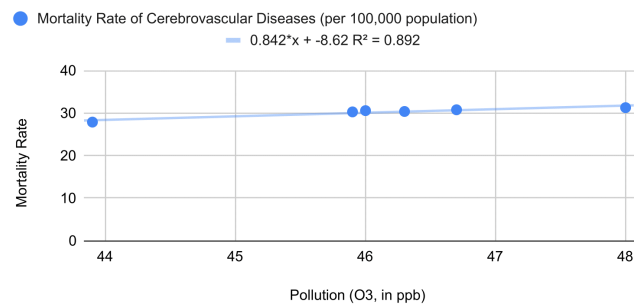


Figure 7: The annual rates of cerebrovascular disease mortality and pollution (O₃), 2010 to 2015.^{49, 53}

Table 1: R² values and correlation coefficients for each pollutant with the mortality rate of cerebrovascular diseases, from highest to lowest correlation:

Pollutant	R ²	Correlation coefficient
NO ₂ (ppb)	0.431	0.66
SO ₂ (ppb)	0.314	0.56
PM _{2.5} (µg/m ³)	0.72	0.85
NO _x (ppb)	0.385	0.62
O ₃ (ppb)	0.892	0.94

Conclusion

The variation in the correlation between pollutant types and the stroke mortality rate has interesting implications. PM_{2.5} and O₃ pollution seemed to be the most correlated with stroke prevalence, with correlation coefficients of 0.72 and 0.892, respectively. O₃ had the highest concentrations overall, which may be the reason behind its higher correlation coefficient. Also, PM_{2.5} not only had higher reported concentrations but is also considered one of the most dangerous pollutants for humans due to its small size and ability to travel deeply into the respiratory tract.³ However, NO_x pollution– which had similar concentrations as PM_{2.5}– did not seem to correlate as strongly. This may be because NO_x, while harmful, is generally considered less dangerous to human health than other forms of pollution, including ozone and particulate matter.

The American Heart Association has found that higher levels of air pollution may trigger cerebrovascular events through both long and short-term exposures.⁵⁴ Major studies

conducted in the U.S., Europe, and Asia found that not only are higher levels of ozone correlated with a risk of premature death but also that lower levels of ozone can still cause serious harm.⁵⁰ A 2017 study in the United States found that older adults faced a higher risk of premature death, even when ozone levels remained well below national standards.⁵¹ PM_{2.5-10} has also been linked to illness, hospitalization, and death.⁵⁰ Researchers in a study of six U.S. cities tracked particle pollution and health outcomes from 1974 to 2009 and estimated that the U.S. could prevent around 34,000 premature deaths yearly by lowering annual particulate matter levels by 1 µg/m³.⁵² In the past three decades, the annual average of PM_{2.5} exposure in Taiwan has ranged from 20 to 30 [µg/m³] (four to six times the World Health Organization's guidelines).^{14, 55} Taiwan's robust industrial sector and its geography and topography exacerbate the population's vulnerability to adverse pollution-related health effects.¹⁵⁻¹⁷ Some studies have even suggested an interaction between pollutants.²⁷ It is plausible that higher correlations between O₃ and PM_{2.5} pollution and stroke are related to both their high concentrations in the atmosphere and the known dangers they pose to human health.

Since the primary data regarding pollutants only spanned from 2010 to 2015, the findings could be more comprehensive in their adaptability. In the future, larger-scale investigations into the link between air pollution and stroke should be explored and analyzed for differences in the types of pollutants and other factors. Additionally, current data and trends should be followed longitudinally to understand the relationship between the variation in pollution and stroke mortality rates. As life expectancies grow, age-related medical conditions, such as stroke, will continue to impact a growing proportion of the global population. Simultaneously, experts are analyzing climate issues— including but not limited to air pollution— more and more for their public health implications. As such, an investigation into the topic of stroke and air pollution in Taiwan has global significance.

■ Acknowledgments

I want to acknowledge my family and friends for their support and encouragement throughout this process.

■ References

- 20six%20pollutants Fuller, R.; Landrigan, P. J.; Balakrishnan, K.; Bathan, G.; Bose-O'Reilly, S.; Brauer, M.; Caravanos, J.; Chiles, T.; Cohen, A.; Corra, L.; Cropper, M.; Ferraro, G.; Hanna, J.; Hanrahan, D.; Hu, H.; Hunter, D.; Janata, G.; Kupka, R.; Lanphear, B.; Lichtveld, M. Pollution and Health: A Progress Update. *The Lancet Planetary Health* 2022, 0 (0). [https://doi.org/10.1016/S2542-5196\(22\)00090-0](https://doi.org/10.1016/S2542-5196(22)00090-0).
- Taiwan: Population Share Aged 65 and Older 1960-2060 <https://www.statista.com/statistics/1112400/taiwan-share-of-persons-in-population-aged-65-and-older/#:~:text=In%202020%2C%20the%20share%20of> (accessed 2022 -11 -08).
- Fine Particles (PM 2.5) Questions and Answers https://www.health.ny.gov/environmental/indoors/air/pm2_5.htm#:~:text=What%20is%20Particulate%20Matter%202.5.
- Lee, K. K.; Miller, M. R.; Shah, A. S. V. Air Pollution and Stroke. *Journal of Stroke* 2018, 20 (1), 2–11. <https://doi.org/10.5853/jos.2017.02894>.
- IQ Air. Interactive Global Map of 2021 PM_{2.5} Concentrations by City <https://www.iqair.com/us/world-air-quality-report>.
- National Institute of Environmental Health Sciences. Air Pollution and Your Health <https://www.niehs.nih.gov/health/topics/agents/air-pollution/index.cfm>.
- World Health Organization. Billions of People Still Breathe Unhealthy Air: New WHO Data <https://www.who.int/news/item/04-04-2022-billions-of-people-still-breathe-unhealthy-air-new-who-data>.
- IQ Air. The Real Cost of Air Pollution <https://www.iqair.com/newsroom/cost-of-air-pollution>.
- Makri, A.; Stilianakis, N. I. Vulnerability to Air Pollution Health Effects. *International Journal of Hygiene and Environmental Health* 2008, 211 (3-4), 326–336. <https://doi.org/10.1016/j.ijheh.2007.06.005>.
- Hajat, A.; Hsia, C.; O'Neill, M. S. Socioeconomic Disparities and Air Pollution Exposure: A Global Review. *Current Environmental Health Reports* 2015, 2 (4), 440–450. <https://doi.org/10.1007/s40572-015-0069-5>.
- Wu, X.; Nethery, R. C.; Sabath, M. B.; Braun, D.; Dominici, F. Air Pollution and COVID-19 Mortality in the United States: Strengths and Limitations of an Ecological Regression Analysis. *Science Advances* 2020, 6 (45), eabd4049. <https://doi.org/10.1126/sciadv.abd4049>.
- Bloomenthal, A. Four Asian Tigers Tend to Promote Roaring Local Economies <https://www.investopedia.com/terms/f/four-asian-tigers.asp>.
- Air quality worst among “Tigers” - Taipei Times <https://www.taipeitimes.com/News/taiwan/archives/2014/05/13/2003590245> (accessed 2022 -11 -08).
- News, T. Taiwanese Non-Smokers Twice as Likely to Get Lung Cancer as Heavy Smokers in West | Taiwan News | 2018-01-24 12:22:00 <https://www.taiwannews.com.tw/en/news/3348480> (accessed 2022 -11 -08).
- Giese-Bogdan, S.; Levine, S. P. From Michigan to Taiwan: Air Pollution Technology. *Journal of the International Institute* 1995, 3 (1).
- Service, NOAA. N. W. Glossary - NOAA's National Weather Service <https://w1.weather.gov/glossary/index.php?word=inversion>.
- Taiwan Air Quality Index (AQI) and Taiwan Air Pollution | Air Visual <https://www.iqair.com/us/taiwan>.
- CDC. Air Quality - Air Pollutants | CDC <https://www.cdc.gov/air/pollutants.htm#:~:text=These%20are%20carbon>.
- European Geosciences Union. Travelling Pollution: East Asian Human Activities Affect Air Quality in Remote Tropical Forests. <https://www.sciencedaily.com/releases/2015/03/150331102451.htm>.
- Ewing, S. A.; Christensen, J. N.; Brown, S. T.; Vancuren, R. A.; Cluff, S. S.; Depaolo, D. J. Pb Isotopes as an Indicator of the Asian Contribution to Particulate Air Pollution in Urban California. *Environmental Science & Technology* 2010, 44 (23), 8911–8916. <https://doi.org/10.1021/es101450t>.
- Team, C. The Traveling Of Air Pollution Around The World: How Air Pollutants From Far Away Can Harm You <https://cleanair.camfil.us/2018/02/19/how-air-pollutants-from-far-away-can-harm-you/#:~:text=Air%20pollution%20is%20distributed%20largely> (accessed 2022 -11 -08).
- Griffith, S. M.; Huang, W.-S.; Lin, C.-C.; Chen, Y.-C.; Chang, K.-E.; Lin, T.-H.; Wang, S.-H.; Lin, N.-H. Long-Range Air Pollution Transport in East Asia during the First Week of the COVID-19 Lockdown in China. *Science of the Total Environment* 2020, 741, 140214. <https://doi.org/10.1016/j.scitotenv.2020.140214>.
- Country: China <https://aqli.epic.uchicago.edu/country-spotlight/china/>.
- Yuan, C.; Sau, C.-C.; Chen, M.-C.; Huang, M.; Chang, S.; Lin,

- Y.; Lee, C. Terrestrial, Atmospheric and Oceanic Sciences (TAO) - Mass Concentration and Size-Resolved Chemical Composition of Atmospheric Aerosols Sampled at the Pescadores Islands during Asian Dust Storm Periods in the Years of 2001 and 2002 <http://tao.cgu.org.tw/index.php/articles/archive/atmospheric-science/item/552> (accessed 2022 -11 -08).
25. Chuang, M.-T.; Fu, J. S.; Lin, N.-H.; Lee, C.-T.; Gao, Y.; Wang, S.-H.; Sheu, G.-R.; Hsiao, T.-C.; Wang, J.-L.; Yen, M.-C.; Lin, T.-H.; Thongboonchoo, N.; Chen, W.-C. Simulating the Transport and Chemical Evolution of Biomass Burning Pollutants Originating from Southeast Asia during 7-SEAS/2010 Dongsha Experiment. *Atmospheric Environment* 2015, 112, 294–305. <https://doi.org/10.1016/j.atmosenv.2015.04.055>.
26. Murray, C. J. L.; Aravkin, A. Y.; Zheng, P.; Abbafati, C.; Abbas, K. M.; Abbasi-Kangevari, M.; Abd-Allah, F.; Abdelalim, A.; Abdollahi, M.; Abdollahpour, I.; Abegaz, K. H.; Abolhassani, H.; Abo yans, V.; Abreu, L. G.; Abrego, M. R. M.; Abualhasan, A.; Abu-Raddad, L. J.; Abushouk, A. I.; Adabi, M.; Adekanmbi, V. Global Burden of 87 Risk Factors in 204 Countries and Territories, 1990–2019: A Systematic Analysis for the Global Burden of Disease Study 2019. *The Lancet* 2020, 396 (10258), 1223–1249. [https://doi.org/10.1016/s0140-6736\(20\)30752-2](https://doi.org/10.1016/s0140-6736(20)30752-2).
27. Romieu, I.; Gouveia, N.; Cifuentes, L. A.; de Leon, A. P.; Junger, W.; Vera, J.; Strappa, V.; Hurtado-Díaz, M.; Miranda-Soberanis, V.; Rojas-Bracho, L.; Carbajal-Arroyo, L.; Tzintzun-Cervantes, G.; HEI Health Review Committee. Multicity Study of Air Pollution and Mortality in Latin America (the ESCALA Study). *Research Report (Health Effects Institute)* 2012, No. 171, 5–86.
28. Orru, H.; Ebi, K. L.; Forsberg, B. The Interplay of Climate Change and Air Pollution on Health. *Current Environmental Health Reports* 2017, 4 (4), 504–513. <https://doi.org/10.1007/s40572-017-0168-6>.
29. Brook, R. D.; Franklin, B.; Cascio, W.; Hong, Y.; Howard, G.; Lipssett, M.; Luepker, R.; Mittleman, M.; Samet, J.; Smith, S. C.; Ta ger, I. Air Pollution and Cardiovascular Disease. *Circulation* 2004, 109 (21), 2655–2671. <https://doi.org/10.1161/01.cir.0000130041.c8>.
30. Kim, D.; Chen, Z.; Zhou, L.-F.; Huang, S.-X. Air Pollutants and Early Origins of Respiratory Diseases. *Chronic Diseases and Translational Medicine* 2018, 4 (2), 75–94. <https://doi.org/10.1016/j.cdtm.2018.03.003>.
31. Clifford, A.; Lang, L.; Chen, R.; Anstey, K. J.; Seaton, A. Exposure to Air Pollution and Cognitive Functioning across the Life Course – a Systematic Literature Review. *Environmental Research* 2016, 147, 383–398. <https://doi.org/10.1016/j.envres.2016.01.018>.
32. Tamayo, T.; Rathmann, W.; Krämer, U.; Sugiri, D.; Grabert, M.; Holl, R. W. Is Particle Pollution in Outdoor Air Associated with Metabolic Control in Type 2 Diabetes? *PLoS ONE* 2014, 9 (3), e01639. <https://doi.org/10.1371/journal.pone.0091639>.
33. Olsson, D.; Mogren, I.; Forsberg, B. Air Pollution Exposure in Early Pregnancy and Adverse Pregnancy Outcomes: A Register-Based Cohort Study. *BMJ Open* 2013, 3 (2), e001955. <https://doi.org/10.1136/bmjopen-2012-001955>.
34. Hansen, C.; Luben, T. J.; Sacks, J. D.; Olshan, A.; Jeffay, S.; Strader, L.; Perreault, S. D. The Effect of Ambient Air Pollution on Sperm Quality. *Environmental Health Perspectives* 2010, 118 (2), 203–209. <https://doi.org/10.1289/ehp.0901022>.
35. Sun, G.; Hazlewood, G.; Bernatsky, S.; Kaplan, G. G.; Eksteen, B.; Barnabe, C. Association between Air Pollution and the Development of Rheumatic Disease: A Systematic Review. *International Journal of Rheumatology* 2016, 2016, 1–11. <https://doi.org/10.1155/2016/5356307>.
36. Xu, X.; Ha, S. U.; Basnet, R. A Review of Epidemiological Research on Adverse Neurological Effects of Exposure to Ambient Air Pollution. *Frontiers in Public Health* 2016, 4. <https://doi.org/10.3389/fpubh.2016.00157>.
37. Weschler, C. J.; Bekö, G.; Koch, H. M.; Salthammer, T.; Schripp, T.; Toftum, J.; Clausen, G. Transdermal Uptake of Diethyl Phthalate and Di(N-Butyl) Phthalate Directly from Air: Experimental Verification. *Environmental Health Perspectives* 2015, 123 (10), 928–934. <https://doi.org/10.1289/ehp.1409151>.
38. Missouri Department of Natural Resources. Air Quality and You: Health Effects of Air Pollution | Missouri Department of Natural Resources <https://dnr.mo.gov/air/get-involved/air-quality-health-effects>.
39. Stanley, M. Air Pollution | National Geographic Society <https://education.nationalgeographic.org/resource/air-pollution>.
40. CDC. About Stroke <https://www.cdc.gov/stroke/about.htm>.
41. World Health Organization. The Top 10 Causes of Death <https://www.who.int/news-room/fact-sheets/detail/the-top-10-causes-of-death>.
42. Krishnamurthi, R. V.; Moran, A. E.; Feigin, V. L.; Barker-Collo, S.; Norrving, B.; Mensah, G. A.; Taylor, S.; Naghavi, M.; Forouzanfar, M. H.; Nguyen, G.; Johnson, C. O.; Vos, T.; Murray, C. J. L.; Roth, G. A.; GBD 2013 Stroke Panel Experts Group. Stroke Prevalence, Mortality and Disability-Adjusted Life Years in Adults Aged 20–64 Years in 1990–2013: Data from the Global Burden of Disease 2013 Study. *Neuroepidemiology* 2015, 45 (3), 190–202. <https://doi.org/10.1159/000441098>.
43. Centers for Disease Control and Prevention. Stroke Facts | cdc.gov <https://www.cdc.gov/stroke/facts.htm#:~:text=Stroke%20Statistics>.
44. Hsieh, F.-I.; Chiou, H.-Y. Stroke: Morbidity, Risk Factors, and Care in Taiwan. *Journal of Stroke* 2014, 16 (2), 59. <https://doi.org/10.5853/jos.2014.16.2.59>.
45. Johns Hopkins Bloomberg School of Public Health. Stroke Risk and Death Rates Fall over Past Two Decades | Johns Hopkins | Bloomberg School of Public Health <https://publichealth.jhu.edu/2014/stroke-risk-and-death-fates-fall-over-past-two-decades> (accessed 2022 -11 -08).
46. European Society of Cardiology. Stroke Incidence Rising in Taiwan Contrary to Falls in Western Countries <https://www.escardio.org/The-ESC/Press-Office/Press-releases/Stroke-incidence-rising-in-Taiwan-contrary-to-falls-in-Western-countries> (accessed 2022 -11 -08).
47. Mehndiratta, M. M.; Khan, M.; Mehndiratta, P.; Wasay, M. Stroke in Asia: Geographical Variations and Temporal Trends. *Journal of Neurology, Neurosurgery & Psychiatry* 2014, 85 (12), 1308–1312. <https://doi.org/10.1136/jnnp-2013-306992>.
48. Kim, Y. D.; Jung, Y. H.; Saposnik, G. Traditional Risk Factors for Stroke in East Asia. *Journal of Stroke* 2016, 18 (3), 273–285. <https://doi.org/10.5853/jos.2016.00885>.
49. Chen, P.-C.; Sung, F.-C.; Mou, C.-H.; Chen, C. W.; Tsai, S. P.; Hsieh, D. H. P.; Hsu, C. Y. A Cohort Study Evaluating the Risk of Stroke Associated with Long-Term Exposure to Ambient Fine Particulate Matter in Taiwan. *Environmental Health: a Global Access Science Source* 2022, 21 (1), 43. <https://doi.org/10.1186/s12940-022-00854-y>.
50. American Lung Association. Particle Pollution. American Lung Association. March 24, 2020.
51. Di, Q.; Dai, L.; Wang, Y.; Zanobetti, A.; Choirat, C.; Schwartz, J. D.; Dominici, F. Association of Short-Term Exposure to Air Pollution with Mortality in Older Adults. *JAMA* 2017, 318 (24), 2446. <https://doi.org/10.1001/jama.2017.17923>.
52. US EPA National Center for Environmental Assessment, R. T. P. N.; Owens, B. Air Quality Criteria for Particulate Matter (Final Report, 2004) <https://cfpub.epa.gov/ncea/risk/recordisplay.cfm?id>

- eid=87903 (accessed 2022 -12 -13).
53. Zhang, W. Taiwan: Cerebrovascular Disease Standardized Mortality Rate 2021 <https://www.statista.com/statistics/860647/taiwan-cerebrovascular-disease-standardized-death-rate/> (accessed 2022 -12 -14).
 54. Kulick, E. R.; Kaufman, J. D.; Sack, C. Ambient Air Pollution and Stroke: An Updated Review. *Stroke* 2022, 54 (3). <https://doi.org/10.1161/strokeaha.122.035498>.
 55. Kan, H. World Health Organization Air Quality Guidelines 2021. *Chinese Medical Journal* 2022, Publish Ahead of Print (5). <https://doi.org/10.1097/cm9.0000000000002014>.
 56. Lin, J.; Pan, D.; Davis, S. J.; Zhang, Q.; He, K.; Wang, C.; Streets, D. G.; Wuebbles, D. J.; Guan, D. China's International Trade and Air Pollution in the United States. *Proceedings of the National Academy of Sciences* 2014, 111 (5), 1736–1741. <https://doi.org/10.1073/pnas.1312860111>.
 57. Shin, D.-C. Hazardous Air Pollutants; CRC Press, 2016; pp. 48–59.
 58. Chien, T.-Y.; Ting, H.-W.; Chan, C.-L.; Yang, N.-P.; Pan, R.-H.; Lai, K. R.; Hung, S.-I. Does the Short-Term Effect of Air Pollution Influence the Incidence of Spontaneous Intracerebral Hemorrhage in Different Patient Groups? Big Data Analysis in Taiwan. *International Journal of Environmental Research and Public Health* 2017, 14 (12), 1547. <https://doi.org/10.3390/ijerph14121547>.
 59. Chiu, H.-F.; Peng, C.-Y.; Wu, T.-N.; Yang, C.-Y. Short-Term Effects of Fine Particulate Air Pollution on Ischemic Heart Disease Hospitalizations in Taipei: A Case-Crossover Study. *Aerosol and Air Quality Research* 2013, 13 (5), 1563–1569. <https://doi.org/10.4209/aaqr.2013.01.0013>.
 60. Tsai, S.-S.; Goggins, W. B.; Chiu, H.-F.; Yang, C.-Y. Evidence for an Association between Air Pollution and Daily Stroke Admissions in Kaohsiung, Taiwan. *Stroke* 2003, 34 (11), 2612–2616. <https://doi.org/10.1161/01.str.0000095564.33543.64>.
 61. Chan, C.-C.; Chuang, K.-J.; Chien, L.-C.; Chen, W.-J.; Chang, W.-T. Urban Air Pollution and Emergency Admissions for Cerebrovascular Diseases in Taipei, Taiwan. *European Heart Journal* 2006, 27 (10), 1238–1244. <https://doi.org/10.1093/eurheartj/ehi835>.
 62. Chang, C.-H.; Chen, S.-H.; Liu, P.-H.; Huang, K.-C.; Chiu, I.-Min.; Pan, H.-Y.; Cheng, F.-J. Ambient Air Pollution and Risk for Stroke Hospitalization: Impact on Susceptible Groups. *Toxics* 2022, 10 (7), 350. <https://doi.org/10.3390/toxics10070350>.
 63. Yang, C.-Y.; Chen, Y.-S.; Chiu, H.-F.; Goggins, W. B. Effects of Asian Dust Storm Events on Daily Stroke Admissions in Taipei, Taiwan. *Environmental Research* 2005, 99 (1), 79–84. <https://doi.org/10.1016/j.envres.2004.12.009>.
 64. Bell, M. L.; Levy, J. K.; Lin, Z. The Effect of Sandstorms and Air Pollution on Cause-Specific Hospital Admissions in Taipei, Taiwan. *Occupational and Environmental Medicine* 2008, 65 (2), 104–111. <https://doi.org/10.1136/oem.2006.031500>.
 65. Tsai, D.-H.; Wang, J.-L.; Chuang, K.-J.; Chan, C.-C. Traffic-Related Air Pollution and Cardiovascular Mortality in Central Taiwan. *Science of The Total Environment* 2010, 408 (8), 1818–1823. <https://doi.org/10.1016/j.scitotenv.2010.01.044>.
 66. Yang, W.-T.; Wang, V.-S.; Chang, L.-T.; Chuang, K.-J.; Chuang, H.-C.; Liu, C.-S.; Bao, B.-Y.; Chang, T.-Y. Road Traffic Noise, Air Pollutants, and the Prevalence of Cardiovascular Disease in Taichung, Taiwan. *International Journal of Environmental Research and Public Health* 2018, 15 (8), 1707. <https://doi.org/10.3390/ijerph15081707>.

■ Author

Audrey Wang is a student at Notre Dame High School who is fascinated by the study of global public health. She hopes to continue studying medicine through an international lens in college and

beyond. In the long term, she hopes to contribute to developing a more equitable future in global health.

IoT - SMART Urinal cum Disinfectant Flush System

Bhupen Sai Bandi

11th Grade, FIITJEE Junior College, Andhra Pradesh - 520010, India; regelelumii4@gmail.com

Mentor: Bhaskar Bandi, B.E (ECE)

ABSTRACT: This paper endeavours to tackle the challenges of poor sanitation and water conservation in public toilets. Inspired by real-world experiences and the critical need to enhance sanitation while conserving essential resources—such as water, human resources, cleaning materials, and time—an IoT device has been conceptualized. The proposed solution is a 'Microcontroller-Based SMART Urinal cum Disinfectant Flush System,' which operates similarly to a sensor-based urinal and also offers automatic cleaning. Moreover, its smartness allows extensive possibilities for further enhancement. It uses microcontrollers (ESP2866, ESP32), Time of Flight (ToF) sensors, Latching Solenoids, Solenoid Drivers, a DC motor, a water flow sensor, a sound recording cum player, and a speaker. The ESP2866 microcontroller continuously measures distance via a ToF sensor installed at the urinal. Suppose a person remains within proximity to the urinal for over 5 seconds. In that case, it triggers the microcontroller to confirm the person's presence and initiate water flushing for a specific duration after leaving. In addition, if the ESP2866 microcontroller detects the presence of any person, it triggers playing customized announcements. Simultaneously, the ESP32 microcontroller oversees water flow using a water flow sensor. If water flow exceeds a specified duration, the ESP32 microcontroller activates a buzzer to indicate potential water leakage. Programmed timings enable the ESP32 to control the central water supply solenoid, turning it OFF, and the ESP2866 activates the urinal flush solenoid and the DC motor submerged in disinfectant flushes disinfectant in the urinal for a set period. After disinfectant flushing, the ESP32 turns ON the central solenoid to restore the main water supply. At the same time, the ESP2866 deactivates the Urinal Flush Solenoid to halt water flow in the urinal and starts performing the routine. The flushing cycle can be changed from post-urination to pre- & post-urination, and it can be customized. Parameters such as the person-sensing distance, water flow duration, disinfectant flushing time and duration, etc, are customizable. The functionality of automated Urinal Flush, Disinfectant Flush, and a customized announcement system were tested using the designed embedded electronic IoT device. Arduino IDE was used to program Microcontrollers ESP32 and ESP2866.

KEYWORDS: Engineering Mechanics, Internet of Things; Smart Urinal; Disinfectant Flush, Microcontroller; ESP32, ESP2866, Solenoid, TOF sensor, Arduino IDE.

■ Introduction

The idea of developing a solution to improve sanitation, hygiene, and water conservation in Public Toilets has come to mind after observing/experiencing poor sanitation and hygiene in several public toilets in various places and cities. The following are a few sample photos (Figure A, Figure B, Figure C, Figure D) of the toilets observed.



Figure A: unhygienic surroundings of Public Toilet



Figure B: unhygienic condition of Urinals



Figure C: unhygienic condition of Urinal



Figure D: unhygienic surroundings of Public Toilet

The Honorable Prime Minister of India, Sri. Naredra Modi Ji launched the Swachh Bharat Mission on 2nd October 2014 to achieve universal sanitation coverage and to put the focus on sanitation, "open-defecation free" (ODF), by 2 October 2019. This has improved sanitation conditions very significantly across all parts of India. However, to make these great efforts sustainable and successful, adopting the latest technologies - Embedded Electronics, Information & Communication Technology; easing the operations, maintenance, and supervision of Public Toilets.

The availability of clean and hygienic toilets is a citizen's fundamental right. However, India's growing urbanization, vast geographical area, prevailing systems, and practices made it an enormous task for Urban Local Bodies to provide hygienic public toilets and maintenance.

Hygiene maintenance is essential in public toilets (Viz.: Schools, Educational Institutions, Hospitals, Hotels, Theatres, Malls, Cities, etc.) to overcome the spread of Covid-19 like a pandemic. Public Toilets are one of the vulnerable places for spread of diseases. The physical touch of taps and faucets increases the spread of harmful bacteria.

Still, people are scared of using public toilets because of poor hygiene and foul smell/odor, causing people to prefer to urinate openly. This is due to poor maintenance, poor supervision, and bad usage of toilets by the public.

Drawbacks of existing traditional Urinals:

1. Manual operation of the valve/faucet, requiring physical touch, posing hygiene concerns.
2. Reluctance to engage with the valve post-urination, leading to incomplete or absent flushing.
3. Necessity for more frequent cleaning of the urinal basin, demanding increased human resources.
4. Unpleasant odors due to inadequate flushing.
5. Potential water wastage caused by valve malfunctions.
6. No mechanism for remote monitoring and supervision..

Drawbacks of existing Sensor based Automatic Urinals:

1. Fixed flush duration without manageability.
2. Predefined time for flush activation, typically occurring 5 to 10 seconds after a person leaves.
3. Lack of control over the triggering distance for the flush mechanism.
4. Absence of a disinfectant flushing system to maintain cleanliness in the urinal basin.
5. Increased maintenance requirements for battery-operated systems, particularly challenging when managing multiple Sensor-based Urinals, demanding more supervision.
6. Inability to monitor water consumption or detect leak-ages.
7. Absence of mechanisms for monitoring usage analytics & remote supervision of toilets.

After exploring various contemporary solutions for automated urinal flush systems, it was found that none addresses all the essential aspects. To overcome these limitations, devised an IoT (Internet of Things) based Smart Urinal cum Disinfectant flush system aimed at addressing the constraints above. This system serves as a foundational step towards developing a more comprehensive solution.

Description of the project:

IoT (Internet of Things) – Smart Urinal cum Disinfectant Flush System (Figure E) consists of three parts and are:

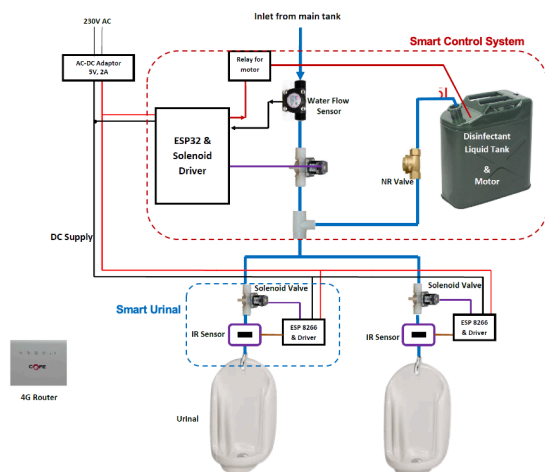


Figure E: Block diagram of IoT based Smart Urinal cum Disinfectant Flush

- a. Smart Urinal.
- b. Smart Control System.
- c. 4G Wi-Fi Hotspot.

Software:

Arduino IDE is used for programming the Microcontrollers in this project.

Working:

Flow chart of Smart Urinal cum disinfectant flush system:

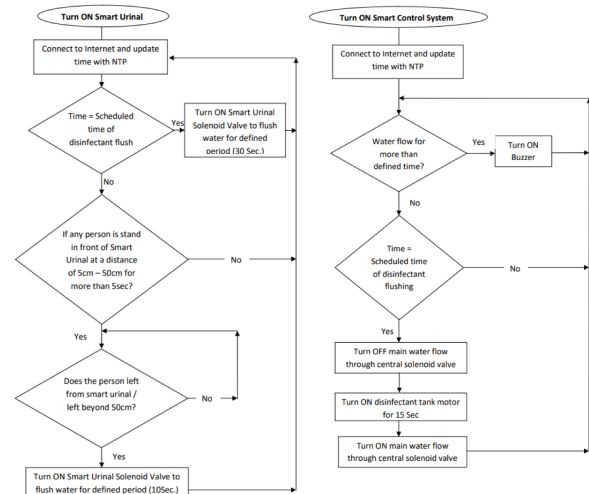


Figure F

Figure F

a. Smart Urinal:

It is designed using microcontroller ESP2866, L9110S – Dual Channel H-Bridge motor driver (as solenoid driver), TOF Sensor –VL5310X, Sound Recorder – ISD 1820, Speaker 0.5W, Latching Solenoid valve. The functioning of the Smart Urinal is explained with a flow chart in Figure F.

1. It establishes an internet connection via a 4G Wi-Fi hotspot and synchronizes its time from an NTP server.

2. It automatically detects a person within a defined proximity for a specified period and initiates water flushing after the person urinates and leaves. In this project, the activation range is set between 5 cm to 50 cm, and the minimum set duration is 5 seconds. If a person enters and exits the proximity in less than 5 seconds within the range of 5 cm to 50 cm, the system will not activate the flush. These parameters are adjustable based on requirements.

3. The flush duration can be customized and it is set as 10 Sec. in this project.

4. As soon as sensor detects a person within specified distance, it plays customised audio. In this project, the announcement is – “**This is an automatic urinal flush system. Please urinate in the urinal only**”. It can be modified as you wish.

5. Distance of activation can be modified through the web page.

b. Smart Control System:

It is designed using microcontroller ESP32, L9110S – Dual Channel H-Bridge motor driver (as solenoid driver), Buzzer, Single Channel Relay, 5V water motor pump, Latching Solenoid valve, tank for disinfectant liquid storage, Non-return Valve, Water Flow Sensor - YF-S201.

The functions of the Smart Control System are explained with a flow chart in Figure G. It performs flushing of disinfectant, Water Leakage detection, and alerting.

1. When the Smart Control System is turned ON, it connects to the internet through a 4G Wi-Fi hotspot and updates its time from the NTP server.

2. When the Smart Control System is turned ON, it connects to the internet through a 4G Wi-Fi hotspot and updates its time from the NTP server.

3. As per the desired schedule, the central water supply solenoid will stop the main water supply, and then the disinfectant motor will be turned ON for a programmed period (for 15 Sec in this project).

4. The disinfectant liquid will be sent into the main water pipeline through a non-return valve, as shown in Figure E.

5. After 15 Sec. the central water supply solenoid will start the flow of water from the main water line.

6. It is programmed to turn ON the Smart Urinal's solenoid valve at the same scheduled time for disinfectant flushing. So that as soon as the main water supply is turned OFF by the Smart Control System, Smart Urinal's solenoid will be continued to be in open for 30 Sec.

7. First, for 15 seconds, the disinfectant will be flushed, and for the next 15 seconds, the water will be flushed. This cleanses the urinal with disinfectant. All the parameters are programmable. After the 30 seconds, Smart Urinal's solenoid valve will be closed automatically.

8. ESP 32 microcontroller continuously receives the water flow rate from the water flow sensor. If the water flows continuously for more than a specified period, it will alert through Buzzer. In this project, 0.5 liters/minute is taken as minimum usage, and the period is taken as 120 seconds. If the use is more than 0.5 liters continuously for more than 120 Sec., it will alert through Buzzer.

c. 4G Wi-Fi hotspot:

It is used for Internet connectivity. Smart Control System and Smart Urinal will work synchronously with the clock synchronized with NTP Server.

Advantages:

1. Improved sanitation and hygiene. Water will be flushed automatically after urination.

2. Water will be conserved. Water will be flushed as programmed.

3. Touchless. No spreading of bacteria/virus through the touch of taps/faucets.

4. Flushing of Disinfectants reduces the frequency of manual cleaning of Urinals.

5. Water leakages can be detected. As a result, water loss can be prevented.

6. All the parameters – Distance of activation, Flush time duration, water leakage rate, Disinfectant, etc. can be programmed.

7. Foul smell/odor can be reduced significantly.

8. Human resources for cleaning can be minimized.

9. The cost of maintenance will be minimized.

10. Much public money can be saved through transparency.

Results:

a.

i. Automatic Urinal Flush is working fine per the programmed parameters, distance of activation, and the time period of flushing.

ii. The minimum time to activate (5 Sec has been set as the minimum time to enable flushing. If the user doesn't

stay 5 Sec., Flusher will not activate)

iii. Tested modification of the distance of activation through the web page.

b. Disinfectant Flush is working well as per the programmed parameters

(Disinfectant flush period).

c. Tested Water Leakage detection alert.

d. Tested customized announcement from Urinal Flushing System.

Conclusion

The IoT - Based SMART Urinal cum Disinfectant Flush System is better than the contemporary Urinal Flush Systems/solutions. It is more manageable and can be customized. It has a disinfectant flush system, differentiating it from any other available solutions. It has tremendous scope for the market in Urban Local Bodies, Universities, Educational Institutions, Hospitals, Hotels, etc. It reduces manual scavenging work. It can be further developed into a more comprehensive solution suitable for smart cities using Artificial Intelligence.

Scope for improvement:

This project holds significant potential for further development, utility enhancement, and market expansion with the adaptation of latest technologies Artificial Intelligence, Data Analytics. Few of them are:

a. Development of a "Data Acquisition, Monitoring & Analytics System – Cloud/Centralized Server" offering the following capabilities:

i. Tracking water consumption on a daily/monthly basis.

ii. Analyzing Smart Urinal Usage Patterns to identify faulty or problematic urinals, simplifying maintenance and planning. Real-time online monitoring of all smart toilets across various geographical scales— individual, street, city, state, country.

b. Development of a Dashboard for centralized monitoring of all the public toilets accessible via a mobile application. This system will monitor Water and Disinfectant levels and the number of flushes per urinal.

c. Integration of provisions for urine sample analysis, potentially alerting individuals using an Ammonia Sensor. For instance, individuals consuming insufficient water could receive alerts prompting them to increase water intake.

d. Monitoring of battery levels remotely and alerting in case of low battery. Utilization of Solar power.

e. Automated sanitizer spraying in toilets and automatic filling of water tanks in Public Toilets.

f. Miniaturization of the device for increased efficiency and practicality.

Prototype Circuit:

Smart Urinal Circuit:



Figure H: Back View

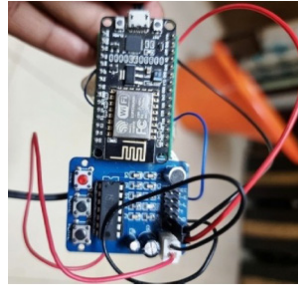


Figure I: Back View

Smart Control System:

Disinfectant Flushing, Water Detection & Water Leakage Alert Board

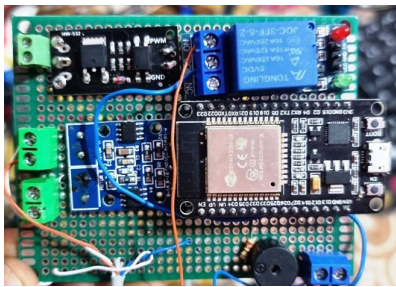


Figure J

Modification of Distance of Operation through Web Page:

Inputted 50cm through the web page, and the result is in Arduino IDE:

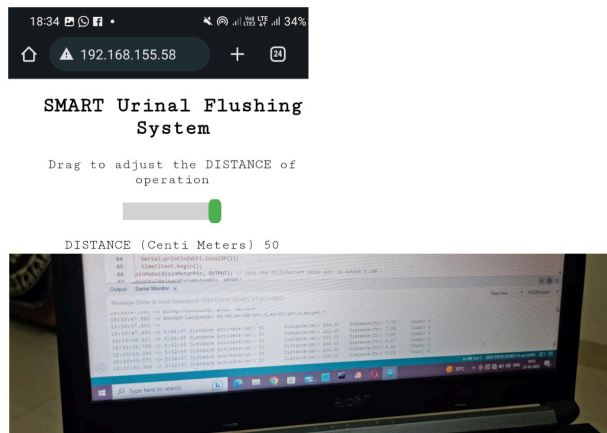


Figure K

References

1. Arduino IDE 2.0.3 downloaded from <https://www.arduino.cc/>-
2. Sample automated Urinal - URS-WHT-13255 for comparison with the proposed Smart Toilet- <https://www.jaquar.com/en/urinal>.
3. Information about bi-stable solenoid drivers: <https://www.hnhcart.com/blogs/pumps-valves/latching-solenoid-valve>
4. Solenoid Valves <https://tameson.com/solenoid-valve-types.html>
5. Latching Solenoid Valves - <https://tameson.com/latching-solenoid-valve.html>
6. ESP8266 PIN out reference - <https://lastminuteengineers.com/es>

p8266-pinout-reference/

7. ESP8266 PIN out reference <https://randomnerdtutorials.com/es-p8266-pinout-reference-gpios/>
8. ESP32 PIN out reference <https://lastminuteengineers.com/esp32-pinout-reference/>
9. Reading distance from the VL53L1X - By: Nathan Seidle, Spark Fun Electronics Date: April 4th, 2018- http://librarymanager/A1l#SparkFun_VL53L1X
10. How to Create ESP8266 Web Server | Complete Beginner's Tutorial <https://www.electronicshub.org/esp8266-web-server/>
11. Water Flow Sensor Interfacing with Arduino – Measure Flow Rate <https://microcontrollerslab.com/water-flow-sensor-pinout-interfacing-with-arduino-measure-flow-rate/>
12. Water Flow Sensor with ESP32 - Idris Cytron/ESP32WaterFlow.ino <https://gist.github.com/IdrisCytron/1b23265ede09577c19ef6acc27ee848d>
13. ESP8266 NodeMCU NTP Client-Server: Get Date and Time (Arduino IDE) <https://randomnerdtutorials.com/esp8266-node-mcu-date-time-ntp-client-server-arduino/>
14. Measuring PPM from MQ Gas Sensors using Arduino (MQ-137 Ammonia) <https://circuitdigest.com/microcontroller-projects/arduino-mq137-ammonia-sensor>
15. Urinal - <https://en.wikipedia.org/wiki/Urinal>

Author

The author of the research paper, Bhupen Sai Bandi, is currently a student at FIITJEE Junior College, Vijayawada, India. He is very much interested in Computer Science Engineering and hopes to pursue higher education in this field. He aimed to combine Computer Science and Electronics engineering to provide the most effective solutions for the betterment and sustainable life worldwide.

Should NBA Teams Sell the Farm for Superstars? Distribution of Player Investment and its Impact on Competitive Outcomes.

Brent A. Dsouza

Deira International School, Al Badia Blvd, Dubai Festival City, Dubai, 79043, United Arab Emirates, brent25may@gmail.com
Mentor: Mr. Samuel Boysel

ABSTRACT: Teams need more ability to invest due to luxury taxes and revenue sharing. Recruiting a star player involves a high opportunity cost to the franchise in the form of diminished cap space or sacrificing future assets like draft picks and possible role players. Therefore, resources must be allocated in a way that would maximize their competitive performance and intern revenue. This research collects archival data from twenty-four teams over thirty-two seasons (1990-2022) and utilizes it to estimate how the allocation of player investment affects a team's competitive outcome. The research uses a panel data regression to analyze the relationship between specific control variables and the outcome variable of interest. The findings of this paper show that marginally increasing the share of salary allocated to the top player increases the regular season winning percentage by 24.35. However, the study finds a weak correlation between paying higher for star-caliber players and a team's postseason performance/likelihood of winning a championship.

KEYWORDS: Behavioral and Social Sciences; Sports Economics; NBA; Salary Allocation; Competitive Performance.

■ Introduction

At the start of the 2020-2021 season, James Harden, 2018 MVP (Most Valuable Player) and six-time All-NBA First Team superstar, signed with the Brooklyn Nets. Harden joined forces with two fellow superstars: Kevin Durant and Kyrie Irving, to form the 'Big 3'.¹ The franchise paid them a whopping \$115 million combined that year, more than 60% of the entire roster salary.² Hence, high expectations were set for the team that season, with some reports even citing them as favorites to win the 2020 championship. However, they crashed out of the playoffs in the second round of the Eastern Conference and, in the following season, were swept four-zero by the Boston Celtics in the first round.

On the other hand, were the 2003-04 Detroit Pistons. The team ranked 17th in spending in the league that year, with only \$53 million spent on players. Yet, despite not having a highly-paid superstar, the team marched into the playoffs, having secured an impressive 54-28 in the regular season.³ The Pistons eventually clinched the title after defeating several notable teams, including the Spurs with Tim Duncan, the Lakers with Shaquille O'Neal, and the Timberwolves with Kevin Garnett. (The three stars have been inducted into the Naismith Memorial Basketball Hall of Fame, arguably the greatest achievement of a basketball player.)

These examples highlight alternative team-building strategies employed by NBA franchises to maximize competitive performance. (It is important to note that competitive performance may not be the franchise's sole objective. While not the direct empirical focus of this paper, the franchise might also employ a specific team-building strategy to maximize game attendance⁴, ticket sales, and merchandise revenue.) One is to recruit a small number of high-salaried, "blue chip" players. This leaves less cap space to pay the remaining players on the

roster. The other is to find better value players, perhaps finding undervalued veterans or developing young players from the draft, and to allocate cap space more evenly across the squad. This paper aims to answer the following questions: what is the return, in terms of competitive performance, to spending a greater share of team salary on top-tier players? Does spreading out investment like the Pistons always pay off? Would better allocation of the Nets' financial resources have enabled them to succeed?

To address these questions empirically, we use data from 24 NBA teams across 32 seasons to explore the relationship between salary allocation to top players and competitive performance (i.e., regular and postseason wins, playoff appearances, and NBA championships). Like any other financial entity, NBA franchises are driven by a profit motive. Using this research's conclusions, teams can identify the best way to utilize resources and available cap space to improve competitive outcomes.

The paper is organized as follows. Section 2 of the introduction covers the background information on various details of the NBA player labor market. Section 3 and section 4 of the introduction review the literature's relevant strands and briefly describe the data, respectively. Section 5 introduces the empirical methodology, and section 6 presents the estimation results and interprets them. Finally, we conclude with discussions and offer suggestions for further research in Section 7.

■ Background

The NBA consists of 30 teams in the Eastern and Western Conferences. Every season, teams in the league compete to win as many games as possible in the regular season. Teams who finish with a regular season record in the top eight of each conference then face off in the playoffs, where teams are

In addition to competitive outcomes, NBA franchises are owned by private citizens and seek to turn a profit. The 2021 season witnessed the NBA generate its highest revenue of \$10 billion, with most teams increasing their valuation.⁵ The question arises: Wouldn't richer teams of the league be able to recruit more skilled workers, i.e., more basketball players and more productive ones? Moreover, how exactly should teams combine players of different skill levels and, therefore, different salaries to maximize competitive performance?

We begin with some details on the labor market of the NBA. Teams can acquire new players through the annual draft, free agency^{6,7}, through trades, and signing up players in the G-league.⁷ Teams get their draft picks out of 60 available players based on their previous season's performance. Through the drafts, they could acquire talent and develop rookies into potential championship players for the team. In addition, teams could strive to have NBA veterans who can help guide the team. Alternatively, teams can settle for recruiting proven superstars to maximize their chances of winning in the season.

While wages have grown for both the highest and lowest-paid players, the distribution of salaries remains highly uneven. For example, the minimum salary for the 1990-1991 season was \$120,000, while the highest-paid player, Patrick Ewing, received \$4.25 million.⁸ When these figures are compared to the 2021-2022 season, where \$925,000 is the minimum salary, and \$45.8 million was the maximum,⁹ it is clear that the pay has skyrocketed, and so have the payment differentials.

A few rules and guidelines have been set to combat this, namely, the Salary Cap, which was reintroduced from the 1984-1985 season onwards.^{10,11} The cap is a "soft" one, which means that teams are not totally restricted by the cap space and will be allowed to exceed it provided they pay a luxury tax (\$1.5-\$4.25) per dollar on the amount exceeded. The salary cap for the 2021-2022 season was \$112.4 million, with the luxury tax threshold at \$136.6 million.¹²

Another policy put into place is the NBA revenue sharing. As part of this, teams are obliged to contribute a percentage of annual revenue to a league-wide pool which is then divided equally among all teams. Revenue sharing aims to bridge the revenue generated by larger market teams, such as the Los Angeles Lakers, and small market teams, like the Cleveland Cavaliers, for instance. The revenue pool is divided equally between each team regardless of their contribution to the pool. The league considers a team a revenue recipient if its contribution is below its average payroll. The revenue given to receiving teams is funded by teams that contribute more than the average payroll.¹³

■ Literature Review

We analyzed some of the peer-reviewed literature on sports economics to give context to our study of the optimal team-building strategy in the NBA. First, concerning how team investment aligns with the profit-maximization objective of the NBA franchise, previous research has found that NBA players are paid approximately their marginal revenue product.^{14,15} In other words, more productive players tend to

bring more value to the franchises' bottom line and therefore are compensated with bigger paychecks.

Liu's¹⁵ key findings show that a team earns 300k more for every win in the regular season and 600k more if the season ends with the team as champions. In addition, teams can earn 5k more annually for every additional seat added to the stadium. It also found that teams earned \$898,070 more for every additional million dollars spent on their roster.

Li¹⁶ uses a regression model to find the relationship between star power, team quality, and attendance. The author finds that for the 2015-16 and 2016-17 seasons, the presence of even one superstar at a game significantly boosted ticket sales, regardless of if the player was on the home or visiting team. This was especially evident in low-level, small-market teams. For example, LeBron James playing against the Milwaukee Bucks would lead to a larger boost in ticket sales when compared to if he were to play against the Miami Heat, a more popular team.

However, this study is most similar in scope to Hatcher,¹⁷ which focuses on the impact of superstars on their team's valuation, wins, and revenue. The top 40 players with the highest player-efficiency rating (PER) were selected and analyzed over five seasons. PER considers field goals, free throws, three-pointers, assists, rebounds, points, steals, missed shots, turnovers, and personal fouls. Like Li,¹⁶ Hatcher finds a great advantage for teams when one superstar plays. However, adding subsequent superstars has only modest marginal benefits. Having more than two superstars on a particular team increases the number of wins but plays a smaller role as a factor in a franchise's revenue or valuation. The lesson learned from this work is that team-building is likely a combinatorial problem: finding the right mix of talent is more important than simply loading a squad with superstars. This study differs from Hatcher's because it examines a franchise's relative salary allocation to top players instead of the player's competitive ranking.

Other work, such as Nourayi's,¹⁶ finds a strong relationship between attendance and winning percentages. Hence, using these results, it can be concluded that teams must aim for a strong performance in the regular and postseason to earn higher revenues. This paper will build on Nourayi's work by seeing if teams can attain these higher records by allotting their financial resources in a particular way.

■ Methodology

Regression is a (1) empirical (2) statistical model: we specify a relationship between variables and then use statistics to estimate the strength and direction of the relationship using real-world data. Our objective is to define a model that captures the relationship between key variables of interest and, given our research question and data at hand, estimate the parameters using statistical techniques. This will inform us of the nature of the relationship between the variables of interest: a team's player investment strategy and the team's competitive performance. Panel Data Regression is a specific class of regression model that uses data varying by entities (e.g., teams) and time (e.g., seasons). This approach has the distinct advantage of allowing us to control for both (1) time-invariant differences between NBA franchises and (2) time-varying in-

fluences that impact all teams. These are commonly known as individual fixed effects and time-fixed effects, respectively.

Let i denote a particular team and t denote season. Let y_{it} denote the outcome variable of interest for team i in season t (e.g., regular season or postseason winning percentage). Let x_{it} denote the explanatory or exogenous variable of interest for team i in season t (e.g., the percentage of team salary allocated to top n players). Our panel data regression model is as follows:

$$y_{it} = \alpha x_{it} + \beta w_{it} + \delta_i + \gamma_t + \varepsilon_{it}$$

In this formulation, α is the effect of increasing the salary allocation towards the highest-paid player on a team's winning percentage, on average, holding all other factors constant. w_{it} is a vector of time and team-varying covariate controls that can potentially explain the competitive outcome. Therefore β is the vector of coefficients associated with covariate influence. Depending on the exact outcome measure considered, the covariates might include current season total team salary expenditures, previous season salary share allocated to the top player, and competitive performance in the previous season, including regular season winning percentage, postseason appearances, and whether the team won the NBA championship last year or not. Finally, δ_i and γ_t are the team and time-fixed effects, respectively. Hence our estimation strategy attempts to control for as much variation in the outcome as possible when estimating the impact of salary allocation, using a combination of covariate controls and fixed effects. Finally, ε_{it} represents all remaining unobserved influences that might possibly drive a team's winning percentage.

We estimate a set of models that follow the panel data econometric specification stated above. In addition, we consider several distinct outcomes: regular and postseason winning percentage, regular and postseason net wins, whether the team made a playoff appearance, and whether the team won the NBA championship that season. For each of the outcome variables, we estimate a sequence of increasingly complete specifications, starting with a bivariate regression using the outcome and the explanatory variable of interest (i.e., the share of team salary allocated to the top player) and subsequently adding covariate controls, team fixed effects and season fixed effects. Our covariate controls include total salary, total salary paid last season, pay paid to the top player last season, regular season winning percentage last season, and whether the team made playoffs or won the championship last season. We include these controls to reduce the possibility of omitted variable bias, which occurs when factors that drive the outcome variable are not included in the regression and lead to incorrect estimates of the effect of the key explanatory variable.

■ Data

The data was collected from multiple sources, including Hoopshype,² Basketball Reference,³ ESPN,¹⁰ and Spotrac.¹² This included data from 24 NBA franchises over 32 seasons (twelve teams selected randomly from each of the two conferences). The observable metrics that we gather are player salary; regular season wins, regular season losses; postseason wins and losses, total postseason games played, whether the team made an NBA finals appearance, and whether the team won the

NBA finals. From this data, we construct our key explanatory and outcome variables of interest. Specifically, our key explanatory metric is the percentage of total team salary taken up by the top 'n' players (where 'n' is some integer $n = 1, 2, \dots$) for a given team. Similarly, we construct our outcome metric as a team's regular season and play-off winning percentage.

One interesting phenomenon in our data is that most variables we consider are relatively symmetric in distribution (Table 1). In other words, the means are similar to their respective medians. While this precludes variation across teams and seasons, it suggests that there are few outlying teams concerning these metrics. In other words, teams are employing slight variations in the player investment strategies with differing results.

Table 1: Summary statistics outline the sample data collected.

Variable	Mean	S.D	Min	Median	Max
Total Salary	\$63,495,769	\$35,834,502	\$7,532,000	\$61,616,409	\$178,980,766
Share of the team salary paid to the top player	0.226	0.0650	0.0992	0.219	1
Net regular season wins	2.16	24.8	-62	4	64
Regular season winning percentage	0.514	0.154	0.122	0.524	0.890
Postseason appearance	0.583	0.493	0	1	1
Net postseason wins	0.203	3.74	-4	-1	15
Postseason winning percentage	0.408	0.207	0	0.429	0.941

■ Results and Discussion

Our core result finds that spending a greater share of team salary on star players significantly impacts regular season winning percentage. The results for a set of regressions in which team salary share allocated to the top player is regressed on the regular season winning percentage is contained in Table 2. In our preferred specification (Column 5 of Table 2, a model with fixed effects and covariate controls), we find that for the average team, marginally increasing the share of salary allocated to the top player increases the regular season winning percentage by 24.35. However, there is not a strong relationship between paying for star-caliber players and postseason performance (Table 3), postseason appearance (Table 4), or the likelihood of winning a championship (Table 5).

Our analysis uncovers some interesting empirical facts to complement our core results. First, a championship won last season improves the chances of winning in the current season. Second, a postseason appearance last season actually negatively impacts your chance of a championship in the current season. Finally, a franchise has a greater chance of being in the postseason this year if they won last year's title. These results suggest that teams who go deep into a postseason likely carry over strong players into the next season but winning a championship still needs to be achieved.

Table 2: Summarizes the coefficient estimates from a regression of regular season winning percentage on the share of a team's salary paid to the highest-paid player for our sample of franchises and season-level outcomes-present alternative specifications with different combinations of fixed effects for each column.

	Regular Season Winning Percentage	Regular Season Winning Percentage	Regular Season Winning Percentage	Regular Season Winning Percentage	Regular Season Winning Percentage
Intercept	0.3921*** (0.0235)	0.1633*** (0.0267)			
Share of salary for the highest-paid player	0.5421*** (0.1025)	0.2480* (0.1014)	0.2225* (0.1070)	0.2700* (0.1073)	0.2435* (0.1145)
Total salary		2.12e-9*** (5.11e-10)	2.22e-9*** (5.78e-10)	2.75e-9*** (6.31e-10)	3.07e-9** (8.59e-10)
Share of salary for the highest-paid player last season		-0.0433 (0.1040)	-0.0673 (0.1409)	-0.0396 (0.1124)	-0.0616 (0.1551)
Total salary last season		-2.31e-9*** (5.43e-10)	-2.39e-9*** (5.56e-10)	-2.56e-9*** (6.39e-10)	-2.49e-9*** (4.83e-10)
Regular season winning percentage last season		0.5846*** (0.0496)	0.5282*** (0.0576)	0.5710*** (0.0574)	0.4996*** (0.0552)
Postseason appearance last season		0.0099 (0.0154)	0.0153 (0.0158)	0.0097 (0.0182)	0.0159 (0.0154)
Reigning champions		0.0093 (0.0189)	0.0119 (0.0154)	0.0077 (0.0185)	0.0109 (0.0152)
Team Fixed Effects	No	No	Yes	No	Yes
Season Fixed Effects	No	No	No	Yes	Yes
Observations	767	742	742	742	742
R Squared	0.03984	0.43434	0.44898	0.44391	0.46012

Note: This Coefficient estimate standard errors are presented in parentheses below the coefficient. Statistical significance codes at the 1- level: 0 ^{***} 0.001 ^{**} 0.01 ^{*} 0.05 [.] 0.1 ['] 1.

Table 3: Summarizes the coefficient estimates from a regression of postseason winning percentage on the share of a team's salary paid to the highest-paid player for our sample of franchises and season-level outcomes-present alternative specifications with different combinations of fixed effects for each column.

	Postseason winning Percentage	Postseason winning Percentage	Postseason winning Percentage	Postseason winning Percentage	Postseason winning Percentage
Intercept	0.2431*** (0.0382)	-0.0033 (0.0623)			
Share of salary for the highest-paid player	0.7139*** (0.1580)	0.4192* (0.1647)	0.3302 (0.2221)	0.4419* (0.2004)	0.2852 (0.2670)
Total salary		6.4e-10 (1.07e-9)	5.58e-10 (1.12e-9)	5.52e-10 (1.17e-9)	4.93e-10 (1.53e-9)
Share of salary for the highest-paid player last season		0.2437 (0.1642)	0.1822 (0.1712)	0.2561 (0.1413)	0.1709 (0.1900)
Total salary last season		-6.9e-10 (1.14e-9)	-5.65e-10 (1.2e-9)	-1.2e-19 (1.34e-9)	-1.51e-9 (1.34e-9)
Regular season winning percentage last season		0.4737*** (0.1141)	0.4273** (0.1154)	0.5159*** (0.1302)	0.4865*** (0.1170)
Postseason appearance last season		-0.0282 (0.0328)	-0.084 (0.0381)	-0.0362 (0.0066)	-0.0176 (0.0386)
Reigning champions		0.0685 (0.0435)	0.0388 (0.0406)	0.0623 (0.0481)	0.0341 (0.0429)

Team Fixed Effects	No	No	Yes	No	Yes
Season Fixed Effects	No	No	No	Yes	Yes
Observations	448	432	432	432	432
R Squared	0.03999	0.13413	0.17942	0.15075	0.19862

Note: Coefficient estimate standard errors are presented in parentheses below the coefficient. Statistical significance codes at the 1- level: 0 ^{***} 0.001 ^{**} 0.01 ^{*} 0.05 ['] 0.1 ['] 1.

Table 4: Summarizes the coefficient estimates from a regression of a postseason appearance on the share of a team's salary paid to the highest-paid player for our sample of franchises and season-level outcomes-present alternative specifications with different combinations of fixed effects for each column.

	Postseason appearance	Postseason appearance	Postseason appearance	Postseason appearance	Postseason appearance
Intercept	0.4125*** (0.0858)	-0.2155* (0.0861)			
Share of salary for the highest-paid player	0.7535* (0.3748)	0.2933 (0.3214)	0.2933 (0.2189)	0.3846 (0.3225)	0.3341 (0.2622)
Total salary		4.52e-9** (1.46e-9)	4.53e-9** 1.42e-9	6.98e-9*** (1.86e-9)	7.09e-9** (2.45e-9)
Share of salary for the highest-paid player last season		-0.2815 (0.3353)	-0.3927 (0.4331)	-0.2354 (0.3311)	-0.3473 (0.4425)
Total salary last season		-4.93e-9** (1.52e-9)	-4.96e-9*** (1.28e-9)	-5.53e-9** (1.79e-9)	-5.66e-9** (1.59e-9)
Regular season winning percentage last season		1.430*** (0.1668)	1.483*** (0.1734)	1.385*** (0.2080)	1.427*** (0.1786)
Postseason appearance last season		0.0934 (0.0592)	0.0500 (0.0649)	0.0888 (0.0636)	0.0475 (0.0651)
Reigning champions		0.0160 (0.0426)	0.0196 (0.0555)	0.0095 (0.0396)	0.0170 (0.0596)
Team Fixed Effects	No	No	Yes	No	Yes
Season Fixed Effects	No	No	No	Yes	Yes
Observations	769	744	744	743	743
R Squared	0.00985	0.29996	0.32009	0.31128	0.33123

Note: Coefficient estimate standard errors are presented in parentheses below the coefficient. Statistical significance codes at the 1- level: 0 ^{***} 0.001 ^{**} 0.01 ^{*} 0.05 ['] 0.1 ['] 1.

Table 5: Summarizes the coefficient estimates from a regression of a championship on the share of a team's salary paid to the highest-paid player for our sample of franchises and season-level outcomes-present alternative specifications with different combinations of fixed effects for each column.

	Championship	Championship	Championship	Championship	Championship
Intercept	-0.0792 (0.0416)	-0.1754** (0.0541)			
Share of salary for the highest-paid player	0.5339** (0.1958)	0.2625 (0.1645)	0.2000 (0.2110)	0.2851 (0.1587)	0.2139 (0.2152)
Total salary		9.18e-10 (6.16e-10)	8.55e-10 (5.54e-10)	1.27e-9 (7.51e-10)	1.01e-9 (8.1e-10)
Share of salary for the highest-paid player last season		0.0684 (0.1674)	-0.0119 (0.1244)	0.0823 (0.1539)	-0.0114 (0.1214)

Total salary last season		-1.05e-9 (6.08e-10)	-9.85e-10 (6.27e-10)	-1.04e-9 (6.95e-10)	-1.13e-9 (8.17e-10)
Regular season winning percentage last season		0.3259*** (0.0838)	0.3392** (0.1198)	0.3187*** (0.0790)	0.3399* (0.1269)
Postseason appearance last season		-0.0535** (0.0191)	-0.0524* (0.0212)	-0.0524* (0.0200)	-0.0537* (0.0222)
Reigning champions		0.2345** (0.0844)	0.1748 (0.1020)	0.2330* (0.0947)	0.1749 (0.1040)
Team Fixed Effects	No	No	Yes	No	Yes
Season Fixed Effects	No	No	No	Yes	Yes
Observations	767	742	742	742	742
R Squared	0.02372	0.13259	0.17416	0.13528	0.17604

Note: Coefficient estimate standard errors are presented in parentheses below the coefficient. Statistical significance codes at the 1- level: 0 ^{***} 0.001 ^{**} 0.01 ^{*} 0.05 [!] 0.1 ['] 1.

■ Discussion

The research results demonstrate a superstar's positive impact on a franchise's regular season record. This effect seems likely to operate over a longer stretch of games, as the player over the regular season would generate higher points per game, assists, and rebounds for the team. However, as teams face off in the postseason, multiple factors come into play. Perhaps it is the fact that postseason success is harder to come by as there are fewer opportunities, there is an increased level of competition, and likely many outcomes come down to chance. It might also be the case that the offensive prowess of superstars is limited in the postseason as teams increase defensive pressure. We find only a weak relationship between increasing the top player's salary and postseason success. Interestingly, there also isn't a strong correlation between star players and postseason appearance. This might be attributed to several factors, including injuries, load management, teams tanking to get better draft picks,^{20,21} and constantly changing rosters.

This study has limitations. Firstly, this research utilizes a limited number of control variables. Additional control variables which can be taken into consideration and may influence the results of the regression include the experience of the coach, the number of years the players have played together (a team's chemistry), investment into facilities, how experienced players are, and the percentage of the roster which is healthy.

The results of this study motivate further research into team building and the economics of sports. First, it would be interesting to delve deeper into the factors that influence the likelihood of postseason performance. What components of team composition increase the likelihood of winning a championship? This kind of research would pair well with the regular season results documented here, as to make it into the postseason, a franchise needs to perform well in the regular season first. Second, the effectiveness of superstars is likely to vary across different professional basketball leagues or even across different sports. Do we still see a positive impact of paying for high-caliber players in leagues outside the NBA? Moreover, do superstars strongly impact competitive perfor-

mance in other sports where team sizes, player roles, and the nature of the game are different? We could easily bring our methodological framework to bear on these different empirical settings.

■ Conclusion

This paper fulfills the objective of finding the best way for franchises to maximize their on-court performance by influencing the distribution of salary allocation of players. Given a team's limited ability to invest, paying for superstars provides the greatest marginal utility for a team in terms of competitive performance. Thus, if a team struggles to make the playoffs, one of the better courses of action would be to allocate a greater percentage of cap space to the top one or two players. This can be done by extending the contract of an existing star-caliber player or acquiring a new player through trades. In addition, teams can also take advantage of increased revenue from a superstar, as shown by Li.¹⁶ While teams not star-studded still win championships occasionally, they are much rarer, and the outcome is less predictable. This study, however, did not find a significant correlation between player investment and postseason performance, indicating that teams may not be able to improve their chance at a championship only by changing their spending patterns alone.

■ Acknowledgments

I want to thank Mr. Samuel Boysel from the University of Southern California for mentoring me. With his constant support and guidance, this paper is possible.

■ References

1. Nets, B. Brooklyn Nets acquire James Harden. <https://www.nba.com/nets/news/2021/01/14/brooklyn-nets-acquire-james-harden> (accessed Oct 15, 2022).
2. HoopsHype. NBA rumors, News, salaries. <https://hoopshype.com/>. (accessed Oct 17, 2022).
3. Basketball Reference. Basketball Statistics and History | Basketball-Reference.com <https://www.basketball-reference.com/>.
4. Humphreys, B. R.; Johnson, C. The Effect of Superstar Players on Game Attendance: Evidence from the NBA. *SSRN Electronic Journal* 2017.
5. NBA reveals record US\$10bn revenue for 2021/22 <https://www.sportspromedia.com/news/nba-revenue-2021-22-season-adam-silver/#:~:text=The%20National%20Basketball%20Association>.
6. Scully, G. W. Player Salary Share and the Distribution of Player Earnings. *Managerial and Decision Economics* 2004, 25 (2), 77–86.
7. Free agency explained. <https://www.nba.com/news/free-agency-explained> (accessed Dec 17, 2022).
8. NBA Trade Rules Overview. <https://cbabreakdown.com/trades#:~:text=Each%20season%2C%20teams%20may%20trade,players%2C%20like%20international%20soccer.> (accessed Dec 17, 2022).
9. Daubs, K. The Highest-Paid Players In The 1990-91 NBA Season: Patrick Ewing Earned The Most, Michael Jordan Was Just 8th With \$2.5 Million <https://fadeawayworld.net/nba/the-highest-paid-players-in-the-1990-91-nba-season-patrick-ewing-earned-the-most-michael-jordan-was-just-8th-with-2-5-million>.
10. ESPN <https://www.espn.com/nba/>.
11. Stanek, T. Player Performance and Team Revenues: NBA Player Salary Analysis. CMC Senior Theses, 2016.
12. NBA2021 Luxury Tax Tracker. <https://222.spotrac.com/nba/tax/2021/#:~:text=NBA%20Team%20Luxury%20Tax%20Tracker>.
13. Pearce, A. NBA Revenue Sharing: Small-Market Teams to Benefit from New Sharing Structure <https://bleacherreport.com/art>

- icles/1039092-nba-revenue-sharing-small-market-teams-to-benefit-from-new-sharing-structure#:~:text=It%20works%20like%20like%20this%3A.
14. Li, H. True Value in the NBA: An Analysis of On-Court Performance and Its Effects on Revenues. Undergraduate Honor Thesis, 2011.
 15. Liu, Y. The Star Effect on Sport Team Revenue: Evidence from the National Basketball Association. MSc Thesis, 2012.
 16. Li, Z. The Impact of Star Power and Team Quality on NBA Attendance. Thesis, 2018.
 17. Hatcher, T.; Michael Seeborg, F. A. What Is the Superstar Effect for an NBA Franchise? *John Wesley Powell Student Research Conference* 2015.
 18. Nourayi, M. M. Profitability in Professional Sports and Benchmarking: The Case of NBA Franchises. *Benchmarking: An International Journal* 2006, 13 (3), 252–271.
 19. Hausman, J. A.; Leonard, G. K. Superstars in the National Basketball Association: Economic Value and Policy. *Journal of Labor Economics* 1997, 15 (4), 586–624.
 20. Taylor, B. A.; Trogdon, J. G. Losing to Win: Tournament Incentives in the National Basketball Association. *Journal of Labor Economics* 2002, 20 (1), 23–41.
 21. Price, J.; Soebbing, B. P.; Berri, D.; Humphreys, B. R. Tournament Incentives, League Policy, and NBA Team Performance Revisited. *Journal of Sports Economics* 2010, 11 (2), 117–135.

■ Author

Brent Dsouza is an IB student at the Deira International School in Dubai. Over the years, he has received several national and international awards. He is a multifaceted individual who loves playing music, creating innovative projects, and researching the NBA as an avid basketball fan.

Development of Polymer-assisted Compaction of DNA Nanoparticles for Cancer Treatment

Caroline Shen

Phillips Academy, 180 Main St., Andover, MA, 01810, USA, carolineshen30@gmail.com

Mentors: Peiru Chen, Prof. Ke Zhang

ABSTRACT: Mutations in Kirsten rat sarcoma virus (KRAS), a protein from the GTPase protein family, are involved in up to 20% of tumors that lead to pancreatic, colorectal, and lung cancers. While it is difficult to directly target KRAS protein with small molecule drugs due to the limited number of active binding sites on KRAS, antisense technology using oligonucleotide drugs has shown promising effects in anti-cancer treatments. To overcome the challenge of natural oligonucleotide intracellular delivery, polymer-assisted compaction of DNA (pacDNA) technology has been developed. pacDNA conjugates are synthesized via click chemistry using an azide functionalized non-cationic PEG (polyethylene glycol)-based nanoparticle and dibenzocyclooctyl (DBCO) conjugated antisense DNA. The pacDNA conjugates showed cytotoxicity in a dose-dependent manner in KRAS-mutated cancer cell lines. In contrast, the PEG-based polymer and naked DNA showed no toxicity as evaluated by a dimethylthiazol-diphenyltetrazolium (MTT) based assay. Furthermore, following protein expression (western blot test) analysis, pacDNA conjugates were shown to downregulate KRAS protein expression; KRAS protein levels in the study were lower than that of the controls. These results indicate that pacDNA comprised of PEG-based polymer and antisense DNA could be potentially effective therapeutics for cancer treatment.

KEYWORDS: Material Science; Nanomaterials; Antisense oligonucleotide; KRAS; PEG; Cancer therapy.

■ Introduction

The human rat sarcoma virus (RAS) gene family is composed of three types, including Neuroblastoma rat sarcoma virus (NRAS), Harvey rat sarcoma virus (HRAS), and Kirsten rat sarcoma virus (KRAS) forms. KRAS is a protein isoform of RAS with the greatest mutability among them. KRAS protein belongs to the GTPase protein family in normal cells, functioning as a signal switch to relay messages from extracellular to intracellular environments.² KRAS proteins are inactive when binding to guanosine diphosphate (GDP) but are active when binding to guanosine triphosphate (GTP).³ KRAS mutations have been discovered to be involved in the pathogenesis of up to 20% of tumors, with their occurrences resulting in high rates of pancreatic, colorectal and lung cancers,⁴ which generally have poor responses to standard anti-cancer therapies such as chemotherapy.⁵ Due to the limited number of active binding sites in KRAS proteins, using them as a potential direct drug target is challenging.⁶ Nonetheless, recent research and development suggest that only a few of potential drug candidates can bind directly to specific KRAS conformations.⁷

In 2021, the Food and Drug Administration (FDA) approved the first drug, sotorasib, a small molecule that targets the KRAS mutant protein, G12C, in treating non-small cell lung cancer.^{8,9} In 2022, FDA granted accelerated approval to another small molecule, adagrasib, targeting the same KRAS mutant protein.¹⁰ As cancer drug resistance is the principal limiting factor for effective treatment in the clinic, developing different chemical modalities or using cocktail therapy is vital in cancer treatment.¹¹ Unlike small molecule drugs, antisense oligonucleotide drugs target mRNA of interest and have

shown to be a promising anti-cancer treatment.¹² Currently, 15 oligonucleotide drugs have been approved by FDA.¹³ Regarded as disruptive therapeutics, oligonucleotide drugs are cost-effective, relatively easy to manufacture, and can target undruggable pathways.¹⁴ AZD4785 is the first anti-KRAS antisense oligonucleotide targeting KRAS mRNA that was put in the clinical study.¹⁵ Unfortunately, the clinical research failed because of lack of efficacy;¹⁶ as oligonucleotides are highly negatively charged and thus pose a challenge for cellular uptake and good distribution. To overcome these difficulties, Professor Zhang's lab at Northeastern University is developing KRAS antisense therapeutics using a platform technology, polymer-assisted compaction of DNA (pacDNA).¹⁷

pacDNA technology leverages the benefit of both nanoparticles and PEG to deliver a target DNA. Nanoparticles showed great potential as drug carriers; currently, several successful liposome-based nanoparticle drugs or vaccines have been approved by FDA, including COVID-19 mRNA vaccines.¹⁸ Recently, a novel polyethylene glycol (PEG) based nanoparticle vehicle was developed and exhibited great activity in drug delivery. The nanostructure provided mounted DNA moiety with enhanced nuclease stability and improved cellular uptake.¹⁹ Using PEG-based nanoparticles as a novel delivery system shows excellent application potential because PEG is an excipient widely used in drug formulations.²⁰

In this study, an antisense DNA oligonucleotide (targeting mouse KRAS mRNA) was conjugated to PEG nanoparticles via non-cleavable bonds. First, the free antisense oligonucleotide was purified with reverse-phase high-performance liquid chromatography (HPLC), and the polymer-DNA conjugate

was synthesized and thereafter purified through gel permeation chromatography (GPC). Then, the final pacDNA was characterized by gel electrophoresis. Lastly, the conjugates were evaluated in a cell-based cytotoxicity assay and western blot analysis of KRAS protein levels.

■ Methods

Oligonucleotide:

The 16-mer KRAS antisense oligonucleotide (ASO) targets mouse KRAS mRNA, and the sequence is 5'-CAT GTA AAT ATA GCC C-3'. The dibenzocyclooctyl (DBCO)-conjugated 16-mer KRAS ASO was synthesized in collaboration with coworkers from Professor Zhang's lab using standard solid-phase phosphoramidite methodology in an Applied Biosystems 391 DNA synthesizer. First, 5'-DBCO was incorporated into the sequence using a commercially available 5'-DBCO-TEG phosphoramidite. Phosphoramidites and supplies for DNA synthesis were purchased from Glen Research Co. All DNA strands were cleaved and deprotected from the CpG support using aqueous ammonia at room temperature for 24 hours. Finally, the crude oligonucleotide mixture was purified through reverse-phase HPLC.

Synthesis of PEG Conjugated Polymer:

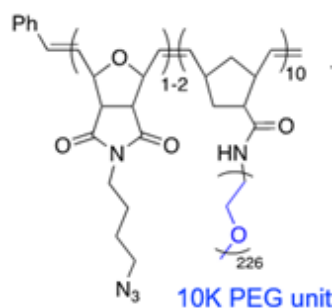


Figure 1: Chemical Structure of PEG-conjugated polymer.

The PEG conjugated polymer (Figure 1) was synthesized in collaboration with coworkers from Professor Zhang's lab according to a previously reported method. The polymer was purified by dialysis and lyophilized for future use.

A General Method for pacDNA Synthesis:

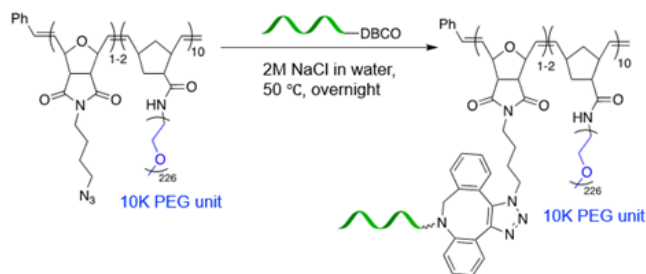


Figure 2: Reaction to produce pacDNA.

Azide-modified brush polymers were dissolved in water to make a 50 μM solution. DBCO-modified DNA (100 nmol) was dissolved in 1 mL azide-brush polymer solution, and ~160 mg of NaCl was added to make a final concentration of 2 M NaCl solution. The mixture was incubated while shaking at 50°C for 16 hours on an Eppendorf Thermomixer. The mixture was purified through GPC with a mobile phase

of 0.1 M NaNO₃. The purification fractions containing the conjugate were collected. After pooling and concentration, the solution was then run through NAP 25 column for desalting. The final solution was lyophilized to form a white powder (Figure 2) and analyzed via gel electrophoresis.

MTT Cytotoxicity Assay:

Free DNA, pacDNA, and polymer were evaluated individually by a dimethylthiazol-diphenyltetrazolium (MTT) cytotoxicity assay in two different cell lines: mouse KRAS cell lines D658 and K273.¹⁶ 1.0×10^4 cells were placed into 96-well plates which were preloaded with 180 μL DMEM medium per well. The plate was then incubated for 24 hrs at 37 °C before free DNA, pacDNA, and the polymer was added to make a final volume of 200 μL . The testing concentration of free DNA, pacDNA and polymer were at 0.1 μM , 0.25 μM , 0.5 μM , 1 μM , 2 μM , 3 μM , 5 μM , 10 μM . Phosphate buffered saline (PBS) was used as the control and added to a 96-well plate. After incubation for 48 hours at 37 °C, MTT stock solution (20 μL , 5 mg/mL) in PBS was added to each well. The plate was then incubated for additional four hours at 37 °C. After removing the medium with unreacted MTT, 200- μL dimethylsulfoxide (DMSO) solution was added to each well to dissolve the purple crystals. The plate was then put in a microplate reader to detect the absorbance at 490 nm.

Western Blot Analysis:

2.0×10^5 cells were placed into 24-well plates, which were preloaded with Roswell Park Memorial Institute (RPMI) medium and incubated overnight at 37 °C with 5% carbon dioxide. Then, free DNA, pacDNA, polymer (10 μM , 500 μL final volume) serum-free medium, and PBS control were added to each well and incubated for 4 hours before the medium was replaced with a complete medium. The 24-well plates were then incubated for 68 hours. Following the manufacturer's protocol (Cell Signaling Technology, Inc), the cells were harvested and lysed with lysis buffer. The extracted protein was then quantified using a BCA kit (Thermo Fisher), and an equal amount of protein (5 μg per lane) was loaded onto sodium dodecyl sulfate (SDS) gel. After gel electrophoresis and electrotransfer to a nitrocellulose membrane, the membrane was incubated with 3% bovine serum albumin (BSA) in Tris buffer with 0.05% Tween-20 for 1 hour at room temperature. After that, the membrane was incubated with primary antibodies overnight at 4°C. The membrane was then washed 3 times and incubated with secondary antibodies for 1 hour at room temperature. Finally, the bands were visualized after incubation with chemiluminescence (ECL western blotting substrate, Thermo Scientific). ImageJ software was used to quantify western blot images by comparing the protein KRAS with that of the housekeeping protein glyceraldehyde 3-phosphate dehydrogenase (GAPDH).

■ Results and Discussion

DBCO-DNA Purification:

The oligonucleotide crude after solid-phase synthesis was purified by reverse phase HPLC (acetonitrile and 0.1 M triethylammonium acetate (TEAA)). The elution of desired product was fractionalized and collected based on UV absorbance at both 260 nm and 310 nm shown in Figure 3. DNA

had an absorbance at 260 nm, while unique DBCO moiety had an absorbance at 310 nm. Therefore, the 310 nm trace indicated a successful DNA strand and signaled that the correct product was generated.

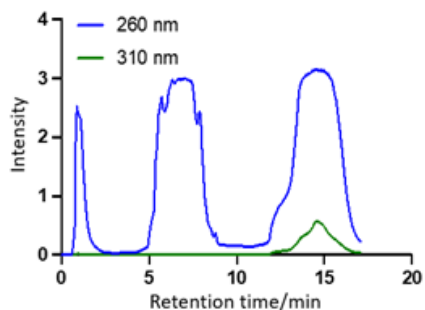


Figure 3: HPLC Chromatogram of DBCO-DNA Purification.

Separation and analysis of pacDNA conjugate:

The pacDNA conjugate was then purified and analyzed by GPC. From Figure 4, pacDNA with a larger size was eluted earlier than unreacted DNA with a smaller size. The conversion of conjugation is around 85% (based on the GPC peak area ratio).

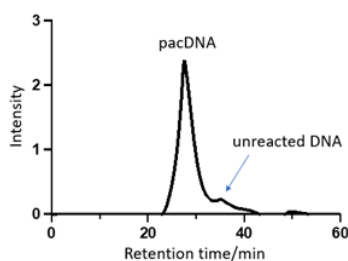


Figure 4: GPC Chromatogram of purified pacDNA conjugate.

Agarose Gel Confirmation:

The purified pacDNA was loaded onto agarose gel with free DNA as control. From Figure 5, after ethyl bromide staining, free DNA and pacDNA showed different locations on the gel, which further confirmed the success of the click reaction and the generation of desired pacDNA conjugate with a significantly larger size.



Figure 5: Ethyl bromide-stained agarose gel.

MTT Assay:

MTT assay is a robust cell proliferation assay that can measure cell viability after treatment. The assay utilizes the yellow tetrazolium (3-(4,5-dimethylthiazolyl-2) - 2,5-diphenyltetrazolium bromide. This tetrazolium salt (MTT) can be reduced

by dehydrogenase enzymes in living cells and change the yellow-colored solution to a purple crystal soluble in DMSO; this color change can be quantified by spectrophotometric means.

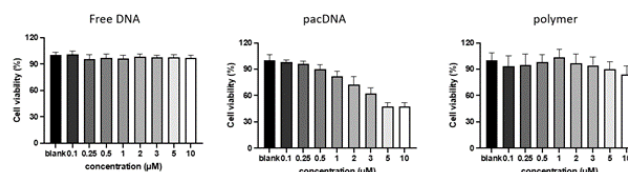


Figure 6: MTT assay of free DNA, pacDNA, polymer in mouse KRAS cell line D658.

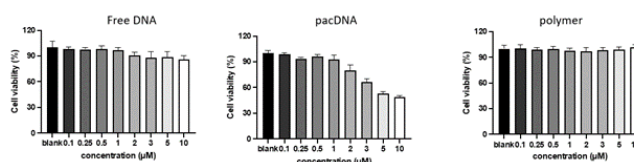


Figure 7: MTT assay of free DNA, pacDNA, polymer in mouse KRAS cell line K273.

In Figure 6 and Figure 7, both free DNA and polymer had over 90% cell viability in mouse KRAS cell lines D658 and K273, whereas, in the case of pacDNA, cell viability decreased depending on the concentration of pacDNA. The cell viability leveled off when pacDNA concentration increased from 0.1 to 10 μM . At 10 μM , the cell viability was below 50% in both cell lines, which confirmed the toxicity against the KRAS-mutated cancer cell line.

Western Blot Analysis:

Western blot is an antibody-based technology to detect proteins of interest, particularly proteins of low abundance.²² From Figure 8, pacDNA showed inhibition of KRAS protein in both D658 and K273 cell lines, while free DNA and polymer showed similar band intensity as blank. GAPDH, which was a housekeeping protein, was used as a loading control

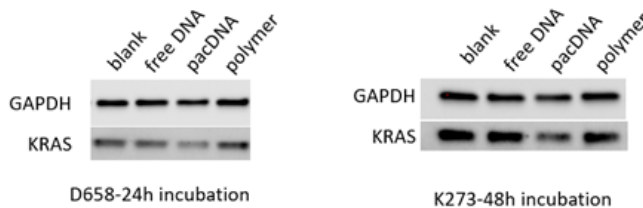


Figure 8: Western blot analysis of 10 μM free DNA, pacDNA, and polymer in both D658 and K273 cell lines.

Discussion

Although two small molecule drugs targeting mutated KRAS have been approved by the FDA most recently, they only target G12C mutated KRAS. Conversely, oligonucleotides offer an expanded range of targeting options for various types of mutations found in the KRAS protein, implying more significant potential as an anti-KRAS therapy for cancer treatment. The major challenge in oligonucleotide application is their low transfection efficiency due to the negative charge of the DNA backbone. Therefore, it is necessary to depend on a delivery vehicle to overcome the barrier of intracellular delivery. Traditional cationic drug delivery carriers for oligonucleotides generally have toxicity issues²³ and are unsafe to

use in anti-cancer therapy. The utilization of non-cationic bottlebrush polymer comprised of biocompatible PEG polymer is shown to be both safe and effective in delivering oligonucleotides. In this study, pacDNA conjugates were synthesized via click chemistry of DBCO-conjugated antisense DNA and PEG-based polymer. The HPLC analysis showed successfully synthesized DBCO-DNA strands. The DNA-polymer conjugates were then subjected to GPC purification and gel electrophoresis analysis as pacDNA had a larger size and was eluted earlier. In contrast, the DBCO-labeled DNA was smaller and was eluted later. Therefore, a desired pacDNA conjugate was prepared.

The MTT cell cytotoxicity assay was tested in both D658 and K273 cell lines, PEG-based polymer and naked DNA showed no toxicity, and the cell viability was above 90% even at the highest concentration (10 μ M), in contrast, pacDNA conjugates showed cytotoxicity in a dose-dependent manner. The cell viability leveled off when increasing dosages; at the highest 10 μ M concentration, both cell lines showed less than 50% cell viability. The cell cytotoxicity results showed that the pacDNA could inhibit the growth of KRAS-mutated cell lines. In contrast, the components in pacDNA did not have nonspecific toxicities against those cell lines.

The pacDNA conjugates inhibition of KRAS protein expression was tested in the Western blot analysis. KRAS protein expression levels were much lower in the pacDNA-treated group than in the control groups. The GAPDH housekeeping gene confirmed the identical protein loading between groups, proving the downregulation of KRAS protein in the pacDNA treatment group is the decrease of KRAS protein expression level. The cellular assays demonstrated that pacDNA could be a promising candidate for further study as an anti-KRAS cancer therapy.

Conclusion

In this study, pacDNA conjugate comprised of PEG-based polymer and antisense DNA has been successfully prepared. Furthermore, the pacDNA conjugate showed cytotoxicity in a dose-dependent manner in two mouse mutated-KRAS cell lines D658 and K273. In addition, it offered to downregulate KRAS protein expression based on Western Blot analysis. These results demonstrate that pacDNA comprised of PEG-based polymer and antisense DNA could be potentially promising effective therapeutics in cancer treatment.

Acknowledgments

The author would like to acknowledge the supervision of Peiru Chen and Professor Ke Zhang at Northeastern University, who suggested the research topic, provided research material and instruments, and provided general guidance on the research process.

References

1. Minati, M.; Assi M.; Libert, M.; Cordi, S.; Lemaigre, F.; Jacquemin, P. KRAS protein expression becomes progressively restricted during embryogenesis and in adulthood. *Front. Cell Dev. Biol.* 2022, 10: 995013. DOI: 10.3389/fcell.2022.995013
2. Timar J.; Kashofer K. Molecular epidemiology and diagnostics of KRAS mutations in human cancer. *Cancer and Metastasis Rev.* 2020, 39(4): 1029-1038. DOI: 10.1007/s10555-020-09915-5
3. Hallin, J.; Engstrom, L.; Hargis, L.; Calinisan, A.; Aranda, R.; Briere, D. M.; Sudhakar, N.; Bowcut, V.; Baer B. R.; Ballard J. A.; Burkard, M. R.; Fell, J. B.; Fischer, J. P.; Vigers, G. P.; Xue, Y.; Gatto, S.; Fernandez-Banet, J.; Pavlicek, A.; Velastagui, K.; Christensen, J. G. The KRAS G12C inhibitor, MRTX849, provides insight toward therapeutic susceptibility of KRAS mutant cancers in mouse models and patients. *Cancer Discov.* 2019,10(1): 54-71. DOI: 10.1158/2159-8290.CD-19-1167
4. Reck, M.; Carbone, D.P.; Garassino, M.; Barlesi, F. Targeting KRAS in non-small-cell lung cancer: recent progress and new approaches. *Ann. Oncol.* 2021, 32(9): 1101-1110. DOI: 10.1016/j.annonc.2021.06.001
5. Lièvre, A.; Bachet, J.; Corre, D.; Boige, V.; Landi, B.; Emile, J-F.; Côté, J-F.; Tomasic, G.; Penna, C.; Ducreux, M.; Rougier, P.; Penault-Llorca, F.; Laurent-Puig, P. KRAS mutation status is predictive of response to Cetuximab therapy in colorectal cancer. *Cancer Res.* 2006, 66(8): 3992-3995. DOI: 10.1158/0008-5472.CAN-06-0191
6. Spoerner M.; Herrmann, C.; Vetter I.R.; Kalbitzer H.R.; Wittinghofer A. Dynamic properties of the Ras switch I region and its importance for binding to effectors. *Proc. Natl. Acad. Sci. USA.* 2002, 98(9): 4944-4949. DOI: 10.1073/pnas.081441398
7. Ostrem, J.; Peters, U.; Sos, M.; Wells, J.; Shokat, K. K-Ras(G12C) inhibitors allosterically control GTP affinity and effector interactions. *Nature.* 2013, 503(7477): 548-551. DOI: 10.1038/nature12796
8. Jaber, N. 2021, FDA approval of KRAS inhibitor sotorasib for lung cancer hailed as milestone. National Cancer Institute. <https://www.cancer.gov/news-events/cancer-currents-blog/2021/fda-sotorasib-lung-cancer-kras>
9. Tanaka, N.; Lin, J.; Li, C.; Ryan, M.; et al, Clinical acquired resistance to KRASG12C inhibition through a novel KRAS switch-II pocket mutation and polyclonal alternations converging on RAS-MAPK reactivation. *Cancer Discovery*, 2021, 11(8): 1913-1922. DOI: 10.1158/2159-8290.CD-21-0365
10. FDA grants accelerated approval to adagrasib for KRAS G12C-mutated NSCLC. 2022, The Food and Drug Administration. <https://www.fda.gov/drugs/resources-information-approved-drugs/fda-grants-accelerated-approval-adagrasib-kras-g12c-mutated-nsclc#:~:text=On%20December%2012%2C%202022%2C%20the,by%20an%20FDA%20approved%20test%2C>
11. Vasan, N.; Baselga, J.; Hyman, D. A view on drug resistance in cancer. *Nature.* 2019, 575(14): 299-309. DOI: 10.1038/s41586-019-1730-1
12. Crooke, S.; Baker, B.; Crooke, R.; Liang, X. Antisense technology: an overview and prospectus. *Nature Rev. Drug Discov.* 2021,20: 427-453. DOI: 10.1038/s41573-021-00162-z
13. Igarashi, J.; Niwa, Y.; Sugiyama, D. Research and development of oligonucleotide therapeutics in Japan for rare diseases. *Future Rare Dis.* 2022, 13: 1006304. <https://www.futuremedicine.com/doi/10.2217/frd-2021-0008>
14. Damase, T.; Sukhovshin, R.; Boada, C.; Taraballi, F.; Pettigrew, R.; Cooke J. The limitless future of RNA therapeutics. *Front. Bioeng. Biotechnol.* 2021, 18(9): 628137. DOI: 10.3389/fbioe.2021.628137
15. Ross, S.; Revenko, A.; Hanson, L.; Ellston, R.; Staniszewska, A.; Whalley, N.; Pandey, S. J.; Revill, M.; Rooney, C.; Buckett, L. K.; Klein, S. K.; Hudson, K.; Monia, B. P.; Zinda, M.; Blakey, D. C.; Lyne, P. D.; Macleod, R. A. Targeting KRAS-dependent tumors with AZD4785, a high-affinity therapeutic antisense oligonucleotide inhibitor of KRAS. *Sci. Transl. Med.* 2017, 9(394): eal5253. DOI: 10.1126/scitranslmed.aal5253
16. Plieth, J. 2019. Astra's first attempt fails, but there's no giving up on KRAS. Evaluate. <https://www.evaluate.com/vantage/articles/n>

- ews/trial-results/astras-first-attempt-fails-theres-no-giving-kras.
17. Wang, D.; Wang, Q.; Wang, Y.; Chen, P.; Lu, X.; Jia, F.; Sun, Y.; Sun, T.; Zhang, L.; Che, F.; He, J.; Lian, L.; Morano, G.; Shen, M.; Ren, M.; Dong, S. S.; Zhao, J. J.; Zhang, K. Targeting oncogenic KRAS with molecular brush-conjugated antisense oligonucleotide. *Proc. Natl. Acad. Sci. USA*. **2022**, *119*(29): 1-12. DOI: 10.1073/pnas.2113180119
18. Park, J. W.; Lagniton, P. N. P.; Liu, Y.; Xu, R.-H. mRNA vaccines for COVID-19: what, why and how. *Int J Biol Sci*. **2021**, *17*(6): 1446-1460. DOI: 10.7150/ijbs.59233
19. Lu, X.; Jia, F.; Tan, X.; Wang, D.; Cao, X.; Zheng, J.; and Zhang, K. Effective antisense gene regulation via noncationic, polyethylene glycol brushes. *J. Am. Chem. Soc.* **2016**, *138*: 9097-9100. DOI: 10.1021/jacs.6b05787
20. D'souza, A.; Shegokaar, R. Polyethylene glycol (PEG): a versatile polymer for pharmaceutical applications. *Expert Opin. Drug Deliv.* **2016**, *13*(9): 1257-75. DOI: 10.1080/17425247.2016.1182485.
21. Lu, X.; Watts, E.; Jia, F.; Tan, X.; Zhang, K. Polycondensation of polymer brushes via DNA hybridization. *J. Am. Chem. Soc.* **2014**, *136*(29): 10214-10217. DOI: 10.1021/ja504790r
22. Kurien, B.T.; Scofield, R.H. Western blotting: an introduction. *Methods Mol. Biol.* **2015**, *1312*: 17-30. DOI: 10.1007/978-1-4939-2694-7_5
23. Lv, H.; Zhang, S.; Wang, B.; Cui, S.; Yan J. Toxicity of cationic lipids and cationic polymers in gene delivery. *J. Control Release* **2006**, *114*(1): 100-109. DOI: 10.1016/j.jconrel.2006.04.014

■ Author

Caroline Shen is a junior student at Phillips Academy in Andover, MA. She enjoys exploring science and has been taking college level chemistry and molecular biology courses.

Variations in Predominant Risk Factors and Interventions for Diarrheal Diseases in Children Under Five Years of Age

Mai Nguyen

Hwa Chong Institution, 661 Bukit Timah Road, Singapore 269734, chimainguyen288@gmail.com

Mentor: Sara Schwetschenau

ABSTRACT: Diarrheal disease, the second highest cause of under-five deaths, is preventable through access to safe water, sanitation, and hygiene (WASH). Since the effectiveness of WASH interventions depends on local risk factors for diarrheal diseases, identifying these risks helps maximize the interventions' benefits. This study investigates the variations of diarrheal disease and the relationship between diarrheal-predominant risk factors and WASH interventions globally from 2000 to 2019. Disease outcomes and intervention data are from the Global Burden of Disease Study 2019 and the WHO/UNICEF Joint Monitoring Programme study, respectively. Changes in the percentage of mortality and Years Lived with Disability (YLD) and their risk factors were calculated to investigate their correlation and predominant risk factors. Globally, after 20 years, under-five diarrheal deaths decreased consistently by 60% from 1,238,822.57 to 500,663.83 deaths, while YLD decreased slowly at an inconsistent rate (3.5% from 1,836,681.85 to 1,771,591.63 YLD). Analysis of WASH intervention data shows that, on average, increasing basic drinking water coverage by 11.2% reduces 142 deaths and 39 YLD per 100,000 under-five children. In addition, a 14.4% increase in basic sanitation coverage reduces 139 fatalities and 38 YLD per 100,000 under-five children. In comparison, a 13% increase in basic hygiene coverage lessens 333 deaths and 90 YLD per 100,000 under-five children. Since interventions are less effective in lowering diarrheal YLD than mortality, more attention should be spent on identifying interventions effective at reducing diarrheal non-fatal health outcomes.

KEYWORDS: Biomedical and Health Sciences; Pathophysiology; Diarrheal Diseases; Mortality; Years Lived with Disability (YLD); Risk Factors; Water, Sanitation, and Hygiene (WASH).

■ Introduction

According to the World Health Organisation, diarrheal diseases are the second leading cause of death among children under five years of age (hereafter referred to as 'under-five'), killing approximately 500,000 children yearly.¹ Though diarrheal diseases are present globally across all countries and regions, the burden is disproportionately placed on areas with poor access to healthcare facilities, clean water, and sanitation.² About 90% of under-five diarrheal deaths occurred in Sub-Saharan Africa and South Asia, and 42% came from only two countries, India and Nigeria.² Hence, identifying the regions with the highest prevalence of diarrheal diseases allows focused interventions to reduce the disease burden effectively.

Since 1980, diarrhea mortality amongst under-five children has decreased thanks to numerous programs on interventions to prevent or treat acute diarrhea.³ Diarrhea mortality per 100,000 under-five children globally decreased by 69.6% between 1990 and 2017, with the most significant absolute decline shown in Nigeria (1344.2 fewer deaths per 100,000 children from 1731.2 deaths per 100,000 children in 1990 to 387.8 deaths per 100,000 children in 2017).⁴

Generally, water, sanitation, and hygiene (WASH) interventions can improve water supply and quality, sanitation, and hygiene.⁵ Improvements to water distribution at both public and household levels, such as establishing a hand pump or a household connection, were considered water supply interventions.⁵ Water quality interventions focused on providing

water treatment, such as chlorine tablets or solutions, on removing bacterial pathogens at the source or household level.^{5,6} Interventions in sanitation include excreta disposal at either public or household levels.⁵ Finally, hygiene improvements combine both education (promotion of handwashing) and facilities-based (provision of soap, access to handwashing facilities).⁷ Therapeutic treatments such as oral rehydration therapy (ORT), zinc, and nutrition supplementation have improved infection recovery and effectively reduced mortality rates.⁸

However, prevention and protection interventions are less effective than treatment interventions, given that diarrhea incidence globally decreased by a modest 9.09% from 1990 to 2019 compared to a significant reduction in diarrhea deaths over the same period.¹⁸ Survivors face both long-term and acute health burdens, including poor physical growth, pneumonia, and other health effects.^{9,10} Diarrhea is a significant cause of malnutrition, and malnourished children are vulnerable to diarrheal diseases due to weaker immunity than normal children.¹ Therefore, the diarrheal burden should be addressed in terms of both mortality and morbidity.

The effectiveness of interventions for diarrhea varies considerably with different risk factors.⁴ Environmental risks such as unsafe water sources and poor hygiene practices have been identified as the primary cause of diarrheal diseases.¹¹ In 2016, an estimated 829,000 deaths and 49.8 million years lived with disability (YLD) were caused by inadequate drinking water, sanitation, and hand hygiene, among which 297,000 under-five

deaths occurred.¹² Accordingly, improving WASH interventions is crucial to reducing disease risk and burden.⁵ Besides environmental risk factors, child and maternal malnutrition, including suboptimal breastfeeding, child growth failure, and vitamin A deficiency, are also risk factors for diarrhea.^{13,14} Inadequate nutrition increases the susceptibility and severity of infectious diseases, including diarrhea.¹⁵ Dietary management for diarrhea, such as promoting breastfeeding or micronutrient supplementation, is essential to control diarrheal diseases and their associated nutritional complications.¹⁶ On the other hand, since WASH interventions are considered the primary approach to treating diarrheal diseases, it is important to understand any correlation between improvements in WASH and changes in exposure to both environmental and nutritional risk factors.

Motivated by the above context, this study aims to provide an up-to-date analysis of changes in diarrhea mortality and YLD from the latest Global Burden of Disease Study (GBD 2019).¹⁸ Furthermore, by identifying the predominant risk factors of diarrheal diseases across all countries and territories and investigating any possible correlation between changing predominant risk factors to significant WASH interventions, this study helps to guide further research and interventions to target communities with different diarrheal risk factors better.

■ Methods

Data sources:

Data about mortality, YLD, and risk factors were obtained from the Global Burden of Diseases, Injuries, and Risk Factors Study 2019 (GBD 2019) from the Institute for Health Metrics and Evaluation (IHME) at the University of Washington. The study estimates prevalence, incidence, mortality, years of life lost (YLLs), years lived with disability (YLD), and disability-adjusted life-years (DALYs) due to 369 diseases and injuries for two sexes and for 204 countries and territories between 1990 and 2019. Data input sources include censuses, household surveys, civil registration and vital statistics, disease registries, health service use, air pollution monitors, satellite imaging, and disease notifications. Methods used to develop these data are described elsewhere.¹⁷ In compliance with the Guidelines for Accurate and Transparent Health Estimates Reporting (GATHER) statement, data and code for the GBD 2019 are publicly available.¹⁸

This study also used data from the WHO/UNICEF Joint Monitoring Programme (JMP) to evaluate the changes in intervention data. The WHO/UNICEF JMP global database established in 1990 estimates improvements in household drinking water, sanitation, and hygiene since 2000. Estimates are derived from over 5,000 national data sources for over 200 countries and territories, including censuses, administrative reports, and nationally representative household surveys. Population-weighted averages for rural and urban areas of each region are calculated and assigned to countries lacking national data for the reference year. Data from JMP are publicly available.¹⁹

Variables

Disease outcome:

WHO defines diarrhea as “the passage of three or more loo-

se or liquid stools per day (or more frequent passage than is normal for the individual).” The GBD uses cause-specific death rates and causes fractions, developed using the Cause of Death Ensemble model and spatiotemporal Gaussian process regression models. YLD data were estimated by multiplying prevalence estimates by disability weights for mutually exclusive sequelae of diseases and injuries. Data obtained were limited to the estimates of deaths and YLD caused by diarrheal diseases by age group (<5 years), sex (both male and female), as well as all WASH and child and maternal malnutrition risk factors available from 2000 to 2019. Classification of regions in this study followed that of WHO, which consists of the African Region, Region of the Americas, South-East Asian Region, European Region, Eastern Mediterranean Region, and Western Pacific Region.

Risk factors:

This study focused on diarrhea-associated risk factors, primarily environmental and nutritional-related risks. GBD 2019 estimates nine diarrhea-associated environmental and nutritional risk factors (unsafe water source, unsafe sanitation, no access to handwashing facility, suboptimal breastfeeding, child growth failure, low birth weight and short gestation, iron deficiency, vitamin A deficiency, zinc deficiency). The modeling framework for the risk factors has been described in other studies.^{20,21} Generally, a comparative risk assessment framework was used in GBD to estimate levels and trends in exposure, attributable deaths, and attributable disability-adjusted life-years (DALYs) for multiple risks from 1990 to 2019. Relative risk and exposure estimates were derived from randomized controlled trials, cohorts, pooled cohorts, household surveys, census data, satellite data, and other sources. Some risk factors, most notably unsafe water, and sanitation, provided little to no data on deaths as the primary study outcome. Hence, diarrheal morbidity was considered the risk of diarrheal mortality for these risks.

Interventions:

Based on the data obtained from the JMP, interventions were categorized into three types: improvement in drinking water, sanitation, and hygiene. Definitions and detailed descriptions of service levels are mentioned in several reports from WHO/UNICEF.²²⁻²⁴ Primary outcomes of this paper are estimates of the percentage of the population having at least basic drinking water, sanitation, and hygiene. Improvements in interventions were considered the increase in basic WASH services coverage between 2000 and 2019. No improvement can be noticed without the exact values from countries with >99% of the population with at least basic services between 2000 and 2019. It is important to note that some countries and territories did not have WASH data recorded. Therefore, these countries and territories were not considered to assess the improvements in basic WASH services coverage.

■ Data analysis

Disease outcome:

In the interest of this study, the primary outcomes were the number of deaths and YLD of under-five children due to diarrheal diseases between 2000 and 2019. The difference in the number of fatalities and YLD in 2000 and 2019 gave the val-

value for change in mortality and YLD. The percentage change in these numbers from 2000 to 2019 was also calculated. Changes in the number of deaths were plotted against those of YLD to assess both fatal and non-fatal outcomes of diarrheal diseases. In map representation, darker colors illustrate a greater magnitude of the values, such as a higher number of deaths and YLD or a greater change in the number of deaths and YLD over time. Where appropriate, diarrhea mortality and YLD rates per 100 000 under-five children were used to improve the comparability of results across locations with different populations.

Predominant risk factors:

The predominant risk factor in a particular year was the risk factor with the highest population-attributable fraction. If the predominant risk factor in 2019 is similar to that in 2000, changes in the prevalence of the predominant risk factor were calculated by the difference in percentages of its population-attributable fractions between 2000 and 2019. If the predominant risk factor changed between 2000 and 2019, the changes in the population attributable fractions of both initial and final risk factors were calculated.

Correlation between changing predominant risk factors to major WASH interventions:

Improvements in WASH intervention were considered in the increased national percentages of access to basic services from 2000 to 2019. These improvements were compared to the changes in the prevalence of risk factors through visual inspection of plots and calculation of correlation coefficients to deduce any possible relationships between WASH interventions and all diarrhea-associated risk factors, including both environmental and nutritional risks.

Results

Disease outcome:

In 2019, diarrheal diseases resulted in 500,663.8 deaths and 1,771,591.6 YLD among under-five children globally. This accounted for 9.92% and 6.5% of global under-five deaths and YLD in 2019, respectively. From 2000 to 2019, under-five diarrheal deaths decreased by 60% from 1,238,822.6 deaths, confirmed by a similar result documented by both UNICEF's Countdown to 2030 report and Jay S. *et al.* (2022).^{25,26} However, under-five diarrheal YLD showed a smaller decrease (3.5% from 2,581,700.3 YLD). While the number of under-five diarrheal deaths continuously declined from 2000 to 2019, the number of YLD remained relatively constant, even though the overall trend was decreasing (Fig. 1).

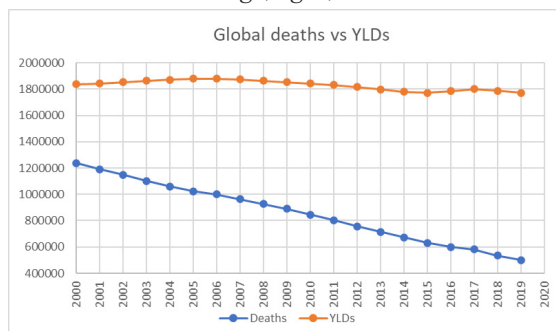
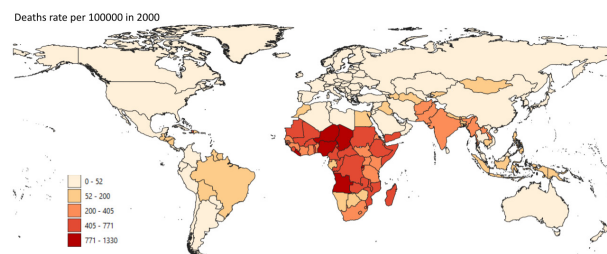


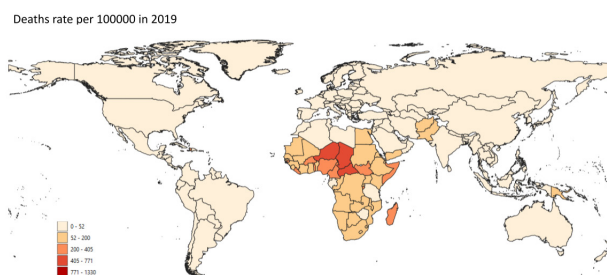
Figure 1: Number of under five diarrheal deaths and YLD globally from 2000 to 2019.

There is substantial variation among countries in the global diarrheal mortality and YLD rate among children under five years of age (Fig. 2). In 2019: the global rate was 75.5 deaths per 100,000 under-five children (Fig. 2C), a 61.9% decrease (Fig. 2B) from 198.3 deaths per 100,000 under-five children in 2000 (Fig 2A). Finland had the lowest mortality rate (0.14 deaths per 100,000 under-five children), while Chad had the highest mortality rate (751.9 deaths per 100,000 under-five children). When comparing the 20-year change in mortality rate among countries, the most significant decline occurred in Liberia, which observed 884.3 fewer deaths per 100,000 under-five children (from 1099.2 deaths to 214.9 deaths per 100,000 under-five children).

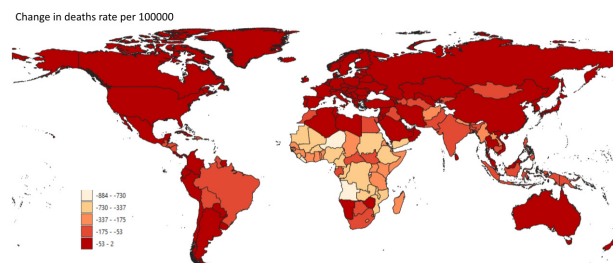
Considering YLD, from 2000 to 2019 observed, a global decline in diarrheal YLD rate among 100,000 children under five years of age was 9.1% (Fig 2F), a shift from 294.0 YLD (Fig. 2D) to 267.3 YLD per 100,000 under-five children (Fig 2E). On the country scale, in 2019, Japan had the lowest YLD rate (7.2 YLD per 100,000 under-five children), while Sudan had the highest YLD rate (627.8 YLD per 100,000 under-five children). Equatorial Guinea saw the most significant decline in YLD with a rate of -231.8 YLD, shifting from 537.6 YLD in 2000 to 305.8 YLD per 100,000 under-five children in 2019.

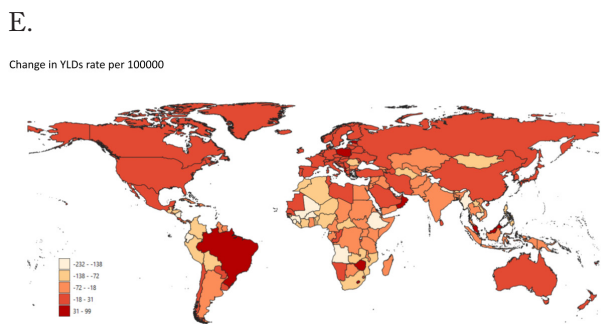
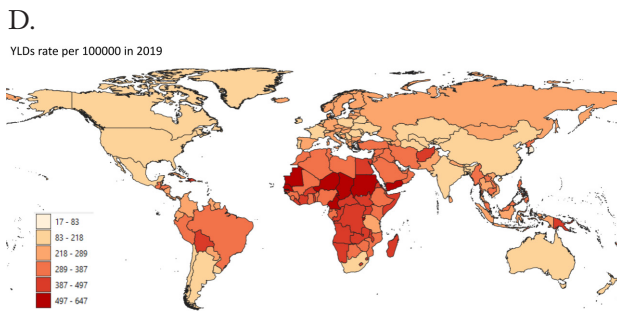
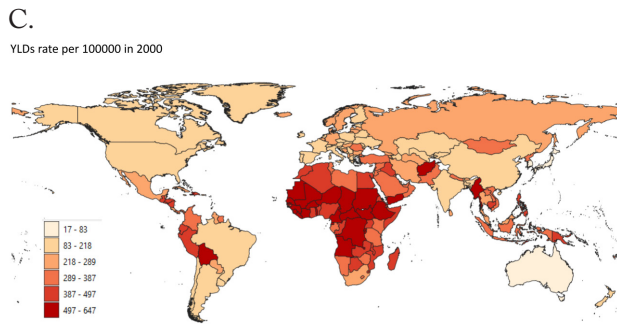


A.



B.

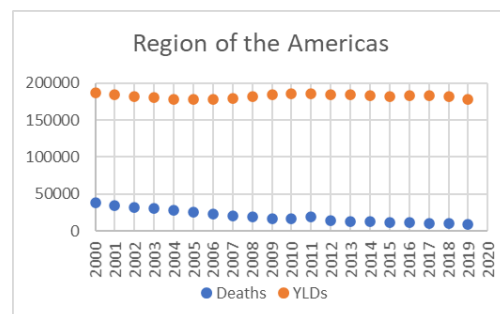
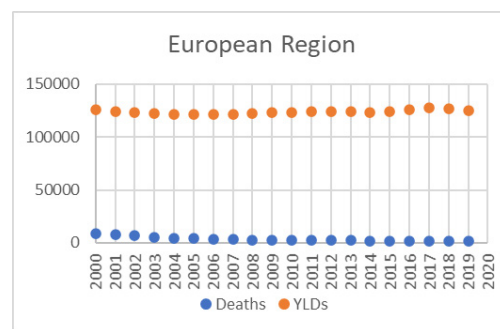
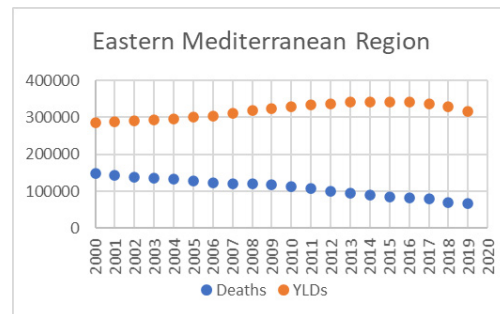
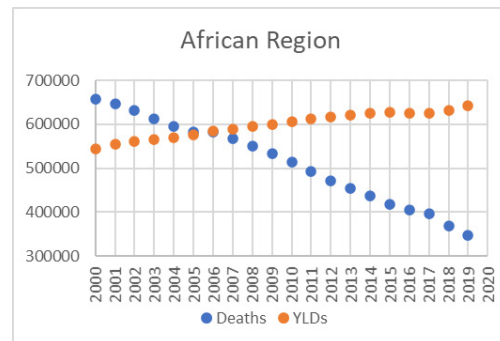
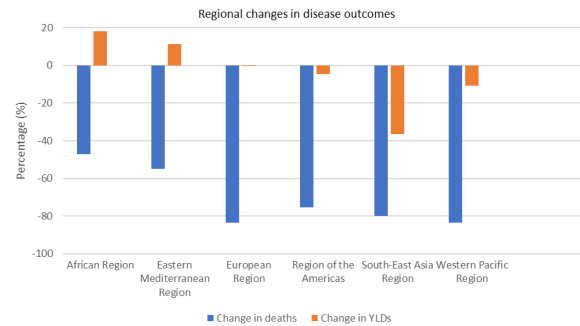




F. **Figure 2:** Maps of mortality and YLD rate between 2000-2019.

Between 2000 and 2019, the most significant regional decrease in diarrheal deaths of 83% occurred in both the European Region (from 9045.9 deaths to 1487.9 deaths) and Western Pacific Region (from 41045.6 deaths to 6791.0 deaths). Regional and temporal trends in fatalities and YLD are shown in Figure 3. Despite the highest percentage decrease in deaths, the European Region had less than a 1% change in YLD (0.56% from 125935.4 YLD to 125229.0 YLD). The South-East Asia Region observed the third most significant decline in the number of deaths (80% from 344158.2 deaths to 68863.9 deaths) and the highest percentage decrease in the YLD (36.5% from 435744.9 YLD to 276691.8 YLD). By contrast, the African Region had the most minor percentage decrease in the number of deaths (47.2% from 656626.8 deaths to 346770.7 deaths) and the highest increase in the number of YLD (18.1% from 544668.6 YLD to 643107.2 YLD). The African and Eastern Mediterranean regions were the only two regions with an increasing number of YLDs from 2000 to 2019. It is also important to note that percentage change may not be representative of absolute difference. For example, despite having the highest percentage decrease in

diarrheal mortality, the European Region observed a smaller reduction in the number of deaths than the African Region (7558.0 deaths compared to 309856.1 deaths).



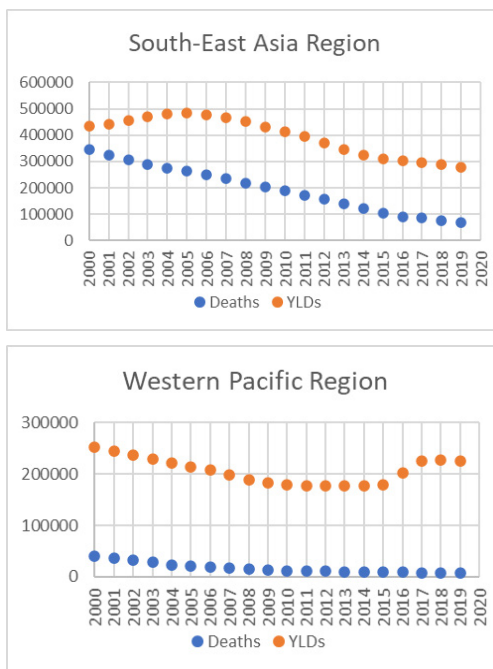


Figure 3: Regional changes in under-five diarrheal deaths and YLD from 2000 to 2019.

Risk factors:

Since a single diarrheal case can be attributed to multiple risks, risk factors are calculated separately. Therefore, the sum of risk-factor attributable fractions is not equal to 100% in a given population.

Globally in 2019, unsafe water, sanitation, and handwashing (WASH) accounted for the most significant proportion of under-five diarrheal deaths at 94.0%, while risk factors related to child and maternal malnutrition, namely suboptimal breastfeeding, child growth failure, low birth weight, and short gestation, iron, vitamin A and zinc deficiencies are associated with 90.4% of deaths. Globally, between 2000 and 2019, a 60% decrease in deaths due to both WASH (from 1,181,128.9 deaths to 470,752.2 deaths) and child and maternal malnutrition risk factors (from 1,133,294.3 deaths to 452,453.5 deaths) resulted in a 59.5% decrease in under-five diarrheal deaths (from 1,238,822.6 to 500,663.8) (Fig. 4).

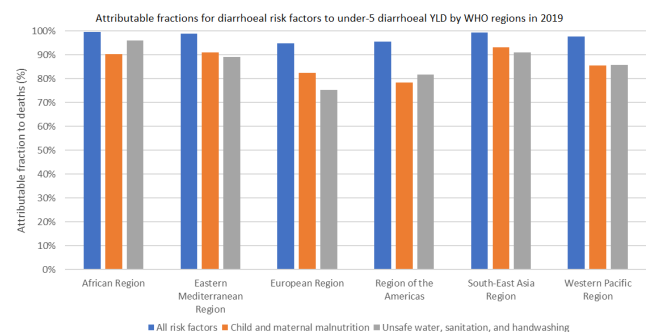
When considering YLD associated with diarrheal diseases, unsafe WASH was attributed to 82.2% of under-five diarrheal YLD worldwide in 2019. By contrast, poor child and maternal nutrition accounted for only 14.7% of diarrheal YLD. From 2000 to 2019, when YLD due to unsafe WASH decreased by 10.1% (from 1619413.5 YLD to 1455623.5 YLD), and child and maternal malnutrition decreased by 21.0% (from 327539.9 YLD to 258890.5 YLD), change in the global number of under-five diarrheal YLD only dropped by 3.5% (from 1836681.9 YLD to 1771591.6 YLD).



Figure 4: Changes in disease outcomes by categories of risk factors.

When considering regional trends in 2019, child and maternal malnutrition was the predominant risk factor in the Eastern Mediterranean Region, European Region, and South-East Asia Region, which accounted for 90.9%, 82.3%, and 93.1% of under-five diarrheal deaths, respectively (Fig. 5). Comparatively, unsafe WASH was the predominant risk factor in the African Region, Region of the Americas, and Western Pacific Region, associated with 96.1%, 81.7%, and 85.7% of under-five diarrheal deaths, respectively (Fig. 5). This marked an improvement from 2000 when unsafe WASH was the predominant risk factor for all regions.

Unsafe WASH was the leading risk factor for under-five diarrheal YLD, accounting for more than 75% of YLD in all regions except the European region. In the European Region, unsafe WASH was responsible for only 41% of diarrheal YLD. Unlike WASH risk factors, nutrition-related risk factors were not a significant risk of diarrheal YLD. Child and maternal malnutrition caused less than one-fifth of diarrheal YLD in all regions, with the highest fraction occurring in the European Region (18.9%).



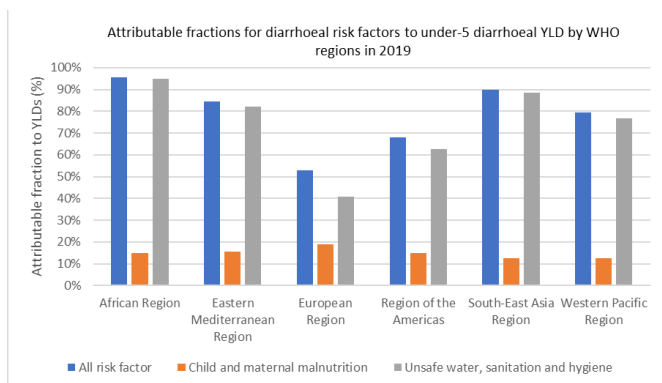


Figure 5: Attributable fractions for diarrhoeal risk factors to under-five diarrhoeal deaths (above) and YLD (below) by WHO regions in 2019

Additional nuance is observed when comparing predominant risk factors among countries. In 2000, there were only two predominant risk factors for under-five diarrhoeal deaths, unsafe water sources, and child growth failure across all countries and territories. Unsafe water sources contributed to the highest percentage of deaths in more countries and territories (108 countries and territories) than child growth failure (96 countries and territories). Comparatively, in 2019, there were three countries and territories with different predominant risk factors from unsafe water sources and child growth failure: Kyrgyzstan (unsafe sanitation), Bosnia and Herzegovina (suboptimal breastfeeding), and Switzerland (low birth weight and short gestation). Furthermore, child growth failure was the predominant risk factor in most countries (113 countries and territories compared to unsafe water sources in 88 countries and territories), over unsafe water sources which dominated in 2000. As a result, 26 countries and territories observed a change in their predominant risk factors for diarrhoeal deaths between 2000 and 2019. Twenty-two had the predominant risk factor changed from unsafe drinking water to child growth failure.

There were three predominant risk factors for under-five diarrhoeal YLD in 2000 and 2019: unsafe water source, suboptimal breastfeeding, and unsafe sanitation. There was no change in the status of these risk factors from 2000 to 2019, with unsafe water sources as the predominant factor (174 countries and territories in 2000 and 170 countries and territories in 2019), followed by suboptimal breastfeeding (28 countries and territories in 2000 and 31 countries and territories in 2019) and unsafe sanitation (2 countries and territories in 2000 and 3 countries and territories in 2019) (Fig. 6). However, nine countries' and territories' predominant risk factors for diarrhoeal YLD changed between 2000 and 2019. In four countries, the predominant risk factor changed from unsafe water and sanitation to suboptimal breastfeeding.

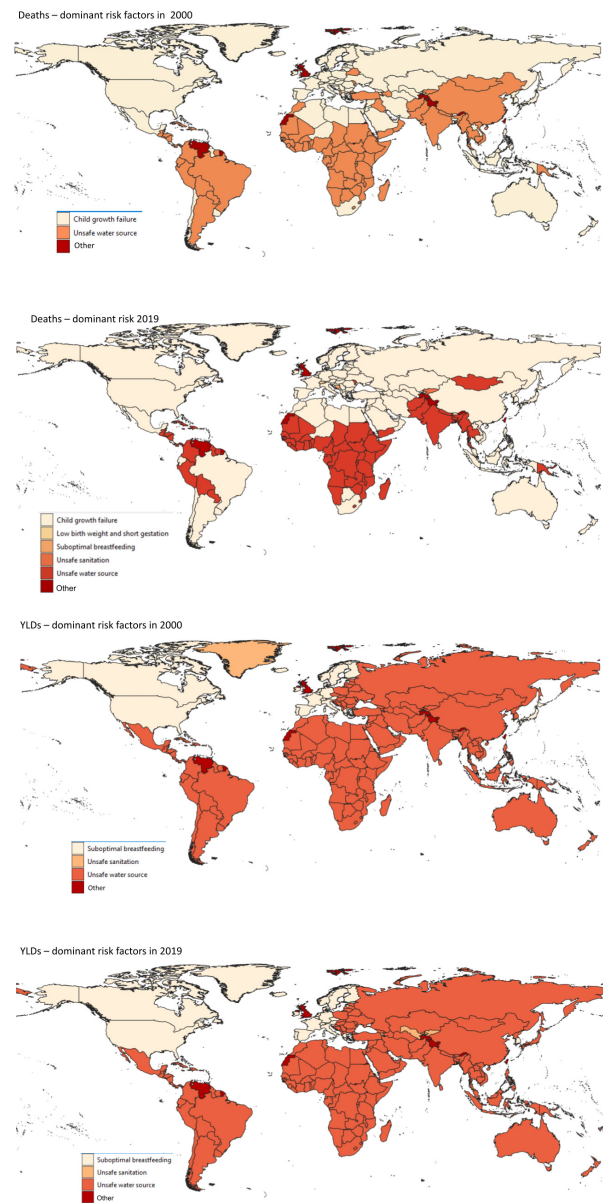


Figure 6: Map of predominant risk factors for under-five diarrhoeal deaths and YLD between 2000-2019.

Improvements in major WASH interventions:

Globally, between 2000 and 2019, the population with access to at least basic drinking water increased by 8.7% from 80.5% to 89.2%. In addition, the population with access to at least basic sanitation and hygiene increased by 22%, from 55% to 77%, and 11%, from 37% to 48%, respectively.

Generally, countries with high coverage of at least basic drinking water, sanitation, and hygiene had relatively lower mortality rates. Conversely, as the percentage of the population with at least basic drinking water decreased, the mortality rate increased (Fig. 7). However, there were considerable variations among countries. For example, Egypt had higher coverage of at least basic drinking water, more than 99% but a mortality rate of 71.4 deaths per 100,000 under-five children, higher than other countries with similar basic drinking water coverage. In comparison, in the United Republic of Tanzania, where

only 60% of the population had at least basic drinking water, a lower mortality rate of 35.5 deaths per 100,000 under-five children was reported. Similar trends were observed for sanitation and hygiene interventions.

In contrast, there was little or no clear relationship between the population percentage with improved WASH interventions and the diarrheal YLD rate (Fig. 8). Overall, there was an upward trend in the YLD rate as the WASH coverage went down. However, there were considerably more country-to-country variations compared to the mortality rate.

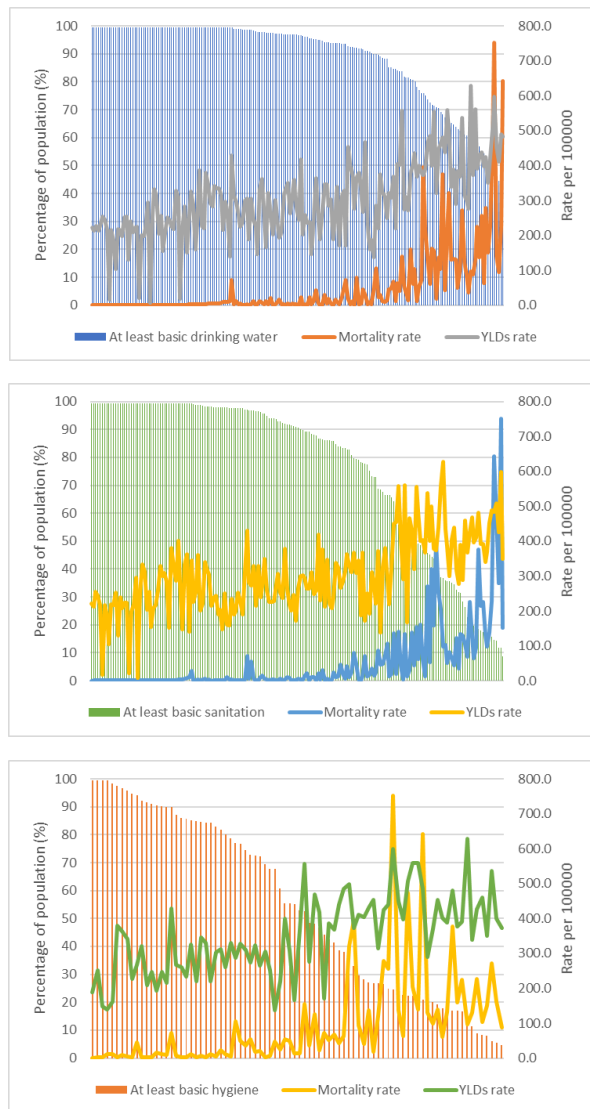


Figure 7: Graph of under-five diarrheal mortality and YLD rates (right y-axis) against the population percentage of countries (left y-axis) with at least basic drinking water (Fig. 7A), sanitation (Fig. 7B) and hygiene (Fig. 7C) across all countries and territories in 2019.

From 2000 to 2019, there were 127, 130, and nine countries and territories with improved drinking water, sanitation, and hygiene interventions, respectively. On average, an 11.2% increase in at least basic drinking water coverage reduces 142 deaths and 39 YLD per 100,000 under-five children. Likewise, at least basic sanitation coverage increased by 14.4% and was associated with 139 fewer deaths and 38 fewer YLD per

100,000 under-five children. Over the same period, access to at least basic hygiene increased by 13% and was associated with 333 fewer deaths and 90 fewer YLD per 100,000 under-five children.

Interestingly, despite the improvements in WASH interventions in many countries and territories, there were limited changes in the predominant risk factors for diarrheal deaths and YLD (Fig. 8). For example, out of 127 and 130 countries and territories with improved drinking water and sanitation, respectively, only 21 of those (17%) had different predominant risk factors for diarrheal deaths. Four countries and territories (3%) showed changes in predominant risk factors for diarrheal YLD between 2000 and 2019. Comparatively, out of nine countries and territories with improved hygiene, no country and territory have different predominant risk factors for diarrheal deaths. Still, one country (Armenia) has its predominant risk factor for diarrheal YLD changed from 2000 to 2019.

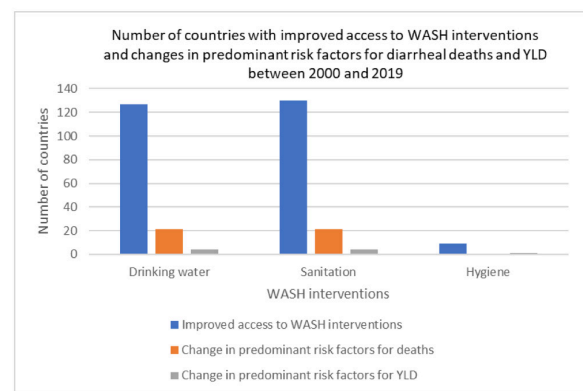


Figure 8: Graph of the number of countries with improved access to WASH interventions and changes in predominant risk factors for diarrheal deaths and YLD between 2000 and 2019.

■ Discussion

Improved access to safe water, sanitation, and hygiene (WASH) has the potential to prevent diarrheal disease, the second highest cause of under-five deaths globally. This study provides an up-to-date analysis of geographical and temporal variations in diarrheal diseases and their associated risk factors globally from 2000 to 2019 from the latest Global Burden of Disease Study (GBD 2019).¹⁸ Intervention efforts have resulted in a greater decrease in under-five deaths from diarrheal diseases than the decrease in YLD. Regionally, the greatest diarrheal death reduction occurred in the European and Western Pacific regions, while YLD happened in the South-East Asia regions.

Predominant risk factors for diarrheal deaths and YLD are also estimated. When considering the regional trends, unsafe WASH was the predominant risk factor in the African Region, Region of the Americas, and Western Pacific Region in 2019, an improvement from 2000 when WASH risk factors were the predominant risk factor for all regions. This trend can also be spotted in national trends when WASH risk factors like unsafe water sources, which dominated in 2000, were no longer the predominant risk factor in most countries in 2019. Conversely, unsafe WASH was the leading risk factor for under-five diarrheal YLD, accounting for more than 75% of

deaths in all regions except the European region. Unlike diarrheal deaths, the unsafe water source was the predominant contributor to YLD in most countries between 2000 and 2019.

As a result, additional efforts are needed to determine the interventions effective at reducing exposure to diarrheal disease pathogens, thereby reducing disease incidence.

Relationship between improvements in WASH interventions and changes in diarrheal deaths:

Globally, between 2000 and 2019, the number of under-five diarrheal deaths decreased continuously over the span of 20 years and dramatically by nearly 60%, which is a testament to serious global efforts to improve access to at least basic drinking water, sanitation, and hygiene, which increased by 8.7%, 22%, and 11%, respectively. However, the number of YLD declined at a slower rate than mortality (3.5% from 1,836,681.9 YLD to 1,771,591.6 YLD), and also the decline was not consistent throughout 20 years. Hence, to better address the impacts of diarrheal diseases, it is important to understand why the declines are unequal and what can be done to lower YLD.

Since the results show that unsafe WASH is associated with 94.0% of deaths, it is reasonable to suggest that improving access to WASH interventions is crucial to lowering diarrheal mortality. Indeed, results indicate a similar trend between the reduction in under-five diarrheal deaths and the attributable fraction of WASH risks to diarrheal mortality. With improved drinking water, even though there were only 21 countries seeing changes in predominant risk factors for under-five diarrheal deaths, 19 out of 21 countries had the predominant risk factor changed from unsafe water source to other risk factors. This is promising and indicates that drinking water treatment can significantly reduce the number of diarrheal deaths. Improving sanitation resulted in a similar reduction in diarrheal deaths due to unsafe water sources. Since sanitation systems reduce contamination of the environment with human waste, sanitation improvements minimize the transmission of pathogens that cause diarrhea into drinking water sources.²⁷ Furthermore, research from the American Journal of Epidemiology has reported that in locations with abysmal sanitation, improving drinking water quality would have little impact, while in places with better community sanitation, improved water treatment would result in a 40% reduction in diarrhea.²⁸

Relationship between improvements in WASH interventions and changes in diarrheal YLD:

Some studies have suggested that mortality data can lead to misrepresentation or even underestimation of the total disease burden without considering the long-term health outcomes of diarrheal diseases, YLD.^{29,30} These studies highlighted mortality and disability due to diarrheal disease.

Beyond acute infection, diarrheal diseases can have long-term impacts, including linear growth faltering, decreased cognitive function, and increased risk of subsequent infectious disease mortality.^{31,32} To address the diarrheal burden, commonly used interventions such as the rotavirus vaccine seem to treat moderate-to-severe diarrheal cases better than non-severe ones.³³ Results of this paper show that WASH-related risk factors are highly associated with diarrheal YLD in all regions. Yet surprisingly, improvements in WASH interventions

do not result in a proportional decrease in the YLD rate. This lack of correlation has been similarly reported in an analysis of the Global Enteric Multicenter Study (GEMS) reporting that there are difficulties in evaluating the effectiveness of WASH interventions in treating non-acute diarrheal cases as survey respondents may overstate water treatment of insufficiently conducted WASH interventions.³⁴ Another possible explanation for this lack of relationship is the exposure to diarrheal transmission on multiple pathways.⁴¹ Hence, no single WASH intervention is enough to eliminate persistent diarrhea completely. In fact, overreliance on one WASH intervention may cause neglect of other transmission pathways, increasing the risk of diarrhea.

As a result, it is necessary to understand and consider the broad range of WASH interventions, from improvements in infrastructures, such as water storage systems, to changes in human behaviors, such as handwashing with soap. It has been found that safe water storage systems, household water treatment, and interventions to enhance water quality at the source can lower diarrhea incidence by as much as 47%.³⁵ In some studies, an estimated median reduction in diarrhea incidence of 36% has been linked to improved sanitation facilities.³⁶ Several studies also pointed out that handwashing with soap can diminish the risk of diarrhea by more than 40%.^{37,38} Hence, to effectively reduce the diarrheal incidence and thus health outcomes like mortality or YLD, there should be a combination of different subcategories of WASH interventions. Beyond WASH interventions, several studies have documented that dietary management, especially with the addition of zinc supplementation, can significantly reduce the diarrheal incidence and thus reduce diarrheal YLD.^{39,40}

Even though WASH risk factors were highly associated with under-five diarrheal YLD, a decrease in YLD due to unsafe WASH did not translate to the same level of decline in the overall YLD due to diarrheal disease. Because multiple risk factors can be attributed to one single diarrheal case, there is an urgent need to improve the current understanding of the factors driving the YLD rate and the effectiveness of interventions in addressing diarrheal YLD. The present analysis was limited by available data and depended on data obtained from two studies. Despite the best efforts to include matching data between the two sources, only some countries and territories were included in both datasets. Omitted countries include Cote d'Ivoire and Taiwan (China), potentially contributing to errors in global trends.

YLD is a relatively new area of study in diarrheal disease research compared to mortality. As a result, risk factors and other drivers of YLD rates have yet to be fully identified. Future work should include further investigation into the total burden of diarrheal diseases and practical solutions to address these non-fatal health outcomes. Moreover, since under-five diarrheal mortality and YLD rates vary from country to country, further evaluation of specific national trends and disease burden associated with subnational variation is needed, such as differences in facilities, different exposure to risk factors, or other ways to target intervention resources better. Finally, to make these studies comparable, authorities and organizations

should provide guidelines on uniform research methods to improve understanding of the results at different spatial scales.

■ Acknowledgments

This paper was finished as a part of the Lumiere Research Scholars Program. I am showing my appreciation to Sara Schwetschenau for her guidance and mentorship and to the academic support team from Lumiere for their constant support.

■ References

1. *Diarrheal disease*. <https://www.who.int/news-room/fact-sheets/detail/diarrheal-disease> (accessed 2022-09-01).
2. Troeger, C.; Forouzanfar, M.; Rao, P. C.; Khalil, I.; Brown, A.; Reiner, R. C.; Fullman, N.; Thompson, R. L.; Abajobir, A.; Ahmed, M.; Alemayohu, M. A.; Alvis-Guzman, N.; Amare, A. T.; Antonio, C. A.; Asayesh, H.; Avokpaho, E.; Awasthi, A.; Bacha, U.; Barac, A.; Betsue, B. D.; Beyene, A. S.; Boneya, D. J.; Malta, D. C.; Dandona, L.; Dandona, R.; Dubey, M.; Eshrati, B.; Fitchett, J. R. A.; Gebrehiwot, T. T.; Hailu, G. B.; Horino, M.; Hotez, P. J.; Jibat, T.; Jonas, J. B.; Kasaeian, A.; Kisosoon, N.; Kotloff, K.; Koyanagi, A.; Kumar, G. A.; Rai, R. K.; Lal, A.; Razek, H. M. A. E.; Mengistie, M. A.; Moe, C.; Patton, G.; Platts-Mills, J. A.; Qorbani, M.; Ram, U.; Roba, H. S.; Sanabria, J.; Sartorius, B.; Sawhney, M.; Shigematsu, M.; Sreeramareddy, C.; Swamina than, S.; Tedla, B. A.; Jagiellonian, R. T.-M.; Ukwaja, K.; Werdecker, A.; Widdowson, M.-A.; Yonemoto, N.; Zaki, M. E. S.; Lim, S. S.; Naghavi, M.; Vos, T.; Hay, S. I.; Murray, C. J. L.; Mokdad, A. H. Estimates of Global, Regional, and National Morbidity, Mortality, and Aetiologies of Diarrheal Diseases: A Systematic Analysis for the Global Burden of Disease Study 2015. *Lancet Infect. Dis.* **2017**, *17* (9), 909–948. [https://doi.org/10.1016/S1473-3099\(17\)30276-1](https://doi.org/10.1016/S1473-3099(17)30276-1).
3. Black, R.; Fontaine, O.; Lamberti, L.; Bhan, M.; Huicho, L.; El Ariefeen, S.; Masanja, H.; Walker, C. F.; Mengestu, T. K.; Pearson, L.; Young, M.; Orobato, N.; Chu, Y.; Jackson, B.; Bateman, M.; Walker, N.; Merson, M. Drivers of the Reduction in Childhood Diarrhea Mortality 1980–2015 and Interventions to Eliminate Preventable Diarrhea Deaths by 2030. *J. Glob. Health* **9** (2), 020801. <https://doi.org/10.7189/jogh.09.020801>.
4. Troeger, C. E.; Khalil, I. A.; Blacker, B. F.; Biehler, M. H.; Albertson, S. B.; Zimsen, S. R. M.; Rao, P. C.; Abate, D.; Admasie, A.; Ahmedi, A.; Ahmed, M. L. C. B.; Akal, C. G.; Alahdab, F.; Alam, N.; Alene, K. A.; Alipour, V.; Aljunid, S. M.; Al-Raddadi, R. M.; Alvis-Guzman, N.; Amini, S.; Anjomshoa, M.; Antonio, C. A. T.; Arablou, J.; Aremu, O.; Atalay, H. T.; Atique, S.; Avokpaho, E. F. G. A.; Awad, S.; Awasthi, A.; Badawi, A.; Balakrishnan, K.; Banoub, J. A. M.; Barac, A.; Bassat, Q.; Bedi, N.; Bennett, D. A.; Bhattacharyya, K.; Bhutta, Z. A.; Bijani, A.; Bills, C. B.; Car, J.; Carvalho, F.; Castañeda-Orjuela, C. A.; Causey, K.; Christopher, D. J.; Cohen, A. J.; Dandona, L.; Dandona, R.; Daryani, A.; Demeke, F. M.; Djalalinia, S.; Dubey, M.; Dubljanin, E.; Duken, E. E.; Zaki, M. E. S.; Endries, A. Y.; Fernandes, E.; Fischer, F.; Frostad, J.; Fullman, N.; Gardner, W. M.; Geta, B.; Ghadiri, K.; Gorini, G.; Goulart, A. C.; Guo, Y.; Hailu, G. B.; Haj-Mirzaian, A.; Haj-Mirzaian, A.; Hamidi, S.; Hassen, H. Y.; Hoang, C. L.; Horita, N.; Hostiuc, M.; Husain, Z.; Irvani, S. S. N.; James, S. L.; Jha, R. P.; Jonas, J. B.; Karch, A.; Kasaeian, A.; Kassa, T. D.; Kassebaum, N. J.; Kefale, A. T.; Khader, Y. S.; Khan, E. A.; Khan, G.; Khan, M. N.; Khang, Y.-H.; Khoja, A. T.; Kimokoti, R. W.; Kisa, A.; Kisa, S.; Kisosoon, N.; Knibbs, L. D.; Kochhar, S.; Kosen, S.; Koul, P. A.; Koyanagi, A.; Defo, B. K.; Kumar, G. A.; Lal, D. K.; Leshargie, C. T.; Lewycka, S.; Li, S.; Lodha, R.; Macarayan, E. R. K.; Majdan, M.; Mamun, A. A.; Manguerra, H.; Mehta, V.; Melese, A.; Memish, Z. A.; Mengistu, D. T.; Meretoja, T. J.; Mestrovic, T.; Miazgowski, B.; Mirzakhimov, E. M.; Moazen, B.; Mohammad, K. A.; Mohammed, S.; Monasta, L.; Moore, C. E.; Morawska, L.; Mosser, J. F.; Mousavi, S. M.; Murthy, S.; Mustafa, G.; Nazari, J.; Nguyen, C. T.; Nguyen, H. L. T.; Nguyen, L. H.; Nguyen, S. H.; Nielsen, K. R.; Nisar, M. I.; Nixon, M. R.; Ogbo, F. A.; Okoro, A.; Olagunju, A. T.; Olagunju, T. O.; Oren, E.; Ortiz, J. R.; A. M. P.; Pakhale, S.; Postma, M. J.; Qorbani, M.; Quansah, R.; Rafiei, A.; Rahim, F.; Rahimi-Movaghar, V.; Rai, R. K.; Reitsma, M. B.; Rezai, M. S.; Rezapour, A.; Rios-Blancas, M. J.; Ronfani, L.; Rothenbacher, D.; Rubino, S.; Saleem, Z.; Sambala, E. Z.; Samy, A. M.; Milicevic, M. M. S.; Sarmiento-Sutó-Suárez, R.; Sartorius, B.; Savic, M.; Sawhney, M.; Saxena, S.; Sbarra, A.; Seyedmousavi, S.; Shaikh, M. A.; Sheikh, A.; Shigematsu, M.; Smith, D. L.; Sreeramareddy, C. T.; Stanaway, J. D.; Sufiyan, M. B.; Temsah, M.-H.; Tessema, B.; Tran, B. X.; Tran, K. B.; Tsodik, A. G.; Ullah, I.; Updike, R. L.; Vasankari, T. J.; Veisani, Y.; Wada, F. W.; Waheed, Y.; Welgan, K.; Wiens, K. E.; Wiysonge, C. S.; Yimer, E. M.; Yonemoto, N.; Zaidi, Z.; Zar, H. J.; Lim, S. S.; Vos, T.; Mokdad, A. H.; Murray, C. J. L.; Kyu, H. H.; Hay, S. I.; Reiner, R. C. Quantifying Risks and Interventions That Have Affected the Burden of Lower Respiratory Infections among Children Younger than 5 Years: An Analysis for the Global Burden of Disease Study 2017. *Lancet Infect. Dis.* **2020**, *20* (1), 60–79. [https://doi.org/10.1016/S1473-3099\(19\)30410-4](https://doi.org/10.1016/S1473-3099(19)30410-4).
5. Fewtrell, L.; Kaufmann, R. B.; Kay, D.; Enanoria, W.; Haller, L.; Colford, J. M. Water, Sanitation, and Hygiene Interventions to Reduce Diarrhea in Less Developed Countries: A Systematic Review and Meta-Analysis. *Lancet Infect. Dis.* **2005**, *5* (1), 42–52. [https://doi.org/10.1016/S1473-3099\(04\)01253-8](https://doi.org/10.1016/S1473-3099(04)01253-8).
6. *WASH Interventions during Disease Outbreaks in Humanitarian Emergencies*. Tufts - Feinstein International Center. <https://fic.tufts.edu/publication-item/wash-interventions-disease-outbreaks/> (accessed 2022-09-01).
7. Garn, J. V.; Wilkers, J. L.; Meehan, A. A.; Pfadenhauer, L. M.; Burns, J.; Imtiaz, R.; Freeman, M. C. Interventions to Improve Water, Sanitation, and Hygiene for Preventing Soil-transmitted Helminth Infection. *Cochrane Database Syst. Rev.* **2022**, *2022* (6), CD012199. <https://doi.org/10.1002/14651858.CD012199.pub2>.
8. *Effect of Community Based Interventions on Childhood Diarrhea and Pneumonia: Uptake of Treatment Modalities and Impact on Mortality*; Centre for Reviews and Dissemination (UK), 2013.
9. Schlaudecker, E. P.; Steinhoff, M. C.; Moore, S. R. Interactions of Diarrhea, Pneumonia, and Malnutrition in Childhood: Recent Evidence from Developing Countries. *Curr. Opin. Infect. Dis.* **2011**, *24* (5), 496–502. <https://doi.org/10.1097/QCO.0b013e328349287d>.
10. Richard, S. A.; Black, R. E.; Gilman, R. H.; Guerrant, R. L.; Kang, G.; Lanata, C. F.; Mølbak, K.; Rasmussen, Z. A.; Sack, R. B.; Valentiner-Branth, P.; Checkley, W.; for the Childhood Malnutrition and Infection Network. Diarrhea in Early Childhood: Short-Term Association With Weight and Long-Term Association With Length. *Am. J. Epidemiol.* **2013**, *178* (7), 1129–1138. <https://doi.org/10.1093/aje/kwt094>.
11. Clasen, T. F.; Alexander, K. T.; Sinclair, D.; Boisson, S.; Peletz, R.; Chang, H. H.; Majorin, F.; Cairncross, S. Interventions to Improve Water Quality for Preventing Diarrhea. *Cochrane Database Syst. Rev.* **2015**, No. 10. <https://doi.org/10.1002/14651858.CD004794.pub3>.
12. Prüss-Ustün, A.; Bartram, J.; Clasen, T.; Colford, J. M.; Cumming, O.; Curtis, V.; Bonjour, S.; Dangour, A. D.; De France, J.; Fewtrell, L.; Freeman, M. C.; Gordon, B.; Hunter, P. R.; Johnston, R. B.; Mathers, C.; Mäusezahl, D.; Medlicott, K.; Neira, M.; Stocks, M.; Wolf, J.; Cairncross, S. Burden of Disease from Inadequate Water, Sanitation and Hygiene in Low- and Middle-Income Settings: A Retrospective Analysis of Data from 145 Countries. *Trop.*

- Med. Int. Health TM IH* **2014**, 19 (8), 894–905. <https://doi.org/10.1111/tmi.12329>.
13. Singh, J. B.; Kumar, M.; Shah Nawaz, K.; Krishna, A. Diarrhea and Malnutrition in Children: A Study from Kishanganj District, Bihar. *J. Evol. Med. Dent. Sci.* **2014**, 3 (14), 3594–3600.
 14. Finlay, J. E.; Özaltın, E.; Canning, D. The Association of Maternal Age with Infant Mortality, Child Anthropometric Failure, Diarrhea and Anaemia for First Births: Evidence from 55 Low- and Middle-Income Countries. *BMJ Open* **2011**, 1 (2), e000226. <https://doi.org/10.1136/bmjopen-2011-000226>.
 15. Beck, M. A.; Levander, O. A. Host Nutritional Status and Its Effect on a Viral Pathogen. *J. Infect. Dis.* **2000**, 182 (Supplement_1), S93–S96. <https://doi.org/10.1086/315918>.
 16. Brown, K. H. Diarrhea and Malnutrition. *J. Nutr.* **2003**, 133 (1), 328S–332S. <https://doi.org/10.1093/jn/133.1.328S>.
 17. Vos, T.; Lim, S. S.; Abbafati, C.; Abbas, K. M.; Abbasi, M.; Abbasifard, M.; Abbasi-Kangevari, M.; Abbastabar, H.; Abd-Allah, F.; Abdelalim, A.; Abdollahi, M.; Abdollahpour, I.; Abolhassani, H.; Aboyans, V.; Abrams, E. M.; Abreu, L. G.; Abrigo, M. R. M.; Abu-Raddad, L. J.; Abushouk, A. I.; Acebedo, A.; Ackerman, I. N.; Adabi, M.; Adamu, A. A.; Adebayo, O. M.; Adekanmbi, V.; Adelson, J. D.; Adetokunboh, O. O.; Adham, D.; Afshari, M.; Afshin, A.; Agardh, E. E.; Agarwal, G.; Agesa, K. M.; Aghaali, M.; Aghami, S. M. K.; Agrawal, A.; Ahmad, T.; Ahmadi, A.; Ahmadi, M.; Ahmadi, H.; Ahmadpour, E.; Akalu, T. Y.; Akinyemi, R. O.; Akin, yemiju, T.; Akombi, B.; Al-Aly, Z.; Alam, K.; Alam, N.; Alam, S.; Alam, T.; Alanzi, T. M.; Albertson, S. B.; Alcalde-Rabanal, J. E.; Alema, N. M.; Ali, M.; Ali, S.; Alicandro, G.; Alijanzadeh, M.; Alinia, C.; Alipour, V.; Aljunid, S. M.; Alla, F.; Allebeck, P.; Almasi-Hashiani, A.; Alonso, J.; Al-Raddadi, R. M.; Altirkawi, K. A.; Alvis-Guzman, N.; Alvis-Zakzuk, N. J.; Amini, S.; Amini-Rarani, M.; Aminorroaya, A.; Amiri, F.; Amit, A. M. L.; Amugsi, D. A.; Amul, G. G. H.; Anderlini, D.; Andrei, C. L.; Andrei, T.; Anjoms, M.; Ansari, F.; Ansari, I.; Ansari-Moghaddam, A.; Antonio, C. A. T.; Antony, C. M.; Antriyandarti, E.; Anvari, D.; Anwer, R.; Arabloo, J.; Arab-Zozani, M.; Aravkin, A. Y.; Ariani, F.; Ärnlöv, J.; Aryal, K. K.; Arzani, A.; Asadi-Aliabadi, M.; Asadi-Pooya, A. A.; Asghari, B.; Ashbaugh, C.; Atnafu, D. D.; Atre, S. R.; Ausloos, F.; Ausloos, M.; Quintanilla, B. P. A.; Ayano, G.; Ayanore, M. A.; Aynalem, Y. A.; Azari, S.; Azarian, G.; Azene, Z. N.; Babae, E.; Badaoui, A.; Bagherzadeh, M.; Bakhshaei, M. H.; Bakhtiari, A.; Bala, krishnan, S.; Balalla, S.; Balassiano, S.; Banach, M.; Banik, P. C.; Bannick, M. S.; Bante, A. B.; Baraki, A. G.; Barboza, M. A.; Barker-Collo, S. L.; Barthelemy, C. M.; Barua, L.; Barzegar, A.; Basu, S.; Baune, B. T.; Bayati, M.; Bazmandegan, G.; Bedi, N.; Beghi, E.; Béjot, Y.; Bello, A. K.; Bender, R. G.; Bennett, D. A.; Bennitt, F. B.; Bensenor, I. M.; Benziger, C. P.; Berhe, K.; Bernabe, E.; Bertolacci, G. J.; Bhageerathy, R.; Bhala, N.; Bhandari, D.; Bhardwaj, P.; Bhattacharyya, K.; Bhutta, Z. A.; Bibi, S.; Biehl, M. H.; Bikbov, B.; Sayeed, M. S. B.; Biondi, A.; Biriha, B. M.; Bisanzio, D.; Bisignano, C.; Biswas, R. K.; Bohlouli, S.; Bohluli, M.; Bolla, S. R. R.; Bolor, A.; Boon-Dooley, A. S.; Borges, G.; Borzi, A. M.; Bourne, R.; Brady, O. J.; Brauer, M.; Brayne, C.; Breitborde, N. J. K.; Brenner, H.; Briant, P. S.; Briggs, A. M.; Briko, N. I.; Britton, G. B.; Brzazka, D.; Buchbinder, R.; Bumgarner, B. R.; Busse, R.; Butt, Z. A.; Santos, F. L. C. dos; Cámera, L. L. A.; Campos-Nonato, I. R.; Car, J.; Cárdenas, R.; Carreras, G.; Carrero, J. J.; Carvalho, F.; Castaldelli-Maia, J. M.; Castañeda-Orjuela, C. A.; Castelpietra, G.; Castle, C. D.; Castro, F.; Catalá-López, F.; Causey, K.; Cederroth, C. R.; Cerci, K. M.; Cerin, E.; Chandan, J. S.; Chang, A. R.; Charlson, F. J.; Chattu, V. K.; Chaturvedi, S.; Chimed-Ochir, O.; Chin, K. L.; Cho, D. Y.; Christensen, H.; Chu, D.-T.; Chung, M. T.; Ciuttini, F. M.; Ciobanu, L. G.; Cirillo, M.; Collins, E. L.; Compton, K.; Conti, S.; Cortesi, P. A.; Costa, V. M.; Cousin, E.; Cowden, R. G.; Cowie, B. C.; Cromwell, E. A.; Cross, D. H.; Crowe, C. S.; Cruz, J. A.; Cunningham, M.; Dahlawi, S. M. A.; Damiani, G.; Dandona, L.; Dandona, R.; Darwesh, A. M.; Daryani, A.; Das, J. K.; Gupta, R. D.; Neves, J. das; Dávila-Cervantes, C. A.; Davletov, K.; Leo, D. D.; Dean, F. E.; DeCleene, N. K.; Deen, A.; Degenhardt, L.; Dellavalle, R. P.; Demeke, F. M.; Demsie, D. G.; Denova-Gutiérrez, E.; Dereje, N. D.; Derveniz, N.; Desai, R.; Desalew, A.; Dessie, G. A.; Dharmaratne, S. D.; Dhungana, G. P.; Dianatinasab, M.; Diaz, D.; Forooshani, Z. S. D.; Dingels, Z. V.; Dirac, M. A.; Djalalinia, S.; Do, H. T.; Dokova, K.; Dorostkar, F.; Doshi, C. P.; Doshmangir, L.; Douiri, A.; Doney, M. C.; Driscoll, T. R.; Dunachie, S. J.; Duncan, B. B.; Duraes, A. R.; Eagan, A. W.; Kalan, M. E.; Edvardsson, D.; Ehrlich, J. R.; Nahas, N. E.; Sayed, I. E.; Tanta, wi, M. E.; Elbarazi, I.; Elgendy, I. Y.; Elhabashy, H. R.; El-Jaafary, S. I.; Elyazar, I. R.; Emamian, M. H.; Emmons-Bell, S.; Erskine, H. E.; Eshtrati, B.; Eskandarieh, S.; Esmailnejad, S.; Esmailzadeh, F.; Esteghamati, A.; Estep, K.; Etemadi, A.; Etillo, A. E.; Farahmand, M.; Faraj, A.; Fareed, M.; Faridnia, R.; Farinha, C. S. e.S.; Farioli, A.; Faro, A.; Faruque, M.; Farzadfar, F.; Fattahi, N.; Fazlzadeh, M.; Feigin, V. L.; Feldman, R.; Fereshtehnejad, S.-M.; Fernandes, E.; Ferrari, A. J.; Ferreira, M. L.; Filip, I.; Fischer, F.; Fisher, J. L.; Fitzgerald, R.; Flohr, C.; Flor, L. S.; Foigt, N. A.; Folyan, M. O.; Force, L. M.; Fornari, C.; Foroutan, M.; Fox, J. T.; Freitas, M.; Fu, W.; Fukumoto, T.; Furtado, J. M.; Gad, M. M.; Gakidou, E.; Galles, N. C.; Gallus, S.; Gamkrelidze, A.; Garcia-Basteiro, A. L.; Gardner, W. M.; Geberemariam, B. S.; Gebrehiwot, A. M.; Gebr emedhin, K. B.; Gebreslassie, A. A. A. A.; Hayoon, A. G.; Gething, P. W.; Ghadimi, M.; Ghadiri, K.; Ghafourifard, M.; Ghajar, A.; Ghamari, F.; Ghashghaee, A.; Ghiasvand, H.; Ghith, N.; Gholami, A.; Gilani, S. A.; Gill, P. S.; Gitimoghaddam, M.; Giussani, G.; Goli, S.; Gomez, R. S.; Gopalani, S. V.; Gorini, G.; Gorman, T. M.; Gottlich, H. C.; Goudarzi, H.; Goulart, A. C.; Goulart, B. N. G.; Grada, A.; Grivna, M.; Grosso, G.; Gubari, M. I. M.; Gugnan, i, H. C.; Guimaraes, A. L. S.; Guimarães, R. A.; Guled, R. A.; Guo, G.; Guo, Y.; Gupta, R.; Haagsma, J. A.; Haddock, B.; Hafezi-Nejad, N.; Hafiz, A.; Hagins, H.; Haile, L. M.; Hall, B. J.; Halvaei, I.; Hamadeh, R. R.; Abdullah, K. H.; Hamilton, E. B.; Han, C.; Han, H.; Hankey, G. J.; Haro, J. M.; Harvey, J. D.; Hasaballah, A. I.; Hasanzadeh, A.; Hashemian, M.; Hassani, S.; Hassankhani, H.; Havmoeller, R. J.; Hay, R. J.; Hay, S. I.; Hayat, K.; Heidari, B.; Heidari, G.; Heidari-Soureshjani, R.; Hendrie, D.; Henrikson, H. J.; Henry, N. J.; Herteliu, C.; Heydarpour, F.; Hird, T. R.; Hoek, H. W.; Hole, M. K.; Holla, R.; Hoogar, P.; Hosgood, H. D.; Hosseini, M.; Hostiu, M.; Hostiu, S.; Househ, M.; Hoy, D. G.; Hsairi, M.; Hsieh, V. C.; Hu, G.; Huda, T. M.; Hugo, F. N.; Huynh, C. K.; Hwang, B.-F.; Iannucci, V. C.; Ibitoye, S. E.; Ikuta, K. S.; Ilesanmi, O. S.; Ilic, I. M.; Ilic, M. D.; Inbaraj, L. R.; Ippolito, H.; Irvani, S. S. N.; Islam, M. M.; Islam, M.; Islam, S. M. S.; Islami, F.; Iso, H.; Ivers, R. Q.; Iwu, C. C. D.; Iyamu, I. O.; Jaafari, J.; Jacobson, K. H.; Jadidi-Niaragh, F.; Jafari, H.; Jafarinaia, M.; Jahagirdar, D.; Jahani, M. A.; Jahanmehr, N.; Jakovljevic, M.; Jalali, A.; Jalilian, F.; James, S. L.; Janjani, H.; Janodia, M. D.; Jayatilake, A. U.; Jee, mon, P.; Jenabi, E.; Jha, R. P.; Jha, V.; Ji, J. S.; Jia, P.; John, O.; John-Akinola, Y. O.; Johnson, C. O.; Johnson, S. C.; Jonas, J. B.; Joo, T.; Joshi, A.; Jozwiak, J. J.; Jürisson, M.; Kabir, A.; Kabir, Z.; Kalan, i, H.; Kalani, R.; Kalankesh, L. R.; Kalhor, R.; Kamiab, Z.; Kanchan, T.; Matin, B. K.; Karch, A.; Karim, M. A.; Karimi, S. E.; Kassa, G. M.; Kassebaum, N. J.; Katikireddi, S. V.; Kawakami, N.; Kayode, G. A.; Keddie, S. H.; Keller, C.; Kereselidze, M.; Khafaie, M. A.; Khalid, N.; Khan, M.; Khatab, K.; Khater, M. M.; Khatib, M. N.; Khayamzadeh, M.; Khodayari, M. T.; Khundkar, R.; Kianipour, N.; Kieling, C.; Kim, D.; Kim, Y.-E.; Kim, Y. J.; Kimokoti, R. W.; Kisa, A.; Kisa, S.; Kissimova-Skarbek, K.; Kivimäki, M.; Kneib, C. J.; Knudsen, A. K. S.; Kocarnik, J. M.; Kolola, T.; Kopec, J. A.;

- Kosen, S.; Koul, P. A.; Koyanagi, A.; Kravchenko, M. A.; Krishan, K.; Krohn, K. J.; Defo, B. K.; Bicer, B. K.; Kumar, G. A.; Kumar, M.; Kumar, P.; Kumar, V.; Kumares, G.; Kurmi, O. P.; Kusuma, D.; Kyu, H. H.; Vecchia, C. L.; Lacey, B.; Lal, D. K.; Laloo, R.; Lam, J. O.; Lami, F. H.; Landires, I.; Lang, J. J.; Lansingh, V. C.; Larson, S. L.; Larsson, A. O.; Lasrado, S.; Lassi, Z. S.; Lau, K. M.-M.; Lavados, P. M.; Lazarus, J. V.; Ledesma, J. R.; Lee, P. H.; Lee, S. W. H.; LeGrand, K. E.; Leigh, J.; Leonardi, M.; Lescinsky, H.; Leung, J.; Levi, M.; Lewington, S.; Li, S.; Lim, L.-L.; Lin, C.; Lin, R.-T.; Linehan, C.; Linn, S.; Liu, H.-C.; Liu, S.; Liu, Z.; Looker, K. J.; Lopez, A. D.; Lopukhov, P. D.; Lorkowski, S.; Lotufo, P. A.; Lucas, T. C. D.; Lugo, A.; Lunevicus, R.; Lyons, R. A.; Ma, J.; MacLachlan, J. H.; Maddison, E. R.; Maddison, R.; Madotto, F.; Mahasha, P. W.; Mai, H. T.; Majeed, A.; Maled, V.; Maleki, S.; Malekzadeh, R.; Malta, D. C.; Mamun, A. A.; Manafi, A.; Manafi, N.; Manguerra, H.; Mansouri, B.; Mansournia, M. A.; Herrera, A. M. M.; Maravilla, J. C.; Marks, A.; Martins-Melo, F. R.; Martopullo, I.; Masoumi, S. Z.; Massano, J.; Massenburg, B. B.; Mathur, M. R.; Maulik, P. K.; McAlinden, C.; McGrath, J. J.; McKee, M.; Mehndiratta, M. M.; Mehri, F.; Mehta, K. M.; Meitei, W. B.; Memiah, P. T. N.; Mendoza, W.; Menezes, R. G.; Mengesha, E. W.; Mengesha, M. B.; Mereke, A.; Meretoja, A.; Meretoja, T. J.; Mestrovic, T.; Miazgowski, B.; Miazgowski, T.; Michalek, I. M.; Mihretie, K. M.; Miller, T. R.; Mills, E. J.; Mirica, A.; Mirzakhimov, E. M.; Mirzaei, H.; Mirzaei, M.; Mirzaei-Alavijeh, M.; Misganaw, A. T.; Mithra, P.; Moazen, B.; Moghadasszadeh, M.; Mohamadi, E.; Mohammad, D. K.; Mohammad, Y.; Mezerji, N. M. G.; Mohammadian-Hafshejani, A.; Mohammadifard, N.; Mohammadpourhodki, R.; Mohammed, S.; Mokdad, A. H.; Molokhia, M.; Momen, N. C.; Monasta, L.; Mondello, S.; Mooney, M. D.; Moosazadeh, M.; Moradi, G.; Moradi, M.; Moradi-Lakeh, M.; Moradzadeh, R.; Moraga, P.; Morales, L.; Morawska, L.; Velásquez, I. M.; Morgado-da-Costa, J.; Morrison, S. D.; Mosser, J. F.; Mouodi, S.; Mousavi, S. M.; Khaneghah, A. M.; Mueller, U. O.; Munro, S. B.; Muriithi, M. K.; Musa, K. I.; Muthupandian, S.; Naderi, M.; Nagarajan, A. J.; Nagel, G.; Naghshtabrizi, B.; Nair, S.; Nandi, A. K.; Nangia, V.; Nansseu, J. R.; Nayak, V. C.; Nazari, J.; Negoi, I.; Negoi, R. I.; Netsere, H. B. N.; Ngunjiri, J. W.; Nguyen, C. T.; Nguyen, J.; Nguyen, M.; Nguyen, M.; Nichols, E.; Nigatu, D.; Nigatu, Y. T.; Nikbaksh, R.; Nixon, M. R.; Nnaji, C. A.; Nomura, S.; Norrvig, B.; Noubiash, J. J.; Nowak, C.; Nunez-Samudio, V.; Ofoi, A.; Oancea, B.; Odell, C. M.; Ogbon, F. A.; Oh, I.-H.; Okunga, E. W.; Oladnabi, M.; Olagunju, A. T.; Olusanya, B. O.; Olusanya, J. O.; Oluwasanu, M. M.; Bali, A. O.; Omer, M. O.; Ong, K. L.; Onwujekwe, O. E.; Orji, A. U.; Orpana, H. M.; Ortiz, A.; Ostroff, S. M.; Otstavnov, N.; Otstavnov, S. S.; Øverland, S.; Owolabi, M. O.; A. M. P.; Padubidri, J. R.; Pakhare, A. P.; Palladino, R.; Pana, A.; Panda-Jonas, S.; Pandey, A.; Park, E.-K.; Parmar, P. G. K.; Pasupula, D. K.; Patel, S. K.; Paternina-Cañedo, A. J.; Pathak, A.; Pathak, M.; Patten, S. B.; Patton, G. C.; Paudel, D.; Toroudi, H. P.; Peden, A. E.; Pennini, A.; Pepito, V. C. F.; Pehrah, E. K.; Pereira, A.; Pereira, D. M.; Perico, N.; Pham, H. Q.; Phillips, M. R.; Pigott, D. M.; Pils, T. M.; Pirsaeheb, M.; Plana-Ripoll, O.; Plass, D.; Polkhor, K. N.; Polibin, R. V.; Polinder, S.; Polkinghorne, K. R.; Postma, M. J.; Pourjafar, H.; Pourmalek, F.; Kalhori, R. P.; Pourshams, A.; Poznańska, A.; Prada, S. I.; Prakash, V.; Pribadi, D. R. A.; Puppillo, E.; Syed, Z. Q.; Rabiee, M.; Rabiee, N.; Radfar, A.; Rafee, A.; Rafei, A.; Raggi, A.; Rahimi-Movaghar, A.; Rahman, M. A.; Rajabpour-Sanati, A.; Rajati, F.; Ramezanzadeh, K.; Ranabhat, C. L.; Rao, P. C.; Rao, S. J.; Rasella, D.; Rastogi, P.; Rathi, P.; Rawaf, D. L.; Rawaf, S.; Rawal, L.; Razo, C.; Redford, S. B.; Reiner, R. C.; Reinig, N.; Reitsma, M. B.; Remuzzi, G.; Renjith, V.; Renzaho, A. M. N.; Resnikoff, S.; Rezaei, N.; Rezaei, M. sadegh; Rezapour, A.; Rhinehart, P.-A.; Riahi, S. M.; Ribeiro, A. L. P.; Ribeiro, D. C.; Ribeiro, D.; Rickard, J.; Roberts, N. L. S.; Roberts, S.; Robinson, S. R.; Roeber, L.; Rolfe, S.; Ronfani, L.; Roshandel, G.; Roth, G. A.; Rubagotti, E.; Rumisha, S. F.; Sabour, S.; Sachdev, P. S.; Sadik, B.; Sadeghi, E.; Sadeghi, M.; Saeidi, S.; Safi, S.; Safiri, S.; Sagar, R.; Sahebkar, A.; Sahraian, M. A.; Sajadi, S. M.; Salahshoor, M. R.; Salamati, P.; Zahabi, S. S.; Salem, H.; Salem, M. R. R.; Salimzadeh, H.; Salomon, J. A.; Salz, I.; Samad, Z.; Samy, A. M.; Sanabria, J.; Santomauro, D. F.; Santos, I. S.; Santos, J. V.; Santric-Milicevic, M. M.; Saraswathy, S. Y. I.; Sarmiento-Suárez, R.; Sarrafzadegan, N.; Sartorius, B.; Sarveazad, A.; Sathian, B.; Sathish, T.; Sattin, D.; Sbarra, A. N.; Schaeffer, L. E.; Schiavolin, S.; Schmidt, M. I.; Schutte, A. E.; Schwebel, D. C.; Schwedde, F.; Senbeta, A. M.; Senthilkumaran, S.; Sepanlou, S. G.; Shackelford, K. A.; Shadid, J.; Shahabi, S.; Shaheen, A. A.; Shaikh, M. A.; Shalash, A. S.; Shams-Beyranvand, M.; Shamsizadeh, M.; Shannawaz, M.; Sharafi, K.; Sharara, F.; Sheena, B. S.; Sheikhtaheri, A.; Shetty, R. S.; Shibuya, K.; Shiferaw, W. S.; Shigematsu, M.; Shin, J. I.; Shiri, R.; Shirkoobi, R.; Shrim, M. G.; Shuval, K.; Siabani, S.; Sigfusdottir, I. D.; Sigurvinsdottir, R.; Silva, J. P.; Simpson, K. E.; Singh, A.; Singh, J. A.; Skiadaresi, E.; Skou, S. T. S.; Skryabin, V. Y.; Sobngwi, E.; Sokhan, A.; Soltani, S.; Sorensen, R. J. D.; Soriano, J. B.; Sorrie, M. B.; Soyiri, I. N.; Sreeramreddy, C. T.; Stanaway, J. D.; Stark, B. A.; Ștefan, S. C.; Stein, C.; Steiner, C.; Steiner, T. J.; Stokes, M. A.; Stovner, L. J.; Stubbs, J. L.; Sudaryanto, A.; Sufiyan, M. B.; Sullo, G.; Sultan, I.; Sykes, B. L.; Sylte, D. O.; Szócska, M.; Tabarés-Sisdedos, R.; Tabb, K. M.; Tadakamadla, S. K.; Taherkhani, A.; Tajdini, M.; Takahashi, K.; Taveira, N.; Teagle, W. L.; Teame, H.; Tehrani-Banhashemi, A.; Teklehaimanot, B. F.; Terrason, S.; Tessema, Z. T.; Thankappan, K. R.; Thomson, A. M.; Tohidinik, H. R.; Tonelli, M.; Topor-Madry, R.; Torre, A. E.; Touvier, M.; Tovani-Palone, M. R. R.; Tran, B. X.; Travillion, R.; Troeger, C. E.; Truelsen, T. C.; Tsai, A. C.; Tsatsakis, A.; Car, L. T.; Tyrovolas, S.; Uddin, R.; Ullah, S.; Undurraga, E. A.; Unnikrishnan, B.; Vacante, M.; Valkilian, A.; Valdez, P. R.; Varughese, S.; Vasankari, T. J.; Vasseghian, Y.; Venketasubramanian, N.; Violante, F. S.; Vlassov, V.; Vollset, S. E.; Vongpradith, A.; Vukovic, A.; Vukovic, R.; Waheed, Y.; Walters, M. K.; Wang, J.; Wang, Y.; Wang, Y.-P.; Ward, J. L.; Watson, A.; Wei, J.; Weintraub, R. G.; Weiss, D. J.; Weiss, J.; Westerman, R.; Whisnant, J. L.; Whiteford, H. A.; Wiangkham, T.; Wiens, K. E.; Wijeratne, T.; Wilner, L. B.; Wilson, S.; Wojtyniak, B.; Wolfe, C. D. A.; Wool, E. E.; Wu, A.-M.; Hanson, S. W.; Wunrow, H. Y.; Xu, G.; Xu, R.; Yadgir, S.; Jabbari, S. H. Y.; Yamagishi, K.; Yaminfirooz, M.; Yano, Y.; Yaya, S.; Yazdi-Feizabadi, V.; Yearwood, J. A.; Yeheyis, T. Y.; Yeshitila, Y. G.; Yip, P.; Yonemoto, N.; Yoon, S.-J.; Lebn, J. Y.; Younis, M. Z.; Younker, T. P.; Yousefi, Z.; Yousefifard, M.; Yousefinezhadi, T.; Yousef, A. Y.; Yu, C.; Yusefzadeh, H.; Moghadam, T. Z.; Zaki, L.; Zaman, S. B.; Zamani, M.; Zamanian, M.; Zandian, H.; Zangeneh, A.; Zastroszhin, M. S.; Zewdie, K. A.; Zhang, Y.; Zhang, Z.-J.; Zhao, J. T.; Zhao, Y.; Zheng, P.; Zhou, M.; Ziapour, A.; Zimsen, S. R. M.; Naghavi, M.; Murray, C. J. L. Global Burden of 369 Diseases and Injuries in 204 Countries and Territories, 1990–2019: A Systematic Analysis for the Global Burden of Disease Study 2019. *The Lancet* **2020**, 396 (10258), 1204–1222. [https://doi.org/10.1016/S0140-6736\(20\)30925-9](https://doi.org/10.1016/S0140-6736(20)30925-9).
18. *GBD Results*. Institute for Health Metrics and Evaluation. <https://vizhub.healthdata.org/gbd-results> (accessed 2022-09-01).
19. *Data | JMP*. <https://washdata.org/data> (accessed 2022-09-01).
20. Gakidou, E.; Afshin, A.; Abajobir, A. A.; Abate, K. H.; Abbafati, C.; Abbas, K. M.; Abd-Allah, F.; Abdulle, A. M.; Abera, S. F.; Abayotans, V.; Abu-Raddad, L. J.; Abu-Rmeileh, N. M. E.; Abyu, G. Y.; Adedeji, I. A.; Adetokunbo, O.; Afarideh, M.; Agrawal, A.; Agrawal, S.; Ahmadieh, H.; Ahmed, M. B.; Aichour, M. T. E.; Aichour, A. N.; Aichour, I.; Akinyemi, R. O.; Akseer, N.; Alahdab, F.; Al-Aly, Z.; Alam, K.; Alam, N.; Alam, T.; Alasfoor, D.; Alene, K. A.

; Ali, K.; Alizadeh-Navaei, R.; Alkerwi, A.; Alla, F.; Allebeck, P.; Al-Raddadi, R.; Alsharif, U.; Altirkawi, K. A.; Alvis-Guzman, N.; Amare, A. T.; Amini, E.; Ammar, W.; Amoako, Y. A.; Ansari, H.; Antó, J. M.; Antonio, C. A. T.; Anwari, P.; Arian, N.; Årnlöv, J.; Ar taman, A.; Aryal, K. K.; Asayesh, H.; Asgedom, S. W.; Atey, T. M.; Avila-Burgos, L.; Avokpaho, E. F. G. A.; Awasthi, A.; Azzopardi, P.; Bacha, U.; Badawi, A.; Balakrishnan, K.; Ballew, S. H.; Barac, A.; Barber, R. M.; Barker-Collo, S. L.; Bärnighausen, T.; Barquera, S.; Barregard, L.; Barrero, L. H.; Batis, C.; Battle, K. E.; Baumgar ner, B. R.; Baune, B. T.; Beardsley, J.; Bedi, N.; Beghi, E.; Bell, M. L.; Bennett, D. A.; Bennett, J. R.; Bensenor, I. M.; Berhane, A.; Ber he, D. F.; Bernabé, E.; Betsu, B. D.; Beurán, M.; Beyene, A. S.; B hansali, A.; Bhutta, Z. A.; Bicer, B. K.; Bikbov, B.; Birungi, C.; Bir yukov, S.; Blosser, C. D.; Boneya, D. J.; Bou-Orm, I. R.; Brauer, M .; Breitborde, N. J. K.; Brenner, H.; Brugha, T. S.; Bulto, L. N. B.; Butt, Z. A.; Cahuana-Hurtado, L.; Cárdenas, R.; Carrero, J. J.; Ca stañeda-Orjuela, C. A.; Catalá-López, F.; Cercy, K.; Chang, H.-Y .; Charlson, F. J.; Chimed-Ochir, O.; Chisumpa, V. H.; Chitheer, A. A.; Christensen, H.; Christopher, D. J.; Cirillo, M.; Cohen, A. J.; Comfort, H.; Cooper, C.; Coresh, J.; Cornaby, L.; Cortesi, P. A .; Criqui, M. H.; Crump, J. A.; Dandona, L.; Dandona, R.; das Nev es, J.; Davey, G.; Davitoui, D. V.; Davletov, K.; de Courten, B.; De fo, B. K.; Degenhardt, L.; Deiparine, S.; Dellavalle, R. P.; Deribe, K.; Deshpande, A.; Dharmaratne, S. D.; Ding, E. L.; Djallalinia, S .; Do, H. P.; Dokova, K.; Doku, D. T.; Donkelaar, A. van; Dorsey, E. R.; Driscoll, T. R.; Dubey, M.; Duncan, B. B.; Duncan, S.; Ebra himi, H.; El-Khatib, Z. Z.; Enayati, A.; Endries, A. Y.; Ermakov, S. P.; Erskine, H. E.; Eshrati, B.; Eskandarieh, S.; Esteghamati, A .; Estep, K.; Faraon, E. J. A.; Farinha, C. S. e S.; Faro, A.; Farzadfa r, F.; Fay, K.; Feigin, V. L.; Fereshtehnejad, S.-M.; Fernandes, J. C .; Ferrari, A. J.; Feyissa, T. R.; Filip, I.; Fischer, F.; Fitzmaurice, C .; Flaxman, A. D.; Foigt, N.; Foreman, K. J.; Frostad, J. J.; Fullman, N.; Fürst, T.; Furtado, J. M.; Ganji, M.; Garcia-Basteiro, A. L.; Ge brehiwot, T. T.; Geleijnse, J. M.; Geleto, A.; Gemechu, B. L.; Gese sew, H. A.; Gething, P. W.; Ghajar, A.; Gibney, K. B.; Gill, P. S.; G illum, R. F.; Giref, A. Z.; Gishu, M. D.; Giussani, G.; Godwin, W. W.; Gona, P. N.; Goodridge, A.; Gopalani, S. V.; Goryakin, Y.; Go ulart, A. C.; Graetz, N.; Gughani, H. C.; Guo, J.; Gupta, R.; Gupt a, T.; Gupta, V.; Gutiérrez, R. A.; Hachinski, V.; Hafezi-Nejad, N .; Hailu, G. B.; Hamadeh, R. R.; Hamidi, S.; Hammami, M.; Han dal, A. J.; Hankey, G. J.; Hanson, S. W.; Harb, H. L.; Hareri, H. A .; Hassanvand, M. S.; Havmoeller, R.; Hawley, C.; Hay, S. I.; Heda yati, M. T.; Hendrie, D.; Heredia-Pi, I. B.; Hernandez, J. C. M.; H oek, H. W.; Horita, N.; Hosgood, H. D.; Hostiuc, S.; Hoy, D. G.; Hsairi, M.; Hu, G.; Huang, J. J.; Huang, H.; Ibrahim, N. M.; Ibur g, K. M.; Ikeda, C.; Inoue, M.; Irvine, C. M. S.; Jackson, M. D.; Ja cobsen, K. H.; Jahanmehr, N.; Jakovljevic, M. B.; Jauregui, A.; Java nbakht, M.; Jeemon, P.; Johansson, L. R. K.; Johnson, C. O.; Jonas , J. B.; Jürisson, M.; Kabir, Z.; Kadel, R.; Kahsay, A.; Kamal, R.; K arch, A.; Karema, C. K.; Kasaeian, A.; Kassebaum, N. J.; Kastor, A .; Katikireddi, S. V.; Kawakami, N.; Keiyoro, P. N.; Kelbore, S. G .; Kemmer, L.; Kengne, A. P.; Kesavachandran, C. N.; Khader, Y. S .; Khalil, I. A.; Khan, E. A.; Khang, Y.-H.; Khosravi, A.; Khubchan dani, J.; Kiadaliri, A. A.; Kieling, C.; Kim, J. Y.; Kim, Y. J.; Kim, D .; Kimokoti, R. W.; Kinfu, Y.; Kisa, A.; Kissimova-Skarbek, K. A .; Kivimaki, M.; Knibbs, L. D.; Knudsen, A. K.; Kopec, J. A.; Kosen, S.; Koul, P. A.; Koyanagi, A.; Kravchenko, M.; Krohn, K. J.; Krom hout, H.; Kumar, G. A.; Kutz, M.; Kyu, H. H.; Lal, D. K.; Lalloo, R .; Lallukka, T.; Lan, Q.; Lansingh, V. C.; Larsson, A.; Lee, P. H .; Lee, A.; Leigh, J.; Leung, J.; Levi, M.; Levy, T. S.; Li, Y.; Li, Y .; Liang, X.; Liben, M. L.; Linn, S.; Liu, P.; Lodha, R.; Logroscino, G .; Looker, K. J.; Lopez, A. D.; Lorkowski, S.; Lotufo, P. A.; Loza no, R.; Lunevicius, R.; Macarayan, E. R. K.; Magdy Abd ElRazek, H .; Magdy Abd El Razek, M.; Majdan, M.; Majdzadeh, R.; Maje ed, A.; Malekzadeh, R.; Malhotra, R.; Malta, D. C.; Mamun, A. A .; Manguerra, H.; Mantovani, L. G.; Mapoma, C. C.; Martin, R. V .; Martinez-Raga, J.; Martins-Melo, F. R.; Mathur, M. R.; Mats ushita, K.; Matzopoulos, R.; Mazidi, M.; McAlinden, C.; McGrat h, J. J.; Mehata, S.; Mehndiratta, M. M.; Meier, T.; Melaku, Y. A .; Memiah, P.; Memish, Z. A.; Mendoza, W.; Mengesha, M. M.; M ensah, G. A.; Mensink, G. B. M.; Mereta, S. T.; Meretoja, T. J.; M erecoja, A.; Mezgebe, H. B.; Micha, R.; Millea, A.; Miller, T. R .; Minnig, S.; Mirarefin, M.; Mirrahimov, E. M.; Misganaw, A.; M ishra, S. R.; Mohammad, K. A.; Mohammed, K. E.; Mohammed, S .; Mohan, M. B. V.; Mokdad, A. H.; Monasta, L.; Montico, M.; Moradi-Lakeh, M.; Moraga, P.; Morawska, L.; Morrison, S. D .; Mountjoy-Venning, C.; Mueller, U. O.; Mullany, E. C.; Muller, K .; Murthy, G. V. S.; Musa, K. I.; Naghavi, M.; Naheed, A.; Nangia, V .; Natarajan, G.; Negoi, R. I.; Negoi, I.; Nguyen, C. T.; Nguyen, Q. L .; Nguyen, T. H.; Nguyen, G.; Nguyen, M.; Nichols, E.; Ning rum, D. N. A.; Nomura, M.; Nong, V. M.; Norheim, O. F.; Norrvi ng, B.; Noubiap, J. J. N.; Obermeyer, C. M.; Ogbo, F. A.; Oh, I.-H .; Oladimeji, O.; Olagunju, A. T.; Olagunju, T. O.; Olivares, P. R .; Olsen, H. E.; Olusanya, B. O.; Olusanya, J. O.; Opio, J. N.; Oren, E .; Ortiz, A.; Ota, E.; Owolabi, M. O.; Pa, M.; Pacella, R. E.; Pan a, A.; Panda, B. K.; Panda-Jonas, S.; Pandian, J. D.; Papachristou, C .; Park, E.-K.; Parry, C. D.; Patten, S. B.; Patton, G. C.; Pereira, D. M .; Perico, N.; Pesudovs, K.; Petzold, M.; Phillips, M. R.; Pilla y, J. D.; Piradov, M. A.; Pishgar, F.; Plass, D.; Pletcher, M. A.; Poli nder, S.; Popova, S.; Poulton, R. G.; Pourmalek, F.; Prasad, N.; Pur cell, C.; Qorbani, M.; Radfar, A.; Rafay, A.; Rahimi-Movaghar, A .; Rahimi-Movaghar, V.; Rahman, M. H. U.; Rahman, M. A.; Rah man, M.; Rai, R. K.; Rajsic, S.; Ram, U.; Rawaf, S.; Rehm, C. D .; Rehm, J.; Reiner, R. C.; Reitsma, M. B.; Remuzzi, G.; Renzaho, A . M. N.; Resnikoff, S.; Reynales-Shigematsu, L. M.; Rezaei, S.; Ri beiro, A. L.; Rivera, J. A.; Roba, K. T.; Rojas-Rueda, D.; Roman, Y .; Room, R.; Roshandel, G.; Roth, G. A.; Rothenbacher, D.; Ruba gotti, E.; Rushton, L.; Sadat, N.; Safdarian, M.; Safi, S.; Safiri, S .; Sahathevan, R.; Salama, J.; Salomon, J. A.; Samy, A. M.; Sanabria, J. R .; Sanchez-Niño, M. D.; Sánchez-Pimienta, T. G.; Santomaur o, D.; Santos, I. S.; Santric Milicevic, M. M.; Sartorius, B.; Satptha thy, M.; Sawhney, M.; Saxena, S.; Schmidt, M. I.; Schneider, I. J. C .; Schutte, A. E.; Schwebel, D. C.; Schwendicke, F.; Seedat, S.; S epanlou, S. G.; Serdar, B.; Servan-Mori, E. E.; Shaddick, G.; Shah een, A.; Shahraz, S.; Shaikh, M. A.; Shamsipour, M.; Shamsizade h, M.; Shariful Islam, S. M.; Sharma, J.; Sharma, R.; She, J.; Shen, J .; Shi, P.; Shibuya, K.; Shields, C.; Shiferaw, M. S.; Shigematsu, M .; Shin, M.-J.; Shiri, R.; Shirkoobi, R.; Shishani, K.; Shoman, H .; Shrime, M. G.; Sigfusdottir, I. D.; Silva, D. A. S.; Silva, J. P .; Silveira, D. G. A.; Singh, J. A.; Singh, V.; Sinha, D. N.; Skiadaresi, E .; Slepak, E. L.; Smith, D. L.; Smith, M.; Sobaih, B. H. A.; Sobn gwi, E.; Soneji, S.; Sorensen, R. J. D.; Sposato, L. A.; Sreeramard dy, C. T.; Srinivasan, V.; Steel, N.; Stein, D. J.; Steiner, C.; Steinke, S .; Stokes, M. A.; Strub, B.; Subart, M.; Sufiyan, M. B.; Skatchi, R . A.; Sur, P. J.; Swaminathan, S.; Sykes, B. L.; Szoeko, C. E. I.; Taba rés-Seisdedos, R.; Takakamadla, S. K.; Takahashi, K.; Takala, J. S .; Tandon, N.; Tanner, M.; Tarekegn, Y. L.; Tavakkoli, M.; Tegegn e, T. K.; Tehrani-Banihashemi, A.; Terkawi, A. S.; Tessema, B.; T hakur, J.; Thamsuwan, O.; Thankappan, K. R.; Theis, A. M.; Tho omas, M. L.; Thomson, A. J.; Thrift, A. G.; Tillmann, T.; Tobe-G ai, R.; Tobollik, M.; Tollanes, M. C.; Tonelli, M.; Topor-Madry, R .; Torre, A.; Tortajada, M.; Touvier, M.; Tran, B. X.; Truelsen, T.; T uem, K. B.; Tuzcu, E. M.; Tyrovolas, S.; Ukwaja, K. N.; Uneke, C. J .; Updike, R.; Uthman, O. A.; van Boven, J. F. M.; Varughese, S .; Vasankari, T.; Veerman, L. J.; Venkateswaran, V.; Venketasubrama nian, N.; Violante, F. S.; Vladimirov, S. K.; Vlassov, V. V.; Vollset, S . E.; Vos, T.; Wadilo, F.; Wakayo, T.; Wallin, M. T.; Wang, Y.-P.; W eichenthal, S.; Weiderpass, E.; Weintraub, R. G.; Weiss, D. J.; Wer

- decker, A.; Westerman, R.; Whiteford, H. A.; Wiysonge, C. S.; Woldeyes, B. G.; Wolfe, C. D. A.; Woodbrook, R.; Workicho, A.; Xavier, D.; Xu, G.; Yadgir, S.; Yakob, B.; Yan, L. L.; Yaseri, M.; Yimam, H. H.; Yip, P.; Yonemoto, N.; Yoon, S.-J.; Yotebieng, M.; Younis, M. Z.; Zaidi, Z.; Zaki, M. E. S.; Zavala-Arciniega, L.; Zhang, X.; Zimsen, S. R. M.; Zipkin, B.; Zodpey, S.; Lim, S. S.; Murray, C. J. L. Global, Regional, and National Comparative Risk Assessment of 84 Behavioural, Environmental and Occupational, and Metabolic Risks or Clusters of Risks, 1990–2016: A Systematic Analysis for the Global Burden of Disease Study 2016. *The Lancet* 2017, 390 (10100), 1345–1422. [https://doi.org/10.1016/S0140-6736\(17\)32366-8](https://doi.org/10.1016/S0140-6736(17)32366-8).
21. Stanaway, J. D.; Afshin, A.; Gakidou, E.; Lim, S. S.; Abate, D.; Abate, K. H.; Abbafati, C.; Abbasi, N.; Abbastabar, H.; Abd-Allah, F.; Abdela, J.; Abdelalim, A.; Abdollahpour, I.; Abdulkader, R. S.; Abebe, M.; Abebe, Z.; Abera, S. F.; Abil, O. Z.; Abraha, H. N.; Abraham, A. R.; Abu-Raddad, L. J.; Abu-Rmeileh, N. M.; Accrombessi, M. M. K.; Acharya, D.; Acharya, P.; Adamu, A. A.; Adane, A. A.; Adebayo, O. M.; Adedoyin, R. A.; Adekanmbi, V.; Ademi, Z.; Adetokunboh, O. O.; Adib, M. G.; Admasie, A.; Adsuar, J. C.; Afanvi, K. A.; Afarideh, M.; Agarwal, G.; Aggarwal, A.; Aghayan, S. A.; Agrawal, A.; Agrawal, S.; Ahmadi, A.; Ahmadi, M.; Ahmadi, H.; Ahmed, M. B.; Aichour, A. N.; Aichour, I.; Aichour, M. T. E.; Akbari, M. E.; Akinyemiju, T.; Akseer, N.; Al-Aly, Z.; Al-Eyadhy, A.; Al-Mekhlafi, H. M.; Alahdab, F.; Alam, K.; Alam, S.; Alami, T.; Alashi, A.; Alavian, S. M.; Alene, K. A.; Ali, K.; Ali, S. M.; Alijanzadeh, M.; Alizadeh-Navaei, R.; Aljunied, S. M.; Alkerwi, A.; Alla, F.; Alsharif, U.; Altirkawi, K.; Alvis-Guzman, N.; Amare, A. T.; Ammar, W.; Anber, N. H.; Anderson, J. A.; Andrei, C. L.; Androudi, S.; Animum, M. D.; Anjomshoa, M.; Ansha, M. G.; Antó, J. M.; Antonio, C. A. T.; Anwari, P.; Appiah, L. T.; Appiah, S. C. Y.; Arabloo, J.; Aremu, O.; Årnlöv, J.; Artaman, A.; Aryal, K. K.; Asayesh, H.; Ataro, Z.; Ausloos, M.; Avokpaho, E. F. G. A.; Awasthi, A.; Ayala Quintanilla, B. P.; Ayer, R.; Ayuk, T. B.; Azzopardi, P. S.; Babazadeh, A.; Badali, H.; Badawi, A.; Balakrishnan, K.; Bali, A. G.; Ball, K.; Ballew, S. H.; Banach, M.; Banoub, J. A. M.; Barac, A.; Barker-Collo, S. L.; Bärnighausen, T. W.; Barrero, L. H.; Basu, S.; Baune, B. T.; Bazargan-Hejazi, S.; Bedi, N.; Beghi, E.; Behzadifar, M.; Behzadifar, M.; Béjot, Y.; Bekele, B. B.; Bekru, E. T.; Belay, E.; Belay, Y. A.; Bell, M. L.; Bello, A. K.; Bennett, D. A.; Bensenor, I. M.; Bergeron, G.; Berhane, A.; Bernabe, E.; Bernstein, R. S.; Beuran, M.; Beyranvand, T.; Bhalla, N.; Bhalla, A.; Bhattarai, S.; Bhutta, Z. A.; Biadgo, B.; Bijani, A.; Bikbov, B.; Bilano, V.; Bililign, N.; Bin Sayeed, M. S.; Bisanzio, D.; Biswas, T.; Bjørge, T.; Blacker, B. F.; Bleyer, A.; Borschmann, R.; Bou-Orm, I. R.; Boufo us, S.; Bourne, R.; Brady, O. J.; Brauer, M.; Brazinova, A.; Breitborde, N. J. K.; Brenner, H.; Briko, A. N.; Britton, G.; Brugha, T.; Buchbinder, R.; Burnett, R. T.; Busse, R.; Butt, Z. A.; Cahill, L. E.; Cahuana-Hurtado, L.; Campos-Nonato, I. R.; Cárdenas, R.; Carreras, G.; Carrero, J. J.; Carvalho, F.; Castañeda-Orjuela, C. A.; Castillo Rivas, J.; Castro, F.; Catalá-López, F.; Causey, K.; Cercey, K. M.; Cerin, E.; Chaiah, Y.; Chang, H.-Y.; Chang, J.-C.; Chang, K.-L.; Charlson, F. J.; Chattopadhyay, A.; Chattu, V. K.; Chee, M. L.; Cheng, C.-Y.; Chew, A.; Chiang, P. P.-C.; Chimed-Ochir, O.; Chin, K. L.; Chittheer, A.; Choi, J.-Y. J.; Chowdhury, R.; Christensen, H.; Christopher, D. J.; Chung, S.-C.; Cicuttini, F. M.; Cirillo, M.; Cohen, A. J.; Collado-Mateo, D.; Cooper, C.; Cooper, O. R.; Coresh, J.; Cornaby, L.; Cortesi, P. A.; Cortinovis, M.; Costa, M.; Cousin, E.; Criqui, M. H.; Cromwell, E. A.; Cundiff, D. K.; Daba, A. K.; Dachew, B. A.; Dadi, A. F.; Damasceno, A. A. M.; Dandona, L.; Dandona, R.; Darby, S. C.; Dargan, P. I.; Daryani, A.; DasGupta, R.; Das Neves, J.; Dasa, T. T.; Dash, A. P.; Davitoutou, D. V.; Davletov, K.; De la Cruz-Góngora, V.; De La Hoz, F. P.; De Leo, D.; De Neve, J.-W.; Degenhardt, L.; Deiparine, S.; Dellavalle, R. P.; Demoz, G. T.; Denova-Gutiérrez, E.; Deribe, K.; Dervenis, N.; Dshpande, A.; Des Jarlais, D. C.; Dessie, G. A.; Deveber, G. A.; Dey, S.; Dharmaratne, S. D.; Dhimal, M.; Dinberu, M. T.; Ding, E. L.; Diro, H. D.; Djalarinia, S.; Do, H. P.; Dokova, K.; Doku, D. T.; Doyle, K. E.; Driscoll, T. R.; Dubey, M.; Dubljanin, E.; Duken, E. E.; Duncan, B. B.; Duraes, A. R.; Ebert, N.; Ebrahimi, H.; Ebrahimipour, S.; Edvardsson, D.; Effiong, A.; Eggen, A. E.; El Bcheraoui, C.; El-Khatib, Z.; Elyazar, I. R.; Enayati, A.; Endries, A. Y.; Er, B.; Erskine, H. E.; Eskandarieh, S.; Esteghamati, A.; Estep, K.; Fakhim, H.; Faramarzi, M.; Fareed, M.; Farid, T. A.; Farinha, C. S. E. S.; Farioli, A.; Faro, A.; Farvid, M. S.; Farzaei, M. H.; Fatima, B.; Fay, K. A.; Fazaeli, A. A.; Feigin, V. L.; Feigl, A. B.; Fereshtehnejad, S.-M.; Fernandes, E.; Fernandes, J. C.; Ferrara, G.; Ferrari, A. J.; Ferreira, M. L.; Filip, I.; Finger, J. D.; Fischer, F.; Foigt, N. A.; Foremant, K. J.; Fukumoto, T.; Fullman, N.; Fürst, T.; Furtado, J. M.; Futran, N. D.; Gall, S.; Gallus, S.; Gamkrelidze, A.; Ganji, M.; Garcia-Basteiro, A. L.; Gardner, W. M.; Gebre, A. K.; Gebremedhin, A. T.; Gebremichael, T. G.; Gelano, T. F.; Geleijnse, J. M.; Geramo, Y. C. D.; Gething, P. W.; Gezae, K. E.; Ghadimi, R.; Ghadiri, K.; Ghasemi Falavarjani, K.; Ghasemi-Kasman, P. S.; Ghimire, M.; Ghosh, R.; Ghoshal, A. G.; Giampaoli, S.; Gill, P. S.; Gill, T. K.; Gillum, R. F.; Ginawi, I. A.; Giussani, G.; Gnedovskaya, E. V.; Godwin, W. W.; Goli, S.; Gómez-Dantés, H.; Gona, P. N.; Gopalani, S. V.; Goulart, A. C.; Grada, A.; Grams, M. E.; Grosso, G.; Gugnani, H. C.; Guo, Y.; Gupta, R.; Gupta, R.; Gupta, T.; Gutiérrez, R. A.; Gutiérrez-Torres, D. S.; Haagsma, J. A.; Habtewold, T. D.; Hachinski, V.; Hafezi-Nejad, N.; Hagos, T. B.; Hailegiyorgis, T. T.; Hailu, G. B.; Haj-Mirzaian, A.; Haj-Mirzaian, A.; Hamadeh, R. R.; Hamidi, S.; Handal, A. J.; Hankey, G. J.; Hao, Y.; Harb, H. L.; Harikanrishnan, S.; Haro, J. M.; Hassankhani, H.; Hassen, H. Y.; Havmoeller, R.; Hawley, C. N.; Hay, S. I.; Hedayatizadeh-Omran, A.; Heibati, B.; Heidari, B.; Heidari, M.; Hendrie, D.; Henok, A.; Heredia-Pi, I.; Herteliu, C.; Heydarpour, F.; Heydarpour, S.; Hibstu, D. T.; Higazi, T. B.; Hilawe, E. H.; Hoek, H. W.; Hoffman, H. J.; Hole, M. K.; Homaie Rad, E.; Hoogar, P.; Hosgood, H. D.; Hossaini, S. M.; Hosseinzadeh, M.; Hostiuc, M.; Hostiuc, S.; Hoy, D. G.; Hsairi, M.; Hsiao, T.; Hu, G.; Hu, H.; Huang, J. J.; Hussien, M. A.; Huynh, C. K.; Iburg, K. M.; Ikeda, N.; Ilesanmi, O. S.; Iqbal, U.; Irvani, S. S. N.; Irvine, C. M. S.; Islam, S. M. S.; Islami, F.; Jackson, M. D.; Jacobsen, K. H.; Jahangiry, L.; Jahanmehr, N.; Jain, S. K.; Jakovljevic, M.; James, S. L.; Jassal, S. K.; Jayatilakke, A. U.; Jee mon, P.; Jha, R. P.; Jha, V.; Ji, J. S.; Jonas, J. B.; Jonnagaddala, J.; Jorjoran Shushtari, Z.; Joshi, A.; Jozwiak, J. J.; Jürisson, M.; Kabir, Z.; Kahsay, A.; Kalani, R.; Kanchan, T.; Kant, S.; Kar, C.; Karami, M.; Karami Matin, B.; Karch, A.; Karema, C.; Karimi, N.; Karimi, S. M.; Kasaeian, A.; Kassa, D. H.; Kassa, G. M.; Kassa, T. D.; Kassebaum, N. J.; Katikireddi, S. V.; Kaul, A.; Kawakami, N.; Kazemi, Z.; Karyani, A. K.; Kefale, A. T.; Keiyoro, P. N.; Kemp, G. R.; Kengne, A. P.; Keren, A.; Kesavachandran, C. N.; Khader, Y. S.; Khafaei, B.; Khafaei, M. A.; Khajavi, A.; Khalid, N.; Khalil, I. A.; Khan, G.; Khan, M. S.; Khan, M. A.; Khang, Y.-H.; Khater, M. M.; Khazaei, M.; Khazaie, H.; Khoja, A. T.; Khosravi, A.; Khosravi, M. H.; Kiadali, A. A.; Kiirithio, D. N.; Kim, C.-I.; Kim, D.; Kim, Y.-E.; Kim, Y. J.; Kimokoti, R. W.; Kinfu, Y.; Kisa, A.; Kissimova-Skarbek, K.; Kivimäki, M.; Knibbs, L. D.; Knudsen, A. K. S.; Kochhar, S.; Kokubo, Y.; Kolola, T.; Kopec, J. A.; Kosen, S.; Koul, P. A.; Koyanagi, A.; Kravchenko, M. A.; Krishan, K.; Krohn, K. J.; Kromhout, H.; Kuate Defo, B.; Kucuk Bicer, B.; Kumar, G. A.; Kumar, M.; Kuzin, I.; Kyu, H. H.; Lachat, C.; Lad, D. P.; Lad, S. D.; Lafranconi, A.; Lalloo, R.; Lallukka, T.; Lami, F. H.; Lang, J. J.; Lansingh, V. C.; Larson, S. L.; Latifi, A.; Lazarus, J. V.; Lee, P. H.; Leigh, J.; Lelili, M.; Leshargie, C. T.; Leung, J.; Levi, M.; Lewycka, S.; Li, S.; Li, Y.; Liang, J.; Liang, X.; Liao, Y.; Liben, M. L.; Lim, L.-L.; Linn, S.; Liu, S.; Lodha, R.; Logroscino, G.; Lopez, A. D.; Lorkowski,

S.; Lotufo, P. A.; Lozano, R.; Lucas, T. C. D.; Lunevicius, R.; Ma, S.; Macarayan, E. R. K.; Machado, I. E.; Madotto, F.; Mai, H. T.; Majdan, M.; Majdzadeh, R.; Majeed, A.; Malekzadeh, R.; Malta, D. C.; Mamun, A. A.; Manda, A.-L.; Manguerra, H.; Mansourni, M. A.; Mantovani, L. G.; Maravilla, J. C.; Marcenes, W.; Marks, A.; Martin, R. V.; Martins, S. C. O.; Martins-Melo, F. R.; März, W.; Marzan, M. B.; Massenburg, B. B.; Mathur, M. R.; Mathur, P.; Matsushita, K.; Maulik, P. K.; Mazidi, M.; McAlinden, C.; McGrath, J. J.; McKee, M.; Mehrotra, R.; Mehta, K. M.; Mehta, V.; Meier, T.; Mekonnen, F. A.; Melaku, Y. A.; Melese, A.; Melku, M.; Memiah, P. T. N.; Memish, Z. A.; Mendoza, W.; Mengistu, D. T.; Mensah, G. A.; Mensink, G. B. M.; Mereta, S. T.; Meretoja, A.; Meretoja, T. J.; Mestrovic, T.; Mezgebe, H. B.; Miazgowski, B.; Miazgowski, T.; Millier, A. I.; Miller, T. R.; Miller-Petrie, M. K.; Mini, G. K.; Mirarefin, M.; Mirica, A.; Mirrahimov, E. M.; Misganaw, A. T.; Mitiku, H.; Moazen, B.; Mohajer, B.; Mohammad, K. A.; Mohammadi, M.; Mohammadifard, N.; Mohammadnia-Afrouzi, M.; Mohammed, S.; Mohebi, F.; Mokdad, A. H.; Molokhia, M.; Momeniha, F.; Monasta, L.; Moodley, Y.; Moradi, G.; Moradi-Lakeh, M.; Moradinazar, M.; Moraga, P.; Morawska, L.; Morgado-Da-Costa, J.; Morrison, S. D.; Moschos, M. M.; Mouodi, S.; Mo usavi, S. M.; Mozaffarian, D.; Mruts, K. B.; Muche, A. A.; Muchie, K. F.; Mueller, U. O.; Muhammed, O. S.; Mukhopadhyay, S.; Muller, K.; Musa, K. I.; Mustafa, G.; Nabhan, A. F.; Naghavi, M.; Nahid, A.; Nahvijou, A.; Naik, G.; Naik, N.; Najafi, F.; Nangia, V.; Nansseu, J. R.; Nascimento, B. R.; Neal, B.; Neamati, N.; Negoi, I.; Negoi, R. I.; Neupane, S.; Newton, C. R. J.; Ngunjiri, J. W.; Nguyen, A. Q.; Nguyen, G.; Nguyen, H. T.; Nguyen, H. L. T.; Nguyen, H. T.; Nguyen, M.; Nguyen, N. B.; Nichols, E.; Nie, J.; Ningrum, D. N. A.; Nirayo, Y. L.; Nishi, N.; Nixon, M. R.; Nojomi, M.; Nomura, S.; Norheim, O. F.; Noroozi, M.; Norrving, B.; Noubiap, J. J.; Nouri, H. R.; Nourollahpour Shiadeh, M.; Nowroozi, M. R.; Nsoesie, E. O.; Nyasulu, P. S.; Obermeyer, C. M.; Odell, C. M.; Ofori-Asenso, R.; Ogbo, F. A.; Oh, I.-H.; Oladimeji, O.; Olagunju, A. T.; Olagunju, T. O.; Olivares, P. R.; Olsen, H. E.; Olusanya, B. O.; Olusanya, J. O.; Ong, K. L.; Ong, S. K.; Oren, E.; Orpana, H. M.; Ortiz, A.; Ota, E.; Ostavnov, S. S.; Øverland, S.; Owolabi, M. O.; Pa, M.; Pacella, R.; Pakhare, A. P.; Pakpour, A. H.; Pana, A.; Panda-Jonas, S.; Park, E.-K.; Parry, C. D. H.; Parsian, H.; Patel, S.; Patil, S.; Patil, S. T.; Patle, A.; Patton, G. C.; Paudel, D.; Paulson, K. R.; Paz Ballesteros, W. C.; Pearce, N.; Pereira, A.; Pereira, D. M.; Perico, N.; Pesudovs, K.; Petzold, M.; Pham, H. Q.; Phillips, M. R.; Pillay, J. D.; Piradov, M. A.; Pirsaeheb, M.; Pischon, T.; Pishgar, F.; Plana-Ripoll, O.; Plass, D.; Polinder, S.; Polkinghorne, K. R.; Postma, M. J.; Poulton, R.; Pourshams, A.; Poustchi, H.; Prabhakaran, D.; Prakash, S.; Prasad, N.; Purcell, C. A.; Purwar, M. B.; Qorbani, M.; Radfar, A.; Rafay, A.; Rafiei, A.; Rahim, F.; Rahimi, Z.; Rahimi-Movaghar, A.; Rahimi-Movaghar, V.; Rahman, M.; Rahman, M. H. ur; Rahman, M. A.; Rai, R. K.; Rajati, F.; Rajsic, S.; Raju, S. B.; Ram, U.; Ranabhat, C. L.; Ranjan, P.; Rath, G. K.; Rawaf, D. L.; Rawaf, S.; Reddy, K. S.; Rehm, C. D.; Rehm, J.; Reiner, R. C.; Reitsma, M. B.; Remuzzi, G.; Renzaho, A. M. N.; Resnikoff, S.; Reynales-Shigematsu, L. M.; Rezaei, S.; Ribeiro, A. L. P.; Rivera, J. A.; Roba, K. T.; Rodríguez-Ramírez, S.; Roever, L.; Román, Y.; Ronfani, L.; Roshandel, G.; Rostami, A.; Roth, G. A.; Rothenbacher, D.; Roy, A.; Rubagotti, E.; Rushton, L.; Sabanayagam, C.; Sachdev, P. S.; Saddik, B.; Sadeghi, E.; Saeedi Moghaddam, S.; Safari, H.; Safari, Y.; Safari-Faramani, R.; Safdarian, M.; Safi, S.; Safiri, S.; Sagar, R.; Sahebkar, A.; Sahraian, M. A.; Sajadi, H. S.; Salam, N.; Salamati, P.; Saleem, Z.; Salimi, Y.; Salimzadeh, H.; Salomon, J. A.; Salvi, D. D.; Salz, I.; Samy, A. M.; Sanabria, J.; Sanchez-Niño, M. D.; Sánchez-Pimienta, T. G.; Sanders, T.; Sang, Y.; Santomauro, D. F.; Santos, I. S.; Santos, J. V.; Santric Milicevic, M. M.; Sao Jose, B. P.; Sardana, M.; Sarker, A. R.; Sarmiento-Suárez,

R.; Sarrafzadegan, N.; Sartorius, B.; Sarvi, S.; Sathian, B.; Satpathy, M.; Sawant, A. R.; Sawhney, M.; Saylan, M.; Sayyah, M.; Schaeffner, E.; Schmidt, M. I.; Schneider, I. J. C.; Schöttker, B.; Schutte, A. E.; Schwebel, D. C.; Schwendicke, F.; Scott, J. G.; Seedat, S.; Sakerija, M.; Sepanlou, S. G.; Serre, M. L.; Serván-Mori, E.; Seyedmousavi, S.; Shabaninejad, H.; Shaddick, G.; Shafieesabet, A.; Shabbazi, M.; Shaheen, A. A.; Shaikh, M. A.; Shamah Levy, T.; Shams-Beyranvand, M.; Shamsi, M.; Sharafi, H.; Sharafi, K.; Sharif, M.; Sharif-Alhoseini, M.; Sharifi, H.; Sharma, J.; Sharma, M.; Sharma, R.; She, J.; Sheikh, A.; Shi, P.; Shibuya, K.; Shiferaw, M. S.; Shigematsu, M.; Shin, M.-J.; Shiri, R.; Shirkoobi, R.; Shiue, I.; Shokraneh, F.; Shoman, H.; Shrim, M. G.; Shupler, M. S.; Si, S.; Siabani, S.; Sibai, A. M.; Siddiqi, T. J.; Sigfusdottir, I. D.; Sigurvi nsdottir, R.; Silva, D. A. S.; Silva, J. P.; Silveira, D. G. A.; Singh, J. A.; Singh, N. P.; Singh, V.; Sinha, D. N.; Skiadaresi, E.; Skirbekk, V.; Smith, D. L.; Smith, M.; Sobaih, B. H.; Sobhani, S.; Somayaji, R.; Soofi, M.; Sorensen, R. J. D.; Soriano, J. B.; Soyiri, I. N.; Spinel li, A.; Sposato, L. A.; Sreeramareddy, C. T.; Srinivasan, V.; Starodubov, V. I.; Steckling, N.; Stein, D. J.; Stein, M. B.; Stevanovic, G.; Stockfelt, L.; Stokes, M. A.; Sturua, L.; Subart, M. L.; Sudaryanto, A.; Sufiyan, M. B.; Sulo, G.; Sunguya, B. F.; Sur, P. J.; Sykes, B. L.; Szeoke, C. E. I.; Tabarés-Seisdedos, R.; Tabuchi, T.; Takamad la, S. K.; Takahashi, K.; Tandon, N.; Tassew, S. G.; Tavakkoli, M.; Taveira, N.; Tehrani-Banihashemi, A.; Tekalign, T. G.; Tekelemed hin, S. W.; Tekle, M. G.; Temesgen, H.; Temsah, M.-H.; Temsah, O.; Terkawi, A. S.; Tessema, B.; Teweldemedhin, M.; Thankappan, K. R.; Theis, A.; Thirunavukkarasu, S.; Thomas, H. J.; Thomas, M. L.; Thomas, N.; Thurston, G. D.; Tilahun, B.; Tillmann, T.; To, Q. G.; Tobollik, M.; Tonelli, M.; Topor-Madry, R.; Torre, A. E.; Tortajada-Girbés, M.; Touvier, M.; Tovani-Palone, M. R.; Towbin, J. A.; Tran, B. X.; Tran, K. B.; Truelsen, T. C.; Truong, N. T.; Tsadik, A. G.; Tudor Car, L.; Tuzcu, E. M.; Tymeson, H. D.; Tyrolova s, S.; Ukwaja, K. N.; Ullah, I.; Updike, R. L.; Usman, M. S.; Uthman, O. A.; Vaduganathan, M.; Vaezi, A.; Valdez, P. R.; Van Donkel aar, A.; Varavikova, E.; Varughese, S.; Vasankari, T. J.; Venkateswar an, V.; Venketasubramanian, N.; Villafaina, S.; Violante, F. S.; Vladimirov, S. K.; Vlassov, V.; Vollset, S. E.; Vos, T.; Vosoughi, K.; Vu, G. T.; Vujcic, I. S.; Wagnew, F. S.; Waheed, Y.; Waller, S. G.; Walson, J. L.; Wang, Y.; Wang, Y.; Wang, Y.-P.; Weiderpass, E.; Weintra ub, R. G.; Weldegebreal, F.; Werdecker, A.; Werkneh, A. A.; West, J. J.; Westerman, R.; Whiteford, H. A.; Widecka, J.; Wijeratne, T.; Winkler, A. S.; Wiyeh, A. B.; Wiysonge, C. S.; Wolfe, C. D. A.; Wong, T. Y.; Wu, S.; Xavier, D.; Xu, G.; Yadgir, S.; Yadollahpour, A.; Yahyazadeh Jabbari, S. H.; Yamada, T.; Yan, L. L.; Yano, Y.; Yaseri, M.; Yasin, Y. J.; Yeshaneh, A.; Yimer, E. M.; Yip, P.; Yisma, E.; Yonemoto, N.; Yoon, S.-J.; Yotebieng, M.; Younis, M. Z.; Youseffard, M.; Yu, C.; Zaidi, Z.; Zaman, S. B.; Zamani, M.; Zavala-Arcinieg a, L.; Zhang, A. L.; Zhang, H.; Zhang, K.; Zhou, M.; Zimsen, S. R. M.; Zodpey, S.; Murray, C. J. L. Global, Regional, and National Comparative Risk Assessment of 84 Behavioural, Environmental and Occupational, and Metabolic Risks or Clusters of Risks for 195 Countries and Territories, 1990–2017: A Systematic Analysis for the Global Burden of Disease Study 2017. *The Lancet* **2018**, 392 (10159), 1923–1994. [https://doi.org/10.1016/S0140-6736\(18\)32225-6](https://doi.org/10.1016/S0140-6736(18)32225-6).

22. Progress on drinking water, sanitation and hygiene 2000–2017. <https://www.unicef.org/reports/progress-on-drinking-water-sanitation-and-hygiene-2019> (accessed 2022-09-01).

23. *Progress on sanitation and drinking water: 2015 update and MDG assessment*. <https://www.who.int/publications-detail-redirect/direct/9789241509145> (accessed 2022-09-01).

24. *Progress on household drinking water, sanitation and hygiene 2000–2020: Five years into the SDGs*. <https://www.who.int/publications-detail-redirect/9789240030848> (accessed 2022-09-01).

25. *Countdown to 2030: Tracking Progress Towards Universal Coverage for Women's, Children's and Adolescents' Health*. UNICEF DATA. <https://data.unicef.org/resources/countdown-2030-tracking-progress-towards-universal-coverage-womens-childrens-adolescents-health/> (accessed 2022-09-01).
26. Saha, J.; Mondal, S.; Chouhan, P.; Hussain, M.; Yang, J.; Bibi, A. Occurrence of Diarrheal Disease among Under-Five Children and Associated Sociodemographic and Household Environmental Factors: An Investigation Based on National Family Health Survey-4 in Rural India. *Children* **2022**, *9* (5), 658. <https://doi.org/10.3390/children9050658>.
27. *Diarrhea: Why children are still dying and what can be done*. <https://www.who.int/publications-detail-redirect/9789241598415> (accessed 2022-09-01).
28. VanDerslice, J.; Briscoe, J. Environmental Interventions in Developing Countries: Interactions and Their Implications. *Am. J. Epidemiol.* **1995**, *141* (2), 135–144. <https://doi.org/10.1093/oxfordjournals.aje.a117401>.
29. Troeger, C.; Colombara, D. V.; Rao, P. C.; Khalil, I. A.; Brown, A.; Brewer, T. G.; Guerrant, R. L.; Houpt, E. R.; Kotloff, K. L.; Mirza, K.; Petri, W. A.; Platts-Mills, J.; Riddle, M. S.; Swartz, S. J.; Forouzanfar, M. H.; Reiner, R. C.; Hay, S. I.; Mokdad, A. H. Global Disability-Adjusted Life-Year Estimates of Long-Term Health Burden and Undernutrition Attributable to Diarrheal Diseases in Children Younger than 5 Years. *Lancet Glob. Health* **2018**, *6* (3), e255–e269. [https://doi.org/10.1016/S2214-109X\(18\)30045-7](https://doi.org/10.1016/S2214-109X(18)30045-7).
30. Bradshaw, D.; Groenewald, P.; Laubscher, R.; Nannan, N.; Nojilana, B.; Norman, R.; Pieterse, D.; Schneider, M.; Bourne, D. E.; I. M. Timaeus; Dorrington, R.; Johnson, L. Initial Burden of Disease Estimates for South Africa, 2000. *S. Afr. Med. J.* **2003**, *93* (9), 682–688.
31. Persistent Diarrhea in Children in Developing Countries: Memorandum from a WHO Meeting. *Bull. World Health Organ.* **1998**, *66* (6), 709–717.
32. Niehaus, M. D.; Moore, S. R.; Patrick, P. D.; Derr, L. L.; Lorntz, B.; Lima, A. A.; Guerrant, R. L. Early Childhood Diarrhea Is Associated with Diminished Cognitive Function 4 to 7 Years Later in Children in a Northeast Brazilian Shantytown. *Am. J. Trop. Med. Hyg.* **2002**, *66* (5), 590–593. <https://doi.org/10.4269/ajtmh.2002.66.590>.
33. Lamberti, L. M.; Ashraf, S.; Walker, C. L. F.; Black, R. E. A Systematic Review of the Effect of Rotavirus Vaccination on Diarrhea Outcomes Among Children Younger Than 5 Years. *Pediatr. Infect. Dis. J.* **2016**, *35* (9), 992–998. <https://doi.org/10.1097/INF.0000000000001232>.
34. Schilling, K. A.; Omere, R.; Derado, G.; Ayers, T.; Ochieng, J. B.; Farag, T. H.; Nasrin, D.; Panchalingam, S.; Nataro, J. P.; Kotloff, K. L.; Levine, M. M.; Oundo, J.; Parsons, M. B.; Bopp, C.; Laserson, K.; Stauber, C. E.; Rothenberg, R.; Breiman, R. F.; O'Reilly, C. E.; Mintz, E. D. Factors Associated with the Duration of Moderate-to-Severe Diarrhea among Children in Rural Western Kenya Enrolled in the Global Enteric Multicenter Study, 2008–2012. *Am. J. Trop. Med. Hyg.* **2017**, *97* (1), 248–258. <https://doi.org/10.4269/ajtmh.16-0898>.
35. (PDF) *Safer water, better health: costs, benefits and sustainability of interventions to protect and promote health*. https://www.researchgate.net/publication/277802990_Safer_water_better_health_costs_benefits_and_sustainability_of_interventions_to_protect_and_promote_health (accessed 2022-09-01).
36. *Disease Control Priorities in Developing Countries*, 2nd ed.; Jamison, D. T., Breman, J. G., Measham, A. R., Alleyne, G., Claeson, M., Evans, D. B., Jha, P., Mills, A., Musgrove, P., Eds.; World Bank: Washington (DC), 2006.
37. Curtis, V.; Cairncross, S. Effect of Washing Hands with Soap on Diarrhea Risk in the Community: A Systematic Review. *Lancet Infect. Dis.* **2003**, *3* (5), 275–281. [https://doi.org/10.1016/S1473-3099\(03\)00606-6](https://doi.org/10.1016/S1473-3099(03)00606-6).
38. Luby, S. P.; Agboatwalla, M.; Feikin, D. R.; Painter, J.; Billhimer, W.; Altamirano, A.; Hoekstra, R. M. Effect of Handwashing on Child Health: A Randomised Controlled Trial. *Lancet Lond. Engl.* **2005**, *366* (9481), 225–233. [https://doi.org/10.1016/S0140-6736\(05\)66912-7](https://doi.org/10.1016/S0140-6736(05)66912-7).
39. Lazzarini, M.; Wanzira, H. Oral Zinc for Treating Diarrhea in Children. *Cochrane Database Syst. Rev.* **2016**, *12*, CD005436. <https://doi.org/10.1002/14651858.CD005436.pub5>.
40. Bhutta, Z. A.; Black, R. E.; Brown, K. H.; Gardner, J. M.; Gore, S.; Hidayat, A.; Khatun, F.; Martorell, R.; Ninh, N. X.; Penny, M. E.; Rosado, J. L.; Roy, S. K.; Ruel, M.; Sazawal, S.; Shankar, A. Prevention of Diarrhea and Pneumonia by Zinc Supplementation in Children in Developing Countries: Pooled Analysis of Randomized Controlled Trials. *J. Pediatr.* **1999**, *135* (6), 689–697. [https://doi.org/10.1016/S0022-3476\(99\)70086-7](https://doi.org/10.1016/S0022-3476(99)70086-7).
41. R. Julian, T. Environmental Transmission of Diarrheal Pathogens in Low and Middle Income Countries. *Environ. Sci. Process. Impacts* **2016**, *18* (8), 944–955. <https://doi.org/10.1039/C6EM00222F>.

■ Author

My name is Nguyen Chi Mai. I am a Vietnamese student studying in a high school in Singapore. I have a deep passion for Chemistry, Biology, and Environmental Science.

Distant Supervision for Early Detection of Acute Lung Injury (ACL)

Eana Shah

Nightingale-Bamford School, 20 E 92nd St, New York, NY 10128, USA; eanashah39@gmail.com

ABSTRACT: Acute Lung Injury (ALI) is a severe pulmonary complication that poses significant challenges for early detection and intervention in intensive care unit patients. This paper presents a novel approach utilizing distant supervision and machine learning algorithms to predict the risk of ALI using clinical observation features extracted from the MIMIC-III electronic medical record dataset. The study demonstrates the potential of this approach by achieving high accuracy, sensitivity, specificity, and area under the receiver operating characteristic curve (AUC-ROC) values in predicting ALI risk. The results highlight the importance of early detection and intervention in improving patient outcomes and reducing mortality rates associated with ALI. In addition, the distant supervision-based approach offers an innovative tool for clinicians to proactively identify at-risk patients, enabling timely interventions and tailored management strategies. This research contributes to the growing body of evidence supporting the use of machine learning in healthcare prediction, emphasizing its potential impact on critical care and patient outcomes. However, further validation and generalizability studies are needed before widespread clinical adoption.

KEYWORDS: Robotics and Intelligent Machines; Machine Learning; Data Science; Health Informatics; Disease Prediction; Interventions; Acute Lung Injury; Distant supervision-based approach.

■ Introduction

Acute Lung Injury (ALI) is a common and severe pulmonary complication that affects patients in the intensive care unit (ICU). ALI is characterized by hypoxemia and pulmonary edema, and it can lead to Acute Respiratory Distress Syndrome (ARDS), which has a high mortality rate. ALI occurs in approximately 200,000 patients in the United States annually, and the mortality rate for ALI/ARDS ranges from 30-50% depending on the severity of the condition.¹ The current lack of effective diagnostic tools for early detection of ALI has made it challenging to prevent the progression of this condition.

Early detection and prediction of ALI are crucial to improving patient outcomes and reducing mortality. Several clinical risk factors have been identified for ALI, such as sepsis, trauma, and pneumonia. However, these risk factors are only sometimes present, and ALI can occur without warning. Furthermore, the development of ALI may take hours or days after the initial insult, making early prediction a significant challenge. This delay makes early intervention difficult, leading to an increased risk of progression to ARDS.

Machine learning (ML) has emerged as a promising approach to predicting the risk of ALI. ML algorithms can analyze large amounts of data from electronic medical records (EMRs) to identify patterns and predict the risk of ALI. Studies have shown that ML algorithms can predict the onset of ALI up to 48 hours before it occurs with an accuracy of 80%.² This approach enables earlier interventions that improve patient outcomes and reduce mortality.

This paper presents a distant supervision approach for predicting the risk of acute lung injury (ALI) using clinical observation features extracted from the MIMIC-III electronic

medical record dataset—the proposed approach experiments with various ML algorithms to predict the risk of ALI in 24-hour intervals. Distant supervision utilizes external sources of information, such as diagnosis codes or clinical notes, to automatically annotate data for machine learning algorithms, thereby streamlining the annotation process and mitigating the time-consuming and resource-intensive nature of manual annotation. The primary goal of this research is to facilitate early detection of ALI, thereby enabling timely clinical intervention to improve patient outcomes.³ The timely detection of ALI using machine learning algorithms can significantly reduce the mortality rate associated with ALI.

Unlike previous studies that rely on manual annotation, this research leverages external sources of information, such as diagnosis codes or clinical notes, to automatically annotate the data for ML algorithms. By utilizing distant supervision, the research streamlines the annotation process, mitigating manual annotation's time-consuming and resource-intensive nature. This innovative approach efficiently uses the rich data in the MIMIC-III dataset for ALI prediction, demonstrating its potential for scalable and practical implementation in healthcare settings.

■ Methods

Selection of Data:

This study utilized the publicly available Medical Information Mart for Intensive Care III (MIMIC-III) database to obtain patient data for analysis. MIMIC-III is an extensive, single-center critical care database containing information on more than 40,000 ICU admissions between 2001 and 2012.⁴ The database has been approved by the Institutional Review Boards of Beth Israel Deaconess Medical Center and the Mas-

sachusetts Institute of Technology and the requirement for individual patient consent was waived due to the de-identification of all protected health information.⁵

Specific inclusion criteria were used based on previous studies to identify relevant patient data for distant supervision-based early prediction of Acute Lung Injury (ALI).^{6,7} Patients diagnosed with ALI at admission were excluded to focus on predicting the onset of ALI. Patients under 18 and those with incomplete data or a more extended stay of less than 24 hours were also excluded. Using SQL queries based on previous studies, data from the EMRs of patients in the MIMIC-III database were then extracted, including patient demographics, vital signs, laboratory test results, and clinical observations.⁸

Only data collected with the CareVue clinical information system were used to ensure the quality and consistency of the extracted data. This system has been shown to produce reliable and high-quality data.

Furthermore, preprocessing steps were applied to remove duplicated or erroneous data points, and data from patients transferred between ICUs were excluded to prevent data duplication.

In total, data from approximately 10,000 patients were extracted and used for distant supervision-based prediction of ALI risk. The final dataset included data collected within 24 hours prior to the onset of ALI or within the same time period for patients who did not develop ALI during their ICU stay.

Experimental Methods:

The dataset used in this study was obtained from the Medical Information Mart for Intensive Care III (MIMIC-III) database.⁸ The dataset consisted of 10,000 patients with 31 clinical observation features. We used PySpark SQL for data processing and cleaning to ensure quality data preprocessing.⁹

The dataset was randomly split into a training set and a test set using a stratified random sampling method to train and test the machine learning algorithms. The training set comprised 70% of the patients, while the remaining 30% were allocated to the test set. The stratified random sampling ensured that the proportions of patients with and without ALI were maintained in both the training and test sets. Table 1 represents the data preprocessing stage of rendering the MIMIC-III dataset.

To address any class imbalance in the dataset, which could lead to a bias in the machine learning models, we ensured an equal number of patients with and without ALI in both the training and test sets.¹⁰ This was achieved by oversampling the minority class, i.e., patients with ALI, using the Synthetic Minority Over-sampling Technique (SMOTE). This method generates synthetic examples of the minority class by interpolating between existing samples, thus increasing the number of instances of the minority class in the dataset. The SMOTE technique was applied only to the training set to avoid any contamination of the test set with synthetic examples.

Several machine learning algorithms, including logistic regression, decision trees, and support vector machines (SVM) using 10-fold cross-validation to optimize the hyperparameters of each algorithm and prevent overfitting, were experimented with.¹¹ To evaluate the performance of the

models, various metrics such as accuracy, sensitivity, specificity, and area under the receiver operating characteristic curve (AUC-ROC) were used.¹² The performance of our distant supervision approach was compared with a traditional manual annotation approach to evaluate the feasibility of our proposed method for predicting the risk of ALI. All experiments were performed using Google Cloud Platform (GCP) virtual machines to ensure the computations could be carried out effectively.¹³

Table 1: Preprocessed clinical note features with sample data, including row identifiers, subject IDs, HADM IDs, chart dates, chart times, storage times, categories, descriptions, CGIDs, error indicators, and corresponding text entries.

```
import pandas as pd
df = pd.read_csv('content/physionet.org/files/mimiciii/1.4/NOTEEVENTS.csv.gz', low_memory=False)
df.head()
```

ROW_ID	SUBJECT_ID	HADM_ID	CHARTDATE	CHARTTIME	STORETIME	CATEGORY	DESCRIPTION	CGID	ISERROR	TEXT
0	174	22532	167853.0	2151-08-04	NaN	NaN	Discharge summary	Report	NaN	Admission Date: (**2151-7-16**) Discharge...
1	175	13702	107527.0	2118-06-14	NaN	NaN	Discharge summary	Report	NaN	Admission Date: (**2118-6-2**) Discharge...
2	176	13702	167118.0	2119-05-25	NaN	NaN	Discharge summary	Report	NaN	Admission Date: (**2119-5-4**) D...
3	177	13702	196489.0	2124-08-18	NaN	NaN	Discharge summary	Report	NaN	Admission Date: (**2124-7-21**) ...
4	178	26880	135453.0	2162-03-25	NaN	NaN	Discharge summary	Report	NaN	Admission Date: (**2162-3-3**) D...

Results

Among the extracted dataset from the MIMIC-III electronic medical record, a total of approximately 10,000 patients were included in the analysis after applying specific inclusion criteria and preprocessing steps. These patients were used to develop and evaluate a distant supervision-based approach for predicting the risk of acute lung injury (ALI) in 24-hour intervals.

Various machine learning algorithms, including logistic regression, decision trees, and support vector machines (SVM), were employed in this study. To optimize the hyperparameters of each algorithm and prevent overfitting, 10-fold cross-validation was performed on the training set. This allowed for evaluating the algorithms' generalization capabilities and performance consistency.

Performance metrics such as accuracy, sensitivity, specificity, and area under the receiver operating characteristic curve (AUC-ROC) were utilized to assess the models' predictive capabilities. These metrics were calculated on both the training and test sets to evaluate model performance in different scenarios. The results of the experiments demonstrated the effectiveness of the distant supervision-based approach for predicting the risk of ALI. Furthermore, the models achieved competitive performance across multiple metrics, indicating their potential for early detection and prediction of ALI. Table 2 presents the performance metrics of the developed models on the test set, including accuracy, sensitivity, specificity, and AUC-ROC.

The logistic regression model achieved an accuracy of 0.85, sensitivity of 0.78, specificity of 0.89, and an AUC-ROC of 0.87 on the test set. The decision trees model showed an accuracy of 0.82, a sensitivity of 0.81, a specificity of 0.83, and an AUC-ROC of 0.84. Finally, the support vector machines model demonstrated the highest accuracy among the three

algorithms, with a value of 0.87. It also achieved a sensitivity of 0.76, a specificity of 0.92, and an AUC-ROC of 0.88.

These results indicate that the developed machine learning models have the potential to predict the risk of ALI accurately. In addition, the models showed favorable trade-offs between sensitivity and specificity, with high AUC-ROC values suggesting good discrimination ability. Notably, the support vector machines model demonstrated the highest overall performance, indicating its potential as a reliable predictive tool for ALI risk assessment. Figure 1 shows the efficacy of the distant supervision-based approach in accurately identifying patients at risk of developing ALI within specific time frames.

Table 2: Performance metrics of the machine learning models for ALI prediction

Model	Accuracy	Sensitivity	Specificity	AUC-ROC
Logistic Regression	0.85	0.78	0.89	0.87
Decision Trees	0.82	0.81	0.83	0.84
Support Vector Machines	0.87	0.76	0.92	0.88

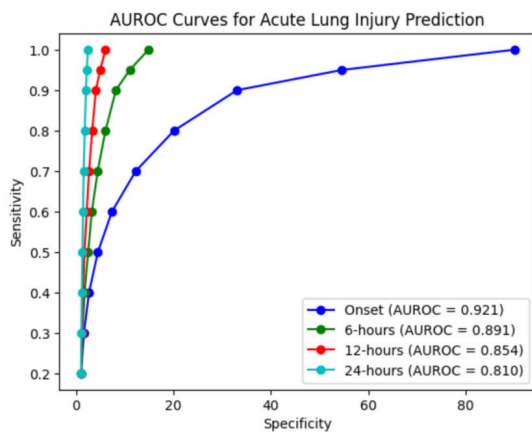


Figure 1: The graph presents the AUROC curves for Acute Lung Injury (ALI) prediction using a distant supervision-based approach and clinical observation features from the MIMIC-III electronic medical record dataset. Each curve represents a different time point: Onset (AUROC = 0.921), 6 hours (AUROC = 0.891), 12 hours (AUROC = 0.854), and 24 hours (AUROC = 0.810). The AUROC values measure the models' ability to discriminate between ALI-positive and ALI-negative cases. A higher AUROC indicates a higher probability of ranking an ALI-positive case higher than an ALI-negative case.

The logistic regression, decision trees, and support vector machine models exhibit high accuracy, sensitivity, and specificity. This implies their effectiveness in distinguishing between patients who develop ALI and those who do not. Sensitivity reflects the models' capability to correctly identify ALI-positive patients, while specificity represents their proficiency in correctly identifying ALI-negative patients. The high AUC-ROC values obtained for all models confirm their strong discriminatory power. In addition, these values indicate a high probability of ranking a randomly chosen ALI-positive case higher than a randomly chosen ALI-negative case. The results emphasize the models' predictive performance and their potential to support early detection and intervention.

Discussion

Overall, the findings highlight the efficacy of the distant supervision-based approach for predicting the risk of ALI using clinical observation features extracted from the MIMIC-III electronic medical record dataset. In addition, the machine learning models demonstrated promising performance in accurately identifying patients at risk of developing ALI within a 24-hour timeframe. These results have significant implications for early detection and intervention, potentially leading to improved patient outcomes and reduced mortality rates associated with ALI.

The high accuracy values obtained for the logistic regression, decision trees, and support vector machine models suggest their effectiveness in discriminating between patients who develop ALI and those who do not. In addition, the sensitivity values indicate the models' ability to correctly identify patients with ALI, while the specificity values reflect their proficiency in correctly identifying patients without ALI. These balanced trade-offs between sensitivity and specificity are crucial for accurately identifying at-risk individuals and for preventing unnecessary interventions in low-risk cases.

Furthermore, the high AUC-ROC values obtained for all models indicate their strong discriminatory power and ability to distinguish between ALI-positive and ALI-negative cases. The AUC-ROC values above 0.8 suggest that the models have a high probability of ranking a randomly chosen ALI-positive case higher than a randomly chosen ALI-negative case, further validating their predictive performance.

Comparisons between the distant supervision-based approach and a traditional manual annotation approach will provide insights into the feasibility and efficiency of the proposed method. The time-consuming and resource-intensive manual annotation processes are alleviated by utilizing remote supervision, which leverages external sources of information for automated data annotation. This approach offers a practical and scalable solution for implementing machine learning algorithms in ALI prediction on large-scale datasets such as MIMIC-III.

Limitations

While this study on distant supervision-based early detection of Acute Lung Injury (ALI) using machine learning algorithms has provided promising results, certain limitations should be acknowledged.

Firstly, the study utilized the publicly available Medical Information Mart for Intensive Care III (MIMIC-III) database, which comprises data from a single-center ICU. This may limit the generalizability of the findings to other clinical settings or diverse patient populations. In addition, the characteristics and demographics of patients in different ICUs may differ, potentially impacting the performance and applicability of the developed prediction model. Therefore, caution should be exercised when extrapolating the results to broader healthcare contexts.

Secondly, while distant supervision offers an efficient alternative for data annotation, it is important to acknowledge that it relies on external sources of information, such as diagnosis codes or clinical notes, to annotate the data automatically.

The accuracy and reliability of these external sources can vary, which may introduce noise or errors in the annotation process. Consequently, the performance of the prediction model could be influenced by the quality and consistency of the distant supervision annotations.

This study focused on predicting the risk of ALI within 24-hour intervals. While this time frame may be suitable for some clinical interventions, it is important to recognize that ALI can have a delayed onset after the initial insult, making early prediction challenging. Extending the prediction window or exploring longitudinal data may enhance the accuracy and timeliness of ALI risk prediction. Future research could explore the optimal prediction timeframe and investigate the impact of longer time intervals on the performance of the developed model.

Lastly, the study utilized retrospective data analysis, which may limit its translation and applicability to prospective clinical settings. The complexity of real-time clinical decision-making and the dynamic nature of patient conditions may introduce additional challenges that must be fully captured in the retrospective analysis. Therefore, it is important to conduct further studies to evaluate the feasibility and effectiveness of the distant supervision approach in real-time clinical practice and assess its impact on patient outcomes and clinical decision-making processes.

■ Conclusion

The results of this research provide compelling evidence for the effectiveness of using distant supervision to predict Acute Lung Injury (ALI) in intensive care unit patients. This innovative method demonstrates promising performance in accurately identifying patients at risk of developing ALI within a 24-hour timeframe. These findings contribute to the growing body of evidence supporting the potential of machine learning algorithms in the early detection and prediction of ALI. Identifying patients at risk of ALI before the onset of symptoms or physiological changes is paramount in critical care. It provides a crucial window for intervention, enabling clinicians to initiate appropriate treatments promptly. Timely interventions may help prevent the progression of ALI to more severe conditions, such as Acute Respiratory Distress Syndrome (ARDS), which is associated with higher mortality rates.

The distant supervision-based approach, utilizing machine learning algorithms, offers a novel and effective tool for detecting and predicting ALI. The models demonstrate high accuracy, sensitivity, specificity, and AUC-ROC values, underscoring their potential in clinical practice. These models present an opportunity for healthcare professionals to proactively identify patients at risk, allowing for timely interventions and tailored management strategies to mitigate the progression and complications of ALI.

While the results of this study are promising, further investigations and validation studies are necessary to assess these models' generalizability and clinical applicability across diverse patient populations and healthcare settings. Ensuring these models perform consistently and effectively in real-world scenarios before widespread adoption in clinical

practice is essential. By leveraging the vast amounts of data available in electronic medical record datasets, such as MIMIC-III, these models can augment clinical decision-making and support healthcare providers in delivering proactive and personalized care to at-risk patients. Moreover, by enabling the identification of high-risk individuals and the implementation of preventive measures, these models can significantly improve patient outcomes and reduce the burden of ALI-related morbidity and mortality.

■ Acknowledgments

I want to thank my teachers at the Nightingale-Bamford School for their ongoing support. I would like to thank my research mentor, who has supported me in understanding health informatics and ALI. I would also like to thank the MIT Raise Initiative and SureStart for allowing me to gain experience in creating machine learning models and rendering datasets.

■ References

1. Matthay, M.A.; Zemans, R.L.; Zimmerman, G.A. Acute respiratory distress syndrome. *Nat. Rev. Dis. Primers* **2019**, *5*(1), 1–22.
2. Calvert, J. S.; Price, D. A.; Chettipally, U. K.; Barton, C. W.; Feldman, M. D. A computational approach to early sepsis detection. *Comput. Math. Methods Med.* **2016**, 2016.
3. Mintz, M.; Bills, S.; Snow, R. Distant supervision for relation extraction without labeled data. In *Proceedings of the Joint Conference of the 47th Annual Meeting of the ACL and the 4th International Joint Conference on Natural Language Processing of the AF NLP: Volume 2*.
4. Abadi, M.; Barham, P.; Chen, J.; Chen, Z.; Davis, A.; Dean, J.; ...; Kudlur, M. TensorFlow: A system for large-scale machine learning. *pp.* 265–283.
5. Johnson, A.E.W.; Pollard, T.J.; Shen, L.; Lehman, L.H.; Feng, M.; Ghassemi, M.; et al. MIMIC-III, a freely accessible critical care database. *Sci. Data* **2016**, *3*, 160035. doi: 10.1038/sdata.2016.35.
6. Mikkelsen, M.E.; Shull, W.H.; Biester, R.C.; et al. Cognitive, Mood, and Quality of Life Impairments in a Select Population of ARDS Survivors. *Respirology* **2009**, *14*(1), 76–82. doi: 10.1111/j.1440-1843.2008.01443.x
7. Laffey, J.G.; Madotto, F.; Bellani, G.; et al. Geo-economic variations in epidemiology, patterns of care, and outcomes in patients with acute respiratory distress syndrome: insights from the LUNG SAFE prospective cohort study. *Lancet Respir. Med.* **2017**, *5*(8), 627–638. doi: 10.1016/S2213-2600(17)30213-8
8. Kang, M.G.; Kim, K.H.; Park, S. Early Prediction of Acute Kidney Injury Using Machine Learning Techniques: A Systematic Review of Methodological Efficacy and Clinical Validity. *J. Clin.*
9. Armbrust, M.; Das, T.; Davidson, A.; Ghodsi, A.; Stoica, I. Scaling Spark in the real world: performance and usability. *Proc. VLDB Endow.* **2015**, *8*(12), 1840–1843.
10. Abadi, M.; Barham, P.; Chen, J.; Chen, Z.; Davis, A.; Dean, J.; ...; Kudlur, M. TensorFlow: A system for large-scale machine learning. *pp.* 265–283.
11. Hastie, T.; Tibshirani, R.; Friedman, J. *The Elements of Statistical Learning*, Vol. 2; Springer, 2009.
12. Fawcett, T. An introduction to ROC analysis. *Pattern Recognition Letters* **2006**, *27*(8), 861–874.
13. Google Cloud Platform. *Compute Engine*. [Online]. Available: <https://cloud.google.com/compute/>

■ **Author**

Eana Shah is a senior at the Nightingale-Bamford School in New York, New York. She plans on majoring in data science and computational biology in the future.

Accessible, AI-enabled TeleMedicine Solution for Multi-organ Dysfunction Caused by SARS Infections

Gatik Trivedi

Dougherty Valley High School, 10550 Albion Rd, San Ramon, CA 94582, USA; gatik.trivedi@gmail.com
Mentor: Mr. Stefan Dunifer

ABSTRACT: SARS patients have common symptoms of Multi-Organ Dysfunction (MOD), including fatigue, difficulty breathing, and fever. Delays in the detection, diagnosis, and treatment of MOD indicators can lead to the inability to manage severe symptoms, conditions worsening, and even deaths that can be prevented. The spirometer, oximeter, and thermal camera are the devices that measure these defined symptoms and were utilized in this solution to output correlative analysis. Code developed in C with the Arduino IDE is used to develop the correlation algorithm to output an “Overall Health” reading for the user to interpret. Integration of these vital elements led to a contactless telemedicine device that can display comprehensive data/results along with the use of IoT and Machine Learning. Lung Capacity, Oxygen Saturation, and temperature reading had an inaccuracy of approximately 1-5%. The correlative analysis provides a precise overall health reading for users to utilize. With the affordable design, we can leverage this to be accessible to low-income and underserved communities. A more sustainable flow of ICU admissions can be achieved because users will have real-time data on their state of being.

KEYWORDS: Biomedical and Health Sciences, Machine Learning; SARS; Multi-Organ Dysfunction; Overall Health Indicator; TeleMedicine; Internet of Things; Regression analysis.

Introduction

Coronavirus is a common, diverse family of viruses. They can cause upper respiratory tract infections. COVID-19 is the name of the infectious disease caused by SARS-CoV-2, a strain of coronavirus. SARS-CoV-2 can cause multi-organ injury via direct infection or through cytokine storms as shown in Figure 1.¹ These injuries entail cardiovascular/respiratory damage, high blood pressure, acute kidney injury (AKI), liver injury, and damage to the central nervous system.² The problem in the status quo is that monitoring is often qualitative, so there is no direct measures to evaluate overall health of the patient during quarantine.

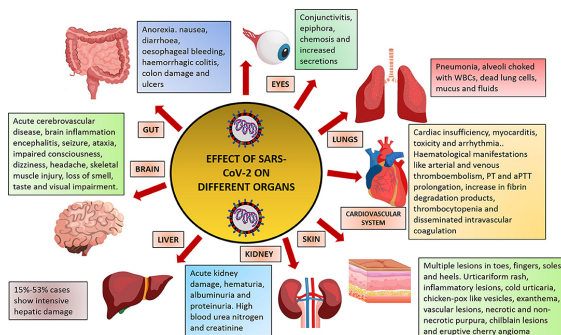


Figure 1: Organs impacted by SARS-CoV-2¹

Table 1: (prepared by student researcher): Key indicators of SARS infections and their impact on organs

Symptoms of COVID-19	Percentage of Patients	Monitorable?	Organs Impacted	Measurement Device
Fever	78%	Yes	Central and Peripheral Nervous Systems	Thermometer / Thermal Sensor
Cough	57%	Yes	Heart Disease	Self Assessment / Clinical Evaluation

Fatigue	31%	Yes	Central nervous and immune system,	Patient Wellness and Oximeter
Loss of smell	25%	No	Tongue and nervous system	Self Assessment / Clinical Evaluation
Difficulty Breathing	23%	Yes	Lungs	Spirometer and Oximeter

Methods

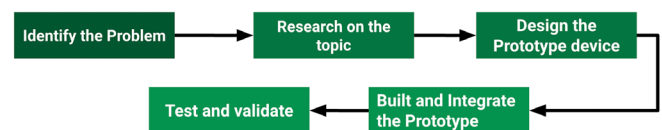


Figure 2: (prepared by student researcher): Development of the Solution

SARS-CoV-2 can be monitored in many ways. My methodology takes it to a MOD (multi-Organ Dysfunction) perspective. First, the trend of body temperature, oxygen levels, and lung capacity was researched, as shown in Figure 1. Then, knowing these common symptoms, the oximeter, spirometer, and thermal sensor were implemented to monitor most of these trends, as depicted in Table 1. The reason why both the spirometer and the oximeter were used is due to the inaccuracy of the individual sensors due to cheap materials. Hence, taking a multiple biosensor approach was best for overall accuracy. Finally, with the three measurement data points, a correlational algorithm was executed that can be used to monitor and track the progress of a person's condition for SARS-related infections. The measurement data points were taken once per

patient for each trial (2 trials). There is also an inclusion of potential SARS patients in the testing with randomly generated readings to demonstrate how the device would work on unwell patients.

A. Solution Components:

Pulse Oximeter:

A Pulse Oximeter measures oxygen saturation in the blood (non-contact). It consists of 2 LEDs that shine red and infrared light through the skin. The Photodetector collects reflected light off the tissues and returns corresponding values. Refer to Figure 3.

Thermal Camera:

A Thermal Camera, also known as an “infrared thermometer,” measures the temperature. An array of infrared detectors detects the radiation given off by objects. The ESP32 maps the values onto a comprehensive grid. Refer to Figure 4.

Spirometer:

A Spirometer measures lung capacity which the user exhales into a sterile tube. The exhaled pressure is sensed by a pressure sensor in the venturi tube and forced vital capacity (FVC) is calculated. Refer to Figure 5

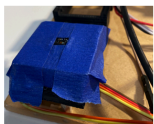


Figure 3 (prepared by student researcher): MAX30102 pulse oximeter

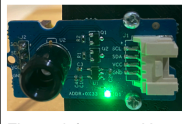


Figure 4 (prepared by student researcher): MLX90640 thermal sensor

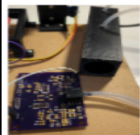


Figure 5 (prepared by student researcher): MPXV7025 spirometer

Building the telemedicine device with these three biotechnologies integrated on a single board with ESP 32 microprocessor and a TFT LCD touchscreen display makes the diagnostic solution both self-contained and accessible for the user’s health monitoring purposes. To ensure the precision of readings taken, optimal distances between the patient and the device are suggested, as illustrated in Figure 6.

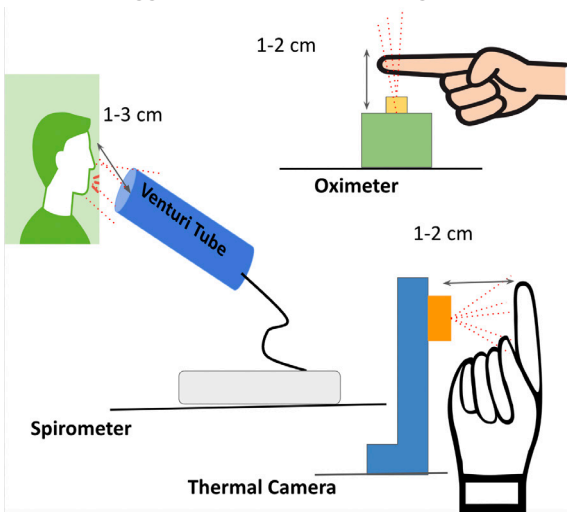


Figure 6: (prepared by student researcher): Optimal distance to obtain precise readings

B. Correlational Algorithm Theory:

To properly assess a user’s well-being through their self-isolation, this device must also calculate overall health. To measure overall health, a weighted average is taken based on a points system out of 100 of the 3 data points that come from the user. These 3 data points come from the Oximeter, Spirometer, and Thermal Sensor. Correlation equation - $(2a + 2b + c)/(a+b+c)$, where a and b are the oximeter and spirometer points, respectively, and where c is the temperature value (as illustrated in Table 2 and Table 3). Lung capacity (spirometer) and Fatigue (oximeter) data points are the same weight because they directly correlate with each other since the oxygen levels in our blood are proportional to the lungs’ capacity to circulate oxygen properly. The thermal temperature is weighed less since viral infections can cause fever.

Table 2: (prepared by student researcher): Table showing the three categories of readings from the three individual biotechnologies.

Readings	Normal	Slightly Abnormal	Abnormal	Severely Abnormal
Temperature	97-99°F	100-101.4°	95.6-96°, 102-104°	Less than 95.5°, Greater than 104°
SpO2	95-100%	Not Applicable	90% - 94%	Less than 90%
Lung capacity (FVC)	80%-120%	70%-79%	60%-69%	35%-59%

Table 3: (prepared by student researcher): Example readings with an overall health indicator.

Readings	Oxygen Levels (SpO ₂)	Lung Capacity (FVC)	Thermal Measurement (°F)	Overall health
Scenario 1	97.5%	98%	97.8	Normal
Scenario 2	95%	96%	97.3	Needs medical attention

Using the Correlational algorithm, the measured values of oxygen levels (SPO2), lung capacity (FVC), and Thermal measurement (degree Fahrenheit) are used, with different weights, to calculate the overall health indicator of the patient. Based on the derived health indicator value, normal (green), slightly abnormal (yellow), and Abnormal/Severely Abnormal (Red) are displayed on the TFT screen, as illustrated in Figure 10.

Results

	Readings	Oxygen Levels (SpO ₂)	Lung Capacity (FVC)	Thermal Measurement (°F)	Indicator results on TFT Screen
Real People	Person 1, Trial 1	97.5%	98%	97.8	Normal
	Person 1, Trial 2	98.3%	96%	97.3	Normal
	Person 2, Trial 1	97.8%	101%	96.7	Normal
	Person 2, Trial 2	96.7%	100%	96.5	Normal
	Person 3, Trial 1	95.3%	91%	98.6	Normal
	Person 3, Trial 2	96.9%	94%	98.2	Normal
	Person 4, Trial 1	98.2%	104%	97.4	Normal
	Person 4, Trial 2	98.7%	103%	97.1	Normal
Hypothetical patients	COVID patient 1	91%	79%	100.4	Slightly Abnormal
	COVID patient 2	92.5%	68%	98.5	Abnormal
	COVID patient 3	87.6%	63.7%	101.1	Severely Abnormal

	Fatigue (Oximeter Reading)	Difficulty Breathing (Spirometer)	Fever (Thermal Camera)	Overall Health Indicator
1	Green	Green	Green	Green
2	Green	Green	Green	Green
3	Green	Green	Green	Green
4	Green	Green	Green	Green
5	Yellow	Grey	Grey	Grey
6	Yellow	Yellow	Green	Yellow
7	Red	Yellow	Grey	Red

A. Statistical Model Leveraged in AI/ML Approach:

The device utilized the Non-linear regression analysis to show predictive analytics of the trend of increasing or decreasing readings depending on the model parameters chosen and the measured variables. Due to the nonlinear nature of the readings taken for a given SARS patient, the nonlinear regression supervised learning algorithm was used, which gave me the best curve-fitting results.

General Formula: $f(x) = A + B \ln(x)$

The general formula is derived from the testing of 50 individual patients. A combination of statistics and ML approaches was used to conclude this general formula that could be applied to all patients. Further testing for how accurate this model is on a large scale is needed.

The A value is changed based on the vertical translation of the values. The value $B > 0$ indicates a growth model, versus $B < 0$ indicates a decay model

Specifics: Based on the given values for a hypothetical patient monitoring their symptoms, the following best-fit curves were determined using the optimal readings (reflected on the graphs below in Figure 7, Figure 8, and Figure 9):

- Spirometer - $[103 + [-13.6 \ln x]]$
- Oximeter - $[98 + [-2.62 \ln x]]$
- Thermal Camera - $[99.1 + [1.62 \ln x]]$

** When actual normal distribution patient data is publicly available, incorporation of 2 standard deviation percentile curves will be leveraged further to validate the accuracy of the current statistical model. All the statistical analysis was performed using Python SciKit learn libraries, and plotted the results in Excel to evaluate best-fit curves.

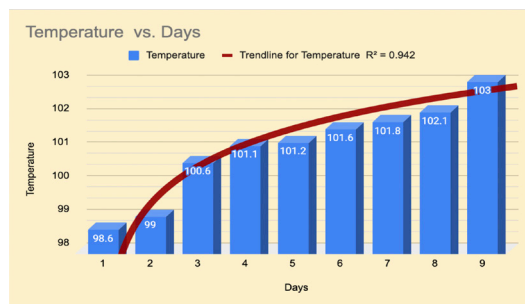


Figure 7: (prepared by student researcher): Temperature simulated reading curve

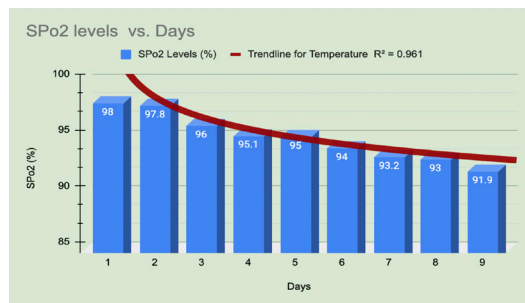


Figure 8: (prepared by student researcher): Oxygen saturation simulated reading graph

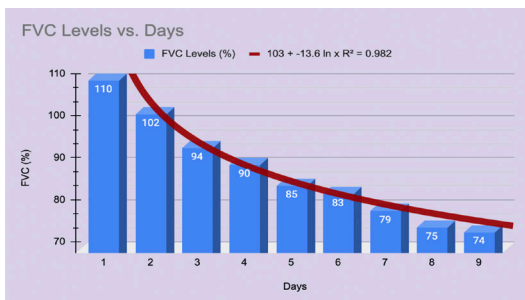


Figure 9: (prepared by student researcher): Lung capacity simulated reading graph

Discussion

Below is the comparison of the triage process as prescribed by the World Health Organization Model and the solution that is being proposed as an outcome of my research:

World Health Organization Model4 -

1. The patient has imposed an onset of 14 days in strict home quarantine without any insight into the ongoing deterioration of the body organs.

2. All the monitoring must be done at the hospital after a patient is forced out of the home due to extreme circumstances and advanced symptoms of SARS-CoV-2.

My Solution -

1. Constant monitoring provides capabilities to record oxygen levels, lung capacity, and body temperature from a single, home-based diagnostic unit. In addition, patients can now get a rough understanding of what their overall condition can become.

2. We are reducing the burden in hospitals by providing at-home diagnostic needs for a more organized triage process.

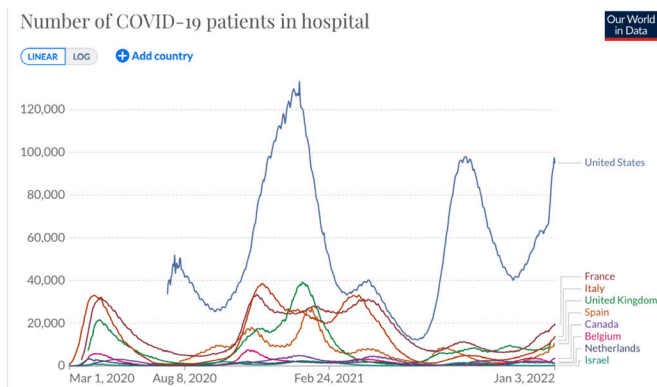


Figure 10: Number of SARS patients admitted to ICUs⁵

The benefits of my solution are:

- ❑ 1. Promote psychological well-being in patients
- ❑ 2. Avoid influxes of SARS cases in ICUs. Refer to Figure 10.
- ❑ 3. Improve patient outcomes resulting in decreased mortality through telemedicine

The Future Growth of Telemedicine Powered by Emerging Technologies:

So far, one of the main hurdles to adopting emerging technologies in the healthcare field has been due to strict government restrictions and guidelines. But recently, the US Food and Drug Administration announced the “Artificial Intelligence/Machine Learning as a Medical Device Action Plan,” which provides a framework for all healthcare providers to encourage the development of intelligent telemedicine applications.

This framework is essential for AI in telemedicine to grow and evolve. Another aspect is the behavioral change for adopting IoT in Healthcare, securing patient data, and developing trust for the new interface between doctors and patients, which are all significant steps. But due to the advancements in the standards and frameworks set by both federal and industry-level participation, the adoption of new technologies like IoT and AI/ML looks promising as the telemedicine industry continues to grow and enable a better patient experience with their healthcare providers.⁶ With all the opportunities that exist and the progress that we have made in modern technologies that can help us make healthcare provisions more efficient, effective, and enjoyable, telemedicine is clearly becoming a leading modality between patients and doctors.

Visual Model of working prototype product:

Below is the visual representation of the final working prototype (Refer to Figure 11) that shows integrated biotechnologies necessary to remotely monitor and diagnose progressing health conditions of patients while quarantined at home or to enable continuous health data sharing mechanisms with their healthcare providers via Mobile Apps (Refer to Figure 12).

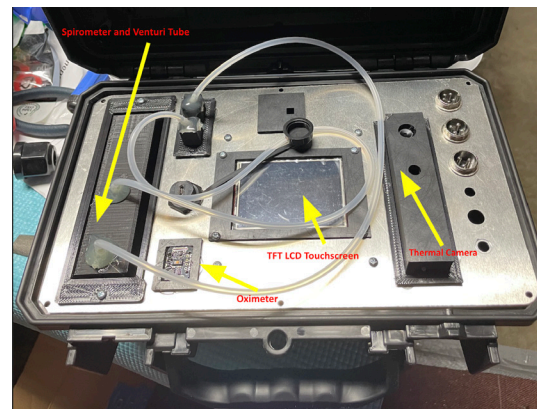


Figure 11: (prepared by student researcher): Prototype Design

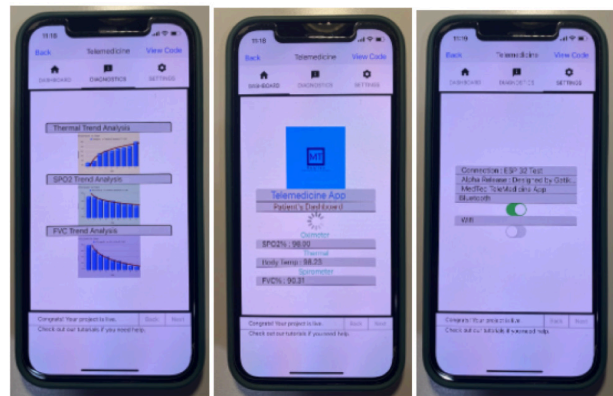


Figure 12: (prepared by student researcher): Mobile app readings

■ **Conclusion**

Successfully developed a novel telehealth solution that incorporates three biosensors onto a single platform for accurate and continuous self-monitoring of patient symptoms. An algorithm using C programming to correlate the data collected was executed as an indicator of overall patient health - critical for timely medical intervention and patient recovery. In addition, preliminary results using a limited number of individuals demonstrated the efficacy of the built solution - further testing of the device on actual patients is needed to corroborate this work's findings further. We successfully integrated machine learning statistical analysis using hypothetical patient data to evaluate predictive trends. To increase user accessibility, a prototype mobile app (alpha release) was developed that leverages patient data and statistical analysis to track health-related trends. Ultimately, a contactless product (with a disposable venturi tube) was achieved to eliminate the risk factors of accidental spread while taking readings.

The Roadmap:

The future area of focus is to explore additional machine learning models further and integrate AI directly into the telemedicine device to help improve the performance and accuracy of the predictive models that could help accurately predict the health progression of patients. It is also imperative to continue improving the device's sensitivity and specificity to enable accurate and rapid diagnosis - which is critical to patient recovery and limiting contagion spread. In the long term, IoT and mobile applications can be utilized to send pa

tient data to doctor's offices for immediate intervention and hospitalization if needed.

Future Telehealth Application:

The current pandemic situation has forced all of us to take a pause and realize the importance of self-management of health and, more importantly, being able to monitor and track the current situation of vital health statistics like blood oxygen levels, lung capacity, and body vitals through remote analysis and monitoring services. Being able to transmit this data via electronic data storage of their healthcare providers can not only ensure timely action can be taken with professional medical advice and intention but also significantly reduce healthcare service costs and potentially eliminate risks of exposure and spreading of viruses due to multiple in-person hospital visits for triage purposes Telehealth also reduces unnecessary non-urgent ER visits and eliminates transportation expenses for regular checkups.

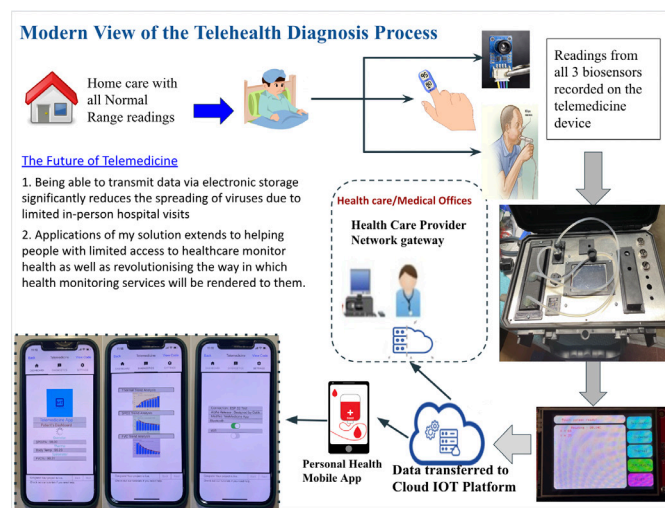


Figure 13: (prepared by student researcher): Future view of Telemedicine based triage process based on IoT capabilities

The evolving IoT capabilities would catalyze the design and deployment of remote diagnostic-based solutions that are both accessible and affordable for use in all parts of society as illustrated in Figure 17. These technologies could become a significant factor in public health mitigation strategies as the Centers for Disease Control and Prevention outlined. In addition, they can help shape future policies in this evolving landscape of medical practice. Regardless of the pandemic situation, the area of telemedicine is being well received by primary healthcare providers due to several factors like health care and insurance costs, timely insights and alerts for the doctor to diagnose a patient, timely intervention for potential life-threatening considerations, and improving overall patient and healthcare provider satisfaction..

Acknowledgments

I would like to thank my honors chemistry teacher, Mr. Estes, for guiding me throughout this project. In addition, I would also like to thank my parents for all the support and encouragement they gave me to pursue my passion.

References

1. Prasad, Ashish, and Manoj Prasad. "Single Virus Targeting Multiple Organs: What We Know and Where We Are Heading?" *Frontiers*, Frontiers, 17 June 2020, www.frontiersin.org/articles/10.3389/fmed.2020.00370/full.
2. Paolo Pelosi, "Multiple Organ Dysfunction in SARS-CoV-2: M ODS-CoV-2." Taylor & Francis, Chiara Robba, 22 June 2020, www.tandfonline.com/doi/full/10.1080/17476348.2020.1778470.
3. Bremer, Andrew, and Jeremy Glynn. "BME Design Projects Better Health by Design." *Low-Cost, Open-Source Spirometer*, 8 Jan. 2009, bmedesign.engr.wisc.edu/projects/s10/spirometer.
4. Ritchie, Research and data: Hannah. "Coronavirus Pandemic (COVID-19) – the Data - Statistics and Research." *Our World in Data*, ourworldindata.org/coronavirus-data.
5. World Health Organisation, "Clinical Care of Severe Acute Respiratory Infections – Tool Kit." World Health Organization, World Health Organization, 11 Apr. 2020, www.who.int/publications/item/clinical-care-of-severe-acute-respiratory-infections-tool-kit
6. Cheng, Matthew P., et al. "Diagnostic Testing for Severe Acute Respiratory Syndrome-Related Coronavirus 2." *Annals of Internal Medicine*, Matthew P. Cheng, 18 Apr. 2020, www.acpjournals.org/doi/10.7326/M20-1301.

Author

Gatik is a Junior at Dougherty Valley High School with a passion for BioMedical and BioTechnology Engineering. He is an aspiring technologist with a deep interest in bio-instrumentation, tissue engineering, biomedical science, and Bioinformatics

Trend and Prediction Analysis of Rainfall and Temperature in Dindigul District, Tamil Nadu, India

Harnishya Palanichamy

Hebron School, Lushington Campus, Ootacamund, Nilgiris District, Tamil Nadu, 643001, India; harnishya.bts@yahoo.com

Mentor: Angel Agnes Mary

ABSTRACT: Climate change is already a fact, where the intensity and frequency of changes in climate extremes and their impacts on various physical and biological systems contribute to global warming. The United Nations Global Sustainable Development Goal 13 calls for urgent action to address climate change and its impacts. The goals call for strengthening resilience and adaptive capacity at the national and local levels. Goal 13- Climate Action, is one of the nine goals for which India has shown a positive push. Tamil Nadu ranked second with a composite score of 74 and is listed as a Front Runner under the Performance towards SDG's goals in 2020-21. The National Action Plan on Climate Change Assessment declares that the climate parameter is important at the regional and local scale to estimate its impacts on various sectors. Hence in the present study, an attempt is made to analyze the trend and prediction of rainfall and temperature using statistical techniques like-Homogeneity test, Box and Whisker Plot test, Coefficient of Variability, Cluster Dendrogram, Mann-Kendall, Sen's slope, and ARIMA model in Dindigul district, Tamil Nadu, India. The rainfall and temperature data are collected from 15 rainfall stations spread across the district for 39 years, from 1981 to 2020. The results can help prioritize new strategies for managing available water resources to sustain the agriculture sector's dependence in the study area. The ongoing Action Plans of the Government of Tamil Nadu to achieve climate change mitigation measures are listed. These recommendations could be utilized by agriculturalists, agro-climatologists, and decision-makers to scientifically support development in the study area.

KEYWORDS: Environmental Sciences, Homogeneity, Box and Whisker Plot, Coefficient of Variability, Cluster Dendrogram, Mann-Kendall, Sen's slope, ARIMA.

■ Introduction

Climate change refers to a continuing shift in weather patterns, and although these may be natural, anthropogenic activities have been the primary cause of climate change since the 1800s.¹ The existence of climate change has already been proven, and the magnitude and occurrence of the variations in climate extremes and their control of various physical and biological systems argue for global warming.² Climate change exacerbates poverty, increases food insecurity and health risks, and thus escalates the overall vulnerability of exposed people.³ It can also pull the community toward factors such as-forced displacement and chronic poverty,⁴ and in the future, climate change will affect the agricultural zone and be the source of the threat of hunger and the increase of water scarcity.⁵ Climate change has emerged as one of the most indispensable concerns in sustainable development⁶, especially in the most vulnerable countries.⁷ The United Nations Global Sustainable Development Goal 13 calls for urgent action to combat climate change and its impacts.⁸ The overall commitment made by the UN is to achieve Goal 13 in an integrated manner focusing on three broad areas- Economic, Social, and Environmental. The goal is to incorporate climate change and disaster risk mitigation measures and sustainable natural resource management into national progress plans.⁹ The goals call for strengthening resilience and adaptive capacity at the national level, as the chain reaction of climate change extends beyond national boundaries.⁹

The highlights of deaths due to extreme weather events in 2018-19 said that, for every one crore population, 15 Indians lost their lives. Hence a target of zero was set, meaning that all States/Union Territories must be adequately prepared to ensure that no lives are lost due to extreme weather events.⁹ The composite score for India has improved from 60 in 2019-20 to 66 in 2020-21, indicating that the country has made overall progress toward achieving the SDGs.⁹ Nine targets are driving the positive push in India with a score between 65 and 99, with Goal 13- Climate Action, being one of them.⁹ Tamil Nadu ranked second with a composite score of 74 and is listed as Front Runner under the Performance of States and Union Territory 2020-21.⁹ The heatmap that displays the performance of each State/Union Territory shows that Tamil Nadu has achieved an Index score of 61, listed as a Performer, under SDG 13- Climate Action in 2020-21 and that the number of lives lost per 1 crore population due to extreme weather events is 12.85 in Tamil Nadu, in 2021-21.⁹ Climate change is occurring on a global scale. Yet its impacts often vary from region to region. Local and regional level studies formulate the development plans that mitigate the fatal consequences of climate change,¹⁰ and the perception of a climate emergency at the regional level has received much attention in the recent past.¹¹ Regional-level studies would help achieve the national level target, and assessment of climate parameters is important at the regional and local levels to estimate the impacts on differ-

ent sectors, according to the National Action Plan on Climate Change.¹²

My mother is a geographer and, interestingly, does research in various areas of her field. In conversations with her, I learned facts about the current global focus on the Sustainable Development Goals. I was amazed to discern the 17 goals, of which Goal 13- Climate Action is closely related to the other SDGs. Goal 13 has five Targets, and each target includes one or more Indicators that can be used to measure and monitor global progress and challenges in achieving the goal. I have read in some articles that the United Nations and Non-governmental Organizations are working on issues related to UN SDG 13. And these details and statistics have always fascinated me.

I chose the study area, the Dindigul district, in Tamil Nadu, India, where my mother was born and where I often visited, especially the rainfall stations in the popular tourist hill station destinations -Berijam and Kodaikanal, where I did my primary education. At that time, I was curious to learn about the changes in the significant climatic variables- rainfall and temperature, in the Dindigul district. For this purpose, I wanted to collect the Rainfall and Temperature data for the study area and apply statistical techniques to analyze these data. It is at this point that I formulated my research question-

"How do climatic variables like Rainfall and Temperature affect climate change in a local area, and what mitigation measures could be taken to address it?"

My research would provide a valuable outcome for understanding climate change at the local level. In addition, I chose to incorporate the Government Action Plans currently being implemented in relation to SDG 13-Action, to combat climate change in the study area. The analysis of the differences in meteorological variables is an important task for the monitoring of climate change. Therefore, an attempt is made to analyze the trend and prediction of Rainfall and Temperature using statistical techniques like the Homogeneity test, Box and Whisker Plot test, Coefficient of Variability, Cluster Dendrogram, Mann-Kendall, Sen's slope, and ARIMA model in Dindigul district, Tamil Nadu, India.

Objectives:

1. To analyze the Uniformity and Variability of Rainfall and Temperature from 1981 to 2020.
2. To study the Pattern and Trend of Rainfall and Temperature from 1981 to 2020.
3. To Predict the Rainfall and Temperature in the study area.
4. To list the Action Plans for SDG 13-Action to Combat Climate Change- those are in progress and undertaken by the Government of Tamil Nadu.

Study Area:

The study area, Dindigul district, is located in the central part of Tamil Nadu, with an extension between 10°14'45" and 10°31'00" North latitudes and 77°45' and 78°4'30" East longitudes, covering an area of 6266.64 sq. Km (Figure 1). It is bordered by Erode, Karur, and Tiruchirappalli districts to the north, Madurai district to the east and south, Coimbatore district, and Kerala state to the west. Dindigul district is covered

by an undulating plain predominantly with red soil.¹³ The study area has a tropical climate, with an average annual temperature of 21.2°C and rainfall of about 700-1400 mm yearly. The population of the Dindigul district is 2159775 persons, according to the 2011 census, ranking 16th among the districts wise of Tamil Nadu.¹⁴ The district is divided into fourteen blocks, namely Attur, Dindigul, Reddiyarchatram, Shanarpatti, Nattam, Nilakkottai, Vathalagundu, Oddanchatram, Palani, Toppampatti, Guziliamparai, Vadamadurai, Vedasandur, and Kodaikanal.

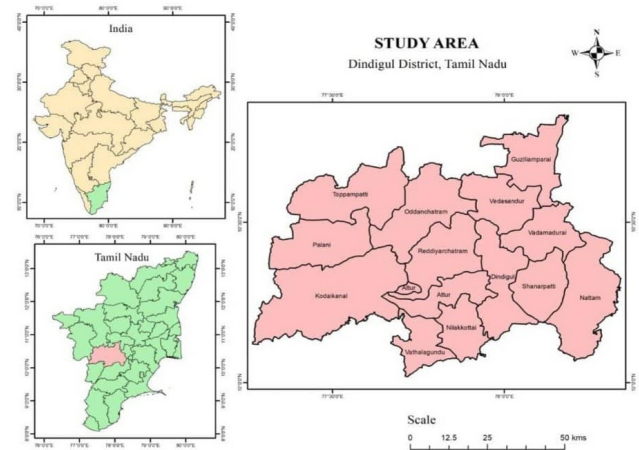


Figure 1: Study Area-Dindigul District.

■ Methodology and Data

The rainfall data were downloaded from NASA/POWER CERES/MERRA2 Native Resolution Average Monthly, from 01/01/1981 to 12/31/2020, with 0.5°*0.625 degrees at approximately 706.32 meters. The rainfall data were collected from 15 rainfall stations for 39 years from 1981 to 2020 in the study area. The 15 rainfall stations are Berijam, Chatrapatti, Dindigul, Kamachipuram, Kodaganar, Kodaikanal, Kuthiraiyur Dam, Marudhanadhi Dam, Nattam, Nilakkotai, Palani, Peeranai, Vedasandur Central Tobacco Institute (CTRI), Vedasandur and Virupachi. The Average Monthly Temperature data were downloaded from the same platform from 01/01/1981 to 12/31/2020, and the data range is 2 meters. ArcMap 10.8 and Microsoft Office 2013 process and calculate the data. The location of the rainfall stations is shown in Figure 2: their latitudes, longitudes, and elevations are listed in Table 1. It is important to note that two hill stations, Berijam and Kodaikanal, are located in the study area. The Homogeneity test, Box and Whisker Plot test, Coefficient of Variability, and Cluster Dendrogram, for both climatic variables, were calculated using simple statistical techniques. Mann-Kendall and Sen's Slope tests analyze monthly rainfall and temperature trends. The precipitation and temperature data prediction analysis were analyzed using the Dickey-Fuller Test, and the ARIMA model was processed with R statistical R program software.

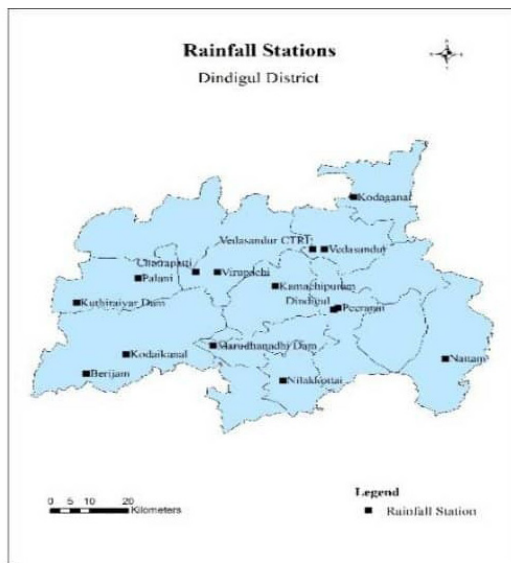


Figure 2: Location of Rainfall Stations

Table 1: Details of Rainfall Stations

Rainfall Stations	Latitude	Longitude	Elevation (in meters)
Vedesandur	10.531066	77.948121	212
Chatrapatti	10.468603	77.649948	136
Nilakkottai	10.165497	77.852450	226
Nattam	10.226478	78.229454	254
Palani	10.450684	77.516048	320
Dindigul	10.362660	77.969458	274
Kodaikanal	10.238674	77.4899095	2088
Berijam	10.185071	77.396134	2150
Kamachipuram	10.428219	77.833957	371
Vedesandur CTRI	10.53155	77.9209	217
Peeranai	10.367312	77.980288	194
Virupachi	10.466667	77.7	306
Marudhanadhi Dam	10.261944	77.69	327
Kodaganar	10.686388	77.969720	427
Kuthiraiyar Dam	10.381944	77.37333	385

■ Review of Literature

Previous studies in Rainfall and Temperature analysis:

Rainfall and temperature are the fundamental physical parameters as they determine the environmental conditions of a given region.¹⁵ Increasing surface temperature leads to changes in rainfall,¹⁶ and the analysis of temperature variations remains an important point of discussion.¹⁷ The effects of climatic changes on rainfall and temperature have received much attention from researchers worldwide¹⁸ and at the regional level.¹⁹ Increased surface temperatures and rainfall variability can lead to crop failure and increased incidents of pests.²⁰ Analysis of long-term temperatures and precipitation trends is extremely important for rain-fed agricultural regions.²¹

Previous studies in Uniformity using Homogeneity Tests in Rainfall and Temperature analysis:

Rainfall records are critical to a climate-related study, and often changes in data collection methods, relocation of stations, and outdated equipment affect the data availability.²²

A data series is “homogenous” only if the recorded data are actually due to climatic variations²³ and not to non-climatic factors (i.e., measurement errors, instrument errors, or errors due to other human-induced changes).²³ The homogeneity of the time series was tested using the Standard Normal Homogeneity Test (SNHT),²⁴ and the Buishand’s Range Test (BRT).²⁵ The results showed that all data sets in Bangladesh²⁶ were homogeneous. Three homogeneity tests, namely, SNHT, BRT, and Pettitt Test (PT), are used to examine the homogeneity of rainfall data.²⁷ The PT and SNHT developed by Alexandersson and Moberg are used to study the changes in annual and seasonal rainfall datasets for all meteorological subdivisions in India.²⁸ Buishand’s Range Test (BRT), Pettitt’s Test (PT), and Von Neumann’s Ratio Test (VNRT) are used along the coastal districts of Maharashtra.²⁹ SNHT has been used to test the homogeneity of long-term data series at a 5% significance level in the northeastern states of India.³⁰

Previous studies in Variability using the Box & Whisker Test and Coefficient of Variability in Rainfall and Temperature analysis:

Analysis of annual rainfall time series from 1980-2013 from many rain gauge stations was carried out using box and whisker plots in the semi-arid region of southern India.²⁷ Monthly, annual, and seasonal rainfall data were presented in box plots in the northeastern states of India.³⁰ Box and whisker plots were constructed for monthly rainfall in Kalahandi, Bolangir, and Koraput districts from 1980 to 2017.³¹ The boxplots are analyzed for the monthly rainfall figures from 1975 to 2009 for the Brong Ahafo Region in Ghana.³²

The coefficient of variation (CV) represents the ratio between the standard deviation and the mean and is used to differentiate the degree of variation from one data series to another.³³ A higher CV value indicates greater variability, and vice versa.³⁴ Analysis of spatiotemporal annual rainfall variability in the Wadi Cheliff Basin, Algeria, from 1970 to 2018 shows an opposite spatial pattern between CV and annual rainfall.³⁵ The CV for rainfall and rainy days is calculated for Ghataprabha River Basin, India.³⁶ The trend, variability, intensity, number of dry days, mean rainfall pattern, and variability in annual and SW monsoon seasons between 1989 to 2018 are analyzed, district-wise, for Kerala and West Bengal.³⁷

Previous studies in Patterns using Cluster Dendrograms in Rainfall and Temperature analysis:

The cluster analysis of 27 rainfall stations was done using the agglomerative hierarchical clustering technique with the criteria of Ward’s minimum variance method and Squared Euclidean Distance method using Statistica for southern India.²⁷

Previous studies in Trends using Mann-Kendall and Sen’s Slope for Rainfall and Temperature analysis:

The Mann-Kendall (MK), a nonparametric test, has been used consistently to detect an upward or downward trend in a range of hydrologic climate and environmental data.³⁸ The MK test can be used for any variable for trend detection.³⁹ The MK test was used to examine rainfall and temperature trends in the southern Gonder zone, Ethiopia.⁴⁰ The MK test

was used to estimate the trend of more than 500 rain gauge stations over 50 years in Italy.⁴¹ The trend of climatic variables between the years 1977 to 2012 in 4 rain gauge stations of Togo, Africa, was analyzed using the MK test.⁴² A study of rainfall trends using the MK test between 1950 and 2015 was researched in the river catchment in the southwestern Ghats, India, for different seasons.⁴³ The Mann-Kendall's test was used to analyze the trend direction of rainfall in India's 12 semi-arid districts of western Rajasthan.⁴⁴

Sen's estimator is a non-parametric method used for trend analysis and magnitude of the hydroclimate dataset.⁴⁵ Sen developed an innovative trend analysis for meteorological, hydrological, and environmental variables.⁴⁶ The trend analysis of temperature and its significance level in Gombe state, Nigeria, was studied using Sen's estimator.⁴⁷ MK and Sen's slope trend analysis are applied to investigate India's seasonal stream flow variability.⁴⁸ Similar studies are done for 21 stations from 1991-2020 in Mandya, Karnataka.⁴⁹, Kashmir Himalayas⁵⁰, and the northeastern states of India and Odisha.^{30,31}

Previous studies in Prediction using ARIMA in Rainfall and Temperature analysis:

Prediction through providing statistics and facts about the future availability of rainfall is critical for managing water supply and demand, mitigating droughts, ensuring water levels in reservoirs, and devising mitigation measures.⁵¹ Together with trend analysis, forecasting future changes in climate variables assists policy planners.⁵² The Coastal Development Strategy prepared by the Water Resources Planning Organization predicts that monsoon rainfall in Bangladesh will increase by 12 % and winter rainfall will decrease by 10 % by 2100.⁵³ Research predicted that a temperature rise would exacerbate urban heat in Addis Ababa, Ethiopia.⁵⁴ The Indian Climate Change Assessment Network from 2010 to 2030 projected an all-around increase in greenhouse gases for the Indian subcontinent, where annual mean surface temperature is projected to increase by 1.7 to 2.0 °C by 2030, which will be felt at higher altitudes.⁵⁵

Various techniques, such as Moving Average (MA), Auto Regressive (AR), Auto Regressive Moving Average (ARMA), and Integrated ARMA (ARIMA), are widely used forecasting methods for analyzing rainfall patterns in different time series.⁵⁶ The autoregressive method assumes that the past can predict the future based on the correlation between the future and the past.²¹ The Auto-Regressive Integrated Moving Average (ARIMA) model is used to predict future rainfall trends for the mean rainfall in Bangladesh.²⁶ The ARIMA model is used to predict rainfall in the Sylhet region⁵⁷ and in the coastal region of the Bay of Bengal.⁵⁸

Results and Discussion

Analysis of Uniformity using Homogeneity Test for Rainfall and Temperature data:

In the study area, the Uniformity of monthly rainfall and temperature was analyzed using the Homogeneity test, at 15 rainfall stations, for 39 years from 1981 to 2020. The results are presented in Table 2 and Table 3. The Standard Normal Homogeneity Test (SNHT) and Buishand Range Test

(BRT) are used to test the homogeneity at a 5 % significance level in all the rainfall stations. The null hypothesis states that the annual rainfall values are independent, identically distributed, and homogeneous, while the alternative hypothesis states that the mean changes abruptly at an unknown time.⁵⁹ The null hypothesis (H0) is accepted if the estimated p-value is greater than the α -value at a 5% significance level: otherwise, it is rejected.²⁷

The results of the homogeneity tests for the rainfall and temperature data are shown in Tables 2 and 3, respectively. The tables show that the results are grouped into two classes depending on whether the hypothesis for both the tests- the homogenous (that accepts the Null hypothesis) and Non-homogenous (that rejects the Null hypothesis). In the analysis of monthly rainfall (Table 2), the highest value (10.063) of SNHT is found in Berijam and Kodaikanal stations. These stations are Non-homogenous, while the remaining 12 stations are homogenous. The non-homogeneity is observed in all rainfall stations for monthly temperature analysis (Table 3), which proves that the availability of daily and hourly data could be more consistent.

Table 2: Homogeneity Test for Rainfall Data

Station	SNHT		BRT		Result
	T-Value	p-Value	Q-Value	p-value	
Berijam	10.063	0.0181	1.5991	0.03065	Non-Homogenous
Chatrapatti	4.9667	0.2927	1.0896	0.4557	Homogenous
Dindigul	4.9667	0.2959	1.0896	0.4617	Homogenous
Kamachipuram	4.9667	0.289	1.0896	0.4629	Homogenous
Kodaganar	4.9667	0.2903	1.0896	0.4618	Homogenous
Kodaikanal	10.063	0.0192	1.5991	0.0317	Non-Homogenous
Kuthiraiyar Dam	5.119	0.2714	1.0512	0.5215	Homogenous
Marudhanadhi Dam	5.119	0.2758	1.0512	0.5214	Homogenous
Nattam	8.1513	0.0584	1.4639	0.07695	Homogenous
Nilakkottai	8.1513	0.0571	1.4639	0.0791	Homogenous
Palani	5.119	0.274	1.0512	0.5173	Homogenous
Peeranai	4.9667	0.2915	1.0896	0.4603	Homogenous
Vedasandur (CTRI)	4.9667	0.2943	1.0896	0.4592	Homogenous
Vedasandur	4.9667	0.292	1.0896	0.4633	Homogenous
Virupachi	5.119	0.2722	1.0512	0.519	Homogenous

Table 3: Homogeneity Test for Temperature Data

Station	SNHT		BRT		Result
	T-Value	p-value	Q-Value	p-value	
Berijam	9.2981	0.03015	2.1263	0.000	Non-Homogenous
Chatrapatti	8.8949	0.03755	1.9762	0.000	Non-Homogenous
Dindigul	9.5101	0.02635	1.8613	0.003	Non-Homogenous
Kamachipuram	9.5101	0.02595	1.8613	0.003	Non-Homogenous
Kodaganar	9.5101	0.02505	1.8613	0.004	Non-Homogenous
Kodaikanal	9.2981	0.03025	2.1263	0.0002	Non-Homogenous
Kuthiraiyar Dam	8.8949	0.03795	1.9762	0.0009	Non-Homogenous
Marudhanadhi Dam	8.8949	0.0345	1.9762	0.0008	Non-Homogenous
Nattam	9.5646	0.0262	1.9089	0.0019	Non-Homogenous
Nilakkottai	9.5646	0.025	1.9089	0.0020	Non-Homogenous
Palani	8.8949	0.0366	1.9762	0.001	Non-Homogenous
Peeranai	9.5101	0.0262	1.8613	0.0036	Non-Homogenous
Vedasandur (CTRI)	9.5101	0.0249	1.8613	0.0035	Non-Homogenous
Vedasandur	9.5101	0.0253	1.8613	0.0031	Non-Homogenous
Virupachi	8.8949	0.0365	1.9762	0.0009	Non-Homogenous

Analysis of Variability using Box & Whisker Test and Coefficient of Variability for Rainfall and Temperature Data:

The variability of monthly rainfall and temperature data for 39 years from 1981 to 2020 is analyzed using the Box & Whisker test and the Coefficient of Variability in the study area.

Box & Whisker Test:

The Box and Whisker test for monthly rainfall data is shown in Figure 3. Studies show that the short boxes have less temporal variation, and the rainfall stations with the long boxes represent a highly dispersed and consistent rainfall pattern.²⁷ Similar conditions prevail in this study, as shown in Figure 3. The median line divides the long and short boxes into upper and lower quartiles. In the study area, four rainfall stations, Berijam, Kodaikanal, Nattam, and Nilakottai, have long boxes, while the remaining 11 stations have short boxes. In the case of Chatrapatti, Dindigul, Kamachipuram, Kodaganar, Peeranai, Vedasandur (CTRI), and Vedasandur rainfall stations, the median line within the boxes is in the upper quartile, which means that these stations have received less rainfall.

The Box and Whisker test for the monthly temperature data is shown in Figure 4. It shows that the long boxes with a highly dispersed temperature variation are found in the Berijam and Kodaikanal rainfall stations. In Palani, Virupachi, and Chatrapatti rainfall stations, the median line is in the lower quartile, exhibiting that these stations have experienced substantial temperature variation.

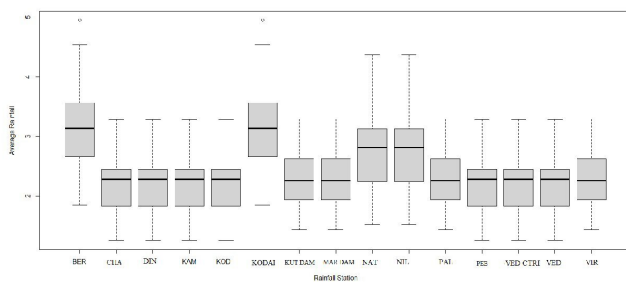


Figure 3: Box & Whisker Test for Rainfall Data

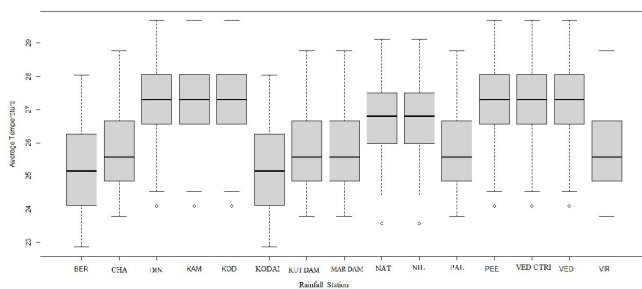


Figure 4: Box & Whisker Test for Temperature Data

Coefficient of Variability (CV):

This study calculated monthly rainfall and temperature variability using the Coefficient of Variability (CV), for 39 years, from 1981 to 2020. CV is calculated to examine the rainfall and temperature variability, and a higher value of CV is an indicator of greater variability, and vice versa, which is calculated as $CV = \frac{\sigma}{\mu} \times 100$, where σ is the standard deviation, and μ is the mean precipitation.⁶⁰

The CV was calculated for the monthly rainfall and temperature data in the study area and is shown in Table 4 and Table 5, respectively. The coefficient of variability for the monthly rainfall data (Table 4) indicates that the Dindigul rainfall station has experienced the higher and Berijam and

Kodaikanal have the lowest variability. The highest rainfall variability is noticed during February, followed by January and March, and the lowest variability is observed in October. The coefficient of variability for monthly temperature data (Table 5) reveals that Berijam & Kodaikanal rainfall stations have higher variability, and Dindigul, Kamachipuram, Kodaganar, Peeranai, Vedasandur CTRI, and Vedasandur rainfall stations, the lowest variability. The highest temperature variability is in October and November, and the lowest is in April.

Table 4: Coefficient of Variability analysis for Rainfall data

Station	Jan	Feb	March	April	May	June	July	Aug	Sep	Oct	Nov	Dec	Annual
Berijam	167	153	122	70	59	61	44	37	57	46	49	93	22
Chatrapatti	165	187	158	98	64	73	65	51	54	46	60	94	21
Dindigul	99	123	129	140	109	121	147	138	94	100	122	101	96
Kamachipuram	165	187	158	98	64	73	65	51	54	46	60	94	21
Kodaganar	165	187	158	98	64	73	65	51	54	46	60	94	21
Kodaikanal	167	153	122	70	59	61	44	37	57	46	49	93	22
Kuthiraiyar Dam	174	160	131	78	57	51	43	36	52	45	52	96	20
Marudhanadhi Dam	174	160	131	78	57	51	43	36	52	45	52	96	20
Nattam	159	175	140	87	62	77	60	47	57	46	58	93	23
Nilakkottai	159	175	140	87	62	77	60	47	57	46	58	93	23
Palani	174	160	131	78	57	51	43	36	52	45	52	96	20
Peeranai	165	187	158	98	64	73	65	51	54	46	60	94	21
Vedasandur (CTRI)	165	187	158	98	64	73	65	51	54	46	60	94	21
Vedasandur	165	187	158	98	64	73	65	51	54	46	60	94	21
Virupachi	174	160	131	78	57	51	43	36	52	45	52	96	20

Table 5: Coefficient of Variability analysis for Temperature data

Station	Jan	Feb	March	April	May	June	July	Aug	Sep	Oct	Nov	Dec	Annual
Berijam	10.02	10.74	7.54	6.77	7.37	12.17	13.47	11.38	12.82	15.03	13.17	12.37	5.16
Chatrapatti	8.95	9.10	7.45	5.96	6.32	11.90	12.16	8.62	11.44	11.48	13.80	12.80	4.82
Dindigul	9.14	8.53	7.80	6.95	6.58	8.30	9.70	6.22	8.76	12.48	15.41	13.01	4.76
Kamachipuram	9.14	8.53	7.80	6.95	6.58	8.30	9.70	6.22	8.76	12.48	15.41	13.01	4.76
Kodaganar	9.14	8.53	7.80	6.95	6.58	8.30	9.70	6.22	8.76	12.48	15.41	13.01	4.76
Kodaikanal	10.02	10.74	7.54	6.77	7.37	12.17	13.47	11.38	12.82	15.03	13.17	12.37	5.16
Kuthiraiyar Dam	8.95	9.10	7.45	5.96	6.32	11.90	12.16	8.62	11.44	11.48	13.80	12.80	4.82
Marudhanadhi Dam	8.95	9.10	7.45	5.96	6.32	11.90	12.16	8.62	11.44	11.48	13.80	12.80	4.82
Nattam	9.36	9.79	8.05	7.07	7.86	8.36	10.84	7.57	10.92	15.15	16.50	14.18	4.81
Nilakkottai	9.36	9.79	8.05	7.07	7.86	8.36	10.84	7.57	10.92	15.15	16.50	14.18	4.81
Palani	8.95	9.10	7.45	5.96	6.32	11.90	12.16	8.62	11.44	11.48	13.80	12.80	4.82
Peeranai	9.14	8.53	7.80	6.95	6.58	8.30	9.70	6.22	8.76	12.48	15.41	13.01	4.76
Vedasandur (CTRI)	9.14	8.53	7.80	6.95	6.58	8.30	9.70	6.22	8.76	12.48	15.41	13.01	4.76
Vedasandur	9.14	8.53	7.80	6.95	6.58	8.30	9.70	6.22	8.76	12.48	15.41	13.01	4.76
Virupachi	8.95	9.10	7.45	5.96	6.32	11.90	12.16	8.62	11.44	11.48	13.80	12.80	4.82

Analysis of Spatial Patterns using Cluster Analysis for Rainfall and Temperature data:

The spatial pattern of monthly rainfall and temperature data, for 39 years, from 1981 to 2020, for the study area is analyzed using Cluster Dendrogram analysis. They are shown in Figure 5 and Figure 6, respectively. Cluster analysis was developed to classify a multivariate data set into homogeneous clusters with minimum dissimilarity within clusters and maximum contrast between clusters.⁶¹ In this study, the R programming software K Means Clustering technique is used to process the data.

The Cluster Dendrogram for monthly rainfall data (Figure 5) reveals the following conclusions. The trails were made by classifying the study area with four rainfall clusters where Cluster 1 consists of Berijam, Kodaikanal; Cluster 2 is found in Nattam, Nilakottai; Cluster 3 includes Kuthiraiyar Dam, Marudhanadhi Dam, Palani, Virupachi and the remaining taluks are classified under Cluster 4. In Kodaikanal and Berijam, classified as cluster 1, the rainfall is highly dispersed, indicating a higher distributed rainfall pattern as these two rainfall stations are located nearly 2088 and 2150 meters above the mean sea level, respectively. The Cluster Dendrogram for monthly temperature analysis (Figure 6) shows that there are four temperature clusters, Cluster 1 includes Berijam and Kodaikanal, Cluster 2 consists of Nattam, Nilakottai, Cluster 3 has Kuthiraiyar Dam, Marudhanadhi Dam, Palani,

fall under cluster 4. The Cluster wise fluctuations in monthly rainfall and temperature in each cluster are oscillatory and do not have a regular pattern, as each cluster has specific rainfall and temperature aspects in the study area.

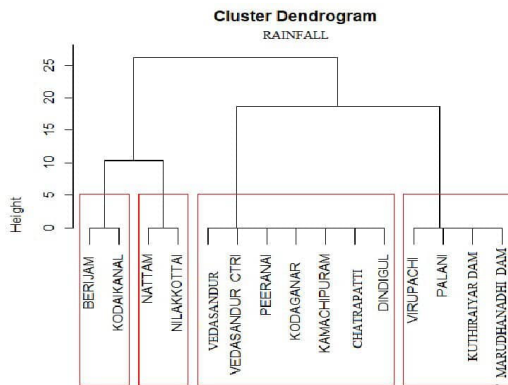


Figure 5: Cluster Dendrogram analysis for Rainfall data

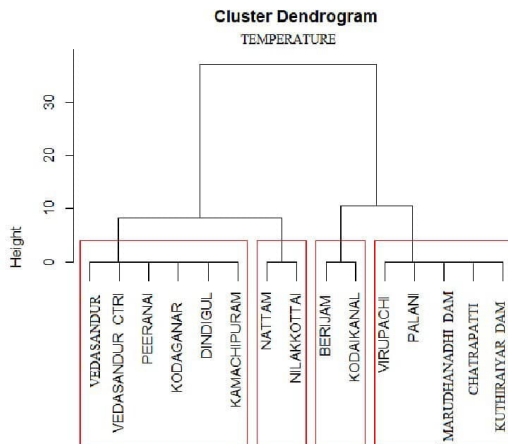


Figure 6: Cluster Dendrogram analysis for Temperature data

Trend analysis using Mann-Kendall and Sen's Slope for Rainfall and Temperature data:

Monthly rainfall and temperature trends are analyzed in the study area from 1981 to 2020 for 15 rainfall stations, using Mann-Kendall and Sen's slope tests. Tables 6 and 7 show the monthly rainfall and temperature patterns obtained in the study area using the Mann-Kendall test and Sen slope estimator, respectively. When performing the Mann-Kendall test, Kendall Tau, a measure of the correlation between two variables, is obtained, and the Kendall Tau takes values between ± 1 .⁶²

The following conclusions can be drawn from Table 6. The results based on the intensity of the z- value of the Mann-Kendall test at the significance level of 0.05 indicate that the monthly rainfall in January, March, June, July, September, and December shows a negative trend (-0.15 to -1.11). The z- value shows a positive trend, varying from 0.38 to 1.78, and observed in February, April, May, August, October, and November, with a strong positive trend (z- value 1.78) in May. Sen slope test shows an increasing trend (0.0051 to 0.0500) in February, April, May, August, October, and November and a decreasing trend, -0.0018 and -0.0486,

in December, September, July, March, January, and June. The annual rainfall trend is increasing as both Sen's slope estimator and Kendall's tau (Z) are positive and found to be 0.00003 and 0.00002, respectively. The results of the Rainfall trend have shown an increase with notable trends perceived at the 95% confidence levels, as recommended.⁶³

From Table 7, the following conclusions are drawn. The results based on the intensity of the z value of the Mann-Kendall test at the 0.05 significance level indicate that the monthly temperature has a negative trend (-0.18 to -2.06) in February, January, March, April, May, June, November, and December. The z value shows a positive trend, varying between 0.34 and 1.37, observed in July, August, September, and October, with a high positive trend (z value 1.37) found during August. Sen's slope test reveals an increasing trend (0.0054 to 0.0244) during September, August, July, and October and a decreasing trend, -0.0065 and -0.0363, February, January, April, May, June, November, December, and March. The trend of annual rainfall is increasing as both the slope estimator of the Sen and the tau (Z) values of Kendall are Negative and found to be -0.0406 and -0.2208, respectively. The results of the Rainfall trend have shown a decrease, with significant trends observed at the 95% confidence levels.

Table 6: Trend analysis for Rainfall data

Months	Z Score	Var S	Mann-Kendall Tau	P-value	Sen's Slope
Jan	-0.86235	7363.67	-0.0963	0.3885	-0.0033
Feb	0.71171	7346.00	0.0802	0.4766	0.0005
March	-0.39616	7365.67	-0.0449	0.692	-0.0023
April	0.38454	7364.67	0.0436	0.7006	0.0051
May	1.7826	7366.67	0.1974	0.0747	0.0276
June	-2.7613	7366.67	-0.3051	0.00 ⁵⁸	-0.0486
July	-1.1186	7365.67	-0.1244	0.2633	-0.0229
Aug	1.4681	7365.67	0.1629	0.1421	0.0225
Sep	-1.1302	7366.67	-0.1256	0.2584	-0.0311
Oct	1.3632	7366.67	0.1513	0.1728	0.0488
Nov	1.503	7366.67	0.1667	0.1328	0.0500
Dec	-0.1515	7366.67	-0.0179	0.8796	-0.0018
Annual	0	7366.67	0.00002	1	0.00003

Table 7: Trend analysis for Temperature data

Months	Z Score	Var S	Mann Kendall Tau	P-value	Sen's Slope
Jan	-0.83916	7361.67	-0.0939	0.4014	-0.0168
Feb	-0.18643	7365.67	-0.0218	0.8521	-0.0065
March	-1.8292	7366.67	-0.2026	0.06737	-0.0363
April	-2.0628	7362.67	-0.2288	0.03913	-0.03349
May	-0.6641	7366.67	-0.0744	0.5066	-0.0086
June	-0.4311	7366.67	-0.0487	0.6664	-0.0081
July	1.0369	7366.67	0.1154	0.2998	0.0186
Aug	1.3749	7365.67	0.1527	0.1692	0.0185
Sep	0.3496	7365.67	0.0398	0.7267	0.0054
Oct	1.0604	7364.67	0.1181	0.289	0.0244
Nov	-1.6428	7366.67	-0.1820	0.1004	-0.0299
Dec	-1.27	7366.67	-0.1410	0.2041	-0.04
Annual	-1.9926	7364.67	-0.2208	0.0463	-0.0406

Prediction analysis using ARIMA Model for Rainfall and Temperature data:

The prediction analysis for rainfall and temperature is done in the study area from 1981 to 2020 for 15 stations, using the ARIMA model that applies the data in the past to prepare forecasts. The data was analyzed with R statistical R program software.

Box Jenkins Algorithm:

The Box Jenkins (1970)^{64,65} advanced the ARIMA model. This method uses ARIMA time series models to systematically Identify, Estimate, and Check (goodness of fit)

procedures.⁶⁶ In the Identifying procedure, the ACF and PACF plots are used. The second procedure estimates the parameters of the identified models. The third procedure helps to assess the most fitted model using Ljung Box Test.⁶⁷ Finally, the best-fitting model is chosen depending on the Akaike Information Criterion (AIC) value.

ARIMA (Auto Regressive Integrated and Moving Average) is an extensively used statistical tool to analyze and predict time series data and consider serial correlation within the time series⁶⁸ and used to initiate forecasts. This approach is typically useful for short to medium-term forecasting.⁶⁹ A set of data obtained sequentially over time is called a Time series. Box Jenkins formula is applied to generate a pattern and structure of the time series data collected and examine the best-fit model and forecast. This process is indicated in Table 8.

Table 8: Box Jenkins Algorithm^{64,70}

1. Plot series.
2. Is variance stable?
 - 2a. No, Apply Transformation, go to 1.
 - 2b. Yes, continue.
3. Obtain ACFs and PACFs.
4. Is mean stationary?
 - 4a. No, Apply Regular and Seasonal differencing.
 - 4b. Yes, continue.
5. Model Selection.
6. Estimate Parameter Values.
7. Are Residuals Uncorrelated?
 - 7a. No, Modify Model, go to 5.
 - 7b. Yes, continue.
8. Are Parameters Significant and Uncorrelated?
 - 8a. No, Modify Model, go to 5.
 - 8b. Yes, continue.
9. Forecast.

Prediction analysis for Rainfall data:

The first step is to plot the data, and as it occurs in time, it is called a time plot. The time series plot for monthly rainfall and temperature calculated from 1981 to 2020 is shown in Figures 7 and 8, respectively. From the figures, it could be observed that the time series plot for rainfall and temperature, which are volatile, is an indication of seasonality. The series generally shows the rise and fall of monthly precipitation and temperature in the study area over the years.

We can endorse the non-seasonality behavior to select the best-fit model by computing the Auto Correlation Function (ACF) and Partial Auto Correlation Function (PACF). As the model selection is vital, and to achieve it, the analysis of ACF and PACF needs to be appropriately applied.⁷⁰ and the ACF and PACF plots for rainfall and temperature in Tables 9 and 10.

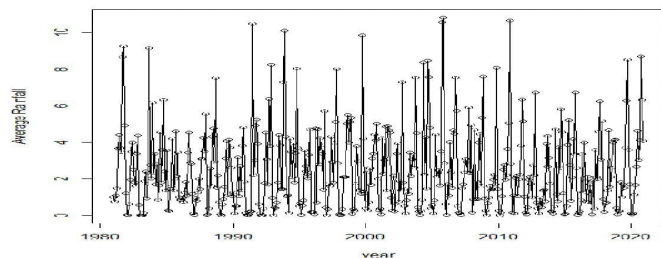


Figure 7: Time series plot for rainfall data

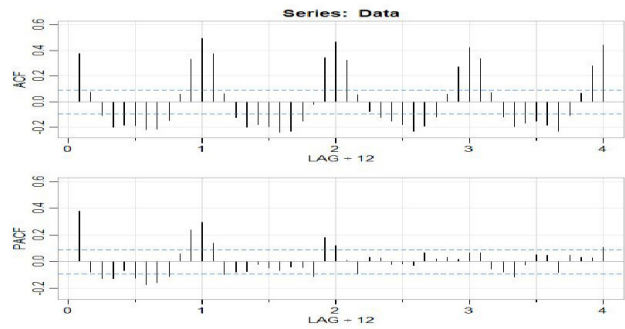


Figure 8: Time series plot for temperature data

Table 9: ACF and PACF plot for rainfall data

Lag	ACF	PACF	Lag	ACF	PACF	Lag	ACF	PACF	Lag	ACF	PACF
1	0.38	0.38	25	0.33	0.01	13	0.38	0.14	37	0.34	0.07
2	0.08	-0.08	26	0.06	-0.09	14	0.06	-0.10	38	0.07	-0.05
3	-0.11	-0.13	27	-0.08	0.03	15	-0.12	-0.08	39	-0.12	-0.08
4	-0.20	-0.13	28	-0.12	0.03	16	-0.20	-0.08	40	-0.19	-0.12
5	-0.18	-0.07	29	-0.15	-0.02	17	-0.18	-0.02	41	-0.17	-0.02
6	-0.19	-0.12	30	-0.18	-0.02	18	-0.19	-0.05	42	-0.15	0.05
7	-0.22	-0.17	31	-0.23	-0.03	19	-0.24	-0.07	43	-0.18	0.05
8	-0.21	-0.16	32	-0.19	0.06	20	-0.23	-0.04	44	-0.23	-0.08
9	-0.15	-0.11	33	-0.12	0.02	21	-0.15	-0.04	45	-0.11	0.05
10	0.06	0.06	34	0.06	0.03	22	-0.02	-0.11	46	0.07	0.03
11	0.33	0.24	35	0.27	0.02	23	0.34	0.18	47	0.28	0.03
12	0.50	0.30	36	0.43	0.07	24	0.47	0.12	48	0.44	0.11

Table 10: ACF and PACF plot for temperature data

Lag	ACF	PACF	Lag	ACF	PACF	Lag	ACF	PACF	Lag	ACF	PACF
1	0.68	0.68	25	0.55	-0.10	13	0.56	-0.07	37	0.53	0.00
2	0.31	-0.27	26	0.26	-0.01	14	0.25	-0.14	38	0.24	-0.09
3	-0.05	-0.28	27	-0.05	-0.02	15	-0.08	-0.09	39	-0.09	-0.11
4	-0.34	-0.21	28	-0.30	-0.02	16	-0.33	-0.04	40	-0.34	-0.06
5	-0.47	-0.10	29	-0.43	0.00	17	-0.47	-0.06	41	-0.46	0.02
6	-0.50	-0.20	30	-0.48	0.03	18	-0.51	-0.04	42	-0.48	0.01
7	-0.49	-0.27	31	-0.45	0.07	19	-0.50	-0.09	43	-0.46	-0.03
8	-0.37	-0.12	32	-0.33	-0.01	20	-0.37	-0.06	44	-0.34	0.02
9	-0.09	0.12	33	-0.08	0.04	21	-0.12	-0.04	45	-0.07	0.07
10	0.25	0.20	34	0.22	-0.07	22	0.23	0.09	46	0.23	-0.04
11	0.56	0.25	35	0.51	0.02	23	0.57	0.19	47	0.54	0.13
12	0.71	0.22	36	0.66	0.12	24	0.70	0.11	48	0.67	0.06

The time series ACF and PACF plots for the monthly rainfall and temperature from 1981 to 2020 are observed, and the same is given in Figures 9 and 10, respectively. From the figures, it could be observed that most of the spikes of ACF and PACF plots are outside the confidence limits. It is also seen that the ACF shows a wave-like pattern of variation. It offers a significant autocorrelation time series plot of monthly Rainfall and temperature from January 1981 to December 2020 with $d = 0$ and $D = 0$.

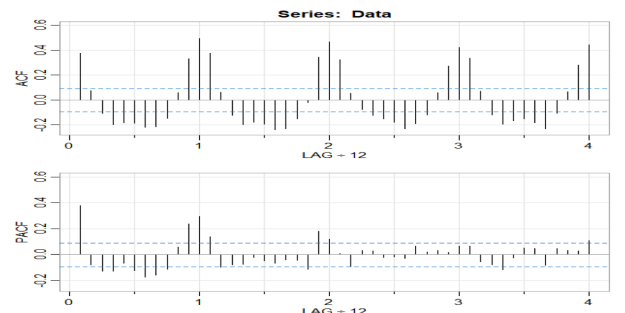


Figure 9: Time series ACF and PACF plot for rainfall data with Seasonal Differencing

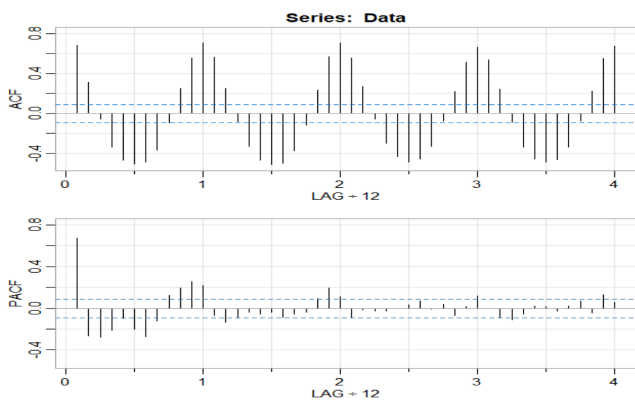


Figure 10: ACF and PACF plot for temperature data with Seasonal Differencing

Augmented Dickey-Fuller Test:

The Augmented Dickey-Fuller test (ADF), a unit root test (whether a time series is stationary or non-stationary), allows accepting or rejecting the null hypothesis of stationarity in a time series for validation⁷¹ and the same method is used in the present study. The ADF test will give a negative number on which the rejection of the hypothesis depends. This test uses two assumptions, the Null hypothesis, where the series is non-stationary, and the Alternative hypothesis, where the series is stationary.⁷² In the present study, the same test is done using an algorithm designed using R programming software.

Stationarity plays an essential role in time series analysis,⁷² and one can test the stationarity of time series data using the unit root test proposed by Dickey and Fuller in 1979.⁷³ The author^{74,75,76} have used Dickey Fuller Test to forecast the rainfall pattern for the monthly weekly, and daily monsoon time series for 14 years. The same methodology is used in this research.

Rainfall

data: Data

Dickey-Fuller = -12.452, Lag order = 7, p-value = 0.01

alternative hypothesis: stationary

The test statistic is -12.452, and the P-value is 0.01

Since the p-value is less than .05, it could be inferred that the Monthly Rainfall data is Stationary.

Temperature

data: Data

Dickey-Fuller = -14.514, Lag order = 7, p-value = 0.01

alternative hypothesis: stationary

The test statistic is -14.514, and the P-value is 0.01

Since the p-value is less than .05, hence, conclude that Monthly Temperature data is Stationary.

Model Fit for Rainfall:

The 8 Identified ARIMA models were listed in Table 11 for monthly rainfall data. It could be observed that only ARIMA (1,0,1)(1,0,1)₁₂ has met the assumptions of the model diagnostics. The Best Model for the data is ARIMA (1,0,1)(1,0,1)₁₂ with an AIC score of 1855.23, as it has met the assumptions of the model diagnostics.

Table 11: ARIMA models for rainfall data

Model	AIC Value
(1,0,1) (1,0,1)₁₂	1855.23
(1,0,2) (1,0,1) ₁₂	1856.78
(1,0,1) (1,0,2) ₁₂	1856.62
(1,0,2) (1,0,2) ₁₂	1858.23
(1,0,0) (1,0,0) ₁₂	1970.18
(1,0,0) (0,0,1) ₁₂	2004.73
(0,0,1) (1,0,0) ₁₂	1970.83
(0,0,1) (0,0,1) ₁₂	2006.48

Model Fit for Temperature:

The 8 Identified ARIMA models were listed in Table 12., for monthly temperature data. It could be observed that only ARIMA (1,0,1)(1,0,1)₁₂ has met the assumptions of the model diagnostics. The Best Model for the data is ARIMA (1,0,1)(1,0,1)₁₂ with an AIC score of 1768.57, as it has met the assumptions of the model diagnostics.

Table 12: ARIMA models for temperature data

Model	AIC Value
(1,0,1) (1,0,1)₁₂	1768.57
(1,0,2) (1,0,1) ₁₂	1770.34
(1,0,1) (1,0,2) ₁₂	1770.53
(1,0,2) (1,0,2) ₁₂	1772.29
(1,0,0) (1,0,0) ₁₂	1941.11
(1,0,0) (0,0,1) ₁₂	2017.60
(0,0,1) (1,0,0) ₁₂	1965.66
(0,0,1) (0,0,1) ₁₂	2065.40

Residual Plot:

The residual plots of monthly rainfall and temperature data are shown in Figures 11 and 12, respectively. The results shown in the figures are derived by following the method adopted by the author.⁷⁷ The mean of the residuals is close to zero, and there is no significant correlation in the residual series in the study area. It can be observed from the figure that, in the Standardized Residuals, a sizeable positive residual is seen in 1992 and 1994 for monthly rainfall and temperature, respectively. The time series showing a wave-like pattern is evidence of seasonality. The ACF of the residuals graph shows a periodic pattern that might be due to the seasonal effect. In this study, the Ljung-Box test (a test employed to check the independence of the residuals) is based on a Q-Q plot where the p-value is proportionately large.

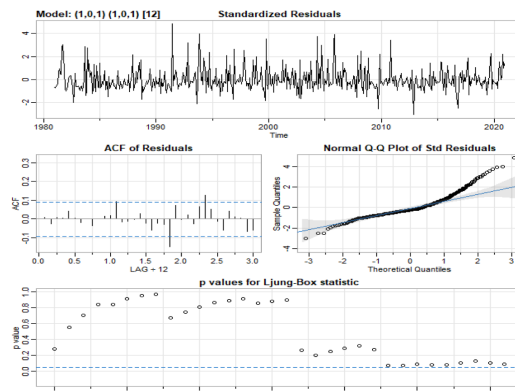


Figure 11: Residual plots for rainfall data

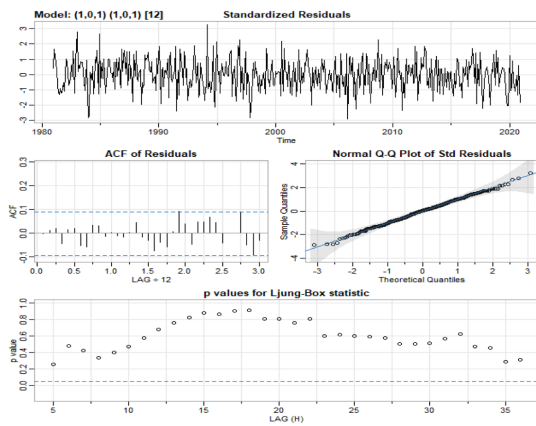


Figure 12: Residual plots for temperature data

Forecast:

The term forecast refers to predicting the future monthly rainfall and temperature of the studied time series. Forecasting is vital in decision-making and planning processes in all socio-economic sectors. The best-fitting model based on AIC is selected. As per the suggestion by the author,⁷⁸ the model with the smallest AIC, and the same procedure is followed in the present research study. The study⁷⁹ also supports that the selection of the best-fit model is strongly associated with the best performance of the residual analysis.

Forecast for monthly Rainfall:

The ARIMA (1,0,1)(1,0,1)₁₂ with the minimum AIC (1855.23), the best model, is used to forecast the Monthly Rainfall for the next five years- 2021, 2022, 2023, 2024, and 2025. Figure 13 and Table 13 show the forecasted plots for monthly rainfall in the study area. The black line indicates the actual values and the red line depicts the predicted values. The monthly rainfall in the study area varies from about 700 mm to 1600 mm. It is maximum during the Northeast Monsoon Seasons- highest in October & November and gradually decreases in December. The rainfall distribution is found to be minimum in the northeast and progressively increases towards the South and Southwestern regions in the study area.

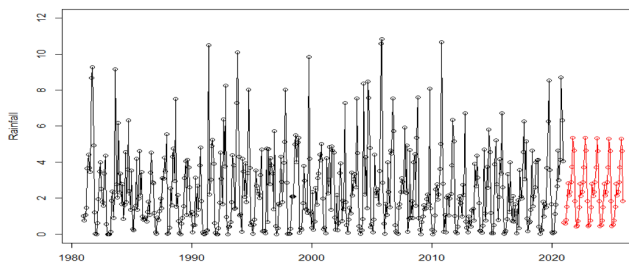


Figure 13: Forecast plots for monthly rainfall

Table 13: Forecast analysis for monthly rainfall

Month	2021	2022	2023	2024	2025
Jan	0.6545544	0.425139	0.4358805	0.4466577	0.4573767
Feb	0.6010922	0.4866647	0.4971189	0.5075653	0.5179553
March	0.791974	0.7361717	0.7453017	0.7544077	0.7634646
April	1.5253757	1.4966402	1.5016751	1.506696	1.5116898
May	2.8277935	2.8081616	2.8061194	2.804095	2.8020816
June	2.1407954	2.1332675	2.1348736	2.1364746	2.138067
July	2.3563189	2.3519925	2.352419	2.3528451	2.3532688
Aug	28.896896	28.84753	28.82303	28.798672	28.774445
Sep	37.260208	37.177482	37.107997	37.038892	36.97016
Oct	536.14982	534.50066	532.92696	531.36178	529.80506

Nov	465.41092	464.17577	462.9819	461.7945	460.6135
Dec	18.290816	18.321541	18.3539	18.386086	18.41181

Forecast for monthly temperature:

The ARIMA (1,0,1)(1,0,1)₁₂ with the minimum AIC (1768.57), the best model, is used to forecast the Monthly Temperature for the next five years- 2021, 2022, 2023, 2024, and 2025. Figure 14 and Table 14 show the forecasted plots for monthly temperature in the study area. The black line indicates the actual values and the red line depicts the predicted values. The average annual temperature in the study area is 21°C. It is maximum during April, followed by May and June.

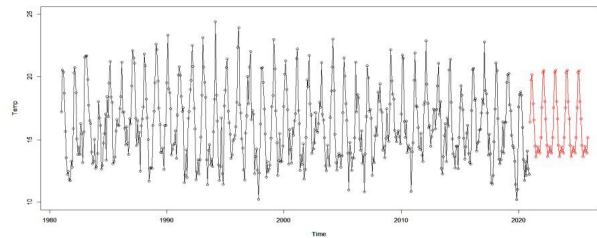


Figure 14: Forecast plots for monthly temperature

Table 14: Forecast analysis for monthly temperature

Month	2021	2022	2023	2024	2025
Jan	16.42864	17.52006	17.51992	17.51889	17.51787
Feb	19.75487	20.35547	20.35282	20.3498	20.34654
March	20.17596	20.50636	20.50337	20.5002	20.49687
April	37.83752	38.02051	38.01926	38.01786	38.01646
May	36.57904	36.68055	36.68023	36.67983	36.67943
June	34.49583	34.55334	34.55457	34.55575	34.55693
July	33.61528	33.64826	33.65015	33.652	33.65388
Aug	20.01704	20.03581	20.03739	20.03896	20.04053
Sep	14.45313	14.46389	14.46515	14.4664	14.46765
Oct	14.15611	14.16273	14.16421	14.16568	14.16715
Nov	13.93113	13.93568	13.93733	13.93897	13.94061
Dec	15.19346	15.19577	15.19648	15.19718	15.19789

Action Plans towards SDG 13-Climate Change, undertaken by the Government of Tamil Nadu:

A. The Centre for Environmental Information System (ENVIS), Tamil Nadu,⁸⁰ has taken steps to combat climate change and those following.

1. Tamil Nadu State Climate Change Cell (TNSCCC)⁸⁰ Realizing the importance of the impact of climate change, the Department of Environment (DoE), Government of Tamil Nadu has initiated Tamil Nadu State Climate Change Cell (TNSCCC) responding to the call of India's National Action Plan on Climate Change (NAPCC). The vision of the cell is to respond to global climate change by building capacity at the local level, particularly in the context of Tamil Nadu State, and to make it a resilient state to combat climate change. This will be addressed through effective climate change governance and climate services by connecting climate change science- policy-society by the climate change cell. However, the cell's mission is to establish a platform to collect, collate and disseminate climate change information about Tamil Nadu State to various stakeholders ranging from farmers, fishermen, general public to policy planners, decision-makers, bureaucrats, and others to enable effective climate change governance and services.

2. Climate Change Adaptation in Rural Areas of India (CCARAI) Project⁸⁰

CCARAI is an Indo-German development project that aims to strengthen the efforts of rural communities in India to cope with climate variability and change. The project has different components, such as preparing action plans on climate change, vulnerability, and risk assessments, climate adaptation measures, climate-proofing public investments, financial instruments for adaptation, information on knowledge management, and human capacity building.

3. State Action Plans on Climate Change (SAPCC)⁸⁰

This would help identify measures that promote development objectives while yielding co-benefits for addressing climate change effectively and outlines particular regional and local characteristics and specific concerns of vulnerable sectors and communities within each State.

B. The Government of Tamil Nadu State Action Plan on Climate Change (TNSAPCC)⁸⁰ has initiated adaptation strategies regarding the Sustainable Development Goal 13-Climate Action, to achieve targets 13.1, 13.2, and 13.3. Those include:

1. Tamil Nadu Green Climate Company (TNGCC)⁸¹ is framed to catalyze public and private financing to implement climate actions. This provides incremental funding for exclusive climate adaptation and mitigation actions and forging partnerships and capacities to implement such measures effectively.

2. The National Adaptation Fund for Climate Change (NAFCC)⁸¹ on Coastal Area Management is framed to assess vulnerability to climate change on coastal ecosystems and coastal communities.

3. Promotion of Electric Vehicles for public and private transport has been another approach to moving towards renewable energy sources to improve climate resilience.⁸¹

4. Promotion of Green spaces and protection of Wetlands are some of the other interventions initiated by the State that are closely linked to climate resilience.⁸¹

5. The Department of Environment and Climate Change works to formulate Early Warning Systems to reduce the impact of extreme weather events. The State will move closer to the Target of "0" as determined by the National Indicator Framework to strengthen the resilience and adaptive capacity to climate-related hazards and natural disasters.⁸¹

6. The State focuses on developing Early Warning Systems and Risk Management to monitor climate shocks.⁸¹

7. The Government of Tamil Nadu has taken the initiative to set up an exclusive Climate Change Research Center, "The Centre for Climate Change and Adaptation Research (renamed as Centre for Climate Change and Disaster Management (CCCDM), to strengthen the understanding of climate change and our capacity to manage and adapt to it. The Climate Studio is one of its kind, established with a high-performance computation facility cluster with storage and accessories for climate modeling at the district and blocks level.⁸¹

8. Tamil Nadu Government started the Eco clubs - National Green Corps (NGC), the first of its kind in India. This program imparts environmental awareness to school students through on-campus and community activities like awareness

programs, tree planting, celebrating Green Days, eco competitions, eco camps, etc., The NGC Eco clubs will also help and support the creation and maintenance of nutri-gardens in the schools with native species of trees and local vegetables wherever possible.⁸¹

9. Chief Minister's Green Fellowship Programme (CMG-FP) aims to disseminate climate change awareness by means and ways to attract younger generations and students and to create a pool of green ideas and technological interventions that will reduce the Environment, Climate change impacts, and conserve Nature.⁸¹

10. The Climate Smart Villages would serve as demo sites to test an approach through participatory methods with various technological and institutional options for dealing with climate change at the community level.⁸¹

11. Sustainable Habitat –Energy saving measures in Government and Private buildings, residents – independent, and apartments are practiced to reduce greenhouse emissions from energy production and consumption to reduce the impacts of Climate Change.⁸¹

■ Conclusion

In the present study, an attempt is made to analyze the trend and prediction of rainfall and temperature using statistical techniques like-Homogeneity test, Box and Whisker Plot test, Coefficient of Variability, Cluster Dendrogram, Mann-Kendall, Sen's slope, and ARIMA model in Dindigul district, Tamil Nadu, India. The rainfall and temperature data are collected from 15 rainfall stations spread across the district for 39 years, from 1981 to 2020. The present study has used techniques admired worldwide by scientists for providing high-precision results. The primary and essential requirement for the management and developmental planning of any region in recent times sectors is the exploration of the spatiotemporal distribution and changing patterns of climatic variables, their trends, and forecast. This study would be helpful to assist the policy and decision-makers establish strategies and priorities to combat the changes in rainfall and temperature patterns in the study area and their stress on global climatic change.

■ Acknowledgments

Harnishya Palanichamy thanks her mother for her guidance in downloading climatic data and preparing the study area map.

■ References

1. United Nations, Climate Action, What is Climate Change? <https://www.un.org/en/climatechange/what-is-climate-change>
2. IPCC, (2007) Climate Change 2007: Impacts, Adaptation and Vulnerability. Contribution of Working Group II to the Fourth Assessment Report of the Intergovernmental Panel on Climate Change. Edited by Parry M, Canziani O, Palutikof J, Linden P, et al, Cambridge University Press, 32 Avenue of the Americas, New York. 10013-2473.
3. UN Fact sheet, (2010). Women, gender inequality and climate change. <http://www.un.org/womenwatch/>. Accessed 15 Apr 2019.
4. Vaibhav Bangar., Rajat Goyal., & Rajiv Pandey. (2020). Climate Change Responses and Sustainable Development: Integration of Mitigation and Adaptation, Chapter 13, Sustainable Development Goals- An Indian Perspective, Edited by Somnath Hazra Anindya

- a Bhukta, ISBN 978-3-030-42488-6 (eBook) <https://doi.org/10.1007/978-3-030-42488-6>
5. IPCC, (2007). Climate Change 2007: Climate Change Impacts, Adaptation and Vulnerability. Working Group II Contribution to the Intergovernmental Panel on Climate Change 4th Assessment Report. Summary for Policymakers. 23.
 6. Diah, M.O., & Kumar, A. (2020). Exploring greenhouse gas mitigation strategies for agriculture in Africa: the case of Nigeria. *Ambio*. <https://doi.org/10.1007/s13280-019-01293-9>
 7. Cherie, G.G., Fentaw, A. (2015) Climate change impact assessment of dire dam water supply. AAUCED HES, Ethiopia.
 8. UN Summit, (2015). Transforming our World: The 2030 Agenda for Sustainable Development, United Nations Summit for the adoption of the post-2015 development agenda. <https://www.un.org/sustainabledevelopment/climate-change/>
 9. SDG India Index & Dashboard (2020-21), Partnerships in the decade of action. NITI Aayog 2021, Government of India, Sansad Marg, New Delhi, India, sdgindiaindex.niti.gov.in.
 10. Babar, S.F., & Ramesh, H. (2013). Analysis of southwest monsoon rainfall trend using statistical techniques over the Nethravathi basin. *International Journal of Advanced Technology in Civil Engineering*, 2(1), 2231-5721.
 11. Kumar, V., Jain, S.K., & Singh, Y. (2010). Analysis of long-term rainfall trends in India. *Hydrological Sciences Journal*, 55(4), 484-496.
 12. NAPCC (2008). <https://www.ncbi.nlm.nih.gov/pmc/articles/PMC2822162>
 13. Brief industrial profile, Dindigul district. (2012-13) <http://dcmsme.gov.in/old/dips/IPS%20dindigul%202012.pdf>
 14. District Diagnostic Report. (2021) <https://www.tnrt.org/documents/>
 15. Kumar, R., & Gautam, H.R. (2014). Climate change and its impact on agricultural productivity in India. *Journal of Climatology and Weather Forecasting*, 2, 109. <https://doi.org/10.4172/2332-2594.1000109>
 16. Birhanu, D., Kima, H., Jangb, C., & Park, P. (2016). Flood risk and vulnerability of Addis Ababa city due to climate change and urbanization. *Proc Eng.*, 154:696-702.
 17. IPCC, (2001). Climate change 2001: the scientific basis. Contribution of working group I to the third assessment report of the Intergovernmental Panel on climate change. Cambridge, United Kingdom and New York, NY, USA: Cambridge University Press.
 18. Karmeshu., & Neha, N. (2015). Trend Detection in Annual Temperature & Precipitation Using the Mann Kendall Test – A Case Study to Assess Climate Change on Select States in the Northeastern United States. *Mausam* 66, no.11-16. http://repository.upenn.edu/mes_capstones/47
 19. Szabó, S., Elemér, L., Kovács, Z., Püspöki, Z., Kertész, A., Singh, S.K. & Balázs, B. (2019). NDVI dynamics as reflected in climatic variables: spatial and temporal trends – a case study of Hungary. *GIS Science & Remote Sensing*, 56, 624-644. <https://doi.org/10.1080/15481603.2018.1560686>
 20. Gromko., Abdurasulova., Gromko, D., & Abdurasulova, G. (2019). Climate change mitigation and food loss and waste reduction: exploring the business case, *Sustainable Development Goals- An Indian Perspective*, Somnath Hazra Anindya Bhukta Editors ISBN 978-3-030-42487-9 ISBN 978-3-030-42488-6 (eBook). <https://doi.org/10.1007/978-3-030-42488-6>
 21. Gary Feng., Stacy Cobb., Zaid Abdo., Daniel K. Fisher, Ying Ouyang., Ardeshir Adeli., & Johnie N. Jenkins (2016). Trend analysis and forecast of precipitation, reference evapotranspiration, and rainfall deficit in the Blackland Prairie of Eastern Mississippi. *J. Appl. Meteorol. Clim.*, 55, 1425-1439, <https://doi.org/10.1175/JAMC-D-15-0265.1>
 22. Jones, P. (1999). The instrumental data record: its accuracy and use in attempts to identify the “CO2 signal”. In: *Analysis of climate variability*. Springer, Berlin, 53-76.
 23. Lazaro, R., Rodrigo, F.S., Gutierrez, L., Domingo, F., & Puigdeabargas, J. (2001). Analysis of a 30-year rainfall record (1967-1997) in semiarid SE Spain for implications on vegetation. *J. Arid Environ.* 48 (3), 373-395.
 24. Hans Alexandersson., (1986). A homogeneity test was applied to precipitation data. *Int J Climatol* 6(6):661-675.
 25. Buishand, T.A. (1982). Some methods for testing the homogeneity of rainfall records. *J Hydrol* 58(1):11-27.
 26. Mohammad Atiqur Rahman., Lou Yunsheng., & Nahid Sultana. (2017). Analysis and prediction of rainfall trends over Bangladesh using Mann–Kendall, Spearman’s rho tests and ARIMA model, *Meteorol Atmos Phys.*, 129:409-424.
 27. Annie Jenifer, M. & Madan, K. Jha. (2021). Assessment of precipitation trends and its implications in the semi-arid region of Southern India, *Environmental Challenges*, 5 100269.
 28. Bushra Praveen., Swapantalukdar., Shahfahad., Susanta Mahato., Jayanta Mondal., Pritee Sharma., Abu Reza Md., Towfiquel Islam & Atiqur Rahman. (2020). Analyzing trend and forecasting of rainfall changes in India using non-parametrical and machine learning approaches, *Scientific Reports* 10:10342 <https://doi.org/10.1038/s41598-020-67228-7>
 29. Amit Gangarde., Saha Dauji., & Londhe, S.N. (2020). Roorkee Water Conclave 2020, Organized by the Indian Institute of Technology Roorkee and the National Institute of Hydrology, Roorkee during February 26-28.
 30. Neel Kamal., & Sanjay Pachauri. (2019). Mann-Kendall, and Sen's Slope Estimators for Precipitation Trend Analysis in the North-Eastern States of India, *International Journal of Computer Applications*, (0975-8887), 177(11).
 31. Arpita Panda & Netranand., (2019). Trend analysis of seasonal rainfall and temperature pattern in Kalahandi, Bolangir and Koraput districts of Odisha, India, *Atmos Sci Lett.* e932.
 32. Afrifa-Yamoah., Ebenezer., Saeed., Bashiru., & Azumah, Karim. (2016). Sarima Modelling and Forecasting of Monthly Rainfall in the Brong Ahafo Region of Ghana. *World Environment*. 6. 1-9. [10.5923/j.env.20160601.01](https://doi.org/10.5923/j.env.20160601.01).
 33. Abha Sinha., Anjani Kumari., Somnath Mahapatra., Singh, H.P., & Birendra Bhart. (2019). Temporal Rainfall Variability and Its Correlation with Temperature over Ranchi, Jharkhand, *International Journal of Engineering and Advanced Technology (IJEAT)* ISSN: 2249-8958 (Online), 9(2), 1099 Published By: Blue Eyes Intelligence Engineering & Sciences DOI: 10.35940/ijeat.B3429.129219
 34. Amogne Asfaw., Belay Simane., Ali Hassen., & Amare Bantide. (2018). Variability and time series trend analysis of rainfall and temperature in northcentral Ethiopia: A case study in Woleka sub-basin. *Weather and climate extremes*, 19, 29-41.
 35. Mohammed Achite., Tommaso Caloiero., Andrzej Wał., Nir Kraukauer & Tarek Hartani. (2021). Analysis of the spatiotemporal Annual Rainfall Variability in the Wadi Cheliff Basin, Algeria, *Water* 2021, 13, 1477. <https://doi.org/10.3390/w13111477>
 36. Abhishek, A., Pathak, B., & Dodamani, M. (2020). Trend analysis of rainfall, rainy days and drought: A case study of Ghataprabha River Basin, India. *Modelling Earth Systems and Environment* 6:1357-1372. <https://doi.org/10.1007/s40808-020-00798-7>
 37. Observed Rainfall Variability and Changes over Kerala State (Met Monograph No.: ESSO/IMD/HS/Rainfall Variability/14(2020)/38) and West Bengal (Met Monograph No.: ESSO/IMD/HS/Rainfall Variability/29(2020)/53), Climate Research and Services India Meteorological Department Ministry of Earth Sciences, Pune.

38. Zinabu Assefa Alemu., & Michael O. Dioha. (2020). Climate change and trend analysis of temperature: the case of Addis Ababa, Ethiopia, *Environ Syst Res.*, 9:27.
39. Sahu, N., Saini, A., Behera, S., Sayama, T., Nayak, S., Sahu, L., Duan, W., Avtar, R., Yamada, M., & Singh, R.B. (2020). Impact of Indo-Pacific climate variability on rice productivity in Bihar, India. *Sustainability*, 12, 7023.
40. Getachew, B. (2018). Trend analysis of temperature and rainfall in south Gonder zone, Ethiopia. *J Degraded Mining Lands Manag.*, <https://doi.org/10.15243/jdmlm.2018.052.1111>
41. Caloiero, T., Coscarelli, R., & Ferrari, E. (2018). Application of the Innovative Trend Analysis Method for the Trend Analysis of Rainfall Anomalies in Southern Italy. *Water Resour. Manag.*, 32, 4971-4983.
42. Agossou Gadedjisso-Tossou., Komlavi Adjegan., & Armand Ketcha Malan Kablan. (2021). Rainfall and Temperature Trend Analysis by Mann-Kendall Test and Significance for Rainfed Cereal Yields in Northern Togo, *Sci*, 3, 17. <https://doi.org/10.3390/sci3010017>
43. Mudbhatal, A., & Amai, M. (2018). Regional climate trends and topographic influence over the Western Ghats catchments of India. *Int. J. Climatol.*, 38, 2265-2279.
44. Meena, H.M., Machiwal, D., Santra, P., Moharana, P.C., & Singh, D.V. (2018). Trends and homogeneity of monthly, seasonal, and annual rainfall over the arid region of Rajasthan, India. *Theor. Appl. Climatol.*, 136, 795-811.
45. Sen, P.K. (1968). Estimates of the regression coefficient based on Kendall's, *Journal of American Statistical Association*, 63:1379-1389.
46. Sen, Z. (2014). Trend identification simulation and application. *J. Hydrol. Eng.*, 19(3), 635-642.
47. Alhaji, U.U., Yusuf, A.S., Edet, C.O., Oche, C.O., & Agbo, E.P. (2018). Trend analysis of temperature in Gombe State using the Mann-Kendall trend test. *J Sci Res Rep.*, 20(3):1-9.
48. Kuriqi, A., Ali, R., & Pham, Q.B. (2020). Seasonality shift and stream flow variability trends in central India. *Acta Geophys.*, <https://doi.org/10.1007/s11600-020-00475-4>
49. Madhusudhan, M., Ningaraju, H.J., & Shashank Patil, M. R. (2021). Analysis of Rainfall Trend Series using Mann-Kendall and Sen's Slope Estimator Statistical Test in Mandya District, Karnataka, *International Research Journal of Engineering and Technology (IRJET)*, 8.
50. Nusrat Batool., Shamim Ahmad Shah., Sajad Nabi Dar., & Safya Skinde.r. (2019). Rainfall variability and dynamics of cropping pattern in Kashmir Himalayas: a case study of climate change and agriculture. *SN Applied Sciences*, 1:606. | <https://doi.org/10.1007/s42452-019-0599->
51. Nury, A. H., Koch, M., & Alam, M. J. B. (2020). In 4th International Conference on Environmental Aspects of Bangladesh. 4 (BE NJapan).
52. Pandey, B. K. & Khare, D. (2018). Identification of trend in long-term precipitation and reference evapotranspiration over Narmada river basin (India). *Global and planetary change* 161, 172-182.
53. WARPO, (2006). Coastal development strategy. National Water Management Plan Project, Water Resources Planning Organization (WARPO), Ministry of Water Resources, Government of Bangladesh.
54. Feyissa, G., Zeleke, G., Bewket, W., & Gebremariam, E. (2018). Downscaling of future temperature and precipitation extremes in Addis Ababa under climate change. *Nature*, MDPI 6:58.
55. INCCA, (2010). Climate change and India: A 4x4 assessment, a sectoral and regional analysis for the 2030s. IOP Conf. Series: Materials Science and Engineering 394. <https://doi.org/10.1088/1757-899X/394/5/052024>
56. Rashid Mahmood, Shaofeng Jia & Wenbin Zhu, (2019). Analysis of climate variability, trends, and prediction in the most active parts of the Lake Chad basin, Africa, *Scientific Reports*. <https://doi.org/10.1038/s41598-019-42811-9>
57. Bari, S.H., Rahman, M.T., Hussain, M.M., & Ray, S. (2015). Forecasting monthly precipitation in Sylhet city using the ARIMA model. *J Civ Environ Res.*, 7(1):69-78.
58. Sultana, N., & Hasan, M.M. (2015). Forecasting temperature in the coastal area of Bay of Bengal-an application of Box-Jenkins seasonal ARIMA model. *J Civ Environ Res.*, 7(8):149-160.
59. Kang, H.M., Yusuf, F. (2012). Homogeneity tests on daily rainfall series in peninsular Malaysia, *International Journal for Contemporary Maths. Sci.* 7(1):9-22.
60. Girma Eshetu, Tino Johansson & Wayessa Garedeew, (2016). Rainfall trend and variability analysis in Setema-Gatira area of Jimma, Southwestern Ethiopia. *African Journal of Agricultural Research*, 11(32):3037-3045.
61. Statistica, (2001). System Reference, StatSoft, Inc, Tulsa, Oklahoma, USA, 1098.
62. Mann, H.B. (1945). Nonparametric tests against trend, *Econometrica*, 13(3):245-259
63. Kendall, M.G. (1990). Rank correlation methods, *British Journal of Psychology*, 25(1):86-91.
64. Box, G. E. P., & Jenkins, G. M. (1976). *Time Series Analysis, Forecasting and Control*, San Francisco: HoldenDay.
65. Lon-Mu Liu & Gregory B. Hudak. (1992). Forecasting and time series analysis using the SCA statistical system. *Scientific Computing Associates Corp. Vol 1:92-161.*
66. The Box- Jenkins Method, Chapter 470, NCSS statistical software.
67. Ljung G. M. & Box G. E. P. (1978). On a Measure of Lack of Fit in Time Series Models. *Biometrika*. 65:297.
68. Yurekli, K., Simsek, H., Cemek, Karaman, S. (2007). Simulating climatic variables by using a stochastic approach. *Build Environ.* 42:3493-3499.
69. Jason Brownlee, (2020). A gentle introduction to the Box and Jenkins methods for time series forecasting, <https://machinelearningmastery.com/gentle-introduction-box-jenkins-method-time-series-forecasting/>
70. Paul Andrew Panga., Shaban Nyimvua., & Isambi Mbalawata (2020). Forecasting Rainfall in Tanzania Using Time Series Approach Case Study: Dar es Salaam. *International Journal of Scientific and Innovative Mathematical Research*, 8(4):14-27.
71. Yugesh Varma. (2021). Complete guide to Dickey-Fuller Test in Time Series Analysis. <https://analyticsindiamag.com/complete-guide-to-dickey-fuller-test-in-time-series-analysis/>
72. Vijaya Kumar., G. (2021). Statistical tests to check Stationarity in Time Series. <https://www.analyticsvidhya.com/blog/2021/06/statistical-tests-to-check-stationarity-in-time-series-part-1/>
73. Erik Erhardt. (2002). Box-Jenkins Methodology vs. Rec.Sport. Unicycling 1999-2001. http://www.statacumen.com/pub/proj/WPI/Erhardt_Erik_tsaproj.pdf (accessed 10- August 2015).
74. Rob J Hyndman & George Athanasopoulos, (2018), *Forecasting: Principles and Practice*, Second Edition, Monash University, Australia.
75. Dabral, P.P., & Murry, M.Z. (2017). Modelling and forecasting of rainfall time series using SARIMA. *Environ. Process*, 4, 399-419.
76. David A. Dickey & Wayne A. Fuller, (1979). Distribution of the Estimators for Autoregressive Time Series with a unit root, *Journal of the American Statistical Association*, 74(366), 427-431 Published By: Taylor & Francis, Ltd. <https://doi.org/10.2307/22863486348>
77. Akpanta, A.C., I. E. Okorie, I.E., & Okoye, N.N. (2015). SARI

- MA Modelling of the Frequency of Monthly Rainfall in Umuahia, Abia State of Nigeria. American Journal of Mathematics and Statistics, 5(2): 82-87.
78. Samuel Olorunfemi Adams & Muhammad Ardo Bamanga, (2020). Modelling and Forecasting Seasonal Behavior of Rainfall in Abuja, Nigeria; A SARIMA Approach. American Journal of Mathematics and Statistics, 10(1): 10-19.
79. Michael Asamoah-Boaheng. (2014). Using SARIMA to Forecast Monthly Mean Surface Air Temperature in the Ashanti Region of Ghana. International Journal of Statistics and Applications, 4(6): 292-299.
80. ENVIS Centre: Tamil Nadu, State of Environment and Related Issues, Hosted by Tamil Nadu State Council for Science, Technology and Environment, Sponsored by Ministry of Environment, Forests & Climate Change, Govt of India. http://tnenvis.nic.in/Database/Climate_1209.aspx
81. Recommendations by- Department of Environment and climate change, Policy Note for 2022-23, Government of Tamil Nadu, (2022). https://cms.tn.gov.in/sites/default/files/documents/eccf_e_pn_2022_23.pdf

■ Author

The author Harnishya Palanichamy is in Grade 10 at Hebron School, Ootacamund, Tamil Nadu, India. She's passionate about computer science and research about Artificial Intelligence. Playing football, piano, debate, hiking, reading, and 3D printing are her pastime activities.

Finding the Exact Value of $\cos(\pi/7)$

Punnawit Kasean

Bowdoin College, 2016 Smith Union, Brunswick, Maine, 04011, USA; punnawit.k@dpst.ipst.ac.th
Mentor: Nantawat Udomchatpitak

ABSTRACT: The values of trigonometry function at $\pi/6$, $\pi/5$, $\pi/4$, and $\pi/3$ have simple root expressions. However, it is not easy to find a record of the value of the trigonometry function $\pi/7$. An article from Wolfram Mathworld states that $\cos(\pi/7)$ is a solution of a cubic equation without giving a root expression of $\cos(\pi/7)$. The objectives of this project are to prove that $\cos(\pi/7)$ is a solution to the cubic equation and to find a root expression $\cos(\pi/7)$. Further investigation into the cubic equation shows that the other two roots are the values of $\cos(3\pi/7)$ and $\cos(5\pi/7)$. Therefore, the scope of the study has been extended to cover the values of cosine at $\pi/7$, $3\pi/7$, and $5\pi/7$. The methods of this study consist of three steps. First, prove that $\cos(\pi/7)$, $\cos(3\pi/7)$, and $\cos(5\pi/7)$ are solutions to the cubic equation using trigonometric identities. Next, find root expressions of the solutions using Cardano's method. Lastly, identify the root expressions with $\cos(\pi/7)$, $\cos(3\pi/7)$, and $\cos(5\pi/7)$. The result shows that the value of $\cos(\pi/7)$ can be written in two forms: one with ω and another without ω ,

where $\omega = \frac{-1+i\sqrt{3}}{2}$. More explicitly,

$$\cos(\pi/7) = \frac{1}{6} \left(1 - \sqrt[3]{\frac{7}{2}} \cdot 2\operatorname{Re}(z\omega) \right) \text{ and } \cos(\pi/7) = \sqrt{\frac{1}{2} - \frac{1}{12} \left(1 - \sqrt[3]{\frac{7}{2}} \cdot 2\operatorname{Re}(z) \right)}$$

where $z = \sqrt[3]{1+3\sqrt{3}i}$. Here $z = \sqrt[3]{1+3\sqrt{3}i}$ is defined to be the cube root of $1+3\sqrt{3}i$ that

lies in the first quadrant of the complex plane and $\operatorname{Re}(z)$ referred to as the real part of the imaginary number z . The exact values of $\operatorname{Re}(z)$, $\operatorname{Re}(z\omega)$, and $\operatorname{Re}(z\omega^2)$, are determined later. Hence, the exact value of $\cos(\pi/7)$ can be rewritten more precisely as

$$\cos(\pi/7) = \frac{1}{6} \left[1 - 2\sqrt{7} \cos\left(\frac{\arctan(3\sqrt{3}) + 2\pi}{3}\right) \right]$$

and

$$\cos(\pi/7) = \sqrt{\frac{1}{2} - \frac{1}{12} \left(1 - 2\sqrt{7} \cos\left(\frac{1}{3} \arctan(3\sqrt{3})\right) \right)}.$$

KEYWORDS: Mathematics; Algebra; Cubic equation; Cardano's method; Exact value of cosine at $\pi/7$, $3\pi/7$, and $5\pi/7$.

■ Introduction

The values of trigonometric functions at $\pi/6$, $\pi/5$, $\pi/4$, and $\pi/3$ have simple root expressions. However, it is not easy to find a record of the values of trigonometric functions at $\pi/7$. That makes this problem interesting and challenging. Moreover, the solution to this problem will broaden trigonometric knowledge. An article from Wolfram Mathworld states that $\cos(\pi/7)$ is a solution of a cubic equation and $\sin(\pi/7)$ is a

solution of a sextic equation without giving root expressions of both quantities¹. It is easier to solve the cubic equation for $\cos(\pi/7)$ and then use a trigonometric identity $\sin^2(x) + \cos^2(x) = 1$ to find $\sin(\pi/7)$. So this project is aimed to find only the exact value of $\cos(\pi/7)$.

Quadratic equations are easy to solve by factoring or using the formula $x = \frac{-b \pm \sqrt{b^2 - 4ac}}{2a}$ where the quadratic equation

is. However, doing so for cubic equations is not easy at all. Therefore, Cardano’s method is introduced in this project to solve the cubic equation.

Several concepts about complex numbers are also introduced in this project. Complex numbers are numbers with a real part and an imaginary part written as $z = a + bi$ where $a, b \in \mathbb{R}$ and i is the $\sqrt{-1}$. a is the real part and b is the imaginary part of the imaginary number z . Imaginary numbers can be expressed in other forms.

$$a + bi = r(\cos \theta + i \sin \theta) = re^{i\theta}$$

Where the radius $r = \sqrt{a^2 + b^2}$ and θ is the angle that a complex vector makes with the real axis in the complex plane counterclockwise.

In addition, cube roots of unity are constantly used throughout the work. Cube roots of unity are the solutions to the equation $x^3 - 1 = 0$. They are $1, \omega$, and ω^2 where $\omega = \frac{-1 + i\sqrt{3}}{2}$ and $\omega^2 = \frac{-1 - i\sqrt{3}}{2}$. Cube roots of unity have a significant geometric application to this project. When we multiply two imaginary numbers, their lengths are multiplied, and their angles are added. ω , and ω^2 with a radius of one make angles of $\frac{2\pi}{3}$ and $\frac{4\pi}{3}$ radians respectively with the real axis in the complex plane. So, when we multiply a complex number with ω , and ω^2 , the result has the same radius but is rotated by $\frac{2\pi}{3}$ and $\frac{4\pi}{3}$ radians respectively.

Methods

Firstly, verify that $\cos(\pi/7), \cos(5\pi/7),$ and $\cos(3\pi/7)$ are solutions of the cubic equation $8x^3 - 4x^2 + 1 = 0$. Then, solve the cubic equation using Cardano’s method.² After that, identify a root expression by algebraic evaluation with $\cos(5\pi/7)$. After obtaining the value of $\cos(5\pi/7)$, use trigonometric identities to derive the value of $\cos(5\pi/7)$ to obtain the values of $\cos(\pi/7)$ and $\cos(3\pi/7)$. Lastly, identify the other two root expressions with $\cos(\pi/7)$ and $\cos(3\pi/7)$ by analyzing in the complex plane

Results and Discussions

Show that $\cos(\pi/7), \cos(3\pi/7),$ and $\cos(5\pi/7)$ are solutions of the cubic equation $8x^3 - 4x^2 + 1 = 0$.

First, define $A = \pi/7$. Get $\pi - 3A = 4A$.

Take cosine function to both sides.

$$\begin{aligned} \cos(\pi - 3A) &= \cos(4A) \\ -\cos(3A) &= \cos(4A) \end{aligned}$$

Since $\cos(4A) = \cos(2 \cdot 2A) = 2\cos^2(2A) - 1$, it follows that $2\cos^2(2A) + \cos(3A) - 1 = 0$.

From $\cos(3A) = 4\cos^3(A) - 3\cos(A)$, get $2\cos^2(2A) + 4\cos^3(A) - 3\cos(A) - 1 = 0$.

Using $(2A) = 2\cos^2(A) - 1$, obtain

$$\begin{aligned} 2[2\cos^2(A) - 1]^2 + 4\cos^3(A) - 3\cos(A) - 1 &= 0 \\ 8\cos^4(A) + 4\cos^3(A) - 8\cos^2(A) - 3\cos(A) + 1 &= 0 \\ (\cos(A) + 1)(8\cos^3(A) - 4\cos^2(A) - 4\cos(A) + 1) &= 0 \end{aligned}$$

Because $\cos(A) = \cos(\pi/7) \neq -1$, therefore

$$8\cos^3(A) - 4\cos^2(A) - 4\cos(A) + 1 = 0$$

Or

$$8x^3 - 4x^2 - 4x + 1 = 0 \text{ when } x = \cos(\pi/7).$$

Later, assume that $B = 3\pi/7$. Get $3\pi - 3B = 4B$. Take cosine function to both sides.

$$-\cos(3\pi - 3B) = \cos(4B)$$

It is the same equation as $-\cos(A) = \cos(4A)$ in the case of angle $\pi/7$ so it leads to the same equation $8x^3 - 4x^2 - 4x + 1 = 0$.

In other words, $\cos(3\pi - 7)$ is another answer of the cubic equation. In the same way, $\cos(5\pi/7)$ is one of the answers of the cubic equation as well. Therefore, the answers of the cubic equation are $\cos(\pi - 7), \cos(3\pi - 7),$ and $\cos(5\pi/7)$.

Solve the cubic equation $8x^3 - 4x^2 - 4x + 1 = 0$ by using Cardano’s method

Define $P(x) = 8x^3 - 4x^2 - 4x + 1 = 0$

Replace x with $t + 1/6$, get

$$P(x) = P\left(t + \frac{1}{6}\right) = 8t^3 - \frac{14}{3}t + \frac{7}{27}$$

Now, know that

$$8t^3 - \frac{14}{3}t + \frac{7}{27} = 0$$

Divided by eight from both sides.

$$t^3 - \frac{7}{12}t + \frac{7}{216} = 0$$

Then, define $t = u + v$, by Cardano’s method², we know that u^3 and v^3 are roots of a quadratic polynomial $y^2 + \frac{7}{216}y + \frac{343}{46,656} = 0$.

Get

$$\begin{aligned} y &= \frac{1}{2} \left(\frac{-7}{216} \pm \sqrt{\left(\frac{7}{216}\right)^2 - 4\left(\frac{343}{46,656}\right)} \right) \\ &= \frac{-7 \pm 21\sqrt{3}i}{432} \end{aligned}$$

That is a set $\{u^3, v^3\} = \left\{ \frac{-7 - 21\sqrt{3}i}{432}, \frac{-7 + 21\sqrt{3}i}{432} \right\}$.

Choose $u^3 = \frac{-7 - 21\sqrt{3}i}{432}$. Obtain

$$\begin{aligned} u &= \frac{-1}{6} \cdot \sqrt[3]{\frac{7}{2}} \cdot \sqrt[3]{1 + 3\sqrt{3}i}, \\ &= \frac{-1}{6} \cdot \sqrt[3]{\frac{7}{2}} \cdot \sqrt[3]{1 + 3\sqrt{3}i\omega}, \\ &= \frac{-1}{6} \cdot \sqrt[3]{\frac{7}{2}} \cdot \sqrt[3]{1 + 3\sqrt{3}i\omega^2} \end{aligned}$$

where $\omega = \frac{-1+i\sqrt{3}}{2}$ and define $\sqrt[3]{1+3\sqrt{3}i}$ as a cube root of $1+3\sqrt{3}i$ that lies in the first quadrant of the complex plane.

There are three different cube roots of $1+3\sqrt{3}i$ as shown in Figure 1 below.

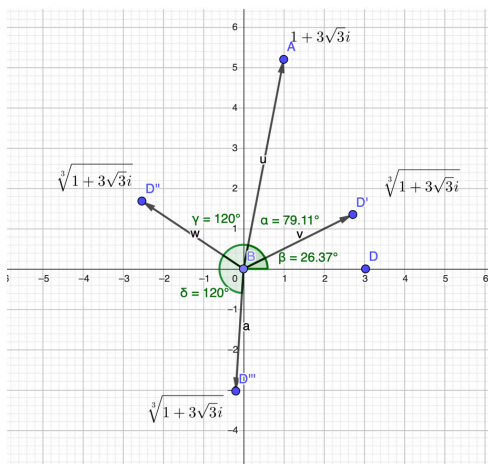


Figure 1: The illustration of $1+3\sqrt{3}i$ and three different cube roots of $1+3\sqrt{3}i$ displayed as $\sqrt[3]{1+3\sqrt{3}i}$ in the complex plane where the horizontal axis is the real axis and the vertical axis is the imaginary axis. The figure was created by the author using Geogebra

From Figure 1, the complex vector $1+3\sqrt{3}i$ makes an angle of $\alpha = 79.11$ degrees with the real axis.

According to the theorem:

If $w = r(\cos \theta + i \sin \theta)$ is a complex number that is not zero, n^{th} root of w has n different roots, which are

$$z = \sqrt[n]{r} \left(\cos \left(\frac{\theta + 2k\pi}{n} \right) + i \sin \left(\frac{\theta + 2k\pi}{n} \right) \right) \quad \text{where } k \in \{0, 1, \dots, n-1\}.$$

From this theorem, we know that the first cube root of $1+3\sqrt{3}i$ is a complex number that makes an angle of $\theta = \frac{79.11}{3} = 26.37$ degrees with the real axis. Then we can find the next cube root of $1+3\sqrt{3}i$ by rotating the first one by 120 degrees counter-clockwise. The last cube root is determined by rotating the second one by 120 degrees counterclockwise. Now we know that there are three different cube roots of $1+3\sqrt{3}i$. However, for the simplicity of further calculations, we define $\sqrt[3]{1+3\sqrt{3}i}$ to be a cube root of $1+3\sqrt{3}i$ that lies in the first quadrant of the complex plane because both real and imaginary parts of this root are positive.

From $r^3 - \frac{7}{12}r + \frac{7}{216} = 0$ which is in the form of $t^3 + pt + q = 0$, know

that $uv = \frac{-p}{3} = \frac{7}{36}$.

That is $v = \frac{7}{36u}$.

Substitute $uv = \frac{-p}{3} = \frac{7}{36}$, obtain

$$\begin{aligned} v &= \frac{7}{36 \cdot \frac{-1}{6} \cdot \sqrt[3]{\frac{7}{2}} \cdot \sqrt[3]{1+3\sqrt{3}i}} \\ &= \frac{-\sqrt[3]{98}}{6} \cdot \frac{1}{\sqrt[3]{1+3\sqrt{3}i}} \cdot \frac{\sqrt[3]{1-3\sqrt{3}i}}{\sqrt[3]{1-3\sqrt{3}i}} \\ &= \frac{-1}{6} \cdot \sqrt[3]{\frac{7}{2}} \cdot \sqrt[3]{1-3\sqrt{3}i} \end{aligned}$$

where $\sqrt[3]{1-3\sqrt{3}i}$ is a conjugate of $\sqrt[3]{1+3\sqrt{3}i}$

From $t = u + v$,

$$t = \left(\frac{-1}{6} \cdot \sqrt[3]{\frac{7}{2}} \cdot \sqrt[3]{1+3\sqrt{3}i} \right) + \left(\frac{-1}{6} \cdot \sqrt[3]{\frac{7}{2}} \cdot \sqrt[3]{1-3\sqrt{3}i} \right)$$

From $x = t + \frac{1}{6}$,

$$\begin{aligned} x &= \frac{1}{6} + \left(\frac{-1}{6} \cdot \sqrt[3]{\frac{7}{2}} \cdot \sqrt[3]{1+3\sqrt{3}i} \right) + \left(\frac{-1}{6} \cdot \sqrt[3]{\frac{7}{2}} \cdot \sqrt[3]{1-3\sqrt{3}i} \right) \\ &= \frac{1}{6} \left[1 - \sqrt[3]{\frac{7}{2}} \cdot \sqrt[3]{1+3\sqrt{3}i} - \sqrt[3]{\frac{7}{2}} \cdot \sqrt[3]{1-3\sqrt{3}i} \right] \end{aligned}$$

$$= \frac{1}{6} \left[1 - \sqrt[3]{\frac{7}{2}} \cdot 2Re \left(\sqrt[3]{1+3\sqrt{3}i} \right) \right].$$

Hence, the first answer to the cubic equation is

$$= \frac{1}{6} \left[1 - \sqrt[3]{\frac{7}{2}} \cdot 2Re \left(\sqrt[3]{1+3\sqrt{3}i} \right) \right].$$

The steps to arrive at the second and third answers are exactly the same as the steps for the first answer except using different values of u . Hence, the calculations for the second and third answers will be omitted and shown in the appendix.

For $u = \frac{-1}{6} \cdot \sqrt[3]{\frac{7}{2}} \cdot \sqrt[3]{1+3\sqrt{3}i\omega}$, the second answer is

$$= \frac{1}{6} \left[1 - \sqrt[3]{\frac{7}{2}} \left(\sqrt[3]{1+3\sqrt{3}i\omega} + \sqrt[3]{1-3\sqrt{3}i\omega^2} \right) \right]$$

For $u = \frac{-1}{6} \cdot \sqrt[3]{\frac{7}{2}} \cdot \sqrt[3]{1+3\sqrt{3}i\omega^2}$, the third answer is

$$= \frac{1}{6} \left[1 - \sqrt[3]{\frac{7}{2}} \left(\sqrt[3]{1+3\sqrt{3}i\omega^2} + \sqrt[3]{1-3\sqrt{3}i\omega} \right) \right].$$

Identify the root expression by algebraic evaluation

Consider

$$\sqrt[3]{1+3\sqrt{3}i} = \sqrt[3]{2\sqrt{7}} \cdot \sqrt[3]{\frac{1}{2\sqrt{7}} + \frac{3\sqrt{3}i}{2\sqrt{7}}}$$

where $\sqrt[3]{\frac{1}{2\sqrt{7}} + \frac{3\sqrt{3}i}{2\sqrt{7}}}$ is the cube root of $\frac{1}{2\sqrt{7}} + \frac{3\sqrt{3}i}{2\sqrt{7}}$

that lies in the first quadrant of the complex plane.

This is similar to the case above. We define $\sqrt[3]{\frac{1}{2\sqrt{7}} + \frac{3\sqrt{3}i}{2\sqrt{7}}}$ to be the cube root of $\frac{1}{2\sqrt{7}} + \frac{3\sqrt{3}i}{2\sqrt{7}}$ that lies in the first quadrant of the complex plane for the simplicity of further calculations since both its real and imaginary parts are positive, although we know that there are three different cube roots of $\frac{1}{2\sqrt{7}} + \frac{3\sqrt{3}i}{2\sqrt{7}}$.

The radius of $\frac{1}{2\sqrt{7}} + \frac{3\sqrt{3}i}{2\sqrt{7}}$ is

$$\sqrt{\left(\frac{1}{2\sqrt{7}}\right)^2 + \left(\frac{3\sqrt{3}}{2\sqrt{7}}\right)^2} = \sqrt{\frac{1}{28} + \frac{27}{28}} = \sqrt{1} = 1$$

And the radius of $\sqrt[3]{\frac{1}{2\sqrt{7}} + \frac{3\sqrt{3}i}{2\sqrt{7}}}$ is the cube root of the radius of $\frac{1}{2\sqrt{7}} + \frac{3\sqrt{3}i}{2\sqrt{7}}$. Therefore, the radius of $\sqrt[3]{\frac{1}{2\sqrt{7}} + \frac{3\sqrt{3}i}{2\sqrt{7}}}$ is $\sqrt[3]{1}$ which is 1. Then, consider the real parts of $\sqrt[3]{\frac{1}{2\sqrt{7}} + \frac{3\sqrt{3}i}{2\sqrt{7}}}$ and $\frac{1}{2\sqrt{7}} + \frac{3\sqrt{3}i}{2\sqrt{7}}$. The real part of $\sqrt[3]{\frac{1}{2\sqrt{7}} + \frac{3\sqrt{3}i}{2\sqrt{7}}}$ is greater than of $\frac{1}{2\sqrt{7}} + \frac{3\sqrt{3}i}{2\sqrt{7}}$ as shown in Figure 2 where $z_1 = \frac{1}{2\sqrt{7}} + \frac{3\sqrt{3}i}{2\sqrt{7}}$ and $z_2 = \sqrt[3]{\frac{1}{2\sqrt{7}} + \frac{3\sqrt{3}i}{2\sqrt{7}}}$.

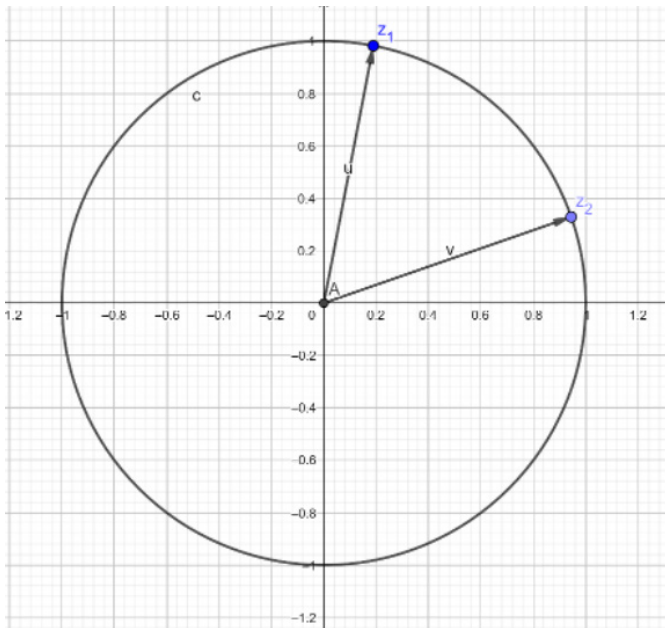


Figure 2: Comparison of the real parts between two complex numbers z_1 and z_2 (not drawn to scale) where the horizontal axis is the real axis and the vertical axis is the imaginary axis. The figure was created by the author using Geogebra.

Therefore,

$$\begin{aligned} \operatorname{Re}\left(\sqrt[3]{1+3\sqrt{3}i}\right) &= \sqrt[3]{2\sqrt{7}} \cdot \operatorname{Re}\left(\sqrt[3]{\frac{1}{2\sqrt{7}} + \frac{3\sqrt{3}i}{2\sqrt{7}}}\right) \\ &> \sqrt[3]{2\sqrt{7}} \cdot \operatorname{Re}\left(\frac{1}{2\sqrt{7}} + \frac{3\sqrt{3}i}{2\sqrt{7}}\right) \\ &= \sqrt[3]{2\sqrt{7}} \cdot \frac{1}{2\sqrt{7}} \\ &= \frac{1}{2^{\frac{2}{3}} \cdot 7^{\frac{1}{3}}} \end{aligned}$$

Consider the first answer $\frac{1}{6} \left[1 - \sqrt[3]{\frac{7}{2}} \cdot 2\operatorname{Re}\left(\sqrt[3]{1+3\sqrt{3}i}\right) \right]$,

$$\frac{1}{6} \left[1 - \sqrt[3]{\frac{7}{2}} \cdot 2\operatorname{Re}\left(\sqrt[3]{1+3\sqrt{3}i}\right) \right] < \frac{1}{6} \left[1 - \sqrt[3]{\frac{7}{2}} \cdot 2 \cdot \frac{1}{2^{\frac{2}{3}} \cdot 7^{\frac{1}{3}}} \right] = 0.$$

Since $\cos(5\pi/7)$ is the only value that is less than zero,

$$\cos(5\pi/7) = \frac{1}{6} \left[1 - \sqrt[3]{\frac{7}{2}} \cdot 2\operatorname{Re}\left(\sqrt[3]{1+3\sqrt{3}i}\right) \right].$$

Consider $\cos(5\pi/7) = -\cos(2\pi/7)$.

Hence,

$$\cos(2\pi/7) = -\frac{1}{6} \left[1 - \sqrt[3]{\frac{7}{2}} \cdot 2\operatorname{Re}\left(\sqrt[3]{1+3\sqrt{3}i}\right) \right].$$

From $\cos\left(\frac{A}{2}\right) = \pm \sqrt{\frac{1+\cos(A)}{2}}$,

$$\cos(\pi/7) = \pm \sqrt{\frac{1}{2} - \frac{1}{12} \left(1 - \sqrt[3]{\frac{7}{2}} \cdot 2\operatorname{Re}\left(\sqrt[3]{1+3\sqrt{3}i}\right) \right)}.$$

Because $\cos(\pi/7) > 0$,

$$\cos(\pi/7) = \sqrt{\frac{1}{2} - \frac{1}{12} \left(1 - \sqrt[3]{\frac{7}{2}} \cdot 2\operatorname{Re}\left(\sqrt[3]{1+3\sqrt{3}i}\right) \right)}.$$

From $\cos(2A) = 2\cos^2(A) - 1$, $\cos(4\pi/7) = 2\cos^2(2\pi/7) - 1$.

$$\begin{aligned} \cos(4\pi/7) &= 2 \left\{ -\frac{1}{6} \left[1 - \sqrt[3]{\frac{7}{2}} \cdot 2\operatorname{Re}\left(\sqrt[3]{1+3\sqrt{3}i}\right) \right] \right\}^2 - 1 \\ &= \frac{1}{18} \left[1 - \sqrt[3]{\frac{7}{2}} \cdot 2\operatorname{Re}\left(\sqrt[3]{1+3\sqrt{3}i}\right) \right]^2 - 1 \end{aligned}$$

From $\cos(3\pi/7) = -\cos(4\pi/7)$,

$$\cos(3\pi/7) = 1 - \frac{1}{18} \left[1 - \sqrt[3]{\frac{7}{2}} \cdot 2\operatorname{Re}\left(\sqrt[3]{1+3\sqrt{3}i}\right) \right]^2$$

Identify the root expressions by analyzing them on the complex plane:

All three answers from solving the cubic equation are

$$\frac{1}{6} \left[1 - \sqrt[3]{\frac{7}{2}} \cdot 2\operatorname{Re}\left(\sqrt[3]{1+3\sqrt{3}i}\right) \right] = \cos(5\pi/7),$$

$$\frac{1}{6} \left[1 - \sqrt[3]{\frac{7}{2}} \cdot \sqrt[3]{1+3\sqrt{3}i\omega} - \sqrt[3]{\frac{7}{2}} \cdot \sqrt[3]{1-3\sqrt{3}i\omega^2} \right],$$

and

$$\frac{1}{6} \left[1 - \sqrt[3]{\frac{7}{2}} \cdot \sqrt[3]{1+3\sqrt{3}i\omega^2} - \sqrt[3]{\frac{7}{2}} \cdot \sqrt[3]{1-3\sqrt{3}i\omega} \right].$$

Since we know one of these three answers is the value of , we have only two answers left to identify.

Consider $\sqrt[3]{1+3\sqrt{3}i}$, $\sqrt[3]{1+3\sqrt{3}i\omega}$, and $\sqrt[3]{1+3\sqrt{3}i\omega^2}$ that appear

on each answer.

And define that

$$\sqrt[3]{1+3\sqrt{3}i} = x + yi \quad \text{where } x, y \in \mathbb{R}^+$$

because $\sqrt[3]{1+3\sqrt{3}i}$ lies on the first quadrant of the complex plane.

Analyze $\sqrt[3]{1+3\sqrt{3}i}$, $\sqrt[3]{1+3\sqrt{3}i\omega}$, and $\sqrt[3]{1+3\sqrt{3}i\omega^2}$ on the complex

plane as shown in Figure 3.

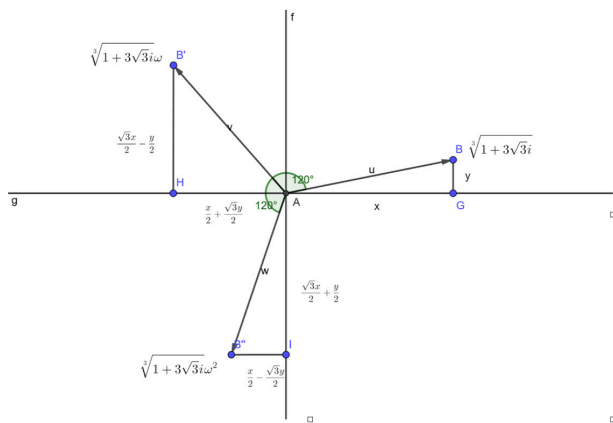


Figure 3: Three complex numbers in the complex plane (not drawn to scale). The figure was created by the author using Geogebra.

Know that

$$\sqrt[3]{1+3\sqrt{3}i\omega} = -\left(\frac{x}{2} + \frac{\sqrt{3}y}{2}\right) + \left(\frac{\sqrt{3}x}{2} - \frac{y}{2}\right)i$$

and

$$\sqrt[3]{1+3\sqrt{3}i\omega^2} = -\left(\frac{x}{2} - \frac{\sqrt{3}y}{2}\right) - \left(\frac{\sqrt{3}x}{2} + \frac{y}{2}\right)i$$

$$\sqrt[3]{1-3\sqrt{3}i} \quad \text{is a conjugate of} \quad \sqrt[3]{1+3\sqrt{3}i}$$

Therefore,

$$\sqrt[3]{1-3\sqrt{3}i} = x - yi.$$

Now, analyze $\sqrt[3]{1-3\sqrt{3}i}$, $\sqrt[3]{1-3\sqrt{3}i\omega}$, and $\sqrt[3]{1-3\sqrt{3}i\omega^2}$

in the complex plane as shown in Figure 4.

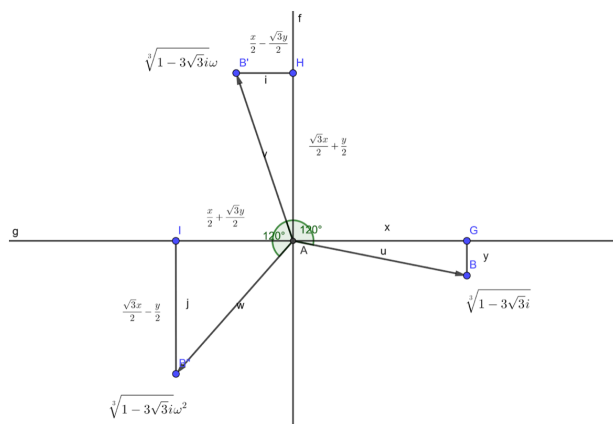


Figure 4: Three complex numbers in the complex plane (not drawn to scale). The figure was created by the author using Geogebra.

Know that

$$\sqrt[3]{1-3\sqrt{3}i\omega} = -\left(\frac{x}{2} - \frac{\sqrt{3}y}{2}\right) + \left(\frac{\sqrt{3}x}{2} + \frac{y}{2}\right)i$$

and

$$\sqrt[3]{1-3\sqrt{3}i\omega^2} = -\left(\frac{x}{2} + \frac{\sqrt{3}y}{2}\right) - \left(\frac{\sqrt{3}x}{2} - \frac{y}{2}\right)i.$$

Since we already know the value of $\cos(5\pi/7)$, we need to analyze only the remaining two answers.

Take a closer look at the second answer.

$$\begin{aligned} & \frac{1}{6} \left[1 - \sqrt[3]{\frac{7}{2}} \left(\sqrt[3]{1+3\sqrt{3}i\omega} + \sqrt[3]{1-3\sqrt{3}i\omega^2} \right) \right] \\ &= \frac{1}{6} \left\{ 1 - \sqrt[3]{\frac{7}{2}} \left[-\left(\frac{x}{2} + \frac{\sqrt{3}y}{2}\right) + \left(\frac{\sqrt{3}x}{2} - \frac{y}{2}\right)i - \left(\frac{x}{2} + \frac{\sqrt{3}y}{2}\right) - \left(\frac{\sqrt{3}x}{2} - \frac{y}{2}\right)i \right] \right\} \\ &= \frac{1}{6} \left\{ 1 - \sqrt[3]{\frac{7}{2}} [-x - \sqrt{3}y] \right\} \end{aligned}$$

And take a closer look at the third answer.

$$\begin{aligned} & \frac{1}{6} \left[1 - \sqrt[3]{\frac{7}{2}} \left(\sqrt[3]{1+3\sqrt{3}i\omega^2} + \sqrt[3]{1-3\sqrt{3}i\omega} \right) \right] \\ &= \frac{1}{6} \left\{ 1 - \sqrt[3]{\frac{7}{2}} \left[-\left(\frac{x}{2} - \frac{\sqrt{3}y}{2}\right) - \left(\frac{\sqrt{3}x}{2} + \frac{y}{2}\right)i - \left(\frac{x}{2} - \frac{\sqrt{3}y}{2}\right) + \left(\frac{\sqrt{3}x}{2} + \frac{y}{2}\right)i \right] \right\} \\ &= \frac{1}{6} \left\{ 1 - \sqrt[3]{\frac{7}{2}} [-x + \sqrt{3}y] \right\} \end{aligned}$$

Since we define that x and y are positive integers when we define $\sqrt[3]{1+3\sqrt{3}i} = x + yi$ where $x, y \in \mathbb{R}^+$,

$$\frac{1}{6} \left\{ 1 - \sqrt[3]{\frac{7}{2}} [-x - \sqrt{3}y] \right\} > \frac{1}{6} \left\{ 1 - \sqrt[3]{\frac{7}{2}} [-x + \sqrt{3}y] \right\}$$

and

$$\cos(\pi/7) > \cos(3\pi/7),$$

$$\cos(\pi/7) = \frac{1}{6} \left\{ 1 - \sqrt[3]{\frac{7}{2}} [-x - \sqrt{3}y] \right\}$$

$$\cos(3\pi/7) = \frac{1}{6} \left\{ 1 - \sqrt[3]{\frac{7}{2}} [-x + \sqrt{3}y] \right\}$$

Moreover, the answers of $\cos(\pi/7)$ and $\cos(3\pi/7)$ can be written in simpler forms.

$$\cos(\pi/7) = \frac{1}{6} \left\{ 1 - \sqrt[3]{\frac{7}{2}} [-x - \sqrt{3}y] \right\}$$

Since $\sqrt[3]{1+3\sqrt{3}i\omega} = -\left(\frac{x}{2} + \frac{\sqrt{3}y}{2}\right) + \left(\frac{\sqrt{3}x}{2} - \frac{y}{2}\right) i$ and

$$Re \left(\sqrt[3]{1+3\sqrt{3}i\omega} \right) = -\frac{x}{2} - \frac{\sqrt{3}y}{2}$$

$$\cos(\pi/7) = \frac{1}{6} \left[1 - \sqrt[3]{\frac{7}{2}} \cdot 2Re \left(\sqrt[3]{1+3\sqrt{3}i\omega} \right) \right]$$

$$\cos(3\pi/7) = \frac{1}{6} \left\{ 1 - \sqrt[3]{\frac{7}{2}} [-x + \sqrt{3}y] \right\}$$

Since $\sqrt[3]{1+3\sqrt{3}i\omega^2} = -\left(\frac{x}{2} - \frac{\sqrt{3}y}{2}\right) - \left(\frac{\sqrt{3}x}{2} + \frac{y}{2}\right) i$ and

$$Re \left(\sqrt[3]{1+3\sqrt{3}i\omega^2} \right) = -\frac{x}{2} + \frac{\sqrt{3}y}{2}$$

Therefore,

$$\cos(3\pi/7) = \frac{1}{6} \left[1 - \sqrt[3]{\frac{7}{2}} \cdot 2Re \left(\sqrt[3]{1+3\sqrt{3}i\omega^2} \right) \right]$$

Answers in these forms also ensure that the value of $\cos(\pi/7)$ and $\cos(3\pi/7)$ are real numbers as expected as a range of trigonometric functions.

Therefore, we can conclude that

$$\begin{aligned} \cos(\pi/7) &= \sqrt{\frac{1}{2} - \frac{1}{12} \left(1 - \sqrt[3]{\frac{7}{2}} \cdot 2Re \left(\sqrt[3]{1+3\sqrt{3}i} \right) \right)} \\ &= \sqrt{\frac{1}{2} - \frac{1}{12} \left(1 - \sqrt[3]{\frac{7}{2}} \cdot 2Re(z) \right)} \end{aligned} \tag{1}$$

$$\begin{aligned} \cos(\pi/7) &= \frac{1}{6} \left[1 - \sqrt[3]{\frac{7}{2}} \cdot 2Re \left(\sqrt[3]{1+3\sqrt{3}i\omega} \right) \right] \\ &= \frac{1}{6} \left[1 - \sqrt[3]{\frac{7}{2}} \cdot 2Re(z\omega) \right] \end{aligned} \tag{2}$$

$$\begin{aligned} \cos(3\pi/7) &= 1 - \frac{1}{18} \left[1 - \sqrt[3]{\frac{7}{2}} \cdot 2Re \left(\sqrt[3]{1+3\sqrt{3}i} \right) \right]^2 \\ &= 1 - \frac{1}{18} \left[1 - \sqrt[3]{\frac{7}{2}} \cdot 2Re(z) \right]^2 \end{aligned} \tag{3}$$

$$\begin{aligned} \cos(3\pi/7) &= \frac{1}{6} \left[1 - \sqrt[3]{\frac{7}{2}} \cdot 2Re \left(\sqrt[3]{1+3\sqrt{3}i\omega^2} \right) \right] \\ &= \frac{1}{6} \left[1 - \sqrt[3]{\frac{7}{2}} \cdot 2Re(z\omega^2) \right] \end{aligned} \tag{4}$$

$$\begin{aligned} \cos(5\pi/7) &= \frac{1}{6} \left[1 - \sqrt[3]{\frac{7}{2}} \cdot 2Re \left(\sqrt[3]{1+3\sqrt{3}i} \right) \right] \\ &= \frac{1}{6} \left[1 - \sqrt[3]{\frac{7}{2}} \cdot 2Re(z) \right] \end{aligned} \tag{5}$$

where $z = \sqrt[3]{1+3\sqrt{3}i}$ and $\omega = \frac{-1+i\sqrt{3}}{2}$.

The exact values of $\cos(\pi/7)$ and $\cos(3\pi/7)$ can be written in two forms: one with ω and another without ω . There is only one form for the exact value of $\cos(5\pi/7)$.

Refer to Figure 1 again and write a polar form of $1+3\sqrt{3}i$.

$$1+3\sqrt{3}i = \sqrt{28}(\cos \theta + i \sin \theta) \quad \text{and} \quad \theta = \arctan(3\sqrt{3})$$

Hence,

$$\begin{aligned} 1+3\sqrt{3}i &= \sqrt{28} \left(\cos \arctan(3\sqrt{3}) + i \sin \arctan(3\sqrt{3}) \right) \\ &= \sqrt{28} e^{i \arctan(3\sqrt{3})} \end{aligned}$$

Recall what we have defined, $\sqrt[3]{1+3\sqrt{3}i}$ is the cube root of

$1+3\sqrt{3}i$ that lies in the first quadrant of the complex plane.

So,

$$\begin{aligned} z &= \sqrt[3]{1+3\sqrt{3}i} = 28^{\frac{1}{6}} e^{\frac{i \arctan(3\sqrt{3})}{3}} \\ Re(z) &= 28^{\frac{1}{6}} \cos \left(\frac{\arctan(3\sqrt{3})}{3} \right) \end{aligned} \tag{6}$$

$$Re(z\omega) = 28^{\frac{1}{6}} \cos \left(\frac{\arctan(3\sqrt{3}) + 2\pi}{3} \right) \tag{7}$$

$$Re(z\omega^2) = 28^{\frac{1}{6}} \cos \left(\frac{\arctan(3\sqrt{3}) + 4\pi}{3} \right) \tag{8}$$

Therefore, the values of $\cos(\pi/7)$, $\cos(3\pi/7)$, and $\cos(5\pi/7)$ listed in the equation numbers (1)-(5) can be written more precisely by substituting $Re(z)$, $Re(z\omega)$, and $Re(z\omega^2)$ with their values above.

Thus,

$$\begin{aligned} \cos(\pi/7) &= \sqrt{\frac{1}{2} - \frac{1}{12} \left(1 - \sqrt[3]{\frac{7}{2}} \cdot 2 \cdot 28^{\frac{1}{6}} \cos \left(\frac{\arctan(3\sqrt{3})}{3} \right) \right)} \\ &= \sqrt{\frac{1}{2} - \frac{1}{12} \left(1 - 2\sqrt{7} \cos \left(\frac{\arctan(3\sqrt{3})}{3} \right) \right)} \end{aligned} \tag{9}$$

$$\begin{aligned} \cos(\pi/7) &= \frac{1}{6} \left[1 - \sqrt[3]{\frac{7}{2}} \cdot 2 \cdot 28^{\frac{1}{6}} \cos \left(\frac{\arctan(3\sqrt{3}) + 2\pi}{3} \right) \right] \\ &= \frac{1}{6} \left[1 - 2\sqrt{7} \cos \left(\frac{\arctan(3\sqrt{3}) + 2\pi}{3} \right) \right] \end{aligned} \tag{10}$$

$$\begin{aligned} \cos(3\pi/7) &= 1 - \frac{1}{18} \left[1 - \sqrt[3]{\frac{7}{2}} \cdot 2 \cdot 28^{\frac{1}{6}} \cos \left(\frac{\arctan(3\sqrt{3})}{3} \right) \right]^2 \\ &= 1 - \frac{1}{18} \left[1 - 2\sqrt{7} \cos \left(\frac{\arctan(3\sqrt{3})}{3} \right) \right]^2 \end{aligned} \tag{11}$$

$$\begin{aligned} \cos(3\pi/7) &= \frac{1}{6} \left[1 - \sqrt[3]{\frac{7}{2}} \cdot 2 \cdot 28^{\frac{1}{6}} \cos \left(\frac{\arctan(3\sqrt{3}) + 4\pi}{3} \right) \right] \\ &= \frac{1}{6} \left[1 - 2\sqrt{7} \cos \left(\frac{\arctan(3\sqrt{3}) + 4\pi}{3} \right) \right] \end{aligned} \tag{12}$$

$$\begin{aligned} \cos(5\pi/7) &= \frac{1}{6} \left[1 - \sqrt[3]{\frac{7}{2}} \cdot 2 \cdot 28^{\frac{1}{6}} \cos \left(\frac{\arctan(3\sqrt{3})}{3} \right) \right] \\ &= \frac{1}{6} \left[1 - 2\sqrt{7} \cos \left(\frac{\arctan(3\sqrt{3})}{3} \right) \right] \end{aligned} \tag{13}$$

Answers to the values of $\cos(\pi/7)$, $\cos(3\pi/7)$, and $\cos(5\pi/7)$ in such forms from above allow us to easily put those expressions into a calculator. Moreover, these expressions reveal relationships among $\cos(\pi/7)$, $\cos(3\pi/7)$, $\cos(5\pi/7)$, and \cos

$\left(\frac{\arctan(\sqrt[3]{3}) + 2\pi k}{3}\right)$ where $k \in \{0,1,2\}$. This could also be future work for me and others to discuss the relationships among those functions.

Conclusion

The exact values of $\cos(\pi/7)$, $\cos(3\pi/7)$, and $\cos(5\pi/7)$ are shown in equation numbers (1)-(5) in two forms: one with ω and another without ω . In equation numbers (1)-(5), those expressions are in terms of $Re(z)$, $Re(z\omega)$, and $Re(z\omega^2)$. Furthermore, since the values of $Re(z)$, $Re(z\omega)$, and $Re(z\omega^2)$ are determined in equation numbers (6)-(8), the exact values of $\cos(\pi/7)$, $\cos(3\pi/7)$, and $\cos(5\pi/7)$ can be rewritten more precisely in equation numbers (9)-(13).

Acknowledgments

I would like to express my very great appreciation to the Institute for the Promotion of Teaching Science and Technology (IPST) and the Development and Promotion of Science and Technology Talents project (DPST) in Thailand for project support and funding. I would also like to offer my special thanks to Dr. Nantawat Udomchatpitak from Mahidol University for his valuable and constructive suggestions and advice during the planning and development of this project.

References

- Weisstein, Eric W. "Trigonometry Angles–Pi/7." MathWorld – a Wolfram Web Resource. <https://mathworld.wolfram.com/TrigonometryAnglesPi7.html>. Accessed 24 Feb. 2023.
- Ratanaprasert, C. พหุนามกำลังสาม Cubic Polynomials. In พีชคณิต [Algebra]. 3rd ed.; The Promotion of Academic Olympiad and Development of Science Education Foundation under the patronage of Her Royal Highness Princess Galyani Vadhana Krom Luang Naradhiwas Rajanagarindra (POSN): Darnsutha Press Co., LTD., 2009; pp 59-65.

Author

Punnawit Kasean is a Thai rising sophomore at Bowdoin College. He plans to major in mathematics and physics with a minor in computer science. He went to Brewster Academy in Wolfeboro, New Hampshire. He won first place in the field of mathematics in the High School Science Symposium 2022. He would like to go to graduate school in either US or UK and become a mathematician and physicist.

Appendix

Calculations of the second and third answers to the cubic equation

For $u = \frac{-1}{6} \cdot \sqrt[3]{\frac{7}{2}} \cdot \sqrt[3]{1+3\sqrt{3}i\omega}$, get

$$\begin{aligned} v &= \frac{7}{36 \cdot \frac{-1}{6} \cdot \sqrt[3]{\frac{7}{2}} \cdot \sqrt[3]{1+3\sqrt{3}i\omega}} \\ &= \frac{-\sqrt[3]{98}}{6} \cdot \frac{1}{\sqrt[3]{1+3\sqrt{3}i\omega}} \cdot \frac{\sqrt[3]{1-3\sqrt{3}i\omega^2}}{\sqrt[3]{1-3\sqrt{3}i\omega^2}} \\ &= \frac{-1}{6} \cdot \sqrt[3]{\frac{7}{2}} \cdot \sqrt[3]{1-3\sqrt{3}i\omega^2}. \end{aligned}$$

From $t = u + v$,

$$t = \left(\frac{-1}{6} \cdot \sqrt[3]{\frac{7}{2}} \cdot \sqrt[3]{1+3\sqrt{3}i\omega}\right) + \left(\frac{-1}{6} \cdot \sqrt[3]{\frac{7}{2}} \cdot \sqrt[3]{1-3\sqrt{3}i\omega^2}\right).$$

From $x = t + \frac{1}{6}$,

$$\begin{aligned} x &= \frac{1}{6} + \left(\frac{-1}{6} \cdot \sqrt[3]{\frac{7}{2}} \cdot \sqrt[3]{1+3\sqrt{3}i\omega}\right) + \left(\frac{-1}{6} \cdot \sqrt[3]{\frac{7}{2}} \cdot \sqrt[3]{1-3\sqrt{3}i\omega^2}\right) \\ &= \frac{1}{6} \left[1 - \sqrt[3]{\frac{7}{2}} \cdot \sqrt[3]{1+3\sqrt{3}i\omega} - \sqrt[3]{\frac{7}{2}} \cdot \sqrt[3]{1-3\sqrt{3}i\omega^2}\right] \\ &= \frac{1}{6} \left[1 - \sqrt[3]{\frac{7}{2}} \left(\sqrt[3]{1+3\sqrt{3}i\omega} + \sqrt[3]{1-3\sqrt{3}i\omega^2}\right)\right]. \end{aligned}$$

For $u = \frac{-1}{6} \cdot \sqrt[3]{\frac{7}{2}} \cdot \sqrt[3]{1+3\sqrt{3}i\omega^2}$, get

$$\begin{aligned} v &= \frac{7}{36 \cdot \frac{-1}{6} \cdot \sqrt[3]{\frac{7}{2}} \cdot \sqrt[3]{1+3\sqrt{3}i\omega^2}} \\ &= \frac{-\sqrt[3]{98}}{6} \cdot \frac{1}{\sqrt[3]{1+3\sqrt{3}i\omega^2}} \cdot \frac{\sqrt[3]{1-3\sqrt{3}i\omega}}{\sqrt[3]{1-3\sqrt{3}i\omega}} \\ &= \frac{-1}{6} \cdot \sqrt[3]{\frac{7}{2}} \cdot \sqrt[3]{1-3\sqrt{3}i\omega}. \end{aligned}$$

From $t = u + v$,

$$t = \left(\frac{-1}{6} \cdot \sqrt[3]{\frac{7}{2}} \cdot \sqrt[3]{1+3\sqrt{3}i\omega^2}\right) + \left(\frac{-1}{6} \cdot \sqrt[3]{\frac{7}{2}} \cdot \sqrt[3]{1-3\sqrt{3}i\omega}\right).$$

From $x = t + \frac{1}{6}$,

$$\begin{aligned} x &= \frac{1}{6} + \left(\frac{-1}{6} \cdot \sqrt[3]{\frac{7}{2}} \cdot \sqrt[3]{1+3\sqrt{3}i\omega^2}\right) + \left(\frac{-1}{6} \cdot \sqrt[3]{\frac{7}{2}} \cdot \sqrt[3]{1-3\sqrt{3}i\omega}\right) \\ &= \frac{1}{6} \left[1 - \sqrt[3]{\frac{7}{2}} \cdot \sqrt[3]{1+3\sqrt{3}i\omega^2} - \sqrt[3]{\frac{7}{2}} \cdot \sqrt[3]{1-3\sqrt{3}i\omega}\right] \\ &= \frac{1}{6} \left[1 - \sqrt[3]{\frac{7}{2}} \left(\sqrt[3]{1+3\sqrt{3}i\omega^2} + \sqrt[3]{1-3\sqrt{3}i\omega}\right)\right]. \end{aligned}$$

Thus, the third answer is

$$= \frac{1}{6} \left[1 - \sqrt[3]{\frac{7}{2}} \left(\sqrt[3]{1+3\sqrt{3}i\omega^2} + \sqrt[3]{1-3\sqrt{3}i\omega}\right)\right].$$

Performance Benefit Analysis of Linked Rainwater Harvesting Systems

Saewoong Ian Park

Seoul International School, 15 Seongnam-daero 1518beon-gil, Sujeong-gu, Seongnam-si, Gyeonggi-do, 13113 Republic of Korea;
ian.park.2102@gmail.com

ABSTRACT: This study investigated the performance of connected rainwater harvesting systems (RWHSs) in regions with different rainfall characteristics. Physical and analytical performance models were developed for modeling reference and connected RWHS performance. Four regions, namely Seoul, Taipei, Los Angeles, and New York were selected to reflect the effects of different rainfall characteristics. The performance efficiency of connected RWHS increased with increased RWHS size, the connected total RWHS size, and combined water demands. The connected RWHS size reduction rate increased with increased water demands, combined water demands, and combined RWHS efficiency. Conclusively, the results of this study imply that connected RWHSs in rainy regions, such as Seoul, Taipei, and NY, show superior benefits with increasing efficiency at a constant RWHS size. Conversely, connected RWHSs in semi-arid or arid regions demonstrate greater benefits with constant efficiency at a reduced RWHS size.

KEYWORDS: Environmental Engineering, Rainwater harvesting system; Performance model; Efficiency; RWHS size.

■ Introduction

Water resource availability, including water use and supply, has become a crucial concern in urban areas due to the population increase. Rainwater harvesting system (RWHS), which stores water in barrels or cisterns, has emerged as a method for promoting water conservation and improving water supply availability. In RWHS, rainwater gathered from the roof of a building or house is used for multiple purposes, including gardening, flushing toilets, and washing cars. Although RWHS is based on a simple concept, measuring the rain barrel performance can be challenging. Most studies have used yield after spillage (YAS) and yield before spillage (YBS) models for the physical performance modeling of RWHS.¹⁻⁶ Rupp *et al.* have suggested a comparative analysis of different methods to estimate the RWHS size.⁷ They used the Netuno program, which calculates the potential for potable water savings for different tank capacities based on daily rainfall. Cordova and Ghisi investigated the difference between the Netuno, YAS, and YBS models and revealed that the results of the three models are statistically equivalent.⁸ Additionally, the Spreadsheet version of the Storage, Treatment, Overflow, Runoff Model (SS STORM) was developed for evaluating the RWHS performance model.^{9,10} This study adopted the SS STORM model to produce a reference result for RWHS performance. The objective of this study was to investigate the efficiency of connected RWHS compared with unconnected RWHS. Specifically, this study analyzed (1) the benefits of connected RWHS efficiency based on RWHSs size, combined RWHSs, and combined water demands, and (2) the benefits of RWHS size reduction based on water demands, combined water demands, and combined efficiency of RWHSs. For this study, the better operation of RWHSs. This study estimates better RWHS operation ef-

ficiencies through the linked existing RWHSs in different rainfall characteristic regions. The results of this study provide a better understanding of RWHS performance and show the optimized RWHS installation approaches based on different water demands.

■ Methods

It is necessary to verify the results of the physical performance and analytical models. In this study, a physical performance model was used as a reference to adjust the analytical performance model. A physical-based RWHS model was used in this study to consider the actual RWHS performance.^{9,10} For evaluating connected RWHS performance, an analytical method was applied.^{11,12} The analytical methods used in this study were calibrated to match the physical model performance results.¹³ The concept of this study is demonstrated in Figure 1. This study compared the performances of two independent RWHSs (Figure 1(a)) and connected RWHSs (Figure 1(b)). Furthermore, RWHS performance efficiency was investigated based on water demand and RWHS size.



Figure 1: Schematic of rainwater harvesting system (RWHS); (a) two single RWHS; (b) connected RWHS

Daily rainfall data were collected from four different cities in East Asia and the USA, including Seoul, Republic of Korea; Taipei, Taiwan; Los Angeles (LA), USA; and New York (NY),

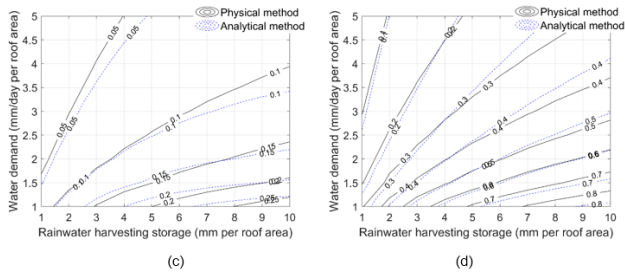


Figure 3: Efficiencies of rainwater harvesting systems between physical and analytical performance models; (a) Seoul, (b) Taipei, (c) Los Angeles, (d) New York. These figures show the RWHS performance efficiencies based on RWHS size and water demand between physical and analytical performance models in each region. These figures also indicate that the results of the analytical performance model are close to the results of the physical performance model in four regions.

2. Efficiency effect of the connected RWHSs:

To quantify the effect of connected RWHS on the efficiency of water demand, two RWHSs of different sizes were investigated. Figure 4 shows that efficiency increases with increased RWHS sizes and combined RWHS sizes. The order of high efficiency is Taipei > NY > Seoul > LA. It was found that annual rainfall and rainy days affect the RWHS efficiency. The RWHS efficiency, based on the RWHS size and combined RWHS size, increased as the annual rainfall and annual rainy days increased. Connected RWHSs in Taipei and NY were 22% more efficient than unconnected RWHSs. Meanwhile, connected RWHSs in Seoul and LA showed higher efficiency compared with unconnected RWHS by 14% and 3.5%, respectively. It was found that Seoul exhibits a lower increasing efficiency compared with NY because the number of annual rainy days in Seoul is much lower than that in NY. Generally, this indicates that connected RWHS in more rainy regions are more beneficial than those in drier regions, based on the RWHS efficiency results.

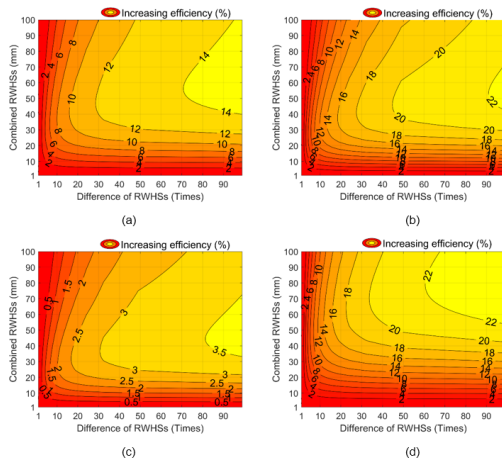


Figure 4: Increasing efficiency percent of combined rainwater harvesting storages and different sizes of RWHSs as a 0.8mm/day combined water demand; (a) Seoul (b) Taipei, (c) Los Angeles, (d) New York. These figures show the increasing efficiencies of the combined RWHSs compared with two single RWHSs based on the difference of RWHS sizes and the combined RWHSs size in each region. These figures indicate that there is an increase in efficiency of the combined RWHSs compared with two single RWHSs as the difference of RWHSs and combined RWHSs size increases. However, the increasing efficiency of the combined RWHSs is different depending on the four rainfalls and their regional characteristics.

Figure 5 shows the increased efficiency of connected RWHSs based on different RWHS sizes and combined water demands in the four regions. Generally, RWHS efficiency increases as the difference, and RWHS sizes and combined water demands increase in all four cities. However, in LA, combined water demands remain the same as the efficiencies of connected RWHS. In contrast, the other three cities show an increasing efficiency of RWHSs depending on the difference in RWHS sizes and combined water demands. It was found that annual rainfall and rainy days in LA are significantly small, and combined water demands do not affect the connected RWHSs.

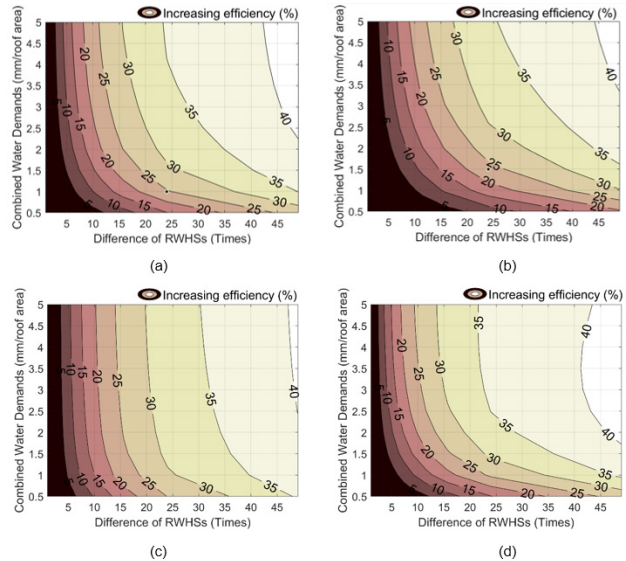


Figure 5: Increasing efficiency of combined rainwater harvesting storages compared with separated rainwater harvesting storages based on combined water demands and difference of connected RWHS in 5 mm/roof area; (a) Seoul, (b) Taipei, (c) Los Angeles, (f) New York. These figures show the increasing efficiencies of the combined RWHSs comparing with two single RWHSs based on the difference of RWHS sizes, and the combined water demands in each region. These figures indicate that the efficiency of the combined RWHSs increases when compared with two single RWHSs as the difference in RWHS size and combined water demands increases. However, the increasing efficiency of the combined RWHSs is different depending on the four rainfalls and their regional characteristics.

3. RWHS Size effect of the connected RWHSs:

Similar to the efficiency variable, it is necessary to analyze the RWHS size reduction effects of connected RWHSs. Therefore, this study investigated the RWHS reduction rate based on the difference in water demands vs. combined water demands and the efficiency of connected RWHSs.

Figure 6 shows the reduction rate of the total connected RWHS size as a function of water demand and total demand. All four regions in Figure 6 show that the RWHS size reduction rate increases as differences in water demands and combined water demand increase. Particularly, LA (Figure 6(c)) produced a much greater RWHS size reduction rate than the other three cities (Figure 6(a), 6(b), and 6(d)). LA in Figure 6(c) shows a higher RWHS storage reduction rate of up to 40%. However, Figures 6(a), 6(b), and 6(d) show low RWHS reduction rates between 0 and 1%. This indicates that the dry region gets advantages from connecting RWHSs in terms of RWHS size reduction. In other words, the LA

region was more sensitive to the RWHS size based on the required efficiency than the other three regions.

Similarly, Figure 7 shows the connected RWHS size reduction as a function of differences in water use and combined efficiency. Overall, the RWHS reduction rate increased as the differences in the water demand and combined efficiency increased. Seoul, Taipei, and NY regions in Figures 7(a), 7(b), and 7(d) show low RWHS storage reduction rates of up to about 3%. However, the LA region in Figure 7(c) produces a high RWHS reduction rate up to approximately 80%. Like Figure 6, the LA region (Figure 7(c)) shows more increase in the RWHS size reduction rate than the other three regions (Figures 7(a), 7(b), and 7(d)). This is because the LA region requires greater RWHS size than the other three regions under the same water demand conditions, as shown in Figure 3.

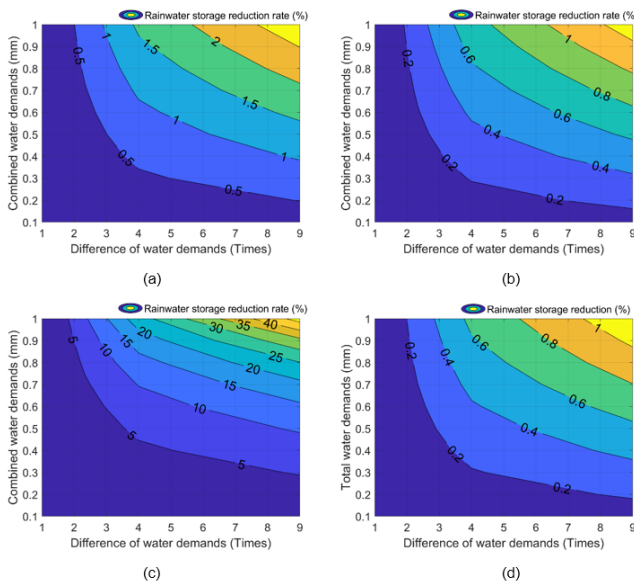


Figure 6: Rainwater storage reduction between the difference of water demands and total water demands in the sharing rainwater harvesting storages system as average efficiency of 30%; (a) Seoul, South Korea, (b) Taipei, Taiwan (c) Los Angeles (d) New York. These figures show the RWHS size reduction rate of the combined RWHSs compared with two single RWHSs based on the difference in water demands and the combined water demands in each region. These figures indicate that the RWHS size reduction rate of the combined RWHSs increases compared with two single RWHSs as the difference between water demands and combined water demands increases. However, the RWHS size reduction rate of the combined RWHSs is different depending on the four rainfalls and their regional characteristics.

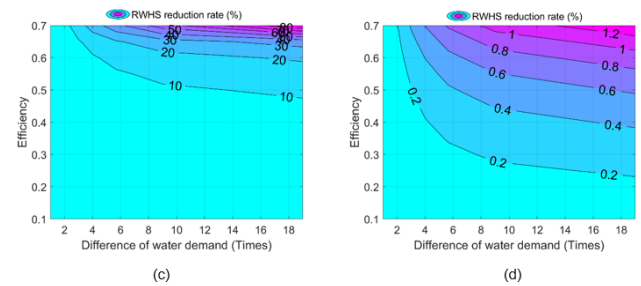
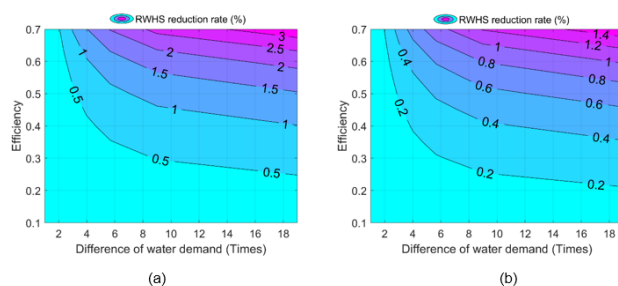


Figure 7: RWHS reduction as a function of the difference of water demand and efficiency for a combined water use of 0.2 mm/day; (a) Seoul, (b) Taipei, (c) Los Angeles, (d) New York. These figures show the RWHS size reduction rate of the combined RWHSs compared with two single RWHSs based on the difference in water demands and the RWHS efficiency in each region. These figures indicate that the RWHS size reduction rate of the combined RWHSs increases compared with two single RWHSs as the difference in water demands and efficiency increases. However, the RWHS size reduction rate of the combined RWHSs is different depending on the four rainfalls and their regional characteristics.

Conclusion

This study investigated the effects of linked RWHS based on differences in combined RWHS sizes, water demands, and RWHS performance efficiencies. To verify the analytical method, this study confirmed that most of the conditions match well with the results of the analytical method and the physical performance model in four cities that represent different rainfall characteristics. This study found that the efficiency of the connected RWHS increased as RWHS size, the connected total RWHS size, and combined water demands increased. In addition, the RWHS size reduction rate increased as the difference in water demands, combined water demands, and combined RWHS efficiency increased. As a result, this study suggests that rainy regions, such as Seoul, Taipei, and NY, show greater benefits in increasing efficiency at a constant RWHS size when RWHSs are connected. In addition, semi-arid or arid regions (e.g., LA) show greater benefits in RWHSs size reduction to satisfy a constant efficiency in the connected RWHSs condition. However, the results of this study need to be verified with actual observed data because the results of the analytical performance model are applied. It will be different from the actual performance, although the analytical performance model is verified with the physical performance model used as reference results.

Acknowledgments

I want to thank my mentor, Sunghoon Jang, from Johns Hopkins University, for his constant support and guidance throughout my endeavors in this project.

References

- Jenkins, D.; Pearson, F., Feasibility of rainwater collection systems in California. *Contribution-California. University* 1978.
- Fewkes, A., Modelling the performance of rainwater collection systems: towards a generalised approach. *Urban Water* 2000, 1 (4), 3 23-333.
- Mitchell, V. G., How important is the selection of computational analysis method to the accuracy of rainwater tank behaviour modelling? *Hydrological Processes: An International Journal* 2007, 21 1 (21), 2850-2861.
- Jones, M. P.; Hunt, W. F., Performance of rainwater harvesting sys

- tems in the southeastern United States. Resources, *Conservation and Recycling* 2010, 54 (10), 623-629.
5. Semaan, M.; Day, S. D.; Garvin, M.; Ramakrishnan, N.; Pearce, A., Optimal sizing of rainwater harvesting systems for domestic water usages: A systematic literature review. *Resources, Conservation & Recycling: X* 2020, 6, 100033.
 6. Imteaz, M. A.; Ahmad, H.; Hossain, I., Pioneer Use of Pseudo Sub-Daily Timestep Model for Rainwater Harvesting Analysis: Acceptance over Hourly Model and Exploring Accuracy of Different Operating Algorithms. *Sustainability* 2023, 15 (5), 3870.
 7. Rupp, R. F.; Munarim, U.; Ghisi, E., Comparison of methods for rainwater tank sizing. *Ambiente construido* 2011, 11, 47-64.
 8. Cordova, M. M.; Ghisi, E., Analysis of potable water savings using behavioural models. *Water conservation. London: INTECH* 2011, 89-97.
 9. Heaney, J. P.; Lee, J. G., *Methods for optimizing urban wet-weather control system*. US Environmental Protection Agency, Office of Research and Development, 2006.
 10. Vargas, D.; Dominguez, I.; Ward, S.; Oviedo-Ocana, E. R., Assising global rainwater harvesting practitioners: a decision support tool for tank sizing method selection under uncertainty. *Environmental Science: Water Research & Technology* 2019, 5 (3), 506-520.
 11. Guo, Y.; Baetz, B. W., Sizing of rainwater storage units for green building applications. *Journal of Hydrologic Engineering* 2007, 12 (2), 197-205.
 12. Pelak, N.; Porporato, A., Sizing a rainwater harvesting cistern by minimizing costs. *Journal of Hydrology* 2016, 541, 1340-1347.
 13. Adams, B. J., *Urban stormwater management planning with analytical probabilistic models*. 2000.
 14. Zhang, S.; Jing, X.; Yue, T.; Wang, J., Performance assessment of rainwater harvesting systems: Influence of operating algorithm, length and temporal scale of rainfall time series. *Journal of Cleaner Production* 2020, 253, 120044.

■ Author

Saewoong Ian Park is a junior at Seoul International School in Seoul, South Korea. He is a student with an avid curiosity in diverse fields of study including environmental science and public policy. He believes that with the combination of STEM and legislative advancements, there will be effective solutions to solving world issues including the shortage and lack of access to water.

Comparative Analysis of the Prevalence of Domestic Violence in India, Basis the NFHS 2015-16 and 2019-21

Jassimrat K. Bhatia

Heritage International Xperiential School, Sector-58, Gurugram, Haryana, 122018, India; jassimratint10206@hixs.org

ABSTRACT: No nation is untouched by domestic violence, and it is well-known that it seriously impacts women's health and well-being. The present study aims to assess the prevalence and characteristics of domestic violence during the COVID-19 pandemic, as compared to the years before, using National Family Health Survey (NFHS) data from 2015-16 and 2019-21. The NFHS collects data nationally through surveys covering various topics, including domestic violence. For this study, graphical representations were created of physical, sexual, and spousal violence and marital control to compare data. Analysis showed that the prevalence of domestic violence has increased during the COVID-19 lockdown, and there has been no significant improvement in domestic violence rates, despite the disparity in the age of respondents between the two surveys. This indicates that more social and governmental programs and policies must be implemented to improve the prevalence of domestic violence in India.

KEYWORDS: Social Science; Sociology; Domestic Violence; NFHS; Data; Prevalence; COVID-19; Lockdown.

■ Introduction

Domestic Violence threatens women's lives, security, and fundamental rights of self-preservation and respect globally. Defined as a pattern of behavior in any relationship—marriages, living together, dating—used to gain or maintain power and control over an intimate partner,¹ Domestic Violence can occur in various forms and undermine through physical, sexual, emotional, economic, or psychological aspects, and even as threats of actions that influence another person.² It may also increase the risk of acquiring HIV in some settings.³

Although prevalent since the 15th century when the Catholic Church established its "Rules of Marriage," recommending husbands beating their wives as an accepted form of discipline that would benefit their soul, Domestic Violence came into light as a significant issue with the influence of the Women's Liberation Movement in the 1960s and 1970s.⁴ Globally, an estimated 736 million women—almost one in three—have been subjected to physical and sexual violence by an intimate partner, non-partner sexual violence, or both at least once in their life (30% of women were aged 15 and older).⁵

Globally, a woman's right to live free from violence is upheld by international agreements such as the Convention on the Elimination of All Forms of Discrimination against Women and the 1993 UN Declaration on the Elimination of Violence against Women.⁶ Social movements such as the #MeToo movement, started by Tarana Burke in 2006, and the UNiTE campaign of 16 days of activism to end violence have also sparked global movements to act upon abuse.⁷

Nationally, The Indian Parliament recognizes domestic violence, a rampant and deep-rooted issue in the Indian subcontinent, as "physical, sexual, verbal, emotional, and economic abuse against women by a partner or family member residing in a joint family."⁸ Women are subjected to violence from both husbands and members of the natal and marital

home. They remain less privileged than boys regarding their position in the family and society and access to material resources.⁹ Marriage continues to be regarded as essential for a girl; to control a woman's sexuality by labeling it as a family reputation that needs to be "handed over" to the husband who practically "owns" their wife.⁹ In India, while boys experience greater freedom, girls face extensive limitations on their ability to make decisions regarding their work, education, marriage, and social relationships.¹⁰ One in three women in India is likely to have been subjected to violence of a physical, emotional, or sexual nature by their partners.¹¹ The differences in educational attainment level or marital age between spouses, lack of autonomy within the home, dowry pressure, childhood abuse, unemployment, alcoholism, and poverty are all linked to high rates of domestic violence in India.⁹

The Constitution of India not only grants equality to women but also empowers the State to adopt measures in favor of women to neutralize the cumulative socio-economic, educational, and political disadvantages faced by them, as is mentioned in articles 14, 15, 16, and 39.¹² Furthermore, the Indian Penal Code condemns various crimes that come under domestic violence such as all forms of rape, torture, and harassment. Apart from the legislation, the government ensures several social policies and grants to protect victims and survivors of domestic violence, like helplines, safe houses, workshops, etc.¹³ However, the gap between laws and their effective enforcement leads to backward traditional and cultural practices, insensitivity of law enforcement machinery, and gender stereotypes.¹⁴

The occurrence of domestic violence differs from state to state in India. At the same time, women in the South report fewer cases of violence against them than their counterparts in the North. In-depth qualitative studies have found considerable under-reporting in the data.⁹ The data peaks in Maharashtra,

Haryana, and their eastern counterparts, with Uttar Pradesh topping the list with 59,853 incidents.¹⁵

The lockdown during the COVID-19 pandemic worsened domestic violence in the country. An increase in the prevalence of domestic violence at 32.5% was seen during the lockdown, with the most common form being verbal abuse and most of the abuse committed by the spouse or mother-in-law. While the medical community focused on controlling the spread of COVID-19, women who experience domestic violence may have been neglected, considering healthcare system challenges caused by the pandemic, as mentioned in the paper.¹⁶ A heightened risk was reported due to house quarantine, living near the abuser 24*7 with no means of escape.¹⁷ Also, it was linked with socio-economic variables such as homelessness and poverty. However, it is reported across all countries and in all socio-economic groups.¹⁸ Additionally, social isolation, exposure to economic and psychological stressors, an increase in negative coping mechanisms (such as alcohol misuse), and an inability to access usual support mechanisms are other cited reasons.¹⁷

Methodology

Research Aim: This research aims to compare the domestic violence stats based on different demographics over the two NFHS reports to identify and understand the possible socio-ecological reasons for the same.

Research Design: This quantitative analysis compares the NFHS India 2015-16 and 2019-21.¹⁹ The NFHS is a large-scale, multi-round survey conducted in a representative sample of households throughout India. The survey provides state and national information on domestic violence statistics across demographics, among other categories. For domestic violence, the NFHS considers physical, sexual, and emotional violence, marital control, and spousal violence. The fourth NFHS, conducted in 2015-16, sheds light on the much-changed state of domestic violence in India, whereas the fifth NFHS, undertaken in 2019-21, accounts for the pandemic in its results. Both surveys present statistics that require to be reflected upon.

Hypothesis: It is hypothesized that domestic violence statistics peaked during the COVID-19 pandemic duration due to restrictions on leaving households.

The results have been divided into four sections: : Physical Violence, Sexual Violence, Marital Control, and Spousal Violence, with further sub-sections within each area.

Results and Discussion

For all the graphs used in this section, blue denotes NFHS 4 (2015-16), and red indicates NFHS 5 (2019-21).

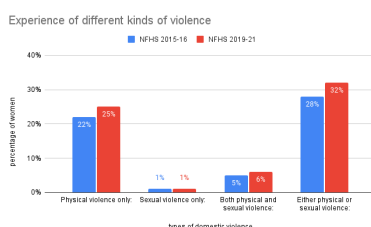


Figure 1 : Graphical representation of different kinds of violence experienced by women according to NFHS data 2015-16 and 2019-21.

In the overall comparison of the experience of different kinds of violence, as seen in Figure 1, NFHS 4 reported that 22% of women were prey to physical violence only, which increased to 25% in the 5th edition of the survey. Interestingly, the percentage of victims of sexual violence only remained constant at 1% for both surveys. While 5% of women experienced physical and sexual violence in 2015-16, the data increased to 6% during 2019-21. There was also an augmentation in the data for the experience of either physical or sexual violence, climbing to 32% in NFHS 5 from 28% in NFHS 4. This indicates a concerning rise in the number of females who experience violence. Sexual violence saw no increase over the two surveys, which means the impact of the COVID-19 pandemic was limited to higher physical aggression tendencies.²⁰ The present study showed an increase in physical aggression during mandatory social isolation, with 56 women reporting physical aggression in 2019 compared to 75 in 2020, an increase of + 32.1%. This result was further supported by the Buss-Perry Aggression Questionnaire (BPAQ), which showed a significant increase in scores for both months of lockdown regarding physical violence.²¹

Physical Violence:

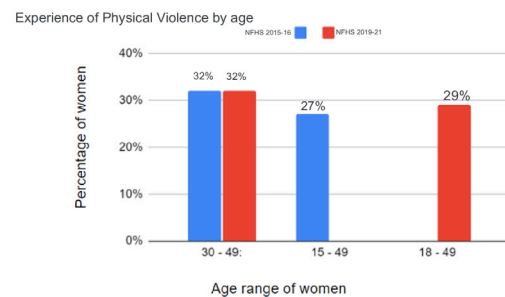


Figure 2: Graphical representation of the experience of physical violence by age according to NFHS data 2015-16 and 2019-21.

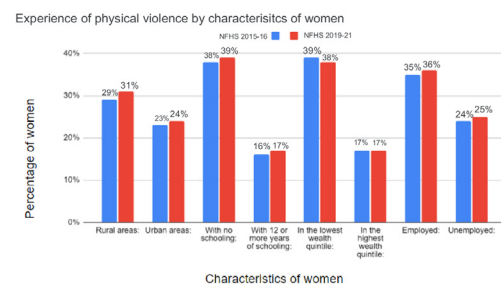


Figure 3: Graphical representation of the experience of physical violence by location, education, wealth, and employment according to NFHS data 2015-16 and 2019-21.

The experience of physical violence against women saw a trend in location, education, wealth, and women's employment over the two surveys, as can be seen in Figure 3.

Women in rural areas were more likely to experience violence, a data point which has only increased from 29% in NFHS 4 to 31% in NFHS 5. Violence in urban areas was also found to increase, but not as significant as in rural areas, with a slight increase from 24% to 25% in 2019-21. Supporting this, small rural and isolated areas reported the highest prevalence of violence (22.5% and 17.9%, respectively) compared to 15.5% for urban women.²² Rural women reported

significantly higher severity of physical abuse than their urban counterparts.²² The mean distance to the nearest inter-partner violence (IPV) resource was three times greater for rural women than for urban women, and rural IPV programs served more counties and had fewer on-site shelter services.²² Over 25% of women in small rural and isolated areas lived >40 miles from the closest program, compared with <1% of women living in urban areas.²²

Uneducated women were more likely to suffer from violence. This could be seen from the statistics, 38% of women with no schooling compared to 16% with 12 or more years of schooling in NFHS 4, and 39% with no schooling as compared to 17% in NFHS 5. Education allows people to understand their rights and empowers them to defend themselves and escape abusive situations.²³ The Centre for Women's Development Studies in New Delhi traced the correlation between education and domestic violence to patriarchal attitudes.²³ "Educated women are aware of their rights," she said. "They are no longer willing to follow commands blindly."²³

The data reported on wealth presented an interesting situation. While it was visible that wealthier women were less likely to be victims of domestic violence, the statistic has not changed over the two surveys (17%). The statistic for less wealthy women who become prey to domestic violence had decreased from 38% in NFHS 4 to 37% in NFHS 5. This indicates an improvement in viewing and considering low wealth in the country. Findings suggest that the relationship between wealth and domestic violence may vary considerably in the included low and middle-income countries. The risk of domestic violence may not necessarily be higher among women in lower wealth brackets.²⁴ Another possibility of the decrease may be due to the loss of wealth during the COVID-19 pandemic. The pandemic has exacerbated global income and wealth inequality, partly reversing the decline of the previous two decades.²⁵

Employed women were more likely to be more prone to domestic violence, 35% in 2015-16 and 36% in 2019-21, than unemployed women, 24% in 2015-16 and 25% in 2019-21. This is an extremely peculiar data point, as across the review of the literature present, employed women are more empowered to prevent and protect themselves against domestic violence. This disagreement between the normal trend and data collected in the NFHS might have emerged from the patriarchal mindsets where a woman is assigned a "typical" role in the family, restricted to the four walls of their houses and housework, and not allowed to work outside. Thus, when a woman sets out of this role, it tends to go against the male ego. Therefore, women who contributed more financially than their partners had a greater domestic violence risk.²⁶ However, to certifiably conclude that employment is a disadvantage when discussing the prevalence of domestic violence would be wrong and adds to the limitation of the study.

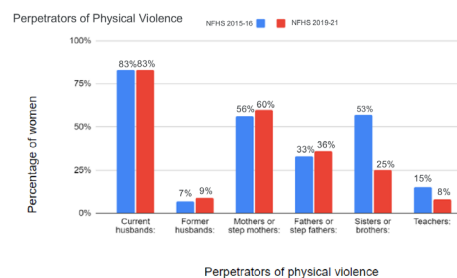


Figure 4: Graphical representation of perpetrators of physical violence according to NFHS data 2015-16 and 2019-2021.

As seen in Figure 4, for every married woman—women who have been married at least once—current husbands and former husbands were categorized as perpetrators. Curiously, the percentage of women who have identified their current husband as the perpetrator remained the same for both surveys, 83%, despite the pandemic and its restrictions.

For unmarried women—mothers or stepmothers, fathers or stepfathers, sisters or brothers, and teachers were categorized as perpetrators. An increase from 56% to 60% by mothers or stepmothers, and 33% to 36% by fathers or stepfathers, was observed during the lockdown. This might have been due to the pandemic restrictions that led to spending more time at home. Mothers or stepmothers were more violent than fathers and showed a 4% increase compared to 3% in the case of fathers. On the other hand, the data for sisters or brothers and teachers showed a cataclysmic fall. From 57% in 2015-16, sisters or brothers as perpetrators had fallen to less than half of that, at 25% in 2019-21. Similarly, teachers as perpetrators almost halved from 15% in 2015-16 to 8% in 2019-21.

Sexual Violence:

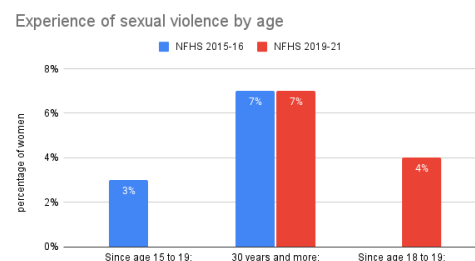


Figure 5: Graphical representation of the experience of sexual violence of age according to NFHS data 2015-16 and 2019-2021.

NFHS 4 and 5 considered the data for age, in terms of the experience of sexual violence, over different age ranges. Figure 5 shows that according to the NFHS 4, 3% of women aged 15-19, 7% aged 30-49, and 9% aged 15-49 had experienced sexual violence. On the other hand, NFHS 5 stated that 4% of women belonging to ages 18-19, 4% of women belonging to ages 20-24, 6% of women belonging to ages 25-29, and 7% of women of ages 30 or more had fallen prey to sexual violence, with 6% of women experiencing it once in their lifetime. The only comparable statistic, of women of ages 30 and above, had remained constant over the two surveys, denoting that there had been no increase or decrease in the sexual violence experience for the women in those ages. However, since 18-19 had a 1% increase in NFHS 5 compared to a more extensive set of 15-19-year-olds in NFHS 4, this indicates that sexual violence is more rampant in the ages of 18 and 19. Furthermore,

the trend in the case of age, for both the surveys, showed an increase in the percentage of women experiencing sexual violence with an increase in their generation.

A detailed study of trial court cases from January 2013 to September 2015 in Delhi State undertaken by the Centre for Child and the Law, National Law School of India University (NLSIU), Bangalore, recorded 526 complaints of sexual assault under POCSO.²⁷ Twenty-eight 28% of these (186 complaints) concerned adolescents between the ages of 16 and 18.²⁷ Data used from 'Crime in India,' an annual publication of the National Crime Record Bureau of India finds that the share of rape of elderly women as a percentage of the total number of rape incidents has increased in the past years, especially since 2014-16.²⁸ It mentions that in 2015, 66% of reported sexual violence cases belonged for the age group of 18 to 50, as compared to 32% of cases below 18 years of age, clearly showing the augmentation in the statistic with age.²⁸ The study concludes by stating that the findings indicate an exponential increase in the incidence of rape and sexual violence against elderly women, both in absolute numbers and as a share of the total number of incidents of rape against women.²⁸ Furthermore, the impact of the pandemic on the cases of sexual violence clearly shows that they have increased. Since the pandemic, an increased statistic of 6 in 10 women said that sexual harassment in public has worsened.²⁹

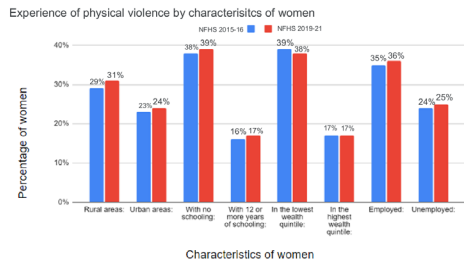


Figure 6: Graphical representation of the experience of sexual violence by education and wealth according to NFHS data 2015-16 and 2019-2021.

Data gathered in 2015-16 from NFHS 4, illustrated in Figure 6, reported that approximately 8% of females with no schooling experienced sexual violence compared to 3% with 12 or more years of schooling. With a similar trend of sexual violence being more prevalent for uneducated females, data gathered in NFHS 2019-21 indicated that 9% of women without schooling fell prey, compared to 3% with 12 or more years of education. The statistics of educated victims of sexual violence had remained the same over both surveys, whereas there had been a 1% increase in the statistics for uneducated victims.

A cross-sectional study on the association between women's level of education and their experience of intimate partner violence (IPV) also concluded that women with higher education have a lower risk of physical and sexual IPV.³⁰ Further, in some aspects of the violence, women's level of education has a protective effect.³⁰ Additionally, less educated women reported more violence, which was statistically significant.³¹

Regarding wealth, 9% of women in the lowest and 3% of women in the highest had faced sexual violence in NFHS 2015-16. In NFHS 5, 10% of women in the lowest wealth

quartile faced sexual violence, along with the constant data of 3% of women in the highest wealth quartile. This establishes that women in the lowest wealth quartile are almost three times more likely to face violence, and the percentage had increased by 1% over the two surveys. A study of 21 cases of sexual assault, out of which 61.9% belong to rural backgrounds, concluded that young girls from poor settlements and lower social strata should especially receive special attention regarding sexual violence.³² Furthermore, violence during the pandemic stated that 66% of women living in rural areas were also more likely to think that sexual harassment in public spaces has worsened, compared to 55% of women living in urban areas.²⁹ And since, in India, the poverty ratio is 32.75% in rural areas against 8.81% in urban areas, the prevalence of sexual violence for unwealthy women has increased, especially during the pandemic.³³ Globally, violence against women disproportionately affects low- and lower-middle-income countries and regions.³⁴ 37% of women aged 15 to 49 living in countries classified by the Sustainable Development Goals as "least developed" have been subject to physical and sexual intimate partner violence in their life.³⁶ 22 % of women in "least developed countries have been subjected to IPV in the past 12 months—substantially higher than the world average of 13%.³⁶

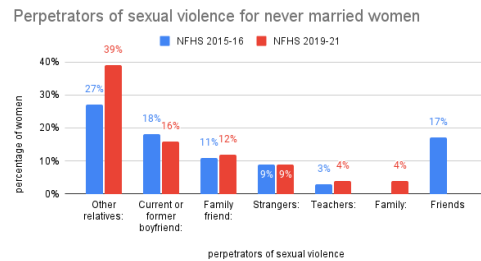


Figure 7: Graphical representation of perpetrators of sexual violence for never-married women according to NFHS data 2015-16 and 2019-2021.

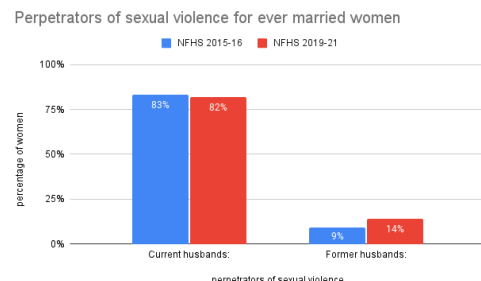


Figure 8 : Graphical representation of perpetrators of sexual violence for ever-married women according to NFHS data 2015-16 and 2019-2021.

Figure 8 portrays that the most common perpetrators of sexual violence for married women were their current husbands- 83% in NFHS 4 and a reduction of just 1% in NFHS 5. An increased statistic of 14% of the former husbands as perpetrators emerged in NFHS 5, compared to 9% in NFHS 4, which is unlikely and needs further speculation. Of those in a relationship, almost one in four adolescent girls aged 15–19 (24%) have experienced physical and sexual violence from an intimate partner or husband.⁵ 16% of young women aged 15 to 24 experienced this violence in the past 12 months.⁵ Globally, 81,000 women and girls were killed in 2020, and around

47,000 of them (58%) died at the hands of an intimate partner or a family member.³⁵

For unmarried women, as seen in Figure 7, other relatives were the most common perpetrator, at 27% in NFHS 4 and 39% in NFHS 5, followed by a current or former boyfriend, which reduced to 16% in NFHS 5 from 18% in NFHS 4, a family friend at 11% in NFHS 4 and 12% in NFHS 5, 9% of strangers over both the surveys, 3% teachers in NFHS 4 and 4% in NFHS 5, 4% for a family in NFHS 5 (not accounted in NFHS 4) and 17% for friends in NFHS 4 (not accounted for NFHS 5). Globally, 6 % of women report they have been subjected to sexual violence from someone other than their husband or partner.³⁶ These statistics for never-married women can be highly influenced by the pandemic. The data for relatives has increased, and family friends and family has grown— all possible due to residence restrictions during the lockdown. Similarly, data for boyfriends and friends has decreased or been disregarded due to its low prevalence, as public meetings were restricted during the pandemic. Interestingly, the data for teachers as perpetrators have increased, even though most schools were online or closed due to COVID-19 and the lockdown.

Marital Control:

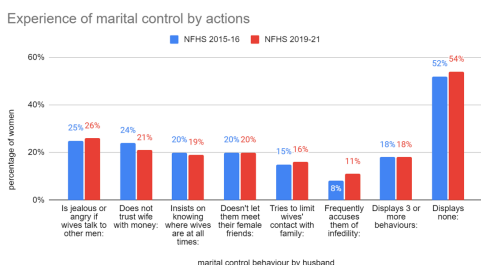


Figure 9: Graphical representation of the experience of marital control by actions according to NFHS data 2015-16 and 2019-2021.

The NFHS survey data also encompasses marital control data, including attempts by husbands to control and monitor their wives' lives and behavior closely; the same is portrayed graphically in Figure 9. If looked at through the lens of actions perpetrated by the husbands, 26% of women reported that their husbands get jealous if they talk to other men in NFHS 5, a 1% increase from the 25% of women in NFHS 4. Additionally, a 3% higher number of 11% of women were frequently accused of infidelity in 2019-21 compared to 2015-16. Jealousy, or the fear of infidelity, in addition to exacerbating relationship conflicts and tension, is described to lead directly to physical inter-partner violence.³⁷ This was often described as a trigger for men, though rarely women, to use violence against their partners in response to actual or suspected infidelity.³⁷

The data point for “insists on knowing where wives are at all times” has also fallen by 1% in NFHS 5, compared to 19% in NFHS 4. Similarly, this could also be related to the restrictions brought upon by the pandemic, strictly limiting any travel outside the home. In both surveys, 20% of women were not allowed to meet their friends. This shows that irrespective of legal restrictions, females are prohibited from meeting their friends. In addition, 16% of women were limited in their

contact with their family in 2019-21, another 1% augmentation from the 2015-16 data.

The percentage of women who reported that their husbands displayed three or more controlling behaviors remained constant at 20%. However, the percentage of women who reported that their husbands demonstrated none of the behaviors increased to 54% in NFHS 5 from 52% in NFHS 4. This shows that the number of males who are less controlling has increased. However, the controlling population has remained constant.

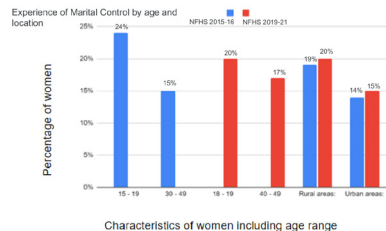


Figure 10: Graphical representation of the experience of marital control by age and location to NFHS data 2015-16 and 2019-2021.

Since the age samples for both surveys are different, they cannot be compared. However, in Figure 10, the percentage of women experiencing marital control during ages 18-19 and 40-49 was 20% and 17%, respectively, in 2019-21, as compared to 24% and 15% in 2015-16; this portrays how older women are more prone to marital control. Suppose the smaller sample sizes carry a large amount of data. In that case, it means that the incidents are concentrated during that period, thus indicating how out of a larger sample, a smaller range is more susceptible— the elder bracket. Such marital control in old age is also related to domestic violence. Furthermore, the data for rural and urban women showed that spousal control is more prominent in rural areas, increased by 1% from 2015-16 to 2019-21— 19% to 20% for rural women and 14% to 15% for urban women. This highlights an apparent increase in the rise of the number of women who experience marital control, regardless of their location. Domestic violence and spousal control were not associated with the tested outcomes among urban women but with rural women.³⁸ Patriarchal views of the family, including traditional roles about gender relations and gender inequality, are commonly held in rural communities.^{39,40} These factors may affect a woman's ability to speak out about abuse, reinforcing the message that what happens between a husband and wife is a private matter.⁴¹ This social structure perpetuates violence as a means of social control.³⁹

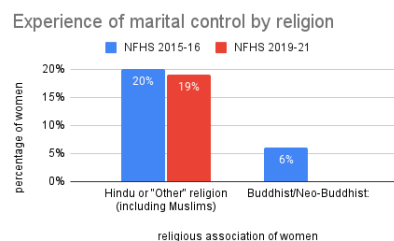


Figure 11: Graphical representation of the experience of marital control by religion according to NFHS data 2015-16 and 2019-2021.

Surprisingly, the NFHS survey data considers only three religions when determining the categories, especially in religiously vibrant demographics like the Indian subcontinent, as seen in Figure 11. Hindus and Muslims make up most of the Indian population; Hindus make up 79.8% of India's population, and Muslims account for 14.2%. Therefore, since the probability of women taking the survey being Hindu/Muslim is higher, their reported cases might be high too. In NFHS 4, 20% of such women reported experiencing marital control, which decreased to 19% in NFHS 5.

As for Buddhism, Buddhist beliefs and gender roles within the Buddhist community perpetuate or silence the issue of violence against women (VAW) and how these beliefs can be used to break the cycle of gender violence.⁴² Buddhism's core values are important in that they may be used to heal and empower survivors of VAW rather than perpetuate violence.⁴³ Thus, it is possible that women of the Buddhist community are more aware and so step forward as victims. 6% of Neo-Buddhist/Buddhist females reported having dealt with marital control, a statistic not collected in 2019-21.

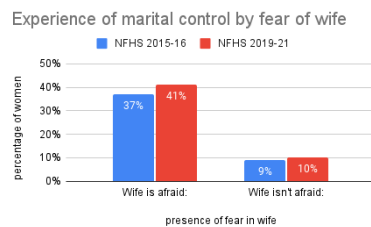


Figure 12: Graphical representation of the experience of marital control by the wife's fear according to NFHS data 2015-16 and 2019-2021.

Data collected shows that marital control is more prevalent if the wife is afraid of the husband, the percentage for which has also increased over the years; this is portrayed through Figure 12. As per NFHS 4, 37% of women reported being fearful of their husbands as a part of marital control, whereas 9% of women did not. In 2019-2021, a significant increase occurred in the percentage of women who were afraid of their husbands, 41%, whereas only a 1% increase was observed in the number of women who said they were not scared of their husbands. This shows that the prevalence of marital control has increased over the two surveys and that more women were afraid of their husbands in NFHS 5.

Spousal Violence:

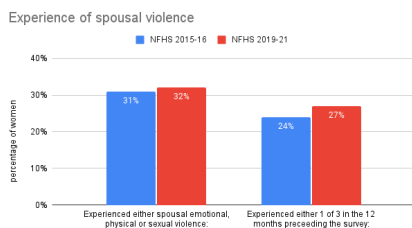


Figure 13: Graphical representation of the experience of spousal violence according to NFHS data 2015-16 and 2019-2021.

Data on spousal violence indicates augmentation between NFHS 4 and 5, as seen in Figure 13. An increase of 1% of women who experienced either spousal sexual, emotional, or physical violence in 2019-21 compared to 31% in 2015-16.

Furthermore, 27% of women experienced it in the 12 months preceding the survey in NFHS 5, and it increased from 24% in 2015-16.

The findings of a rapid 8-day online survey on spousal violence against women during the COVID-19 lockdown in India support this analysis.⁴⁴ Of the 101 positive responses, the rates of physical, sexual, verbal, and emotional violence were 34.7%, 10.9%, 65.3%, and 43.6%, respectively.⁴⁴ While 13.6% (n=76) reported spousal violence experienced before the lockdown, 4.5% (n=25) said it to have begun since the lockdown.⁴⁴ This indicates a 33.1% increase in the rates since the lockdown.⁴⁴ Of those who reported spousal violence to be present before the lockdown, 77.6% (n=59) reported increased violence since the lockdown was enforced.⁴⁴ The study concluded that the responses they received reflected an increase in spousal violence since the COVID-19 lockdown in India.⁴⁴

Slapping was the most common form of spousal physical violence (25%), followed by pushing, shaking, and having something thrown at you (12%). This more than 10% difference between the two most common forms portrays slapping as a rapidly occurring and widespread action. Arm twisting or hair pulling closely follow (10%), with punching and beating (8%) and choking or burning being the least common (2%). The gap of 6% between the least two common forms portrays the extremely rare prevalence of choking or burning—meaning when it is exercised, the situation is dire. However, the interesting detail is that none of the actions has seen a percentage increase over the two surveys. This indicates that the trends of physical abuse have remained the same, despite the lockdown. Almost 50% of women out of a sample of 500 in Maharashtra reported being slapped at a point in their marriage, the most common prevalence of physical violence in the model.⁴⁵ This evidences the high prevalence of slapping as part of spousal physical violence, which hasn't changed during the lockdown.

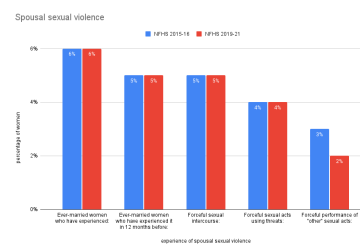


Figure 14: Graphical representation of the experience of spousal sexual violence according to NFHS data 2015-16 and 2019-2021.

Figure 14 shows that data collected on spousal sexual violence indicate either no change or decrease over the period of NFHS 4 and NFHS 5. 6% of ever-married women had experienced spousal sexual violence, and 5% had experienced it in the 12 months preceding the survey over the course of both surveys. Although this shows no increase in spousal sexual violence due to the lockdown, it does mean that occurrences of sexual violence are more rampant, as out of the 6% who had ever experienced it, 83% of them experienced it in the 12 months preceding the survey.

Forced sexual intercourse was the most common method of spousal sexual violence, at 5%. Experiences of forced sexual relations, often perpetrated by an intimate partner, have been increasingly documented over the last decade. An analysis of over fifty population-based surveys revealed, for example, that between 10 and 50% of adult women globally reported having been physically assaulted by an intimate male partner, including husbands, at some point in their lives and in more than one-third of these cases sexual abuse was also experienced.⁴⁶ A recent review of non-consensual sexual experiences of young people, primarily those aged thirteen to twenty-four, also suggests that between 2 and 20% of adolescent and young women have experienced non-consensual sexual relations.⁴⁷ Although significant proportions of sexually active adolescents and young women (fifteen to twenty-four-year-olds) in developing-country settings are married, the literature is surprisingly silent on the sexual experiences of these young women and the extent to which these experiences are wanted or consensual.⁴⁷ Evidence on forced sexual experiences within marriage among adolescents and young women in India comes mainly from qualitative studies.⁴⁷ Quantitative data are also available from three small-scale surveys highlighting such experiences' prevalence. These surveys, conducted in the states of Gujarat and West Bengal, observe that between 6 and 13% of young married women reported forced sexual experiences perpetrated by their husbands.^{48,49}

Interestingly, the percentage data for "forced sexual performance of 'other' acts" saw a fall of 1%, from 3% in NFHS 4 to 2% in NFHS 5, meaning that forceful performances of such acts were reduced over the course of the lockdown. Although there is no certified reasoning as to why this has decreased, a changed age sample may play a role. If that is the case, then it would imply that women between the ages of 15 and 18 years old are more likely to be forced to perform 'other' sexual acts, as compared to women above 18 years of age. Furthermore, this may also indicate how the development of the human mind and maturity of the body can influence a woman's experience of domestic spousal violence.

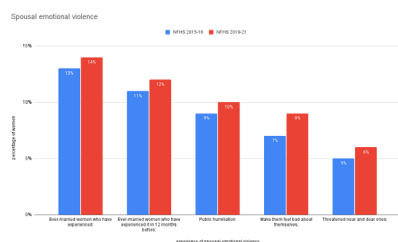


Figure 15: Graphical representation of the experience of spousal emotional violence according to NFHS data 2015-16 and 2019-2021.

Data collected on spousal emotional violence had increased over the period of NFHS 4 and 5, as seen in Figure 15. For example, ever-married women who experienced it in NFHS 4 were 13%, which increased to 14% in NFHS 5. Similarly, ever-married women who experienced it in the 12 months preceding the survey in NFHS 4 was 11%, which increased to 12% in NFHS 5. This indicates that spousal emotional

violence increased during the lockdown but also saw more rampant incidences, as 85% occurred in the recent past.

A cross-sectional study conducted in June–August 2020 on married Indian women of reproductive age who attended the obstetrics-gynecology outpatient department during the COVID-19 pandemic using The Abuse Assessment Screening questionnaire had 412 women included in the study.¹⁶ The prevalence of domestic violence in any form was 32.5%, with one of the majority being public humiliation.¹⁶ Furthermore, the percentage of making wives feel bad about themselves was the highest, from 7% in NFHS 4 to 9% in NFHS 5. This means that feelings of superiority, disrespect, and ego were heightened in husbands during the lockdown. Lastly, threatening near and dear ones also increased to 6% in NFHS 5 from 5% in NFHS 4.

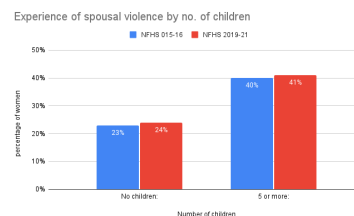


Figure 16: Graphical representation of several children's experience of spousal violence according to NFHS data 2015-16 and 2019-2021.

Women with five or more children are almost twice as likely to experience spousal violence as women without children, as seen in Figure 16. These data points saw an increase over the two surveys. In NFHS 4, 23% of women with no children faced spousal violence, and 40% of women with five or more children. In NFHS 5, increased figures of 24% and 41% were observed. However, literature on the link between the number of children and violence experienced by women is lacking in context to the Indian scenario so no conclusion could be drawn from this data.⁵¹

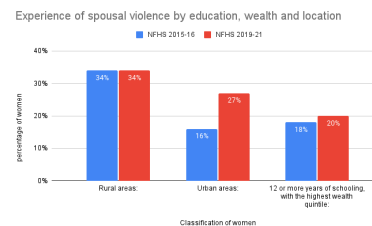


Figure 17: Graphical representation of the experience of spousal violence by education, wealth, and education according to NFHS data 2015-16 and 2019-2021.

Figure 17 portrays that spousal violence is more prevalent in uneducated women who reside in rural areas, the percentage of which remained constant for both surveys (34%). A community-based cross-sectional study was carried out in a rural area of Puducherry, South India.⁵⁰ Married women in the reproductive age group were interviewed using a structured pretested questionnaire.⁵⁰ Of 310 study participants, 56.7% reported some form of domestic violence, 51.3% said psychological violence, 40% reported physical violence, and 13.5% reported sexual violence.⁵⁰ A statistically significant association was found between women's illiteracy and domes-

tic violence (AOR: 4.3, 95% confidence interval: 1.1–15.7 P: 0.03).⁵⁰ The prevalence of domestic violence was found to be high in this rural setting.⁵⁰

However, data about the experience of spousal violence in urban areas saw a significant increase during the lockdown, from 16% in NFHS 4 to 27% in NFHS 5. This evidence can be seen in heightened statistics from major Indian metropolitan cities. For example, data showed that domestic violence complaints doubled after the nationwide lockdown was imposed in India.⁵² Tamil Nadu Police reported an increase in domestic violence complaints. They received approximately 25 calls daily during the lockdown period and registered at least 40 such cases.⁵³ Similarly, Bangalore Police reported a spike in complaints from 10 calls to 25 calls every day from the victims of domestic violence.⁵⁴ These data from different sources indicate that domestic violence incidents increased nationwide during the lockdown.

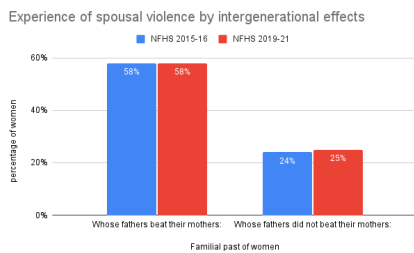


Figure 18: Graphical representation of the experience of spousal violence by intergenerational effects according to NFHS data 2015-16 and 2019-21.

Women whose fathers beat their mothers were more likely to experience spousal violence, 58% of which was consistent throughout both surveys, as is visible in Figure 18. Childhood exposure to parental and spousal violence plays a vital role in shaping conformation to the gender role norms in India.⁵⁵ Moreover, the findings suggest that exposure to childhood violence has a more devastating effect on building women's understanding of gender norms.⁵⁵ Also, there is high concordance in the recent experience of spousal violence against women and spousal violence faced by their mothers.⁵⁵ The risk of a lifetime and past-year physical and sexual violence was significantly higher for those who witnessed interparental violence during childhood than those without such experience.⁵⁶ Women with experience of interparental violence during childhood reported acceptance of violence within an intimate relationship to a greater extent than those without such experience.⁵⁶ This indicates that intergenerational effects have a strong influence over spousal violence.

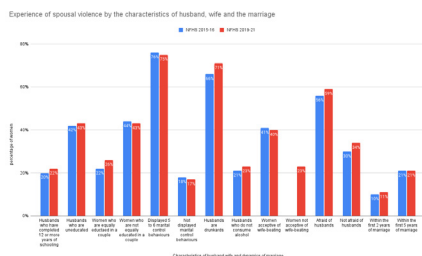


Figure 19: Graphical representation of the experience of spousal violence by the characteristics of husband, wife, and the marriage according to NFHS data 2015-16 and 2019-2021.

As shown through Figure 19, literacy and levels of education attained by men also have a significant impact on reducing the incidence of domestic violence.⁵⁷ Spousal violence was almost twice as prevalent when the husband is not educated (42% in NFHS 4, 43% in NFHS 5) than when husbands have completed 12 or more years of schooling (20% in NFHS 4, 22% in NFHS 5). Their study concludes that husbands with higher levels of education are less likely to engage in violence.⁵⁷

Furthermore, evidence from other countries indicates a lower incidence of domestic abuse in couples where the woman is more educated than the husband or partner compared to equally low-educated spouses.⁵⁷ This supports the findings from NFHS 4 and 5, where women who are equally educated in a couple were less likely to suffer spousal violence (22% in NFHS 4 and 26% in NFHS 5) as compared to women who are not equally educated (44% in NFHS 4 and 43% in NFHS 5). While the statistic for equally educated women who suffer spousal violence had risen during the lockdown, the statistic for unequally educated women who suffer spousal violence had decreased. This indicates how restrictions due to the COVID-19 pandemic have negatively impacted literate females in terms of the violence faced and positively impacted illiterate females.

Data on the relationship between marital control behaviors and spousal violence decreased over the two surveys. For example, couples, where the husband displayed five or more marital control methods were more likely to suffer spousal violence, 76% in NFHS 4 to 75% in NFHS 5, as compared to couples where the husband did not display any marital control behavior, 18% in NFHS 4 to 17% in NFHS 5.

Data reflects that husbands with a drinking addiction were more likely to propel spousal violence, an increased statistic of 71% in 2019-21 from 66% in 2015-16, as compared to husbands that do not drink, which also saw an increase from 21% in 2015-15 to 23% in 2019-21. Although there are mixed findings concerning changes in the quantity of drinking, there are reports of binge/heavy drinking during the lockdown and relapse post-lockdown.⁵⁸ Furthermore, positive, zero-order correlations were found between antisocial behavior, long-term alcohol involvement, family conflict, and husbands' reports of violent behavior toward their wives.⁵⁸ A history of alcohol-related troubles was associated with a hostile family environment and increased violence in the home.⁵⁹

In NFHS 4, 41% of women acceptive wife-beating suffered spousal violence. Data for women not acceptive of wife-beating was not recorded then. This is a research gap. In NFHS 5, 40% of women acceptive of wife-beating suffered spousal violence, 1% lesser than last year. 23% of women not acceptive of wife-beating suffered spousal violence in 2019-21. This shows that women accepting of beating are more likely to suffer spousal violence. This statistic has seen a reduction, and this can be because more women are now becoming self-aware of their rights and are standing up against violence.

Conclusion

A pattern has emerged from the findings of the two surveys on the parameters that make women more prone to

experiencing domestic violence. Aged, married, uneducated, employed, poor, and rural women are more prone to violence. However, how the lockdown has impacted the severity of these factors differs for each. While most categories saw an increase during the pandemic years, some, especially those that included literacy aspects, saw a fall. This implies that while overall, the pandemic caused a rise in violence, it led to improvements in categories due to situational problems such as mass unemployment, financial stress, and fear of disease also impacting the psyche. Different factors were found to play a role; hence, there is a need for social revolution for this public health concern.

■ Limitations

This paper has some potential limitations. Firstly, the data analysis is primarily based on secondary data collected from a restricted sample. This may lead to problems in generalization due to the extensive nature of the Indian population and also because many study victims reside in rural areas that are remote and unreachable. Secondly, the data gathered is spread over a large span of years and does not consider other changes that might have occurred over the two surveys, such as economic and demographic changes. Similarly, the paper's analysis is primarily based on the assumption that the lockdown restrictions led to an increase in the statistics. However, there is no primary data evidence of the same. Lastly, limitations in the analysis also arose from gaps in the available research knowledge.

This includes that change in sample size over the two surveys, making it impossible for data to be compared and analyzed at par. NFHS 4 considered women from age 15 onwards; NFHS changed that to age 18, completely disregarding three years of probable violence. While there has been no mention of an apparent reason, the legal age of marriage might play a role. For example, NFHS 4 stated that 27% of women aged 20-24% got married before the legal age of 18. However, this had decreased to 23% in NFHS 5. Therefore, the sample could have changed since more women were getting married at 18. This is also indicated in the fact that 16% of women had experienced violence in both 15-19 and 18-19. Since 18-19 is a more concentrated sample, this would mean that similar statistics data shows more rampant violence for that age group.

The lack of data on non-spousal emotional violence also makes it difficult to compare married and unmarried individuals, or establish a relationship, if any, between marriage and the occurrence of emotional violence. Additionally, a minimal scope of religious categorization has been presented by NFHS, despite the immensely varied religious population of the Indian subcontinent. This also makes it challenging to analyze the link between religion and violence and research the causes and consequences of different faiths for the same.

■ Implications

The paper brings to light various gaps in the NFHS data like the difference in age groups, making it difficult to compare data across years, and increasing religious variety that would be critical in helping to understand the implication of religion on the occurrence of domestic violence, and also data

on non-spousal emotional violence, which may help bring to light a large sample of women being neglected. Furthermore, the stagnant or increasing data points call for greater government programs to manage and control domestic violence. Therefore, the paper may help in policy creation.

■ Acknowledgments

My gratitude remains with my research team for guiding me every step of the way and making this paper truly a pleasure to work on, as well as my parents, who have remained as supportive and motivating throughout this process as they have been for everything I have done in my life.

■ References

1. United Nations. What Is Domestic Abuse? UNITED NATION S. <https://www.un.org/en/coronavirus/what-is-domestic-abuse>.
2. Kaur, R.; Garg, S. Addressing Domestic Violence against Women: An Unfinished Agenda. *Indian Journal of Community Medicine* 2008, 33 (2), 73. <https://doi.org/10.4103/0970-0218.40871>.
3. World Health Organization. Violence against women. www.who.int. <https://www.who.int/news-room/fact-sheets/detail/violence-against-women#:~:text=Estimates%20published%20by%20WHO%20indicate>.
4. Fader, S. A History of Domestic Violence: How Much Have Things Changed? | Betterhelp. www.betterhelp.com. <https://www.betterhelp.com/advice/domestic-violence/a-history-of-domestic-violence-how-much-have-things-changed/>.
5. UN Women. Facts and figures: Ending violence against women. UN Women. <https://www.unwomen.org/en/what-we-do/ending-violence-against-women/facts-and-figures>.
6. UN Women. What we do: Ending violence against women. UN Women. <https://www.unwomen.org/en/what-we-do/ending-violence-against-women>
7. Nations, U. International Day for the Elimination of Violence against Women. United Nations. <https://www.un.org/en/observances/ending-violence-against-women-day>.
8. THE PROTECTION of WOMEN from DOMESTIC VIOLENCE ACT, 2005. https://www.indiacode.nic.in/bitstream/123456789/15436/1/protection_of_women_from_domestic_violence_act%2C_2005.pdf.
9. A Summary Report of a Multi-Site Household Survey Domestic Violence in India; 2000. <https://www.icrw.org/wp-content/uploads/2016/10/Domestic-Violence-in-India-3-A-Summary-Report-of-a-Multi-Site-Household-Survey.pdf>.
10. UNICEF. Gender equality. www.unicef.org. <https://www.unicef.org/india/what-we-do/gender-equality>.
11. 1 in 3 women in India is likely to have been subjected to intimate partner violence | BMJ. [BMJ](http://www.bmj.com). <https://www.bmj.com/company/newsroom/1-in-3-women-in-india-is-likely-to-have-been-subjected-to-intimate-partner-violence/>.
12. Violence against women in India and the remedies as per the Indian Constitution - A Critical Analysis. [legalserviceindia.com](http://www.legalserviceindia.com/legal/article-4208-violence-against-women-in-india-and-the-remedies-as-per-the-indian-constitution-a-critical-analysis.html). <https://www.legalserviceindia.com/legal/article-4208-violence-against-women-in-india-and-the-remedies-as-per-the-indian-constitution-a-critical-analysis.html>
13. English Releases. pib.gov.in. <https://pib.gov.in/newsite/erelcontent.aspx?relid=35773#:~:text=Article%2042%20directs%20the%20State> (accessed 2023-04-14).
14. Sharma, I. Violence against Women: Where Are the Solutions? *Indian Journal of Psychiatry* 2015, 57 (2), 131. <https://doi.org/10.4103/0019-5545.158133>.
15. राशक्य अपराध *रकॉड. /यूरो. ncrb.gov.in. <https://ncrb.gov.in/sites/default/files/CII%202019%20Volume%201.pdf>.
16. Kamath, A.; Yadav, A.; Baghel, J.; Mundle, S. Locked Down: Ex

- periences of Domestic Violence in Central India. *Global Health: Science and Practice* 2022, 10 (4), e2100630. <https://doi.org/10.745/ghsp-d-21-00630>.
17. Gulati, G.; Kelly, B. D. Domestic Violence against Women and the COVID-19 Pandemic: What Is the Role of Psychiatry? *International Journal of Law and Psychiatry* 2020, 71, 101594. <https://doi.org/10.1016/j.ijlp.2020.101594>.
 18. Thompson, R. S.; Bonomi, A. E.; Anderson, M.; Reid, R. J.; Dimer, J. A.; Carrell, D.; Rivara, F. P. Intimate Partner Violence. *American Journal of Preventive Medicine* 2006, 30 (6), 447–457. <https://doi.org/10.1016/j.amepre.2006.01.016>
 19. National Family Health Survey. Rchiips.org. <http://rchiips.org/nfhs/>.
 20. Araujo, S. C. S.; de Souza, A. A. B.; Coelho, L. V.; Ramos, G. V.; Silveira, R. L.; Amaral, M. B. F. Did Physical Aggression in Women Increase during the Novel Coronavirus 2019 (COVID-19) Pandemic? A Perspective of Facial Trauma. *Oral and Maxillofacial Surgery* 2022. <https://doi.org/10.1007/s10006-022-01118-2>.
 21. Killgore, W. D. S.; Cloonan, S. A.; Taylor, E. C.; Anlap, I.; Dailey, N. S. Increasing Aggression during the COVID-19 Lockdowns. *Journal of Affective Disorders Reports* 2021, 5, 100163. <https://doi.org/10.1016/j.jadr.2021.100163>.
 22. Peek-Asa, C.; Wallis, A.; Harland, K.; Beyer, K.; Dickey, P.; Saftlas, A. Rural Disparity in Domestic Violence Prevalence and Access to Resources. *Journal of Women's Health* 2011, 20 (11), 1743–1749. <https://doi.org/10.1089/jwh.2011.2891>.
 23. Development of Women through Education Against Domestic Violence. *International Journal of Education and Information Studies* 2011, 1 (1), 1–5.
 24. Kebede, S.; Van Harmelen, A.-L.; Roman-Urrestarazu, A. Wealth Inequality and Intimate Partner Violence: An Individual and Ecological Level Analysis across 20 Countries. *Journal of Interpersonal Violence* 2021, 36(10), 1088626052110163. <https://doi.org/10.1177/08862605211016337>.
 25. Adarov, A. Global income inequality and the COVID-19 pandemic in three charts. [blogs.worldbank.org](https://blogs.worldbank.org/developmenttalk/global-income-inequality-and-covid-19-pandemic-three-charts). <https://blogs.worldbank.org/developmenttalk/global-income-inequality-and-covid-19-pandemic-three-charts>.
 26. Abramsky, T.; Lees, S.; Stöckl, H.; Harvey, S.; Kapiga, I.; Ranganathan, M.; Mshana, G.; Kapiga, S. Women's Income and Risk of Intimate Partner Violence: Secondary Findings from the MAISH A Cluster Randomised Trial in North-Western Tanzania. *BMC Public Health* 2019, 19 (1). <https://doi.org/10.1186/s12889-019-7454-1>.
 27. Pitre, A.; Lingam, L. Age of Consent: Challenges and Contradictions of Sexual Violence Laws in India. *Sexual and Reproductive Health Matters* 2021, 29 (2), 1–19. <https://doi.org/10.1080/26410397.2021.1878656>.
 28. Singh, T. Geriatric Sexual Violence in India: Studying State-Wise and Year-Wise Trends. <http://maitreyi.ac.in/Datafiles/cms/2020/magzine/issue%202020-1/geriatric.pdf> (accessed 2023-04-14).
 29. VIOLENCE against WOMEN during COVID 19 MEASURING the SHADOW PANDEMIC: 2. <https://data.unwomen.org/sites/default/files/documents/Publications/Measuring-shadow-pandemic.pdf>.
 30. Loembe, D. Association between Women's Level of Education and Their Experience of Intimate Partner Violence in Nigeria: A Cross-Sectional Study. <https://www.diva-portal.org/smash/get/diva2:1472860/FULLTEXT01.pdf>.
 31. Shetty, S.; Kundapur, R.; Kempaller, V.; Kumar, A.; Anurupa, M. Violence against Educated Women by Intimate Partners in Urban Karnataka, India. *Indian Journal of Community Medicine* 2017, 42 (3), 147. https://doi.org/10.4103/ijcm.ijcm_41_16.
 32. Aggarwal, A. D.; Singh, P.; Walia, D. S.; Kukreja, S. Study of Sexual Assault Cases among below 18 Years Age Group during September 2018 to September 2020 in Government Medical College, Patiala, Punjab, India: Cross-Sectional Study. *Pan African Medical Journal* 2022, 41. <https://doi.org/10.11604/pamj.2022.41.15.29852>.
 33. Dhasmana, I. Poverty Ratio 32.75% in Rural Areas against 8.81% in Urban: NITI Report. *Business Standard India*. December 5, 2021. https://www.business-standard.com/article/economy-policy/poverty-ratio-32-75-in-rural-areas-against-8-81-in-urban-niti-report-121120500971_1.html.
 34. UN Women. Facts & Figures. UN Women. <https://www.unwomen.org/en/news/in-focus/commission-on-the-status-of-women-2012/facts-and-figures>
 35. UNODC Research: 2020 saw a woman or girl being killed by someone in their family every 11 minutes. United Nations: Office on Drugs and Crime. https://www.unodc.org/unodc/frontpage/2021/November/unodc-research_-2020-saw-every-11-minutes-a-woman-or-girl-being-killed-by-someone-in-their-family.html.
 36. World Health Organization. Devastatingly pervasive: 1 in 3 Women Globally Experience Violence. [www.who.int](https://www.who.int/news/item/09-03-2021-devastatingly-pervasive-1-in-3-women-globally-experience-violence). <https://www.who.int/news/item/09-03-2021-devastatingly-pervasive-1-in-3-women-globally-experience-violence>.
 37. Kyegombe, N.; Stern, E.; Buller, A. M. "We Saw That Jealousy Can Also Bring Violence": A Qualitative Exploration of the Intersections between Jealousy, Infidelity and Intimate Partner Violence in Rwanda and Uganda. *Social Science & Medicine* 2021, 114593. <https://doi.org/10.1016/j.socscimed.2021.114593>.
 38. Meiksin, R.; Meekers, D.; Thompson, S.; Hagopian, A.; Mercer, M. A. Domestic Violence, Marital Control, and Family Planning, Maternal, and Birth Outcomes in Timor-Leste. *Maternal and Child Health Journal* 2014, 19 (6), 1338–1347. <https://doi.org/10.1007/s10995-014-1638-1>.
 39. Gagné, P. L. Appalachian Women: Violence and Social Control. *J. Contemp. Ethnogr.* 1992, 20 (4), 387–415. <https://doi.org/10.1177/089124192020004001>.
 40. Websdale, N. *Rural Women Battering and the Justice System: An Ethnography*; SAGE, 1998.
 41. Riddell, T.; Ford-Gilboe, M.; Leipert, B. Strategies Used by Rural Women to Stop, Avoid, or Escape from Intimate Partner Violence. *Health Care for Women International* 2008, 30 (1-2), 134–159. <https://doi.org/10.1080/07399330802523774>.
 42. Eisenbruch, M. The Cultural Epigenesis of Gender-Based Violence in Cambodia: Local and Buddhist Perspectives. *Culture, Medicine, and Psychiatry* 2018, 42 (2), 315–349. <https://doi.org/10.1007/s11013-017-9563-6>.
 43. Kanukollu, S. N.; Epstein-Ngo, Q. Violence against Women through a Buddhist Lens. *Religion and Men's Violence Against Women* 2015, 343–355. https://doi.org/10.1007/978-1-4939-2266-6_21.
 44. Patojoshi, A.; Sidan, A.; Garg, S.; Mishra, S. N.; Singh, L. K.; Goyal, N.; Tikka, S. K. "Staying Home Is NOT Staying Safe": A Rapid 8-Day Online Survey on Spousal Violence against Women during the COVID-19 Lockdown in India. *Psychiatry and Clinical Neurosciences* 2020. <https://doi.org/10.1111/pcn.13176>.
 45. Jain, D.; Sanon, S.; Sadowski, L.; Hunter, W. Violence against Women in India: Evidence from Rural Maharashtra, India. *Rural Remote Health* 2004, 4 (4), 304. <https://doi.org/10.22605/rrh304>.
 46. Heise, L., Ellsberg, M. and Gottemoeller, M. (1999) *Ending Violence Against Women. Population Reports, Series L, No.11*. http://www.vawnet.org/assoc_files_vawnet/populationreports.pdf
 47. Jejeebhoy, S. J.; Shah, I.; Thapa, S. *Sex without Consent: Young People in Developing Countries*; Zed Books, 2005.
 48. Dhingra, S. *Criminalisation of Marital Rape in India*. [papers.ssrn.com](https://papers.ssrn.com/sol3/papers.cfm?abstract_id=1000000).

- n.com. https://papers.ssrn.com/sol3/papers.cfm?abstract_id=2604919.
49. Visaria, L. Violence against Women in India: Is Empowerment a Protective Factor? *Economic and Political Weekly* 2008, 43 (48), 60–66.
 50. Chinnakali, P.; George, J.; Nair, D.; Premkumar, N.; Saravanan, N.; Roy, G. The Prevalence of Domestic Violence and Its Associated Factors among Married Women in a Rural Area of Puducherry, South India. *Journal of Family Medicine and Primary Care* 2016, 5 (3), 672. <https://doi.org/10.4103/2249-4863.197309>.
 51. Solanke, B. L.; Bisiriyu, A. L.; Oyedokun, A. Is the Likelihood of Spousal Violence Lower or Higher among Childless Women? Evidence from Nigeria Demographic and Health Surveys. *BMC Women's Health* 2018, 18 (1). <https://doi.org/10.1186/s12905-018-0514-3>.
 52. vora, M.; Malathesh, B. C.; Das, S.; Chatterjee, S. S. COVID-19 and Domestic Violence against Women. *Asian Journal of Psychiatry* 2020, 53, 102227. <https://doi.org/10.1016/j.ajp.2020.102227>.
 53. Domestic Violence Cases in Chennai Up, Cops Get 25 Calls a Day. *The Times of India*. April 15, 2020. <https://timesofindia.indiatimes.com/city/chennai/domestic-violence-cases-in-chennai-up-cops-get-25-calls-a-day/articleshow/75153610.cms>.
 54. Domestic Violence Calls up from 10 to 25 a Day during Lockdown in Bengaluru. *The Times of India*. April 10, 2020. <https://timesofindia.indiatimes.com/city/bengaluru/domestic-violence-calls-up-from-10-to-25-a-day-during-lockdown/articleshow/75073669.cms>.
 55. Mukherjee, A. Transmission of Intergenerational Spousal Violence against Women in India. *Gender-Based Violence* 2015, 215-238. https://doi.org/10.1007/978-3-319-16670-4_10.
 56. Vung, N. D.; Krantz, G. Childhood Experiences of Interparental Violence as a Risk Factor for Intimate Partner Violence: A Population-Based Study from Northern Vietnam. *Journal of Epidemiology & Community Health* 2009, 63 (9), 708–714. <https://doi.org/10.1136/jech.2008.076968>.
 57. Mona, S. S. and D. S. and. Domestic Violence and Women's Health in India: Insights from NFHS-4. ORF. <https://www.orfonline.org/research/domestic-violence-and-womens-health-in-india-insights-from-nfhs-4/>.
 58. Murthy, P.; Narasimha, V. L. Effects of the COVID-19 Pandemic and Lockdown on Alcohol Use Disorders and Complications. *Current Opinion in Psychiatry* 2021, 34 (4), 376–385. <https://doi.org/10.1097/ycp.0000000000000720>.
 59. *****A*****It*****. <https://files.eric.ed.gov/fulltext/ED315151.pdf>

■ Author

Jassimrat is 16, and a passionate spokesperson for gender equality. She is finishing her sophomore year in high school. As someone with a creative bent of mind, Jassimrat wishes to explore Literature, History or PPE as an international student. She enjoys writing and reading outside of school and is dabbling in photography and filmmaking.

Anxiety about COVID-19 and Future Expectations among High School Students

Justin J. Shin

Ames High School, 1801 Ridgewood Ave, Ames, Iowa, 50014, USA; justinshin1117@gmail.com
Mentor: Dr. Chengxin Cao

ABSTRACT: COVID has had a profound impact on mental health among high school students. This study examines the overall level of anxiety related to COVID-19 among high school students. The paper explores gender and racial differences in anxiety related to COVID-19. Furthermore, I investigated the link between concerns related to COVID-19 and future expectations and savings intentions. High school students in the U.S. were given an online survey with questions about their worries about COVID-19, future expectations, and savings intentions. Findings from several linear regressions indicate that high school students' anxiety and concern about COVID-19 are linked with negative future expectations. That is, high school students with higher fear were likely to report lower expectations about their family, work, and future health. In addition, their worry and concern about COVID predicted their perceptions about future finances and savings intentions. The findings suggest that mental health resulting from COVID-19 could have implications on future life and financial consumption expectations. The implications for understanding the impact of mental health issues are discussed, and future research directions are offered. This study provides important contributions to literature by demonstrating the pervasive effect of anxiety on future expectations and perceptions and savings intention.

KEYWORDS: Behavioral and Social Science COVID-19; Future Expectation; Mental Health; Financial Expectation; Saving Intentions.

■ Introduction

COVID-19 has brought several mental health challenges worldwide. These rising mental health issues were termed the "second pandemic" for children and adolescents. Subsequently, COVID-19 has left the younger generation with increased worries and anxiety, negatively impacting students. Furthermore, as the global spread of COVID-19 continued, it disproportionately affected individuals from lower socioeconomic status or sexual/racial minorities.¹ Again, the widespread increase in pandemic-related worry may have other cascading consequences. For example, the uncertainty and anxiety about the future due to COVID-19 may affect how youth see their future beyond the pandemic.

Thus, the current investigation aims to understand the unequal effect of anxiety about COVID-19 by examining gender and racial differences. Further, I examine the impact of the COVID-19 pandemic-related fear among adolescents on their future expectations and perceptions of financial future and saving intentions. Finally, the study will help us to understand the impact of mental health resulting from COVID-19 and the need to develop interventions and policies to address this issue.

Racial and Gender Differences in Worry about COVID-19:

All studies consistently identified a clear relationship between mental health and the onset of the COVID-19 pandemic. Although worsened mental health has been documented across the lifespan, several studies have found that young adults are experiencing the greatest deterioration in mental health.^{2,3} Due to this unprecedented pandemic and the following eco-

nomical consequences, adolescents may worry about not having adequate academic or financial resources, which could result in feelings of anxiety. Mental health issues may also arise from other social consequences, such as losing social opportunities and their parents' employment change. Similar psychological effects have been found from wars and previous disease outbreaks after the SARS and economic recession in 2008.⁴ Several longitudinal studies examined the association between psychological well-being and economic pressures.⁵⁻⁷ These studies showed that young adults with higher levels of depressive mood and anxiety reported higher economic pressures and concerns about their future. Subsequently, it is expected that an unstable economic situation after the breakout of COVID-19 could lead to severe financial and emotional problems.

However, some populations are more vulnerable to COVID-19.⁸ As the pandemic has caused many social changes, such as school closures and social isolation, adverse mental health outcomes may be elevated among female or minority students. Campbell *et al.*⁹ found that female students report higher anxiety and depressive symptoms than male students after COVID-19. Scholars speculated that it could be due to their higher prevalence of the internalizing disorder or lack of social support and contacts, which are crucial for the psychological well-being of female students.¹⁰ As most studies have utilized general anxiety measures to assess mental health outcomes among adolescents, the current study would test the gender differences using the measure of worry specific to COVID-19.¹¹

In addition, recent surveys show that minority students were more severely impacted by COVID-19.¹² Due to the stigma and discrimination associated with the coronavirus, Asian students in the States reported higher anxiety and concern about the impact of COVID-19.¹⁰ Again, other studies with similar designs have used other general anxiety measures; this study employs anxiety measures specific to COVID-19 rather than general anxiety.

Impact of Worry about COVID-19 on Future Expectations and Economic Outlook:

Although recent studies examined the anxiety about COVID-19 on health behaviors or health outcomes, few studies addressed the impact of anxiety on future expectations in adolescence.¹³ However, given its impact on our society, the pandemic and its induced anxiety can disrupt the future aspiration among adolescents. This is critical because adolescence is a crucial period in developing future orientation.

In 2008, when the economic recession hit the U.S., parents experienced higher stress levels, leading to increased stress levels for the children.¹⁴ Drawing on the long-lasting effect of economic recession on mental health outcomes and behavioral outcomes of young adults, it is reasonable to expect a similar impact during and post-pandemic: a negative impact of the macroeconomic situation on anxiety among adolescents, which, in turn, affects their expectations and future aspirations. Thus, this paper will examine the effect of fear of COVID-19 on adolescents' future work, family, and health expectations.

Economic outlook and perceptions about the future financial situation are crucial for adolescents because they may make a difference between reaching career goals or educational attainment. Researchers found that optimistic financial and economic expectations may motivate adolescents to work harder and pursue job opportunities.¹⁵

Previously, studies have shown the relationship between sociodemographic factors and perceptions of the financial future. For example, Schmitt-Wilson¹⁶ found that economic expectations are usually influenced by their parents' education and social advantage. However, it is also possible that the economic outlook could be influenced by uncertainty and anxiety, as observed after the economic recession in 2008.¹⁴ To address this question, I examined the association between anxiety about COVID-19 and perceptions about the future financial situation and controlled sociodemographic factors.

Finally, attitudes about the saving of adolescents predict financial behavior and planning in young adulthood. Saving-oriented attitudes include avoiding buying, cutting spending, and savings for future events.¹⁷ As saving-oriented attitudes often predict financial security and well-being in adulthood, it is important to consider assessing this orientation among adolescents who will be future consumers and labor force workers.

Less is known about the relationship between anxiety about COVID-19 and financial behavior or intentions. However, previous studies indicated that students who exhibited higher anxiety were less likely to revolve a balance on credit cards.¹⁸ It was also found that those with lower anxiety levels tend to engage in more recommended financial management be-

haviors (e.g., savings and financial goal setting). In addition, results from the survey with college students, Sages *et al.*¹⁹ found that higher anxiety levels were related to financial management behaviors such as spending more than earnings and less saving among young adults. Based on these reports, this paper explores further the relationship between worry about COVID-19 and saving attitudes.

■ Methods

This cross-sectional study uses an anonymous questionnaire with multiple choices questions and convenience snowball sampling across the States.

Hypothesis:

The current study explores the association between anxiety about COVID-19 and mental health well-being among high school students. Given the evidence that COVID-19 has adverse mental health effects on high school students, the first hypothesis is that female and sexual minority high school students will report higher anxiety about COVID-19 (Hypothesis 1a). In addition, it is expected that Asian students would report higher levels of anxiety compared to other races (Hypothesis 1b). Second, there will be a negative association between anxiety about COVID-19 and future expectations about work, family, and health among high school students (Hypothesis 2). The third hypothesis is that anxiety about COVID-19 is negatively associated with perceptions of their financial futures (Hypothesis 3). The final hypothesis was to predict whether more profound concern about COVID-19 would predict lower levels of future savings intention among high school students experiencing COVID-19 (Hypothesis 4). Additionally, I control various demographic factors such as race, gender, health status, and work status.

Sample:

The study sample of high school students (N = 380; see Table 1) was obtained through a Qualtrics survey. First, I searched relevant literature to find the survey items that have been validated and used in prior research. Then, I distributed the survey to several high schools across the States using social networks and the national high school registry. Participants completed the eligibility questions before accessing the full survey measure.

Table 1: Univariate descriptions of study variables (N=380)

Variable	%	Mean	SD	Range
Age		17.5	.942	15-19
Gender (Female)	45.8			
Race				
White	54.2			
Asian	6.8			
African American	18.4			
Hispanic	12.6			
Others	7.9			
Worry about COVID-19		80.27	24.11	19-182
Future Expectations				
Family		17.23	5.13	4-28
Work		35.61	5.03	10-70
Health		16.55	5.46	4-28
Financial Perceptions		9.64	2.34	4-15
Consumption Attitudes				
Savings		12.44	2.97	4-20

^aNote. S.D. stands for standardized deviation.

The inclusion criteria for the study were that participants: (a) are currently high school students and (b) reside in the USA territory. They were recruited through a convenience/snowball sampling method. Participants were allowed to discontinue the survey and skip questions if they were uncomfortable answering. Data were collected over two months period from July 2021 to September 2021. Participants were told that the purpose of the survey was to understand better if their COVID-19 experiences are related to their current and future perceptions of their work and family. Participants in the study remained anonymous.

Measures:

Pandemic-Related Worries Questionnaire (PRWQ). Participants completed the initial 30-item PRWQ questionnaire, which measured various concerns about the pandemic. To cover the full breadth of potential anxiety that could be experienced, the items were generated for areas that consistently emerge as common topics, as previously identified in the Worry Domains Questionnaire.²⁰ This measure identifies anxiety across five key domains, including anxiety about social relationships, academic and occupational performance, financial concerns, disrupted or aimless future goals, and lack of confidence. As several domains of concern were included, this measure represented pandemic-related worries rather than focusing on the direct worry or anxiety trait of participants. The response to each item was along a Likert Scale ranging from 'Not Distressed' (1) to 'Extremely Distressed'(10) for how they felt over the past month. All twenty items were summed to create the scores representing anxiety about COVID-19 so that higher scores indicate higher anxiety about COVID-19. The internal consistency was generally good ($\alpha=.82$). The full PRWQ-20 scale is listed in Appendix A.

Future Expectation Scale for Adolescents (FESA) The FESA is a 25-item measure developed by McWhirter and McWhirter¹⁵ to assess the degree to which the respondent believes a series of statements about their future. Among 25 items, I have selected three dimensions with 18 items: Work/Educational attainment, Family and Marriage, and Health. Participants rated from 1 (I do not believe this at all) to 7 (I certainly think this). Sum scores for each category were calculated, such that higher scores mean higher future expectations about their future. The internal consistency coefficient was good ($\alpha=.81$). The items of the scale are included in Appendix A.

Perceptions of Financial Future Participants were asked to rate their perceptions of future financial situations from 'Very Bad' (1) to 'Very good' (5). This measure was originally from Financial Well-being Scale for Emerging Adults (MS-FWBS, Sorgente & Lanz, 2019). However, for the purpose of this study, I revised three questions that were asked about their current perception of the future financial situation after COVID-19. Internal consistency was good ($\alpha=.80$). Sum scores were created so that higher scores mean optimistic views about their financial future.

Attitudes toward Saving. Participants were presented with nine statements concerning attitudes toward consumption

(see Appendix A). Scholars who developed this scale found several domains in the survey.¹³ Out of three domains, I used one dimension, attitudes toward saving. Participants evaluated each statement on a five-point Likert scale, with values ranging from 1 ("Never") to 5 ("Often"). Thus, four items related to saving were summed to create the score. Higher scores indicate higher intentions to save in their consumption behavior.

Demographic Information Participating high school students completed a brief demographic survey concerning their gender, self-rated health (from 1=very bad, 5=very good), race (1=White, 2=Black, 3=Hispanic, 4=Asian, 5=other), number of siblings, mother's education (1=no school completed, 8=Master's, professional or doctoral degree), and work status (employed=1, not employed =0).

Statistical analyses:

The data were analyzed using the Statistical Package for Social Sciences software (SPSS), version 26. Before the main analysis, descriptive analyses were conducted to describe the demographic characteristics of high school students who participated in the online survey. Second, a one-way ANOVA was performed to compare gender and racial differences in the worry about COVID-19 to test the first hypothesis. Finally, I used a linear regression model to examine the effect of apprehension and concern about COVID-19 on high school students' expectations about the future, financial future, and saving intentions (Hypothesis 2-4). Each hypothesis was tested using a two-tailed analysis at $\alpha=.05$ level of statistical significance.

Results and Discussion

Table 1 presents 380 respondents of the survey's demographics, including their age, self-identified gender, race, and mother's education. Respondents included 164 female and 194 male high school students. Twenty-two students did not wish to answer or skip the gender questions. In terms of race, the majority of participants ($N=206$, 54.2%) were White. For Hypothesis 1, Race category (1=White, 2=Black, 3=Hispanic, 4=Asian, 5= Other) had recoded them into two categories (1=Asian, 2=other race). In other analyses, race was included as a covariate. Given that the sample did not have enough participants per racial category and most students were White (54.2%), race was dichotomized as White and minority (0=White, 1=Minority). As hypotheses 2-4, race was not the main predictor and covariate.

Results from the ANOVA tests are in Figures 1-2. As can be seen, a one-way ANOVA revealed that there was a statistically significant difference in worry between the two groups ($F(1,378) = [6.894]$, $p = [.008]$). Furthermore, female students had higher levels of anxiety ($M=83.87$, $SD=31.42$) than male students ($M=74.5$, $SD=31.42$), supporting Hypothesis 1a. In terms of race (Hypothesis 1b), there was a significant difference between Asian and other race students ($F(1,378) = [4.16]$, $p=.042$). As the size of each group was different, I checked the variance and normality of each race. The test of homogeneity of variances was non-significant, indicating similar variances between groups.

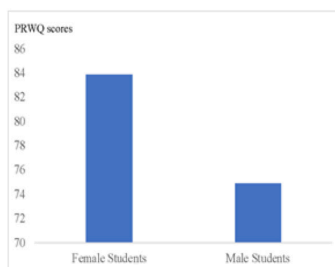


Figure 1: Gender differences in PRWQ

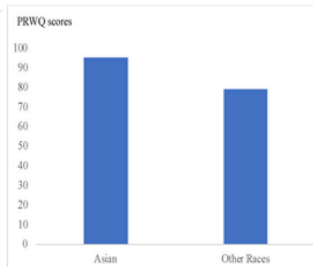


Figure 2: Racial differences in PRWQ

To examine hypotheses 2-4, I conducted multiple regression to determine if anxiety about COVID-19 predicted the future expectation about their family, work, health, financial future, and savings intentions. The tested models and predictors for future expectations and financial perceptions are seen in Table 2, where each column represents a different regression. In all the regression models, possible demographic covariates, including gender, race, health, and work status, were included.

The second hypothesis on the future expectation was supported. Table 2 shows that anxiety about COVID-19 significantly predicted future expectations about work, family, and health while controlling several demographic variables. In particular, students who reported more profound concern about COVID-19 reported lower levels of future expectations about family ($\beta = -.115, p < .01$), work ($\beta = -.141, p < .01$), and health ($\beta = -.155, p < .01$). In terms of control variables, race was negatively associated with future expectations about the family ($\beta = -.190, p < .001$), indicating the influence of social disadvantage on the projection of their family situation in the future. In addition, self-rated health was also associated with future expectations of health ($\beta = -.257, p < .001$). This suggests that current health status is also related to their future expectations about their health. Interestingly, I found no significant association between gender and future expectations.

Table 2: Predicting Future Expectations and Saving Intentions with COVID-19 Worries

Variables	Future expectations about work	Future expectations about family	Future expectations about health	Perception of financial Future	Saving Intention
	β	β	β	β	β
Gender	.023	-.029	-.020	-.069	-.019
Race	-.016	-.190***	-.064	-.112*	-.176**
Self-rated health	-.216	-.161	-.257***	-.124*	.014
Work Status	-.144	-.062	-.058	.020	.027
Worry	-.115**	-.141**	-.155**	-.018*	-.318***
Adjusted R ²	.12	.28	.32	.52	.68
N	380	380	380	375	369

Note. * $p < .05$, ** $p < .01$, *** $p < .001$. N = sample size

Similar results were noted for perceptions of the future financial situation (Hypothesis 3). As seen in Table 2, the third hypothesis was also supported. The linear regression results suggest a significant negative relationship between anxiety

about COVID-19 and perceptions about the future financial situation ($\beta = -.018, p < .05$) while controlling demographic variables. Students who reported higher COVID-19 reported lower perceptions of their financial future. For covariates, I found a significant relationship between race/self-rated health and perception of financial future ($\beta = -.112, -.124, p < .05$). That is, minority participants reported lower perceptions of financial future ($\beta = -.112, p < .05$) -and participants reporting lower self-rated health also reported lower perceptions of their financial future ($\beta = -.124, p < .05$).

Finally, I found support for the final hypothesis (Hypothesis 4). Results showed that anxiety about COVID-19 was negatively associated with their future savings intention ($\beta = -.318, p < .001$). Furthermore, students with higher COVID-19-related concerns reported lower levels of saving intention in the future. Furthermore, regarding control variables, race was negatively associated with future intentions about saving ($\beta = -.176, p < .001$). That is, minority adolescents reported lower intentions to save in the future than their White counterparts.

Overall, all of our hypotheses were supported. Furthermore, these findings indicate that worry about COVID-19 tends to be associated with overall negative expectations about the future in several domains, including family, health, work, and economic situation.

Discussion

This study aimed to determine whether COVID-19-related concerns are related to future expectations and consumption behaviors among high school students amid COVID-19. Using a convenience sample of 380 high school students in the U.S., this study provides insight into the adverse mental health resulting from the pandemic, predicting future expectations across several life domains.

First, our results reveal that high school students were generally worried about COVID-19 and its impact, with approximately 35% reporting moderate to severe concern about COVID-19 over the last six months. This finding is consistent with previous studies demonstrating poor mental health during the COVID-19 pandemic among young adults.

Consistent with the hypothesis on gender and racial differences, female students reported higher anxiety levels than male students. As female students tend to report higher anxiety symptoms in general, anxiety about COVID-19 may have emerged as an emotional response among female students more than male students. This finding suggests that sociodemographic factors such as gender may be additional sources of disparities in how the pandemic affected adolescents' mental health outcomes. Our results align with the recent studies demonstrating widening gender gaps in mental health during the pandemic.^{21, 22}

Consistent with recent studies, the findings showed that Asian students were more worried about COVID-19 than other races.²³ The growing discrimination against the Asian community, combined with pressure from COVID-19, appears to make Asian students more vulnerable to mental health problems. Scholars speculated that Asians tend to use social media for COVID-19-related information, which ex

poses them to discrimination-related news. Thus, this finding has implications for Asian Americans who may continue to have this prejudice against them. Future policies or programs should support the population heavily impacted by the pandemic. Given the small size of this group, however, this study needs to be replicated with bigger samples.

As expected, it was shown that greater anxiety about COVID-19 was related to lower levels of future expectations in many domains, such as family, work, and health, even after controlling the sociodemographic factors. This finding has an important implication for young adults' mental and physical health in the long run. In addition, Kim and Kim²⁴ found that adolescents' orientation toward the future affects their health-related behaviors and, consequently, their health status in adulthood. Finally, following up on adolescents to adulthood, Ashby & Schoon²⁵ also found that future expectations would play a more significant role than educational expectations in predicting physical health in adulthood.

Our findings concerning the perceptions of future financial situations and savings intentions also highlight the negative implication of anxiety about COVID-19. This finding relates to previous studies on the effects of stressful life events and mental health issues in early life on pessimistic perceptions about the financial future.²⁶ In line with prior studies on the effect of anxiety on the lower intention to save¹⁸, this study provides strong evidence that pandemic-related anxiety is associated with financial well-being. However, the current study did not include any data on parental job loss, unemployment, or recent family financial situation change, such as significant loss of savings. Thus, anxiety about COVID-19 could reflect the perception of the economic situation resulting from the pandemic. Therefore, additional research on how these other circumstances affect their anxiety, future expectations, and perception of their financial situation is needed.

In sum, the current study findings highlight the potential adverse consequences that the COVID-19 pandemic has on future expectations and financial intentions among adolescents. The adverse effects of COVID-19 may be long-lasting and negatively affect young students far beyond the duration of the pandemic. To mitigate this, developing and implementing public health interventions or programs should be planned and implemented to buffer these adverse effects for adolescents facing challenges. Based on these findings, it is also necessary to monitor the mental health of high school students. In addition, as the pandemic slows down, implementing interventions, programs, and education about economic situations in school should be carried out to improve the psychological well-being of high school students.

The current study has several limitations. First, the present study was limited to the United States of America. Therefore, caution regarding generalization to other countries needs to be acknowledged. Second, our study relied on a cross-sectional correlational design, so I cannot rule out the reverse pattern. Relatedly, the connection between Pandemic related anxiety and future expectations may depend on factors not included in this study, such as parents' job insecurity or unemployment due to COVID-19. It is known that students with lower SES

were more affected by the impact of COVID-19. Although our results including covariates were not significant, it is still possible that sociodemographic factors may have directly influenced their anxiety and concern about COVID-19.²³ Finally, there could be a reporting bias such that high school students with mental health issues would report lower expectations about the future and financial situation. Thus, future studies should consider separating worry about COVID-19 from the personality or general tendency to write future expectations negatively.

■ Conclusion

COVID-19 brought a significant challenge that forced young adolescents to adjust their lifestyles. While COVID-19 has impacted everyone, our studies show that these challenges impacted some high school students more than others. The current study's findings could help us understand how concern about COVID-19 affects teenagers' future aspirations and economic outlook. Given that future expectations play a key role in the motivations of people and the actions that follow, this is a critical issue. If adolescents can no longer expect a positive future for themselves, they will lack the motivation to pursue goals. As a result, we could see subsequent negative impacts cascading from worry and anxiety to adverse health and education outcomes in young adulthood.

■ Acknowledgments

I want to thank Dr. Cao for her support during the process. I am also grateful for Dr. Cao's guidance throughout this paper. Additionally, I am thankful for the high school students across the U.S. who participated in the online survey.

■ References

1. Singu, S.; Acharya, A.; Challagundla, K.; Byrareddy, S. N., Impact of Social Determinants of Health on the Emerging COVID-19 Pandemic in the United States. *Front Public Health* **2020**, *8*, 406.
2. Elharake, J. A.; Akbar, F.; Malik, A. A.; Gilliam, W.; Omer, S. B., Mental Health Impact of COVID-19 among Children and College Students: A Systematic Review. *Child Psychiatry Hum Dev* **2022**, *1-13*.
3. Graupensperger, S.; Calhoun, B. H.; Patrick, M. E.; Lee, C. M., Longitudinal effects of COVID-19-related stressors on young adults' mental health and wellbeing. *Appl Psychol Health Well Being* **2022**, *14* (3), 734-756.
4. Johnson, M. K.; Staff, J.; Patrick, M. E.; Schulenberg, J. E., Adolescent adaptation before, during and in the aftermath of the Great Recession in the USA. *Int J Psychol* **2017**, *52* (1), 9-18.
5. Hoyt, L. T.; Cohen, A. K.; Dull, B.; Maker Castro, E.; Yazdani, N., "Constant Stress Has Become the New Normal": Stress and Anxiety Inequalities Among U.S. College Students in the Time of COVID-19. *J Adolesc Health* **2021**, *68* (2), 270-276.
6. Mouza, A.-M., Perceived Stress of the Undergraduate Students in Greece Due to the Economic Crisis. *Procedia - Social and Behavioral Sciences* **2015**, *177*, 265-272.
7. Stein, C. H.; Hoffmann, E.; Bonar, E. E.; Leith, J. E.; Abraham, K. M.; Hamill, A. C.; Kraus, S. W.; Gumber, S.; Fogo, W. R., The United States Economic Crisis: Young Adul

- VID-19 for adolescents: Follow-up of a four-wave longitudinal study during the pandemic. *Am Psychol* **2022**, *77* (1), 85-99.
22. Glowacz, F.; Schmits, E., Psychological distress during the COVID-19 lockdown: The young adults most at risk. *Psychiatry Res* **2020**, *293*, 113486.
23. Trammell Ph, D. J.; Joseph Ph, D. N.; Harriger Ph, D. J., Racial and ethnic minority disparities in COVID-19 related health, health beliefs and behaviors, and well-being among students. *J Am Coll Health* **2023**, *71* (1), 242-248.
24. Kim, T.; Kim, J., Linking adolescent future expectations to health in adulthood: Evidence and mechanisms. *Soc Sci Med* **2020**, *263*, 113282.
25. Ashby, J. S.; Schoon, I., Career success: The role of teenage career aspirations, ambition value and gender in predicting adult social status and earnings. *Journal of Vocational Behavior* **2010**, *77* (3), 350-360.
26. Bartholomae, S.; Fox, J. J., A Decade Review of Research on College Student Financial Behavior and Well-Being. *Journal of Family and Economic Issues* **2021**, *42* (1), 154-177.

■ Author

Justin Shin, a junior at Ames high school, is committed to business and marketing. A swimmer with a business mindset, Justin shows a keen interest in the motivation process and how it can impact the business world. He is looking to pursue a career in psychology and business in the future.

Efficacy of Si-Wu-Tang on Treating Primary Dysmenorrhea: A Systematic Review and Meta-Analysis

Yiyi Liu

Beijing Haidian Foreign Language Academy, Beijing, China; liuyiyiangel@sina.com
Mentor: Ms. Hongging Yao

ABSTRACT: According to prescriptions from famous gynecologists, Si-Wu-Tang (SWT) has been one of the main treatments for primary dysmenorrhea (PD). This systematic review and meta-analysis aim to test the efficacy and safety of SWT in treating PD. First, randomized controlled trials (RCTs) of SWT in treating PD were researched. Data were from the Year 2000 to June 2022. A cumulative meta-analysis was then performed based on those data. A total of 228 potential studies relevant to this study were searched, and 22 RCTs were included. Twenty studies compared the effect of SWT with Western medicine (WM) in treating PD. In addition, two studies compared the effect of SWT with Danggui Shaoyao San (DSS) in treating PD. The results revealed that SWT was more effective than Nonsteroidal anti-inflammatory drugs (NSAIDs), and SWT was more effective than DSS in treating PD. These results indicate that SWT might be effective in treating PD.

KEYWORDS: Transactional Medical Science; Disease Treatment and Therapies; Si-Wu-Tang; Primary Dysmenorrhea; Chinese Herbal Medicine.

■ Introduction

Background:

Dysmenorrhea refers to cyclic cramping pain in the lower abdomen of a woman's body. Symptoms of sweating, tachycardia, headaches, nausea, and vomiting are often accompanied after or during menstruation periods. Primary Dysmenorrhea (PD) is pain without significant pathological pelvic disease. Several studies have shown the prevalence of dysmenorrhea to range from 16% to 90% in populations of students, teenagers, their mothers, and other individuals from special groups like industrial workers.¹ According to a meta-analysis of 20,813 young women, 71.1% were impacted by dysmenorrhea. Within the meta-analysis, across 11,226 women, 20.1% recorded absenteeism from school due to dysmenorrhea, and a report that 40.9% of them had their class performance impaired due to dysmenorrhea.² Although pains from dysmenorrhea are not life-threatening, they can be very distracting in women's lives and activities.³

The pathogenesis of primary dysmenorrhea is unclear. However, Dawood found a positive correlation between vasoactive prostanoid secretion and primary dysmenorrhea.⁴ Therefore, Nonsteroidal anti-inflammatory drugs (NSAIDs) were the primary therapy for primary dysmenorrhea. NSAIDs are prostaglandin synthetase inhibitors (PGSIs) that can relieve the symptoms.¹ Furthermore, Owen found that significant pain was relieved by PGSIs for most women.⁵ However, some NSAIDs appeared to have side effects on women. A study showed that indomethacin was likely to cause slight gastrointestinal discomfort. Moreover, there was also a lack of sufficient evidence to prove the safety of some of the NSAIDs like flurbiprofen.⁶

Chinese Herbal Medicine (CHM) has long been used in East Asia. Currently, some Chinese herbs have already been

used to treat Primary Dysmenorrhea. The efficacy of Chinese Herbal Medicine (Danggui Shaoyao San) in treating primary dysmenorrhea has been systematically reviewed.³⁹ Compared with the placebo, CHM was significantly ($P < 0.01$) more effective in relieving pain. Moreover, within the comparison with conventional therapies (NSAIDs), CHM also showed significantly stronger effects in ($P < 0.01$) pain relief, compared with conventional therapies (NSAIDs), and its benefit could last for more than three months or more in most cases.⁷ Si-Wu-Tang (SWT) was one of the main treatments for primary dysmenorrhea, according to prescriptions from famous gynecologists.⁹ SWT is mainly composed of 4 types of herbs: prepared Rehmanniae Radix Praeparata (Shudihuang), Paeoniae Radix Alba (Baishao), Angelicae Sinensis Radix (Danggui), and Chuanxiong Rhizoma (Chuanxiong).⁴⁰ To clearly show the efficacy and safety of SWT, meta-analysis and systematic review are needed, such as the previous study on Danggui Shaoyao San for treating PD.³⁹ However, such existing studies with high statistical homogeneity were limited. Furthermore, more recent evidence and subgroup comparisons were needed to be included in the test of the SWT efficacy. Randomized Controlled Trials of SWT in treating SWT studies existed. However, there was no analysis to compare subgroups with different types of interventions. Moreover, existing meta-analyses or systematic reviews only take account of a single type of SWT, but no combination studies of different kinds of SWT are conducted. Therefore, the study's objective was to make a systematic review and meta-analysis of the efficacy and safety of SWT with the most recent studies and data. The efficacy is measured by the total effective rate of overall symptom reduction. The safety is evaluated by the adverse effect description being recorded in the study.

Abbreviations:

SWT= Si-Wu-Tang, PD= Primary Dysmenorrhea, NSAIDs= Nonsteroidal Anti-inflammatory Drugs, RR= Relative Risk, CI= Confidence Interval, RCT= Randomized Controlled Trials, PRISMA= Preferred Reporting Items for Systematic Reviews and Meta-Analyses, TER= Total Effective Rate, PGSI= Prostaglandin Synthetase Inhibitor, DSS= Danggui Shaoyao San.

Research Method

Data Collection and Data Selection:

This study researched randomized control trials (RCTs) of Si-Wu-Tang (SWT) as a treatment for PD from the Year 2000 to June 2022. Databases were derived from PubMed, the Cochrane Library, Elsevier, China National Knowledge Infrastructure, and JSTOR.

The used terms include: (Primary dysmenorrhea OR menstruation OR menstrual pain OR menstrual disorders OR dysmenorrhea) AND (Si-Wu-Tang OR Four-agents-decoction OR Si-Wu-decoction OR Chinese Herbal Medicine OR Chinese Traditional Medicine OR Herbal Medicine) in English or Chinese.

The data was selected, and the quality of the data was assessed. This process was performed individually by the researcher. To determine the data quality, the study used the “revised Cochrane risk of bias tool for randomized trials (rob2)” to measure the risk of bias.³⁶ The following domains are being assessed: randomization process, deviations from the intended interventions, missing outcome data, measurement of the outcome, and selection of the reported result. Each domain is rated as “low risk,” “high risk,” or “some concerns.” If the study was scored as “high risk,” it means it did not include enough information for some domains.

Criteria for inclusion in the meta-analysis:

1. The type of study was Randomized Controlled Trials (RCTs) or other quasi-RCTs. Studies written in Chinese and English would be accepted. However, case studies, case series, qualitative studies, or similar studies that cannot provide detailed information on the efficacy of SWT would be excluded.

2. All participants in the study were patients of primary dysmenorrhea.

3. The experiment interventions were SWT alone or with some additions due to the difference in the condition of patients. All kinds of formulations would be accepted. The control interventions were Western medicine, other CHM, or placebo.

4. Results of the study need to be measured by the following methods: pain level, treatment response rate, the use of other pain-reliever, or the quality of life. Therefore, data were either dichotomous or quantitative.

Data Analysis

The statistical analysis was performed using RStudio 2022.02.3+492. Since all data were either dichotomous or qualitative, relative risks and 95% confidence intervals (CIs) are used to express treatment effects. Subgroup analysis was performed based on the type of medicine, control type, or clinical heterogeneity. Risk ratio (RR) (or Relative risk) was

calculated using the ratio of patients in the experimental group that reflect treatment as effective treatment divided by the ratio of patients in the control group that reflect treatment as effective. The total effective rate (TER) recorded in the study is used to calculate the RR.

Results and Discussion

Results of the study search:

The study search results are shown in Figure 1 as a PRISMA flowchart. The search identified 228 potential study that was relevant to this study. At last, 22 studies met the inclusion criteria of this study.⁹⁻³⁰ The included types of SWT are ‘Taohong Si-Wu-Tang,’ ‘Danggui Si-Wu-Tang,’ and ‘Xiangfu Si-Wu-Tang.’

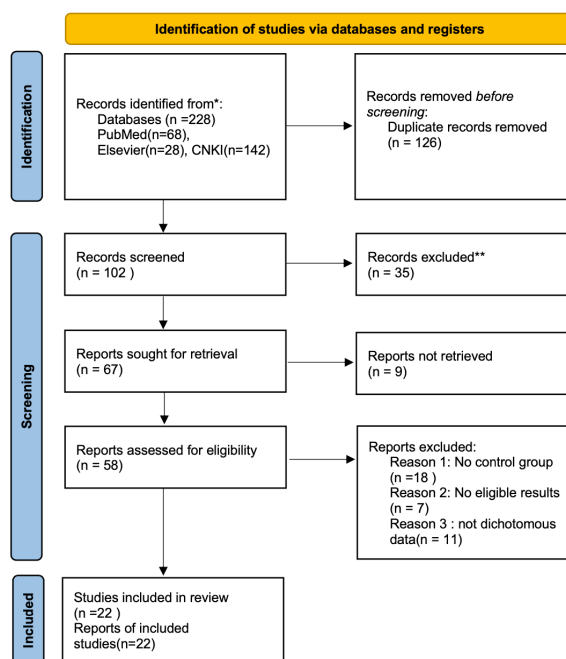


Figure 1: The flow chart of the study process. CNKI = Chinese National Knowledge Infrastructure

Risk of bias:

The overall risk of bias graph is shown in Figure 2. The risk of bias was moderate or low for most cases. However, all data were at high risk for bias due to deviations from intended interventions. The reason was that all studies did not adequately address the method of randomization or the RCTs were not conducted in a single or double-blind way.

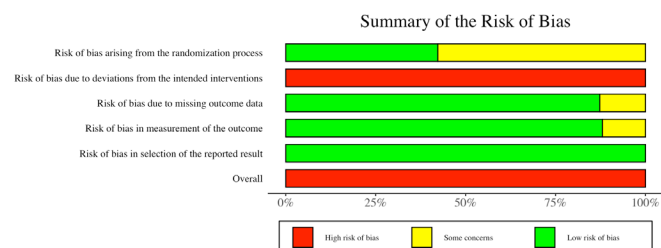


Figure 2: Summary of the Risk of Bias: author’s judgment about each risk of bias domain is presented as a percentage across all studies included.

Effects of SWT

SWT vs. NSAIDs:

A total of 20 studies⁹⁻²⁸ (2275 women) compared the effects of SWT with NSAIDs (Ibuprofen, Flufenamic acid capsules, or Indomethacin). All studies reported a total effective rate (TER). In TER, the results revealed that SWT was more effective than NSAIDs (RR 2.36, 95% CI 1.92-2.92, $P < .0001$). The statistic I^2 for heterogeneity was high ($I^2 = 57.2\%$). (Figure 3)

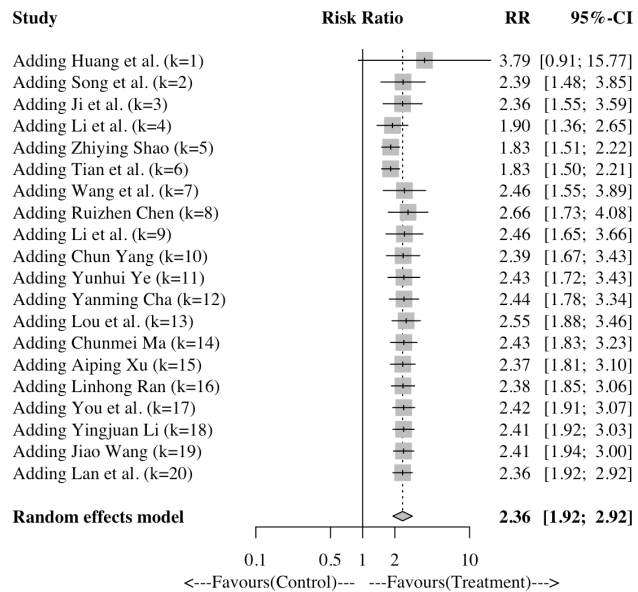


Figure 3: Forest plot of SWT vs. NSAIDs. RR = Relative Risk, CI= Confidence Interval

SWT vs. other CHM:

Two studies^{29,30} (179 women) compared the effect of SWT on Danggui Shaoyao San (DSS). Both studies reported TER and the results revealed that SWT was more effective than DSS in treating PD (RR 3.2130, 95% CI 1.9534-5.3338, $P < .0001$). The statistic I^2 for heterogeneity was low, with almost no heterogeneity ($I^2 = 0.00\%$). (Figure 4)

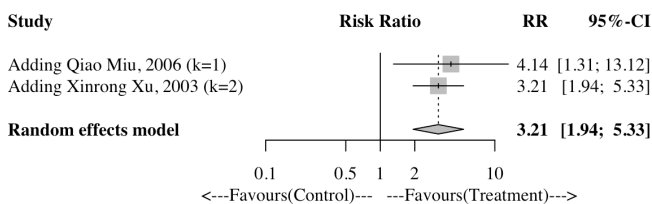


Figure 4: Forest graph for SWT vs. DSS. RR= Relative Risk, CI=Confidence Interval.

Discussion

This systematic review and meta-analysis analyzed 22 studies with 2454 women on the effect of SWT in treating PD. The results showed that SWT was more effective in treating PD than NSAIDs or DSS.

SWT and NSAIDs were compared in 20 studies. SWT was more effective in treating PD than NSAIDs (RR 2.36, 95% CI 1.92-2.92, $P < .0001$). However, the heterogeneity was high ($I^2 = 57.2\%$). According to Western medicine, the

mechanism of this disease was the enhanced contraction of the smooth muscle of the uterus and the small arteries of the myometrium, resulting in pain due to ischemia and hypoxia in the uterus. Therefore, most of the symptomatic treatment was taken to treat this disease. Currently, three major categories of drugs are recognized as major treatments for primary dysmenorrhea, namely NSAIDs, contraceptives, and calcium channel blockers, which are effective and fast, but have greater side effects, and treat the symptoms but not the root cause and are prone to recurrent attacks.³² Studies have also shown that CHM significantly improved pain relief with long-term efficacy compared to conventional therapies.⁷ Results revealed in this study also proven this statement.

According to the theory of Traditional Chinese Medicine, Si-Wu-Tang is a good formula for tonifying the blood, invigorating the blood, and regulating menstruation compared to other CHMs since it focuses more on dealing with patients with deficiency of both qi and blood symptoms.³³ Two studies compared the effect of SWT or DSS in treating PD. The results displayed a more favorable outcome toward SWT in treating PD (RR 3.2130, 95% CI 1.9534-5.3338, $P < .0001$). The heterogeneity is low ($I^2 = 0.00\%$). All those results showed the significant effect of SWT in treating PD. The pharmacology of SWT could be interpreted. In previous research, it has shown that the main component, *Semen persicae* contains aromatic cyanophoric glycoside extract that can increase the activity of cytochrome oxidase in energy metabolism and inhibit ADP-induced platelet aggregation; *Danggui* (*Angelica*) contains aromatic acids that inhibit platelet aggregation and inhibits vascular smooth muscle proliferation; *Paeonia lactiflora* composed mainly of monoterpene glycosides has vasodilatation, anti-thrombosis, anti-platelet aggregation, and inhibition of angiotensin-converting enzyme activity.³³ That information on the mechanism of SWT in treating PD would make SWT a promising safe drug for PD. Moreover, recent research has also shown that SWT inhibits oxytocin-induced uterus contraction in women.³⁴ Also, SWT improved the blood coagulation function in women, improving their quality of life.³⁵

Although this study included plenty of observations on the efficacy of SWT in treating PD, many limitations still exist. First, all data in this study were dichotomous, and all patients were Chinese. So, whether there was variability due to different regions' patients could not be determined, and the conclusion from the present study could not be applied to other areas of the world until further relevant studies confirmed it. Second, the studies included in our meta-analysis did not specifically describe the process of randomization, and the blindness of studies could not be determined. This would reduce the reliability of the study since the risk of bias due to the blinding of patients or researchers was high. Third, all data were measured in TER instead of other methods, such as pain intensity in scale. Again, this would reduce the reliability and validity of the study. A more specific pain measurement should be adopted in further studies to improve reliability.

■ Conclusion

The systematic review included 22 RCTs that showed a higher total effective rate in the SWT treatment group than in the control group being treated by NSAIDs or DSS in treating dysmenorrhea. However, this study had a high risk of bias due to the need for more description in the randomization process and blinding in all the included studies. Therefore, more reliable and detailed RCTs had to be conducted and analyzed to prove better SWT's reliability in treating PD.

■ Acknowledgments

I sincerely thank my mentor, Ms. Yao, for her suggestions and guidance for my research.

■ References

1. Stenchever, M. A. (2001). *Comprehensive gynecology*. St. Louis, Mo: Mosby. 815-28.
2. Armour, M., Parry, K., Manohar, N., Holmes, K., Ferfolja, T., Curry, C., ... Smith, C. A. (2019). The Prevalence and Academic Impact of Dysmenorrhea in 21,573 Young Women: A Systematic Review and Meta-Analysis. *Journal of Women's Health*.
3. Ward, R. M., & Beachy, J. C. (2003). Neonatal complications following preterm birth. *BJOG: An International Journal of Obstetrics & Gynaecology*, 110, 8-16.
4. Dawood MY, Khan-Dawood FS. Differential suppression of menstrual fluid prostaglandin F2a, prostaglandin E2, 6-keto prostaglandin F1a and thromboxane B2 by suprofen in women with primary dysmenorrhea. *Prostaglandins Other Lipid Mediate* 2007;83:146-53.
5. Owen PR. Prostaglandin synthetase inhibitors in the treatment of primary dysmenorrhea. Outcome trials reviewed. *Am J Obstet Gynecol*. 1984 Jan 1;148(1):96-103.
6. Feng, X., & Wang, X. (2018). Comparison of the efficacy and safety of non-steroidal anti-inflammatory drugs for patients with primary dysmenorrhea: A network meta-analysis. *Molecular Pain*, 14, 174480691877032.
7. Zhu, X., Proctor, M., Bensoussan, A., Wu, E., & Smith, C. A. (2008). Chinese herbal medicine for primary dysmenorrhea. *Cochrane Database of Systematic Reviews*.
8. Cao, W.M., Yu, ll, Zhang KM, Zhang SL. A study on the pattern of medication used by famous Chinese gynecologists in the treatment of dysmenorrhea based on the data mining method. *Med Data Min*. 2022;5(1):3.
9. Cha, Y.M. Clinical efficacy of Siwu Tang with addition and subtraction in the treatment of dysmenorrhea in adolescent females. *Journal of Baotou Medical College*, 2015; 31(3): 80. (Chinese)
10. Chen, R.Z. (2013). Clinical efficacy of Tao Hong Si Wu Tang with addition and subtraction in the treatment of 76 cases of dysmenorrhea. *Guide of China Medicine*, 2013 April; 11(10):276. (Chinese)
11. Hao, G.X., Xu, Y.H. Analysis of 58 cases of primary dysmenorrhea treated with Si Wu Tang with addition and reduction. *Inner Mongolia Chinese Medicine*. 2000 April; 04(15):14. (Chinese)
12. Ji, Y.X., & Jiang X.D. Treatment of primary dysmenorrhea in 50 cases with addition and subtraction of Tao Hong Si Wu Tang. *Qingdao Med J*, 2006; 38(6):424 (Chinese)
13. Lan, Y.B., & Wang, D.M. 180 cases of primary dysmenorrhea treated with Tao Hong Si Wu Tang combined with Wen Jing Tang. *Guangming Journal of Medicine*, 2020 May; 35(9):1282. (Chinese)
14. Li, G.F., & Zhou, X.L. Clinical observation on the treatment of primary dysmenorrhea with addition and subtraction of Tao Hong Si Wu Tang. *Chinese Journal of Basic Medicine in Traditional Chinese Medicine*, 2011 May; 17(5):583. (Chinese)
15. Li, H.Y., & Yao, Q.F. Treatment of primary dysmenorrhea in 70 cases with the addition Siwu Tang. *Journal of Practical Traditional Chinese Medicine*, 2013 May; 29(5): 35. (Chinese)
16. Li, Y.J. 57 cases of primary dysmenorrhea treated with addition Siwu Tang. *Journal of North Pharmacy*, 2018; 15(3): 71. (Chinese)
17. Lou, H.Y., & Liang, L.Q. Clinical observation of 42 cases of primary dysmenorrhea treated with Tao Hong Si Wu Tang. *Journal of Guangdong Medical College*, 2011 June; 29(3):285. (Chinese)
18. Ma, C.M. Clinical study on the treatment of primary dysmenorrhea with Chinese medicine. *ACTA Chinese Medicine*, 2016 October; 10(31):1600. (Chinese)
19. Ran, L.H. Clinical efficacy analysis of Siwu Tang with addition and subtraction in the treatment of dysmenorrhea in adolescent women. *Journal of Clinical Medical*, 2017; 4(4): 741. (Chinese)
20. Shao, Z.Y. Clinical experience in the treatment of primary dysmenorrhea with addition and subtraction of Tao Hong Si Wu Tang. *Chinese and Foreign Medical Research*, 2011 May; 9(13):48. (Chinese)
21. Song, X.M., & Kang, Q.Y. 70 cases of dysmenorrhea treated with Tao Hong Si Wu Tang. *Journal of Liaoning College of TCM*, 2003 August; 5(3):248. (Chinese)
22. Tian, F., Long, J.P., & Li, J. 25 cases of primary dysmenorrhea treated with Four Herbs Decoction. *Henan Traditional Chinese Medicine*, 2011 July; 31(7):751. (Chinese)
23. Wang, C.X., & Li, Y.W. 159 cases of dysmenorrhea in adolescent girls treated with Siwu Tang. *Chinese Journal of Experimental Traditional Medical Formulae*, 2011 December; 17(24):212. (Chinese)
24. Wang, J. Clinical observation of 84 cases of primary dysmenorrhea treated with addition and subtraction of Tao Hong Si Wu Tang. *China Continuing Medical Education*, 2019; 11(29):147. (Chinese)
25. Xu, A.P. 72 cases of primary dysmenorrhea treated with Tao Hong Si Wu Tang with addition. *China's Natropathy*, 2016; 24(11):53. (Chinese)
26. Yang, C. 40 cases of primary dysmenorrhea with blood stasis treated with Siwu Tang-like formula. *Chinese Medicine Modern Distance Education of China*, 2013 May; 11(10): 24. (Chinese)
27. Ye, Y.H. Clinical study on the treatment of primary dysmenorrhea with Siwu Tang. *Guangming Journal of Chinese Medicine*, 2014 July; 29(7):1443. (Chinese)
28. Yang, A.J., & Xu, F. Clinical observation of 48 cases of dysmenorrhea in adolescents treated with Siwu Tang plus reduc

- tion. Chinese Journal of Ethnomedicine and Ethnopharmacology, 2017; 3. (Chinese)
29. Miu, Q. Clinical Observation on Primary Dysmenorrhea Treated with Tao-Hong Si-Wu Tang Plus. Chinese Archives of Traditional Chinese Medicine, 2006 October; 24(10): 1926. (Chinese)
 30. Xu, X.R. Treatment of Dysmenorrhea with Addition and Reduction of Tao Hong Si Wu Tang Clinical experience of dysmenorrhea. 2003; Journal of Emergency in Traditional Chinese Medicine, 2003; 5:428. (Chinese)
 31. Li, J. *et al.* Obstetrics and Gynecology. People's Medical Publishing House, 201:318-319. (Chinese)
 32. Li, M.X., Zhang, X.T., & Liu, J.C. Advances in the treatment of primary dysmenorrhea in Chinese and Western medicine. Xinjiang Journal of Traditional Chinese Medicine, 2018; 36(1):142. (Chinese)
 33. Ju Y.C., & Li, X. Progress of research on chemical composition of Tao Hong Si Wu Tang. Herald of Medicine, 2008 May; 27(5):575. (Chinese)
 34. Liu, P., Duan, J., Hua, Y., Tang, Y., Yao, X., & Su, S. (2001). Effects of Xiang-Fu-Si-Wu Decoction and its main components for dysmenorrhea on uterus contraction. Journal of Ethnopharmacology, 133(2), 591-597.
 35. Fang, F. Exploring the effect of Siwu Tang on coagulation function in patients with primary dysmenorrhea. Guide of Chinese Medicine, 2018 January; 16(1):8. (Chinese)
 36. Julian H., Jonathan S., ... Roy E. Revised Cochrane risk-of-bias tool for randomized trials(Rob2). Cochrane Methods Bias.
 37. Balduzzi S, Rücker G, Schwarzer G. Evid Based Ment Health 2019;22:153-160.
 38. Zhu, X., Proctor, M., Bensoussan, A., Wu, E., & Smith, C. A. (2008). Chinese herbal medicine for primary dysmenorrhoea. Cochrane Database of Systematic Reviews.
 39. Lee, H. W., Jun, J. H., Kil, K.-J., Ko, B.-S., Lee, C. H., & Lee, M. S. (2016). Herbal medicine (Danggui ShaoyaoSan) for treating primary dysmenorrhea: A systematic review and meta-analysis of randomized controlled trials. Maturitas, 85, 19-26. doi:10.1016/j.maturitas.2015.11.013
 40. Li, G., Liu, A., Lin, M., Liao, S., & Wen, Z. (2020). Chinese herbal formula siwutang for treating primary dysmenorrhea: A systematic review and meta-analysis of randomized controlled trials. Maturitas, 138, 26-35. doi:10.1016/j.maturitas.2020.03.009
 41. Liu, L. *et al.*, Research progress on Siwu Tang-like formula for dysmenorrhea with blood stasis evidence in gynecology. Chinese Journal of Traditional Chinese Medicine, 40.5 (2015):8.

■ Author

I'm Yiyi Liu, a Beijing Haidian Foreign Language Academy senior student. I'm interested in biology, specifically pharmacology, and I seek to become a biology major.

Deep Learning-based Automatic Measures of Spinal Curvature in Idiopathic Scoliosis

Yubeen Lee, Seoyoung Park, Seunghoon Han

Saint Paul Preparatory Seoul, 14-8, Seocho Jungang-ro 31-gil, Seocho-gu, Seoul, 06593, Korea; maeveyblee@gmail.com

Mentors: Dr. Jae-Hun Kim, Hyoungmin Kim

ABSTRACT: This study aimed to evaluate the accuracy of a proposed method for measuring scoliosis curvature and its level of agreement with the traditional method of experts' Cobb angle measurements, which serves as the reference standard. This study included 301 whole-spine radiographs of 86 patients with idiopathic scoliosis. The proposed method used a deep-learning model to measure spinal curvatures automatically. In addition, segmentation of the entire spine, extraction of the central line, detection of inflection points, and measurement of the curvature angle were performed. The proposed method was more reliable than the traditional Cobb angle measurement method. The intraclass correlation coefficient for absolute agreement between the two methods was 0.969 (95% confidence interval: 0.957~0.977), indicating excellent agreement. Bland-Altman analysis showed no specific pattern, with a mean difference of -1.29 and 95% limits of agreement ranging from -9.49 to 6.91. The accuracy of the proposed method for detecting scoliosis with a Cobb angle ≥ 40 degrees was 88.4%, with a sensitivity and specificity of 95.9% and 83.2%, respectively. The accuracy of the proposed method for detecting spinal curve progression was 84.9%, with a sensitivity and specificity of 63.6% and 90.5%, respectively. The proposed model for automatic spinal curvature measurement using deep learning showed acceptable accuracy and excellent agreement with the traditional method for Cobb angle measurement. The proposed method may be useful for detecting severe scoliosis and monitoring moderate scoliosis that may progress over time.

KEYWORDS: Biomedical Engineering; Biomedical Imaging; Scoliosis; Cobb Angle Measures; Deep Learning.

■ Introduction

Scoliosis is a type of spinal deformity that causes lateral curvature of the spine. It can occur in people with conditions such as cerebral palsy and muscular dystrophy; however, most cases are idiopathic, meaning the cause is unknown. Idiopathic scoliosis is usually diagnosed in adolescents during their growth spurt and affects approximately 3% worldwide.¹ It is characterized by a lateral deviation of the spine greater than 10 degrees, measured using the Cobb angle on an X-ray image.² Also, scoliosis can cause various complications, such as back pain, respiratory problems, cosmetic issues, and psychological distress.³ Therefore, accurate diagnosis and scoliosis monitoring are essential for effective treatment planning.

The Cobb angle measurement is the gold standard for evaluating scoliosis in clinical practice.⁴ However, this method has several drawbacks that could be improved to maintain its reliability and validity. First, it is subjective and prone to interobserver and intraobserver variability.⁵ Second, it is influenced by the patient's position and degree of rotation during X-ray image acquisition.⁶ Third, it does not capture the three-dimensional nature of a spinal deformity.⁷

Several computer-assisted methods to measure the Cobb angle more objectively and accurately have been proposed to overcome these limitations. These methods typically involve manual or semiautomatic detection of vertebral landmarks on X-ray images using graphical user interfaces or image processing techniques.⁸⁻¹⁰ However, these methods require human intervention and expertise to select appropriate landmarks and

curves on the spine. Moreover, these methods are sensitive to image quality and resolution and may need to be revised in complex or atypical cases. In this study, we proposed a model for the automatic measurement of spinal curvature using the U-Net model, which simplifies the process and reduces error by segmenting the entire spine, extracting the central line, detecting inflection points, and measuring the curvature angle.

This study was designed to (a) evaluate the reliability between the traditional experts' Cobb angle measurements and the proposed measurements, (b) investigate the accuracy of the proposed method for detecting severe scoliosis that may require surgery and monitoring moderate scoliosis that may progress over time, using the traditional Cobb angle measurement method as the reference standard, and (c) determine the interobserver reliability of Cobb angle measurements among novices who are not trained in radiology, compared to experts' Cobb angle measurements.

■ Methods

Data Collection:

Our Institutional Review Board approved this retrospective study (No. 2010-124-1166). A total of 301 whole-spine anteroposterior (AP) radiographs of 86 patients with idiopathic scoliosis obtained from the Department of Orthopedics, Seoul National University Hospital, were used for the study. Inclusion criteria for this study include patients between the ages of ten and nineteen who have been diagnosed with idiopathic scoliosis. Exclusion criteria consist of patients who have undergone spine surgery, those with infantile idiopathic scoliosis,

and individuals with scoliosis resulting from certain conditions such as cerebral palsy and muscular dystrophy. Whole-spine AP radiographs were taken with patients in the conventional standing posture at a fixed distance of 228 cm from the X-ray source.

Deep-learning-based Computation of Spinal Curvature:

The automatic measurement of the Cobb angle consisted of four steps (Figure 1): segmenting the entire spine, extracting the central line, detecting the inflection points, and measuring the Cobb angle. First, the U-Net model was trained using 200 radiographic images and manually segmented spine masks to automatically segment the entire spine. The 200 radiographs used for spine auto-segmentation were patients who were diagnosed with adolescent idiopathic scoliosis with their x-rays, and they were not used for results analysis. Next, morphological operations were used to produce a skeleton of the spine from the segmented areas, and a seventh-order polynomial curve-fitting method was used to extract the points on the skeleton. After, the first derivative of the spinal curve was computed to detect the inflection points on the skeleton curve. The Cobb angle was then calculated automatically based on the detected inflection points.

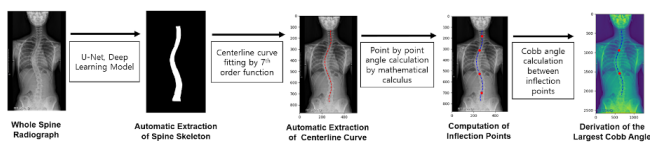


Figure 1: Overview of spinal curvature evaluation. A U-Net model was trained for automatic spine segmentation, followed by morphological operations and curve-fitting techniques to extract the central line, detect inflection points, and automatically measure the Cobb angle.

Cobb Angle Measurement by human readers:

Blinding of the observers was performed. All 301 radiographs were numbered and analyzed in consensus by an experienced orthopedic surgeon and an experienced radiologist using an electrical tool for Cobb angle measurements embedded in the Picture Archiving and Communication System (PACS) (INFINITT PACS; INFINITT Healthcare, Seoul, Korea). Lines were manually drawn through the endplates of the curve's upper and lower end vertebrae on the monitor, and the Cobb angle was automatically generated on the screen. These results were considered the reference standard for Cobb angle measurements. Additionally, four novice observers analyzed the Cobb angles in 30 randomly selected radiographs using the same method. They were blinded to the results obtained by the experts or the proposed method. However, they were educated on how to measure the Cobb angles and tested using five radiographs before proceeding with the primary analysis.

Statistical Analysis:

Data were presented as means and standard deviations. A comparison between the proposed method and the traditional experts' Cobb angle measuring method was performed using the paired t-test. Agreement between the two methods in measuring spinal curvature was evaluated using the intraclass correlation coefficient (ICC) two-way mixed model on the absolute agreement and Bland–Altman plots. An ICC less

than 0.2 was considered unacceptable; 0.2 to 0.39 questionable; 0.4 to 0.59 good; 0.6 to 0.74 very good; and 0.75 to 1.00 excellent. Using Bland–Altman analysis, the mean difference and 95% confidence limits of agreement were calculated. The accuracy, sensitivity, specificity, negative predictive value, and positive predictive value of the proposed method for detecting scoliosis with an angle of 40 degrees or greater were assessed using the Cobb angles obtained from the traditional method as the reference standard. Likewise, the accuracy, sensitivity, specificity, negative predictive value, and positive predictive value of the proposed method for detecting spinal curve progression were assessed using the traditional Cobb angles obtained by experts as the reference standard. An increase of five degrees or more of the Cobb angle in the follow-up radiograph was defined as progression, and radiographs with an interval of more than six months from the first radiograph were included. Frequencies of Cobb angle of 40 degrees or greater, or the progression in scoliosis in the follow-up, were compared between the measurements by experts and those by the proposed method using the McNemar test. Finally, the mean values of the Cobb angles from the reference standard and those from each novice were compared using the paired t-test, and the interobserver reliability between the measurements from the reference standard and those from each novice was evaluated using the ICC two-way mixed model on the absolute agreement. All statistical analyses were performed using SPSS software (version 25.0; IBM, Armonk, NY, USA). A p-value < 0.05 was considered statistically significant.

Results and Discussion

Table 1 shows the basic characteristics of the 86 patients and the distribution of the Cobb angles of the 301 radiographs. Although the mean values of the results from the proposed method were significantly greater than those from the traditional method (39.01 ± 12.85 vs. 37.7 ± 12.42 ; mean difference, -1.29 ± 4.18 [$p < 0.001$]), an agreement between the two methods was excellent (ICC, 0.969; 95% confidence interval, 0.957–0.977 [$p < 0.001$]) (Figure 2). In Figure 3, Bland–Altman plots between Cobb angles and the proposed method show no specific pattern, with a mean difference of -1.29 and 95% limits of agreement ranging from -9.49 to 6.91 .

Table 1: Baseline characteristics and distribution of the Cobb angles in 301 radiographs of 86 patients: People with severe scoliosis with an angle of 40 or greater comprised 40.5% of the study population.

Baseline characteristics	
Female (%)	74 (86.1)
Age, years* (range)	14.0 \pm 2.6 (5.6–21.3)
No. of follow-up radiographs* (range)	3.5 \pm 3.1 (1–16)
Cobb angle	
<20°	23 (7.6)
20–<40°	156 (51.8)
40–<60°	113 (37.5)
$\geq 60^\circ$	9 (3.0)

*mean \pm standard deviations

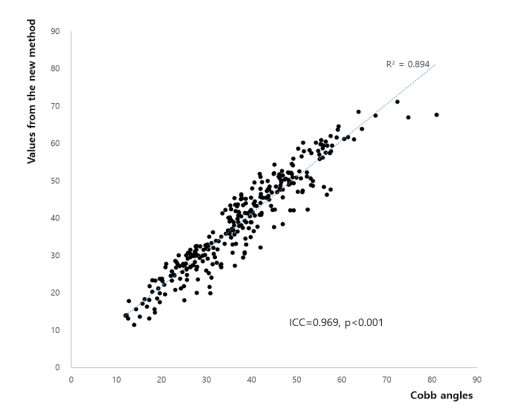


Figure 2: Agreement between measurements using the traditional experts' Cobb angle method and the proposed method. High agreement between the newly proposed measurements and the traditional Cobb angle measurements is shown with an ICC of 0.969.

The performance of the proposed method for the detection of scoliosis with an angle of 40 degrees or greater in the 301 radiographs was acceptable: accuracy, 88.4%; sensitivity, 95.9%; specificity, 83.2%; negative predictive value, 96.7%; and positive predictive value, 79.6% (McNemar test, $p < 0.001$) (Table 2). In terms of performance of the proposed method for detection of progression of more than five degrees in a total of 159 follow-up radiographs of 52 patients, accuracy, sensitivity, specificity, positive predictive value, and negative predictive value were 84.9%, 63.6%, 90.5%, 63.6%, and 90.5%, respectively (McNemar test, $p = 1.0$) (Table 2).

Table 2: Performance of the proposed method for detecting scoliosis with a Cobb angle of 40 degrees or greater ($n = 301$ radiographs) and for detecting progression in scoliosis ($n = 159$ radiographs). Accuracies for detecting severe scoliosis and progression are respectively 88.4% and 84.9%.

Accuracy for the detection of scoliosis with 40 degrees or greater		
Cobb angles by experts		
The proposed method	40° or more	117
	Less than 40°	5
		Less than 40°
		40° or more
		149
		30

Accuracy for the detection of the progression in scoliosis		
Cobb angles by experts		
The proposed method	Progression	21
	No progression	12
		No progression
		Progression
		114

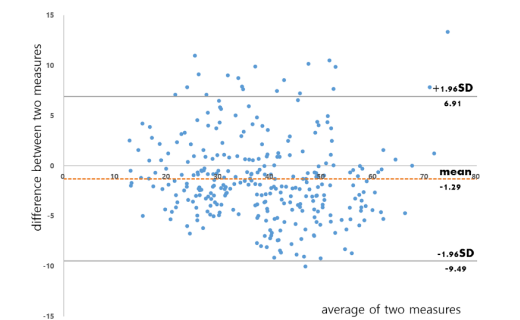


Figure 3: Bland-Altman plots between the Cobb angle measurement by experts and those by the proposed method. The graph shows no specific pattern, with a mean difference of -1.29 and 95% limits of agreement ranging from -9.49 to 6.91.

The interobserver reliability of the four novices, using the Cobb angle measurements obtained by the experts as the reference standard, is shown in Table 3. Again, all novice results differed significantly from the experts, with the mean difference ranging from 2.26 to 9.98.

Table 3: Interobserver reliability of four novices, using the Cobb angle measurements obtained by experts as the reference standard. The Cobb angle measurements obtained by four inexperienced individuals differed significantly from those obtained by the expert.

	Expert	Observer 1	Observer 2	Observer 3	Observer 4
Cobb angles*	38.39±15.29	36.13±16.02	32.96±15.62	35.52±14.22	28.41±13.58
Difference* (range)†	NA	2.26±4.13 (0.55-14.05)	5.43±7.73 (0.35-22.24)	2.87±3.33 (0.14-9.99)	9.98±5.45 (0.53-26.18)
P value‡	NA	0.006	0.001	<0.001	<0.001
ICC	NA	0.978	0.905	0.978	0.858
(95% CIs)		(0.938-0.991)	(0.678-0.963)	(0.873-0.993)	(-0.14-0.965)
P value§	NA	<0.001	<0.001	<0.001	<0.001

*mean ± standard deviations (SD)
 †Difference between expert's and each novice's Cobb angles
 The parenthesis range indicates the absolute difference between the expert's and each novice's Cobb angles.
 ‡Paired t-test between the expert's and each observer's measures
 §P value for ICC between the expert's and each observer's measures
 CI, confidence interval
 NA, non-applicable

The principal findings of the present study can be summarized as (a) the proposed method for the automatic quantification of the spinal curvature showed excellent agreement (ICC, 0.969) with the traditional method for Cobb angle measurement by experts, (b) the accuracy of the proposed method for detecting scoliosis with a Cobb angle of 40 degrees or greater was good (88.4%), with a sensitivity of 95.9% and a specificity of 83.2%, (c) the accuracy of the proposed method for monitoring spinal curve progression was modest (84.9%), with a sensitivity of 63.6% and a specificity of 90.5%, and (d) interobserver reliability of the four novices showed different ICC values ranging from 0.858 to 0.978, with a comprehensive 95% confidence interval of -0.14 to 0.991. In contrast, the proposed method always provides consistent results.

In our proposed model, segmentation of the entire spine using deep-learning technology was implemented, eliminating the requirement for the manual detection of the anatomical landmarks, which was present in previous computational methods.¹¹ Previous models implemented partial division of each spinal column because of the complexity of the spine and the number of calculations required. Calculating the curvature is more complex and prone to errors from segmenting individual vertebrae. Instead of manually connecting the midpoints, this deep-learning model automatically draws the midline and converts it into a seventh-order function, which becomes the basis for measuring the spinal curvature, thereby minimizing the impact of segmentation errors on the Cobb angle measurement. In addition, this model resolves the problem of interobserver variability because a machine automatically conducts the measurement. The simplicity of the proposed model saves time and resources and offers convenience by using a functional graph to calculate the spinal curvature. The severity of the curvature can also be observed from the shape of the automatic line, which makes the detection process more accessible.

This study had some limitations. First, although the proposed method is simple, fully automated, and generates consistent measurements of spinal curvatures, the accuracy levels for detecting severe scoliosis and monitoring progression must be sufficiently high to replace the traditional Cobb angle measurement method. Thus, additional modifications are required to enhance the accuracy of the proposed method. Second, this was a single-center study. Therefore, external validation is necessary to ascertain whether similar results can be replicated in other institutions. Lastly, it's important to note that our model was primarily trained to measure adolescent idiopathic scoliosis, and we lack the data necessary to confirm its accuracy in detecting degenerative changes in the spine that typically occur after the 30s-40s. Therefore, our model may not be optimal for diagnosing degenerative scoliosis, as it was specifically designed to measure adolescent idiopathic scoliosis patients who generally have more severe conditions.

■ Conclusion

The proposed method for automatic spinal curvature measurement using the U-Net model showed acceptable accuracy and excellent agreement with the traditional method for Cobb angle measurement by experts. The proposed method may be useful for detecting severe scoliosis and monitoring moderate scoliosis that may progress over time.

■ Acknowledgments

This study was conducted through scoliosis research club activities at Saint Paul Preparatory Seoul High School. Professor Hyoungmin Kim, one of the advisors of this study and an orthopedic surgeon, performed scoliosis surgery on Yubeen Lee, the club's leader. Through this relationship, he provided an opportunity for collaborative research with Professor Jae-Hun Kim, Ph.D., Engineering at Samsung Medical Center. We sincerely thank the two professors who served as advisors for this study. With their guidance, this study was conducted. We are grateful for the opportunity to conduct this study under their supervision. In addition, the three authors who participated in the club activities contributed equally to this study.

■ References

- Weinstein, S. L.; Dolan, L. A.; Cheng, J. C.; Danielsson, A.; Morcuende, J. A. Adolescent Idiopathic Scoliosis. *The Lancet* 2008, 371 (9623), 1527–1537. DOI:10.1016/s0140-6736(08)60658-3.
- Cobb JR. Outline for the study of scoliosis. *Instr Course Lect.* 1948;5:261-75.
- Negrini, S.; Donzelli, S.; Aulisa, A. G.; Czaprowski, D.; Schreiber, S.; de Mauroy, J. C.; Diers, H.; Grivas, T. B.; Knott, P.; Kotwicki, T.; Lebel, A.; Marti, C.; Maruyama, T.; O'Brien, J.; Price, N.; Parent, E.; Rigo, M.; Romano, M.; Stikeleather, L.; Wynne, J.; Zaina, F. 2016 SOSORT Guidelines: Orthopaedic and Rehabilitation Treatment of Idiopathic Scoliosis during Growth. *Scoliosis and Spinal Disorders* 2018, 13 (1). DOI:10.1186/s13013-017-0145-8.
- Konieczny, M. R.; Senyurt, H.; Krauspe, R. Epidemiology of Adolescent Idiopathic Scoliosis. *Journal of Children's Orthopaedics* 2013, 7 (1), 3–9. DOI:10.1007/s11832-012-0457

-4.

- Vrtovec, T.; Pernuš, F.; Likar, B. A Review of Methods for Quantitative Evaluation of Spinal Curvature. *European Spine Journal* 2009, 18 (5), 593–607. DOI:10.1007/s00586-009-0913-0.
- La Maida, G. A.; Zottarelli, L.; Mineo, G. V.; Misaggi, B. Sagittal Balance in Adolescent Idiopathic Scoliosis: Radiographic Study of Spino-Pelvic Compensation after Surgery. *European Spine Journal* 2013, 22 (S6), 859–867. DOI: 10.1007/s00586-013-3018-8.
- Ilharreborde, B.; Even, J.; Lefevre, Y.; Fitoussi, F.; Presedo, A.; Souchet, P.; Penneçot, G.-F.; Mazda, K. How to Determine the Upper Level of Instrumentation in Lenke Types 1 and 2 Adolescent Idiopathic Scoliosis. *Journal of Pediatric Orthopaedics* 2008, 28 (7), 733–739. DOI:10.1097/bpo.0b013e318185a36b.
- Chockalingam, N.; Dangerfield, P. H.; Giakas, G.; Cochrane, T.; Dorgan, J. C. Computer-Assisted Cobb Measurement of Scoliosis. *European Spine Journal* 2002, 11 (4), 353–357. DOI:10.1007/s00586-002-0386-x.
- Zhang, J.; Lou, E.; Le, L. H.; Hill, D. Computer-Assisted Cobb Angle Measurement on Posteroanterior Radiographs. *Studies in Health Technology and Informatics* 2008, 140, 151–156. DOI:10.3233/978-1-58603-888-5-151.
- Papaliadis, D. N.; Bonanni, P. G.; Roberts, T. T.; Hesham, K.; Richardson, N.; Cheney, R. A.; Lawrence, J. P.; Carl, A. L.; Lavelle, W. F. Computer Assisted Cobb Angle Measurements: A Novel Algorithm. *International Journal of Spine Surgery* 2017, 11 (3), 21. DOI:10.14444/4021.
- Chi, W.-M.; Cheng, C.-W.; Yeh, W.-C.; Chuang, S.-C.; Chang, T.-S.; Chen, J.-H. Vertebral Axial Rotation Measurement Method. *Computer Methods and Programs in Biomedicine* 2006, 81 (1), 8–17. DOI:10.1016/j.cmpb.2005.10.004.

■ Authors

Yubeen Lee, Seoyoung Park, and Seunghoon Han are high schoolers at Saint Paul Preparatory Seoul who participated in this research as members of the Scoliosis Research club with deep interests in biology, statistics, and computer science.

Prediction of a City's Power Consumption by Artificial Neural Networks

Maxwell Y. Chen

Georgiana Bruce Kirby Preparatory School, 425 Encinal Street, Santa Cruz, California 95060, USA; maxwellyhchen@gmail.com
Mentors: Shourya Bose, Yu Zhang

ABSTRACT: Electricity is the most important and useful energy form for our modern society. This calls for smart management to have optimal usage. Artificial neural networks (ANNs) have emerged as a powerful tool in forecasting power demand, especially when multiple variables are involved. In this paper, taking a city in Morocco as an illustrating example, a long short-term memory (LSTM) neural network is developed to predict power consumption via five weather factors. Our numerical results corroborate the merits of LSTM in forecasting the load demand with which temperature exhibits the strongest correlation.

KEYWORDS: Robotics and Intelligent Machines; Machine Learning; Artificial Neural Networks; LSTM; Power Consumption Prediction.

■ Introduction

Electricity is indispensable in our society, giving life to our appliances and electronic gadgets and powering our critical infrastructure. Therefore, developing effective technologies to protect our electrical grid is important. One strategy is to accurately predict spikes and dips in power consumption, preventing property damage and ensuring that every customer has electricity access. Indeed, power consumption forecasting is an important task in the energy industry, enabling energy providers to allocate their resources and optimize their operations efficiently. This can be achieved using statistical methods, such as linear regression, polynomials, and ARIMA (autoregressive integrated moving average). For instance, in a previous study,¹ we demonstrated that ARIMA was a reasonably reliable tool in predicting power consumption by using data from several California counties as the illustrating examples. Nevertheless, ARIMA-based forecasting performs best on data points strongly correlated to each other in the time domain. Thus, expanding the prediction toolset that can be applied to a wide range of data and variables and producing accurate results is important.

Recently, there has been a growing interest in using artificial neural networks (ANN) to forecast power consumption.² Neural networks are a class of machine learning algorithms that are particularly well-suited for complex, non-linear data patterns, making them an ideal choice for forecasting power consumption. By analyzing historical data on power consumption, weather patterns, and other relevant variables, neural networks can accurately predict future power demand with a high degree of accuracy. In this way, power providers can adjust their energy generation and distribution strategies to meet the changing needs of their customers while minimizing waste and improving overall efficiency. Notably, ANN can be used for a wide range of systems. For instance, Stošović *et al.*³ employed five different network structures, i.e., ordinary

recurrent neural network (RNN), long short-term memory (LSTM), gated recurrent units (GRU), bidirectional LSTM, and bidirectional GRU, to predict the electricity consumption of a cold storage facility. The results showed that the modifications of RNN performed much better than ordinary RNN, and more significantly, GRU and LSTM exhibited the best performances. Chen *et al.*⁴ constructed an ANN to predict the electricity demands in several office buildings by splitting the time variable for different occupancy rates within the context of multiple weather factors. Adhiswara *et al.*⁵ developed an ANN algorithm to predict long-term electricity consumption in Indonesia for 2019-2025. Jamii *et al.*⁶ propose an ANN-based paradigm to effectively and accurately predict wind power generation and load demand.

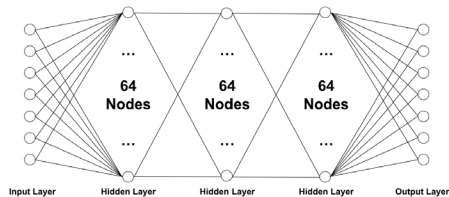
Motivated by these successes, in the present study, an LSTM-based ANN is constructed for power demand forecasting using data from a city in Morocco as the illustrating example. Unlike a feed-forward network that only allows data to move in a single direction, an LSTM has many feedback loops that will enable past data to influence the data being inputted, allowing for more accurate output. The results indeed show that LSTM is a reliable and feasible tool for predicting power consumption within the context of multiple weather factors.

■ Methods

The dataset selected for this project is from a city in Morocco called Tetuan City.⁷ This dataset contains five environmental variables along with power consumption. These are time, temperature in Celsius, humidity in percentage, wind speed in kilometers per hour, and diffuse flow and general diffuse flow, which are related to groundwater flow. It is also important to note that the data spans from the entirety of 2017, and is in 10-minute intervals, therefore amounting to over 52,000 data points.

Four tools were used to write the LSTM neural network (Scheme 1). The first tool is the Pycharm IDE, an application to create and run Python programs. The second is NumPy, a Python library that gives access to many useful mathematical functions. The third is matplotlib, another Python library that allows one to plot custom graphs using data points and equations. Finally, the most important tool is Pytorch, another Python library. This library provides neural network functions that one can use to create the program's framework.

Before inputting data into the neural network, they needed to be converted into the appropriate format for the LSTM. This was done by writing code to scale data to a range from 0 to 1 to lower the resources used and make the training much more efficient. The data was then sorted into two matrices directly used in the neural network. The first matrix was the input matrix. This matrix contained a series of consecutive data points that corresponded with the length of the specified input length. The next matrix was the input comparison matrix. This matrix had the same data points as the input matrix and contained additional data that would be used to compare with the neural network's output. By comparing the output with the comparison matrix, the neural network lowered the validation loss and therefore increased the accuracy of the prediction. Overall, 700 iterations of the training loop were run, in conjunction with the use of the Adam activation function and the Smooth L1 Loss function in order to produce high-quality results.



Scheme 1: Schematic representation of an LSTM neural network.

Results and Discussion

Analysis was first carried out to evaluate the correlation of these weather factors to power consumption. Figure 1 shows the comparison graphs where the red curves are the power consumption (in kilowatt, kW) and the blue ones are the respective weather factors for the entire time period. Of course, some variables are more related to power consumption than others. For example, the patterns of temperature variation rather closely resembled those of power consumption, whereas only a weak correlation was observed with wind speed and diffuse flow.

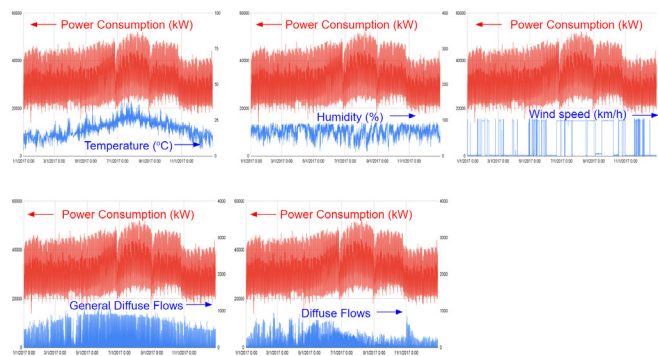


Figure 1: Comparison of power consumption (red curves) with various weather factors (blue curves) within the year 2017, such as temperature, humidity, general diffuse flows, wind speed, and diffuse flows. The results show that temperature exhibits the highest correlation with power consumption, whereas wind speed and diffuse flow are weakly correlated.

This can be further confirmed by calculating the r^2 coefficient of each variable in relation to power consumption. For example, from Figure 2, one can see that the r^2 value decreases in the order of temperature (0.194) > humidity (0.083) > general diffuse flow (0.035) > wind speed (0.028) > diffuse flow (0.006). This suggests that power consumption is correlated to multiple weather factors, and temperature exhibits the highest r^2 value and is hence the most correlated to power consumption.

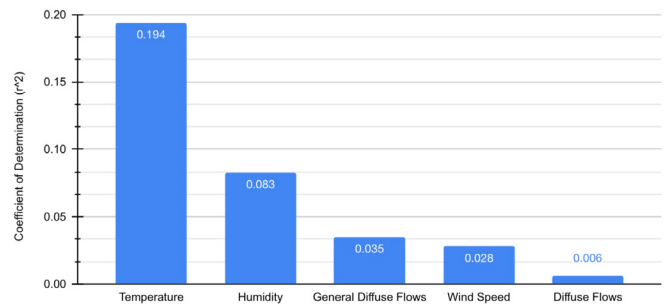


Figure 2: Comparison of the r^2 coefficient of each weather factor in relation to power consumption. Values are obtained from statistical calculations of data in Figure 1. The results show that power consumption is the most correlated with temperature, followed by humidity, general diffuse flow, wind speed, and diffuse flow.

Since these weather factors are correlated with power consumption, they must all be included for prediction when the dataset is input into the LSTM. However, to ensure that the neural network can adequately follow the trends of the dataset, it was programmed to have one data point as an input and then output the next predicted point. This was done for every data point in the dataset, and the result is shown in Figure 3, with the blue being the original data and the red being the predicted LSTM points. One can see that the neural network followed the data patterns very closely and matched many of the spikes and dips in power consumption. This suggests that the obtained LSTM algorithm may be an effective tool in reproducing the power consumption data, a critical step in implementing LSTM for power consumption forecasting.

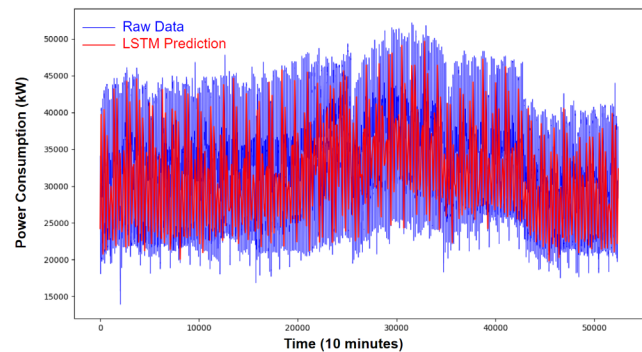


Figure 3: Comparison of raw data versus LSTM prediction using a single previous data point as input, which outputs one prediction data point. Blue curves are raw data, and red curves are LSTM predictions. The similarities between the raw data and LSTM predictions indicate that this algorithm is an effective tool for reproducing power consumption.

Since the LSTM neural network could learn the trends of the dataset, it was then used to predict power demand. This was done by using a train-test split, where 1200 consecutive data points were allocated for training, and the subsequent 252 data points were selected for testing. The training portion of the dataset was input into the LSTM for training, and the testing portion was purely for comparing the output results and was not used for machine learning. The results are shown in Figure 4, where the blue represents the training data, the green represents the testing data, and the red represents the output of the LSTM. One can see that the LSTM output closely follows the patterns of the testing data and suggests that this LSTM is adequate for predicting power consumption.

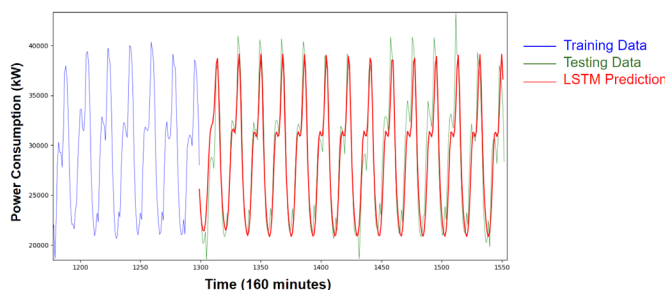


Figure 4: With part of the actual data as training data (blue curve), the remaining data is used as testing data (green curve) to compare the accuracy of LSTM prediction (blue curve). Only a portion of the training data is shown to highlight the details of the comparison. The close agreement of the LSTM prediction to the testing data indicates that this ANN can be used for accurate power consumption prediction.

■ Conclusion

In summary, an LSTM neural network was developed to analyze the correlation between the power consumption of a Moroccan city with various weather factors within the span of a whole year. The results showed that power consumption depended on these weather variables, with temperature showing the strongest correlation. ANNs were also shown as a powerful tool for forecasting power demand by leveraging these correlated variables, allowing it to be applicable to a wider spectrum of communities, ranging from an apartment complex to an entire nation. The predicted patterns and trends will be important in optimizing power management and developing a smart power grid.

■ Acknowledgments

M.Y.C. would like to thank Prof. Yu Zhang and Shourya Bose for their mentorship in this project. Some of the programs were run using the UCSC Lux Supercomputer.

■ References

1. M. Y. Chen, S. Bose, Y. Zhang, AI-Based Power Demand Forecasting of California Counties, *International Journal of High School Research*, 5 (2022) 83-85.
2. O. I. Abiodun, A. Jantan, A. E. Omolara, K. V. Dada, A. M. Umar, O. U. Linus, H. Arshad, A. A. Kazaure, U. Gana, M. U. Kiru, Comprehensive Review of Artificial Neural Network Applications to Pattern Recognition, *IEEE Access*, 7 (2019) 158820-158846.
3. M. A. Stošovic, N. Radivojevic, M. Ivanova, Electricity

Consumption Prediction in an Electronic System Using Artificial Neural Networks, *Electronics* 11 (2022) 3506.

4. S. Chen, Y. Ren, D. Friedrich, Z. Yu, J. Yu, Prediction of office building electricity demand using artificial neural network by splitting the time horizon for different occupancy rates, *Energy and AI*, 5 (2021) 100093.
5. R. Adhiswara, A. G. Abdullah and Y. Mulyadi, Long-term electrical consumption forecasting using Artificial Neural Network (ANN), *Journal of Physics: Conference Series*, 1402 (2019) 033081.
6. J. Jamii, M. Mansouri, M. Trabelsi, M. F. Mimouni, W. Shatanawi, Effective artificial neural network-based wind power generation and load demand forecasting for optimum energy management, *Frontiers in Energy Research*, 10 (2022) 898413.
7. <https://www.kaggle.com/datasets/fedesoriano/electric-power-consumption>

■ Author

Maxwell Y. Chen is a junior at the Georgiana Bruce Kirby Preparatory School. He wants to pursue a computer science major in college and is very interested in modern technological advancements. In his spare time, he likes to experiment with software and hardware.

Nutritional Status of Sickle Cell Disease Patients: A Literature Review

Minjoon Hur

Raffles Christian School Pondok Indah, Jalan Gedung Hijau Raya No.1, Jakarta Selatan, DKI Jakarta, 12310, Indonesia;

hurminjoon0705@gmail.com

Mentor: Dr. Boluwatiwi Durojaye

ABSTRACT: Sickle cell disease (SCD) is a lethal, life-long condition characterized by a mutation in the gene that codes for hemoglobin. To alleviate the pain experienced by sickle cell (SC) patients, adequate nutrition levels are vital as deficiencies of vitamins or minerals may cause other symptoms. This review aims to provide an overview of the nutrient status of SC patients and propose research areas where further study is required. The review summarizes twelve primary research papers that assessed the levels of vitamins A, C, D, E, B-2, B-6, B-12, folate, magnesium, iron, zinc, and copper in SC patients. Most SC patients exhibited suboptimal levels of vitamin A, while deficiencies in vitamin D and B-2 were prevalent. Their zinc and vitamins B-6, B-12, C, and E levels were generally adequate, while elevated folate and copper levels were observed. The magnesium levels in SC patients were lower than those in the healthy population. Determining the status of iron concentration in SC patients was challenging due to the limitations associated with the measurement methods employed in the reviewed papers. There were notable differences in some of the measurement methods used for the same nutrient levels. More research is needed to find the optimal amount of vitamin A supplement for SC patients. The effect of zinc supplementation on copper levels and the cause of low zinc levels in SC patients remains unexplored.

KEYWORDS: Translational Medical Sciences, Sickle Cell Disease; Malnutrition; Vitamins; Minerals.

■ List of Abbreviations

Sickle Cell (SC)
Sickle Cell Disease (SCD)
Sickle Cell Anemia (SCA)
Red Blood Cell (RBC)
Hemoglobin (Hb)
Hemoglobin S (HbS)
Recommended Daily Allowance (RDA)
Vitamin D Deficiency (VDD)
Serum 25-hydroxyvitamin D (25(OH)D)
Transferrin Soluble Receptors (sTfR)
Erythrocyte Glutathione Reductase activation coefficient (EGRac)

■ Introduction

Sickle cell disease (SCD) is a group of inherited genetic disorders characterized by a mutation in the gene that codes for hemoglobin subunit β .^{1,2} The gene mutation replaces the glutamic acid with valine at position 6 in the β -globin chain.¹ The change in the primary structure of the polypeptide alters the product from Hemoglobin A to Hemoglobin S (HbS), producing erythrocytes with sickle shapes under low oxygen tension.² Increased sickle erythrocyte concentration causes vaso-occlusion (blockage of blood vessels), which leads to insufficient oxygen transport to tissues and organs.² Vaso-occlusion causes frequent pain in bones and joints, inflammatory response, and oxidative stress.² These symptoms lower the life expectancy of SCD patients to 54 years, making it a lethal condition as those without SCD have a life expectancy of 76 years.⁴ The trait for

SCD is not uncommon, as about one in twenty people in the human population carries the trait gene for hemoglobin (Hb) disorders: HbS.³

The severity of the SCD is determined by the concentration of HbS, which depends on the patient's genotype.² The most severe genotype is HbSS, followed by HbS β 0-thalassemia, HbS β +thalassemia, and HbSC.²

Proper nutrition is vital for overall health and in decreasing the morbidity of diseases.⁶ This is particularly relevant for individuals with SCD, as maintaining optimal nutritional status can significantly enhance their quality of life with the widely accessible cure for SCD remaining as an unresolved issue.⁵ This paper focuses on examining the significance of specific essential nutrients in SC patients, namely vitamins A, C, D, E, B-2, B-6, B-12, folate, magnesium, iron, zinc, and copper. When one lacks adequate intake of any or some of these essential nutrients, one may develop deficiency symptoms, which will be discussed in detail in the subsequent sections dedicated to each nutrient. To reduce the risk of an individual developing these symptoms, the Recommended Daily Allowance (RDA) has been established.⁵ However, the RDA may not be sufficient for SCD patients as it is made for the general healthy population rather than individuals with specific medical conditions.⁵

To prevent SC patients from developing nutritional diseases, this paper will outline the nutrient deficiencies and elevations present in SC patients using the primary data gathered by researchers. Most of the primary data will be from papers published after 2010, as a review paper on nutrition in SCD was published that year.⁵ With the latest primary data, this paper

will provide an updated review of the nutrition status of SC patients.

■ Methods

Twelve primary research papers that investigated nutrient levels in SC patients were collected and summarized. Two of the 12 research papers collected were randomized clinical trials; the rest were cross-sectional studies. The nutrients evaluated in the papers were vitamins A, C, D, E, B-2, B-6, B-12, folate, magnesium, iron, zinc, and copper. For each nutrient, the nutrient deficiency cutoff was researched and noted. Units of the deficiency cutoff values were manually converted to match the units of the measured values in the primary research papers. The cutoff values were then compared to those obtained from SC patients to determine whether deficiencies or elevations of the nutrient were evident in SC patients.

■ Results and Discussion

Zinc:

Zinc is essential for cellular and subcellular metabolism; it is an integral component of the catalytic sites of some enzymes and may have a specific role in many other biological proteins.⁹ Zinc is also responsible for the absorption, mobilization, transport, and metabolism of vitamin A.¹⁰ The serum zinc test is commonly used to measure zinc status in the body, with a serum zinc concentration of $<60 \mu\text{g/dL}$ considered deficient.¹¹ This method was used by a cross-sectional study in India.¹⁰ After recruiting 33 homozygous SC patients and 33 age and sex-matched healthy controls, the study compared the serum zinc level in SC patients to that of normal controls.¹⁰ The paper's main objective was to evaluate plasma vitamin A, C, and E levels and serum zinc and copper levels in adolescent patients with HbSS.¹⁰ All subjects were aged 10–20 years and had no history of blood transfusion within three months, a factor that may significantly affect zinc concentration.^{10,49} Subjects with chronic ailments, diabetes mellitus, or SCD cases with an acute crisis, together with patients on multivitamin supplementation, were excluded from the patient and control groups.¹⁰ The serum zinc concentration in SCD and healthy controls were $83 \pm 9 \mu\text{g/dl}$ and $104 \pm 6 \mu\text{g/dl}$, respectively.¹⁰ The serum concentration in healthy controls was significantly higher than those in SCD patients ($p < 0.001$).¹⁰ Also, the values shown above suggest that no SC patients were zinc deficient because their serum zinc concentrations were greater than $60 \mu\text{g/dL}$.^{10, 11}

A cross-sectional study that took place in Saudi Arabia also concluded that there was no zinc deficiency in SC patients.¹² Using the same measurement method with 25 SC patients that have severe sickle cell anemia (SCA), the study was designed to evaluate levels of vitamins A, C, and E and elements zinc and copper.¹² The exclusion criteria of the study were individuals younger than 15 years of age, the presence of β - or α -thalassemia trait, glucose-6-phosphate dehydrogenase deficiency, regular blood transfusion, treatment with hydroxyurea, use of vitamin and trace element supplements other than folic acid, illness other than sickle cell manifestations, or pregnancy.¹² The mean measured serum zinc level was about $65 \mu\text{g/dL}$, which is above the deficiency cutoff.¹²

Nevertheless, the results still show that SCA patients have lower serum zinc levels than the controls.

Both papers show that SC patients have serum zinc levels lower than the normal controls but above the zinc deficiency cutoff value. Therefore, the SC patients in these studies do not have a zinc deficiency.

Vitamin A:

Vitamin A is responsible for immune function, growth, development, reproduction, and, most importantly, vision.¹³ The plasma retinol test commonly measures its concentration in the body, with a concentration of $<20 \mu\text{g/dL}$ considered deficient and a concentration of $20\text{--}29 \mu\text{g/dL}$ considered suboptimal.¹³ Vitamin A deficiency in patients may lead to night blindness, a decrease in growth rate, and a reduction in bone development rate.¹⁴ To determine whether SC patients are also at risk of developing disorders related to vitamin A deficiency, a randomized controlled trial in the United States investigated the effect of giving supplemental vitamin A to children with SCD by measuring their plasma levels before and after the supplementation.¹³

The study aimed to determine whether three doses of supplemental vitamin A (300, 400, or 600 μg of retinyl palmitate per day for twelve months) on SCD would optimize vitamin A status in SC patients with the HbSS genotype. Subjects aged 2–13 years were enrolled.¹³ The exclusion criteria were chronic transfusion therapy or a transfusion within the past two months, hydroxyurea therapy, history of stroke, liver enzymes >3 times the reference range, height >2.0 standard deviations above the age and sex mean, participation in another intervention study, pregnancy, and other chronic conditions known to affect growth, dietary intake, or nutritional status.¹³ The mean initial plasma retinol concentration of children with SCD was $26 \pm 8 \mu\text{g/dL}$: a level considered suboptimal but not deficient.¹³ Though the mean plasma retinol concentration was above the deficiency cutoff value, 22 out of 96 patients were vitamin A deficient. After the twelve-month supplementation of 300/400/600 $\mu\text{g/d}$, the serum retinol values changed by $-2.8 \pm 2.4 \mu\text{g/dL}$, $0.9 \pm 4.1 \mu\text{g/dL}$, and $3.6 \pm 2.8 \mu\text{g/dL}$, respectively.¹³ The patients still had suboptimal vitamin levels after the supplementations, though.¹³ Low vitamin A levels were also witnessed by Hasanato *et al.*, as their SC patients also had a lower mean plasma retinol concentration than normal, healthy controls.¹²

Both papers lean towards the conclusion that SC patients have lower vitamin A levels than healthy controls and that there are some patients who are vitamin A deficient.^{12,13}

Vitamin E:

Vitamin E is the major lipid-soluble component in the cell antioxidant defense system.¹⁵ As an antioxidant, it is effective against diseases caused by oxidation.^{15,16} The most widely used method for its measurement is the serum α -tocopherol test, with a concentration of $<5 \mu\text{g/ml}$ marking vitamin E deficiency.¹⁷ This test was used by Wasnik *et al.* in 2017 to evaluate the vitamin E status of SC patients.¹⁰ The design for this study has been thoroughly described in the subsection on zinc. The serum α -tocopherol count in SC patients and controls in the study were $9 \pm 1 \mu\text{g/mL}$ and $12 \pm 2 \mu\text{g/mL}$, respectively.¹⁰

The serum concentration in healthy controls was significantly higher than those in SCD patients ($p < 0.001$).¹⁰ Also, as the values shown were greater than 5 $\mu\text{g}/\text{mL}$, most SC patients in the study were not vitamin E deficient.¹⁷ They were not expected to experience the symptoms of vitamin E deficiency.¹⁷ Even so, lower levels of vitamin E should not be ignored as tissues needing α -tocopherol may be damaged when needs exceed the amounts available.¹⁷

Low levels of vitamin E in SC were also witnessed by Hasanato *et al.*, as the mean serum vitamin E concentration of SC patients was about 2 $\mu\text{g}/\text{mL}$.¹² This value is far below the cutoff marking deficiency, and if the measurement was accurate, SC patients are at risk of experiencing increased infection, anemia, and stunting of growth.¹⁷ The difference between the measured values may be due to their different measurement methods: the study of Wasnik *et al.* used the modified method of serum vitamin E estimation, while the study of Hasanato *et al.* used the long-term freezer storage method.^{10,12,39,40} As the long-term freezer storage method may be erroneous due to the potential degradation of the sample over time, the values obtained by Wasnik *et al.* are probably more accurate.³⁹ Though their measurement methods differ, both papers show suboptimal vitamin E levels in SC patients.^{10,12} Therefore, it is likely for SC patients to have suboptimal vitamin E levels.

Vitamin C:

As an antioxidant, vitamin C is a micronutrient with pleiotropic functions.¹⁹ It supports the human immune system and is a cofactor for a family of biosynthetic and gene-regulatory enzymes.¹⁹ It is commonly measured by plasma ascorbic acid (vitamin C), with a cutoff value for deficiency of $< 11 \mu\text{mol}/\text{L}$.²¹ Hasanato *et al.* examined the vitamin C status of 25 SC patients by measuring their plasma levels of ascorbic acid.¹² The design for this study has been thoroughly described in the subsection on zinc. The study found that the mean plasma vitamin C in patients was approximately 57 $\mu\text{mol}/\text{L}$, indicating that SC patients were not vitamin C deficient.¹² However, the mean plasma level of vitamin C in the SC patients was about half that of the non-SC, healthy controls.¹²

A cross-sectional study in Nigeria also observed low vitamin C levels.⁴⁴ 80 SC patients with HbSS aged 1-15 years and 80 age and gender-matched healthy HbAA controls were recruited.⁴⁴ The exclusion criteria included the presence of febrile illness, history of blood transfusion in the past three months, history of hydroxyurea or chronic blood transfusion, and history of taking antioxidant supplements.⁴⁴ The study explored the relationship between the frequency of vaso-occlusive crises and plasma levels of antioxidant micronutrients, including vitamin C.⁴⁴ The vitamin C level of SC patients and controls in the study was $38 \pm 10 \mu\text{mol}/\text{L}$ and $63 \pm 17 \mu\text{mol}/\text{L}$ respectively.⁴⁴ The plasma concentration in healthy controls was significantly higher than those in SCD patients ($p < 0.001$).⁴⁴ These values support the ones obtained by Hasanato *et al.* as the vitamin C levels in SC patients are above the deficiency cutoff but are lower than the controls.

The big difference between the ascorbic plasma levels in patients and controls made researchers conclude that SC patients have vitamin C deficiency; but as their plasma vitamin

C levels are higher than the deficiency cutoff, SC patients have adequate vitamin C and are unlikely to experience the common symptoms of vitamin C deficiency.^{12,20}

Copper:

Copper is required in redox chemistry to produce many proteins, including enzymes.²² The most widely used biomarker for evaluating copper status is serum copper, with a value of 64-140 $\mu\text{g}/\text{dL}$ considered adequate.^{23,41} By measuring this biomarker, a cross-sectional study in Ghana measured and compared copper levels in 90 SC patients aged 14-53 and 50 healthy controls aged 22-43.²² Of the 90 SC patients, 41 had the HbSC genotype, and 49 had the HbSS genotype.²² All 50 controls held the HbAA genotype, and any subjects with diabetes, renal disease, gastrointestinal disease, or coronary artery disease were excluded from the study.²² As it aimed to evaluate serum iron, copper, and zinc levels in SC patients, the study also excluded patients with a history of blood transfusion three months before the study.²² The mean serum copper levels of SC patients and controls were $221 \pm 28 \mu\text{g}/\text{dL}$ and $114 \pm 16 \mu\text{g}/\text{dL}$, respectively.²² The serum concentration in healthy controls was significantly lower than those in SCD patients ($p < 0.001$).²² As the mean copper level of SC patients in this study was elevated, SC patients were at risk of developing stomach pain, extreme thirst, and changes in taste that may lead to decreased appetite.^{23,24}

Elevated copper levels in SC patients were also seen in research done by Emokpae and Fatimehin.⁴⁵ Seeking to evaluate the serum copper and zinc levels in SC patients, 100 confirmed SC patients with a mean age of 19 ± 1 years and age-matched healthy subjects were recruited in the study.⁴⁵ The mean serum copper levels in SC patients and the controls were 184 $\mu\text{g}/\text{dL}$ and 107 $\mu\text{g}/\text{dL}$, respectively.⁴⁵ The mean copper level of SC patients in this study, too, was elevated.^{23,45}

Both papers show higher levels of copper in SC patients, so there was a copper elevation in SC patients in the studies reviewed.

Vitamin D:

Vitamin D is crucial for calcium absorption and maintaining normal serum calcium and phosphate levels.²⁵ It also plays a vital role in immune function, cell proliferation, differentiation, and apoptosis.²⁶ These crucial tasks may not be completed efficiently when an individual is vitamin D deficient. Vitamin D deficiency (VDD) may also lead to osteoporosis (brittle bones) and increased fragility fractures.⁴² VDD is commonly diagnosed by measuring the biomarker serum 25-hydroxyvitamin D (25(OH)D).²⁶ A serum 25(OH)D concentration of 30-60 ng/mL is optimal, while values below 30 ng/mL and 20 ng/mL are considered suboptimal and deficient, respectively.²⁶ By measuring and comparing the serum 25(OH)D level of 640 SC patients to the cutoff values, a cross-sectional study in Saudi Arabia evaluated the vitamin D status in SC patients.²⁶ All patients enrolled in the study were 12 years old and older, and there were no controls.²⁶ About 82% of the patients had suboptimal 25(OH)D, while 67% were deficient.²⁶ Middle-aged (45-65 years) and elderly (>65 years) patients had higher 25(OH)D levels than young patients, with females having slightly higher 25(OH)D levels than males.²⁶ Furthermore,

SC patients with crisis had higher average 25(OH)D levels than those in steady state condition.²⁶ As most SC patients have insufficient serum 25(OH)D levels, they are also vitamin D deficient.

Folate, vitamins B-2, B-6, and B-12:

Folate (vitamin B-9) is essential for producing red blood cells.²⁷ It is also vital in one-carbon metabolism, which is essential for synthesizing DNA and RNA.²⁷ Vitamins B-2, B-6, and B-12 are required to produce the universal methyl donor, S-adenosylmethionine.²⁷ To determine whether these metabolic reactions were carried out efficiently in SC patients, a cross-sectional study in Canada measured the folate concentrations and B-vitamin levels in the blood of Canadian children with SCD supplemented with 1 mg of folic acid daily as their regular treatment.²⁷ All 11 patients were aged 2-19 years, with 8 holding the HbSS genotype, 2 holding the HbSC genotype, and 1 holding the HbS β 0 -Thalassemia genotype.²⁷ The obtained mean concentration and the deficiency cutoff value of each B vitamin are listed below:

Table 1: Obtained mean concentrations and the cutoff values for B vitamins in SC patients taking folate supplements. B-vitamin biomarker concentrations were measured in plasma (n = 8) and serum (n = 3) for folate forms, in plasma (n = 10) and serum (n = 1) for vitamin B-12, and in plasma for pyridoxal 5'-phosphate (n = 11) and vitamin B-2 (n = 11).²⁷

Vitamin	Obtained mean concentration (nmol/L)	Deficiency cutoff value ²⁷ (nmol/L)
B-2 riboflavin	15.9	26.5
B-6 pyridoxine	36.9	30
B-9 folic acid	62.0	10
B-12	0.4	0.15

As seen in Table 1, SC patients supplemented with 1 mg/d of folic acid were not deficient in vitamin B-6, B-9, or B-12, but were deficient in vitamin B-2.²⁷ However, without the supplement, an increase in patients with vitamin B-6 deficiency is expected as supplemental folic acid can reduce plasma levels of pyridoxal 5'-phosphate, an activated form of vitamin B-6.^{27,46} None of the patients showed folate deficiency.²⁷ The mean total folate level (62.0 nmol/L) exceeded the limit for normal folate (45.3 nmol/L), indicating that the patients had elevated folate after the supplement.

Magnesium:

Magnesium is key in many cellular processes, including intermediary metabolism, DNA replication and repair, and transporting potassium and calcium ions.²⁸ Serum magnesium measures magnesium levels in the body, with a deficiency cutoff value of 0.85 mmol/L.²⁹ Using serum magnesium as an indicator of magnesium status in subjects, a cross-sectional study measured the magnesium content in 120 SC patients with HbSS and HbSC genotypes and 48 healthy controls with the HbAA genotype.³² Patients with coronary artery disease, diabetes mellitus, hypertension, renal failure, pregnancy, and a history of blood transfusion within three months before the study were excluded.³² The patients and the controls had serum magnesium levels of 0.80 ± 0.24 mmol/L and 0.90 ± 0.11 mmol/L, respectively.³² As the mean serum magnesium level of SC patients is below the deficiency cutoff value, SC patients in the study were magnesium deficient.

The lower serum/plasma magnesium content in SC patients was also shown by a randomized trial that measured the plasma and red blood cell (RBC) magnesium content in 10 HbSS treated with oral magnesium supplements (0.6 meq/kg per day of magnesium pidolate).³⁰ The study aimed to evaluate whether magnesium supplementation to SC patients reduces the number of sickled erythrocytes. The trial enrolled 45 patients who were 19 years and older, along with 17 non-SC controls with a mean age of 32 ± 9 years.³⁰ The inclusion criteria were normal renal and liver function, 70% or greater performance status, and no blood transfusions during the preceding three months.³⁰ Using plasma magnesium and erythrocyte magnesium as the biomarkers, the authors measured the magnesium content in HbSS and HbSC patients before the supplementation, 14 days after the supplementation, and 28 days after the supplementation.³⁰ The initial erythrocyte magnesium levels in HbSS and HbSC patients and the controls were 7 ± 1 mmol/kg Hb, 6 ± 1 mmol/kg Hb, and 9 ± 1 mmol/kg Hb respectively ($p < 0.05$).³⁰ The paper does not show the data on plasma magnesium as there were no significant differences between the plasma magnesium levels of HbSS patients, Hb SC patients, and normal controls.³⁰ The magnesium RBC content after 14 and 28 days of supplementation was only measured on 10 HbSS patients, and this data is represented in the table below.³⁰

Table 2: Mean plasma and erythrocyte (RBC) magnesium concentrations in HbSS patients on oral magnesium supplementation at baseline, 14, and 28 days after the supplementation

Time (days)	Plasma Magnesium (mmol/L)	Erythrocyte Magnesium (mmol/kg Hb)
Baseline	0.86 ± 0.06	5.18 ± 0.24
14	0.95 ± 0.11	9.34 ± 2.30
28	0.94 ± 0.09	11.40 ± 1.20

As shown in Table 2, there was a significant increase in erythrocyte magnesium content in HbSS patients ($p < 0.05$, $p < 0.005$ for days 14 and 28, respectively).³⁰ There was no significant change in the plasma magnesium level, but this may be due to the fact that it generally takes three months to see the rise in plasma magnesium level for patients who took oral magnesium therapy.^{30,51}

The first paper shows that SC patients have a magnesium level below the deficiency cutoff, while the other shows that SC patients have a magnesium level above the deficiency cutoff.^{30,32} However, both papers agree that the mean serum magnesium value of SC patients is below or very close to the deficiency cutoff value. This indicates that SC patients are at risk of developing chronic diseases, insulin resistance, and type-2 diabetes.³³

Iron:

Iron is an essential element as it is responsible for blood production as it is a component of hemoglobin.³⁴ It is also an essential component for electron transport and DNA synthesis.⁴³ An individual's iron status is commonly assessed by measuring the biomarker serum ferritin, with a reference range of 12-300 ng/mL.³⁵

Two studies with differing opinions regarding iron deficiency in SC patients were studied. The first study was a

cross-sectional study that took place in Nigeria.³⁶ The authors investigated whether iron was deficient in patients with SCD by measuring serum ferritin concentration in 43 HbSS patients aged over 14 years and 43 age and sex-matched HbAA controls.³⁶ Exclusion criteria included a history of blood transfusion in the previous three months or any form of SC crisis within two weeks of the study. The results showed that only 7% of the SC patients were iron-deficient and that the mean serum ferritin in SC patients and in the healthy controls was 559 ± 428 ng/mL and 185 ± 120 ng/mL, respectively.³⁶ The serum ferritin concentration in healthy controls was significantly lower than those in SCD patients ($p < 0.001$).³⁶ Also, the value from SC patients was even higher than the upper limit of the reference range (300 ng/mL). This indicates iron elevation, which may be caused by vitamin B 12 deficiency, folate deficiency, myelodysplastic syndrome, or malignancy in SC patients.³⁷

The other study was also cross-sectional, with 40 SCD patients and 30 age-matched controls enrolled.³⁸ All subjects were 3-18 years old and had hemoglobin levels < 11 g/dL.³⁸ The study measured the level of transferrin soluble receptors (sTfR) to determine whether iron was deficient. As the body increases the production of sTfR in response to low iron levels, iron deficiency is marked by an sTfR value greater than 1.8 mg/L.^{47,48} The authors of the cross-sectional study found that 97.5% of the patients had higher sTfR values than the threshold indicative of iron deficiency.⁴⁸ Still, it is difficult to say that SCD is solely responsible for this increase, as hemolysis (destruction of red blood cells) could also affect sTfR values.^{38,48}

The differences in the results and conclusions of the two papers confirm the limitations of usual biochemical parameters in the diagnosis of iron deficiency in homozygous drepanocytosis.

Overview, Limitations:

Table 3: Overview of Nutrient Status of SC patients.

Nutrient	Measurement Method/Biomarker used	Measured value in SC patients	Measured value in healthy controls	Cutoffs	Deficient/Suboptimal/Elevated for SC patients
Vitamin A	Plasma Retinol	26 ± 8 µg/dL	No controls used	- Suboptimal if 20-29 µg/dL - Deficient if < 20 µg/dL	Suboptimal
Vitamin B-2	Plasma Riboflavin	15.9 nmol/L	No controls used	- Deficient if < 25.5 nmol/L	Deficient
Vitamin B-6	Plasma P-5-P	28.9 nmol/L	No controls used	- Deficient if < 30 nmol/L	Adequate
Vitamin B-12	Serum Vitamin B-12	405 pmol/L	No controls used	- Deficient if < 150 pmol/L	Adequate
Vitamin C	Plasma Vitamin C	38.38 ± 9.81 µmol/L	93.20 ± 16.96 µmol/L	- Deficient if < 11 µmol/L	Adequate
Vitamin D	Serum 25-hydroxyvitamin D	14.3 ng/mL	No controls used	- Optimal if 30-80 ng/mL - Suboptimal if < 30 ng/mL - Deficient if < 20 ng/mL	Deficient
Vitamin E	Serum Tocopherol count	8.662 ± 1.137 µg/ml	11.782 ± 1.846 µg/ml	- Deficient if < 5.165 µg/ml	Adequate
Folate (vitamin B-9)	Total Folate level	62.0 nmol/L	No controls used	- Deficient if < 10.0 nmol/L - Elevated if > 45.3 nmol/L	Elevated
Magnesium	Serum Magnesium level	0.80 ± 0.24 mmol/L 0.88 ± 0.08 mmol/L	0.90 ± 0.11 mmol/L	- Deficient if < 0.85 mmol/L	Unable to Determine
Copper	Serum Copper level	220.9 ± 27.8 µg/dL	114 ± 18.3 µg/dL	- Optimal if 63.7-140.12 µg/dL	Elevated
Zinc	Serum Zinc level	83.09 ± 9.28 µg/dl	104.06 ± 9.27 µg/dl	- Deficient if < 80 µg/dl - Optimal if ≥ 80 µg/dl	Adequate
Iron	Serum Ferritin	550.33 ± 427.01 ng/mL	184.53 ± 119.74 ng/mL	- Elevated if > 300 ng/mL	Elevated
Iron	Transferrin Soluble Receptors (sTfR)	Not reported	Not reported	- Deficient if > 1.8 mg/L	Deficient

As shown by Table 3, it was clear that most SC patients had suboptimal vitamin A levels and were vitamin D and B-2 deficient. However, their zinc and vitamins B-6, B-12, C, and E levels were adequate, while their folate and copper levels were elevated. It is not possible to conclude the iron status of SC patients as the results of the papers agreed on the limitations of usual biochemical parameters in the diagnosis of iron deficiency in SC patients.^{35,38} The same goes for magnesium, as the papers had different conclusions and results.^{30,32}

There were some limitations in some of these research papers: sample sizes were often small,^{12,27} the most accurate method may have yet to be used,^{30,36} and exact numerical values were not recorded.¹² For instance, for iron, two studies used different biomarkers to assess iron status in SC patients,^{36,38} one used the serum ferritin method, while the other used sTfR. Ironically, both authors favored the other method over the method they used. The author, who used serum ferritin, stated that measuring sTfR is a more reliable index of iron status in SC patients than serum ferritin due to the low sensitivity of serum ferritin in SCA.³⁶ The author who used sTfR, on the other hand, stated that serum ferritin is a better biomarker for iron deficiency as sTfR could be affected by hemolysis and therefore has limits in accuracy.^{22,38}

The differences in methods used were also seen in papers that measured magnesium content in SC patients.^{30,32} Both papers measured serum magnesium,^{30,32} but only one measured erythrocyte magnesium.³⁰ It has been suggested that measuring the erythrocyte magnesium content is not the most accurate way to represent magnesium content in one's body,³¹ so data on serum magnesium could be considered more reliable. Despite the difference in their measurement methods, both papers claimed that SC patients had a mean serum magnesium value that is very close to the deficiency cutoff value.^{30,32}

There were limitations in other reviewed studies as well. The study that measured vitamin D did not analyze other factors that may have affected the vitamin D levels in the subjects.²⁶ These factors include nutritional status, physical activity, lack of sun exposure, medications that alleviate SCD crises, and other illnesses.²⁶

For the measurement of the vitamin C level in SC patients, none of the studies used the most accurate method, which is measuring vitamin C in lymphocytes.⁸ This may be because the equipment required to ensure vitamin C in lymphocytes is not widely available. Therefore, researchers who conducted the studies used the plasma vitamin C level instead to determine whether SC patients were vitamin C deficient.^{12,44}

For vitamin B-2, its status is usually determined using the erythrocyte glutathione reductase activation coefficient (EGRac), which was not available in the study conducted by Williams *et al.*²⁷ Consequently, the alternative value of 26.5 nmol/L has been used instead of the EGRac of 1.25, which indicates vitamin B-2 deficiency.

For the majority of the studies, SC patients with a history of blood transfusion months before the study were excluded.^{10,12,13,22,30,36,44} For studies that measure the concentrations of iron, zinc, and copper, patients with a history of blood transfusion were excluded as blood transfusion may heavily alter the levels of these elements.^{7,10,12,22,36,49} This may also mean that the studies did not include the sickest of the SC patients who are transfusion-dependent, indicating that the serum status of these nutrients may be worse among those with a more severe state of the disease.^{7,49} Blood transfusion does not alter the levels of folic acid and vitamin B-12, so the study of Williams *et al.* may not have had a history of blood transfusion as an exclusion criterion due to this reason.⁵⁰ The effect of blood transfusion on antioxidant levels and magnesium seems to be

a field yet to be explored, and Dougherty *et al.*, De Franceschi *et al.*, and Smith *et al.* may have excluded patients who have received a blood transfusion to eliminate this risk factor.^{13,30,44}

■ Conclusion

Though many nutrient deficiencies in SC patients were initially suspected, SC patients were only deficient in vitamin D and B-2. Instead: they had elevated levels of vitamin B-9 and copper. Low levels of magnesium in the patients were shown,²⁷ and it is impossible to confirm iron deficiency as the results of the papers highlight the limitations of usual biochemical parameters in the diagnosis of iron deficiency in SC patients.^{35,38} The patients had adequate levels of vitamins B-6, B-12, C, and E, and zinc, as none of the measured values of these nutrients were below the deficiency cutoffs. However, though they had adequate levels of these nutrients, SC patients generally had lower levels than the healthy population. As both lower and elevated nutrient levels impede normal body function, SC patients risk experiencing various toxic effects. More research is required to understand the sodium/magnesium transporter to find the cause of reduced magnesium content in SC patients.³⁰ There is also a need for another study involving age and sex-matched healthy control to determine whether SCD is solely responsible for VDD, not other factors. Furthermore, further research is needed to confirm whether VDD worsens chronic pain in SC patients.²⁶ With no improvement of vitamin A status in those taking 600 µg of vitamin A daily, a study that tests the effect of a daily supplemental dose of retinyl palmitate of over 600 µg on those aged 14-18 years with SCD must be conducted. Such an age group is selected based on the National Institutes of Health's recommendation that individuals aged 14 years and above not exceed a daily intake of 900 µg of supplemental vitamin A.¹⁸ The effect of zinc supplements on the vitamin A levels of SC patients must also be explored. The confirmation of whether low zinc levels in SC patients are due to excessive destruction of red blood cells or excessive excretion is required.¹⁰ The effect of zinc supplementation on copper levels in SC patients must also be studied.²² As shown by Table 3, SC patients generally have a lower level of micronutrients. This supports the claim made by Hyacinth *et al.*: the RDAs for the essential nutrients are only for healthy people and that these requirements for optimal intakes may be higher for SC patients.⁵ As the studies reviewed by this paper only focus on patients with SCD and not those in a carrier state, there is more research needed to confirm whether low micronutrient levels are also observed in populations with only the sickle cell trait but not the disease. This literature review analyzed the existing studies that measured the nutrient status in SC patients.

■ Acknowledgments

The author would like to thank Dr. Boluwatiwi Durojaye for introducing the author to the art of secondary review papers and reviewing the article.

■ References

- Kavanagh, P. L.; Fasipe, T. A.; Wun, T. Sickle Cell Disease: A review. *JAMA*. **2022**, *328* (1), 57-68. DOI: 10.1001/jama.2022.10233
- Tebbi, C. K. Sickle Cell Disease, a Review. *Hemato*. **2022**, *3* (2), 341-366. DOI: 10.3390/hemato3020024
- Xu, J. Z. and Thein, S. L. The carrier state for sickle cell disease is not completely harmless. *Haematologica*. **2019**, *104* (6), 1106-1111. DOI: 10.3324/haematol.2018.206060
- Lubeck, D.; Agodoa, I.; Bhakta, N.; Danese, M.; Pappu, K.; Howard, R.; Gleeson, M.; Halperin, M.; Lanzkron, S. Estimated Life Expectancy and Income of Patients with Sickle Cell Disease Compared with Those Without Sickle Cell Disease. *JAMA Network Open*. **2019**, *2* (11), e1915374. DOI: 10.1001/jamanetworkopen.2019.15374
- Hyacinth, H. I.; Gee, B. E.; Hibbert, J. M. The Role of Nutrition in Sickle Cell Disease. *Nutr. Metab. Insights*. **2010**, *3*, 57-67. DOI: 10.4137/NMI.S5048
- Ohlhorst, S. D.; Russell, R.; Bier, D.; Klurfeld, D. M.; Li, Z.; Mein, J. R.; Milner, J.; Ross, A. C.; Stover, P.; Konopka, E. Nutrition research to affect food and a healthy lifespan. *Adv Nutr*. **2013**, *4*(5), 579-584. DOI: 10.3945/an.113.004176
- Rasel, M. and Mohammad R. Transfusion Iron Overload. In *Stat Pearls [Internet]*, Year 2023 ed.; StatPearls Publishing, 2023. <https://www.ncbi.nlm.nih.gov/books/NBK562146/>
- Emadi-Konjin, P.; Verjee, Z.; Levin, A. V.; Adeli, K. Measurement of intracellular vitamin C levels in human lymphocytes by reverse phase high performance liquid chromatography (HPLC). *Clin Biochem*. **2005**, *38* (5), 450-456. DOI: 10.1016/j.clinbiochem.2005.01.018.
- Hambidge, M. Human zinc deficiency. *J. Nutr*. **2000**, *130* (5S Suppl), 1344S-9S. DOI: 10.1093/jn/130.5.1344S
- Wasnik, R. R. and Akarte, N. R. Evaluation of Serum Zinc and Antioxidant Vitamins in Adolescent Homozygous Sickle Cell Patients in Wardha, District of Central India. *J. Clin. Diagn. Res*. **2017**, *11* (8), BC01-BC03. DOI: 10.786060/JCDR/2017/30855.10320
- Yokokawa, H.; Fukuda, H.; Saita, M.; Miyagami, T.; Takahashi, Y.; Hisaoka, T.; Naito, T. Serum zinc concentrations and characteristics of zinc deficiency/marginal deficiency among Japanese subjects. *J. Gen. Fam. Med*. **2020**, *21* (6), 248-255. DOI: 10.1002/jgf2.377
- Hasanato, R. M. W. Zinc and antioxidant vitamin deficiency in patients with severe sickle cell anemia. *Ann. Saudi. Med*. **2006**, *26* (1), 17-21. DOI: 10.5144/0256-4947.2006.17
- Dougherty, K. A.; Schall, J. I.; Kawchak, D. A.; Green, M. H.; Ohene-Frempong, K.; Zemel, B. S.; Stallings, V. A. No Improvement in suboptimal vitamin A status with a randomized, double-blind, placebo-controlled trial of vitamin A supplementation in children with sickle cell disease. *Am. J. Clin. Nutr*. **2012**, *96* (4), 932-940. DOI: 10.3945/ajcn.112.035725
- World Health Organization-Vitamin A deficiency. <https://www.who.int/data/nutrition/nlis/info/vitamin-a-deficiency>. Accessed on 23rd December 2022
- Rizvi, S.; Raza, S. T.; Ahmed, F.; Ahmad, A.; Abbas, S.; Mahdi, F. The Role of Vitamin E in Human Health and Some Diseases. *Sultan Qaboos Univ. Med. J*. **2014**, *14* (2), e157-e165
- Miyazawa, T.; Burdeos, G. C.; Itaya, M.; Nakagawa, K.; Miyazawa, T. Vitamin E: Regulatory Redox Interactions. *IUBMB Life*. **2019**, *71* (4), 430-441. DOI: 10.1002/iub.2008
- Traber, M. G. Vitamin E inadequacy in humans: causes and consequences. *Adv. Nutr*. **2014**, *5* (5), 503-514. DOI: 10.3945/an.114.006254
- National Institutes of Health-Vitamin A and Carotenoids. <https://ods.od.nih.gov/factsheets/VitaminA-HealthProfessional/>. Accessed on 13th February 2023
- Carr, A. C. and Maggini, S. Vitamin C and Immune Function. *Nutrients*. **2017**, *9* (11), 1211. DOI: 10.3390/nu9111211

20. McCall, S. J.; Clark, A. B.; Luben, R. N.; Wareham, N. J.; Khaw, K. T.; Myint, P. K. Plasma Vitamin C and Functional Health: Results from the European Prospective Investigation into Cancer-Norfolk. *Nutrients*. **2019**, *11* (7), 1552. DOI: 10.3390/nu11071552
21. Rowe, S.; Carr, A. C. Global Vitamin C Status and Prevalence of Deficiency: A Cause for Concern? *Nutrients*. **2020**, *12* (7), 2008. DOI: 10.3390/nu12072008
22. Antwi-Boasiako, C.; Dankwah, G. B.; Aryee, R.; Hayfron-Benjamin, C.; Doku, A.; N'guessan, B. B.; Asiedu-Gyekye, I. J.; Campbell, A. D. Serum Iron Levels and Copper-to-Zinc Ratio in Sickle Cell Disease. *Medicina*. **2019**, *55* (5), 180. DOI: 10.3390/medicina55050180
23. Kennelly, P. J.; Murray, R. K.; Jacob, M. Plasma Proteins and Immunoglobulins. *Harper's Illustrated Biochemistry*, 30th ed.; Cenveo Publisher Services. 2011. <https://accessmedicine.mhmedical.com/content.aspx?bookid=1366§ionid=73247095#1106060414>
24. Royer, A. and Sharman, T. Copper Toxicity. In *StatPearls [Internet]*, Year 2022 ed.; StatPearls Publishing, 2022. <https://www.ncbi.nlm.nih.gov/books/NBK557456/>
25. Lee, H. C.; Chang, S. W. Vitamin D and health - The missing vitamin in humans. *Pediatr. Neonatol.* **2019**, *60* (3), 237-244
26. AlJama, A.; AlKhalifah, M.; Al-Dabbous, I. A.; Alqudaihi, G. Vitamin D deficiency in sickle cell disease patients in the Eastern Province of Saudi Arabia. *Ann. Saudi. Med.* **2018**, *38* (2), 130-136. DOI: 10.5144/0256-4947.2018.130
27. Williams, B. A.; Mayer, C.; McCartney, H.; Devlin, A. M.; Lamers, Y.; Vercauteren, S. M.; Wu, J. K.; Karakochuck, C. D. Detectable Unmetabolized Folic Acid and Elevated Folate Concentrations in Folic Acid-Supplemented Canadian Children With Sickle Cell Disease. *Front. Nutr.* **2021**. DOI: 10.3389/2021/642306
28. Blaszczyk, U.; Duda-Chodak, A. Magnesium: its role in nutrition and carcinogenesis. *Rocz. Panstw. Zakl. Hig.* **2013**, *64* (3), 165-71.
29. Rosanoff, A.; West, C.; Elin, R. J.; Micke, O.; Baniyadi, S.; Barbagallo, M.; Campbell, E.; Cheng, F.; Costello, R. B.; Gamboa-Gomez, C.; Guerrero-Romero, F.; Gletsu-Miller, N.; Ehrlich, B. V.; Iotti, S.; Kahe, K.; Kim, D. J.; Kisters, K.; Kolisek, M.; Kraus, A.; Maier, J. A.; Maj-Zurawska, M.; Merolle, L.; Nechifor, M.; Pourdowlat, G.; Shechter, M.; Song, Y.; Teoh, Y. P.; Touyz, R. M.; Wallace, T. C.; Yokota, K.; Wolf, F. Recommendation on an updated standardization of serum magnesium reference ranges. *Eur. J. Nutr.* **2022**, *61* (7), 3697-3706. DOI: 10.1007/s00394-022-02916-w
30. De Franceschi, L.; Bachir, D.; Galacteros, F.; Tcherna, G.; Cynober, T.; Alper, S.; Platt, O.; Beuzard, Y.; Brugnana, C. Oral magnesium supplements reduce erythrocyte dehydration in patients with sickle cell disease. *J. Clin. Invest.* **1997**, *100* (7), 1847-52. DOI: 10.1172/JCI119713
31. Arnaud, M. J. Update on the assessment of magnesium status. *Br. J. Nutr.* **2008**, *99* (3S Suppl), S24-36. DOI: 10.1017/S000711450800682X
32. Antwi-Boasiako, C.; Kusi-Mensah, Y. A.; Hayfron-Benjamin, C.; Aryee, R.; Dankwah, D. B.; Kwawukume, L. A.; Darkwa, E. O. Total Serum Magnesium Levels and Calcium-To-Magnesium Ratio in Sickle Cell Disease. *Medicina*. **2019**, *55* (9), 547. DOI: 10.3390/medicina55090547
33. Gröber, U.; Schmidt, J.; Kisters, K. Magnesium in Prevention and Therapy. *Nutrients*. **2015**, *7* (9), 8199-226. DOI: 10.3390/nu7095388
34. Naigamwalla, D. Z.; Webb, J. A.; Giger, U. Iron deficiency anemia. *Can. Vet. J.* **2012**, *53*(3), 250-256.
35. Pagana, K. D.; Pagana, T. J.; Pagana, T. N. Mosby's Diagnostic & Laboratory Test Reference, 14th ed.; Elsevier. 2019.
36. Sani, M. A.; Adewuyi, J. O.; Babatunde, A. S.; Olawumi, H. O.; Shittu, R. O. The Iron Status of Sickle Cell Anaemia Patients in Ilorin, North Central Nigeria. *Adv. Hematol.* **2015**. DOI: 10.1155/2015/386451.
37. Lanier, J. B.; Park, J. J.; Callahan, R. C. Anemia in Older Adults. *Am. Fam. Physician.* **2018**, *98* (7), 437-442.
38. Lopez-Sall, P.; Diop, P. A.; Diagne, I.; Cissé, A.; Mahou, C. M. S.; Sylla-Niang, M.; Guéye, P. M.; Diarra, M. Transferrin soluble receptors' contribution to the assessment of iron status in homozygous drepanocytic anemia. *Ann. Biol. Clin. (Paris)*. **2004**, *62* (4), 415-421.
39. Comstock, G. W.; Alberg, A. J.; Helzlsouer, K. J. Reported effects of long-term freezer storage on concentrations of retinol, beta-carotene, and alpha-tocopherol in serum or plasma summarized. *Clin. Chem.* **1993**, *39* (6), 1075-1078.
40. Jargar, J. G.; Hattiwale, S. H.; Das, S.; Dhundasi, S. A.; Das, K. K. A modified simple method for determination of serum α -tocopherol (vitamin E). *J. Basic Clin. Physiol. Pharmacol.* **2012**, *23* (1), 45-48. DOI: 10.3390/ma14133691
41. Olivares, M.; Méndez, M. A.; Astudillo, P. A.; Pizarro, F. Present situation of biomarkers for copper status. *Am. J. Clin. Nutr.* **2008**, *88* (3), 859S-862S. DOI: 10.1093/ajcn/88.3.859S
42. Sizar, O.; Khare, S.; Goyal, A.; Givler, A. Vitamin D Deficiency. In *StatPearls [Internet]*, Year 2022 ed.; StatPearls Publishing, 2022. <https://www.ncbi.nlm.nih.gov/books/NBK532266/>
43. Lieu, P. T.; Heiskala, M.; Peterson, P. A.; Yang, Y. The roles of iron in health and disease. *Mol. Aspects Med.* **2001**, *22* (1-2), 1-87. DOI: 10.1016/s0098-2997(00)00006-6
44. Smith, O. S.; Ajose, O. A.; Adegoke, S. A.; Adegoke, O. A.; Adediji, T. A.; Oderinu, K. A. Plasma level of antioxidants is related to frequency of vaso-occlusive crises in children with sickle cell anemia in steady state in Nigeria. *Pediatric Hematology Oncology Journal*. **2019**, *4* (1) 17-22. DOI: 10.1016/j.phoj.2019.03.003
45. Emokpae, M. A. and Fatimehin, E. B. Copper-To-Zinc Ratio as an Inflammatory Marker in Patients with Sickle Cell Disease. *Sci.* **2020**, *2* (4), 89. DOI: 10.3390/sci2040089
46. Tsang, B.; Sandalinas, F.; De-Regil, L. M.; Folate supplementation in women of reproductive age. *Cochrane Database Syst Rev.* **2015**, *2015* (6), CD011766. DOI: 10.1002/14651858.CD011766
47. Bermejo, F. and García-López, S. A guide to diagnosis of iron deficiency and iron deficiency anemia in digestive diseases. *World J Gastroenterol.* **2009**, *15* (37), 4638-4643. DOI: 10.3748/wjg.15.4638
48. Oustamanolakis, P.; Koutroubakis, I. E.; Messaritakis, I.; Niniraki, M.; Kouroumalis, E. A. Soluble transferrin receptor-ferritin index in the evaluation of anemia in inflammatory bowel disease: a case-control study. *Ann. Gastroenterol.* **2011**, *24* (2), 108-114.
49. Alhillawi, Z. H.; Al-Hakeim, H. K.; Moustafa, S. R.; Maes, M. Increased zinc and albumin but lowered copper in children with transfusion-dependent thalassemia. *J Trace Elem Med Biol.* **2021**. DOI: 10.1016/j.jtemb.2021.126713
50. Ho, C. H. The effects of blood transfusion on serum ferritin, folic acid, and cobalamin levels. *Transfusion.* **1992**, *32* (8), 764-765. DOI: 10.1046/j.1537-2995.1992.32893032107.x.
51. Zhang, X.; Li, Y.; Gobbo, L. C. D.; Rosanoff, A.; Wang, J.; Zhang, W.; Song, Y. Effects of Magnesium Supplementation on Blood Pressure: A Meta-Analysis of Randomized Double-Blind Placebo-Controlled Trials. *Hypertension.* **2016**, *68* (2), 324-333. DOI: 10.1161/HYPERTENSIONAHA.116.07664.

■ Author

The author, Minjoon Hur, is a high schooler at Raffles Christian School in Indonesia passionate about nutrition science and biomedical sciences. He hopes to become a pharmaceutical researcher or a nutritionist and plans to conduct quantitative primary research in the near future.

The Effect of Autoinducer Analogs on the Quorum Sensing Systems of *E. coli* K12

Sai Ashutosh Chellarapu, Eswar Pondugula

Rock Ridge High School, 43460 Loudoun Reserve Dr, Ashburn, VA 20148, USA; saishutosh.c@gmail.com

Mentor: Dylan Cashman

ABSTRACT: Virulent *E. coli* in clinic settings causes UTIs, meningitis, among others. Novel drugs to combat these bacteria are developed, but a resistant strain will inevitably arise. Therefore, a non-antibiotic approach using autoinducer analogs (AIAs) was taken to inhibit the biofilms of *E. coli* K12. The effects of the AIAs N-Acetylglucosamine and S-(5'-Adenosyl)-L-homocysteine on the LuxI/LuxR and LuxS quorum sensing systems of *E. coli* K12 were studied to determine which quorum sensing system of *E. coli* K12 is most susceptible to inhibition. This experiment measured the reduction of biofilm formation of *E. coli* K12 using AIAs on the strain's quorum sensing systems: LuxI/LuxR and LuxS. *E. coli* K12 had a 10-sample control group along with a 10-sample AIA group for each AIA. The biofilm counts were recorded for all three groups in 24-hour intervals. The LuxI/LuxR group resulted in the greatest biofilm inhibition meaning the LuxI/LuxR quorum sensing system of *E. coli* is most susceptible to inhibition. This non-antibiotic approach for inhibition will save millions of dollars for pharmaceutical companies that are spent on developing antibiotics to combat multidrug-resistant bacteria.

KEYWORDS: Biochemistry; General Biochemistry; Autoinducer Analogs; *E. coli*; Quorum Sensing.

■ Background

A study done by Microbiologists in Japan was on the effects of autoinducer analogs on both the free-floating (planktonic) and concentrated (biofilms) cells of *Pseudomonas aeruginosa*. This gram-negative bacterium can cause serious illnesses such as cystic fibrosis.¹ In general, bacteria can be divided into two types: gram-positive and gram-negative. The key difference between both types of bacteria is that gram-positive bacteria have a thicker layer of peptidoglycan than gram-negative bacteria in the extracellular matrix area. Regardless, both types of bacteria use the process of quorum sensing to form biofilms, which cause infections. A biofilm is an aggregation of bacteria with a slimy layer of proteins that covers the bacteria. Using quorum sensing, bacteria release autoinducers: ligands that bind to specific receptors with similar signaling pathways. Thus, these ligands act as indicators that alert the bacteria to move to a common location forming adhesive clumps known as biofilms.² Biofilms are multi-drug resistant from garnering many bacterial strains effective against antibiotics, especially in clinical settings. Novel antibiotics are similar to pre-existing ones in terms of chemical composition, thereby allowing biofilms to continue their resistance. Additionally, antibiotics are developed at a slow rate because of the US Food and Drug Administration's limited approvals contributing to the quick adaptability of biofilms.

A possible solution to stop the formation of biofilms is to stop the autoinducer ligands from binding to the receptors. Thus, autoinducer analogs are competitive inhibitors that prevent the binding of autoinducers to the receptors and help stop the aggregation of bacteria. The researchers purchased two autoinducers (AIA-1 and AIA-2) analogs from Meiji

Seika Pharmaceuticals and two antibiotics called azithromycin (AZM) and clarithromycin (CLR). The control group *P. aeruginosa* was grown without antibiotics. They used the killing assay to determine the biofilm cells after using AIA-1 plus various concentrations of AZM, CLR, and AIA-2 plus multiple concentrations of AZM and CLR. The results were that there was at least 100 times less formation of biofilms for both antibiotics. For AZM, specifically, on the highest dosage of 256 micrograms/milliliter, there was at least 100,000 times less biofilm formation.

According to a study on QS and biofilms, the three general classes of signaling pathways for the gram-positive and gram-negative bacteria are defined: LuxI/LuxR, Oligopeptide-two-computing-type, and LuxS.³ Each of these signaling pathways has its own autoinducer for which respective autoinducer analogs can be used to inhibit the signaling pathways, thereby ceasing biofilm formation. Usually, the bacteria have at least two of the three signaling pathways.⁴

From our background research, discovering which signaling pathways of critical multi-drug resistant bacteria such as *E. coli* are most susceptible to autoinducer analogs would help identify which signaling pathways are most relevant for biofilm inhibition and paving future research in a methodical manner. A Time Kill Assay would be used to measure the reduction of biofilm formation over time with and without the addition of AIAs respective to *E. coli*'s quorum sensing systems of LuxI/LuxR and LuxS. Furthermore, the Time Kill Assay is adept at only measuring biofilm inhibition and not the killing of bacteria as biofilms exposed to AIAs may exist in a planktonic state where they are separated from biofilms and alive partially but not visible in the field view, making such bacteria untraceable and unethical to count.⁵ The experiment is feasible as all mate

rials are within reach for a low price. Additionally, the studies formerly stated are thorough and provide a solid foundation for the experiment.

Methods

An inoculation loop was heated using a Bunsen burner until it was hot red for sterilization and was left alone for a 5-minute cooldown. *E. coli* K12 from its growth medium was transferred to 10 Petri dishes and cultured using the 4-quadrant streaking method in a fume hood, also where all Petri dishes were stored and monitored for biofilm formation. The average number of visible biofilms (Table 1) was calculated from the control groups after 24, 48, and 72 hours. Experimental Petri dishes were prepared for *E. coli* K12's (LuxI/LuxR and LuxS) quorum sensing systems with the autoinducer analogs for *E. coli* K12's (N-Acetylglucosamine and S-(5'-Adenosyl)-L-homocysteine) quorum sensing systems. A precision scale was used to weigh 1000x Minimum Inhibitory Concentration (MIC) for each AIA (Figure 1), which was the most precise level of AIA, in grams, obtainable. MIC values were obtained from IC values initially (maximal inhibitory concentration). The IC100 (100% of maximal inhibition) for LuxS and IC50 (50% of maximal inhibition) values for LuxI/LuxR were converted to MIC values. The measured amounts were diluted by 1mL of DI water for the concentrations of 1.8 mM and 0.5 mM for LuxI/LuxR and LuxS groups. Each AIA solution was transferred using sterile pipettes to their respective groups on the 3rd and 4th quadrants of the Petri dishes, as that is the area of bacterial growth. The number of isolated colonies formed for both autoinducer analog groups of *E. coli* K12 were averaged after 24, 48, and 72 hours. The averaged biofilm counts of the autoinducer analog groups for *E. coli* K12 were compared to each other and their control using an ANOVA test and Tukey's HSD to identify the significance of the results. In addition, a Time Kill Assay was generated to determine which quorum sensing system was most susceptible to inhibition.

Results

Table 1: The table shows the recorded number of biofilms for each group (Control, LuxS, and LuxI/LuxR) for all ten samples of each group over 24-hour intervals (0, 24, 48, and 72 hours). LuxI/LuxR showed the lowest number of biofilms or the greatest susceptibility.

Sample #	Number of Biofilms by Group								
	Control			LuxS			LuxI/LuxR		
	24 hrs	48 hrs	72 hrs	24 hrs	48 hrs	72 hrs	24 hrs	48 hrs	72 hrs
1	0	105	297	0	300	450	0	5	180
2	0	237	435	0	70	220	0	35	250
3	0	138	415	0	150	350	0	120	150
4	0	300	595	0	200	396	0	15	250
5	0	204	600	0	147	358	0	19	50
6	0	196	572	0	133	305	0	57	80
7	0	203	543	0	62	172	0	69	130
8	0	300	589	0	119	208	0	19	260
9	0	99	225	0	118	210	0	14	200
10	0	23	189	0	48	90	0	16	80

Table 2: The table shows an ANOVA test for the three groups: Control, LuxS, and LuxI/LuxR. The null hypothesis is rejected, and the result is a p-value of less than 0.05, indicating the statistical significance of the data.

	Groups			Total
	Control (T1)	LuxS (T2)	LuxI/LuxR (T3)	
N	20	20	20	60
ΣX	6225	4106	1999	12330
Mean	311.25	205.3	99.95	205.5
ΣX ²	2610473	1107384	344759	4062616
Std.Dev.	188.1967	117.9702	87.3465	160.9717
f-ratio	11.75677			
p-value	0.000053			

Table 3: The table shows Tukey's HSD, which identified the significance of every pair in this study. As indicated in blue, the p values are less than 0.05 for the possible combinations of Control (T1), LuxS (T2), and LuxI/LuxR (T3) groups.

Pairwise Comparisons		HSD _{.05} = 104.8609 HSD _{.01} = 132.2162	Q _{.05} = 3.4032 Q _{.01} = 4.2910
T ₁ :T ₂	M ₁ = 311.25 M ₂ = 205.30	105.95	Q = 3.44 (p = .04714)
T ₁ :T ₃	M ₁ = 311.25 M ₃ = 99.95	211.30	Q = 6.86 (p = .00003)
T ₂ :T ₃	M ₂ = 205.30 M ₃ = 99.95	105.35	Q = 3.42 (p = .04870)

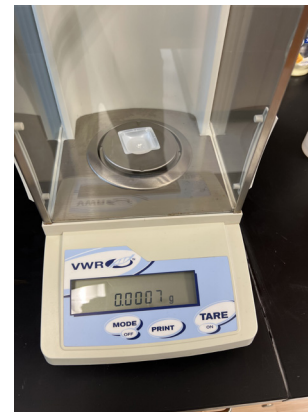


Figure 1: 1000x MIC of LuxS was 0.0007g which was weighed using the shown VWR precision scale.

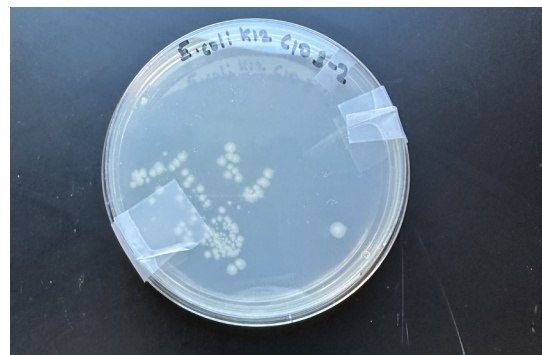


Figure 2: Sample #10 of Control after 72 hrs. of incubation.

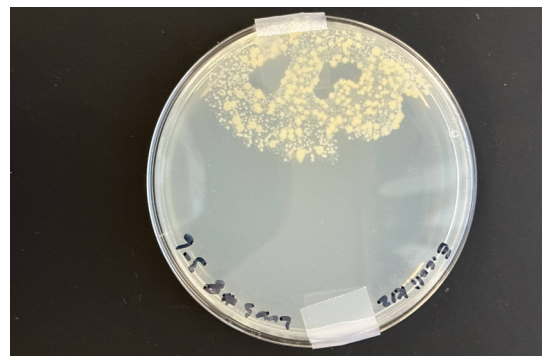


Figure 3: Sample #8 of LuxS after 72 hrs. of incubation.

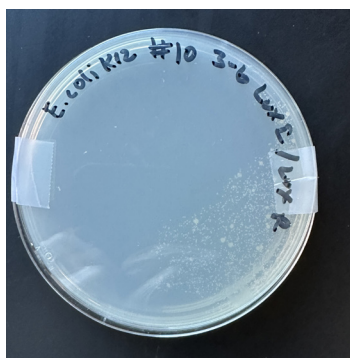


Figure 4: Sample #10 of LuxI/LuxR after 72 hrs. of incubation.

Average Biofilm Count for 0, 24, 48, and 72 hrs for Control, Lux S, and Lux I/Lux R Quorum Sensing Systems of *E. coli* K12

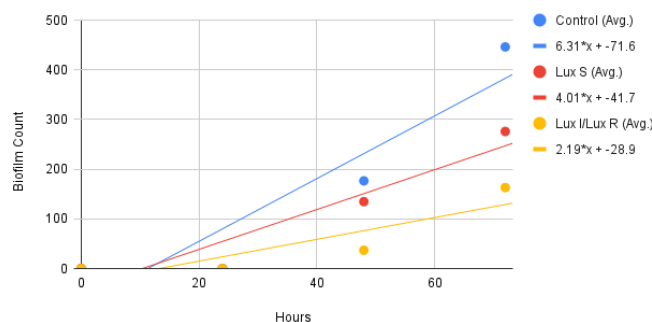


Figure 5: The Time Kill Assay of *E. coli* K12 biofilm count over 24-hour intervals (0, 24, 48, and 72) of the average number of biofilms for the groups of control, LuxS, and LuxI/LuxR shows that the LuxI/LuxR quorum sensing system is more susceptible to inhibition than the LuxS quorum sensing system of *E. coli* K12.

■ Results and Discussion

Data Significance Validation:

To understand if our results are significant, we conducted an ANOVA test for which we received a p-value of 0.000053, as shown in Table 1, which is significant when p is less than 0.05. To further verify the significance of our results, we conducted Tukey's HSD, shown in Table 2, which compared all possible combinations of pairs of the three groups. The result was once again p values of less than 0.05 which are shown to the immediate right of the Q values in blue. Once again, our data has shown to be statistically significant at p less than 0.05.

Data Interpretation:

As our results were significant, we interpreted our data by generating a Time Kill Assay (Figure 5), which shows the averages of the biofilm counts of all ten samples for each group in 24-hour intervals along with their lines of best-fit or trendlines. The number of biofilms was not referred to as CFUs as we did not count for the number of cells in total but instead for the number of isolated colonies. Once again, it is important to note that the Time Kill Assay measures biofilm inhibition rather than the killing of bacteria. Furthermore, the counted number of biofilms is equivalent to the number of isolated colonies visible in the 3rd and 4th quadrants of the Petri dishes. Distinctive biofilm - multiple isolated colonies - growth in the 1st and 2nd quadrants of the Petri dishes would lead to discarding the Petri dishes. As shown in Figure 5, the overall virulence of *E. coli* has decreased as the biofilm concentration

has seen inhibition which can be seen as the trendlines for both the LuxS and LuxI/LuxR groups are significantly lower than the control group's trendline.

Initially, when deciding between spread plating, a common technique used to measure antibiotic effectiveness, and 4-quadrant streaking for proper biofilm yield, we concluded with 4-quadrant streaking because we considered not only the distribution of the bacteria but also the distribution of the compound. spread plating considers antibiotic effectiveness based on the diameter of the zone of inhibition. As AIAs are not like commonly tested antibiotics, there is no existing research on pre-established diameters for zones of inhibition. Additionally, the AIA solutions would not fully dissolve after dilution, so it would have been difficult to disperse the undissolved compounds evenly across a Petri dish as done in spread plating. In contrast, the spreading is limited to only the 3rd and 4th quadrants in 4-quadrant streaking, which was our method of biofilm growth. From this experiment, we identified the quorum sensing system of *E. coli* that is most susceptible to inhibition: LuxI/LuxR. This result can be observed in the Time Kill Assay (Figure 5) as the trendline for the biofilm count for the LuxI/LuxR group has the lowest slope meaning that it was the group with the greatest amount of inhibition.

Potential Errors and Growth:

Our experiment may have been prone to potential errors. First, some biofilms were not separate but rather one big chunk of overlapping biofilms, making it difficult to separate for some. For instance, one chunk may have been three biofilms combined as one but could have been considered 2 or 4 biofilms in the counting process, which is not the most accurate.

Another error would be the cooling time of the inoculation loops. The 5-minute cooling period for the 4-quadrant streaking method was used for the control group. Still, the cooling period was shortened to approximately 3 to 4 minutes for the experimental groups to increase work efficiency. This may have resulted in some bacteria not being killed by the heat, meaning there could have been a greater parent population size for the experimental groups relative to that of the control group.

Additionally, we can observe from Figures 2, 3, and 4 that the biofilms of the LuxI/LuxR sample are smaller than those of the control and LuxS samples, which showed that the partial inhibition of quorum sensing from inhibiting one of the two quorum sensing systems led to the breakdown of more extensive biofilms to smaller biofilms some of which may not have been visible to the naked eye. As the visible larger biofilms were counted, the smaller biofilms were not, which could be made more accurate using microscopy techniques in the future. Although our data were statistically significant, future studies should have more data samples, high-end microscopy techniques, and tests for a larger representation and greater accuracy in counting biofilms to answer the research question better.

■ Conclusion

Previous research not only for *E. coli* but also for infectious bacteria has tested the efficacy of certain antibiotics of the popular *Pseudomonas aeruginosa* model.¹ The lack of research in clinical bacteria such as *E. coli* prompted us to identify autoin-

ducer analogs that would inhibit the growth of *E. coli*. Additionally, there needed to be more research on identifying the sensitivity of the quorum sensing systems to inhibitors. As we were looking forward to researching non-antibiotic methods of inhibiting biofilm growth, we decided to conduct this specific experiment to discover the quorum sensing system of *E. coli* most susceptible to inhibiting biofilm growth.

Our experiment showed that inhibiting the LuxI/LuxR system led to the greatest decrease in biofilm count. As the autoinducer analogs were specific inhibitors of their quorum sensing pathways, we concluded that the LuxI/LuxR pathway is more susceptible to inhibition than the LuxS pathway.

This experiment is crucial for pharmaceutical companies developing antibiotics to inhibit biofilm growth. Our experiment solidifies the concept that autoinducer analogs may be the future of non-antibiotic approaches to inhibition of *E. coli* and such bacteria, thereby saving millions of dollars in the drug development process. Identification of the LuxI/LuxR quorum sensing system as more susceptible to inhibition than the LuxS quorum sensing system forecasts for the development of compounds targeted towards the LuxI/LuxR quorum sensing system for greater efficacy against *E. coli*, thereby lowering nosocomial infections and encouraging similar research for other infectious bacteria.

■ Acknowledgments

We thank the Rock Ridge High School Science Dept., especially Mr. Dylan Cashman, Dr. Mithra Marcus, and Ms. Madina Mamatova, for their guidance. We also thank the Joanne Nagurny Memorial Fund for recognizing our work at the Loudoun County Public Schools Regional Science and Engineering Fair. Furthermore, we thank Dr. Stephen Burton of George Mason University for providing us this research opportunity.

■ References

1. Li, Y.-H., & Tian, X. (2012). Quorum sensing and bacterial social interactions in biofilms. *Sensors*, *12*(3), 2519–2538. <https://doi.org/10.3390/s120302519>
2. Guo, M., Gamby, S., Zheng, Y., & Sintim, H. (2013). Small molecule inhibitors of AI-2 signaling in bacteria: State-of-the-art and future perspectives for Anti-Quorum Sensing Agents. *International Journal of Molecular Sciences*, *14*(9), 17694–17728. <https://doi.org/10.3390/ijms140917694>
3. Antunes, L. C., Ferreira, R. B., Buckner, M. M., & Finlay, B. B. (2010). Quorum sensing in bacterial virulence. *Microbiology*, *156*(8), 2271–2282. <https://doi.org/10.1099/mic.0.038794-0>
4. Wang, S., F., Payne, G., & E. Bentley, W. (2019). Repurposing *E. coli* by engineering quorum sensing and Redox Genetic Circuits. *Gene Expression and Control*. <https://doi.org/10.5772/intechopen.81245>
5. Abe, M., Murakami, K., Hiroshima, Y., Amoh, T., Sebe, M., Katakami, K., & Fujii, H. (2021). Autoinducer analogs can provide bactericidal activity to macrolides in *Pseudomonas aeruginosa* through antibiotic tolerance reduction. *Antibiotics*, *11*(1), 10. <https://doi.org/10.3390/antibiotics11010010>

■ Authors

Sai Ashutosh Chellarapu is a senior at Rock Ridge High School. He is a USABO Semifinalist, DECA ICDC Qualifier, and EMT, and he co-founded a charity organization known

as HeartSaver for CPR education. With a passion for applying theoretical knowledge to lab work, he hopes to pursue medicine as a career pathway.

Eswar Pondugula is a senior at Rock Ridge High School. He is a 2-time DECA ICDC Qualifier, plays volleyball at the national level, and participates in varsity lacrosse. In his free time, he works on his personal business venture.

Using Biomimetics to Mimic Bamboo to Create a More Robust and More Durable Material

Sean Jung

Punahou School, 1601 Punahou St, Honolulu, HI 96822, USA; seanminjung@gmail.com

Mentor: Dr. Jong Seol Jeong

ABSTRACT: Through biomimetics, numerous contraptions and inventions inspired by nature and its processes have revolutionized the world. A quick pan around any room will reveal an abundance of cylindrical tubes or rods. Whether it is used in construction equipment or holding up large, heavy structures, the sheer quantity of the cylindrical tube begs for improvement. Nature's cylindrical tube is the bamboo plant. Bamboo plants are durable and have extreme structural and tensile strength. The source of the bamboo's strength is a diaphragm or node. Three specimen types with varying frequencies and numbers of diaphragms were synthesized and tested. We hypothesize that placing "diaphragms" in tubes would increase the structural strength of the tube as a whole. We also hypothesize that more diaphragms would increase overall structural strength. Experiment results are consistent with the hypothesis. There is a drastic difference in tensile and compressive strength between a tube with no diaphragm and one with one. However, interestingly, adding more diagrams only increases the structural strength marginally. It is likely that, like the bamboo plant, the perfect ratio of diaphragms is the strongest the tube could ever be.

KEYWORDS: Materials Science; Biomimicry; Biomimetics; Bamboo; Diaphragm.

■ Introduction

Since the dawn of human civilization, humans have been constructing marvelous inventions and contraptions that have benefited our species dramatically. Though we may credit Leonardo DaVinci or Thomas Edison as the greatest inventors of all time, mother nature is the most significant inventor.^{1,2} While we may have gone from the wheel to the Metaverse in a couple of thousand years,³ nature has constantly evolved for billions of years. While humanity was in its infancy, nature had built up billions of years of research and development that natural selection coaxed out.^{4,5} This means scientists can look back into nature to determine how we could copy and use it to our advantage. We call this concept *biomimetics*.^{6,7}

According to the Oxford Dictionary, biomimicry is the design and production of materials, structures, and systems mimicking biological entities and processes. Though we may not realize it, countless crucial inventions that improve our lives daily are the outcome of what nature inspires.⁸ During the 1990s in Japan, Japanese scientists and engineers were looking to make their trains faster and more efficient. As it turned out, speed came with one main problem: sound.⁹ A deafening sonic boom was heard throughout the surrounding areas when the trains exited tunnels at high speeds.¹⁰⁻¹² Puzzled, one of the Japanese scientists looked to nature to find the key. As the story goes, while observing the Kingfisher bird hunt for fish in the lake, the Japanese scientist was hit with a realization.¹³ As he observed, the Kingfisher bird could enter the water with little sound not to scare its prey away. After several experiments, the scientist found that the beak of the Kingfisher bird allowed it

to break the water's surface with minimal resistance. By applying the design of the Kingfisher bird's beak onto a train, the Japanese scientists found that the noise was drastically lower.¹⁴ To this day, the bullet train glides at speeds up to 320 km/hour (Figure 1).¹⁵

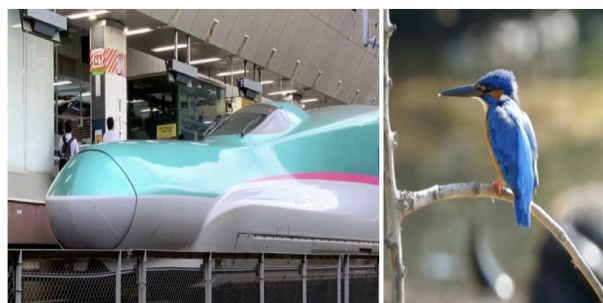


Figure 1: Using biomimicry in building and developing Japan's famous bullet train.

Furthermore, in the case of military aircraft, speed is also an essential factor. Though the Wright Brothers have been up in the air hundreds of years ago, nature has been creating aircraft of its own.¹⁶ The B-2 Stealth Bomber is a military aircraft that mimics the world's fastest animal on earth: the Peregrine Falcon.¹⁷ Similarities are apparent when comparing the B-2 Stealth Bomber and the Peregrine Falcon side-by-side comparison. The Stealth Bomber has a similar "head" shaped portion near the cockpit, while its wings mirror those of a fully extended Peregrine Falcon (Figure 2).¹⁸

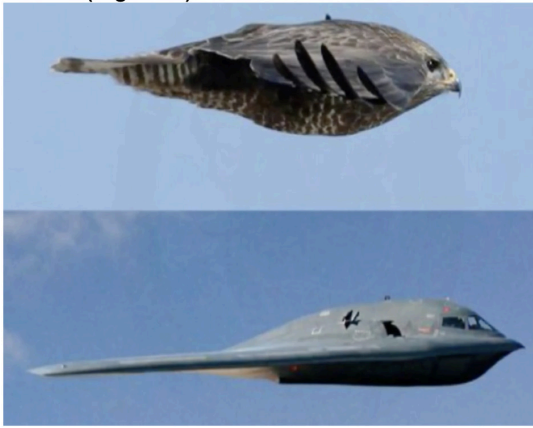


Figure 2: The United States military developed the Northrop Grumman B-2 Spirit, or the Stealth Bomber, to mimic the fastest animal in the world: the Peregrine Falcon.

Every day scientists search for new and inventive ways to incorporate biomimicry into our lives.^{19,20} Like any inventor will say, however, the first step in solving a problem is identifying that there is one in the first place. A quick scan around any room will reveal that rods or bars are a big part of our daily lives. Whether the bars holding up a table or the rods holding up construction workers, cylindrical shapes are a crucial part of daily living.^{21,22} With such an essential role in our lives, it is evident that the safety of these bars is also necessary. We professionally describe this bar shape as a cylindrical rod. When manufacturing equipment, structural integrity is crucial.²³ This is especially true in scenarios where the health and safety of people are at stake.^{24,25} With this in mind, the question is how the cylindrical rod could be improved in terms of structural strength to benefit us.

The bamboo plant is the most remarkable example of a cylindrical rod in nature. During the end of the second world war, the United States had created a bomb so powerful that they believed it could end the war that had claimed millions of lives.²⁶ Pushing closer and closer to the mainland of Japan, the United States military did not find evidence that the Japanese were slowing down.²⁷ With the permission of President Harry S. Truman, the U.S. detonated two atomic bombs on Hiroshima and Nagasaki.^{28,29} Though every free-standing structure was obliterated, bamboo groves stood proud and tall. Even through immense stress and pressure, the bamboo plant withstood it all, which is no surprise, as bamboo is flexible.³⁰ It possesses an outer surface that is strong and dense, but as you go in, the density gets lower but stays durable and enduring.³¹ This is why it bends well and absorbs external force. Bamboo is highly elastic and has a higher tensile strength than some alloys.³² Bamboo has higher compressive strength than many mixtures of concrete. For this very reason, people use bamboo to assist construction workers in many countries in Asia, primarily Southeast Asia.^{33,34}

With this data in mind, using biomimicry, bamboo's structural strength could be synthesized and applied to modern science to create stronger, more durable materials. Bamboo gets its unique strength from the "nodes" placed intricately

throughout its internal structure. These nodes are disc-shaped. Scientists call these "diaphragms" (Figure 3).

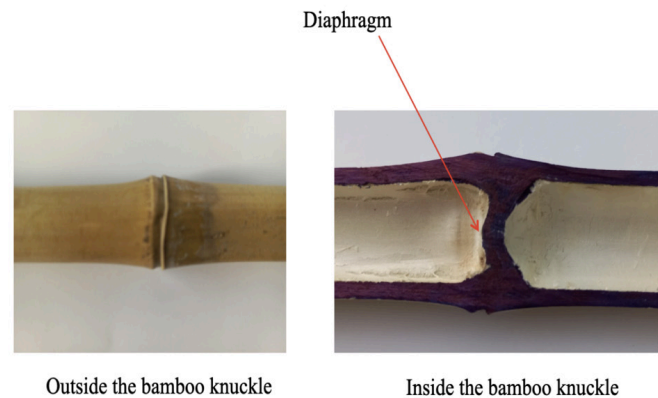


Figure 3: Bamboo's external surface is hard and durable. On the outside of the bamboo, there is a "knuckle." This knuckle bears a striking resemblance to the human knuckle. On the internal surface of the bamboo, there is a disc called the "diaphragm." This diaphragm is a circular node located on the inner surface of the bamboo.

Based on the previous research,³⁵⁻³⁷ this study examined whether placing "diaphragms" in tubes would increase the structural strength of the tube as a whole. With cylindrical shapes so prevalent in our lives, this study contributes to the research and development of everything, which includes rods and tubes. From construction equipment to pull-up bars to NASA spacecraft,³⁸ the structural integrity of such objects is crucial to the safety of everyone around and using them. Furthermore, we can save money and resources by making rods more structurally strong without making solid rods, which can lead to environmental and economic benefits.³⁹

Research Question and Hypothesis:

The research question asked is: "How could the structural strength of a bar be improved by synthesizing the biomimicry of bamboo?" We hypothesize that placing "diaphragms" in tubes would increase the structural strength of the tube.^{40,41} It was further hypothesized that more diaphragms would increase overall structural strength. More specifically, a tube with three diaphragms would be more structurally stable than a tube with one diaphragm and a tube without any diaphragm. Furthermore, by the same logic, the tube with one diaphragm would be more robust than a tube without any diaphragm.

Methods

Study Sites:

We collected data from the experiment performed at the Seoul National University of Science and Technology research laboratory. We chose this location due to its access to the INSTRON tensile, compression, fatigue, impact, rheology, and structural testing machine (Figure 4).



Figure 4: The INSTRON 4467 machine performing the three-point bending test.

Experimental Design:

Using the INSTRON tensile, compression, fatigue, impact, rheology, and structural testing machine, a "three-point bending test" was performed.^{42,43} The "three-point bending test" is designed to test the structural strength of a given specimen. As two pillars held up the specimen, a third pillar was lowered into the middle, adding weight to the tube until it fractured. We refer to the two pillars that held up the specimen as "supporting anvils" and refer to the third as the "load anvil" (Figures 5 and 6). Using the "three-point bending test," both compressive and tensile stresses were measured. As the INSTRON 4467 loaded on weight via the "load anvil," the structural strength was recorded and collected (Figure 5).

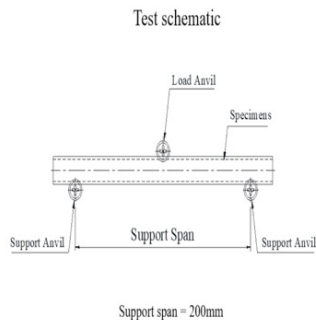


Figure 5: Inner workings of the three-point bending test.⁴⁴

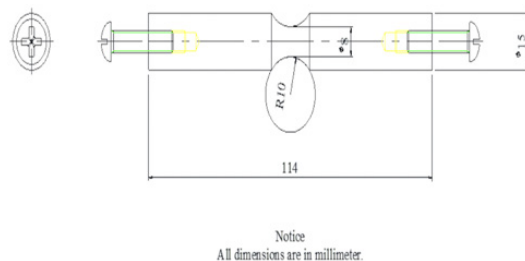


Figure 6: The load and support anvils of the INSTRON 4467 Tensile Testing machine are identical and contain a 'divot' in the center where we locate the specimen. The 'divot' is made for the specimen to fit precisely for the three-point bending test.

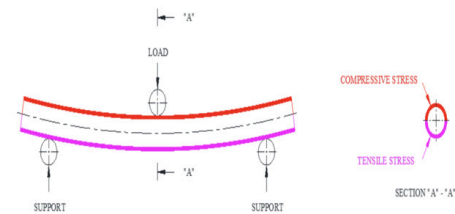
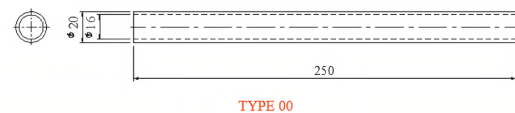


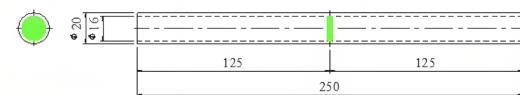
Figure 7: The three-point bending test shows two types of stress on the specimen. On the lower side of the specimen, tensile stress (σ_{bt}) occurs, while compressive stress (σ_{bc}) occurs on the upper side. Tensile stress is the stress that causes the length of the specimen to increase, while compressive stress is the stress that causes the length of the specimen to decrease.⁴⁵

Three types of specimens were developed and tested. We made the body of each specimen out of a standard clear, plastic, acrylic pipe (PMMA, Poly methyl methacrylate). We used the same material to construct the diaphragms inside each specimen. The three types of specimens vary in frequency and distance of diaphragms - Type 00, Type B1, and Type B3. While Type 00 is just a pipe with no diaphragm, Type B1 and B3 contain one and three diaphragms, respectively. All pipes are 250 mm in length and 20 mm in diameter. The internal diameter of the pipes is 16 mm across. Type 00 is an empty acrylic pipe 250 mm long (Figure 8). In Type B1, one singular diaphragm in the center equidistant from the sides is located precisely in the middle or 125 mm from each edge (Figure 9). In Type B3, there are three diaphragms. One is directly in the center, and two are 100 mm from the center (Figure 10). Each diaphragm is 16 mm in height and 8 mm in length (Figure 11). To reduce the effect of measurement errors on experiment results, we made five specimens for each type, thus, 15 specimens.



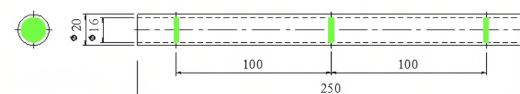
TYPE 00

Figure 8: Type 00 specimen design consists of an empty acrylic plastic tube with no diaphragm. It is 250 mm in length and 20 mm in diameter. The internal diameter of the pipe is 16 mm across.



TYPE B1

Figure 9: Type B1 specimen design consists of an acrylic plastic tube with one diaphragm. One singular diaphragm in the center equidistant from the sides is located precisely in the middle or 125 mm from each edge. It is 250 mm in total length and 20 mm in diameter. The internal diameter of the pipe is 16 mm across.



TYPE B3

Figure 10: Type B3 specimen design consists of an acrylic plastic tube with one diaphragms. One is directly in the center, and two are 100 mm from the center. It is 250 mm in total length and 20 mm in diameter. The internal diameter of the pipe is 16 mm across.

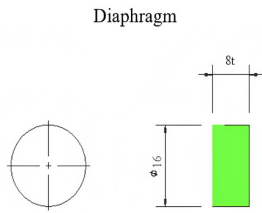


Figure 11: Each diaphragm is 16 mm in height and 8 mm in length.

We collected data from the testing device INSTRON 4467 (3 tons) at pressure speeds of 2 mm per minute. The support span of the INSTRON 4467 is 200 mm. The lab's temperature at the time of testing was 27~29°C (80.6~84.2°F), with a lab humidity of 62~64%.

Results and Discussion

Results:

As mentioned, five specimens were made for each type – TYPE 00, TYPE B1, and TYPE B3 to reduce measurement errors in experimental results. Since we inserted one diaphragm for TYPE B1 and three diaphragms for TYPE B3, specimens for TYPE B1 and TYPE B3 are heavier than those for TYPE00. We report these results in Table 2 below (column entitled 'weight of tube').

The INSTRON 4467 machine produced data on the maximum force endured by each specimen in both kg (kilograms) and N (newtons). We calculated the maximum tensile and compressive stress values to test hypotheses using this data. From the point where the load anvil touches each specimen, we could identify each specimen's maximum compressive and tensile stress points. The side of the load anvil is called the maximum compressive stress point, and the opposite side is called the maximum tensile stress point (in Figure 12).

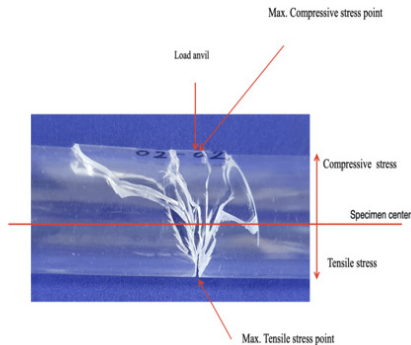


Figure 12: The fracture point on the lower side of the specimen is called the maximum tensile stress point. The point where the load anvil weighs on the specimen is called the maximum compressive stress point.

The values for maximum bending moment, M_{max} , were first needed to get the values of these stresses. To calculate M_{max} , the following equation is used (in Figure 13).⁴⁵ We computed the maximum bending moment, M_{max} , by multiplying the distance between the support anvil and the center of the specimen (i.e., the half of the support span), or $L/2$, and load, the pressure of load anvil (P). Since each half of the specimen experiences half of the load ($= P/2$), $M_{max} = P/2 * L/2 = P * L / 4$. The bottom panel of Figure 13 graphically shows how P and L are defined.

$$M_{max} = \frac{P * L}{4}$$

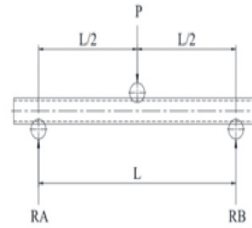


Figure 13: Equation to calculate maximum bending moment, M_{max} ⁴⁵.

$$\sigma_{bt}, \sigma_{bc} = \frac{M_{max} * y}{I_x}$$

$$I = \frac{\pi}{64} (d_o^4 - d_i^4)$$

where d_o = specimen outside diameter and d_i = specimen inside diameter

Figure 14: We show the equation to calculate the maximum tensile and compressive stresses on the top.⁴⁹ While both maximum tensile (σ_{bt}) and compressive stresses (σ_{bc}) have the same magnitude, their signs are opposite - the maximum tensile stress (σ_{bt}) has a positive value; and the compressive stress (σ_{bc}) has a negative value. Finally, we show the formula to calculate the moment of inertia (I_x) used in computing maximum tensile and compressive stresses on the bottom.

Then, as shown in Figure 14, both maximum tensile and compressive stresses are computed by multiplying the maximum bending moment (M_{max}) and the coordinate from the center of the specimen (y) divided by the moment of inertia (I_x). Since all specimens are identical in length and location in the testing machine, by experimental design, y should be the same for all types of specimens. While the value of I_x should be different theoretically for each type due to the existence and frequency of diaphragms, the difference in I_x between types is statistically insignificant in this experiment, potentially due to the nature of the material for specimens (i.e., plastic). In addition, the difference is too small to be detected by the testing machine. Thus, we assume that those values are the same for all types. Therefore, according to the equation below, since the coordinate from the center of the specimen (y) and the moment of inertia (I_x) remain the same for all the types, as the maximum bending moment (M_{max}), the numerator of the equation increases, the maximum tensile (σ_{bt}) and compressive stresses (σ_{bc}) increase.

Figure 14 shows how to calculate the moment of inertia (I_x) based on the formula.⁴⁵ As explained, the outside diameter of the specimen is 20mm, and the inside diameter of the specimen is 16mm. Pi is simplified to be 3.14. Plugging these numbers in the equation, the value of inertia (I_x) is 4,636.91 throughout all specimens in the experiment. We used this value when calculating the maximum tensile (σ_{bt}) and compressive stresses (σ_{bc}).

Table 1 below shows how to calculate the maximum bending moment and maximum tensile and compressive stresses based on results obtained from the experiment for the TYPE 00 - specimen without a diaphragm. For the value, P , also known as the maximum load, the average maximum load of all five Type 00 specimens is used in the units Newton (= the absolute unit

of force in the International System of Units), which is 683.2 L (= support span), y (= the coordinate from the center of the specimen), and I_x (= the moment of inertia), remain the same for all the types. In this example, we plugged 200.0 for L, 10.0 for y, and 4,636.9 for I_x , respectively, in the equations to compute the maximum bending moment and maximum tensile and compressive stresses. After computations, 34,160.0 N.mm and 73.7 MPa were obtained for maximum bending moment and maximum tensile and compressive stresses, respectively, for Type 00 (specimen without a diaphragm).

Table 1: Example calculating maximum bending moment and maximum tensile and compressive stresses for TYPE 00.

1. Design Data	
1) Load	P = 660.0 N = 67.4 kg
2) Support Span	L = 200.0 mm
3) Tensile Strength of PMMA	σ_{max} = 71.0 MPa = 723.9 kg/cm ²
4) Specimens Out Dia.	D = 20.0 mm
5) Specimens In Dia.	d = 16.0 mm y = 10.0 mm
6) 2nd Moment of Area(I_x)	I_x = 4,636.9 mm ⁴
7) Reaction force $R_A = R_B$	$R_A = R_B$ = 330.0 N = 33.7 kg
2. Moment	
1) Maximum Bending Moment	
$M_{max} = \frac{P \cdot L}{4} = \frac{660.0 \cdot 200.0}{4} = 33,000.0$ N mm	
3. Stress	
1) Maximum Tensile & Compressive Stress ($\sigma_{t,c}$)	
$\sigma_{t,c} = \frac{M_{max} \cdot y}{I_x} = \frac{33,000.0 \cdot 10.0}{4,636.9} = 71.2$ MPa	

In the same way, we computed the values for the maximum bending moment and maximum tensile and compressive stresses of all types of specimens. As explained, since support span (= L), the coordinate from the center of the specimen (= y), and the moment of inertia (= I_x) are constant for all types, P (maximum load) determines the values of maximum bending moment and maximum tensile and compressive stresses. For Type B1, the testing machine generated the value of 908.5 N, on average, for P (= maximum load). For Type B3, the value of P is 923.5 N. Table 2 summarizes all the results based on the above equations.

Table 2: Data to calculate the values of all types' maximum bending moment and maximum tensile and compressive stresses.

TYPE	Specimen number	Maximum load (kg)	Average maximum load (kg)	Maximum load (N)	Average maximum load (N)	Weight of specimen (g)	I_x (mm ⁴)	y(mm)	M_{max}	σ_{max} (MPa)
TYPE 00	00-01	70	68.47	686.47	34.355	34.355	4,636.99	10	34.1	73.7
	00-02	75	73.50	735.50	34.454	34.454				
	00-03	64	62.73	627.63	32.724	32.724				
	00-04	65	63.74	637.43	32.862	32.862				
	00-05	74	72.89	725.89	34.390	34.390				
TYPE	Specimen number	Maximum load (kg)	Average maximum load (kg)	Maximum load (N)	Average maximum load (N)	Weight of specimen (g)	I_x (mm ⁴)	y(mm)	M_{max}	σ_{max} (MPa)
TYPE B1	B1-01	88.27	85.63	865.63	36.131	36.131	4,636.99	10	45.4	98.0
	B1-03	89.31	87.83	893.79	35.997	35.997				
	B1-04	95.03	93.19	931.93	36.005	36.005				
	B1-05	93.58	91.71	917.71	35.659	35.659				
	B1-06	98.82	96.09	969.09	36.046	36.046				
	B1-02	88.27	85.63	865.63	36.131	36.131				
TYPE	Specimen number	Maximum load (kg)	Average maximum load (kg)	Maximum load (N)	Average maximum load (N)	Weight of specimen (g)	I_x (mm ⁴)	y(mm)	M_{max}	σ_{max} (MPa)
TYPE B3	B3-01	91.89	90.13	901.13	39.920	39.920	4,636.99	10	46.1	99.6
	B3-02	96.24	94.79	943.79	39.633	39.633				
	B3-03	94.39	92.65	925.65	39.807	39.807				
	B3-04	102.12	100.46	1001.46	39.627	39.627				
	B3-05	87.22	85.34	855.34	39.385	39.385				

Results in Table 2 show that the average maximum load for TYPE 00 is 69.7kg or 683.2 N (Newton). Consistent with the hypothesis, the results show that the average maximum load for TYPE B1 is much higher than that for TYPE 00. Since the maximum load is the most critical determinant of both maximum bending moment and maximum tensile and compressive stresses, and the higher maximum load indicates structural

strength, these results support the hypothesis. Specifically, the average maximum load based on five specimens of TYPE B1 is 92.6kg, which increases by 32.9% (= (92.6 - 69.7)/69.7, or 908.5 N, which increases by 33% (= (908.5 - 683.2)/683.2), compared to TYPE 00. This increase of approximately 33% in the average maximum load appears meaningful. Furthermore, the average maximum load for TYPE B3 is 94.2 kg or 923.5 N, which is higher than those for both TYPE 00 and TYPE B1. However, the increase in the average maximum load for TYPE B3, relative to TYPE B1, seems to be marginal, considering that TYPE B3 has three diaphragms while TYPE B1 has only one diaphragm.

More importantly, we found similar results when comparing maximum bending moment (M_{max}) and maximum tensile and compressive stresses (σ_{max} (MPa)) among specimens of three types. Specifically, maximum tensile and compressive stresses (σ_{max} (MPa)) for TYPE B1 increase by 33% relative to TYPE 00. Maximum tensile and compressive stresses (σ_{max} (MPa)) for TYPE B3 are increased by 35.2% relative to TYPE 00. Again, the difference in maximum tensile and compressive stresses (σ_{max} (MPa)) between TYPE B1 and TYPE B3 do not appear significant. Inferences based on the maximum bending moment (M_{max}) are similar.

The fracture points for each type of specimen were also examined since this examination may corroborate inferences from Table 2. Figure 15 contains photos of the fracture points for each type. It becomes apparent that the fracture in the specimen of TYPE 00 is the most severe (on the left side of Figure 15). On the contrary, the fractures of both TYPE B1 and TYPE B3 are not as severe (on the middle and the right sides of Figure 15).

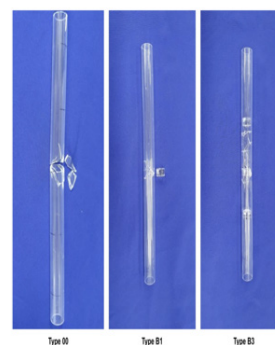


Figure 15: The fracture points for each type are different. The fracture in TYPE 00 is the most severe. On the contrary, the fractures of both TYPE B1 and TYPE B3 are not as severe.

Discussion

Interestingly, there is no significant improvement in structural integrity from one diaphragm to three diaphragms. We like to explore why this is the case further. Structural integrity should increase with more diaphragms, but the marginal increases from adding more diaphragms may decrease. One plausible reason for these results may be the length of the specimen. Due to the size of the INSTRON 4467 Tensile Tester device, the maximum length of each specimen was 250 mm. In the future, we would like to test the effect of length

on each specimen variation's tensile strength and durability. Increasing the length proportionately to the number of diaphragms in a specimen would generate more consistent results with the hypothesis - more diaphragms increase the structural strength proportionately. Looking back into nature, we see that bamboo follows a similar pattern. As it grows, bamboo stays consistent with the length between each diaphragm. Mimicking nature in that way may yield a more favorable outcome toward the hypothesis. At the same time, these results provide intriguing implications - simply adding more diaphragms does not significantly improve the structural strength.

Considering the cost of diaphragms, finding an optimal number of diaphragms in the given length is essential. To address this, we plan to design and develop fourth and fifth types of specimens, namely Type B4 and Type B5. Type B4 has four diaphragms with an even spread of diaphragms in a tube. Type B5 contains five diaphragms, and in this type, we will add two more diaphragms to the end of each side of Type B3 (specimen with three diaphragms). Testing hypotheses with these new types of specimens will shed more light on this research question.

We made each specimen out of acrylic plastic tubing due to the budget and manufacturing difficulties when this project started. In the future, we also like to test metal's tensile strength and structural integrity instead of plastic. Since we make most cylindrical tubes used in real life out of metal, these results would yield a more valuable diagnosis of the effect of diaphragms. Testing whether what we found with the plastic tubes is also applied to metal would be very intriguing. Considering that metal is already strong, it is also possible that the results - more diaphragms improve the strength of plastic tubes - may not exist with metal.

To mimic bamboo more closely, we also like to create more similar diaphragms to the ones in real life. For example, when splitting bamboo down the middle, one can observe that the diaphragms of bamboo are not entirely straight and perpendicular to the cylindrical tube. In the future, we would like to design a specimen that more closely mimics the angle and shape of natural bamboo (Figure 3). In addition, on the outside of the bamboo plant, there is a "knuckle": a thicker portion of the plant in the diaphragms' external surface. We also want to mimic this knuckle and test how much strength this knuckle can provide with diaphragms combined.

We also need to test whether a rod with diaphragms is more robust (or equally strong) than a solid rod to compare the tensile strength of specimens used in this project with that of a solid rod. Again, this test could have substantial real-world implications. For example, we can make rods with less material but more or similar structural strength. In that case, they will require less money and resources, leading to positive economic and environmental outcomes.

■ Conclusion

This paper used biomimicry to improve the cylindrical rod's structural strength. While we can see many solid cylindrical rods in real life, there are also many tube-type, empty cylindrical rods. If we can make tube-type cylindrical rods

as strong as solid ones, we can reduce the material costs to make solid cylindrical rods. Considering a recent supply chain disruption in many natural resources due to Covid-19, this research is critical and can significantly contribute to the economy and society. In addition, by reducing materials to make products of cylindrical rods, this research can also significantly contribute to protecting our environment.

Natural characteristics of bamboo are adopted to make empty cylindrical rods stronger. Bamboo is robust due to its diaphragms. Thus, we are interested in how much adding diaphragms can increase the structural strength of empty tubes. Therefore, we hypothesized that a tube with one diaphragm would be more robust than that without one. We also hypothesized that the more diaphragms a tube has, the greater its structural strength is. To test this hypothesis, we made three plastic tube types - a tube without a diaphragm, a tube with one diaphragm, and a tube with three diaphragms and five specimens for each type.

Consistent with the hypothesis, experiment results show that adding diaphragms to an empty tube does improve the structural integrity and tensile strength of a cylindrical tube. However, interestingly, there are non-significant changes in structural integrity between three diaphragms and one diaphragm. Specifically, both TYPE B1 (i.e., a tube with one diaphragm) and TYPE B3 (i.e., a tube with three diaphragms) are more robust than TYPE 00 (i.e., a tube without a diaphragm). However, when comparing TYPE B1 and TYPE B3, the difference is insignificant, based on average maximum load and maximum tensile and compressive stresses. While the average maximum load for TYPE B3 is higher than that for TYPE B1, the increase is only 1.7% ($= (94.2 - 92.6)/92.6$). These results suggest a possibility that there is an optimal number or ratio of diaphragms in the given length to maximize the structural strength.

■ Acknowledgments

We are grateful for the help of the Seoul National University of Science and Technology research laboratory for allowing us to use the INSTRON 4467 Tensile Tester they possess. More specifically, Sean Jung would like to thank Dr. Jong Seol Jeong for his guidance and assistance in allowing him to conduct and explore this experiment. Sean Jung would also like to acknowledge Mr. Johannes Adams for his help in getting me involved in this science fair. Finally, Sean Jung would like to thank the Hawaii Academy of Science for listening and giving him a platform to share his passion for science.

■ References

1. Benyus, J. *Biomimicry: Innovation Inspired by Nature*. Harper Collins Publisher. 2002.
2. Tittmann, B.R.; C.J. Bryan. *Biomimicry: Using nature as a model for design*. *ACS Central Science*. 2019. 5(11), 1805-1816.
3. Ansary, T. *The Invention of Yesterday: A 50,000-Year History of Human Culture, Conflict, and Connection*. *Public Affairs*. 2019.
4. Wade, M.J.; S. Kalisz. The causes of natural selection. *Evolution*. 1990,44(8),1947-1955. DOI:https://doi.org/10.1111/j.1558-5646.1990.tb04301.x
5. French, M. *Invention and evolution*. Cambridge University Press. 1994.

6. Vincent, J. F.V.; O.A. Bogatyreva; N.R. Bogatyrev; A. Bowyer; A-K. Pahl. Biomimetics: its practice and theory. *Journal of the Royal Society Interface*. 2006. DOI: <https://doi.org/10.1098/rsif.2006.0127>
7. Barthelat, F. Materials by design: lessons from nature. *Advanced Materials*, 2016. 28(24), 5187-5189.
8. Bar-Cohen, Y. Biomimetics – using nature to inspire human innovation. *Bioinspiration and Biomimetics*. 2006, 1(1).
9. Hargroves, K.; M.H. Smith. Innovation inspired by nature biomimicry. *Ecos*. 2006,129.
10. Liu, B.; C. Li; J. Li. Numerical Study of Pressure Waves Generated by High-Speed Train Entering and Exiting Tunnels. *Journal of Fluids and Engineering*. 2017, 139, 011106-1-011106-12.
11. Fan, J.; J. Xie.; H. Chen. Aerodynamic Performance of High-Speed Trains Entering and Exiting Tunnels. Proceedings of the Institution of Mechanical Engineers, Part F: *Journal of Rail and Rapid Transit*. 2014, 228, 255-265.
12. Yoshida, Y.; T. Iida. The aerodynamic design of high-speed trains for tunnel safety and comfort. *Journal of Wind Engineering and Industrial Aerodynamics*, 2015, 145, 126-133.
13. Lee, D. Biomimicry: Inventions Inspired by Nature. Kids Can Press. 2011.
14. Dicks, H. The Biomimicry Revolution: Learning from Nature How to Inhabit the Earth. United States: Columbia University Press. 2023.
15. AskNature. High-Speed Train Inspired by the Kingfisher. The Biomimicry Institute. 2021. Obtained from <https://asknature.org/innovation/high-speed-train-inspired-by-the-kingfisher/>.
16. Wu, F., A. Han, W., Jiang, Y., Yue, and D. Xie. A biomimetic design of steam turbine blade to improve aerodynamic performance. *International Journal of Thermal Science*. 2022, 181, DOI: <https://doi.org/10.1016/j.ijthermalsci.2022.107782>
17. Levine, J. The fastest animals in the world. Cell Mentor from Cell Press and Cell Signaling Technology. 2016.
18. Magazine, Smithsonian. How Biomimicry Is Inspiring Human Innovation. Smithsonian.com, Smithsonian Institution, obtained from 1 Sept. 2012, <https://www.smithsonianmag.com/science-nature/how-biomimicry-is-inspiring-human-innovation-17924040/>.
19. Speck, T.; O. Speck. Biomimetics in architecture: architecture of life and buildings. Springer. 2016.
20. Bhusan, B. Biomimetics: lessons from nature - An overview. *Philosophical Transactions of the Royal Society A: Mathematical, Physical and Engineering Sciences*. 2016, 374(2063).
21. Hecht, E. E.; Cree, G. S. The role of cylindrical objects in human culture and evolution. *Journal of Cognition and Culture*. 2015, 15 (1-2), 1-26.
22. Cho, K. H.; J.H. Lee. Cylindrical objects in everyday life. *International Journal of Industrial Ergonomics*, 2008, 38(7-8), 578-585.
23. Kusiak, A.; J. Wang. Structural Integrity and Failure Prevention in Manufacturing Processes. *Journal of Manufacturing Systems*. 2011, 30(3), 144-152.
24. Lourenço, P.B.; G. Milani. Structural integrity of masonry buildings. *International Journal of Architectural Heritage*. 2012, 6(1), 85-104.
25. Hassan, M. A.; A.A. Ali. Structural integrity of concrete structures. *Journal of Materials and Structures*. 2015, 48(5), 1255-1267.
26. Reed, B.C. The History and Science of the Manhattan Project. Springer Berlin, Heidelberg. 2019. DOI: <https://doi.org/10.1007/978-3-662-58175-9>
27. Feifer, G. The Battle of Okinawa: The Blood and the Bomb. United States: Lyons Press. 2001.
28. Stimson, H.L.; H.S. Truman. The Decision to Use the Atomic Bomb. *Bulletin of the Atomic Scientists*. 1947, 3:2, 37-67, DOI: 10.1008/00963402.1947.11455840
29. Selden, M. A Forgotten Holocaust: US Bombing Strategy, the Destruction of Japanese Cities and the American Way of War from World War II to Iraq. *The Asia-Pacific Journal*. 2007, 5(5)
30. Obataya, E.; P. Kitin; H. Yamauchi. Bending characteristics of bamboo (*Phyllostachys pubescens*) with respect to its fiber-foam composite structure. *Wood Sci Technol*. 2007, 41, 385-400. DOI: <https://doi.org/10.1007/s00226-007-0127-8>
31. Lessard, G.; A. Chouinard. *Bamboo research in Asia*: Proceedings of a workshop held in Singapore, 28-30 May 1980. Ottawa, Ont., IDRC, 1980, p.228.
32. Elert, G. Elasticity Summary. The Physics Hypertextbook. 2021. Obtained from <https://physics.info/elasticity/summary.shtml>.
33. Huang, Z. Resource-Driven Sustainable Bamboo Construction in Asia-Pacific Bamboo Areas. Germany: Springer International Publishing, 2021.
34. Tewari, D. N. Bamboo in building and construction in Southeast Asia. *Construction and Building Materials*. 2004, 18(6), 447-452.
35. Krawczak, P. Diaphragms in tubes as a measure increasing the energy absorption capacity of structures. *Journal of Theoretical and Applied Mechanics*. 2017, 55(3), 813-823.
36. Marques, R. A.; A.P. Silva. Effect of diaphragms on the strength of steel pipes under axial compression. *Journal of Construction Steel Research*. 2018, 141, 67-76.
37. Lin, Z.; J. Han; X. Yu; Y. Wang. Effects of diaphragm parameters on ultimate strength of thin-walled tubes. *Thin-Walled Structures*. 2017, 111, 45-54. DOI: <https://doi.org/10.1016/j.tws.2016.10.1003>
38. Davidson, J.R. Reliability and structural integrity. NASA *Technical Memorandum*, 1974. 14 p
39. Ciriacy-Wantrup, S.V. Resource Conservation: Economics and Policies. United States: University of California, Division of Agricultural Sciences, Agricultural Experiment Station, 1968.
40. Hu, J.; L. Ma; Z. Li. Numerical study on the effect of diaphragm position on the mechanical behavior of thin-walled tubes. *Thin-Walled Structures*, 2021, 160. DOI: <https://doi.org/10.1016/j.tws.2020.107757>
41. Xu, S.; J. Deng. Experimental and numerical investigation of thin-walled steel tubes with corrugated diaphragms under axial compression. *Journal of Construction Steel Research*. 2016, 120, 162-175. DOI: <https://doi.org/10.1016/j.jcsr.2016.01.024>
42. Cordero, R.M.; J.C. Polanco; J.A. Montalvo. Structural behavior of cold-formed steel members with circular holes subjected to bending. *Journal of Construction Steel Research*, 2017,137, 100-110.
43. D. M. Souza; L.M. Correia; E.R.M. Filho. Experimental analysis of composite columns with steel and concrete using full-scale specimens. *Engineering Structures*. 2016, 119, 438-449.
44. ASTM International, Designation D 790-03: Standard test methods for flexural properties of unreinforced and reinforced plastics and electrical insulating materials.
45. Gere, J.M.; B.J. Goodno. Mechanics of Materials. Brief Edition. CENGAGE Learning. 2011.

■ Author

Sean Jung is a senior at Punahou School. A pursuit in biomedical engineering interests me the greatest. I want to focus on biology and how it could be synthesized to improve the world. I wish to be a part of that conversation.

Arsenic in Groundwater and Its Carcinogenicity

Shriya Raja

Coppell High School, 185 W Parkway Blvd, Coppell, TX 75019, USA; dallasshriya@gmail.com

Mentor: Professor Jerome Nriagu

ABSTRACT: Due to groundwater contamination and runoff from certain mining operations, populations are exposed to detrimental levels of arsenic daily. The effects of arsenic exposure on the human epigenome are extensive, and some are still unknown. It can alter DNA methylation, inhibiting specific tumor suppressor genes and increasing the risk of neoplasia. This can be drawn back to certain crucial factors of DNA methylation, such as CpG Binding Proteins or DNA Methyl-transferases, all of which have shown linkage to carcinogenesis. Arsenic can also cause an overproduction of free radicals and a reduction of antioxidant production, causing oxidative stress. Lastly, it has also been associated with specific chromosomal abnormalities. All of these factors, which will be discussed in further detail, have been shown to contribute to the progression of cancer.

KEYWORDS: Biomedical and Health Sciences, Epigenetics; Arsenic Carcinogenicity; DNA Methylation; Methyl CpG Binding Proteins; DNA Methyltransferases.

■ Introduction

Arsenic is a naturally occurring and extensively distributed element found in the earth's crust. It comes in a multitude of forms, some of them being organic (Arsenite (AsIII) and Arsenate (AsV)) and others being inorganic (Dimethylarsinic acid (DMA) and Monomethylarsonic acid (MMA)).¹ Organic arsenic is metabolized by being absorbed into the bloodstream and reduced from Arsenate to Arsenite, which then allows for its methylation and detoxification.² In its inorganic form, however, arsenic can be extremely harmful to the human body, causing the development of skin lesions, cardiovascular diseases, and cancer.³ The health defects of chronic exposure to arsenic are relatively well-known. What is little known about Arsenic, however, is its prevalence in our daily lives. It is said that the average daily dietary intake of Arsenic through food ingestion in adults is 40 micrograms.⁴ This is in addition to levels of arsenic found in drinking water, which in some areas of the United States exceeds the maximum contaminant level of 10 µg/L.⁵ It is worth noting that certain populations are more susceptible to arsenic exposure than others, namely, lesser-developed countries that rely on mining and other industrial processes to fuel their economies. Mining has served as a significant economic resource and has allowed numerous countries to prosper. It provides many employment opportunities and will enable countries that were once economically stagnant to flourish. However, some of its environmental effects must be addressed due to its pervasiveness. Acid Mine Drainage (AMD) is the process of newly exposed iron sulfides oxidizing to create sulfuric acid, a corrosive acid capable of weathering nearby rocks and leaching toxic metals into rivers and streams.⁶ Certain populations, having no choice but to drink this contaminated water and not being given enough information by the government to deem the water undrinkable, may be at risk of developing diseases associated with increased arsenic exposure. The International Agency for Research on

Cancer (IARC) has identified arsenic and arsenic compounds as carcinogens. This is also applicable to when arsenic is ingested through drinking water, where it has been known to cause cancers of the bladder and lungs.⁷ However, in studies regarding the carcinogenicity of arsenic, there have been a few uncertainties about whether arsenic in itself is a carcinogen or whether it works synergistically with other carcinogens. Furthermore, in studies involving laboratory animals, where arsenic is administered as a single agent, it has generally been found to be nongenotoxic. In a study conducted by Xie *et al.*, both organic and inorganic forms of arsenic were administered to mice for a 17-week period. After the initial 4 weeks of administering arsenic, phorbol 12-myristate 13-acetate (TPA), a tumor promoter, was given to the mice. At the end of the 17-week period, global hypomethylation (contributor to carcinogenesis) was found in the mice for all forms of arsenic.⁸ Therefore, research in animal models does not demonstrate the carcinogenicity of arsenic as a single agent but rather its ability to serve as a co-carcinogen along with other carcinogenic environmental factors.⁹

One such population that suffers from frequent exposure to carcinogenic environmental factors is that of Mongolia¹⁰; Mining accounts for 20-30% of Mongolia's national GDP and 90% of its annual exports.¹¹ Mongolia places great importance on its mining activities but fails to recognize its effect on the welfare of its people. Mongolia has the highest incidence rate for stomach cancer in the whole world.¹² Bangladesh, a country infamous for its "Arsenic Incident" of 1993, discovered arsenic in their tube wells, the primary source of drinking water for rural populations.¹³ Bangladesh is ranked second worldwide for Mouth and Oral Cancer incidence rates.¹² It is essential to note that mining is not the sole contributor to arsenic in drinking water. Even countries that don't depend on mining, such as the United States, have unhealthy levels of arsenic in their groundwater.¹⁴ Therefore, this is not only a local phe-

nomenon but a global one. Cancer is said to be the product of multistage developments and changes in gene expression.¹⁵ This paper aims to identify such developments and how arsenic contributes to their progression. Exposure to arsenic and other toxic metals through mining operations and groundwater contamination increases susceptibility and mortality to certain forms of cancer.

■ Discussions

Epigenetics:

The term “epigenetics” was introduced in 1942 by embryologist Conrad Waddington, who related the term to the 17th-century concept of “epigenesis” since it was known to show the developmental processes connecting one’s genotype to their phenotype.¹⁶ Since then, the definition of epigenetics has evolved into the study of how behavioral and environmental factors can affect genetic processes. These changes, although reversible, are extremely prominent and can go so far as to turn genes “on” or “off,” either stimulating or inhibiting genetic functionality.¹⁷ There are different forms of epigenetic alteration, including DNA methylation, histone modification, and non-coding RNA. DNA Methylation, the most extensively discussed form in this paper, involves methyl groups being added to genes in order to repress their activity. When gene expression is suppressed too much or, in some cases, not enough, it can greatly change regular gene development and can lead to unwanted processes. It is important to note, however, that not all methylation leads to gene silencing. When taking place in locations outside promoter regions, methylation does not necessarily lead to gene silencing and may not impact gene expression as extensively.¹⁸ Another form of epigenetic alteration is histone modification, which involves the attachment of chemical groups to histone proteins, making them more closely packed together. This hinders the ability of other proteins to “read” the genes and assist in their development. Lastly, there is a form of epigenetic alteration that takes place using non-coding RNA. While the main role of non-coding RNA is to break down coding RNA to stop the production of certain proteins, it can also recruit proteins to modify histones, again rendering certain genes defective.¹⁷

DNA Methylation and Cancer:

DNA methylation plays an important role in regulating genes that control cell proliferation, differentiation, and overall development. These alterations can be passed down to daughter cells during DNA replication.¹⁹ DNA promoter hyper-methylation has been linked to the loss of tumor suppressor gene expression, specifically the production of the p53 gene. An article by Esteller *et al.* covers a study regarding the prevalence of DNA hyper-methylation in lung cancer patients. The study tested 22 non-small cell lung cancer patients for aberrant methylation in a couple of tumor suppressor/detoxification genes. 68% of the patients presented with signs of hyper-methylation in all tumor stages. Genes such as tumor protein p53 and p16 genes have been proven fundamental to neoplasm prevention, but all are affected by hyper-methylation.²⁰ Another study by Kroeger *et al.* observes DNA hyper-methylation in the progression of acute myeloid leukemia (AML). A genome-wide screening was conducted

to reveal the methylated CpG sites in AML patients. 23% to 83% of patients with AML showed signs of abnormal methylation at diagnosis, and 47% to 93% of patients with AML showed signs of abnormal methylation at relapse. To assess the correlation between the hyper-methylated genes and cancer progression, a total of 9 genes were tested in a group of AML patients for abnormal methylation. It was found that all patients had at least 1 of the 9 genes methylated at diagnosis and at least 2 of the 9 genes methylated during relapse. In addition, many of the methylated genes played crucial roles in tumor suppression, such as the p15 gene and the CDH13 gene. During AML relapse, a 15% increase in the number of p15 genes methylated was shown. This shows a positive correlation between the hyper-methylation of tumor-suppressor genes and cancer progression.²¹

Another topic related to genetic alteration and DNA methylation is hypo-methylation. There have been studies associating hypo-methylation with oncogenic transformation. One such study is that of Good *et al.* In the study, patients with Triple-negative breast cancer (TNBC) were said to have an over-expression of TET1 DNA demethylase, along with hypo-methylation of up to 10% of CpG sites. Through further study of breast and ovarian cancers, scientists have found a connection between TET1 and hypo-methylation and the activation of cancer-specific oncogenic pathways such as PI3K, EGFR, and PDGF.

Furthermore, after a CRISPR-mediated removal of TET1, there was a significant decrease in the usage of oncogenic pathways and a substantial increase in immune response genes. This suggests a dependence of cancer cell proliferation on TET1 over-expression.²² Another correlation worth considering is that of hypo-methylation and tumorigenesis. Though it is clear that neoplasm formation is strongly associated with hypo-methylation, the underlying mechanism is still not understood. Some studies, such as that of Tongelen *et al.*, relate tumorigenesis to the activation of “cancer germline genes,” which are genes of the germ-line that utilize DNA methylation as a method of repression. When affected by hypo-methylation, these genes can stimulate oncogenic pathways and catalyze processes such as cell proliferation, angiogenesis (blood cell formation), and metastasis (malignant growths at a distance from the primary site of cancer).²³ Lastly, there are studies connecting hypo-methylation of the LINE-1 repetitive element to tumorigenesis, such as that of Ehrlich.²⁴ The LINE-1 repeat promoter has the main function of mediating tumor suppressor deletion. When this gene is methylated, this function is inhibited, and tumor suppressor genes can perform their respective functions. However, when the LINE-1 promoter is hypo-methylated, there is a more rapid and frequent deletion of tumor suppressor genes, which can lead to oncogenic formation. The hypo-methylation of LINE-1 affects the human genome depending on the condition. For example, LINE-1 hypo-methylation significantly affects lymph node involvement in prostate adenocarcinomas. Another instance is hepatocellular carcinoma, which shows the hypo-methylation of repetitive sequences (such as LINE-1) in relation to the recurrence of the disease.

Epigenetic Machinery:

There are other facets to DNA methylation to be considered, such as methyl CpG binding proteins, that can potentially lead to cancer. Methyl CpG binding proteins (MBPs) recognize the CpG sites during DNA methylation. Therefore, they play a major role in identifying where to attach methyl groups. There are three categories into which methyl CpG binding proteins are divided: MBD-containing proteins, methyl-CpG binding zinc fingers, and the SRA domain-containing proteins.²⁵ The first category, MBD-containing proteins, is further divided into three subdivisions: histone methyl-transferases (HMT_MBD), the MeCP2_MBD proteins, and histone acetyltransferases (HAT_MBD). However, not all members of this group interact directly with CpG sites. HMT_MBD, which has been shown to interact with CpG sites, contains two categories: *SETDB1* and *SETDB2*, affecting chromosomes 1 and 13, respectively. *SETDB1*, on its own, has not been proven to cause cancer but has been associated with proteins that play a significant role in neoplasia. For example, its association with *DNMT3A* has been proven to repress the *p53* gene in breast and ovarian cancer cell lines. *SETDB1* has also been proven to interact with the protein MCAF1. Along with MBD1 (another transcriptional repressor), *SETDB1* and MCAF1 form a complex (*SETDB1:MCAF1:MBD1*). This complex has been shown to result in heterochromatin formation and gene repression.²⁶ Although the evidence linking *SETDB2* and cancer is limited compared to that of *SETDB1*, there is evidence associating *SETDB2* with a 1-Mb deletion on chromosome 13q, which is related to the progression of lymphocytic leukemia.²⁶ Another study by Yang *et al.* observes the over-expression of the CXXC zinc finger protein 1 (CFP1) in ovarian cancer tissues and cells. To ascertain the role of CFP1 in ovarian cancer progression, immunohistochemistry was performed on ovarian cancer tissues. A strong CFP1 signal was found in 125 samples; of those, over 30% showed a moderately strong signal, and just over 5% showed a powerful signal. Therefore, the overexpression of CFP1, a CpG-binding protein, can negatively affect DNA methylation, potentially leading to cancer. This evidence is only amplified when considering the high expression of CFP1 in endometroid carcinoma and serous cystadenoma.²⁷

There is also the catalyst of DNA methylation, DNA methyl-transferases (DNMTs) to consider. It is no doubt that when considering the consequences of methylation, DNMTs should be analyzed as well. The methyl-transferase family generally has five members: *DNMT1*, *DNMT2*, *DNMT3A*, *DNMT3B*, and *DNMT3L*. *DNMT1* is a maintenance methyl-transferase, identifying a hemimethylated site and establishing the methylation pattern for the *de novo* methyl-transferases. *DNMT3A* and *DNMT3B* focus on un-methylated CpG sites, predominantly active in embryonic stem cells.²⁸ Since exposure to arsenic has well-established effects on DNA methylation, it is highly plausible that it affects the expression or activity of DNA methyltransferases. Over-expression of these methyl-transferases can cause the methylation of CpG sites within tumor suppressor genes, which represses their activity and can cause tumorigenesis. For example, the over-expression of *DNMT1* can silence tumor suppressor genes *p16*, *CDH13*, and

CDH1, which can lead to pituitary adenoma.²⁹ Furthermore, mutations in *DNMT3A* can cause DNA hypo-methylation through *DNMT3A R882* mutation and can potentially lead to acute myeloid leukemia.³⁰ The process through which hyper-methylation can occur evolves around densely packed CpG dinucleotides known as CpG islands. CpG islands, in the normal methylation process, are usually un-methylated, while dispersed CpG sites are hyper-methylated. When CpG islands, especially those in tumor suppressor genes, are hyper-methylated, it can silence the tumor suppressor gene and lead to neoplasm formation.³¹ The carcinogenicity of DNA methyl-transferase over-expression was further proven using animal models. Belinsky *et al.* used a mouse model to observe the role of *DNMT1* in tumor formation. It was found that the reduction of *DNMT1* correlated with the reduction of incidence rates for lung cancer.³² However, though the correlation between DNMTs and cancer is undeniable, there is a certain contradiction. Husni *et al.* found that the lack of *DNMT3A* can facilitate tumorigenesis.³³ Various other studies have verified that *DNMT3A* deficiency can promote tumor growth and cause overall genomic instability. This calls to question whether *DNMT3A* is an oncogene or a tumor suppressor gene. In some cases, depending on the cancer type, stage, and other factors, *DNMT3A* and other proteins might be considered oncogenes, whereas, in others, they might be considered tumor suppressors. Furthermore, scientists have yet to discover if the other DNA methyltransferases abide by this paradox.³⁴

Arsenic and Epigenetic Changes:

Arsenic has been known to cause changes in DNA methylation, possibly hyper or hypo-methylating certain genes. This is shown in a study conducted by Intrasananont *et al.*, which shows the in utero effects of chronic arsenic exposure in newborn babies.³⁵ The study involved fifty-five newborn babies exposed to levels of arsenic and sixteen newborns that have not been exposed to arsenic. An *in vitro* study was conducted as well. Results showed increased levels of arsenic in the cord blood, hair, fingernails, and toenails in the newborn exposed to arsenic, as well as an increase in promoter methylation of *p53*. (hyper-methylation) In the *in vitro* study, there was a global hypomethylation, showing reductions in repetitive elements such as LINE-1, as well as *p53* hypermethylation once again. This shows that in utero exposure to arsenic could make certain people more susceptible to carcinogenesis. Another study conducted by Enith Nava-Rivera *et al.*, discusses the transgenerational effects of arsenic exposure in rats.³⁶ A group of rats were chronically exposed to arsenic, and four generations of their offspring were observed. Results showed declining levels of concentration, motility, vitality, and morphology in the generations. Exposure to arsenic caused genotoxic damage, aberrant methylation patterns, and an overall decrease in the quality of the sperm. This shows that the epigenetic alterations caused by arsenic not only affect those exposed but also future generations. Chronic arsenic exposure negatively affects the quality of life and endangers future generations, possibly increasing their susceptibility to certain forms of cancer.

Free Radical Production and Oxidative Stress:

Exposure to arsenic has been linked to the increased production of free radicals derived from the superoxide radical and reactive oxygen species (ROS).³⁷ Free radicals are unpaired electrons that, under certain circumstances, can cause cell damage and oxidative stress. Reactive oxygen species are those that contain oxygen, which easily reacts with other molecules.³⁸ In addition to this, arsenic has also been associated with the depletion of glutathione and other antioxidants responsible for regulating free radicals.³⁹ Therefore, the combination of increased free radicals and decreased antioxidants causes oxidative stress. Oxidative stress has many negative consequences, the majority of which encompass the inability of free radicals to perform their usual functions of defending the body against pathogens. This can cause atherosclerosis, diabetes, hypertension, and even cancer.⁴⁰ More specifically, ROS has been known to cause DNA strand breaks and damage to nucleotides. Many studies have shown significant DNA oxidation in cancer tissues leading to malignant progression in breast cancer and hepatocellular carcinoma. ROS can also modify regulatory proteins and enzymes in non-cancerous cells, causing carcinogenesis. Furthermore, carcinogenesis, through a study regarding colorectal cancer, has been linked with lipid peroxidation. This was found through thiobarbituric acid-reactive substances in the colorectal cancer patient, which are by-products of lipid peroxidation. This process generates many genotoxic molecules and can alter cellular membrane structure, affecting membrane permeability and recognition by the immune system.⁴¹ Although the correlation between free radicals and cancer is widely unrefuted, some studies link free radical usage to chemotherapeutics, providing a contradictory function to the free radicals. It is well acknowledged that the overproduction of ROS can cause genetic alterations, but these alterations can be lethal to cancer cells. Therefore, ROS has a dual role in both initiating and suppressing carcinogenesis. This is shown through evidence that ROS participates both in the Ras-Raf-MEK1/2-ERK1/2 oncogenic pathway and in the p38 MAPK tumor-suppressing pathways. So, depending on the cell type, ROS function may vary.⁴²

Chromosomal Aberrations:

Exposure to arsenic and arsenic compounds has been found to cause chromosomal aberrations. In a study by Beckman *et al.*, short-cultured lymphocytes of nine workers exposed to arsenic at the Rönnskär smeltery in northern Sweden were observed. Eighty-seven aberrations were found in 819 mitoses.⁴³ Despite the numerous developmental problems associated with chromosomal aberrations, it has also been linked to cancer. Two predominant factors of cancer cells are aneuploidy (an abnormal number of chromosomes) and structural reorganization of the chromosomes. Aneuploidy has been identified in most tumor cases and half of all leukemia and lymphoma cases. Its underlying cause is an erosion of mitotic fidelity, a condition called chromosomal instability (CIN). This produces alarmingly high losses and gains of chromosomes. Both aneuploidy and CIN have been associated with poor patient prognosis and resistance to chemotherapeutics.⁴⁴ There have also been studies, such as that of Moore *et al.*, that have con-

nected arsenic exposure and chromosomal alterations. This connection was determined by examining 123 patients in Argentina and Chile exposed to arsenic. In general, chromosomal abnormalities were higher in those exposed to arsenic. The deletion of chromosome 17p was the most predominant result of the exposure. This study also found an association between these chromosomal alterations and tumorigenesis. The mean number of chromosomal changes increased along with the tumor age and grade, showing a positive correlation between tumor progression and chromosomal abnormalities.⁴⁵

Conclusion

In conclusion, exposure to arsenic can cause a multitude of physiological difficulties and could potentially lead to cancer. Through its effect on DNA methylation, chromosomes, and ROS-mediated oxidative stress, arsenic can permanently alter the human genome. This affects not only those exposed to arsenic but also their offspring. There are, however, ways to remedy this widespread phenomenon. In areas with arsenic in groundwater, populations can use low-arsenic water sources such as purified surface water or rainwater. Testing water for arsenic is also important to distinguish between drinking water and water used for other purposes.⁴⁶ Although all the alterations to the genome induced by arsenic have not yet been identified, scientists continue to explore genomic patterns about arsenic and other toxic metals. There are even non-epigenetic effects of arsenic that are yet to be explored thoroughly.⁴⁷ When discovered, they can revolutionize epigenetics and etiology, potentially saving many lives.

Acknowledgments

Shriya Raja acknowledges and thanks Professor Jerome Nriagu from the University of Michigan for dedicating his time to guide and support her in writing this paper. She also thanks her parents for encouraging and supporting her throughout writing this paper.

References

1. P S Analytical "Applying the Power of Atomic Fluorescence." <http://www.psanalytical.com/products/arsenic-speciation.html#:~:text=Up%20to%20four%20arsenic%20species,separated%20on%20a%20simple%20system.> (accessed 2023-06-04).
2. Arsenic Toxicity: What Is the Biologic Fate of Arsenic in the Body? https://www.atsdr.cdc.gov/csem/arsenic/biologic_fate.html#:~:text=and%20Dart%202001%5D.-,Metabolism,Carter%201995%3B%20Wang%20et%20al. (accessed 2023-06-04).
3. Arsenic. <https://www.who.int/news-room/fact-sheets/detail/arsenic> (accessed 2023-06-04).
4. Arsenic Toxicity: What Are the Routes of Exposure for Arsenic? https://www.atsdr.cdc.gov/csem/arsenic/what_routes.html (accessed 2023-06-04).
5. Arsenic and Drinking Water Active. <https://www.usgs.gov/mission-areas/water-resources/science/arsenic-and-drinking-water> (accessed 2023-06-04).
6. Abandoned Mine Drainage. <https://www.epa.gov/nps/abandoned-mine-drainage> (accessed Jan 27, 2023).
7. Arsenic and Cancer Risk. [https://www.cancer.org/healthy/cancer-causes/chemicals/arsenic.html#:~:text=International%20Agency%20for%20Research%20on%20Cancer%20\(IARC\)&text=One%20of%20its%20major%20goals,Bladder%20cancer](https://www.cancer.org/healthy/cancer-causes/chemicals/arsenic.html#:~:text=International%20Agency%20for%20Research%20on%20Cancer%20(IARC)&text=One%20of%20its%20major%20goals,Bladder%20cancer) (accessed Jan 7, 2023).
8. Xie Y; Trouba KJ; Liu J; Waalkes MP; Germolec DR; Biokinetics

- and Subchronic Toxic Effects of Oral Arsenite, Arsenate, Monomethylarsonic Acid, and Dimethylarsinic Acid in V-Ha-Ras Transgenic (TG.AC) MICE. <https://pubmed.ncbi.nlm.nih.gov/15345372/> (accessed 2023-06-04).
9. Reichard, J. F.; Puga, A. Effects of Arsenic Exposure on DNA Methylation and Epigenetic Gene Regulation. <https://www.ncbi.nlm.nih.gov/pmc/articles/PMC2877392/> (accessed 2023-06-04).
 10. Boehm, S.; Moses, E.; Excell, C. Left in the Dark on Pollution, Mongolia's Poorest Communities Must Use Contaminated Water. <https://www.wri.org/insights/left-dark-pollution-mongolias-poorest-communities-must-use-contaminated-water> (accessed 2023-06-04).
 11. Canada, G. A. Mining Market in Mongolia. <https://www.tradecommissioner.gc.ca/mongolia-mongolie/market-reports-etudes-de-marches/0006654.aspx?lang=eng> (accessed 2023-06-04).
 12. Stomach Cancer Statistics. <https://www.wcrf.org/cancer-trends/stomach-cancer-statistics/> (accessed 2023-06-04).
 13. Ahmad, S. A.; Khan, M. H.; Haque, M. Arsenic Contamination in Groundwater in Bangladesh: Implications and Challenges for Healthcare Policy. <https://www.ncbi.nlm.nih.gov/pmc/articles/PMC6281155/#:~:text=Fifty%20million%20people%20of%20Bangladesh,toxicity%20are%20evident%20in%20Bangladesh.> (accessed 2023-06-04).
 14. Arsenic. <https://www.niehs.nih.gov/health/topics/agents/arsenic/index.cfm#:~:text=There%20are%20no%20arsenic%20water,EP A%20standard%20of%2010%20ppb.> (accessed 2023-06-04).
 15. Smith, M. T.; Guyton, K. Z.; Gibbons, C. F.; Fritz, J. M.; Portier, C. J.; Rusyn, I.; DeMarini, D. M.; Caldwell, J. C.; Kavlock, R. J.; Lambert, P. F.; Hecht, S. S.; Bucher, J. R.; Stewart, B. W.; Baan, R. A.; Coglian, V. J.; Straif, K. Key Characteristics of Carcinogens as a Basis for Organizing Data on Mechanisms of Carcinogenesis. <https://www.ncbi.nlm.nih.gov/pmc/articles/PMC4892922/> (accessed 2023-06-04).
 16. U; D. Epigenetics: The Origins and Evolution of a Fashionable Topic. <https://pubmed.ncbi.nlm.nih.gov/27291929/#:~:text=The%20term%20epigenetics%20was%20introduced,between%20the%20genotype%20and%20phenotype.> (accessed 2023-06-04).
 17. What Is Epigenetics? <https://www.cdc.gov/genomics/disease/epigenetics.htm#:~:text=Epigenetics%20is%20the%20study%20of,body%20reads%20a%20DNA%20sequence.> (accessed 2023-06-04).
 18. PA.; J. Functions of DNA Methylation: Islands, Start Sites, Gene Bodies and Beyond. <https://pubmed.ncbi.nlm.nih.gov/22641018/> (accessed 2023-06-04).
 19. DNA methylation. <https://www.whatisepigenetics.com/dna-methylation/> (accessed Jan 27, 2023).
 20. Detection of Aberrant Promoter Hypermethylation of Tumor Suppressor Genes in Serum DNA from Non-Small Cell Lung Cancer Patients. <https://aacrjournals.org/cancerres/article/59/1/67/505065/Detection-of-Aberrant-Promoter-Hypermethylation-of> (accessed Jan 27, 2023).
 21. Kroeger, H.; Jelinek, J.; Estécio, M. R. H.; He, R.; Kondo, K.; Chung, W.; Zhang, L.; Shen, L.; Kantarjian, H. M.; Bueso-Ramos, C. E.; Issa, J.-P. J. Aberrant CPG island methylation in acute myeloid leukemia is accentuated at relapse. <https://www.ncbi.nlm.nih.gov/pmc/articles/PMC2515110/> (accessed Jan 30, 2023).
 22. Good, C. R.; Panjarian, S.; Kelly, A. D.; Madzo, J.; Patel, B.; Jelinek, J.; Issa, J.-P. J. Tet1-mediated hypomethylation activates oncogenic signaling in triple-negative breast cancer. <https://aacrjournals.org/cancerres/article/78/15/4126/544595/TET1-Mediated-Hypomethylation-Activates-Oncogenic> (accessed Jan 27, 2023).
 23. Van Tongelen A; Loriot A; De Smet C; Oncogenic roles of DN A hypomethylation through the activation of cancer-germline genes. <https://pubmed.ncbi.nlm.nih.gov/28342986/> (accessed Jan 27, 2023).
 24. Ehrlich, M. DNA hypomethylation in cancer cells. <https://www.ncbi.nlm.nih.gov/pmc/articles/PMC2873040/> (accessed Jan 30, 2023).
 25. Du, Q.; Luu, P.-L.; Stirzaker, C.; Clark, S. J. Methyl-CPG-Binding Domain Proteins: Readers of the Epigenome. <https://www.futuremedicine.com/doi/10.2217/epi.15.39> (accessed 2023-06-05).
 26. Parry, L.; Clarke, A. R. The Roles of the Methyl-CPG Binding Proteins in Cancer. <https://www.ncbi.nlm.nih.gov/pmc/articles/PMC3174265/> (accessed 2023-06-04).
 27. Yang, L.-Q.; Hu, H.-Y.; Han, Y.; Tang, Z.-Y.; Gao, J.; Zhou, Q.-Y.; Liu, Y.-X.; Chen, H.-S.; Xu, T.-N.; Ao, L.; Xu, Y.; Che, X.; Jiang, Y.-B.; Xu, C.-W.; Zhang, X.-C.; Jiang, Y.-X.; Heger, M.; Wang, X.-M.; Cheng, S.-Q.; Pan, W.-W. CPG-binding protein CFP1 promotes ovarian cancer cell proliferation by regulating BST2 transcription. <https://www.nature.com/articles/s41417-022-00503-z> (accessed Jan 30, 2023).
 28. Jin, B.; Robertson, K. D. DNA Methyltransferases, DNA Damage Repair, and Cancer. [https://www.ncbi.nlm.nih.gov/pmc/articles/PMC3707278/#:~:text=DNA%20methyltransferases%20\(DNMTs\)%2C%20responsible,%2C%20DNMT3A%2C%20DNMT3B%20and%20DNMT3L.](https://www.ncbi.nlm.nih.gov/pmc/articles/PMC3707278/#:~:text=DNA%20methyltransferases%20(DNMTs)%2C%20responsible,%2C%20DNMT3A%2C%20DNMT3B%20and%20DNMT3L.) (accessed 2023-06-04).
 29. Ma, H.-S.; Wang, E. L.; Xu, W.-F.; Yamada, S.; Yoshimoto, K.; Qian, Z. R.; Shi, L.; Liu, L.-L.; Li, X.-H. Overexpression of DNA (Cytosine-5)-Methyltransferase 1 (Dnmt1) and DNA (Cytosine-5)-Methyltransferase 3A (DNMT3A) Is Associated with Aggressive Behavior and Hypermethylation of Tumor Suppressor Genes in Human Pituitary Adenomas. <https://www.ncbi.nlm.nih.gov/pmc/articles/PMC6069575/> (accessed 2023-06-04).
 30. Ley, T. J.; Li Ding; Walter, M. J.; McLellan, M. D. DNMT3A Mutations in Acute Myeloid Leukemia | *Nejm*. <https://www.nejm.org/doi/full/10.1056/NEJMoa1005143> (accessed 2023-06-05).
 31. Esteller, M. CPG Island Hypermethylation and Tumor Suppressor Genes: A Booming Present, a Brighter Future. <https://www.nature.com/articles/1205600> (accessed 2023-06-04).
 32. Belinsky SA; Klinge DM; Stidley CA; Issa JP; Herman JG; March TH; Baylin SB; Inhibition of DNA methylation and histone deacetylation prevents murine lung cancer. <https://pubmed.ncbi.nlm.nih.gov/14612500/> (accessed Jan 27, 2023).
 33. Husni RE; Shiba-Ishii A; Iiyama S; Shiozawa T; Kim Y; Nakagawa T; Sato T; Kano J; Minami Y; Noguchi M; DNMT3a expression pattern and its prognostic value in Lung Adenocarcinoma. <https://pubmed.ncbi.nlm.nih.gov/27237029/> (accessed Jan 27, 2023).
 34. Zhang, J.; Yang, C.; Wu, C.; Cui, W.; Wang, L. DNA methyltransferases in cancer: Biology, paradox, aberrations, and targeted therapy. <https://www.ncbi.nlm.nih.gov/pmc/articles/PMC7465608/#:~:text=DNMT%20aberrations%20usually%20affect%20tumor,th e%20difficulty%20of%20cancer%20therapy.> (accessed Jan 27, 2023).
 35. Intarasunanont, P.; Navasumrit, P.; Waraprasit, S.; Chaisatra, K.; Suk, W. A.; Mahidol, C.; Ruchirawat, M. Effects of Arsenic Exposure on DNA Methylation in Cord Blood Samples from Newborn Babies and in a Human Lymphoblast Cell Line - Environmental Health. <https://ehjournal.biomedcentral.com/articles/10.1186/1476-069X-11-31> (accessed 2023-06-04).
 36. Nava-Rivera, L. E.; Betancourt-Martínez, N. D.; Lozoya-Martínez, R.; Carranza-Rosales, P.; Guzmán-Delgado, N. E.; Carranza-Torres, I. E.; Delgado-Aguirre, H.; Zambrano-Ortiz, J. O.; Morán-Martínez, J. Transgenerational Effects in DNA Methylation, Ge

- nototoxicity and Reproductive Phenotype by Chronic Arsenic Exposure. <https://www.nature.com/articles/s41598-021-87677-y> (accessed 2023-06-04).
37. Jomova K; Jenisova Z; Feszterova M; Baros S; Liska J; Hudecova D; Rhodes CJ; Valko M; Arsenic: Toxicity, oxidative stress, and human disease. <https://pubmed.ncbi.nlm.nih.gov/21321970/> (accessed Jan 27, 2023).
38. NCI Dictionary of Cancer terms. <https://www.cancer.gov/publications/dictionaries/cancer-terms/def/reactive-oxygen-species> (accessed Jan 27, 2023).
39. Hall, M. N.; Niedzwiecki, M.; Liu, X.; Harper, K. N.; Alam, S.; Slavkovich, V.; Ilievski, V.; Levy, D.; Siddique, A. B.; Parvez, F.; Me y, J. L.; van Geen, A.; Graziano, J.; Gamble, M. V. Chronic arsenic exposure and blood glutathione and glutathione disulfide concentrations in Bangladeshi adults. <https://www.ncbi.nlm.nih.gov/pmc/articles/PMC3764071/> (accessed Jan 27, 2023).
40. Dix, M. Oxidative stress: Definition, effects on the body, and prevention. <https://www.healthline.com/health/oxidative-stress> (accessed Jan 27, 2023).
41. Pizzino, G.; Irrera, N.; Cucinotta, M.; Pallio, G.; Mannino, F.; Arcoraci, V.; Squadrito, F.; Altavilla, D.; Bitto, A. Oxidative stress: Harms and benefits for human health. <https://www.ncbi.nlm.nih.gov/pmc/articles/PMC5551541/> (accessed Jan 27, 2023).
42. Gupta, N.; Verma, K.; Nalla, S.; Kulshreshtha, A.; Lall, R.; Prasad, S. Free radicals as a double-edged sword: The cancer preventive and therapeutic roles of curcumin. <https://www.ncbi.nlm.nih.gov/pmc/articles/PMC7698794/> (accessed Jan 27, 2023).
43. I; B. G. B. L. N. Chromosome aberrations in workers exposed to arsenic. <https://pubmed.ncbi.nlm.nih.gov/908292/> (accessed Jan 27, 2023).
44. Thompson, S. L.; Compton, D. A. Chromosomes and cancer cells. <https://www.ncbi.nlm.nih.gov/pmc/articles/PMC3770937/> (accessed Jan 27, 2023).
45. Moore LE; Smith AH; Eng C; Kalman D; DeVries S; Bhargava V; Chew K; Moore D; Ferreccio C; Rey OA; Waldman FM; Arsenic-related chromosomal alterations in bladder cancer. <https://pubmed.ncbi.nlm.nih.gov/12441324/> (accessed Jan 30, 2023).
46. Arsenic. <https://www.who.int/news-room/fact-sheets/detail/arsenic> (accessed Jan 27, 2023).
47. Björklund, G.; Aaseth, J.; Chirumbolo, S.; Urbina, M. A.; Uddin, R. Effects of Arsenic Toxicity beyond Epigenetic Modifications-Environmental Geochemistry and Health. <https://link.springer.com/article/10.1007/s10653-017-9967-9> (accessed 2023-06-04).

■ Author

Shriya Raja is a sophomore at Coppell High School. She is highly interested in the medical field, especially oncology research. Shriya plans to pursue a career in either medical research or surgery. In addition, she loves to read, sing, and volunteer.

Investigation of Functional Role of a Novel Biomarker: CCNC Gene Deletion on Human Leukemia Cancer

Sooah Yoo

St. Mark's School, 25 Marlboro Rd, Southborough, MA 01772, USA; gosityber1@gmail.com
Mentor: Prof. Woo Rin Lee

ABSTRACT: Leukemia is deadly cancer that increases the number of leucocytes in the blood or bone marrow. Even though the recent improvements in treatment protocols, the survival rate for five years after diagnosis is only 29.5%. Therefore, it is crucial to understand the biomarker and its molecular mechanism of how leukemia develops tumor progression. This study analyzed the genomic alteration and clinical profiles of 1978 leukemia patients using the cBioPortal database. We found that nine out of ten genes were deleted in chromosome 6q16.1-2. Also, we discovered that the CCNC gene deletion is enriched in deceased patients (9.09%) compared to living patients (1.33%). To further understand how CCNC gene deletion affects leukemia cancer progression, we silenced the CCNC gene using small interfering RNA (siRNA) to mimic CCNC gene deletion using the Jurkat leukemia cancer cell line. Our result showed that CCNC knockdown significantly increased cancer cell migration. We found that CCNC deletion or knockdown is a crucial novel biomarker that increases cancer cell migration and may cause poor prognosis in leukemia patients. This finding may support the current limitation of diagnosis and improve the accuracy of predicting the prognosis of leukemia patients.

KEYWORDS: Cellular and Molecular Biology, Cancer Biology, Genetics, Leukemia, CCNC, Patient Survival.

■ Introduction

Leukemia is cancer found in blood and blood-forming tissues, including the bone marrow and the lymphatic system.¹ Leukemia usually involves white blood cells, as the bone marrow of leukemia patients produces an excessive amount of abnormal white blood cells that cannot function properly. Leukemia is the most common cancer in childhood and teens, accounting for almost one out of three cancers.² Most childhood leukemias are acute lymphocytic leukemia (ALL). On the other hand, Acute Myeloid Leukemia (AML) is more common in older adults. Leukemia accounts for 10% of all diagnosed cancers in the United States. Currently, leukemia has a relative survival rate of 5 years, about 29.5% after diagnosis.³

A cancer biomarker refers to a substance or a process indicative of cancer in the body, including proteins or genes.⁴ Biomarkers help detect cancer; about 40% of cancers can be cured if they are detected early enough through biomarkers. There are cancer biomarker types: Genetic, epigenetic, proteomic, and glycomic.⁵ This study focused on genetic biomarkers, which refer to genes enriched in deceased cancer patients.

Genes are commonly deleted in leukemia patients. Gene deletions, which occur because of mutations, can eliminate tumor-suppressor genes and promote cancer.⁶ Gene deletions refer to the loss of both copies of genes, thus leaving zero copies of the gene. Previous research showed that 68.2% (144/211) of adult B-ALL patients carried gene deletions, and the frequency is much higher in Ph+B-ALL patients.⁷ IKZF1 gene deletion is the most common gene deletion in adult B-ALL, followed by CDKN2A/B deletion.⁷

Searching for a novel biomarker is essential to develop a novel leukemia diagnosis method and treatment. Therefore, we searched for a novel biomarker significantly affecting the leukemia patient's survival. Consequently, we analyzed 1978 leukemia patient genomics and found that the CCNC gene was deleted in deceased patients. Next, we analyzed the functional role of CCNC gene deletion in leukemia cells using siRNA transfection. Overall, this study found that CCNC gene deletion or knockdown is a crucial biomarker that increases cancer cell migration in leukemia cancer cells.

■ Methods and Materials

cBioPortal patient data analysis:

cBioPortal is an open-source platform that provides access to comprehensive cancer genomics data and allows users to visualize, analyze, and interpret cancer genomics data. Therefore, it can be used to analyze patient survival data in the context of cancer genomics. A total of 1,551 leukemia patients' information and genomic data were retrieved from cBioPortal.

Cell culture and maintenance:

The human leukemia cancer cell line Jurkat was purchased from the Korean Cell Line Bank (Seoul, Korea). Jurkat cells were cultured in RPMI-1640 medium (Gibco) supplemented with 10% HyClone™ fetal bovine serum (Thermo Fisher Scientific) and 1% penicillin and streptomycin (Gibco) in a 5% CO₂ incubator at 37 °C.

siRNA transfection in Jurkat cells:

A total of 100,000 cells were prepared in each well on a 6-well culture plate. Then the siRNA stock was prepared with 10 pmole/μL. In the separate tube, 1 nM of siRNA was prepared with different volumes of INTERFERin reagent (Polyplus), each with 8 μL, 4 μL, and 12 μL, as well as siRNA

negative control with 8 μ L. The mixture samples were then incubated for 10 minutes at room temperature. Finally, the transfection mix was added to the cells in serum containing RPMI-1640 medium. The cells were incubated for 48 hours. The following siRNA sequence targeting CCNC was used: 5'-CUGUAUCCUCCUUUGAUGA=tt-3'(anti-sense), 5'-UCAUGAAAGGAGGAUACAG=tt-3' (sense).

Total RNA extraction:

AccuPrep Universal RNA Extraction Kit (Bioneer) was used to extract total RNA from the Jurkat cultured cells, followed by the manufactured protocol.

cDNA synthesis:

To synthesize the cDNA library, TOPscript™ Reverse Transcriptase (Enzymatics) was used, and a total of 10 μ L reaction condition was prepared with 10X reaction buffer, reverse transcriptase enzyme, dNTP, oligo dT primer, and 1 μ g of extracted RNA were used for each sample to proceed cDNA synthesis. The samples were incubated in the following condition: 45 °C for 1 hour, 95 °C for 5 minutes, and infinite for storage at 15 °C.

Polymerase chain reaction:

AccuPower® PCR PreMix (Bioneer) was used to amplify CCNC and GAPDH cDNA. A total of 20 μ L reactions were made. 10 pmol of forward primer and reverse primer were added with 100 ng of cDNA. The PCR reaction proceeded in the following condition: 95 °C for 5 minutes (step 1), 95 °C for 30 seconds (step 2), 58 °C for 30 seconds (step 3), 72 °C for 15 seconds (step 4), repeat from step 2 to 4 for 29 times, 72 °C for 5 minutes (step 5), and infinite for storage at 12 °C.

Cell migration:

The cell migration was analyzed using the transwell assay (Corning). First, Jurkat cells were added with cell media without fetal bovine serum cell media in the upper chamber. Then, the cell media with fetal bovine serum was added to the bottom chamber to stimulate cell migration. Finally, the cells were incubated for 96 h, and the cells migrated to the bottom chamber was imaged.

Results and Discussion

Table 1: Top 10 deleted genes that are significantly enriched in deceased leukemia patients.

Gene	Cytoband	Living group	Deceased group	p-Value	q-Value	Most enriched in
CCNC	6q16.2	7 (1.33%)	14 (9.09%)	5.86E-06	8.27E-04	DECEASED
EPHA7	6q16.1	7 (1.33%)	14 (9.09%)	5.86E-06	8.27E-04	DECEASED
PRDM13	6q16.2	7 (1.33%)	14 (9.09%)	5.86E-06	8.27E-04	DECEASED
USP45	6q16.2	7 (1.33%)	14 (9.09%)	5.86E-06	8.27E-04	DECEASED
COQ3	6q16.2	8 (1.52%)	14 (9.09%)	1.73E-05	2.27E-03	DECEASED
FAXC	6q16.2	8 (1.52%)	14 (9.09%)	1.73E-05	2.27E-03	DECEASED
MCHR2	6q16.2	8 (1.52%)	14 (9.09%)	1.73E-05	2.27E-03	DECEASED
PNISR	6q16.2	8 (1.52%)	14 (9.09%)	1.73E-05	2.27E-03	DECEASED
SIM1	6q16.3	8 (1.52%)	14 (9.09%)	1.73E-05	2.27E-03	DECEASED
ADD3	10q25.1-q25.2	16 (3.04%)	19 (12.34%)	2.45E-05	3.17E-03	DECEASED

We analyzed leukemia patients' genomics using the cBioPortal genomic database to find the novel leukemia biomarker. Through this, we further investigated the deletion of genes from the DNA of the leukemic patients. As a result, we found the top ten deleted genes at a higher level in deceased leukemia patients: CCNC, EPHA7, PRDM13, USP45, COQ3, FAXC,

MCHR2, PNISR, SIM1, and ADD3. Nine of these genes are located in chromosome 6, with one exception, which is located in chromosome 10 (Table 1). This study focused on CCNC gene deletion, as CCNC has not been well studied in leukemia cancer cells. Also, CCNC was one of the top-ranked enriched deleted genes in the deceased group: comparing the data from living and deceased categories, only 1.33% were living, while 9.09% were deceased. Thus, we found ten novel genes were deleted in deceased leukemia patients, making them novel leukemia biomarkers.

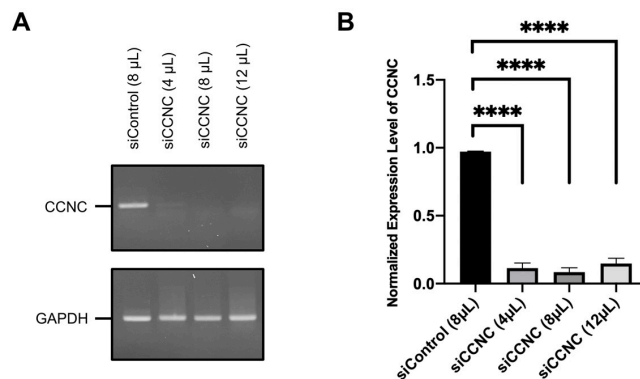


Figure 1: siRNA targeting CCNC decreased CCNC expression level in human leukemia Jurkat cells (A) Agarose gel representing the amplified CCNC and GAPDH cDNA. (B) Bar graph illustrating mean and standard deviation of the normalized expression level of CCNC. One-way ANOVA with Tukey's post hoc test was performed to calculate the p-value. $p < 0.0001$ (****).

We found that CCNC gene deletion was enriched in deceased leukemia patients. To further investigate the function of CCNC deletion on leukemia cancer cell development, we silenced the CCNC gene using siRNA transfection. Four siRNA transfection conditions were tested for this experiment to optimize the siRNA transfection: siControl, siCCNC (4 μ L, 8 μ L, 12 μ L). Then, the amplification of two genes (CCNC and GAPDH) was analyzed in agarose gel electrophoresis. GAPDH was used to normalize the CCNC expression level. Finally, the band intensity of CCNC was quantified, and the normalized expression level of CCNC was calculated. The results show that all three CCNC siRNA transfection conditions significantly decreased the expression level of CCNC in human leukemia Jurkat cells (Figure 1). Thus, our designed siRNA targeting CCNC successfully silenced the CCNC gene expression.

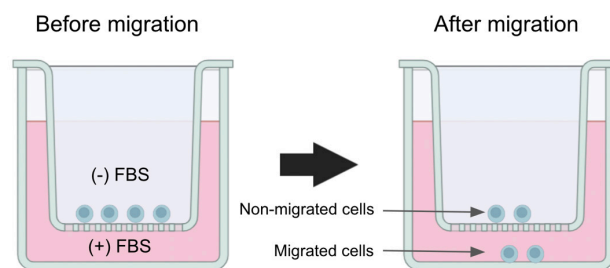


Figure 2: The representation of the concept of migration assay using transwell. Jurkat cells were placed on the upper chamber of the transwell, which has small holes that cancer cells can pass through to the bottom chamber. The migration of cells towards FBS-containing media was measured as an indicator of cell migration ability.

Cell migration is essential in many biological processes, such as embryological development, tissue formation, immune defense or inflammation, and cancer progression. Especially cell migration is one of the initial processes of cancer metastasis. Since CCNC deletion was enriched in deceased leukemia patients, we hypothesize that CCNC silencing may increase cell migration. Cancer cells are known to localize around the human blood vessels, which contain abundant nutrients such as glucose and oxygen. Cancer cells can sense the nutrients and move towards high-nutrition conditions. Therefore, in this experiment, we designed a transwell experiment that provides two different conditions: with and without FBS, which contains high nutrition for cancer cells. First, we placed the Jurkat cells on the upper chamber of the transwell (Figure 2). The upper chamber transwell has small holes that cancer cells can pass through to the bottom chamber. This transwell assay can measure the cell migration ability that cancer cells move towards the nutrition full environment.

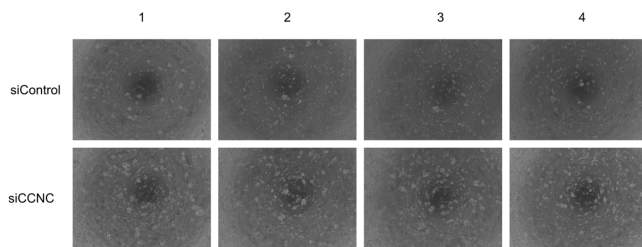


Figure 3: CCNC gene silencing increased Jurkat leukemia cell migration. The migrated cells were then photographed, and the number of migrated cells was quantified. Four replicate samples were analyzed after transfecting siControl and siCCNC.

We underwent CCNC silencing to find the novel function of the CCNC gene in leukemia cells. CCNC silencing increased cell migration in leukemia cells, as shown in Figure 3. A greater number of leukemia cells were found in the siCCNC transfected sample compared to the siControl transfected sample. This means the increased number of CCNC silenced cells have migrated from (-) FBS to (+) FBS. We repeated the experiment four times and had the same result. Therefore, our results show that inhibiting the expression of CCNC enhanced cell migration and may lead to decreased leukemia patient survival.

■ Conclusion

This study aimed to identify novel genes deleted in leukemia patients that could serve as important biomarkers for the disease. The study identified ten such genes by analyzing genomic data, and one of them, CCNC, was investigated further for its functional role in leukemia. In addition, the study aimed to understand how the deletion of CCNC affects the migration ability of leukemia cells and whether it could be used as a potential biomarker for leukemia prognosis.

As shown in Table 1, we have found ten novel genes deleted in leukemia patients that make them important biomarkers for leukemia. In Figure 1, the agarose gel represents how CCNC siRNA transfection significantly decreases the normalized expression level of CCNC, indicating successful silencing of CCNC gene expression. Figure 2 shows our concept of migration assay using transwell to measure the

cell migration ability toward the environment with richer nutrients. Finally, Figure 3 demonstrates the result in which silencing CCNC increases the migration of the leukemia cells. Overall, the deletion of CCNC acts as a novel biomarker for leukemia, as it contributes to enhanced cancer cell migration and eventually decreased chance of survival.

Nevertheless, we acknowledge some limitations to our experiment. First, eight other gene deletions in chromosome 6 other than CCNC are significantly enriched in deceased leukemia patients. Therefore, we need to analyze the function of the other deleted genes. Second, only one type of leukemia cell line was used, which was Jurkat. Therefore, we need to verify our results using different types of leukemia cancer cell lines. Also, we only investigated the functional role of CCNC on cell migration. Investigation into the functional role in cell proliferation, cell invasion, and chemoresistance is also needed. Finally, we only performed an *in vitro* experiment and must complete a mouse experiment to verify our results further.

The findings of our study have significant implications for the diagnosis and treatment of leukemia. Our identification of CCNC deletion as a novel biomarker for leukemia patients provides an easier and more accurate diagnosis method using genomic information, leading to a more precise prognosis prediction. Furthermore, personalized treatments based on genomic information can increase the efficacy of cancer therapy drug and minimize the side effects.

Additionally, our study highlights the association between CCNC deletion and poor prognosis in leukemia patients. The deletion of CCNC increases cancer cell migration and promotes metastasis. Thus, our findings suggest that targeting CCNC could be a potential therapeutic strategy to prevent metastasis and improve the survival rate of leukemia patients.

Overall, our study contributes to advancing the understanding of the genetic mechanisms underlying leukemia, which can significantly impact the development of diagnosis and treatment options for patients. In addition, by identifying novel biomarkers and elucidating their functional roles, we pave the way for developing personalized medicine that considers each patient's unique genetic makeup, leading to more effective and targeted treatments.

■ Acknowledgments

I thank my research advisor, Prof. Woo Rin Lee, at the University of Suwon, for supporting this research.

■ References

1. Pelcovits, A.; Niroula, R. Acute Myeloid Leukemia: A Review. *R. I. Med. J.* (2013) 2020, 103 (3), 38–40.
2. Tebbi, C. K. Etiology of Acute Leukemia: A Review. *Cancers (Basel)* 2021, 13 (9).
3. Redaelli, A.; Laskin, B. L.; Stephens, J. M.; Botteman, M. F.; Pashos, C. L. A Systematic Literature Review of the Clinical and Epidemiological Burden of Acute Lymphoblastic Leukaemia (ALL). *Eur J Cancer Care (Engl)* 2005, 14 (1), 53–62.
4. Bhatt, A. N.; Mathur, R.; Farooque, A.; Verma, A.; Dwarakanath, B. S. Cancer Biomarkers - Current Perspectives. *Indian J. Med. Res.* 2010, 132, 129–149.
5. Wu, L.; Qu, X. Cancer Biomarker Detection: Recent Achievements and Challenges. *Chem. Soc. Rev.* 2015, 44 (10), 2963–2997.

6. Zhang, Y.; Liu, D.; Li, F.; Zhao, Z.; Liu, X.; Gao, D.; Zhang, Y.; Li, H. Identification of Biomarkers for Acute Leukemia via Machine Learning-Based Stemness Index. *Gene* 2021, 804, 145903.
7. Fang, Q.; Song, Y.; Gong, X.; Wang, J.; Li, Q.; Liu, K.; Feng, Y.; Hao, Q.; Li, Y.; Wei, H.; et al. Gene Deletions and Prognostic Values in B-Linage Acute Lymphoblastic Leukemia. *Front. Oncol.* 2021, 11, 677034.

■ Author

Sooah Yoo is a current high school junior at St. Mark's School, MA. As a student who enjoys diving into scientific research, she aims to major in biology and medical science, pursuing a passion for neuroscience and genetics. She is willing to continue her research on cancer and leukemia in the future to improve human health.

A new approach to Turing completeness in *Baba is You*

Caleb J. Su

Mercer Island High School, 8219 SE 28th Street, Mercer Island, Washington, 98040, USA; calebjzs@gmail.com

Mentors: Dr. Jim Purbrick, Dr. Chaitanya Mishra, Dr. Dan Grossman, Alvin Shi

ABSTRACT: *Baba is You* is a 2019 indie puzzle game whose levels are two-dimensional grids of objects. This paper demonstrates how a universal Turing machine could be created as a custom level in the game if a specific in-game limit were to be removed. A player could perform any computation by playing this level, allowing infinitely many new and meaningful puzzles to be created. Furthermore, the construction is such that the level is won if and only if the Turing machine halts, proving perfect play of the game to be unattainable by any computer. The machine is found to be exponentially time-complex, and the paper concludes with a discussion of the practical feasibility of in-game computation.

KEYWORDS: Systems Software; Other; Logic in Computer Science; Computational Complexity; Turing Completeness.

■ Introduction

Baba is You is a puzzle game released in 2017. Like many puzzle games, it is turn-based, and playable characters in its levels can push objects.¹ However, *Baba is You* contains a type of object that can alter the properties of the level and change, for instance, which characters are playable and which objects are solid. Furthermore, if a level meets certain conditions, its objects can move autonomously without player input. The emergent dynamics of such a system have led to some consideration among players of the computational complexity of *Baba is You* levels.

Previous Work:

In 2019, the game was considered Turing complete on an infinite grid. The cellular automaton, Rule 110, has been proven Turing complete, and Matthew Rodriguez demonstrated how it could be simulated in a custom level.² Rodriguez's design required the *Baba is You* grid to be extended to an infinite size, though the game's maximum level size is 33 by 18 squares. Thus, his proof presented an application of general *Baba is You* rules rather than a level usable for computation in the actual game.

New Contributions:

This paper demonstrates for the first time how Turing completeness can be achieved in standard *Baba is You* by describing the first universal Turing machine that fits within the game's native level size. The effects of this proof are that one can calculate anything computable simply by playing vanilla *Baba is You* and that future expansions or online content for the vanilla game could contain levels provably unsolvable by any computer. Unfortunately, the design cannot store large Turing machine configurations because of a limitation on in-game object stacking. However, after learning of this design, the developer of *Baba is You* considered removing this limitation in a future port of the game precisely because of the potential to create such levels.³

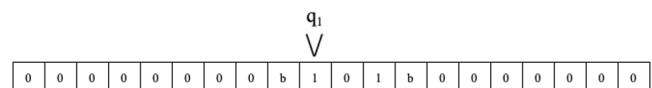


Figure 1: A representation of a finite portion of a Turing machine. The tape head is represented by a ∇ and q_1 refers to its state. It is currently above a square with the symbol “1”.

Preliminaries:

A Turing machine is a theoretical model of computing first proposed in 1936. It can be described as a tape and a tape head.

The tape is divided into squares and extends infinitely in both directions. Each square is marked with a symbol. Before starting the machine, the user may write their own symbols on a finite portion of the tape beyond which zeroes are assumed to extend infinitely in both directions.

At all times, the tape head is occupying one (and only one) square of the tape. The tape head also keeps track of a state: at all times, the tape head is in one (and only one) state. A construction is shown in Figure 1.

The tape head is capable of “writing” symbols that replace symbols on the squares it occupies, as well as moving one square to the left or to the right, before altering its own state. It can also halt the Turing machine permanently. The tape head determines which of these actions to take based on its current state and the symbol it is on. It will keep reading and editing the tape in a deterministic, repeating, and sometimes infinitely long process.

Meanwhile, *Baba is You* is a turn-based puzzle game consisting of objects on a rectangular grid. It is a Nomic game, meaning that almost all of its “rules” can be changed, from the playable character to the win condition.⁴ *Baba is You* implements its system of “rules” using “text” objects. At the start of each turn, the game examines all text objects to find which ones form what it defines as rules. Rules declare a type of object to have a specific behavior. Rules can be read left-to-right or top-to-bottom.

Figure 2 contains three text objects that create a rule, “BABA IS YOU,” which declares baba objects in the level to be playable. Since the rule exists on the level, the two babas will move with directional input from the player.

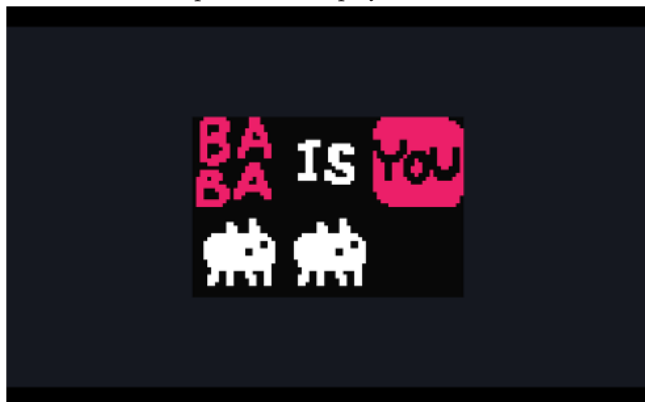



Figure 2: A level containing two “baba” objects (), as well as three text objects (which spell “BABA IS YOU”).



Figure 3: A level containing two baba objects and five text objects.

If the player somehow breaks the sentence (e.g., by separating or destroying a word), the rule that babas are playable will no longer apply, and the babas will no longer respond to directional input from the player.

Rules can be conditional, only applying to objects when they are “on” or “near” an object of a given type. For instance, the rule “ROCK NEAR BABA IS PUSH” means that all “rock” objects adjacent to baba objects are pushable.

A mechanic essential to the design of this universal Turing machine is the property “WORD.” Objects defined as “WORD” can be used in sentences as if they were their text counterparts.

The rule at the top of Figure 3 declares all babas to have the property “WORD.” Thus, both babas in the level can be used in sentences as if they were text. This allows the second line to be interpreted as “baba IS YOU”.^a Thus, both babas become playable as in the first example.

^a For clarity, text objects are named in capital letters, but all other objects are named in lowercase, even when they function as WORDs.

The Design:

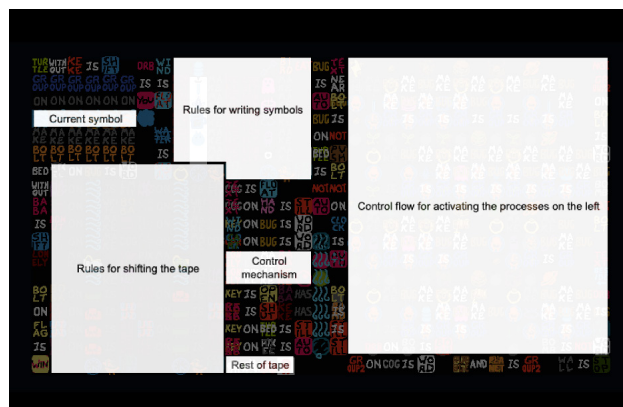


Figure 4: A schematic of the design overlaid with an image of the in-game level, meant to highlight the machine’s basic structure.

Size constraints of the level prevent an arbitrarily large physical tape from being laid out across the level with a physical tape head moving along it. Instead, the design uses overlapping objects so it can store both the tape to the left of the tape head and the tape to the right of the tape head on single squares.^b (The symbol directly under the tape head is stored separately.) This storage method can hold arbitrarily large amounts of tape in fixed amounts of space, at the cost of turning simple operations like shifting the tape into complex conversion processes. Indeed, far more of the level is devoted to implementing operations than to storing the tape itself, as seen in Figure 4.

The Turing machine the design simulates is Rogozhin’s four-state, six-symbol universal Turing machine from his 1996 paper, *Small universal Turing machines*. It comes from a set of universal Turing machines that simulate string-modification algorithms called “tag systems” that have been proven to be universal.⁵ The process requires more setup for initializing the tape but contains fewer states and symbols than a direct emulation of other Turing machines.⁶ (Rogozhin’s six-symbol machine contains the fewest total instructions and thus takes up the least in-game space in *Baba is You*.)

To closer match the *Baba is You* objects chosen to represent them, the states q_1 , q_2 , q_3 , and q_4 in Rogozhin’s machine have been renamed to q_{seed} , q_{sprout} , q_{tree} , and q_{trees} respectively. Furthermore, to better fit the arithmetic method used to express the symbols, Rogozhin’s symbols 1, b, b [right], b [left], c, and 0 have been renamed to 1, 2, 3, 4, 5, and 0 respectively.

Storing the Current Symbol:

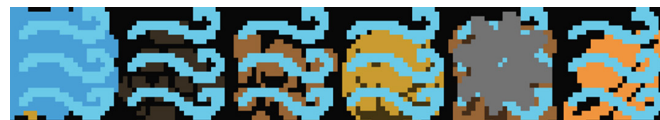



Figure 5: Part of the level featuring a cog () on a track of six wind objects. The cog is on the fifth tile, so the Turing machine’s current symbol is a 5.

The symbol the tape head is on is stored using a cog’s position on one of the six tiles in Figure 5. A cog on the first tile means that the current symbol is a 1, a cog on the second tile represents the symbol 2, and so on through the symbols 3, 4, 5, and 0.

^b This section explains how the design would work if the limit on stacking copies of a single object were arbitrarily high. Currently, the limit is 6.

Unique identifying objects on each square help the game determine the placement of the cog. The first tile (for the symbol 1) contains a dust object (☐), the second tile (for the symbol 2) contains a brick object (■), and so on through rubble (☐), rock (⬛), cliff (⬛), and planet (☐).

Storing the Rest of the Tape:

This design stores the tape to the left of the tape head using the number of babas on the cart seen in Figure 6. The number of babas is set to the base 6 number created by reading each

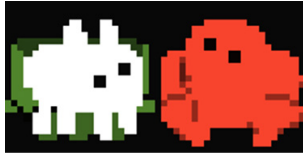


Figure 6: Part of the level featuring several babas (☐) on a cart and several kekes (⬛) on a car^c.

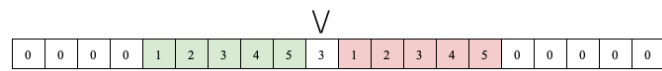


Figure 7: A sample Turing machine tape. V represents the position of the tape head, and the area from the leftmost nonzero symbol to the symbol directly to the left of the tape head is highlighted in green. The area from the rightmost nonzero symbol to the symbol directly to the right of the tape head is highlighted in pink.

symbol from the leftmost nonzero symbol to the symbol directly to the left of the tape head. The tape to the left of the tape head in Figure 7 can be read as the number 12,345 in base 6 or 1,865 in base 10. Thus, it is encoded as a stack of 1,865 babas on the cart.

Similarly, the design stores the tape to the right of the tape head using the number of kekes on the car seen in Figure 6. The number of kekes is set to the base 6 number created by reading the symbols from the rightmost nonzero symbol to the symbol directly to the right of the tape head. The tape to the right of the tape head in Figure 7 can be read (right to left) as 54,321 in base 6 or 7,465 in base 10. Thus, it is encoded as a stack of 7,465 kekes on the car.

Each finite configuration of the left or right side of the tape can thus be read as a unique number and represented with a unique number of objects.

Performing Operations:

Instead of writing a symbol, shifting the tape, and then reading the new symbol, this design executes instructions by shifting the tape, reading the new symbol, and then writing a symbol on the space it just left.

The “shift left” operation, for instance, works by dividing the



Figure 8: Another sample Turing machine tape.

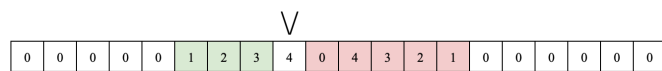


Figure 9: The Turing machine tape from Figure 8 after a “shift left” operation as this design implements it.

number of babas by six (rounding down), setting the current

symbol to the remainder, and multiplying the number of kekes by six. Because of the base six arithmetic, this serves to remove the last digit from the number of babas and set the current symbol to said digit. It also adds a 0 to the end of the number of kekes. The result is shown in Figure 9: it almost completes the shift operation but puts a 0 in the square the tape head leaves.

Writing a symbol in the square the tape head leaves is now a matter of changing the last digit of the number of kekes. It is a 0, so the design can change it to a number from 1 to 5 simply by adding that number of kekes to the car.

The right-shifting functions work equivalently to the left-shifting functions except that they divide the kekes by six, multiply the babas by six, and add up to five babas to the cart.

Splitting objects into copies is a relatively common gimmick in *Baba is You* levels. This design uses the most common technique of abusing how the game resolves conflicting rules about baba or keke transformation when such rules are created on the same turn.

Dividing stacks of objects, however, is featured in almost no *Baba is You* level solutions, because losing objects is usually counterproductive. This design accomplishes division using the “OPEN” mechanic: when an object is “opened” in *Baba is You*, it is destroyed, unless a rule specifies that the opened object “HAS” another object (in which case the opened object instead becomes the object that it “HAS”). In this design, such a rule is active only once every six turns, allowing only one in six babas or kekes to survive being opened.

Control Flow:

Typical *Baba is You* puzzles expect the rules of the level to be modified primarily by the playable character pushing text objects around the level, moving them into and out of sentences. While some in-game objects can be programmed to move autonomously, the level of control over them is insufficient to facilitate the sort of strategic text placement and displacement expected of a user.

Thus, instead of featuring movable text objects, this design lays out rows of incomplete rules that substitute one piece of text with the object the text describes, as in Figure 10. The design goes on to define as “WORD” any objects overlapping a bug object (☐) placed in the level. Thus, while the bug is on one of these objects, the rule applies because the object



Figure 10: An almost complete rule from the design. It spells “wind MAKE HAND”, where the word “WIND” is replaced with a wind object.

can be used interchangeably with text to complete the rule (in Figure 10’s case, as “wind MAKE HAND”). However, the rule deactivates as soon as the bug moves off of the object (the object will no longer be “WORD” and the game will go back to interpreting the rule as incomplete).

^c It is worth clarifying that in *Baba is You*, a stack of objects looks the same as a single object. The game knows how many objects are on each tile, but it is impossible to tell visually.

The result of this is that the bug can execute entire algorithms simply by moving along a straight path through preset arrangements of incomplete rules, as can be seen in Figure 11.

The bug is controlled by a bolt object (■) which follows a similar process of completing rules using the WORD mechanic. The bolt can follow one of 24 tracks in the level – one for each of the six symbols Rogozhin’s tape head can read in each of its four states.

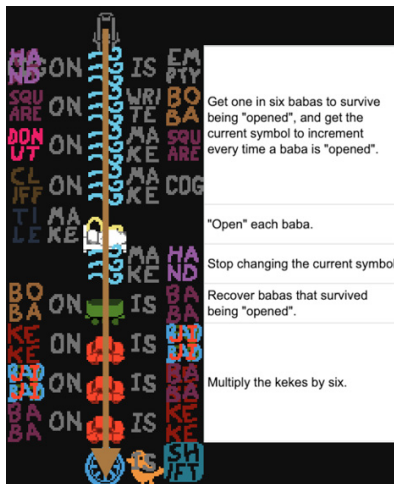


Figure 11: A bug’s path through a set of incomplete rules (left) and a rough translation of what the rules would do when the bug activates them (right). A bug summoned to move through these carefully designed rules will induce specific object interactions that simulate shifting the tape to the left.

Changing State:

At the end of its current instruction, the bolt coordinates with the cog that stores the current symbol in order to create a specific rule that forms one bolt in the square at the beginning of the Turing machine’s next instruction.

When the bolt gets to the end of its instruction, it will define objects representing the Turing machine’s next state as part of a custom “GROUP”. For instance, to switch into the q_{seed} state, it will activate the rule “seed IS GROUP”.

Meanwhile, the cog that stores the tape head’s current symbol (as shown in Figure 4) activates a rule that directs objects of said GROUP to spawn bolts if they overlap with objects that represent the tape head’s current symbol. For instance, if the current symbol is 1 (represented by dust objects) the cog would form “GROUP ON dust MAKE BOLT”^d. Continuing the previous example, this would mean that SEED ON DUST MAKE BOLT.

The result of such a rule is that the next bolt is created in squares containing both an object representing the Turing machine’s next state and an object representing the Turing machine’s current symbol. In this design, there will only ever be one such square in the level, and it will always be directly above the rules for the appropriate next instruction.

Halting:

A level is won in *Baba is You* when an object defined as AUN and an object defined as WIN both occupy the same tile. The design contains the rules BOLT ON FLAG IS YOU and BOLT ON FLAG IS WIN, so the level is won instantly (and the Turing machine stops) when the bolt moves onto a

flag. The design contains these flags at the end of instructions in which the Turing machine is to halt.

Setup:

When the Turing machine is first loaded, there are neither babas on the cart nor kekes on the car, and the bolt is in a paused state. There is a playable “orb” that the user can control (i.e., “ORB IS YOU.”) By moving it, the user can add any number of babas to the cart and any number of kekes to the car. The starting current symbol, however, is always assumed to be 1, as Rogozhin’s machine expects to only start on a 1.

By controlling the orb, the user may also unpause the bolt and start the machine. Doing so destroys the playable orb so the user cannot tamper with the tape while the machine runs. This sets the machine into a completely deterministic state – the only legal move on all subsequent turns is to wait (and to let the autonomous parts of the level run their courses).

Reading the Tape:

The user may count how many babas are opened and how many kekes are opened and thus keep track of the entirety of the tape. If the user ignores the tape for a while and then starts reading at an arbitrary point in time, they can figure out the contents of the tape as soon as they watch long enough to see one left shift and one right shift occur.

The Full Construction:



Figure 12: The entire Turing machine level when it is first loaded.

■ Results and Discussion

Time-complexity of the Machine:

As explained in a previous section, writing symbols requires adding between zero and five babas or kekes to the stacks of objects. Adding zero babas or kekes is equivalent to leaving the stack unchanged, and will require zero turns, while adding between one and five babas will take between three and seven turns.

However, the slowest part of the machine’s execution is performing the shift operations. Multiplying the babas or kekes by six will take a fixed twelve turns.

But dividing the babas or kekes by six will take one turn per baba or keke. In the best case, the symbols on the tape that the tape head moves towards read “1000...”, which, using the base 6 conversion explained in a previous section, will be stored as $6^n - 1$ babas or kekes, where n is the number of symbols (so opening all of them would take $6^n - 1$ turns)^e.

In the worst case, the symbols on the tape that the tape head moves towards read “5555...”, which will be stored as

^d The cog would accomplish this using a similar process to that of the bug and bolt: by letting the dust object in the middle of the sentence be used as a WORD so it can finish an otherwise incomplete rule.

^e Of course, when the tape the tape head moves towards is completely blank (and thus stored as zero babas or kekes), opening them will take zero turns (and not the “one sixth of a turn” that the best-case model suggests).

$6^n - 1$ babas or kekes, where n is the number of symbols (so opening all of them would take $6^n - 1$ turns).

Thus, the number of turns to execute an instruction, where n is the number of symbols the tape head moves towards, can be expressed as:

$$(\text{number from } 0 \text{ to } 7) + 12 + (\text{number from } (6^n - 1) \text{ to } (6^{n-1} - 1))$$

When the input repeat delay is set to a minimum, holding the spacebar will allow turns to run about nine times per second, about as fast as a human tapping the spacebar repeatedly. As shown in Table 1, this combined with the exponential time-complexity of the shift operation has alarming implications for the practical efficiency of the machine.

On *Baba is You* Limits:

Table 1: The time-complexity of the machine.

Length of nonzero tape towards which tape head moves	Turns to execute instruction	Approximate time to execute instruction
0	12 to 19	1.33 to 2.11 seconds
2	18 to 54	2.00 to 6.00 seconds
4	228 to 1314	25.33 seconds to 2 minutes, 26 seconds
6	7,788 to 46,674	14 minutes, 25 seconds to 1 hour, 26 minutes
8	279,948 to 1,679,634	8 hours, 38 minutes to 2 days, 4 hours
10	1,007,708 to 60,466,194	12 days, 23 hours to 2 months, 17 days

The limit on stacking copies of the same object seems unusually low. Many limitations in *Baba is You* are very large and seem to be determined directly by memory and performance (meaning that they might increase if *Baba is You* was ported to more robust systems). Levels will end with a “Too Complex!” message if one of the following conditions occurs:

- There are more than 5,000 first words of rules in the level,
- There are more than 2,000 objects in the level,
- A single rule has more than 3,000 ways it could be read (because of combinatorics with overlapping text), or
- A “level” object from a custom world is transformed into more than 50 objects simultaneously.

Furthermore, there is no limit on overlapping objects of different types.

These generous restrictions allow things like Five Nights at Freddy’s, Pac-Man, Tetris, Bloons Tower Defense, Donkey Kong, sliding puzzles, Bomberman, and even a variant of Super Mario Brothers to be created in *Baba is You*.⁷⁻¹⁴ The advanced projects that push *Baba is You* to its literal limits show that the game was indeed willing to sacrifice performance to allow for creativity. These projects lag the game significantly but are still allowed by the constraints of *Baba is You*.

However, levels in *Baba is You* have a set maximum size of 33 spaces wide by 18 spaces tall. This limit is more restrictive – complex custom levels (including this one) almost always use maximum size levels and fill their entireties. Despite this, there are multiple reasons why the developer, Arvi Teikari, would enforce this limit. Perhaps they believed that vast levels (or even the very concept of scrolling) departed from the puzzle-based essence of *Baba is You*. Or maybe they did not want hubs containing many smaller areas to fit in single levels, in-

stead wanting players to utilize the built-in “custom world” mechanic to hold small areas.

The limit on stacks of identical objects (currently 6) was likely set merely because Teikari did not see the potential of utilizing large stacks of identical objects. This may have been because stacks of the same object in *Baba is You* function identically to single objects in almost all cases except OPEN/SHUT. For instance, a stack of multiple babas will move as if it were one baba, push things as if it were one baba, and can be destroyed by a single object (e.g., one skull that IS DEFEAT) as if it were one baba. Moreover, in most *Baba is You* puzzles, working with separated objects is strictly advantageous over working with overlapping objects, especially if they are YOU.

However, allowing arbitrarily large stacks of identical objects (because it enables the full functionality of this design) allows *Baba is You* to support new logical and mathematical puzzles that would not otherwise work in a block-pushing game. For example, consider a custom world where each level asks the player to compute a number, say, the sum of the first 20 primes. The player may input a guess at the number into the level by creating that number of objects. The level is won if and only if the number inputted is equal to the number that the level wants (in this case, 77). The level checks each attempt by repeatedly dividing it by ten and comparing the remainders with hardcoded ones for the answer (in this case, seven and seven). This comparison process is hidden from the player’s view with the HIDE property to prevent cheating. The player is instead supposed to solve the number puzzle by exiting the level, traversing the custom world to enter the universal Turing machine level, and calculating the answer there. After finding the answer to the computation, the player may go back to the number puzzle level and input the answer.

Indeed, removing the stacking limit allows for infinitely many significant new puzzles. The puzzles would have to already be solved beforehand, but of course, this could also be done using this universal Turing machine level. If the stacking limit were removed, any question solvable by computation whose answer is somehow expressible as a number could be turned into a playable, winnable *Baba is You* level that can be beaten without leaving the game. These puzzles could include graphing the Mandelbrot set to a certain precision, running von Neumann’s universal constructor for a set number of turns, or even (once this is solved) attempting to find the winning first move in chess.

Admittedly, even calculating addition in this design would require excruciatingly tedious conversions – after a Turing machine is created, it would have to be converted into a 2-tag system, which would need to be formatted as an input for Rogozhin’s machine. Any computation a user insisted on performing in *Baba is You* would require laying on the virtual starting tape an unreadable symbol monstrosity and then waiting cosmic amounts of time for single instructions to complete.

However, it is worth noting that Turing machines are themselves extremely inefficient compared to modern forms of computation. Contributions of this paper’s nature are valued, if at all, because they demonstrate the expressive potential of

the Turing-complete systems and not because the operation of the simulated machines will cause paradigm shifts in how the systems are actually used.

Teikari learned of this design in August of 2022 and said it inspired them to consider removing the stacking limit if the *Baba is You* were ported to new platforms.³

The Unsolvability of Baba is You:

If the stacking limitation were removed, *Baba is You* would be computationally unsolvable. Any Turing machine could be simulated in this level, and a move (if it starts the Turing machine and destroys the playable orb character) could put the level into a state where it will be won if and only if the Turing machine halts. This proves that *Baba is You* without the stacking limitation is unsolvable: a computer that could decide with certainty whether a *Baba is You* move is winning would be able to solve the halting problem.

Comparison with Rodriguez's machine:

Rodriguez's design simulates the cellular automaton Rule 110, which was proven Turing complete in 2004 by Matthew Cook. Cook created a way for Rule 110 to simulate any "cyclic tag system," which in turn simulates a regular tag system.¹⁵ Regular tag systems were proven Turing complete in 1961 by Marvin Minsky.¹⁶

Minsky's tag systems are linearly larger than the Turing machines they simulate, and Cook's cyclic tag systems are linearly larger than the regular tag systems they simulate. However, Cook's starting configurations of Rule 110 must contain two infinitely long patterns no matter which cyclic tag systems they simulate. If the patterns were to be abbreviated, the cyclic tag systems might stop before the Turing machines they are simulating have halted.

This creates a practical problem. Rodriguez proposes that the starting Rule 110 configurations for his level be created one object at a time, either in the level editor or by playing the level itself. The user must, therefore, manually create an infinite number of objects in the level before the Rule 110 simulation can even be started. Thus, even if *Baba is You* were, as Rodriguez proposes, extended to an infinite grid, his design as it is formulated is not only impractical but entirely impossible to run.

This design improves on Rodriguez's in one more way. In Rodriguez's design, the Turing machine has halted when a particular pattern appears in the level. The user may find it tedious to check large swaths of the level every turn for a fourteen-object-long pattern. In this design, on the other hand, it is readily apparent when the Turing machine has halted, because this wins the level (which makes the game play a sound and display "CONGRATULATIONS!" before returning the player to the custom world).

Conclusion

This paper has demonstrated that if a hardcoded stacking limit is removed from the game, a Turing complete custom level can be created in *Baba is You*, meaning that the game is capable of universal computation. It has found the proposed custom level vastly superior to a previous attempt at Turing completeness in the game. Furthermore, it has proposed theories about possibilities for unprecedented computation-based

puzzle levels that the design unlocks. Moreover, it has proven that a game long known to be challenging for humans would be ultimately unsolvable by computers.

Acknowledgments

Many thanks to Alvin Shi for his guidance on the paper's structure, and to Dr. Jim Purbrick, Dr. Chaitanya Mishra, and Dr. Dan Grossman for reviewing this paper and providing key guidance on what to simplify and what to clarify. Thanks to Arvi "Hempuli" Teikari for reading a first draft of this paper and somewhat popularizing the machine.

References

1. Game Maker's Toolkit. How Baba Is You Makes Brain Busting Puzzles. <https://www.youtube.com/watch?v=7zLwa4bztWs> (accessed 2023-05-25).
2. Rodriguez, M. BABA IS TURING COMPLETE: A Sketch of a Proof (v2) https://www.twitlonger.com/show/n_1sqrh1m (accessed February 1, 2023).
3. You, B. I. And re: The stacking limit; ideally in a future reimplement of the engine stacked objects would be combined into a single object with knowledge of the stack size instead of being deleted, allowing for arbitrarily-sized stacks. it'd be a big undertaking but it's in my mind [sic]
4. Suber, P. In *The Paradox of Self-Amendment: A Study of Law, Logic, Omnipotence, and Change*; Peter Lang Publishing, 1990; 362.
5. Rogozhin, Y. Small Universal Turing Machines. *Theoretical Computer Science*. [Online] **1996**, *168*, 215-240. Science Direct. <https://www.sciencedirect.com/science/article/pii/S0304397596000771> (accessed February 5, 2023).
6. Turing, A. On Computable Numbers, with an Application to the Entscheidungsproblem (1936). *The Essential Turing* **2004**, 244. DOI:10.1093/oso/9780198250791.003.0005. Turing lays out his own universal Turing machine in the same paper where he introduces regular Turing machines. It is very difficult to read, primarily because of his (by modern standards) unusual language and syntax used to describe them (e.g., he refers to as "m-configurations" what nearly all computer scientists now call "states").
7. Su, C. J.-Z. I Created the Entirety of Five Nights at Freddy's in Baba Is You. <https://steamcommunity.com/app/736260/discussions/0/3372657079037273155/> (accessed 2023-05-25). Although the mechanics are ported faithfully (Bonnie and Chica move along the correct paths, Freddy can be camera stunned, and blocking Foxy with the door drains power), the port of a point-and-click game into a tile-based puzzle game renders it very confusing, even to series veterans.
8. Germaphobe2. Pac-Man in Baba Is You (Custom Level). https://www.youtube.com/watch?v=97BhtVA0E_0 (accessed 2023-05-25).
9. CavoX5. Baba Is You Improved Tetris. <https://www.youtube.com/watch?v=FEKD3MM5rsA> (accessed 2023-05-25).
10. TeslaPenguin1. Baba Is Bloon. https://www.youtube.com/watch?v=g1reHDw_8rY (accessed 2023-05-25).
11. Semicolon, G. Donkey Kong Recreated in Baba Is You (Custom Level). <https://www.youtube.com/watch?v=v1m26xUYeRY> (accessed 2023-05-25).
12. Mu, M. [Baba Is You] New Adventures - Arcade A - Baba hour (449b). <https://www.youtube.com/watch?v=YVIBMS0pgdk> (accessed 2023-05-25).
13. GincenVeez. Bomberman in Baba Is You. https://www.youtube.com/watch?v=IHOTyF7S_vg (accessed 2023-05-25).
14. Mu, M. [Baba Is You] New Adventures - Arcade G - Jump up, Babastar (Orb) (449b) <https://www.youtube.com/watch?v=rbuJFrDS1kI> (accessed 2023-05-25).

15. Cook, M. A concrete view of Rule 110 computation. <https://arxiv.org/abs/0906.3248> (accessed Feb 5, 2023).
16. Minsky, M. Recursive Unsolvability of Post's Problem of "Tag" and Other Topics in Theory of Turing Machines. *The Annals of Mathematics* 1961, 74 (3), 437–455. Minsky published a simpler second proof in 1964.

■ Author

Caleb Su is a senior at Mercer Island High School in Washington State. He is currently creating a working Python interpreter in Scratch and hopes to study computer science in college.

How Does Trust In Government Institutions Affect The Demand For Cryptocurrencies?

Veer Krishan Choudhari

Vidyashilp Academy, Govindapura, Yelahanka, Bangalore, Karnataka, India - 560064

Mentor: Mimansa Bhairati

ABSTRACT: A cryptocurrency is a digital, decentralized currency that runs on networks based on blockchain technology. The study covers three years, from 2018 to 2021, during which cryptocurrencies reached monetary values of up to 66,002 USD. However, there still needs to be a greater understanding of these digital assets and their underlying technology, including how they work and why people are driven to invest in them. I hypothesize that trust in institutions affects the demand for cryptocurrencies in different regions across the globe. I analyze data on cryptocurrency usage and adoption, and provide insights into the factors that drive the demand for cryptocurrencies. The findings of this study are important for policymakers, financial institutions, and investors seeking to understand the relationship between trust in institutions and the demand for cryptocurrencies. Finally, this paper also contributes to the ongoing discourse on the role of cryptocurrencies in the global financial system.

KEYWORDS: Behavioral and Social Sciences; Digital Currencies; Cryptocurrencies; Trust; Trust in Institutions; Factors affecting demand for Cryptocurrencies.

■ Introduction

In this study, I focus on cryptocurrencies. Cryptocurrencies are a form of decentralized digital currency that rely on complex blockchain technology for their operation.¹ This technology uses encryption algorithms to create alternative payment systems and virtual accounting systems. Unlike traditional currencies, they are highly volatile and not managed directly by central banks. As a result, they can be easily transferred from one place to another and have the potential to be quite profitable.

Due to the unpredictability of cryptocurrencies, investing in them requires careful consideration and research. Additionally, the history of cryptocurrencies is shrouded in mystery, with their origins and early development still needing to be discovered.² Due to this, the relationship between trust in institutions and cryptocurrencies is unclear.

Cryptocurrencies are also important as their transactions are fast, digital, secure, and worldwide, and due to various contingencies, fraud is negligible. Cryptocurrencies use various encryption technologies, such as public-key cryptography, hash functions, and digital signatures, to secure transactions and prevent counterfeiting. It is also important because of the digital platform it uses, which is known as blockchain. Blockchain is a platform that allows cryptocurrencies and their digital tokens to operate within it.³ Blockchain technology is used by cryptocurrency to provide a decentralized, secure, transparent, and efficient system for recording and verifying transactions. Any transaction capable of being recorded can look to the use of blockchain, whether medical records, immigration information, birth certificates, insurance policies, etc. All of their data can be stored over a blockchain. According to various articles, Cryptocurrencies have created a paradigm shift in how we view

money. The way we look at buying it and the way we look at spending it.³

This currency goes against one of the founding ideologies of modern society, and that is trust. Human beings have been pioneers throughout history in promoting trust.⁴ We have created multiple organizations that push individuals and societies towards trust.

'Trust' is defined as a firm belief in a particular organization or idea, leading to complete reliability.⁵ While an 'institution' is defined as any establishment that has been set up for a religious, educational, professional, or social purpose.⁶ For example, when citizens of a country are voting, they usually choose a reliable candidate who provides them a sense of comfort; therefore, they trust their country in that candidate's hand and vote for them.

In this literature review, I focus on trust in public institutions and its effect on the demand for cryptocurrencies. I define trust as the trust that citizens of a country have in their government and its institutions. These include public banks, government-issued standardized currencies, and other government-owned or managed institutions.⁷ The psychological phenomenon of trust in the public is affected by numerous factors that range from government policies and programs to the country's economic history.

I base this study on the observation that the value of various cryptocurrencies, such as Bitcoin, rose significantly during the pandemic, leading to the number of investors in it increasing rapidly. This is where the relation between trust in institutions and cryptocurrencies comes in. Most surveys show that the pandemic decreased confidence in public institutions as governments were considered incompetent and unreliable when their lack of infrastructure to fight the virus was exposed. This, in turn, led to a reduction in the usage of public institutions

and led to people investing in decentralized and unstandardized assets such as cryptocurrencies.⁸ This resulted in a massive surge in their value, with Bitcoin increasing in value by 1,788% from Jan 2019 - Jan 2021.

Through this literature review, I will investigate how trust in public institutions affects the demand for cryptocurrencies and the various factors affecting this phenomenon.

■ Discussion

Demand For Cryptocurrencies:

A cryptocurrency is a digital currency in which all transactions are maintained by a decentralized system using cryptography technology. They are based on digital coding, also known as blockchain technology, a decentralized, distributed ledger system that is used to record transactions securely and transparently.⁹ Cryptocurrencies are generated through a process called mining. This does not refer to mining in caves but instead to massive, decentralized networks of computers located all over the world, which initiate a cryptocurrency transaction; the transaction is broadcast to the network of users, who then validate it using complex mathematical algorithms. After the user solves the algorithm and validates the transaction, the user is rewarded with a certain amount of cryptocurrency, which is newly created as a reward for their efforts. Investments can be made in cryptocurrencies through various mobile apps and online platforms such as Coinbase, Binance, Kraken, Robinhood, and eToro. These platforms allow users to buy, sell, and store cryptocurrencies.¹⁰ The value of cryptocurrencies differs from one type to another. As of 2022, over 1,583 types of cryptocurrencies are listed in the market, which all differ in their code.¹¹ Some of the most popular types include Bitcoin, Ethereum, Tether, and Dogecoin.¹² Another thing to consider is that each Cryptocurrency is in limited supply; Bitcoin, for example, only has a stock of 21 million coins, of which 90% have already been produced. Bitcoin is in short supply because of its design. The creator of Bitcoin, known by the pseudonym Satoshi Nakamoto, set a limit on the total number of bitcoins that can ever exist. This limit is 21 million bitcoins, which is hard-coded into the Bitcoin protocol.¹³ Cryptocurrencies work very differently from any centralized or government-regulated form of currency. It does not have a geographically or politically discreet real economy in which it is dominant, as stated in the paper written by Brett Scott.¹⁴ This has led to people characterizing cryptocurrencies as digital assets instead of currency. However, there is no denying that cryptocurrencies are a perfect alternative to the current system of government-regulated currency.

These digital currencies have many advantages, including facilitating cheaper and faster money transfers, and they are useful as remittance tools. As they are decentralized, they do not collapse at a single point of failure. Cryptocurrencies showcase a high-risk and reward system, sometimes leading to high profits. Bitcoin, one of the most popular cryptocurrencies, has been used as an intermediary currency to help facilitate trade between other currencies. It also has the potential to facilitate small-scale international commerce.¹⁵

However, with these advantages come some drawbacks. These include cryptocurrencies' highly unpredictable nature and how quickly their value can rise and fall. Cryptocurrencies are thus highly volatile. Another major drawback is that digital currencies need to be regulated. The lack of regulation of cryptocurrency refers to the absence of clear and specific rules and laws that govern the use and trading of cryptocurrencies. In many countries, investments in cryptocurrencies are illegal. Another major factor that leads to decreased cryptocurrency usage is highly conservative people, who are cautious about changing technology. For example, the older generation is apprehensive about using technology and investing online as they like to do things 'the old-fashioned way.' Lastly, very little is known to the general public about the origin of cryptocurrencies and the method by how their value is decided. This goes against the current system of centralized currencies, where it is known which factors affect the value of that currency, and its regulators are known in the form of the government. It also goes against one of the founding ideologies of human society, and that is trust. Also, since it is not well known who runs these currencies, investors usually invest knowing only the high risk involved with dealing with this currency.¹⁶

Now that we understand what cryptocurrencies are and how they work, we have to look into the factors affecting the demand for them.

The main factor that affects the demand for cryptocurrencies is their value: the higher the value, the more demand. Indeed, this is a fairly obvious factor. The next factor which affects cryptocurrencies is their limited supply. The currency's demand will increase if there is a limited supply of cryptos. Meanwhile, if more cryptos are supplied, the demand will decrease.¹⁷

Another major factor contributing to the demand for cryptocurrencies is the psychological factor called 'fear of missing out' and curiosity. Fear of missing out is the feeling of apprehension that one is missing out on information, events, experiences, or life decisions that could make one's life better.¹⁸ This factor indicates that a person will invest in crypto simply because they do not want to miss out on purchasing them. They believe that if they do not invest in cryptocurrencies, they will live to regret it. This psychological factor is especially apt for these digital currencies as they are something that not only has great potential but also are something very different from anything that exists in the world at this moment. This leads to curiosity and more people investing in cryptocurrencies and therefore leads to higher demand for them.¹⁹

Another factor that affects the demand for cryptocurrencies is the ease of transfer of money from one place to another. According to Brett Scotts, cryptocurrencies are one of the most popular means of transferring money as they have the potential for small-scale international trade and to be used as an intermediary currency between other, more dominant currencies. Thus, they may be useful for remittances. Also, Bitcoin and other cryptocurrencies also have the potential to serve as mobile wallets and as a replacement currency for countries with an unstable national currency. Various other uses of Cryptocurrencies also affect their demand.

I hypothesize that a decrease in people's trust in their government and institutions affects the demand for cryptocurrencies. The main reason for this is when people lose confidence in their government, and the government's monetary institutions. This could be due to various reasons, including but not limited to the head of the government then, lack of effort to improve the country's financial state after previous financial issues, poor dealing with the pandemic, and the form of government in which the person lives. All these issues lead to more and more people moving away from centralized currencies and moving to non-government-regulated and decentralized digital currencies.²¹ I will discuss this in more detail in the section titled – How does trust in institutions affect the demand for cryptocurrencies?

Trust In Institutions:

Trust in institutions is essential for the progress of any country. Trust is the very foundation upon which the world's public institutions are built. Trusting in a public institution is important as it helps maintain social cohesion.²² Simply put, when the public trusts government institutions, it leads to the success of the government's policies and regulations. If trust in these institutions were lost, it would lead to chaos in that specific region. Trust in institutions is also crucial in providing a sense of safety for citizens of that country.²³

Trust in institutions has always been unpredictable, as it depends not only on people's beliefs but also on the reliability of the government. This trust also varies from country to country. Countries with financial issues in the past usually have citizens who need to be more trusting in their public institutions. While countries, where the government has been more stable tend to have citizens who are more trusting of their institutions.²⁴

During the pandemic, it was observed that there was a massive decline in the trust in the government and its institutions. It was recorded to be the lowest that this trust has ever been. This was because governments needed to handle the COVID-19 virus better. People felt as though their governments were incompetent and unreliable.²⁵ The methods of stopping the spread of the virus were considered poor, and the lack of proper infrastructure in many countries was exposed to the waves of the virus as there needed to be more oxygen cylinders or beds in hospitals for most of the population in many countries. In European countries, millions of people saw a pay cut or lost their jobs. These people were supposed to be reimbursed by the government. However, when 3,000 households in Italy were surveyed, it was shown that only 12% of people were fully compensated.²⁶ This led to an even greater decline in trust in public institutions.

As we move towards a new normal, trust must be rebuilt between the government and the public. This will take a very long process. Matthew Bishop takes the view,²⁷ and examines various factors which need to be fixed to rebuild trust in governments, such as the construction of better health facilities, promotion of social welfare, and compensation for all economic losses.

In conclusion, when there is a decline in the trust in institutions, people move away from the conventional centralized currencies from governments to decentralized cryptocurrencies, which are almost entirely different from the current system of currencies. Only little is known about how cryptocurrencies function and their existence, but investing in them completely abandons the ideology of trust. As discussed in a paper by economist Greg Rosalsky,²⁸ in which, he talks not only about the importance of trust in our society but also about how we are moving towards cryptocurrencies and their digital blockchain coding, which does not focus on trust.

How Does Trust in Institutions Affect the Demand for Cryptocurrencies?:

According to most sources, cryptocurrencies were first introduced in the year 1990 through the first-ever cryptocurrency called eCash.²⁹ However, until 2018, most cryptocurrencies were almost entirely worthless and showed minimal real potential to be worth any amount. However, since 2019 various cryptocurrencies have gone up in value to almost 50,000 US Dollars, as per CNBC, and some even surpassed this value.³⁰ This coincidentally is the time when the pandemic began. The theory that I want to put forth is that during the pandemic, due to various governments worldwide failing to control the COVID-19 outbreak, there was a massive decline in the trust citizens had not only for their government but also for its institutions. Trust in institutions has always been inconsistent, sometimes citizens trust their government altogether, and sometimes they need to trust them more. However, the pandemic led to one of the most significant government trust declines ever recorded.³¹ This directly relates to a massive increase in the demand for cryptocurrencies.

Trust in institutions also depends on the country's financial past and present government policies. The article published by IE University's global and public affairs shows this.³² Trust in institutions varies from country to country. This is especially true for Latin American, European, and North American countries. The divide is caused in countries where central banks experience lower social trust. These countries have citizens more open to adopting new digital currencies issued by alternative, decentralized institutions.

According to this survey, 27% of Brazilians, 20% of Argentinians, and 18% of Mexican citizens own cryptocurrencies in Latin America. For those citizens who do not own cryptocurrencies in these three countries in Latin America, the study found that the main reason for not holding digital currencies was not due to a lack of interest but simply needing to know how to buy them. In fact, 79% of Argentinians, 78% of Mexicans, and 75% of Brazilians, who do not yet own cryptocurrencies, would be willing to own a digital currency. The reason for this high demand for cryptocurrencies is due to low trust in the government and its institutions. This lack of confidence comes due to the government's response to the financial crisis, as many of the people surveyed felt that authorities had not taken meaningful steps in fixing the issues caused in the year 2008, the year of the great recession. As a result, these countries' governments remain highly unstable, leading to low trust in institutions and higher demand for digital currencies.

On the other hand, most European and US citizens do not own cryptocurrencies because they consider them too risky. Only 29% of Germans, 32% of Britons, 33% of US, 36% of French, and 49% of Spaniards are willing to use a new effective cryptocurrency. These results prove that countries with a more stable monetary history are less open to new digital currencies. These countries also have much more stable and efficient governments and therefore have greater trust in their institutions, leading to lower demand for cryptocurrencies.

This comparative survey further suggests that trust in institutions plays a part in the demand for cryptocurrencies.

One major problem that has come up while talking about the demand for cryptocurrencies is their regulation by the government and the fact that in many countries, trading, owning, and investing in cryptocurrencies has become illegal. The main reason is that these countries' governments have taken this step because they are wary of cryptocurrencies' high volatility and decentralized nature.³³ These countries where cryptocurrencies are illegal can thus not come under this theory's classification.

Lastly, high social trust lowers the demand for various financial assets, including cryptocurrencies. This can be seen especially in China according to a research study about this topic.³⁴ In this research study, we see that higher trust in institutions in China has a negative impact on cryptocurrencies. In comparison, lower trust in social institutions positively impacts cryptocurrencies.

All this data and research show that my inference is correct and that trust in institutions does affect the demand for cryptocurrencies.

■ Conclusion

Therefore, in this study, I can provide evidence to support my hypothesis that trust in Institutions impacts the demand for cryptocurrencies. There is an inverse relationship between them; in areas with a higher rate of trust in public institutions, there is a lower demand for cryptocurrencies. On the other hand, in areas where the rate of trust is lower in public institutions, the demand for cryptocurrencies is high.

However, as trust in institutions is dynamic and likely to change over time, it is difficult to find regions where the demand for cryptocurrencies is consistently high over a long period of time. Further, as shown by the data, regions with issues with their governments remain the regions with the highest demand for cryptocurrencies. This is because citizens of these regions usually feel that their government will let them down again, leading them to invest in a currency not regulated by them.

This is the conclusion brought out by my research study.

■ Acknowledgments

I take this opportunity to thank the management of Lumiere for allowing me to undertake this research study in the form titled "How does trust in government institutions affect the demand for cryptocurrencies?"

I want to express my deepest gratitude to my mentor, Mrs. Mimansa Bhairati, for all the guidance, and continued encouragement, and support throughout this study.

I would also like to express my gratitude to my reviewers, publication specialist Tyler Moulton, writing coach Caryn Mckenzie and program manager Shreya Urvashi without whom this project would not have been possible. Only with the help of their feedback have I been able to complete this literature review.

Last but not least, I would like to thank and express my regards to my family and all my friends for their exclusive contributions, without which the project would not have been completed efficiently.

■ References

1. Bornstein, Brian H., and Alan J. Tomkins. "Institutional Trust: An Introduction." SpringerLink. Springer International Publishing, January 1, 1970. https://link.springer.com/chapter/10.1007/978-3-319-16151-8_1.
2. "Dataspac: Decrypting Crypto: Analyzing Trust, Corruption and the Formation of Speculative Bubbles in the Bitcoin Market." Princeton University. The Trustees of Princeton University. Accessed August 4, 2022. <https://dataspac.princeton.edu/handle/88435/dsp013n204180t>.
3. *Why is crypto so important and should I care?* Conyers. (2021, November 15). Retrieved September 4, 2022, from <https://www.conyers.com/publications/view/why-is-crypto-so-important-and-should-i-care/>
4. Bornstein, Brian H., and Alan J. Tomkins. "Institutional Trust: An Introduction." SpringerLink. Springer International Publishing, January 1, 1970. https://link.springer.com/chapter/10.1007/978-3-319-16151-8_1.
5. Oxford languages and Google - English. Oxford Languages. (n.d.). Retrieved August 4, 2022, from <https://languages.oup.com/google-dictionary-en/>
6. Bornstein, Brian H., and Alan J. Tomkins. "Institutional Trust: An Introduction." SpringerLink. Springer International Publishing, January 1, 1970. https://link.springer.com/chapter/10.1007/978-3-319-16151-8_1.
7. Bornstein, Brian H., and Alan J. Tomkins. "Institutional Trust: An Introduction." SpringerLink. Springer International Publishing, January 1, 1970. https://link.springer.com/chapter/10.1007/978-3-319-16151-8_1.
8. "Dataspac: Decrypting Crypto: Analyzing Trust, Corruption and the Formation of Speculative Bubbles in the Bitcoin Market." Princeton University. The Trustees of Princeton University. Accessed August 4, 2022. <https://dataspac.princeton.edu/handle/88435/dsp013n204180t>.
9. Bornstein, Brian H., and Alan J. Tomkins. "Institutional Trust: An Introduction." SpringerLink. Springer International Publishing, January 1, 1970. https://link.springer.com/chapter/10.1007/978-3-319-16151-8_1.
10. "Cryptocurrency." Wikipedia. Wikimedia Foundation, August 2, 2022. <https://en.wikipedia.org/wiki/Cryptocurrency>.
11. Aguirre, Fernando Gonzalez. "Why Are There So Many Cryptocurrencies?" Bob's Guide, May 13, 2021. <https://www.bobsguide.com/articles/why-are-there-so-many-cryptocurrencies/>.
12. Stump, Westley. "9 Of the Most Well-Known Types of Cryptocurrencies." Equity Trust, May 9, 2022. <https://www.trustetc.com/blog/cryptocurrency-types/>.
13. SPOTLIGHT / Oct 26, 2021. "Times of India." The Times of India. TOI. Accessed August 4, 2022. <https://m.timesofindia.com/business/cryptocurrency/blockchain/tokenomics-demand-and-supply-of-cryptocurrencies/articleshow/87273549.cms>.
14. How can cryptocurrency and blockchain technology play a role in ... (n.d.). Retrieved August 7, 2022, from <https://www.weusecoi>

- ns.org/assets/pdf/library/Cryptocurrency%20and%20Blockchain%20-%20Role%20in%20Building%20Social%20and%20Solidarity%20Finance.pdf
15. SoFi. "12 Benefits of Cryptocurrency in 2022." SoFi. SoFi, February 2, 2022. <https://www.sofi.com/learn/content/benefits-of-crypto/>.
 16. "Top 5 Disadvantages of Cryptocurrency." How many disadvantages of cryptocurrency | Motilal Oswal. Accessed August 7, 2022. <https://www.motilaloswal.com/blog-details/top-5-disadvantages-of-cryptocurrency/20617>.
 17. Bloomenthal, Andrew. "What Determines Bitcoin's Price?" Investopedia. Investopedia, July 8, 2022. <https://www.investopedia.com/tech/what-determines-value-1-bitcoin/#:~:text=The%20combination%20of%20supply%2C%20demand,significant%20factor%20affecting%20cryptocurrency%20prices>.
 18. "Fear of Missing Out." Wikipedia. Wikimedia Foundation, August 1, 2022. https://en.wikipedia.org/wiki/Fear_of_missing_out.
 19. Limited, Bangkok Post Public Company. "Cryptocurrency Curiosity Ramping Up." <https://www.bangkokpost.com>, March 18, 2022. <https://www.bangkokpost.com/business/2281054/cryptocurrency-curiosity-ramping-up>.
 20. How can cryptocurrency and blockchain technology play a role in ... (n.d.). Retrieved August 7, 2022, from <https://www.weusecoins.org/assets/pdf/library/Cryptocurrency%20and%20Blockchain%20-%20Role%20in%20Building%20Social%20and%20Solidarity%20Finance.pdf>
 21. IE University. "Lack of Trust in Public Institutions Leads to Cryptocurrencies." IE University. IE University, January 31, 2020. <https://www.ie.edu/university/news-events/news/lack-trust-public-institutions-leads-higher-use-cryptocurrencies/>.
 22. Rosalsky, Greg. "Stranger Danger: An Economist's Guide to Overcoming Distrust." NPR. NPR, April 6, 2021. <https://www.npr.org/sections/money/2021/04/06/984040411/stranger-danger-an-economist-s-guide-to-overcoming-distrust>.
 23. "Key Resources." OECD. Accessed August 7, 2022. <https://www.oecd.org/governance/trust-in-government/>.
 24. "Trust in Public Institutions: Trends and Implications for Economic Security | DISD." United Nations. United Nations. Accessed August 7, 2022. <https://www.un.org/development/desa/dspd/2021/07/trust-public-institutions/>.
 25. "How the Coronavirus Crisis Affects Citizen Trust in Institutions and in ..." Accessed August 7, 2022. <https://ejpr.onlinelibrary.wiley.com/doi/10.1111/1475-6765.12419>.
 26. "Working Paper No 646 - CSEF." Accessed August 7, 2022. <https://www.csef.it/WP/wp646.pdf>.
 27. Rosalsky, Greg. "Stranger Danger: An Economist's Guide to Overcoming Distrust." NPR. NPR, April 6, 2021. <https://www.npr.org/sections/money/2021/04/06/984040411/stranger-danger-an-economist-s-guide-to-overcoming-distrust>.
 28. "What Will It Take to Rebuild Trust in 2022?" World Economic Forum. Accessed August 7, 2022. <https://www.weforum.org/agenda/2022/01/rebuilding-trust-government-society-2022/>.
 29. Reiff, Nathan. "What Was the First Cryptocurrency?" Investopedia. Investopedia, July 26, 2022. <https://www.investopedia.com/tech/were-there-cryptocurrencies-bitcoin/#:~:text=The%20first%20cryptocurrency%20was%20eCash%2C%20created%20by%20David%20Chaum's%20company,and%20accepted%20cryptocurrency%20before%20Bitcoin>.
 30. Edwards, John. "Bitcoin's Price History." Investopedia. Investopedia, July 4, 2022. <https://www.investopedia.com/articles/forex/121815/bitcoins-price-history.asp>.
 31. "Covid-19 Eroding Youth Trust in Political Leadership and Institutions: LSE Research." COVID-19 eroding youth trust in political leadership and institutions | LSE Research. Accessed August 8, 2022. <https://www.lse.ac.uk/research/research-for-the-world/politics/the-political-scar-of-epidemics-why-covid-19-is-eroding-youth-peoples-trust-in-their-leaders-and-political-institutions>.
 32. IE University. "Lack of Trust in Public Institutions Leads to Cryptocurrencies." IE University. IE University, January 31, 2020. <https://www.ie.edu/university/news-events/news/lack-trust-public-institutions-leads-higher-use-cryptocurrencies/>.
 33. Bajpai, Prableen. "Countries Where Bitcoin Is Legal and Illegal." Investopedia. Investopedia, July 13, 2022. <https://www.investopedia.com/articles/forex/041515/countries-where-bitcoin-legal-illegal.asp>.
 34. Gu, Leilei, Zhongyang Liu, Sichao Ma, and Hongyu Wang. "Social Trust and Corporate Financial Asset Holdings: Evidence from China." International Review of Financial Analysis. North-Holland, April 22, 2022. <https://www.sciencedirect.com/science/article/abs/pii/S105752192200134X>.

■ Author

Veer Krishan Choudhari is a student at Vidyashilp Academy, Bangalore, in grade 12, studying under the ISC board. The subjects in his course include Economics, Commerce, Accounting, Mathematics, and English. He undertook this project to understand better how to write a research paper and learn about cryptocurrencies.

Evaluating Beyond Meat's Success in the Consumer Market for Plant-Based Meat

Victor T. Weng

TFS - Canada's International School, 306 Lawrence Ave E, Toronto, Ontario, M4N 1T7, Canada; VictorWengVTW@gmail.com

Mentor: Susan Tonin

ABSTRACT: Behavioral economics theories were used to evaluate Beyond Meat's success in changing consumer tastes and preferences for plant-based protein in North America—mainly through its retail presence and partnerships with fast-food restaurants. Conclusions were drawn through the analysis of Beyond Meat's corporate decisions and various secondary sources, such as research conducted by Cattlemen's Beef Promotion and Research Board, Kansas University, and Purdue. The study revealed that biases, including status quo, distinction, familiarity, anchoring, and confirmation, are extensive in consumer perceptions of plant-based meats, often requiring immense efforts in choice architecture and nudging to create changes in pre-established habits such as meat consumption. However, by leveraging theories such as advertised responsibility, framing, nudging, herd behavior, and FOMO, Beyond Meat has significantly impacted the industry and the acceptance of plant-based meats. Biases pose problems in our day-to-day lives as change is required for improvement. Through exploring the factors in decision-making that influence human stagnance, we could alter the environment and context in which choices are presented through choice architecture, “nudging” consumers in the right direction. This can lead to low-cost and wide-scale change, such as more sustainable diets and reducing the impacts of imminent issues such as climate change.

KEYWORDS: Behavioral and Social Sciences; Other (Behavioral Economics); Nudge Theory; Choice Architecture; Plant-based Meat Market.

■ Introduction

To reduce human behavior within a set of given rules would do injustice to the complexity of our minds; equally inaccurate would be the theories based upon such assumptions. Traditionally, economists have studied an abstraction of human behavior referred to as ‘*homo economicus*’—a term first used by economist John Stuart Mill in the 19th century.¹ The model assumes that humans are purely driven by self-interest, make decisions with perfect rationality and information, and have unlimited cognitive capacity. However, observation of our world and ourselves reveals that this is not entirely the case. We engage in altruistic behavior, such as charity or making purchasing decisions based on the ethical origins of products. We have limited thinking capabilities, are often flawed by cognitive biases and heuristics, and can only make choices from the information available.² Popularized in recent decades, behavioral economics develops and evaluates policies based on a more accurate reflection of human behavior—expanding upon the traditional model of ‘*Homo economicus*’ by considering how humans respond and react to various circumstances. Given the immense influence of cognitive decision-making in markets, a review would be important for furthering the applications of these theories in present-day issues such as climate change. By leveraging the interconnection of psychology and economics, policymakers and companies can guide the general public toward more beneficial outcomes without the need for as great of a monetary incentive, which would otherwise be costly to implement.³ As a basis for this essay, I will use such behavioral economic theories to evaluate Beyond Meat's success in changing consumer tastes

and preferences for plant-based protein in North America, mainly through its retail presence and partnerships with fast-food restaurants. Our various human cognitive biases, leading to resistance to unfamiliarity, pose problems in our day-to-day lives as change is required for innovation and improvement. By exploring and recognizing the factors in decision-making that influence human stagnance, we could alter the environment and context in which choices are presented through choice architecture, “nudging” consumers to make more environmentally sustainable decisions.⁴ One area that could benefit from this is the food industry as “the global production of food is responsible for a third of all planet-heating gases emitted by human activity.”⁵ While behavioral economics has seen a strong emergence in recent years, very few resources have been allocated regarding the plant-based meat market. Although behavioral economics can be used subconsciously as marketing tactics, a more thorough acknowledgment and understanding of these theories will allow greater efficiency and effectiveness in applying these theories. Given the substantial influence of cognitive decision-making in consumer markets, a detailed review of its applications can further reveal its impact in present-day issues such as climate change and socioeconomic inequality.

To conduct a market analysis, background information was gathered through research, articles, news outlets, and readings of Beyond Meat's own statements—while being cognizant of their potential bias. These sources may refer to changes in the plant-based industry or focus on Beyond Meat's products specifically. In both cases, Beyond Meat maintains a significant

products specifically. In both cases, Beyond Meat maintains a significant market share in the industry, and changes to the entire sector will reflect their products to a certain extent. The applicable behavioral economic theories will be analyzed through research articles and publications describing the biases and their effects, such as *Nudge* by Richard Thaler or *Thinking, Fast and Slow* by Daniel Kahneman. The review will evaluate possible short-term and long-term barriers to transforming consumer habits due to bias and relevant economic factors from the currently available data.

■ Discussion

Context and Beef Market Analysis:

With technological developments and an increased population, our global meat consumption has tripled in the last 50 years.⁶ This poses issues as meat production leads to various negative externalities, defined as the cost to third parties not involved in producing and consuming goods. This occurs at the free market equilibrium price and quantity, which is where supply meets demand in a market without external interference from actors such as the government. As these negative external costs are not reflected in the market price of meat, the quantity being produced and consumed exceeds the socially optimum level, leading to market failure.

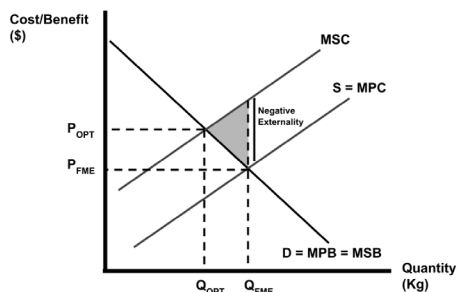


Figure 1: Negative externalities of beef production in the United States.

The negative externalities of beef production, labeled in **Figure 1**, come from sources such as the land and irrigation required for livestock feed, the release of methane from cows, pollution from machine operation, eutrophication, and fertilizer use, all contributing to increasingly prevalent environmental issues. Furthermore, modern farms are often unsanitary and overcrowded, raising ethical questions. These practices have led to various diseases, such as AIDS, SARS, Ebola, and COVID-19, with “three out of every four emerging infectious diseases in humans originating in animals,” according to PETA.⁷ The repercussions of pandemics are immense, causing supply-chain disruptions and the loss of lives, economic potential, and GDP. These consequences result in welfare loss: the total cost to society, shown in gray. This signals that beef is overproduced and overconsumed at the current free market equilibrium P_{FME} and Q_{FME} . In the interest of sustainability, it should be shifted toward the optimal equilibrium at P_{OPT} and Q_{OPT} .

However, meat production on a large scale is necessary to keep up with the population growth in the United States of 68.9% since 1970,⁸ with the average person in the country consuming 274 pounds of meat every year, a 40% increase

increase from 1961.⁹ While researchers have proven that meat consumption is not necessary to maintain a healthy diet from 1961.⁹ While researchers have proven that extensive meat consumption is not necessary to maintain a healthy diet and that protein can be obtained through other foods such as seitan, tofu, and beans, various factors such as habit, culture, taste, preference, and marketing have led to meat remaining in most US consumers’ diets.

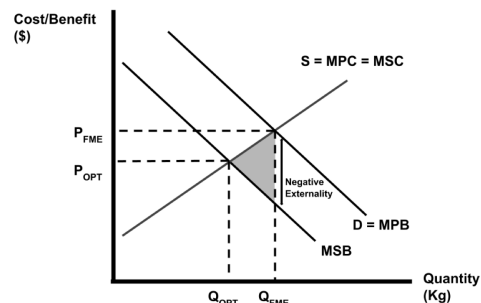


Figure 2: Negative Externalities of Beef Consumption in the United States.

According to Oxford University, consuming too much meat leads to heart disease, pneumonia, and diabetes.¹⁰ As illustrated in **Figure 2**, this further acts as a negative externality from the consumption side as the U.S. healthcare system spends an estimated USD 180-250 billion annually treating meat-consumption-related illnesses.¹¹ Funded through taxpayers, the welfare loss, shaded in gray, is equally significant.

If consuming meat poses so many issues, and there are so many alternatives, why aren’t most consumers switching? Vegetarian, vegan, and keto are among various plant-based diets that have surfaced, yet, groups such as vegetarians represent only 5% of all US consumers.¹² Through a behavioral lens, this may result from status-quo bias, which is rooted in several underlying psychological factors. Examples include loss aversion, where embracing alternative options such as plant-based meats pose a greater perceived risk than the apparent benefits, or from habits, where the comfort and familiarity of the current state create a resistance to change. Consequently, those who have grown up with meat may tend to stick with it throughout their lives.

The issue of convenience also exists—you would not have trouble finding a restaurant selling meat options. However, vegetarian or vegan alternatives are a lot more scarce, with only 1471 purely vegetarian and vegan restaurants in the United States (2020) out of more than 1 million in total.¹³ This makes it difficult for consumers to switch, and thus, it is also unappealing for producers to offer such options due to the small consumer base. Suppose we are not leaving meat anytime soon: would it be possible to develop a substitute product that is almost identical in taste, texture, smell, and look, addressing the issue of human stagnancy? This introduces plant-based meat, aiming to address the aforementioned negative externalities while developing a product that consumers may find easier to switch to. Founded in 2009, Beyond Meat pioneered a new approach to the plant-based meat industry. The CEO of Beyond Meat, Ethan Brown, believes that they can change consumer tastes and preferences

through their pea-based patties. And so far, it is working, finding itself in supermarkets, media headlines, and large-name partnerships with fast-food restaurant chains such as A&W, KFC, McDonald's, and Tim Hortons. Since then, various companies such as Impossible Meats have looked to compete in the global plant-based meat industry valued at USD 8.5 billion (2021) and expected to reach USD 24.8 billion by 2030.¹⁴ However, Beyond Meats remains a significant player in the industry, holding a 22% market share as seen in Figure 3.

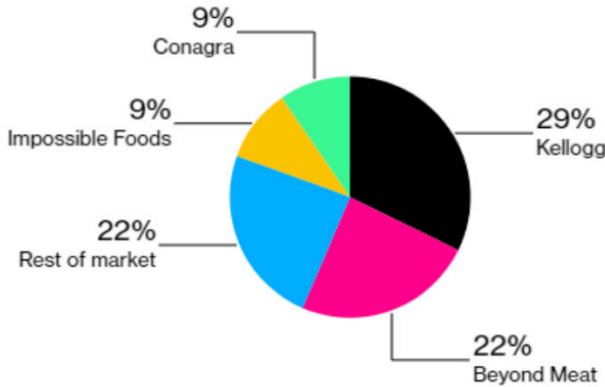


Figure 3: Market share for plant-based meats.¹⁵

Even though plant-based meat has been around since the 1970s, the primary difference between the Californian start-up and previous attempts is that pre-existing plant-based burgers had a small market of vegetarians and vegans and a poor reputation for having bad taste, with 90% of respondents claiming that beef burgers tasted better than plant-based alternatives.¹⁶ On the other hand, Beyond Meat targets meat-eaters and flexitarians: a primarily plant-based diet with the occasional incorporation of meat. This is done by trying to imitate the look and taste of actual meat, providing a healthier, more appealing, and more environmentally sustainable substitute for consumers. While a possible and commonly suggested solution to reducing meat consumption would be to increase taxation, this may pose downsides for low-income families as food, a necessity, would become less affordable. An alternative would be to offer a substitute for consumers who can afford it, decreasing the demand for meat consumption, reducing its negative externalities from Ne to Ne1 and welfare loss from the darker to the lighter shaded region in Figure 4.

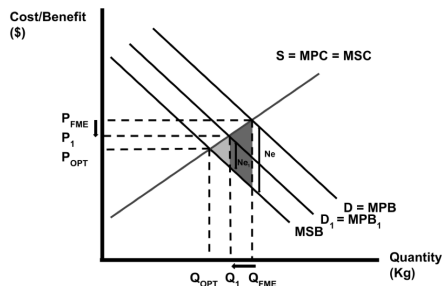


Figure 2: Negative externalities of beef consumption in the United States with the introduction of substitute goods.

However, as of 2022, rising food prices, living costs, supply-chain disruptions, and international conflicts, among various factors, have led to Beyond Meat incurring net losses of USD 100.5 million, leading to plummeting shares and doubts raised by investors. Despite the current economic environment, however, approaching the issue through the lens of behavioral economics may provide further insight into the industry's long-term prosperity.

Short-term Analysis:

Partnerships with fast-food restaurant chains, constituting USD 304.8 billion in U.S. consumer spending,¹⁷ have allowed Beyond Meat to access a more extensive consumer base. Targeting the fast-food industry may be beneficial as there is a smaller focus on meat quality compared to other preparation methods. Consumers eat for taste, enjoyment, convenience, and lower prices in the fast-food industry. The taste of the patties is often hidden behind sauces, condiments, and a subconscious taste bias from marketing strategies due to an already existing habit for producers to disguise low-quality meat. Analyzing this approach, the primary focus will be the data collected from consumer demand for Beyond Meat burgers in both fast-food restaurants and retail stores, where meat quality is less of a focus. This section draws four barriers to converting consumer choice in the short-run: anchoring, status quo, distinction, and familiarity bias.

Proposition 1: Anchoring Bias:

Anchoring bias refers to the human tendency to over-rely on initial pieces of information, the “anchor,” when making decisions or estimates. This is particularly prevalent when consumers encounter unfamiliar environments and situations, seeking out reference points to make judgments. Consequently, this may lead to biased decisions as the consumer strays from rational reasoning. Within the plant-based meat market, consumers may experience anchoring bias when confronted with the choice of plant-based meat alternatives as it is considered to be relatively new. In this case, the closest anchors can be either the last vegetarian burger the consumer has tried, which is different from Beyond Meat’s line of products, or the information they have received from their external sources such as advertisements or word of mouth.

The effect of this bias is noticeable in a research survey conducted by Kansas University and Purdue on consumer perceptions of meat compared to plant-based alternatives. It is important to note that it was funded by Cattlemen’s Beef Promotion and Research Board, a “research program designed to increase the demand for beef,”¹⁸ signifying that the results may be skewed in preference for traditional meat.

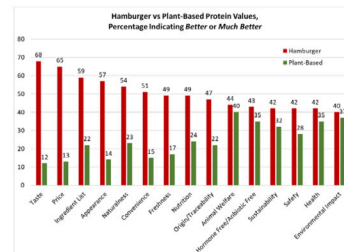


Figure 5: Hamburger vs. plant-based protein value perceptions indicating Better or Much Better.¹⁹

Figure 5 indicates the percentage of survey participants that ranked either plant-based (green) or hamburgers (red) as “Better” or “Much Better” compared to each other for specific categories, with the remaining respondents falling somewhere in between. It should be noted that while hamburgers are rated higher than plant-based burgers in every aspect, there are categories where the results are comparable. As expected, the most appealing factors of plant-based meats rely on consumer morals, with animal welfare rated at 40%, environmental impact at 37%, and sustainability at 32%. That being said, the ratings of plant-based burgers on taste, price, appearance, convenience, freshness, origin, ingredient list, naturalness, and nutrition fall significantly behind that of hamburgers. This poses a significant issue as consumers generally would place heavier emphasis on taste and price when purchasing food, as opposed to environmental impact. This may point to a setback of advertised responsibility, where consumers may only feel inclined to buy one good over another from a moral perspective if both goods are relatively similar in their primary utility, in this case, taste.

However, anchoring bias is particularly noticeable for the more objective categories, such as animal welfare or environmental impact. While taste may be subjective, it is nearly indisputable that plant-based meats—involving no animal killing in their production—should be rated higher than hamburgers for animal welfare. Yet, of the participants, 44% believed that hamburgers, relying on animal slaughter, were either “Better” or “Much Better” than plant-based alternatives for animal welfare and the environment. This points to the significance of both imperfect information and biases, going against the previously made assumption of homo-economicus, where all actors can make perfectly rational decisions. Consequently, we can observe an over-reliance on unverified information or beliefs when forming consumer perceptions. Most of the results could be attributed to anchoring bias, as seen in the following Figure 6, 65% of the survey respondents have not consumed plant-based meat within the last month.

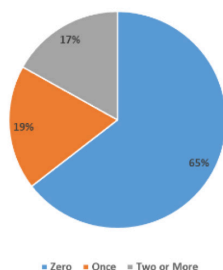


Figure 6: Consumption in the past month of plant-based burger patties or ground crumbles.

Thus, some participants would be relying on previous experiences with plant-based burgers or perceptions developed through interactions with others. Therefore, imperfect knowledge and anchoring bias toward plant-based hamburgers may play a significant role in these survey results.

Seen as the lowest consumer perception rating for traditional meat is 40% for Environmental Impact and approximately the same for similar categories; around 40% of respondents

appear to be biased in favor of traditional meat. However, bias can go both ways. A similarly objective category is price. Plant-based burgers are, on average, 70% more expensive than regular-meat hamburgers.²⁰ Factoring extreme deviations from this average, plant-based burgers would, at the very least, be expected to have a similar price to regular burgers due to their higher production costs. Either way, respondents should not perceive plant-based alternatives as “Better” or “Much Better” in terms of price compared to regular meat, leading to approximately 10-15% of consumers being irrationally biased in favor of plant-based burgers. Overall, these results point to a growing plant-based meat consumer base and the remaining work to do in converting the population to new habits against various biases.

Proposition 2: Status Quo Bias:

As explained in Kahneman’s *Anomalies*: “[...] individuals have a strong tendency to remain at the status quo, because the disadvantages of leaving it loom larger than advantages.” (197-198)²¹ In the case of regular meat consumption, there would need to be a change in dietary, cooking, and purchasing habits if consumers were to switch to plant-based meats. The effort required to change will likely dissuade most consumers from converting to a new diet, even with advertised and proven benefits. However, as seen in the first proposition, most consumers may not even have access to or accept these advantages. Consequently, anchoring bias and a lack of information may cause apparent disadvantages to seem even greater, furthering the effects of the status quo bias and the resistance to change.

A solution Beyond Meat has pursued is reducing the significance of change and normalizing eating plant-based meats, such as attempting to replicate the taste, texture, and cooking style of regular meat. However, they have also placed significant care in the choice architecture surrounding its products by “organizing the context in which people make decisions”²² to influence consumer decision-making. Choice architecture aims to design environments that help individuals make beneficial choices without restricting freedom, often employing nudges. As stated by Richard Thaler, “to count as a mere nudge, the intervention must be easy and cheap to avoid. Nudges are not mandates: Putting apples at eye level counts as a nudge.”²² In this case, Beyond Meat prides itself as the “world’s first plant-based burger sold in the meat case”²³ in North American grocery stores.



Figure 7: Beyond Meat burger patties at Canadian Loblaws in the meat freezer the author took the photo on May 8th, 2022.



Figure 8: Beyond Meat sausages at Canadian Loblaws next to the real meat, the photo was taken on on May 8th, 2022, by the author

This is a significant step in increasing accessibility and convenience for consumers. As seen in the above Figure 7 and Figure 8, consumers can follow their purchasing habits of visiting the meat section and still encounter the option of plant-based patties. Although this has raised controversy as the product is not actually “meat,” it exposes the target audience of meat-eaters and flexitarians to this substitute good, facilitating the change by making the product align with established habits. The exposure is furthered by the company’s partnerships with fast-food restaurants such as Mcdonald’s to ensure that the alternatives are offered widely at established locations. This collaboration increases the likelihood of consumers trying the new alternatives as fast-food restaurants already have a regular consumer base. By readily offering these products at convenient locations, consumers may be more inclined to try plant-based meat instead of exerting the additional effort of going through a plant-based aisle or entering vegetarian restaurants when searching for alternatives. However, this may lead to other barriers such as distinction bias that counteract this goal.

Proposition 3: Distinction Bias:

Placing plant-based and regular burgers in the same context could lead to distinction bias, where two options are considered more different when compared side by side. This is due to individuals evaluating and making decisions based on relative differences rather than the absolute values of either choice. Where plant-based meats may have been an appealing choice on their own, the presence of traditional meat may lead to consumers becoming more aware of the differences between Beyond Meat burgers and traditional meat, driving the negative stigma around plant-based meats being unnatural and, thus, irrationally assumed to be less healthy. Plant-based patties are considered processed and are often referred to in the media as “lab-grown.” This contributes to a negative perception of plant-based meat as less natural, as indicated by a significant gap in “naturalness” perception shown in Figure 5 of 54% compared to 23%. This framing of information draws a difference between the two products and contributes to the negative stigma surrounding plant-based meat being “fake.” Consequently, this may decrease the effectiveness of the choice architecture surrounding plant-based meats next to traditional meat. As a result, consumers have become more conscious of the exact contents of plant-based alternatives. According to Market Research Firm Mintel, consumers are looking for

recognizable ingredients and packaging similar to real meat, with over 70% of consumers reading the label before buying a meat alternative they’ve never had before.²³ This plays on the familiarity bias, where consumers feel more comfortable purchasing and consuming what they know.

Proposition 4: Familiarity Bias:

Being able to recognize certain ingredients reduces the “unnaturalness” that is often associated with plant-based meats. These variables were also studied in the research survey conducted by Kansas University and Purdue,¹⁹ where respondents were presented with choices in two contexts. The first is Figure 10, with the nutrient contents of two burgers and their calorie count—the second, in Figure 11, with the ingredient list.

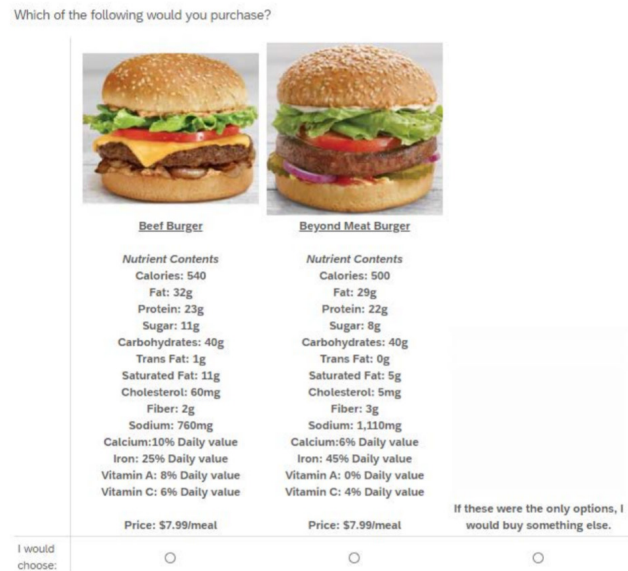


Figure 9: Choice option between beef and Beyond Beef in the presence of nutrient contents.



Figure 10: Choice option between beef and Beyond Beef in the presence of an ingredient list. The respondent data is recorded below in Figure 11.

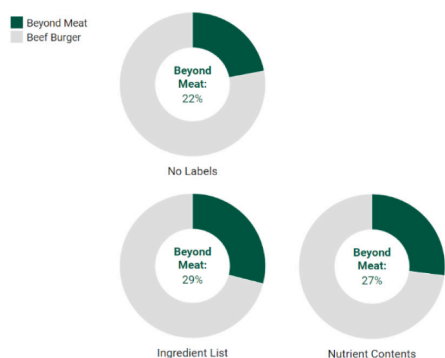


Figure 11: Respondent choice distribution in different testing conditions.

Both ingredient lists and nutrient contents yield higher choice levels from respondents than with no labels: in the presence of more information, consumers are more likely to pick the healthier alternative of Beyond Meat. According to research by The Food Information Council on U.S. households, 47.9% of consumers wanted access to more information on plant-based meat, such as the complete ingredient content, before trying them.²⁴ Despite the difference in respondent choice with more information, the nutrient contents shown in Figure 10 were somewhat misleading as regular beef can also be broken down into constituent parts, such as being 75% water, rather than exaggerating the differences between the choices.²⁵ This may further the distinction bias as many of the listed ingredients for plant-based meats such as water or sodium are also present in regular meat, which on the other hand, is listed as “100% Beef.” While certain consumers may be more attracted to familiar ingredients in the plant-based patty, others may be dissuaded by the long list of scientific jargon, causing important differences to be downplayed as it is saturated by less relevant and possibly unfamiliar information. Thus, in a market environment, packaging could highlight the health benefits of Beyond Meat more explicitly, such as the ones found at a Canadian Loblaws shown below in Figure 12 emphasizing the reduced saturated fat content (in turquoise), which could otherwise be lost in the information overload.



Figure 12: Beyond Meat burger patties at Canadian Loblaws with “New Look” packaging, the author took the photo on May 8th, 2022.

Thus, the presence of increased information can be effective in reducing consumer irrationality as it can lead to more educated and informed purchases. However, there could be further research exploring if effective packaging and presentation of information to greater change in consumer behavior.

Beyond leads the personal incentives of healthier purchasing decisions, humans are also susceptible to judgment from others, resulting in herd behavior. The heuristic describes the human tendency to act similarly to the majority or what they perceive to be the majority. This is particularly problematic in creating change from a pre-established context, such as a culture embedded in meat consumption, as most actions go against the change. However, herd behavior also leads to trends. Over the past decade, the media has given significant attention to imminent environmental issues. Thus, Beyond Meat is equally advertised as a means for consumers to save the environment through their diet. Consumers feel inclined to participate in this trend while also feeling good about themselves due to an apparent environmental benefit. However, movements, while effective in the short term, may be less effective in the long-term, which is necessary for permanent changes in consumer tastes and preferences. As seen by the recent decline of Beyond Meat, one questions whether the plant-based diet shift will last.

Long-term Analysis:

Having experienced a 46% increase in dollar sales from 2019 to 2020, the sudden flattening of growth from 2020 to 2021 may indicate a decline in the industry as seen in Figure 13.

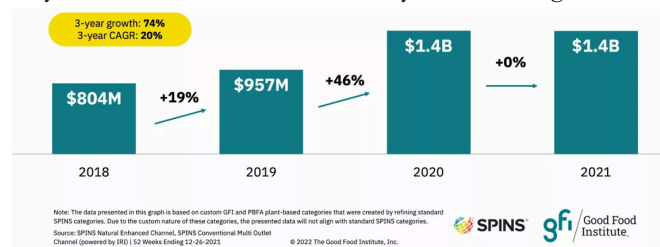


Figure 13: Plant-based meat and seafood dollar sales, U.S. retail, 2018-2021.²⁶

However, this can be attributed to various factors, such as FOMO (Fear of Missing Out) only being effective in the short-term, inflation levels, increased competition, supply-chain disruptions, and counter-advertising from the meat industry—revealing that the sale stagnancy may be short-term and not as concerning.

Proposition 1: Fear of Missing Out:

Firstly, partnerships with fast-food restaurants have been advertised as “limited time” deals, which use the FOMO and loss aversion bias by encouraging consumers to try the Beyond Meat products before they are gone. Fear of Missing Out is a psychological unease coming from the anxiety that others have rewarding experiences or opportunities that one is absent from. Whether it be due to societal influence and pressure or the fear of regret, consumers can be influenced into purchasing goods that are only available temporarily. While this technique seems to be effective in the short-run with about two-thirds of Americans having tried plant-based meats in the past year, the long-run change in consumer behavior remains for only 20% of Americans who eat it once a week.²⁴ From a sustainability standpoint, the lack of long-term commitments to the product is concerning, particularly as the trend fades from media coverage. Thus, certain approaches may need to be taken, such as re-framing the consumption of plant-based meat products as

long-term commitments or even reworks to the product itself. This is necessary for not only the plant-based meat industry but others based on environmental sustainability, as trends are insufficient to create permanent change. However, while biases may be at play, there are other significant economic factors that may be responsible for the recent slowing in growth.

Proposition 2: Competition, Inflation, and Supply-Chain Issues:

Firstly, the recent decline of 13.9% in Beyond Meat year-over-year sales²⁷ could also be associated with the increased competition that the start-up is facing. Although the plant-based industry experienced no expansion, specific competitors, such as Impossible Foods, gained USD 500 million in funding during a period of “record growth.”²⁸ As other companies battle for market share, Beyond Meat may experience decreased revenues.

Secondly, as the decline has been particularly prevalent in recent years, it could be associated with supply-chain issues and rising food prices. The high level of inflation has been steadily increasing, reaching as high as 8.5% in the United States²⁹ and 7.6% in Canada as of July 2022.³⁰ This may lead to an increase in consumer price awareness and decreased spending due to higher costs. However, inflation represents a persistent increase in the average price levels of most goods and services. Thus, it is not unique to plant-based meat sales and would require a larger context of analysis. The following data table from Good Food Institute draws a comparison between the market changes in plant-based meat to conventional meat.

Category	Dollar sales, 1-year change	Unit sales, 1-year change	Average price per unit, 1-year change
Total food	2%	-3%	+5%
Frozen & refrigerated conventional meat*	1%	-4%	+6%
Plant-based meat	0%	-3%	+3%

Figure 14: Dollar sales, unit sales, and average price per unit of plant-based meat and conventional meat 2020 to 2021.²⁶

As seen in Figure 14, while frozen and refrigerated conventional meat dollar sales increased by 1%, their unit sales decline was larger than that of plant-based meats: -4% compared to -3%. As well, the average price unit change of 6% indicates that increased prices completely drove the conventional meat’s dollar sales growth. Although the plant-based meat industry had no change in dollar sales over 2020–2021, it performed better than conventional meat in consumer demand as it experienced a lower loss of unit sales. The decreased unit sales of conventional meat would also reduce negative externalities associated with meat consumption and production, possibly indicating a more sustainable trend to emerge.

Finally, inflation may result from supply chain disruptions and ingredient shortages, demonstrating that the decrease in demand for Beyond Meat products may be price-driven and unrelated to the consumer’s tastes and preferences. Canada, the largest producer of yellow peas, experienced an extreme drought over the 2020–2021 summer.

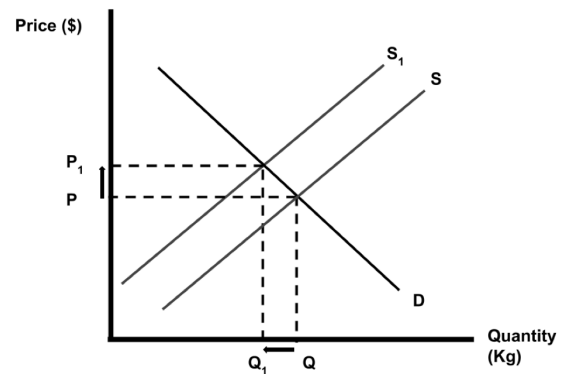


Figure 15: Effects of extreme drought in Canada on the yellow pea market.

The extreme weather conditions led to a decrease in supply (S to S_1) in Figure 15, causing a 45% decrease in yellow pea production (Q to Q_1) and an increase in pea prices by 120% (P to P_1) compared to last year.³¹ Overall, this would contribute to higher production costs for Beyond Meat as yellow peas are their primary ingredient, leading to higher prices. However, such extreme weather conditions can be considered short-term and unpredictable, indicating that the fall in Beyond Meat sales may be temporary. With climate change leading to harsher weather conditions and impacting industries trying to address the issue, the concern of environmental harm appears to be self-perpetuating and only furthers our need to take prompt action.

Proposition 3: Counter-Advertising from an Established Meat Industry:

There exist advertising campaigns from a well-established meat industry. The firms want to increase demand for traditional meat and, by doing so, may use methods to decrease the need for substitute goods. With substantial funding due to their scale, the firms can run expensive ad campaigns that criticize plant-based meat for being “unnatural.” This contributes to confirmation bias, where consumers are more likely to remember and favor information that agrees with their previous beliefs and values. If past convictions consist of negative perceptions of plant-based meats, as some may result from previous vegetarian burgers, then consumers may become more hesitant towards change. As explored throughout the analysis, many of the barriers to transforming consumer habits are due to biases involving ideologies and the lack of factually correct information. Consequently, in a free market, traditional meat firms that have the necessary resources and economies of scale to maintain control over the industry may continue to do so by playing on psychological factors that influence human decisions. However, with plant-based meat being considered a possible solution to the negative externalities of meat production and consumption, governments may need to implement policies that support plant-based firms. Whether it be increased spending on research and development, advertisement, or subsidies for crop farmers, the free market may take too long to accept plant-based alternatives as the standard. However, despite the concerns about the sudden halt of growth, many factors appear to be widespread and short-term, shedding a positive light on the issue.

Recommendations for Future Research:

The plant-based industry is just emerging, and like the products and firms, there remains significant work and areas to explore. As there is insufficient information within the field to confidently reach certain conclusions, I have proposed recommendations for future research based on the findings in this review.

1. A more balanced comparison of choice options between Beef and Beyond Meat Burgers:

a. As discussed in **Proposition 4: Familiarity Bias Figure 10**, the presentation of the ingredients list for both types of beef burgers is unjustly exaggerated, potentially leading to inaccurate results. A survey that takes into account all the ingredients within traditional beef patties in the same manner that plant-based meat was presented may lead to a more balanced comparison of the two products. This may increase the familiarity that consumers feel towards Beyond Meat as it would closer resemble traditional meat, leading to a greater, and more equitable change in favor of Beyond Meat burgers as an option. In addition to this fact, the images presented are also unjustly compared as different elements are present in the burgers, such as cheese being in the traditional burger. Therefore, a new survey with more variables being controlled would also be beneficial.

2. Evaluating the effectiveness of packaging and presentation of information to highlight important benefits of plant-based alternatives:

a. As discussed in **Proposition 4: Familiarity Bias Figure 12**, Beyond Meat implemented packaging that highlights the low saturated fat content, among other incentives to encourage the consumer to purchase the beef. As the survey from Kansas University and Purdue presented the nutrient contents and ingredients list in a linear and cluttered way, consumers may default to their habits as information was not appealing to read and not reflective of an the actual product at the grocery store. Instead, a survey with Beyond Meat's packaging should be compared to traditional meat's packaging to create a more accurate representation of consumer choice, while also allowing necessary information and comparisons to be highlighted for the consumer.

3. Understanding why consumers fail to integrate plant-based meat into their diets:

a. With around 67% of Americans having tried plant-based meats last year and only 20% who continue to consume it once a week, it would be important to understand why plant-based meat fails to remain in consumers' diets. Whether it be the product itself, the price, availability, or biases, there is insufficient available information to make necessary adjustments and changes. Therefore, a point of further research could be a survey that seeks to understand the reasons why respondents who have tried a plant-based product once opted not to do so again.

Conclusion

The current state of meat consumption is unsustainable, producing various negative externalities. As a result, numerous efforts have been made to shift consumer behavior towards more sustainable diets involving meat substitutes. However, as demonstrated through Beyond Meat's successes

and downturns, biases such as status quo, distinction, familiarity, anchoring, and confirmation, are extensive and often require immense efforts in choice architecture and nudging to create changes in pre-established habits such as meat consumption. Nevertheless, Beyond Meat has significantly impacted the industry by improving consumer taste and preferences for plant-based products. Behavioral economic theories such as advertised responsibility, framing, nudging, herd behavior, and FOMO, whether applied intentionally or not, can be used extensively to evaluate Beyond Meat's expansions—being conscious of such notions can lead to more effective changes moving forward. Looking into subsequent years, whether the decrease in sales of Beyond Meat and the plant-based meat industry is short-term or long-term will play a significant role in the future health of our environment and climate. As research in the field improves the quality and price of the products, and as the firms develop economies of scale, it could be expected that the demand would re-increase, considering that the environmental and health benefits are undeniable. However, considering barriers such as biases and the meat industry, the time needed for changes as immense as altering human nature, and the tradition of meat consumption, this change may take generations to form.

Acknowledgments

This study would not have been possible without the support and mentorship of Susan Tonin, my Higher-Level Economics teacher in the International Baccalaureate academic diploma program, and peer review from professors Albert Malkin from Western Ivey, Nicholas Ajzenman from McGill University and Joshua Foster from Western Ivey.

References

1. The Decision Lab. "Homo Economicus." The Decision Lab Reference Guide. The Decision Lab, n.d. <https://thedecisionlab.com/reference-guide/economics/homo-economicus>.
2. Kahneman, Daniel. *Thinking, Fast and Slow*. New York: Farrar, Straus and Giroux, 2011.
3. University of Chicago News. "What Is Behavioral Economics?" University of Chicago, n.d. <https://news.uchicago.edu/explainer/what-is-behavioral-economics>. Accessed 18 December 2022.
4. Thaler, Richard H., and Cass R. Sunstein. *Nudge: Improving Decisions about Health, Wealth, and Happiness*. Yale University Press, 2008.
5. Milman, O. "Meat accounts for nearly 60% of all greenhouse gases from food production, study finds," The Guardian, www.theguardian.com/environment/2021/sep/13/meat-greenhouses-gases-food-production-study Accessed May 26, 2022.
6. Ritchie, H., and Roser, M. "Meat and Dairy Production," Our World in Data, www.ourworldindata.org/meat-production Accessed May 8, 2022.
7. PETA. "Animal Agriculture Increases the Risk of Pandemics," www.peta.org/issues/animals-used-for-food/animals-used-food-factsheets/animal-agriculture-and-pandemics/ Accessed May 12, 2022.
8. Macrotrends. "U.S. Population Growth Rate 1970-2022 | Macro Trends," www.macrotrends.net/countries/USA/united-states/population-growth-rate Accessed May 8, 2022.
9. Sentient Media. "Meat Consumption in the U.S.: Is It Increasing or Decreasing?" www.sentientmedia.org/meat-consumption-in-the-us/ Accessed March 17, 2022.

10. Papier, K. Fensom, G.K., Knuppel, A. et al. "Meat consumption and risk of 25 common conditions: outcome-wide analyses in 475,000 men and women in the UK Biobank study." *BMC Med* 19, 53 (2021). <https://doi.org/10.1186/s12916-021-01922-9>. Accessed May 9, 2022.
11. The Atlantic. "The Economic Value of Giving Up Meat," www.theatlantic.com/business/archive/2016/03/the-economic-case-for-worldwide-vegetarianism/475524/ Accessed May 11, 2022.
12. Jacimovic, D. "Vegetarian Statistics," *Deals On Health*, www.dealsonhealth.net/vegetarian-statistics/ Accessed May 11, 2022.
13. Kateman, B. "Vegan Restaurants Are On The Rise," *Forbes*, www.forbes.com/sites/briankateman/2019/08/21/vegan-restaurants-are-on-the-rise/ Accessed May 14, 2022.
14. Bloomberg.com. "Plant-based Meat Market Size Worth \$24.8 Billion By 2030: Grand View Research, Inc.," www.bloomberg.com/press-releases/2022-02-01/plant-based-meat-market-size-worth-24-8-billion-by-2030-grand-view-research-inc Accessed May 14, 2022.
15. Hirtzer, M. *et al.* "Tyson Takes on Beyond Meat, Impossible Foods With Plant-Based Burger, Fake Meat," *Bloomberg.com*, www.bloomberg.com/news/articles/2021-05-03/tyson-takes-on-beyond-meat-impossible-foods-with-plant-based-burger-fake-meat Accessed May 14, 2022.
16. Slade, P. (2018). *If You Build It, Will They Eat It? Consumer Preferences For Plant-based And Cultured Meat Burgers*. *Appetite*, 125. 428-437. Accessed June 19, 2023.
17. Statista. "QSR sector consumer spending US 2021." 25 Apr. 2022, www.statista.com/statistics/259148/consumer-spending-us-qsr-sector/. Accessed 15 May 2022.
18. Cattlemen's Beef Board. "What is the Beef Checkoff?" www.beefboard.org/checkoff/. Accessed 14 May 2022.
19. Tonsor, Glynn, *et al.* "Impact of New Plant-Based Protein Alternatives on US Beef Demand - Full Report." *AgManager.info*, 12 Feb. 2021, www.agmanager.info/livestock-meat/meat-demand/meat-demand-research-studies/impact-new-plant-based-protein-0. Accessed 30 Mar. 2022.
20. Alini, Erica. "Can't afford steak? Don't even think about buying veggie burgers." *The Globe and Mail*, 7 May 2022, www.theglobeandmail.com/investing/personal-finance/household-finances/article-eating-vegetarian-not-cheaper-than-meat/. Accessed 15 May 2022.
21. Kahneman, Daniel, Jack L. Knetsch, and Richard H. Thaler. 1991. "Anomalies: The Endowment Effect, Loss Aversion, and Status Quo Bias." *Journal of Economic Perspectives*, 5 (1): 193-206. Accessed 14 May 2022.
22. Thaler, Richard H., and Cass R. Sunstein. *Nudge: Improving Decisions about Health, Wealth, and Happiness*. Yale University Press, 2008. 428
23. Michail, Niamh. "What do consumers really think of meat alternatives?" *Food Navigator*, 28 Sept. 2021, www.foodnavigator.com/Article/2018/07/27/What-do-consumers-really-think-of-meat-alternatives. Accessed 14 May 2022.
24. Food Insight. "Plant-Based Meat Survey." Nov. 2021, foodinsight.org/wp-content/uploads/2021/11/IFIC-Plant-Based-Meat-Survey-November-2021.pdf. Accessed 15 May 2022.
25. American Meat Science Association. "Water in Meat and Poultry Products." 12 Apr. 2017, meatscience.org/TheMeatWeEat/topics/fresh-meat/article/2017/04/12/water-in-meat-and-poultry-products. Accessed 31 Aug 2022.
26. Ignaszewski, Emma. "A deeper dive into plant-based meat sales in 2021 - The Good Food Institute." *Good Food Institute*, 24 Mar. 2022, gfi.org/blog/a-deeper-dive-into-plant-based-meat-sales-in-2021/. Accessed 15 May 2022.
27. CNBC. "Beyond Meat (BYND) Q3 2021 earnings miss." www.cnbc.com/2021/11/10/beyond-meat-bynd-q3-2021-earnings.html Accessed May 15, 2022.
28. Business Wire. "Impossible Foods Closes \$500M in New Funding Amid Record Growth." www.businesswire.com/news/home/20211123005589/en/Impossible-Foods-Closes-500M-in-New-Funding-Amid-Record-Growth Accessed May 15, 2022.
29. Bureau of Labor Statistics. "Consumer prices up 8.5 percent for year ended March 2022: The Economics Daily: U.S." www.bls.gov/opub/ted/2022/consumer-prices-up-8-5-percent-for-year-ended-march-2022.htm Accessed May 14, 2022.
30. Bank of Canada. "Key Inflation Indicators and the Target Range." www.bankofcanada.ca/rates/indicators/key-variables/key-inflation-indicators-and-the-target-range/ Accessed September 10, 2022.
31. Food Navigator. "Roquette warns of soaring pea prices." www.foodnavigator.com/Article/2021/10/01/Roquette-warns-of-soaring-pea-prices Accessed May 15, 2022.

■ Author

Victor Weng is a high-school graduate of TFS - Canada's International School in Toronto, Canada, class of 2023, and is pursuing higher education at the University of Toronto's Engineering Science program. He is interested in behavioral economics, psychology, and artificial intelligence. His research projects primarily focus on the applications of psychology in fields such as economics, computer science, and engineering.

Review of the Neural Correlates of Intelligence and Convergence on a Holistic Approach

Quinn B. Smith

South Western High School, 200 Bowman Rd, Hanover, Pennsylvania, 17331, USA; Smith.Quinn7810@gmail.com
Mentor: Mrs. Wimssett

ABSTRACT: For over a century, scientists have sought to uncover the neurological correlates of intelligence. With recent advancements in neuroimaging technology, neuroscientists have been converging upon the neurological correlates of intelligence. This review compiles the most current and relevant evidence, from all perspectives, concerning the manifestation of intelligence in the brain. A network-based approach to intelligence was utilized during this review, relying on the flexible interactions between the intrinsic connectivity networks to explain intelligence. Indeed, the brain's most important intrinsic connectivity networks were the frontoparietal control network and the cingulo-opercular network, the brain's two control networks. The review begins with understanding the neural correlates of intelligence task processing and intelligence differences. Then, the final section of this review reveals the two most important threads connecting the various perspectives on intelligence: neural networks and neural flexibility. Through these threads, this review attempts to identify the neurological core of intelligence, opening the door for convergence upon a holistic approach to intelligence in the near future.

KEYWORDS: Behavioral and Social Sciences, Neuroscience; Intelligence; Perspectives; Networks; Flexibility.

■ Introduction

Intelligence, defined by the American Psychological Association as “the ability to derive information, learn from experience, adapt to the environment, and correctly utilize thought and information,” has remained a topic of debate within the neuroscientific community. There have been many prominent theories that attempt to understand the neurological basis of intelligence, including the Neural Efficiency Hypothesis,¹ Parieto-Frontal Integration Theory (P-FIT),² and the Multiple-Demand (MD) Theory,³ the Process Overlap Theory,⁴ and The Network Neuroscience Theory of Intelligence.⁵ This review attempts to cover the extensive evidence pertaining to intelligence to combine these various theories of intelligence into a more holistic view of intelligence in the brain. By no means will this review be able to cover every finding and every aspect of the neurological correlates of intelligence, but this review serves to highlight the most important aspects of the brain for intelligence.

Broadly, this review will analyze the neural correlates of intelligence through the connectivity of the major intrinsic connectivity networks (ICNs) within the brain. First, the review will examine the neural correlates of intelligence task processing through the functional and structural connectivity of the brain's ICNs. Next, the neural correlates of intelligence differences will be investigated, examining how the system outlined in the first section is augmented in higher-intelligent individuals. Last, the various intelligence models will be connected to produce a more holistic approach to the neural correlates of intelligence. Because this review doesn't attempt to propose a new theory of intelligence but rather identify the most important neural components for intelligence, this review will be more descriptive of intelligence than prescriptive.

■ Discussion

In 1904, Spearman recognized that a common factor, *g*, existed among the diverse cognitive abilities contributing to intelligence.⁶ Jung & Haier in 2007 felt poised to answer the question regarding the neural correlates of intelligence (*g*). Similarly, I am poised to expand upon their model and others by combining the regional associations of intelligence with the connectivity dynamics associated with intelligence. This analysis will explain multiple questions related to the neural correlates of intelligence: what neural dynamics underlie the human ability to approach a task? How are the functional and structural dynamics of the ICNs manipulated to increase human intelligence capabilities? Finally, how do these findings bring together the theories of intelligence?

Intelligence Task Processing :

This section attempts to answer the first question: *what neural dynamics underlie the human ability to approach an intelligence task?* In 2007, Jung & Haier compiled an extensive review of studies that examined the regions involved in intelligence. Combining functional and structural associations, Jung & Haier implicated regions within the dorsolateral prefrontal cortex (DLPFC), superior parietal lobule, inferior parietal lobule, anterior cingulate cortex (ACC), temporal lobes, and occipital lobe.² Jung & Haier compile these regions into the Parieto-Frontal Integration Theory (P-FIT), which outlines six stages of intelligence processing. This stage of the review will be similar in that respect, with the following stages of intelligence processing: (1) Humans gather and process sensory information through auditory and visual means, triggering a task-positive neural state; (2) As basic perceptual processing is fed forward to the control regions, downstream control is initiated; (3) Rule generation begins, with the control regions

flexibly recruiting downstream regions to obtain task-relevant information; (4) Once a rule is reached, this rule is applied through downstream working memory manipulation to find a solution; (5) The cingulo-opercular network (CON) sends this solution down towards the striatum which sends the motor response down to deeper subcortical structures; (6) Errors in intelligence processing are recognized by the CON and the frontoparietal control network (FPCN) facilitates the changes in downstream control necessary to correct the mistake.

It is important to note that the research devoted to task-processing dynamics associated with intelligence is relatively small. So, this section primarily consists of studies on cognitive control, which will be augmented by the few studies that discuss relevant task-processing features of intelligence. Since intelligence is a flexible means of implementing cognitive control, this approach is relevant, and I believe I can elucidate many important facets of intelligence that otherwise go unrecognized. Further, minute temporal dynamics are largely unknown for the neural processes in intelligence tasks. Using more recent scientific evidence, this section proposes a model for the processes our brain undergoes in attempting to solve intelligence tasks and suggests possible mechanisms that these networks use to achieve these functions. This model does not try to explain the temporal dynamics for intelligence tasks fully but instead organizes our current evidence of neural processing during intelligence tasks into a coherent temporal framework.

As individuals prepare for an intelligence task, the brain must be driven into a task-positive state from a resting state. Recent evidence has suggested that the dorsal posterior cingulate cortex (dPCC) is a perfect candidate for this function. With the PCC being the central hub of the default mode network (DMN), the dPCC has extensive connections to DMN nodes. Still, it is also widely connected with many other intrinsic connectivity networks, including the FPCN, CON, and dorsal attention network (DAN).⁷⁻¹¹ The widely integrative functional connectivity of the dPCC indicates greater functional relevance beyond the DMN, and recent evidence supports this claim. The dPCC is very active when individuals wait for an external cue to action, which involves high vigilance. However, activity falls when externally-directed attention on a specific task has been initiated.¹⁰ From these results, Leech and colleagues conclude that the dPCC controls the balance between internally and externally directed control.¹⁰ The mechanisms through which the dPCC enables the transition between attentional states is by influencing global metastability within the brain.¹² Metastability is a vague concept in the neuroscientific literature. However, this review utilizes Leech and Sharps' definition of metastability, where metastability reflects the variability of neural activity within the ICNs over time.¹² High metastability, reflecting highly variable neural activity, was associated with high PCC activity and enabled rapid transitions between neural states.¹³ Therefore, the PCC likely tunes the brain's metastability, enabling the brain to enter a broadly focused state that enables highly flexible adjustments of neural connectivity to meet incoming demands.

Once the task begins, sensory stimuli flood our cortical sensory systems. Since the visual system is the most likely source

of task-relevant information during intelligence tasks, this review will focus on its mechanisms specifically. The visual system hierarchy begins with specific feature processing in the striate and extrastriate cortex. The feedforward projections then divide along the ventral and dorsal pathways, encapsulating the visual system's 'what' and 'where' pathways, responsible for object recognition and the spatial location of an object, respectively.¹⁴ With greater relevance later in the review, the temporal cortex is involved in object recognition processing, while the parietal cortex is responsible for the spatial location processing for visual stimuli. As the stimuli are fed forward, the attention networks likely become activated and begin the downstream control of visual regions. Indeed, evidence suggests that the ventral attention network (VAN) can redirect the DAN to unexpected or unattended stimuli,¹⁵ providing a mechanism for attentional resources being directed towards new task-relevant stimuli. The initial attentional focus would aid in identifying the object and spatial location identification.

The right anterior insula (aINS) likely enables the switch between DMN and FPCN activity, initiating control signals and giving the FPCN access to salient external and internal information.¹⁶ This evidence implicates the CON in utilizing the high metastability facilitated by the dPCC to transition global network activity into the specific task-relevant activation patterns necessary to meet task demands. The CON is responsible for task-set maintenance and control allocation,^{29, 32-35} and the ability to direct global network activity to task-relevant states might be a mechanism the CON uses to achieve these functions.

Proper modulation of incoming information is necessary to prevent the control networks from reaching cognitive capacity. It provides the control networks with sufficient information to direct their neural control in behaviorally salient ways. The feedforward communication to the prefrontal cortex occurs through both corticocortical connections and subcortical modulatory pathways. Cocchi and colleagues demonstrated that the FPCN and CON could rapidly and flexibly obtain information processed by other specialized systems such as DMN, visual, and sensorimotor systems to achieve optimal goal-directed behavior.¹⁷ In filtering unnecessary information, the subcortical systems direct the control systems in goal-oriented ways while reducing the control systems' cognitive load. The mesocortical dopamine system has been demonstrated to be one of the significant modulatory systems. It initiates and maintains motivation in the brain,¹⁸ and prepares the prefrontal cortex (PFC) for incoming sensory information through dopaminergic pathways connecting the midbrain to the PFC.^{19,20} Indeed, dopamine can excite or inhibit information transmission, filtering sensory information received by the PFC and enabling information to be encoded into the working memory.²¹⁻²³ Another region within the mesocortical dopamine system, the striatum, is also relevant for directing the control networks toward task goals. Importantly, it must be noted that the striatum plays a more fundamental role in neural function than what will be covered in this review, with neuroscientists only beginning to understand its functions. With respect to intelligence, the striatum generates a future

response strategy faster than the prefrontal cortex.²⁴ When approaching an intelligence-based cognitive task, the problem is usually novel, requiring a rapidly constructed strategy for task completion that could not have been planned previously. Thus, the striatum is crucial in biasing control networks towards behaviorally salient processing according to rapidly constructed plans for goal completion.

More broadly, the basal ganglia likely functions like a switchboard activating the control networks while deactivating the DMN.²⁵ This function is very similar to the function of the CON described above, and it is unclear how these two mechanisms relate to one another; however, the basal ganglia may prime the control regions for incoming information, for which the CON is responsible for more direct activation of the FPCN. As such, the basal ganglia likely capitalize on the metastability provided by the dPCC to coordinate a goal-oriented plan and activate the control networks to assert control. A recent review outlined the importance of the thalamus as a gated relay station for cortical and subcortical connections.²⁶ Specifically, the thalamus has modulatory mechanisms that regulate the relay of information from sensorimotor regions and the basal ganglia to the brain's frontal regions. Recent evidence also points to bilateral regions in the anterior thalamus as being a critical node of the CON,^{27,28} and the anterior thalamus likely assists in the functions of the CON that will be discussed later.

With information being fed to the control networks, control must be implemented by the control networks to achieve task goals. Understanding the structural connections of CON regions is critical for understanding how the CON functions during intelligence tasks. The dorsal anterior cingulate cortex (dACC) has a much more isolated role, likely being responsible for determining the when, where, and how of control allocation;²⁹ meanwhile, the aINS has a much more integrated role, detecting salient features for additional processing and directing other brain networks.^{16,30,31} Together, these two regions are important for task-set maintenance and control allocation.^{29,32-35} Task-set maintenance requires the maintenance of task state network dynamics and determining the relevant information. Downstream, the CON likely achieves stable implementation of task sets in sensorimotor regions,³⁶ serving as a mechanism for deciding relevant externally derived information. Upstream, the CON mediates the antagonism between the DMN and the FPCN,^{37,38} regulating the influence of internal cognition on task sets. The CON's ability to successfully mediate the activity and connectivity of the FPCN and DMN regulates the flow of internal information toward the FPCN. It maintains the control network dynamics necessary for the task set. Implicit in the CON's ability to maintain the task set upstream is its ability to regulate control allocation. Evidence suggests that both the aINS and dACC influence control signals in the DLPFC,^{16,39,40} with task-based integration between dACC, DLPFC, and aINS being critical for guiding and supporting phasic control according to task goals.¹⁷ The influence of the dACC and aINS likely serve different roles in influencing DLPFC control, routed in the dACC's ability to allocate control and the aINS' ability to provide working

memory and attentional processes access to salient, bottom-up information.^{16,29}

Intelligence tasks often require manipulating an individual's internal representation of external stimuli according to some externally-presented or internal-generated rule. When a rule is given in the task, the mechanisms for generating the rule are likely to be bypassed; however, most tasks require individuals to uncover the rule. Among the two control networks, the FPCN likely generates a rule^{41,42} using behaviorally salient information that must be maintained. At the same time, external stimuli are manipulated within our working memory based on the rule.^{41,43-45} To understand how the FPCN obtains the necessary information to generate a rule, we must understand the functional connectivity of the FPCN regions. Recent evidence suggests that the FPCN exerts control on a rostral-caudal axis of abstraction,⁴⁶⁻⁵² and this axis roughly aligns with its two distinct subnetworks.⁵³⁻⁵⁶ The rostral-caudal axis of abstractness contains rostral regions that are responsible for temporal control, facilitating the maintenance of internal representation for future-oriented processing; intermediary zones that are responsible for contextual control, enabling the integration of internal and external representations according to prevailing context; and caudal regions that are responsible for sensorimotor control, asserting attention directed towards stimulus-action selection. Interestingly, the cerebellum has also been found to exhibit the same rostral-caudal axis of control during cognitively demanding tasks,⁵⁷ and has even been implicated in working memory manipulation.⁵⁸⁻⁶⁰ However, research on the cerebellum's role in intelligence is still relatively small, with more research required to understand the cerebellum's precise functional role in intelligence. The two distinct subnetworks, roughly aligned along this rostral-caudal axis, are defined by their coactivation patterns with other neural networks: the FPCN A is strongly connected to the DMN, while the FPCN B is strongly connected to the DAN.⁵³⁻⁵⁶ Nee found that FPCN A is most strongly implicated in temporal control and FPCN B is most strongly implicated in sensorimotor control, consistent with their connectivity profiles and alignment to the rostral-caudal axis. Contextual control requires the involvement of both networks, but FPCN B is more aligned with contextual control activation.⁶¹ These results make sense, considering that FPCN A aligns more with the rostral regions, whereas FPCN B aligns more with the caudal regions. This network alignment also ties the internally-oriented rostral regions to DMN connectivity and the externally-directed caudal regions to the DAN. Additionally, the rostral and caudal extremes of this axis show greater segregation of connectivity representing their more specialized functions, tied to their specific network connectivity profiles, whereas the intermediary zone, responsible for contextual control, is the central integrative region of the FPCN.⁶¹ These results indicate that the two subnetworks can operate in segregative or integrative fashions according to task demands, but the integrative functioning of the FPCN in contextual control is crucial for higher-level cognitive abilities.⁶¹⁻⁶⁴

The cortical structure of the FPCN intimates a potential mechanism that the FPCN could use to generate a rule re

quired for task completion. The FPCN potentially mediates the activation of DMN and DAN nodes and facilitates the transfer of internal and external information to control regions from the DAN and DMN nodes.⁶⁵ Hearne and colleagues suggest that transient, task-specific activations of DMN regions are critical for task performance under specific contexts. Further, the transient recruitment of DMN nodes is mediated by the rostrolateral prefrontal cortex (RLPFC) - also known as the anterior prefrontal cortex (aPFC) and Brodmann Area (BA) 10.²⁵ For example, one region of the DMN recruited by the control networks is the PCC.^{38,66,67} However, opposite functional connectivity patterns between the dPCC and ventral posterior cingulate cortex (vPCC) occur as cognitive demands increase.¹¹ The differing functional connectivity patterns reflect the importance of the RLPFC to effectively mediate DMN nodes relevant for intelligence processing. Further, the function of the angular gyrus in comprehending event concepts and mentally manipulating representations is advantageous in some contexts,⁶⁸ but the increased functional connectivity of the AG as complexity increases also appears to interfere with task performance.²⁵ Therefore, not all DMN connections to the FPCN are advantageous. At the same time, some are advantageous only in specific contexts, and proper mediation of the DMN nodes' functional connectivity with the FPCN is necessary for task goals. With the caudal regions of the FPCN being more connected to the DAN,^{55,61} these regions are responsible for collecting externally salient information for task goals. With the DAN being considered a task-positive network, its involvement in intelligence is more straightforward than the DMN, epitomized by a recent study that demonstrated DAN activity most strongly correlated with fluid intelligence.⁶⁹ The internal and external information collected by the FPCN requires assimilation, considering this information is collected mainly in the more segregated regions of the FPCN. The intermediary zones are a perfect place for such integration since it is known for top-down modulations that sharpen representations.^{70,71} Assimilating and subsequently sharpening the distinct internal and external representations would serve as a perfect mechanism to generate a rule given the specific task demands. Preliminary evidence supports this proposition, with the mid-DLPFC being responsible for hypothesis generation during inductive reasoning.⁴² More research should be done to support these results across a broader range of cognitive abilities. Further, the left DLPFC is likely critical for integrating FPCN and CON activity for optimal control,¹⁷ suggesting that this region integrates relevant information from the CON on top of the collected externally and internally relevant information when generating a rule and asserting downstream control.

Recent evidence has elucidated the potential functions of DMN nodes in intelligence tasks beyond feeding internal information toward frontal DMN regions. Transient, task-dependent coupling between the dPCC, DMN, and FPCN nodes enables the integration of externally and internally directed thought.¹¹ The dPCC may be the centerpiece of this coupling due to its ability to coordinate the activity of ICNs to achieve effective control.¹² Integrating internally and exter-

nally directed thought in the DMN, specifically, could tribute to its function in idea generation,⁷² suggesting an alternative route outside of the FPCN for aiding the generation of a hypothesis. Recent evidence by Dixon and colleagues indicates that DMN-DAN functional connectivity isn't always anticorrelated, expressing windows of positive correlation which the authors suggest represents information transfer between the networks;⁷³ so, the DMN has a mechanism for incorporating external information independent of FPCN connections. However, the PCC's role in the DMN's generation of ideas isn't entirely independent of the FPCN since the PCC can transition from a DMN node to an FPCN node during task states.^{10,11,74} The task-dependent recruitment of the PCC and its involvement in integrating internally and externally-directed thought suggests that the PCC is a connector between internally-generated ideas and the FPCN, potentially aiding in the FPCN's generation of task rules. Indeed, Beatty and colleagues suggest that the FPCN evaluates the ideas generated by the DMN,⁷² proposing a mechanism through which the FPCN and DMN could work together on certain tasks. The specific dynamics between the DLPFC and PCC in facilitating rule generation aren't entirely clear; the PCC's recruitment and relay of ideas may be reserved for more internally demanding intelligence tasks. It is important to note that there are no functional associations between DMN nodes and working memory manipulation, supporting evidence indicating that working memory processes are externally oriented.⁶⁹ In contrast, the PCC and its involvement in intelligence tasks will be internally oriented.

The process of determining the rule for a given task likely falls under the step of rule inference since a few rules may be generated that require testing before the best rule for the task can be identified. The process of testing and weeding through hypotheses requires the process of conflict monitoring, something that will be described later. Santarnecchi and colleagues conclude that FPCN and DAN activity is geared towards generating a rule. As individuals transition to the rule application phase, frontal lobe activity decreases while occipital lobe activity increases.⁶⁹ Recent evidence attempting to model the function of the neocortex based on its columnar structure provides a possible explanation for these frontal lobe results. Hawkins and colleagues simulated the ability of the neocortex to recognize objects in our environment.⁷⁵ When scanning an object, initial sensory input constitutes common feature detection, causing dense activation. This dense activation reflects the uncertainty of failing to recognize an object rooted in the lack of information. However, as we scan the object, we accumulate features of the object until we reach enough features to adequately recognize an object, usually occurring when at least one sufficiently uncommon feature allows us to recognize the object. Broad inhibition within the output layer helps to maintain the sparsity of activation patterns,^{76,77} likely representing the need to maintain a specific representation, spread this information, and inhibit other representations. With the significant homogeneity of the neocortex,⁷⁸ some neuroscientists have claimed that the entirety of the neocortex functions in the same way,⁷⁹ and the synaptic connections are what differ

entiate regional differences in observed functions. Considering these implications, the LPFC, implicated in generating and maintaining the rule governing a task, would undergo the same process for rule generation as posterior regions undergo for object recognition. The maintenance of a specific representation through inhibition would explain decreased frontal activation during rule application compared to rule inference; the uncertainty regarding the rule required for a task generates dense activation within the LPFC, causing continued recruiting of internal and external information until a rule is reached and activation is diminished to only a single representation.

With convergence on a rule, the way our brain manipulates behavior to achieve task goals must be explored. However, understanding this requires understanding the mechanisms with which the control networks exert control. Cole and colleagues posited the “flexible hub theory,” asserting that the FPCN is composed of “brain regions that flexibly and rapidly shift their brain-wide functional connectivity patterns to implement cognitive control across a variety of tasks.”⁸⁰ This hypothesis attempts to answer questions regarding the FPCNs importance in adaptive control tasks using two FPCN mechanisms: global variable connectivity and compositional coding. The FPCN has been found to have extensive global connectivity and the highest global variability connectivity,⁸¹ meaning the vast cortical connections of the FPCN are highly susceptible to rapidly and flexibly changing during intelligence tasks. Further, global connectivity differences of the FPCN have been correlated with cognitive control abilities and intelligence,⁸² demonstrating its importance in intelligence tasks. Compositional coding requires the reuse of task elements across task contexts,⁸³⁻⁸⁵ and these functions have been found within the FPCN.⁸⁶ Indeed, compositional coding appears to be analogous to object compositionality explored by Hawkins and colleagues,⁷⁵ who posit that novel objects can be identified through the composition of already-learned objects that comprise the novel object. Using their example, let’s say we see a coffee cup with a logo on it that we have not seen before. We can utilize our pre-existing knowledge to create a representation of this coffee cup by identifying its component parts, namely, the plain coffee cup and the logo. Using this model, compositional coding allows the FPCN to combine previously existing task elements to construct a rule, or combination of rules, required to complete a novel task. Therefore, compositional coding has massive implications for intelligence, potentially explaining how the FPCN enables unique and flexible control according to a generated rule to meet novel task goals. The Flexible Hub Theory also supports the cognitive epochs proposed for the MD system of the primate brain. Duncan explains that different cognitive epochs during task states are represented by overlapping neuronal populations within the frontal brain regions,³ findings supported by other recent research.^{87,88} The overlapping neuronal populations explain the mechanism underlying compositional coding, and the unique activity patterns demonstrate how novel and flexible downstream control can be achieved.

The vast cortical control of the FPCN mediates two critical functions required for cognitive tasks: working memory and

attention. While the DLPFC is a critical frontal component in the FPCN and is essential for both working memory and attentional tasks,⁸⁹⁻⁹¹ Watanabe and Funahashi demonstrated that these two functions recruited the activation of largely overlapping prefrontal populations.^{92,93} Two important conclusions can be made from these results. First, attention and working memory are two closely related cognitive processes mediated by the FPCN; second, working memory and attentional allocation must fight for resources within the FPCN. The dACC, a region of the CON, has been implicated in inhibitory control and suppressing irrelevant information,⁹⁴ which was recently found to be important in rule application.⁶⁹ It is possible that the CON takes on the most crucial role in attentional control during rule application, enabling more neural space for the working memory processes of the FPCN. Still, more research is required to support this claim.

To meet task demands, rule application requires that the internal representation of external stimuli is manipulated in an individual’s working memory according to the rule maintained. The FPCN has been implicated in manipulating information according to goal-directed behavior.⁹⁵ This section discusses the mechanism employed by the FPCN and regulated by the CON to facilitate mental manipulation toward task completion. The LPFC coordinates the working memory manipulation required to meet task goals, while the visual and language processing regions are the template where representations are manipulated. With the mid-LPFC being the main integration center of the FPCN and the major region in contextual control, it is likely the most important frontal region in asserting the working memory manipulation; however, the rostral and caudal regions undoubtedly assist the mid-LPFC in its downstream control and exert downstream control on their own. The RLPFC is unique to humans and is critical for higher cognitive abilities in humans.⁹⁶ The RLPFC mediates the context-specific implementation of a rule and the maintenance of that rule.^{17,61} These results suggest that the RLPFC does the “thinking” we associate with facilitating the timely implementation of a rule. The RLPFC is vital for higher relational thinking,^{97,98} making it important for functions such as analogical reasoning, applying rules to novel features, and reasoning using compound rules.⁹⁹⁻¹⁰³ These functions of the RLPFC epitomize the adaptability required of human intelligence networks, allowing humans to apply rules to novel features, a necessity for most intelligence tasks. The caudal regions of the LPFC likely coordinate with the DAN to enable the requisite eye movements and downstream enhancement required to focus on the salient stimuli from one moment to the next. However, more research needs to be done on the specific downstream function of the caudal LPFC. While contextual control activation patterns suggest the mid-LPFC actively coordinates both internal and external working memory faculties, it is also possible that these results reflect the overlapping of FPCN A and FPCN B nodes within the mid-LPFC, representing separate internal and external access within the region. Whether the internal and external control remains segregated or becomes integrated into the mid-DLP

FC, this region is undoubtedly the most important region for downstream working memory control.

Being the other region within the FPCN, the PPC has also been found to have the same rostral-caudal axis for cognitive control abstraction as the LPFC,¹⁰⁴ and it is tightly linked to the LPFC in facilitating the maintenance and manipulation of information in subserving goal-directed behavior.¹⁰⁵ Further, recent evidence suggests that the superior parietal cortex (SPC) is important for working memory manipulation;⁴⁵ however, it is still being determined whether the SPC exerts downstream control to achieve this or if it is the interface where working memory is manipulated. More work will need to be done to understand which possibility is correct for SPC functioning. Still, it is also possible that the SPC both exerts downstream control on more basic processing regions and serves as an interface for working memory manipulation. In line with the evidence presented above, the rostral PPC regions appear to play less of a role in intelligence tasks, likely due to their connections with internally-oriented cognition, which is reduced during intelligence tasks in most contexts.

Within this section, most of the discussion has focused on the individual functions of the FPCN and CON networks; however, their interplay is important for understanding task dynamics. As previously discussed, Cocchi and colleagues found that phasic, task-specific control according to task goals depends on the task-based integration of the dACC, aINS, and DLPFC.¹⁷ This evidence directly links the CON's role as a control allocator to the downstream control by the FPCN. Throughout the duration of the task, one way in which the CON manages the control allocated is through the dACC's likely role in evaluating response conflict, encompassing both attentional processes and error detection.¹⁰⁶ While both generating and implementing a rule, this CON function ensures that the cognitive process is consistent and in accordance with external information. Notably, the RLPFC is an important region for mediating the task-dependent integration of the CON and FPCN, with increased integration with both the dACC and DLPFC as task difficulty increases.¹⁷ This integration likely reflects increased response conflict and, therefore, an increased need to adjust control, emphasizing that the importance of FPCN-CON connectivity only goes so far with too much integration worsening performance.¹⁷ Despite the maladaptiveness of too much integration, the connectivity serves an important purpose, allowing the FPCN to update downstream control by cognitive systems and flexibly adapt throughout a task and correct mistakes, critical functions of intelligence.

Assem and colleagues attempted to refine and update the MD system of the primate brain,^{3,107} finding a network consisting almost exclusively of FPCN and CON regions associated with intelligence. The willingness to classify the FPCN and CON as one network during intelligence tasks underscores the importance of their interconnectedness during a task state. This tight association reflects the significance of the CON in setting parameters for information recruitment, maintaining the task set, allocating control, and responding to conflict. The possibility of the FPCN updating the CON when switching

task sets provides further avenues for FPCN and CON connectivity to be adaptive during task states. Further research should be dedicated to expanding our understanding of the connectivity dynamics of these two control regions during intelligence tasks.

A vital strategy for approaching intelligence tasks appears to be dividing cognitive tasks into simpler subcomponents. This strategy has been implicated in better task performance and has correlated with fluid intelligence.¹⁰⁸ For example, in number sequence tasks where an individual is required to guess the following number in the sequence based upon the rule for the sequence, let us say the rule is +2, then -5. Humans divide the problem into +2 and THEN -5: we don't do these operations simultaneously. The division of a task into task components reduces cognitive load, explaining its utility during intelligence tasks. Neurologically, the cognitive epochs previously discussed provide a viable mechanism for dividing a task into components. The CON has been considered a flexible integrator of task-based goals,¹⁰⁹⁻¹¹¹ so the CON could signal slight adjustments of control within the FPCN during the transition between different cognitive epochs of a single task. It is also possible that the striatum plays a role in the shift between task components considering the association between the striatum and intelligence in humans and the association between the striatum and the capacity to set-shift in rats.¹¹²⁻¹¹⁷ The CON's function in detecting conflict may provide an avenue for its ability to transition between task components, where previously relevant information is no longer relevant and previously irrelevant information is now relevant. Thus, the CON recognizes the need for a change in activity and facilitates the required modification for the next cognitive epoch.

Further, the transition between task components can be eased if we are aware of the rule governing the next component and, for example, holding the rule -5 in our mind while we apply the rule +2. The RLPFC is likely responsible for maintaining an alternative course of action,¹¹⁸ potentially providing a neural storage system for the rule governing the next task component.

Once a solution to an intelligence task has been identified, the internal solution must be converted into a behavior. This review has widely established that the control systems connect with subcortical structures, enabling the onset of task control, transitions between task sets, and potential transitions between task components. The subcortical structures have also been found to mediate the connection between the cortical systems and motor outputs. Hearne and colleagues found that linking acquired representations with specific actions depends on striatal activity.²⁵ Further, Bonelli and Cummings reviewed multiple frontal-subcortical circuits relevant to behavior. For example, the ACC circuit appears important in enabling motivated behavior, while the DLPFC circuit allows information organization to facilitate a response.¹¹⁹ Another important control region with connections to subcortical structures is the pre-supplementary motor area (preSMA). A few recent studies suggest that the pre-supplementary motor area (preSMA) is within the CON and has connections to both the FPCN and caudate.¹²⁰⁻¹²³ The cortical and subcortical connections of

the preSMA are important for its possible functions in higher-level aspects of motor control, including updating motor plans and learning new motor sequences.¹²⁴ These results demonstrate that multiple cortical-subcortical pathways enable the proper motor response necessary for intelligence tasks. Furthermore, dynamic interactions between these various circuits likely enable the unique motor outputs necessary depending on the task context.

The final important function of the control systems in relation to intelligence tasks is the ability to recognize and adapt following errors. As discussed earlier, Cohen and colleagues characterized the ACC as functioning in evaluating response conflict, encompassing both attentional processes and error detection.¹⁰⁶ Therefore, the CON is likely responsible for recognizing these errors and adjusting the attentional control to minimize the conflict. This hypothesis is supported by more recent findings in a decision-making task that suggests the CON functions as a performance report measure.¹²⁵ These results indicate the ubiquity of this ACC function that is critical for adequately completing intelligence tasks. Interestingly, the same study identifies the right FPCN, but not the left, in bringing about behaviorally salient changes.¹²⁵ These results have not been replicated in studies testing intelligence, so this functional lateralization may not apply to intelligence tasks. However, the results suggest that the FPCN is critical for making the required changes to support goal-directed behavior. This finding is consistent with this review thus far.

Intelligence Differences:

To examine the neural correlates of intelligence, it is not enough to only discuss the underlying network mechanisms that facilitate intelligence task completion; instead, neural correlates of intelligence differences must also be analyzed. The neural correlates of intelligence differences have primarily been examined through functional and structural associations between brain regions and psychometric intelligence tests. This review section will attempt to contextualize these regional findings into their underlying networks. Further, intelligence differences have also been examined through the speed of processing metrics. Notably, there has been discussion as to whether more general or specific tract efficiency is more beneficial. Last, the recent work in network neuroscience has introduced a third perspective on the neural correlates of intelligence differences. Overall, this section attempts to answer this question: *How are the functional and structural dynamics of the ICNs manipulated to increase human intelligence capabilities?*

The Parieto-Frontal Integration Theory:

While the steps of processing proposed in the P-FIT were expanded upon in the previous section, this section addresses the structural and functional differences subserving intelligence differences. Recently, the P-FIT was updated, and these updates included the introduction of results from studies after the P-FIT was published, the pruning of studies only to include those that involved intelligence differences, and the division of the negative functional associations, positive functional associations, and positive structural associations with psychometric intelligence.¹¹⁶ The regions that Basten and colleagues have implicated in intelligence include the frontopolar

cortex (RLPFC), the lateral PFC, the ACC, the preSMA, the insula, the parietal cortex, the PPC/precuneus, the temporal cortex, the occipital cortex, the caudate nuclei, and the mid-brain. Since Basten and colleagues' revisions are more recent and narrowed towards the focus of this section - intelligence differences - the regional associations with intelligence analyzed in this paper will originate from their revisions rather than from Jung and Haier. In light of the updates to task-processing stages proposed in this review, the regional associations proposed by Basten and colleagues will be analyzed by the ways in which they augment network functioning within their task-processing roles.

Beginning with the visual processing system, positive functional and structural associations with intelligence were found in both the 'what' and 'where' visual pathways. For the structural associations, Basten and colleagues used only voxel-based morphometry (VBM) studies measuring gray matter volume,¹¹⁶ so this analysis will focus solely on the utility of differences in gray matter volumes. Recent evidence suggests that the positive structural associations increased these regions' feature and object recognition capabilities. In a recent study, capacity was defined as the number of objects a network can learn and recognize without confusion.¹²⁶ Their results indicated that increasing the number of neurons in either the input or output layers of a cortical column or increasing the number of cortical columns within the region, given the column sizes are fixed, can all increase neural capacity.¹²⁶ So, the greater gray matter volume within the visual system would likely enable more efficient and accurate identification of objects and relevant features. This structural advantage could reduce demand on higher cognitive regions by reducing unnecessary information being relayed to these regions through more efficient identification of salient stimuli. Positive functional associations with intelligence were found in both the temporal cortex's object identification regions and the parietal cortex's spatial attention regions. These activation correlates are unlikely to reflect initial processing stages; instead, they potentially reflect a more robust recruitment of these regions in maintaining salient information or utilizing these regions' representations for working memory manipulation. Along these lines, the positive structural associations in the temporal cortex could increase the capacity for working memory manipulation, easing the transition between object representations.

Looking at the DMN, there were regional associations in the PCC and precuneus with intelligence. To begin, the PCC experienced positive structural associations with intelligence. Applying the findings for neural capacity to the PCC, the greater gray matter volume in the PCC facilitates greater neural capacity for PCC functions, including generating global metastability for shifts in attentional focus and integrating information necessary for control from various brain regions. The efficiency of these processes would enable greater global network flexibility in shifting attentional state and integrating control processes. The precuneus is a DMN hub that increases connectivity with FPCN during a task,¹²⁷ and Basten and colleagues found both positive and negative functional associations with intelligence.¹¹⁶ Along with the PCC, the precuneus

is important for integrating information from systems segregated at rest.^{11, 128-130} Further, the precuneus is implicated in a wide array of functions, with spatial functions and navigation being the two most relevant for intelligence tasks.^{131,132} The positive and negative functional associations with intelligence could relate to the selective recruitment of this region depending on task context or fine-grained activation and inhibition of precuneus subregions. Both selective recruitment and fine-grained recruitment would reflect the control networks' flexibility of regional recruitment according to task goals and suggest that higher-intelligent individuals can better recruit the precuneus functions and information necessary for a given task.

Looking at the FPCN, all three types of associations were present. In the FPCN's frontal regions, both the RLPFC and the LPFC experienced positive structural associations with intelligence. Fewer features were required to identify an object as the number of cortical columns increased during the simulation run by Hawkins and colleagues,¹²⁶ and viewing these results from the perspective of the FPCN's frontal regions, the larger number of cortical columns may reflect more efficient identification of the rule in a task, requiring less external and internal information to reach the rule. Not only can a rule be identified through fewer features, but increased gray matter volume in the caudal and rostral regions also allows for the more precise input of information. This is rooted in the mechanism through which capacity increases: greater gray matter volume warrants activity profiles of representations to have fewer overlapping patterns. This means that the information sent to the frontal regions is also likely to be more precise in higher-intelligent individuals, further quickening rule identification. The greater efficiency of rule generation is highly cost-effective, spending fewer resources on generating the rule and more on the downstream control required to complete task goals. Beyond structural associations, both positive functional and negative functional associations exist between the LPFC and intelligence. There are multiple ways to interpret the functional associations of the LPFC and psychometric intelligence. The LPFC likely experiences both stable and dynamic activation throughout a task and across task components due to properties outlined in the Flexible Hub Theory and this review. These activation patterns would make functional associations hard to parse, and it is possible that some studies found positive associations while others found negative associations due to varying contexts. It is also possible that finer-grained regions within the LPFC were associated with positive and negative associations, respectively. Second, the neural efficiency hypothesis suggests that higher-intelligent individuals experience less cortical activation than average-intelligence individuals on the same task.¹ The idea behind these results is that these tasks would require less cognitive demand of the higher-intelligent individuals, warranting less activation. Recent evidence also suggests the opposite is the case, where higher-intelligent individuals experience greater cortical activation than average-intelligent individuals.¹³³ These results were contingent upon the task's complexity, suggesting that the average-intelligent individuals gave up, demonstrating

less LPFC activation. In contrast, higher-intelligent individuals were engaged in the task since they had the capabilities to solve the problem. So, the positive and negative functional associations found could depend upon the difficulty of the tasks used in the studies Basten and colleagues analyzed.¹¹⁶ Both the flexible hub explanation and the neural efficiency explanation are plausible, and it is also possible that both are true simultaneously; however, further research is necessary to understand the cause of the findings.

Beyond the frontal lobe, the FPCN also contains regions within the PPC. The positive functional associations within the PPC were present along the entirety of the rostral-caudal gradient.¹¹⁶ It is possible that these results support the feedforward recruitment of internally and externally salient information in the frontal lobe during rule generation; however, it is also possible that these associations relate to the manipulation of representations in one's working memory during Rule Application. Recent evidence may support the second possibility. As problems become more challenging, lower-intelligent individuals struggle more with task solving, likely routed in their worse ability to divide problems into simpler components or plan a problem-solving strategy.^{108,134} Thus, higher-intelligent individuals are more likely to reach the mental manipulation stage of task completion. These results are supported by the notion that Rule Inference is marked by a high amount of frontal activation. In contrast, Rule Application sees a reduction in that frontal activity as resources are devoted to posterior regions.⁶⁹ Since lower-intelligent individuals spend longer in Rule Inference than higher-intelligent individuals, the lower-intelligent individuals would have frontal-heavy activation profiles that would cause them to have less parietal activation than higher-intelligent individuals. Further, positive functional associations in object recognition or language regions could reflect the active manipulation of these areas according to task goals. Research should be done to understand the temporal dynamics of these associations further.

The results of Basten and colleagues in the LPFC and PPC could also indicate activation patterns within the DAN.¹¹⁶ Some regions associated with intelligence in the LPFC and PPC could overlap with DAN regions, such as the frontal eye fields, ventral premotor area, and the superior parietal lobule. The associations within these regions are predominately positive functional associations and suggest that greater DAN activity is associated with intelligence. These results would indicate that higher-intelligent individuals have greater resources directed toward the attentional processing of sensory stimuli, a finding supported by associations between DAN activity and fluid intelligence.⁶⁹ However, it is likely that the positive functional associations in these regions are indicative of both FPCN and DAN activity, subserving the overall goal of task completion. While the DAN maintains attentional focus on the external stimuli, the FPCN can manipulate this information with the working memory to meet task goals.

The CON was associated with all three types of associations. Beginning with the dACC, both positive and negative functional associations were found with intelligence. The most likely explanation relates to the flexible nature of the CON,¹⁰⁹⁻

¹¹¹ causing flexible activation of the dACC that subserves its main functions in conflict resolution, control allocation, and task-set maintenance. Another explanation could be rooted in the adjacency of ACC regions implicated in the CON and salience network (SN) networks. The SN is involved in “representing and responding to homeostatically relevant internal or external stimuli and imbuing these stimuli with emotional weight.”¹³⁵ Emotional interference has been proven to affect cognitive control negatively,¹³⁶ so the emotional functioning of the SN is counterproductive to the completion of intelligence tasks. In contrast, CON activity is advantageous considering its functions in conflict resolution and task-set maintenance. Therefore, dACC functional associations may reflect better inhibition of SN and better activation of CON.

The preSMA regions experienced all three associations with intelligence. These associations likely aid in this region’s motor preparation and execution. Applying the cortical column mechanism previously discussed,¹²⁶ both the functional associations exhibited by the preSMA and the structural associations within the SMA likely reflect greater convergence onto one motor plan. Greater convergence in higher-intelligent individuals could be caused by better problem-solving abilities, reducing uncertainty about what action to take, or through the more distinct neural activity of specific motor plans. Finally, the aINS didn’t experience any associations with intelligence. Considering its integrative role in CON functions, the amount of aINS activity is likely less important than the quality of that activation. Controlling global dynamics in a behaviorally salient way requires unique and flexible activation patterns but not necessarily more or less activation.

Additionally, reduced activation within the posterior insula (pINS) was associated with intelligence. Some studies have implicated the pINS in the CON.^{35,125} Regardless of the pINS’ connectivity to the CON, its role in representing interoceptive information about the body’s physiological status isn’t necessarily relevant in intelligence tasks.¹³⁷ So, the negative functional associations with intelligence could be due to a reduction in resources dedicated to this function, preventing these regions from interfering with the control required for task goals. In the CON broadly, functional and structural differences within the dACC appear most advantageous for intelligence. This suggests that the core for improving CON function is enhancing its specific cognitive abilities more than its global influence on brain dynamics.

What most differentiated the results from the P-FIT and its revisions is the addition of the caudate and the midbrain.^{2,116} Basten and colleagues suggest that the structural associations of these two regions relate to their involvement in the mesocortical dopamine system.¹¹⁶ For the caudate, recent evidence suggests that increased gray matter volume is correlated with better delay discounting and decreased impulsivity.^{138,139} These studies indicate that gray matter volume in the caudate is critical for maintaining long-term goals. Applying these results to intelligence tasks, increased gray matter volumes in the caudate may enable higher-intelligent individuals to maintain focus on task completion better. The structural associations of the midbrain are also likely to aid in maintaining long-term

goals during task conditions. In their review, Ott and Nieder demonstrate how the dopaminergic connections from the midbrain to the PFC reflect the perception of behaviorally salient information by the PFC, and the dopamine released enables the encoding of this information into working memory.¹⁴⁰ Indeed, the midbrain aids in directing the PFC towards behaviorally salient stimuli, maintaining the long-term goals through the mediation of feedforward processes.

Modularity:

The past few years have seen a shift from examining intelligence concerning associations in regional gray matter volume and activation to instead examining associations of structural connectivity and modularity with intelligence. While this line of research is still a region-based approach, it lies within a network neuroscience perspective, epitomizing the recent shift to network neuroscience to tackle one of neuroscience’s most significant challenges: uncovering the neural basis of intelligence. Thus, the structural connectivity and modularity of specific regions will be examined through their influence on the intrinsic networks they subserve and broader task dynamics discussed in the first section.

Recent research seeks to discover intelligence associations between node-specific measures of within- and between-module connectivity from cortical and subcortical regions previously implicated in intelligence.¹⁴¹ Within the CON, Hilger and colleagues have found that intelligence was associated with lower within-module connectivity and higher between-module connectivity of the aINS. They reasoned that the aINS’ connectivity pattern facilitated the processing of salient information between modules.¹⁴¹ This conclusion is supported by the evidence proposed in the first section of the discussion. However, the global connectivity of the aINS does more. The aINS is also responsible for downstream task set maintenance and facilitating the proper allocation of control. Thus, the greater integrative capabilities of the aINS in higher-intelligent individuals not only enable the processing of salient information but it tries to maximize the efficiency and effectiveness of the attentional and working memory processes.

Interestingly, there were no associations found between the dACC and intelligence.¹⁴¹ These results suggest that the connectivity of the dACC is relatively stable across intelligence levels and that variances in the connectivity of the dACC aren’t as critical of a determinant for proper CON functioning as variances in the connectivity of the aINS. These results make sense, considering that the specialized functions of the dACC require a relatively isolated position in the brain. Still, the dACC also needs its between-module connections with the DLPFC and aINS to fulfill its functions. With respect to modularity differences, the ability of the CON to adjust global brain dynamics appears most critical to its role in task-set maintenance, control allocation, and conflict resolution. Interestingly, activation pattern differences suggest a mechanism for the enhancement of CON’s specific functions, meanwhile modularity differences of the CON account for the enhancement of its global functions. Indeed, these results highlight the importance of multiple perspectives for

studying the neural correlates of intelligence differences in generating a complete picture of neural enhancements in higher intelligent individuals.

Continuing the discussion on the control networks, many within- and between-network associations within the FPCN and intelligence are primarily centered within their frontal regions. For example, the anterior tip of the superior frontal gyrus, a region within the RLPFC, had both negative between-network and positive within-network modularity.¹⁴¹ Hilger and colleagues understood this to represent the inhibition of distracting information from the DMN interfering with goal-directed behavior. The evidence suggested in this review would support this notion since interference by the DMN on the RLPFC has been proven to interfere with goal-directed behavior.¹⁷ However, this review wouldn't support their suggestion that the RLPFC's influence in task contexts must be diminished. Instead, the RLPFC has been proven to play an integral role in the FPCN, supplying the higher-order abstract abilities required to complete tasks. So, the increased modular structure in higher-intelligent individuals may facilitate the RLPFC's specialized higher-order functions. Interestingly, the middle frontal gyrus (MFG) and inferior frontal gyrus (IFG) displayed positive within-module connectivity associations with intelligence. Both regions are a part of the LPFC, widely considered the central integrative hub of the FPCN, and a major connector hub,^{82,111,142} so these results may initially appear contradictory to previous evidence, but they are not. There was no positive or negative association for these regions with between-module connectivity and intelligence, indicating that the integrative functions of the LPFC are relatively consistent regardless of intelligence level. According to recent network neuroscientific evidence, greater within-module connectivity produces more efficient processing,¹⁴³ potentially explaining the results within the LPFC. Greater efficiency supports critical functions of the LPFC by allowing greater capacity to generate task rules, meet working memory demands, and organize the downstream control required to complete task goals. Therefore, these results suggest that higher-intelligent individuals don't have an advantage in the integrative connectivity of the FPCN, instead showing benefits in the capacity for the higher-order thinking and control planning required to utilize their integrative functions most effectively.

Hilger and colleagues distinguished between two overlapping regions of the brain: the tempoparietal junction (TPJ) and the inferior parietal lobule (IPL). However, the results for both the TPJ and IPL were focused on the angular gyrus and supramarginal gyrus. These two regions are traditionally considered the IPL,¹⁴⁴ so this review will collectively refer to these regions as the IPL. During the initial processing stages, the IPL likely functions in language comprehension, processing language from simple sounds and phonemes to syntax and the meaning of information.¹⁴⁵ During rule application stages, the angular gyrus (AG) is likely responsible for comprehending event concepts and mentally manipulating representations. The supramarginal gyrus (SMG) is likely responsible for verbal working memory processes,^{68,146}

accessible by the FPCN during intelligence tasks. Hilger and colleagues found the IPL to have negative between-module connectivity and positive within-module connectivity associated with intelligence, and these associations were interpreted as reducing the IPL's influence during intelligence tasks, minimizing the interference of irrelevant processes on task goals.¹⁴¹ It is unclear how much of a role the IPL plays in intelligence; but, considering that the IPL broadly overlaps with the FPCN,⁵⁴ has positive functional associations with intelligence,¹¹⁶ and is responsible for functions important for specific intelligence tasks, it is unlikely that the functional connectivity variances serve an isolating role. So, the structural variances of the IPL may serve to aid in the specialized functioning of the IPL, enhancing functions that are advantageous for intelligence in specific contexts.

The last important finding involves the modularity of sub-cortical regions associated with intelligence; both the caudate and hippocampus had increased within-module connectivity associated with intelligence that Hilger and colleagues related to requiring a more independent position within their functional modules.¹⁴¹ This conclusion is reasonably substantiated by the evidence presented throughout this review. To begin, the caudate has been implicated in imbuing the frontal control regions with the necessary motivation to complete task-relevant goals, facilitating both initiation and updates to these goals. So, greater within-module connectivity would increase the efficiency and effectiveness of the caudate's specialized function,¹⁴³ namely, generating the necessary goal-directed behavior. The results also indicate that the caudate has already established all the required between-module connections, regardless of intelligence level, required for its functions. This suggests that generating goal-directed signals within the caudate, more so than their propagation, is critical for explaining variation in intelligence. On the other hand, the within-module associations between the hippocampus and intelligence appear to follow the conclusion presented by Hilger and colleagues.¹⁴¹ All major studies examining functional associations with intelligence find no functional associations between the hippocampus and intelligence.^{2,3,107,116} Therefore, the hippocampus isn't significantly involved in intelligence, and its isolation from task-positive regions during a task, indicated by the increased within-module connectivity, would be advantageous during intelligence tasks.

The region-specific modularity correlates with intelligence are crucial for understanding how specific regions function within their broader network to facilitate critical task-relevant functions; meanwhile, general modularity correlates with intelligence and explores the underlying global mechanisms that drive the brain towards completing intelligence-based tasks. These general correlates have been studied in recent years.

A theme throughout the review has been the necessity of integration to facilitate high cognitive performance on intelligence tasks, with both the FPCN and CON having been demonstrated to have vast connections throughout the brain. Recent evidence has supported this position, finding that the

brain can flexibly shift between segregated (high modularity) and integrated (low modularity) states, with the integrated states being associated with high cognitive performance.⁶¹⁻⁶⁴ This push towards a more integrated topology is complementary to evidence that low rates of high-modularity states are associated with intelligence, better protecting higher intelligent individuals from network fragmentation that interferes with network communication required for task goals.¹⁴⁷ The topological patterns during task conditions allow for effective inter-regional communication by promoting integration and preventing fragmentation of specialized regions. These results underscore the need for long-range communication and the integration of vast cortical activation to meet task goals.

Hilger and colleagues also found that greater stability of network segregation over time was associated with intelligence and that the DAN was driving this network stability.¹⁴⁷ Their findings support results that implicated the DAN as having the most significant functional associations with fluid intelligence.⁶⁹ The DAN's association with fluid intelligence reflects greater attentional focus, which requires stable activation throughout the entirety of the task. Thus, the necessity for the DAN to maintain a stable attentional focus drives the stability of network segregation. Importantly, Santarnecchi and colleagues suggested that the weaker functional associations between FPCN and CON with intelligence reflected less important implications for these networks and intelligence than previously reported.⁶⁹ However, the lack of temporal stability for network integration suggests that the major connector hubs don't have temporally stable connections throughout task demands. In conjunction with the flexible hub theory and the CONs flexible connectivity,^{80,109-111} these results suggest that control networks provide flexible connectivity required to meet the dynamic control demands throughout a given task. So, these networks are no less important for intelligence tasks than the DAN. Still, their integrative demands create flexible topological patterns during tasks that won't likely manifest in functional associations with intelligence. While both integrative and segregative patterns are important for intelligence, these patterns also provide a plausible avenue to connect previous intelligence studies, such as the study by Santarnecchi and colleagues,⁶⁹ to the evidence within network neuroscience.

The results connecting modularity with resting states and task states further the complexity of network dynamics facilitating intelligence. Unlike task conditions, intelligence lacks intrinsic associations with either segregation or integration at rest.^{141,148-150} Despite discrepancies between the task and rest states, temporal stability of network organization from resting to task state is associated with intelligence, interpreted as requiring less network reconfiguration, and presumably cognitive effort, to switch from a resting state to a task state.¹⁵¹ It is possible that higher-intelligent individuals possess a more effective resting state connectivity profile among the intrinsic connectivity networks that enables the minimal network reconfiguration required for intelligence tasks. Evidence supporting this claim comes from Hearne and colleagues, who found that greater connectivity between

the FPCN and DMN during rest was associated with higher intelligence.¹⁵² Higher-intelligent individuals have greater connectivity of intrinsic networks at rest, possibly explaining the greater stability from resting to task state. In contrast, lower intelligent individuals require greater network configuration when transitioning into a task state, requiring greater cognitive demand and creating a less efficient processing system. The results found by Hearne and colleagues may relate to the functioning of the PCC in facilitating the transition from resting to task states, where greater connectivity to the PCC by task-positive networks during rest eases the demand on transitioning between states. Notably, too much functional connectivity of intrinsic connectivity networks is suboptimal, impairing cognitive abilities as humans age and suggesting that higher-intelligent individuals likely obtain a near-optimal level of connectivity.¹⁵³

Neural Efficiency:

Decades of research have examined how metrics of neural efficiency relate to intelligence differences. A pivotal trigger for this line of research was the Neural Efficiency Hypothesis, which proposed that higher intelligence was associated with less neural activation, interpreted as less neural effort.¹ In the more than three decades since this paper, many researchers have expanded upon these results by tying other variables to neural efficiency and intelligence, including speed of processing,¹⁵⁴ shorter characteristic path length and greater global efficiency,¹⁵⁵ and global white matter integrity.^{156,157} However, a recent study has elucidated event-related potential (ERP) latencies as a highly reliable measure to explain variation in intelligence.

Schubert and colleagues examined whether higher intelligent individuals expressed global information processing correlations with intelligence or specific information processing correlates with intelligence using ERP latencies.¹⁵⁸ Their study indicated that the latter was true, finding that the latencies of later components explained 80% of the variance in general intelligence. Specifically, the P300 latencies showed the most significant association with the intelligence of all the ERP latencies. P300 is proposed to reflect the inhibition of extraneous processes to transmit information from frontal attention and working memory areas to temporal-parietal memory storage regions.¹⁵⁹ Since short-term/working memory has also been associated with more than half of the variance in general intelligence, and there has been an abundance of correlations between the speed of information-processing and short-term/working memory, Schubert and colleagues propose that the speed of higher-order processing aids working memory by facilitating faster inhibition of irrelevant information.¹⁵⁸ Further, they claim these processes serve intelligence by increasing the efficiency of selective attention and memory updating. Within the purview of this review, these results emphasize the importance of the allocation of resources on intelligence task completion. Funahashi details evidence that both attentional control and working memory capacity rely on overlapping neural populations within the LPFC, a pivotal FPCN region.¹⁶⁰ P300 appears to make the frontal cortex's downstream working

memory and attentional control more efficient. Specifically, P300 appears to reflect the greatest efficiency on the attentional control aspects that can most effectively inhibit the influence of irrelevant information. This efficiency will open greater neural space for working memory, increasing its capacity and influence on downstream regions. These results underscore the importance of working memory capacity in intelligence tasks, explaining the importance of processing speed on this capacity.

The variances in ERP latencies found by Schubert and colleagues support the notion that higher-intelligent individuals have greater neural capacity caused by the increased efficiency of attentional processes. Along these lines, recent work has updated the Neural Efficiency Hypothesis by demonstrating that the pattern of neural effort reversed as task complexity increased, where higher-intelligent individuals showed increased activity in both FPCN and CON regions. In contrast, lower-intelligent individuals saw decreased activity in these regions.¹³³ These authors interpreted these results as increasing cognitive effort in higher-intelligent individuals as complexity increases, whereas lower-intelligent individuals cease to try after reaching their cognitive capacity.¹³³ Among many factors, the ERP latencies studied by Schubert and colleagues likely enable this cognitive capacity, reflecting the greater working memory capacity of higher intelligence individuals that allows them to take on cognitively complex tasks; meanwhile, the inefficiencies of these same processes causes lower intelligent individuals to reach capacity and give up on the task.

While the results previously discussed reflect neurological processes that amend the Neural Efficiency Hypothesis,^{133,158} current research also suggests that a cognitive practice can influence our understanding of neural efficiency. During response selection, average-intelligent (A-IQ) individuals experience greater response conflict and greater working memory load, reflected in greater ACC and ventrolateral prefrontal cortex (VLPFC) activation, respectively, than higher-intelligent (H-IQ) individuals. Further, H-IQ individuals demonstrated greater activation during feedback evaluation, reflecting formulation of response strategies (caudate), motor planning (middle frontal gyrus), and task set reconfiguration (superior parietal cortex) than A-IQ individuals. These authors concluded that higher-intelligent individuals diverted greater cognitive resources toward planning the next response, reducing the activity required during response selection.¹³⁴ Devoting more resources to planning reflects a cognitive mechanism employed by higher-intelligent individuals to reduce neural demand and allow for greater efficiency during rule application. Notably, this is only possible when the rule for the upcoming task can be predicted; however, repeated efforts to encode task rules to memory could aid in rule generation for future, unpredicted tasks.

In this section of the review, it has been demonstrated that greater neural efficiency provides space for greater neural capacity, which is concentrated almost entirely in the frontal regions. For example, P300 makes inhibition of irrelevant processes more efficient,¹⁵⁸ opening up greater neural space

for working memory in prefrontal neuronal populations; greater cognitive planning in H-IQ individuals enabled less prefrontal activation than found in A-IQ individuals,¹³⁴ reflecting more efficient processing of salient information and control; and this efficiency means that high-intelligent individuals had a greater capacity for increasingly complex tasks, allowing them to solve complex tasks that lower-intelligent individuals were unable to solve.¹³³ All of these results indicate that the most critical point is the transition from rule generation to rule application. This transition into rule application requires both the successful generation of a rule and the production of a response strategy based on the generated rule, with greater neural efficiency proven to aid both processes.

The Network Neuroscience Theory of Intelligence:

The Network Neuroscience Theory of Intelligence is the most comprehensive theory put forth in the network neuroscience field for the neural correlates of intelligence. While this review has discussed previous evidence related to network neuroscience - namely, variances in modularity - the Network Neuroscience Theory of Intelligence attempts to explain intelligence through network neuroscience rather than describe characteristics of intelligence.^{5,141,147} The two central tenants of the Network Neuroscience Theory of Intelligence are that intelligence relies on the small-world model of cortical structure and that the capacity to transition between network states rapidly explains variances in intelligence.

The small-world structure of the cortex explains that the brain is comprised of densely interconnected modules that contain sparser, long-distant connections connecting modules from across the cortex. Barbey suggests that the densely interconnected modules enable specific cognitive operations; meanwhile, the long-range connections provide the integrative faculties to enable broad cognitive abilities, including intelligence.⁵ Evidence presented throughout this review supports the importance of specialized cognitive abilities and their integrative recruitment. For example, the ACC's important role in conflict detection is crucial for the adaptive adjustments of control necessary for task completion.¹⁰⁶ The IPL's role in abstract and concrete language comprehension is vital for generating relevant information during rule generation and may be dynamically recruited during rule application depending on task demands.¹⁴⁵ In contrast, the LPFC and aINS have extensive global connectivity that warranted more integrative functions,^{81,82,161-163} dynamically recruiting specialized functions such as those within the dACC and IPL. Indeed, the importance of the integrative and segregative functions of the cortex is exemplified by variances in regional modularity found to be advantageous for intelligence. Therefore, the small-world model of the brain relies on a balance among regions expressing more regular or random network structures. This variation of the small-world model creates the flexibility expressed during intelligence tasks, enabling integrative and segregative capabilities in the brain.

According to the Network Neuroscience Theory of Intelligence, general intelligence depends upon the dynamic reorganization of ICNs in service of system-wide

flexibility and adaptability.⁵ The control networks provide the integrative template upon which task-specific connectivity is constructed from the dynamic recruitment of specific cognitive abilities. The control system's dynamic recruitment of specific cognitive abilities is rooted in the topological reorganization of the ICNs during intelligence tasks. For example, the FPCN can recruit specific DMN nodes according to task demands,^{10,11,25,164} illustrating the accessibility of pre-existing knowledge and internal-oriented representations necessary for intelligence tasks. Further, the sensory regions recruited during task demands depend on the external stimuli present and the sensory manipulations upon one's internal representation necessary for task demands.

Beyond the reorganization of ICNs, intelligence difference relies on the capacity to flexibly transition between mental states.⁵ Barbey suggests that the control systems enable these flexible transitions between network states since they exhibit greater degrees of variability that manifest in time-varying profiles of functional connectivity.^{165,166} The control systems were explicitly tied to the capacity to reach difficult-to-reach states,¹⁶⁷ indicative of their vast long-range connections throughout the brain. Indeed, these weak, long-distant connections explained variance in general intelligence better than the strong, short connections.¹⁶⁸ So, the long-range connections of the control networks are crucial for general intelligence and enable the global shifts in network states. Within the context of this review, two network states critical for intelligence coincides with rule generation and rule application, where the brain strives to obtain a rule and manipulate working memory to achieve task goals. The initial feedforward processes that activate the control regions are likely direct, representing easy-to-reach states. From there, the control networks dynamically recruit brain regions upon the intelligence-general integrative template of connectivity. The convergence on a rule depends upon the proper recruitment of internally and externally sourced information, the specific downstream control characteristic of the different FPCN and CON subnetworks,^{55,169} and the short-range interactions between the different subregions of the.^{170,171} Indeed, rule generation relies on short- and long-range connections to traverse an indirect but necessary path to converge upon the rule. The frontal activity diminishes once the rule is reached, reflecting a more direct maintenance path. By its nature, this direct path represents an easing of the network state, and maintaining this pathway likely strengthens the connections as well, further easing the demand for its maintenance. Once again, the brain strives towards difficult-to-reach states, reflecting the long-range, downstream control by the frontal control regions to manipulate the working memory according to the rule acquired. At this stage, segregating the task into simpler subcomponents is advantageous and is correlated with intelligence.¹⁰⁸ Neurologically, these subcomponents manifest in cognitive epochs described by the MD Theory that activate respective neural ensembles,^{3,43} flexibly asserting downstream control.⁸⁰ These neural mechanisms are designed to reduce demand, making it easier to reach a difficult-to-reach state. Each subcomponent may work the same

way as rule convergence, where a subcomponent's completion coincides with slightly diminished activity, reflecting neural rewiring to create a more direct path and strengthening of the connection, which must be maintained during future components. However, the nature of this mechanism suggests that the greater numbers of components, indicative of increasingly complex tasks, reflect more and more indirect pathways to maintain our working memory. This mechanism could explain the benefits of dividing a task into subcomponents for higher intelligent individuals, where periodically easing the network state could allow higher-intelligence individuals to more effectively reach the difficult-to-reach state that enables the completion of task goals.

Beyond task components, the brain employs other mechanisms to ease transitions towards difficult-to-reach states required for intelligence tasks. The ERP latencies studied indicate that the best component in explaining variances in general intelligence is P300, which is implicated in more efficient inhibition of irrelevant information. This downstream control by the control networks contributes to its ability to reach difficult-to-reach states. As demonstrated in this review, more efficient downstream attentional control opens greater neural space for working memory, increasing working memory capacity. The DAN, responsible for attentional control, exhibits stable within-network functional connectivity and segregation during intelligence tasks.^{147,172,173} These results indicate that the DAN cannot significantly contribute to the control network's ability to drive the brain into difficult-to-reach states because any significant changes in functional connectivity would not occur during task states. Despite the importance of the DAN's attentional control on intelligence,⁶⁹ the DAN's role appears to be rooted in creating more efficient attentional control to provide greater capacity for the control networks to drive the brain into difficult-to-reach states through their manipulation of working memory.

The significance of P300 doesn't stop at attentional efficiency; instead, Schubert and colleagues suggest that P300 also contributes to memory updating.¹⁵⁸ These results propose another insufficiently researched mechanism for easing transitions toward difficult-to-reach states: memory. Graham and colleagues found that planning during delay periods was associated with intelligence.¹³⁴ While intelligence tasks don't usually have delay periods, this planning indicates an effort to encode a rule to memory for future use. Encoding a rule to memory would be highly advantageous to intelligence tasks, allowing our control networks to converge more efficiently on a rule. While memory relies on easy-to-reach states, the memory must be applied to a novel task, requiring a difficult-to-reach state and giving memory room to contribute to intelligence.

A Holistic View?:

Thus far, this review has elucidated countless connections between the various theories of intelligence, augmenting our understanding of the neural correlates of intelligence. In addition, a few neural characteristics have been reoccurring threads, connecting these multiple theories and perspectives.

Understanding these threads will augment our understanding of the neural correlates of intelligence, bringing us closer to a holistic view.

The first thread that was pervasive throughout all neuroscientific theories was neural networks. For both task processes and intelligence differences, global and regional neural dynamics were most effectively analyzed by tying these dynamics to their respective neural networks and explaining the significance of these results to intelligence. Analyzing the neural dynamics of the various neural networks proved crucial for tying the prominent theories together: The Network Neuroscience Theory of Intelligence,⁵ the Process Overlap Theory,⁴ the MD Theory,³ and P-FIT all rely on neural networks to neurologically explain their theories.² The dynamic interplay between the brain networks was extensively discussed in the previous two sections and would be too extensive to outline here. However, the most important network findings discussed here, and prevalent throughout the various theories, is the importance of the control networks, specifically, how the control networks dynamically recruit other networks or network nodes to enable intelligence processing.

The control networks' ability to dynamically recruit other cortical networks and nodes requires understanding the second thread connecting the various theories of intelligence: flexibility. The control networks displayed flexibility in activation during task processes,^{3,43,80,109-111} and displayed task-specific, time-varying functional connectivity.^{43,165,166} Indeed, this review explains how these processes enable the domain-general integrative template upon which specific cognitive abilities are recruited for intelligence, providing up-to-date neural support for the Process Overlap Theory and explaining the mechanism that the P-FIT couldn't yet supply for the control network's ability to produce responses.^{2,4} Further, this flexibility enables the brain to drive toward a difficult-to-reach state,⁵ and higher-intelligent individuals can more efficiently drive the brain into these states. As previously discussed, P300,¹⁵⁸ planning,¹³⁴ and task components reflect three of the likely many ways that higher-intelligent individuals can more efficiently reach difficult-to-reach states.¹⁰⁸

With the power to connect all perspectives of the neural correlates of intelligence, neural networks, and network flexibility could provide the foundation for a holistic perspective of intelligence. Indeed, recent papers are converging upon these two threads, most notably the Process Overlap Theory.⁴ This pattern suggests that neuroscience is already converging upon the core of intelligence in the brain. These positive strides are very promising for the future of neuroscience.

■ Conclusion

With decades of research dedicated to identifying the neural correlates of intelligence, the neuroscientific community continues to refine its understanding of intelligence in the brain. This review has compiled the most up-to-date and relevant research on the neural correlates of intelligence task processing and intelligence differences. Notably, the evidence compiled in this review covered many different perspectives on intelligence, requiring analysis of the crossroads between

these perspectives. The first two sections culminated in this review's final section, which covered the threads that most consistently connected the various perspectives of intelligence: neural networks and neural flexibility.

More important than this review's time-tested accuracy is the potential for further refinement of our understanding of intelligence due to the threads identified in this review. Indeed, this review opens exciting new possibilities for the future of intelligence research in neuroscience.

■ Acknowledgments

I want to thank Mrs. Wimsett at South Western High School. Despite having minimal knowledge of neuroscience, she supported my efforts by helping me gain access to the papers cited in this review and asking great questions that challenged me to construct a better paper.

■ References

- Haier, R.; Siegel, B.; Nuechterlein, K.; Hazlett, E.; Wu, J.; Paek, J.; Browning, H.; Buchsbaum, M. Cortical Glucose Metabolic Rate Correlates of Abstract Reasoning and Attention Studied with Positron Emission Tomography. *Intelligence* **1988**, *Volume 12, Issue 2* (1988), Pages 199-217.
- Jung, R. E.; Haier, R. J. The Parieto-Frontal Integration Theory (P-FIT) of Intelligence: Converging Neuroimaging Evidence. *Behavioral and Brain Sciences* **2007**, *30* (2), 135-154. <https://doi.org/10.1017/S0140525X07001185>.
- Duncan, J. The Multiple-Demand (MD) System of the Primate Brain: Mental Programs for Intelligent Behaviour. *Trends Cogn Sci* **2010**, *14* (4), 172-179. <https://doi.org/10.1016/j.tics.2010.01.004>.
- Kovacs, K.; Conway, A. R. A. Process Overlap Theory: A Unified Account of the General Factor of Intelligence. *Psychological Inquiry* **2016**, *27* (3), 151-177. <https://doi.org/10.1080/1047840X.2016.1153946>.
- Barbey, A. K. Network Neuroscience Theory of Human Intelligence. *Trends in Cognitive Sciences* **2018**, *22* (1), 8-20. <https://doi.org/10.1016/j.tics.2017.10.001>.
- Spearman, C. "General Intelligence," Objectively Determined and Measured. *The American Journal of Psychology* **1904**, *15* (2), 201. <https://doi.org/10.2307/1412107>.
- Parvizi, J.; Van Hoesen, G. W.; Buckwalter, J.; Damasio, A. Neural Connections of the Posteromedial Cortex in the Macaque. *Proc. Natl. Acad. Sci. U.S.A.* **2006**, *103* (5), 1563-1568. <https://doi.org/10.1073/pnas.0507729103>.
- Vincent, J. L.; Snyder, A. Z.; Fox, M. D.; Shannon, B. J.; Andrews, J. R.; Raichle, M. E.; Buckner, R. L. Coherent Spontaneous Activity Identifies a Hippocampal-Parietal Memory Network. *Journal of Neurophysiology* **2006**, *96* (6), 3517-3531. <https://doi.org/10.1152/jn.00048.2006>.
- Margulies, D. S.; Vincent, J. L.; Kelly, C.; Lohmann, G.; Uddin, L. Q.; Biswal, B. B.; Villringer, A.; Castellanos, F. X.; Milham, M. P.; Petrides, M. Precuneus Shares Intrinsic Functional Architecture in Humans and Monkeys. *Proc. Natl. Acad. Sci. U.S.A.* **2009**, *106* (47), 20069-20074. <https://doi.org/10.1073/pnas.0905314106>.
- Leech, R.; Kamourieh, S.; Beckmann, C. F.; Sharp, D. J. Fractionating the Default Mode Network: Distinct Contributions of the Ventral and Dorsal Posterior Cingulate Cortex to Cognitive Control. *J. Neurosci.* **2011**, *31* (9), 3217-3224. <https://doi.org/10.1523/JNEUROSCI.5626-10.2011>.
- Leech, R.; Braga, R.; Sharp, D. J. Echoes of the Brain within the Posterior Cingulate Cortex. *J. Neurosci.* **2012**, *32* (1), 215-222. <https://doi.org/10.1523/JNEUROSCI.3689-11.2012>.
- Leech, R.; Sharp, D. J. The Role of the Posterior Cingulate Cor

- tex in Cognition and Disease. *Brain* **2014**, *137* (1), 12–32. <https://doi.org/10.1093/brain/awt162>.
13. Hellyer, P.; Scott, G.; Shanahan, M.; Sharp, D.; Leech, R. Local Network Dynamics and Structural Connectivity during Task Based Activity in The Brain. *Human Brain Mapping* **2012**.
 14. Ungerleider, L.; Haxby, J. “What” and “Where” in the Human Brain. *Current Opinion in Neurobiology* **1994**, *4* (2), 157–165. [https://doi.org/10.1016/0959-4388\(94\)90066-3](https://doi.org/10.1016/0959-4388(94)90066-3).
 15. Corbetta, M.; Shulman, G. L. Control of Goal-Directed and Stimulus-Driven Attention in the Brain. *Nat Rev Neurosci* **2002**, *3* (3), 201–215. <https://doi.org/10.1038/nrn755>.
 16. Menon, V.; Uddin, L. Q. Salience, Switching, Attention and Control: A Network Model of Insula Function. *Brain Struct Funct* **2010**, *214* (5–6), 655–667. <https://doi.org/10.1007/s00429-010-0262-0>.
 17. Cocchi, L.; Halford, G. S.; Zalesky, A.; Harding, I. H.; Ramm, B. J.; Cutmore, T.; Shum, D. H. K.; Mattingley, J. B. Complexity in Relational Processing Predicts Changes in Functional Brain Network Dynamics. *Cerebral Cortex* **2014**, *24* (9), 2283–2296. <https://doi.org/10.1093/cercor/bht075>.
 18. Kim, S. Neuroscientific Model of Motivational Process. *Front. Psychol.* **2013**, *4*. <https://doi.org/10.3389/fpsyg.2013.00098>.
 19. Redgrave, P.; Gurney, K. The Short-Latency Dopamine Signal: A Role in Discovering Novel Actions? *Nat Rev Neurosci* **2006**, *7* (12), 967–975. <https://doi.org/10.1038/nrn2022>.
 20. De Lafuente, V.; Romo, R. Dopamine Neurons Code Subjective Sensory Experience and Uncertainty of Perceptual Decisions. *Proc Natl. Acad. Sci. U.S.A.* **2011**, *108* (49), 19767–19771. <https://doi.org/10.1073/pnas.1117636108>.
 21. Cohen, J. D.; Braver, T. S.; O’Reilly, R. C. A Computational Approach to Prefrontal Cortex, Cognitive Control and Schizophrenia: Recent Developments and Current Challenges. *Phil. Trans. R. Soc. Lond. B* 1996, *351* (1346), 1515–1527. <https://doi.org/10.1098/rstb.1996.0138>.
 22. Cohen, J. D.; Braver, T. S.; Brown, J. W. Computational Perspectives on Dopamine Function in Prefrontal Cortex. *Current Opinion in Neurobiology* **2002**, *12* (2), 223–229. [https://doi.org/10.1016/S0959-4388\(02\)00314-8](https://doi.org/10.1016/S0959-4388(02)00314-8).
 23. Braver, T. S.; Cohen, J. D. Chapter 19 Dopamine, Cognitive Control, and Schizophrenia: The Gating Model. In *Progress in Brain Research*; Reggia, J. A., Ruppini, E., Glanzman, D., Eds.; Disorders of Brain, Behavior and Cognition: The neurocomputational Perspective; Elsevier, 1999; Vol. 121, pp 327–349. [https://doi.org/10.1016/S0079-6123\(08\)63082-4](https://doi.org/10.1016/S0079-6123(08)63082-4).
 24. Pasupathy, A.; Miller, E. K. Different Time Courses of Learning-Related Activity in the Prefrontal Cortex and Striatum. *Nature* **2005**, *433* (7028), 873–876. <https://doi.org/10.1038/nature03287>.
 25. Hearne, L.; Cocchi, L.; Zalesky, A.; Mattingley, J. B. Interactions between Default Mode and Control Networks as a Function of Increasing Cognitive Reasoning Complexity. *Hum. Brain Mapp.* **2015**, *36* (7), 2719–2731. <https://doi.org/10.1002/hbm.22802>.
 26. Sherman, S. M.; Guillery, R. W. Distinct Functions for Direct and Trans-thalamic Corticocortical Connections. *Journal of Neurophysiology* **2011**, *106* (3), 1068–1077. <https://doi.org/10.1152/jn.00429.2011>.
 27. Sadaghiani, S.; Scheeringa, R.; Lehongre, K.; Morillon, B.; Giraud, A.-L.; Kleinschmidt, A. Intrinsic Connectivity Networks, Alpha Oscillations, and Tonic Alertness: A Simultaneous Electroencephalography/Functional Magnetic Resonance Imaging Study. *J. Neurosci.* **2010**, *30* (30), 10243–10250. <https://doi.org/10.1523/JNEUROSCI.1004-10.2010>.
 28. Dosenbach, N. U. F.; Fair, D. A.; Miezin, F. M.; Cohen, A. L.; Wenger, K. K.; Dosenbach, R. A. T.; Fox, M. D.; Snyder, A. Z.; Vincent, J. L.; Raichle, M. E.; Schlaggar, B. L.; Petersen, S. E. Distinct Brain Networks for Adaptive and Stable Task Control in Humans. *Proc. Natl. Acad. Sci. U.S.A.* **2007**, *104* (26), 11073–11078. <https://doi.org/10.1073/pnas.0704320104>.
 29. Shenhav, A.; Botvinick, M. M.; Cohen, J. D. The Expected Value of Control: An Integrative Theory of Anterior Cingulate Cortex Function. *Neuron* **2013**, *79* (2), 217–240. <https://doi.org/10.1016/j.neuron.2013.07.007>.
 30. Sridharan, D.; Levitin, D. J.; Menon, V. A Critical Role for the Right Fronto-Insular Cortex in Switching between Central-Executive and Default-Mode Networks. *Proc. Natl. Acad. Sci. U.S.A.* **2008**, *105* (34), 12569–12574. <https://doi.org/10.1073/pnas.0800005105>.
 31. Uddin, L. Q. Salience Processing and Insular Cortical Function and Dysfunction. *Nat Rev Neurosci* **2015**, *16* (1), 55–61. <https://doi.org/10.1038/nrn3857>.
 32. Seeley, W. W.; Menon, V.; Schatzberg, A. F.; Keller, J.; Glover, G. H.; Kenna, H.; Reiss, A. L.; Greicius, M. D. Dissociable Intrinsic Connectivity Networks for Salience Processing and Executive Control. *J. Neurosci.* **2007**, *27* (9), 2349–2356. <https://doi.org/10.1523/JNEUROSCI.5587-06.2007>.
 33. Dosenbach, N. U. F.; Visser, K. M.; Palmer, E. D.; Miezin, F. M.; Wenger, K. K.; Kang, H. C.; Burgund, E. D.; Grimes, A. L.; Schlaggar, B. L.; Petersen, S. E. A Core System for the Implementation of Task Sets. *Neuron* **2006**, *50* (5), 799–812. <https://doi.org/10.1016/j.neuron.2006.04.031>.
 34. Dosenbach, N. U. F.; Fair, D. A.; Cohen, A. L.; Schlaggar, B. L.; Petersen, S. E. A Dual-Networks Architecture of Top-down Control. *Trends in Cognitive Sciences* 2008, *12* (3), 99–105. <https://doi.org/10.1016/j.tics.2008.01.001>.
 35. Power, J. D.; Cohen, A. L.; Nelson, S. M.; Wig, G. S.; Barnes, K. A.; Church, J. A.; Vogel, A. C.; Laumann, T. O.; Miezin, F. M.; Schlaggar, B. L.; Petersen, S. E. Functional Network Organization of the Human Brain. *Neuron* **2011**, *72* (4), 665–678. <https://doi.org/10.1016/j.neuron.2011.09.006>.
 36. Cole, M. W.; Bassett, D. S.; Power, J. D.; Braver, T. S.; Petersen, S. E. Intrinsic and Task-Evoked Network Architectures of the Human Brain. *Neuron* **2014**, *83* (1), 238–251. <https://doi.org/10.1016/j.neuron.2014.05.014>.
 37. Bressler, S. L.; Menon, V. Large-Scale Brain Networks in Cognition: Emerging Methods and Principles. *Trends in Cognitive Sciences* **2010**, *14* (6), 277–290. <https://doi.org/10.1016/j.tics.2010.04.004>.
 38. Bonnelle, V.; Ham, T. E.; Leech, R.; Kinnunen, K. M.; Mehta, M. A.; Greenwood, R. J.; Sharp, D. J. Salience Network Integrity Predicts Default Mode Network Function after Traumatic Brain Injury. *Proc. Natl. Acad. Sci. U.S.A.* **2012**, *109* (12), 4690–4695. <https://doi.org/10.1073/pnas.1113455109>.
 39. Gehring, W. J.; Knight, R. T. Prefrontal–Cingulate Interactions in Action Monitoring. *Nat Neurosci* **2000**, *3* (5), 516–520. <https://doi.org/10.1038/74899>.
 40. Kerns, J. G.; Cohen, J. D.; MacDonald, A. W.; Cho, R. Y.; Stenger, V. A.; Carter, C. S. Anterior Cingulate Conflict Monitoring and Adjustments in Control. *Science* **2004**, *303* (5660), 1023–1026. <https://doi.org/10.1126/science.1089910>.
 41. Ridderinkhof, K. R.; Van Den Wildenberg, W. P. M.; Segalowitz, S. J.; Carter, C. S. Neurocognitive Mechanisms of Cognitive Control: The Role of Prefrontal Cortex in Action Selection, Response Inhibition, Performance Monitoring, and Reward-Based Learning. *Brain and Cognition* **2004**, *56* (2), 129–140. <https://doi.org/10.1016/j.bandc.2004.09.016>.
 42. Crescentini, C.; Seyed-Allaei, S.; De Pisapia, N.; Jovicich, J.; Amati, D.; Shallice, T. Mechanisms of Rule Acquisition and Rule Following in Inductive Reasoning. *J. Neurosci.* **2011**, *31* (21), 7763–7774. <https://doi.org/10.1523/JNEUROSCI.4579-10.2011>.

43. Buschman, T. J.; Denovellis, E. L.; Diogo, C.; Bullock, D.; Miller, E. K. Synchronous Oscillatory Neural Ensembles for Rules in the Prefrontal Cortex. *Neuron* **2012**, *76* (4), 838–846. <https://doi.org/10.1016/j.neuron.2012.09.029>.
44. Petrides, M. The Role of the Mid-Dorsolateral Prefrontal Cortex in Working Memory. *Exp Brain Res* **2000**, *133* (1), 44–54. <https://doi.org/10.1007/s002210000399>.
45. Koenigs, M.; Barbey, A. K.; Postle, B. R.; Grafman, J. Superior Parietal Cortex Is Critical for the Manipulation of Information in Working Memory. *J. Neurosci.* **2009**, *29* (47), 14980–14986. <https://doi.org/10.1523/JNEUROSCI.3706-09.2009>.
46. Badre, D.; Nee, D. E. Frontal Cortex and the Hierarchical Control of Behavior. *Trends in Cognitive Sciences* **2018**, *22* (2), 170–188. <https://doi.org/10.1016/j.tics.2017.11.005>.
47. Badre, D.; D'Esposito, M. Is the Rostro-Caudal Axis of the Frontal Lobe Hierarchical? *Nat Rev Neurosci* **2009**, *10* (9), 659–669. <https://doi.org/10.1038/nrn2667>.
48. Koechlin, E.; Ody, C.; Kouneiher, F. The Architecture of Cognitive Control in the Human Prefrontal Cortex. *Science* **2003**, *302* (5648), 1181–1185. <https://doi.org/10.1126/science.1088545>.
49. Nee, D. E.; D'Esposito, M. The Hierarchical Organization of the Lateral Prefrontal Cortex. *eLife* **2016**, *5*, e12112. <https://doi.org/10.7554/eLife.12112>.
50. Nee, D. E.; D'Esposito, M. Causal Evidence for Lateral Prefrontal Cortex Dynamics Supporting Cognitive Control. *eLife* **2017**, *6*, e28040. <https://doi.org/10.7554/eLife.28040>.
51. Badre, D.; D'Esposito, M. Functional Magnetic Resonance Imaging Evidence for a Hierarchical Organization of the Prefrontal Cortex. *Journal of Cognitive Neuroscience* **2007**, *19* (12), 2082–2099. <https://doi.org/10.1162/jocn.2007.19.12.2082>.
52. Badre, D. Cognitive Control, Hierarchy, and the Rostro-Caudal Organization of the Frontal Lobes. *Trends in Cognitive Sciences* **2008**, *12* (5), 193–200. <https://doi.org/10.1016/j.tics.2008.02.004>.
53. Braga, R. M.; Buckner, R. L. Parallel Interdigitated Distributed Networks within the Individual Estimated by Intrinsic Functional Connectivity. *Neuron* **2017**, *95* (2), 457–471.e5. <https://doi.org/10.1016/j.neuron.2017.06.038>.
54. Thomas Yeo, B. T.; Krienen, F. M.; Sepulcre, J.; Sabuncu, M. R.; Lashkari, D.; Hollinshead, M.; Roffman, J. L.; Smoller, J. W.; Zöllei, L.; Polimeni, J. R.; Fischl, B.; Liu, H.; Buckner, R. L. The Organization of the Human Cerebral Cortex Estimated by Intrinsic Functional Connectivity. *Journal of Neurophysiology* **2011**, *106* (3), 1125–1165. <https://doi.org/10.1152/jn.00338.2011>.
55. Dixon, M. L.; De La Vega, A.; Mills, C.; Andrews-Hanna, J.; Spreng, R. N.; Cole, M. W.; Christoff, K. Heterogeneity within the Frontoparietal Control Network and Its Relationship to the Default and Dorsal Attention Networks. *Proc. Natl. Acad. Sci. U.S.A.* **2018**, *115* (7). <https://doi.org/10.1073/pnas.1715766115>.
56. Murphy, A. C.; Bertolero, M. A.; Papadopoulos, L.; Lydon-Staley, D. M.; Bassett, D. S. Multimodal Network Dynamics Underpinning Working Memory. *Nat Commun* **2020**, *11* (1), 3035. <https://doi.org/10.1038/s41467-020-15541-0>.
57. D'Mello, A. M.; Gabrieli, J. D. E.; Nee, D. E. Evidence for Hierarchical Cognitive Control in the Human Cerebellum. *Current Biology* **2020**, *30* (10), 1881–1892.e3. <https://doi.org/10.1016/j.cub.2020.03.028>.
58. Malm, J.; Kristensen, B.; Karlsson, T.; Carlberg, B.; Fagerlund, M.; Olsson, T. Cognitive Impairment in Young Adults with Infarcted Frontal Cortex. *Neurology* **1998**, *51* (2), 433–440. <https://doi.org/10.1212/WNL.51.2.433>.
59. Stoodley, C.; Schmahmann, J. Functional Topography in the Human Cerebellum: A Meta-Analysis of Neuroimaging Studies. *NeuroImage* **2009**, *44* (2), 489–501. <https://doi.org/10.1016/j.neuroimage.2008.08.039>.
60. Marvel, C. L.; Desmond, J. E. Functional Topography of the Cerebellum in Verbal Working Memory. *Neuropsychol Rev* **2010**, *20* (3), 271–279. <https://doi.org/10.1007/s11065-010-9137-7>.
61. Nee, D. E. Integrative Frontal-Parietal Dynamics Supporting Cognitive Control. *eLife* **2021**, *10*, e57244. <https://doi.org/10.7554/eLife.57244>.
62. Cohen, J. R.; Gallen, C. L.; Jacobs, E. G.; Lee, T. G.; D'Esposito, M. Quantifying the Reconfiguration of Intrinsic Networks during Working Memory. *PLoS ONE* **2014**, *9* (9), e106636. <https://doi.org/10.1371/journal.pone.0106636>.
63. Braun, U.; Schäfer, A.; Walter, H.; Erk, S.; Romanczuk-Seiferth, N.; Haddad, L.; Schweiger, J. I.; Grimm, O.; Heinz, A.; Tost, H.; Meyer-Lindenberg, A.; Bassett, D. S. Dynamic Reconfiguration of Frontal Brain Networks during Executive Cognition in Humans. *Proc. Natl. Acad. Sci. U.S.A.* **2015**, *112* (37), 11678–11683. <https://doi.org/10.1073/pnas.1422487112>.
64. Cohen, J. R.; D'Esposito, M. The Segregation and Integration of Distinct Brain Networks and Their Relationship to Cognition. *J. Neurosci.* **2016**, *36* (48), 12083–12094. <https://doi.org/10.1523/JNEUROSCI.2965-15.2016>.
65. Spreng, R. N.; Sepulcre, J.; Turner, G. R.; Stevens, W. D.; Schacter, D. L. Intrinsic Architecture Underlying the Relations among the Default, Dorsal Attention, and Frontoparietal Control Networks of the Human Brain. *Journal of Cognitive Neuroscience* **2013**, *25* (1), 74–86. https://doi.org/10.1162/jocn_a_00281.
66. Weissman, D. H.; Roberts, K. C.; Visscher, K. M.; Woldorff, M. G. The Neural Bases of Momentary Lapses in Attention. *Nat Neurosci* **2006**, *9* (7), 971–978. <https://doi.org/10.1038/nn1727>.
67. Bonnelle, V.; Leech, R.; Kinnunen, K. M.; Ham, T. E.; Beckmann, C. F.; De Boissezon, X.; Greenwood, R. J.; Sharp, D. J. Default Mode Network Connectivity Predicts Sustained Attention Deficits after Traumatic Brain Injury. *J. Neurosci.* **2011**, *31* (38), 13442–13451. <https://doi.org/10.1523/JNEUROSCI.1163-11.2011>.
68. Seghier, M. L. The Angular Gyrus: Multiple Functions and Multiple Subdivisions. *Neuroscientist* **2013**, *19* (1), 43–61. <https://doi.org/10.1177/1073858412440596>.
69. Santarnecchi, E.; Emmendorfer, A.; Pascual-Leone, A. Dissecting the Parieto-Frontal Correlates of Fluid Intelligence: A Comprehensive ALE Meta-Analysis Study. *Intelligence* **2017**, *63*, 9–28. <https://doi.org/10.1016/j.intell.2017.04.008>.
70. Miller, E. K.; Cohen, J. D. An Integrative Theory of Prefrontal Cortex Function. *Annu. Rev. Neurosci.* **2001**, *24* (1), 167–202. <https://doi.org/10.1146/annurev.neuro.24.1.167>.
71. Miller, B. T.; D'Esposito, M. Searching for “the Top” in Top-Down Control. *Neuron* **2005**, *48* (4), 535–538. <https://doi.org/10.1016/j.neuron.2005.11.002>.
72. Beaty, R. E.; Benedek, M.; Barry Kaufman, S.; Silvia, P. J. Default and Executive Network Coupling Supports Creative Idea Production. *Sci Rep* **2015**, *5* (1), 10964. <https://doi.org/10.1038/srep10964>.
73. Dixon, M. L.; Andrews-Hanna, J. R.; Spreng, R. N.; Irving, Z. C.; Mills, C.; Girn, M.; Christoff, K. Interactions between the Default Network and Dorsal Attention Network Vary across Default Subsystems, Time, and Cognitive States. *NeuroImage* **2017**, *147*, 632–649. <https://doi.org/10.1016/j.neuroimage.2016.12.073>.
74. Spreng, R. N.; Schacter, D. L. Default Network Modulation and Large-Scale Network Interactivity in Healthy Young and Old Adults. *Cerebral Cortex* **2012**, *22* (11), 2610–2621. <https://doi.org/10.1093/cercor/bhr339>.
75. Hawkins, J.; Lewis, M.; Klukas, M.; Purdy, S.; Ahmad, S. A Framework for Intelligence and Cortical Function Based on Grid Cells in the Neocortex. *Front. Neural Circuits* **2019**, *12*, 121. <https://doi.org/10.3389/fncir.2018.00121>.
76. Helmstaedter, M.; Sakmann, B.; Feldmeyer, D. L2/3 Interneuro

- n Groups Defined by Multiparameter Analysis of Axonal Projection, Dendritic Geometry, and Electrical Excitability. *Cerebral Cortex* **2009**, *19* (4), 951–962. <https://doi.org/10.1093/cercor/bhn130>.
77. Meyer, H. S.; Schwarz, D.; Wimmer, V. C.; Schmitt, A. C.; Kerr, J. N. D.; Sakmann, B.; Helmstaedter, M. Inhibitory Interneurons in a Cortical Column Form Hot Zones of Inhibition in Layers 2 and 5A. *Proc. Natl. Acad. Sci. U.S.A.* **2011**, *108* (40), 16807–16812. <https://doi.org/10.1073/pnas.1113648108>.
78. Buxhoeveden, D. P.; Casanova, M. F. The Minicolumn Hypothesis in Neuroscience. *Brain* **2002**, *125* (5), 935–951. <https://doi.org/10.1093/brain/awf110>.
79. Mountcastle, V. An Organizing Principle for Cerebral Function: The Unit Module and the Distributed System. **1978**.
80. Cole, M. W.; Reynolds, J. R.; Power, J. D.; Repovs, G.; Anticevic, A.; Braver, T. S. Multi-Task Connectivity Reveals Flexible Hubs for Adaptive Task Control. *Nat Neurosci* **2013**, *16* (9), 1348–1355. <https://doi.org/10.1038/nn.3470>.
81. Cole, M. W.; Pathak, S.; Schneider, W. Identifying the Brain's Most Globally Connected Regions. *Neuroimage* **2010**, *49* (4), 3132–3148. <https://doi.org/10.1016/j.neuroimage.2009.11.001>.
82. Cole, M. W.; Yarkoni, T.; Repovs, G.; Anticevic, A.; Braver, T. S. Global Connectivity of Prefrontal Cortex Predicts Cognitive Control and Intelligence. *J Neurosci* **2012**, *32* (26), 8988–8999. <https://doi.org/10.1523/JNEUROSCI.0536-12.2012>.
83. Cole, M. W.; Etzel, J. A.; Zacks, J. M.; Schneider, W.; Braver, T. S. Rapid Transfer of Abstract Rules to Novel Contexts in Human Lateral Prefrontal Cortex. *Front Hum Neurosci* **2011**, *5*, 142. <https://doi.org/10.3389/fnhum.2011.00142>.
84. Singley, M. K.; Anderson, J. R. The Transfer of Text-Editing Skill. *International Journal of Man-Machine Studies* **1985**, *22* (4), 403–423. [https://doi.org/10.1016/S0020-7373\(85\)80047-X](https://doi.org/10.1016/S0020-7373(85)80047-X).
85. Hebb, D. O. The Organization of Behavior: A Neuropsychological Theory; John Wiley and Sons, Inc., 1949.
86. Cole, M. W.; Laurent, P.; Stocco, A. Rapid Instructed Task Learning: A New Window into the Human Brain's Unique Capacity for Flexible Cognitive Control. *Cogn Affect Behav Neurosci* **2013**, *13* (1), 1–22. <https://doi.org/10.3758/s13415-012-0125-7>.
87. Sigala, N.; Kusunoki, M.; Nimmo-Smith, I.; Gaffan, D.; Duncan, J. Hierarchical Coding for Sequential Task Events in the Monkey Prefrontal Cortex. *Proc. Natl. Acad. Sci. U.S.A.* **2008**, *105* (33), 11969–11974. <https://doi.org/10.1073/pnas.0802569105>.
88. Rigotti, M.; Barak, O.; Warden, M. R.; Wang, X.-J.; Daw, N. D.; Miller, E. K.; Fusi, S. The Importance of Mixed Selectivity in Complex Cognitive Tasks. *Nature* **2013**, *497* (7451), 585–590. <https://doi.org/10.1038/nature12160>.
89. Funahashi, S.; Bruce, C. J.; Goldman-Rakic, P. S. Mnemonic Coding of Visual Space in the Monkey's Dorsolateral Prefrontal Cortex. *Journal of Neurophysiology* **1989**, *61* (2), 331–349. <https://doi.org/10.1152/jn.1989.61.2.331>.
90. Funahashi, S. Functions of Delay-Period Activity in the Prefrontal Cortex and Mnemonic Scotomas Revisited. *Front. Syst. Neurosci.* **2015**, *9*. <https://doi.org/10.3389/fnsys.2015.00002>.
91. Rossi, A. F.; Bichot, N. P.; Desimone, R.; Ungerleider, L. G. Top-Down Attentional Deficits in Macaques with Lesions of Lateral Prefrontal Cortex. *J. Neurosci.* **2007**, *27* (42), 11306–11314. <https://doi.org/10.1523/JNEUROSCI.2939-07.2007>.
92. Watanabe, K.; Funahashi, S. Neural Mechanisms of Dual-Task Interference and Cognitive Capacity Limitation in the Prefrontal Cortex. *Nat Neurosci* **2014**, *17* (4), 601–611. <https://doi.org/10.1038/nn.3667>.
93. Watanabe, K.; Funahashi, S. A Dual-Task Paradigm for Behavioral and Neurobiological Studies in Nonhuman Primates. *Journal of Neuroscience Methods* **2015**, *246*, 1–12. <https://doi.org/10.1016/j.jneumeth.2015.03.006>.
94. Petersen, S. E.; Posner, M. I. The Attention System of the Human Brain: 20 Years After. *Annu. Rev. Neurosci.* **2012**, *35* (1), 73–89. <https://doi.org/10.1146/annurev-neuro-062111-150525>.
95. Damoiseaux, J. S.; Rombouts, S. A. R. B.; Barkhof, F.; Scheltens, P.; Stam, C. J.; Smith, S. M.; Beckmann, C. F. Consistent Resting-State Networks across Healthy Subjects. *Proc. Natl. Acad. Sci. U.S.A.* **2006**, *103* (37), 13848–13853. <https://doi.org/10.1073/pnas.0601417103>.
96. Neubert, F.-X.; Mars, R. B.; Thomas, A. G.; Sallet, J.; Rushworth, M. F. S. Comparison of Human Ventral Frontal Cortex Areas for Cognitive Control and Language with Areas in Monkey Frontal Cortex. *Neuron* **2014**, *81* (3), 700–713. <https://doi.org/10.1016/j.neuron.2013.11.012>.
97. Wendelken, C.; Nakhabenko, D.; Donohue, S. E.; Carter, C. S.; Bunge, S. A. “Brain Is to Thought as Stomach Is to ??”: Investigating the Role of Rostrolateral Prefrontal Cortex in Relational Reasoning. *J Cogn Neurosci* **2008**, *20* (4), 682–693. <https://doi.org/10.1162/jocn.2008.20055>.
98. Wendelken, C.; Bunge, S. A.; Carter, C. S. Maintaining Structure d Information: An Investigation into Functions of Parietal and Lateral Prefrontal Cortices. *Neuropsychologia* **2008**, *46* (2), 665–678. <https://doi.org/10.1016/j.neuropsychologia.2007.09.015>.
99. Christoff, K.; Prabhakaran, V.; Dorfman, J.; Zhao, Z.; Kroger, J.; Holyoak, K. J.; Gabrieli, J. D. Rostrolateral Prefrontal Cortex Involvement in Relational Integration during Reasoning. *Neuroimage* **2001**, *14* (5), 1136–1149. <https://doi.org/10.1006/nimg.2001.0922>.
100. Christoff, K.; Gabrieli, J. D. E. The Frontopolar Cortex and Human Cognition: Evidence for a Rostrocaudal Hierarchical Organization within the Human Prefrontal Cortex. *Psychobiology*, **2000**, *28* (2), 168–186. <https://doi.org/10.3758/BF03331976>.
101. Kroger, J. K.; Sabb, F. W.; Fales, C. L.; Bookheimer, S. Y.; Cohen, M. S.; Holyoak, K. J. Recruitment of Anterior Dorsolateral Prefrontal Cortex in Human Reasoning: A Parametric Study of Relational Complexity. *Cereb Cortex* **2002**, *12* (5), 477–485. <https://doi.org/10.1093/cercor/12.5.477>.
102. Smith, R.; Keramatian, K.; Christoff, K. Localizing the Rostrolateral Prefrontal Cortex at the Individual Level. *NeuroImage* **2007**, *36* (4), 1387–1396. <https://doi.org/10.1016/j.neuroimage.2007.04.032>.
103. Bunge, S. A.; Helskog, E. H.; Wendelken, C. Left, but Not Right, Rostrolateral Prefrontal Cortex Meets a Stringent Test of the Relational Integration Hypothesis. *Neuroimage* **2009**, *46* (1), 338–342. <https://doi.org/10.1016/j.neuroimage.2009.01.064>.
104. Choi, E. Y.; Drayna, G. K.; Badre, D. Evidence for a Functional Hierarchy of Association Networks. *Journal of Cognitive Neuroscience* **2018**, *30* (5), 722–736. https://doi.org/10.1162/jocn_a_01229.
105. Uddin, L. Q.; Supekar, K. S.; Ryali, S.; Menon, V. Dynamic Reconfiguration of Structural and Functional Connectivity Across Core Neurocognitive Brain Networks with Development. *J. Neurosci.* **2011**, *31* (50), 18578–18589. <https://doi.org/10.1523/JNEUROSCI.4465-11.2011>.
106. MacDonald, A. W.; Cohen, J. D.; Stenger, V. A.; Carter, C. S. Dissociating the Role of the Dorsolateral Prefrontal and Anterior Cingulate Cortex in Cognitive Control. *Science* **2000**, *288* (5472), 1835–1838. <https://doi.org/10.1126/science.288.5472.1835>.
107. Assem, M.; Blank, I. A.; Mineroff, Z.; Ademoğlu, A.; Fedorenko, E. Activity in the Fronto-Parietal Multiple-Demand Network Is Robustly Associated with Individual Differences in Working Memory and Fluid Intelligence. *Cortex* **2020**, *131*, 1–16. <https://doi.org/10.1016/j.cortex.2020.06.013>.
108. Duncan, J.; Chylinski, D.; Mitchell, D. J.; Bhandari, A. Complexity and Compositionality in Fluid Intelligence. *Proc. Natl. Acad. Sci. U.S.A.* **2017**, *114* (20), 5295–5299. <https://doi.org/10.1073/p>

- nas.1621147114.
109. Bertolero, M. A.; Yeo, B. T. T.; D'Esposito, M. The Diverse Clusters of the Human Brain. *Nat Commun* **2017**, *8* (1), 1277. <https://doi.org/10.1038/s41467-017-01189-w>.
 110. Bertolero, M. A.; Yeo, B. T. T.; D'Esposito, M. The Modular and Integrative Functional Architecture of the Human Brain. *Proc. Natl. Acad. Sci. U.S.A.* **2015**, *112* (49). <https://doi.org/10.1073/pnas.1510619112>.
 111. Gratton, C.; Sun, H.; Petersen, S. E. Control Networks and Hub Regions. *Psychophysiol* **2018**, *55* (3), e13032. <https://doi.org/10.1111/psyp.13032>.
 112. Rhein, C.; Mühle, C.; Richter-Schmidinger, T.; Alexopoulos, P.; Doerfler, A.; Kornhuber, J. Neuroanatomical Correlates of Intelligence in Healthy Young Adults: The Role of Basal Ganglia Volume. *PLoS ONE* **2014**, *9* (4), e93623. <https://doi.org/10.1371/journal.pone.0093623>.
 113. Burgaleta, M.; MacDonald, P. A.; Martínez, K.; Román, F. J.; Alvarez-Linera, J.; González, A. R.; Karama, S.; Colom, R. Subcortical Regional Morphology Correlates with Fluid and Spatial Intelligence: Basal Ganglia and Cognitive Abilities. *Hum. Brain Mapp.* **2014**, *35* (5), 1957–1968. <https://doi.org/10.1002/hbm.22305>.
 114. Melrose, R. J.; Poulin, R. M.; Stern, C. E. An fMRI Investigation of the Role of the Basal Ganglia in Reasoning. *Brain Research* **2007**, *1142*, 146–158. <https://doi.org/10.1016/j.brainres.2007.01.060>.
 115. Schlagenhaut, F.; Rapp, M. A.; Huys, Q. J. M.; Beck, A.; Wustenberg, T.; Deserno, L.; Buchholz, H.; Kalbitzer, J.; Buchert, R.; Bauer, M.; Kienast, T.; Cumming, P.; Plotkin, M.; Kumakura, Y.; Grac, A. A.; Dolan, R. J.; Heinz, A. Ventral Striatal Prediction Error Signaling Is Associated with Dopamine Synthesis Capacity and Fluid Intelligence. *Hum. Brain Mapp.* **2013**, *34* (6), 1490–1499. <https://doi.org/10.1002/hbm.22000>.
 116. Basten, U.; Hilger, K.; Fiebach, C. J. Where Smart Brains Are Different: A Quantitative Meta-Analysis of Functional and Structural Brain Imaging Studies on Intelligence. *Intelligence* **2015**, *51*, 10–27. <https://doi.org/10.1016/j.intell.2015.04.009>.
 117. Aoki, S.; Liu, A. W.; Zucca, A.; Zucca, S.; Wickens, J. R. Role of Striatal Cholinergic Interneurons in Set-Shifting in the Rat. *Journal of Neuroscience* **2015**, *35* (25), 9424–9431. <https://doi.org/10.1523/JNEUROSCI.0490-15.2015>.
 118. Koechlin, E. Frontal Pole Function: What Is Specifically Human? *Trends in Cognitive Sciences* **2011**, *15* (6), 241. <https://doi.org/10.1016/j.tics.2011.04.005>.
 119. Bonelli, R. M.; Cummings, J. L. Frontal-Subcortical Circuitry and Behavior. *Dialogues Clin Neurosci* **2007**, *9* (2), 141–151. <https://doi.org/10.31887/DCNS.2007.9.2/rbonelli>.
 120. Brown, J. W.; Braver, T. S. Learned Predictions of Error Likelihood in the Anterior Cingulate Cortex. *Science* **2005**, *307* (5712), 1118–1121. <https://doi.org/10.1126/science.1105783>.
 121. O'Reilly, J. X.; Schuffelgen, U.; Cuell, S. F.; Behrens, T. E. J.; Mars, R. B.; Rushworth, M. F. S. Dissociable Effects of Surprise and Model Update in Parietal and Anterior Cingulate Cortex. *Proc. Natl. Acad. Sci. U.S.A.* **2013**, *110* (38). <https://doi.org/10.1073/pnas.1305373110>.
 122. Johansen-Berg, H.; Behrens, T. E. J.; Robson, M. D.; Drobniak, I.; Rushworth, M. F. S.; Brady, J. M.; Smith, S. M.; Higham, D. J.; Matthews, P. M. Changes in Connectivity Profiles Define Functionally Distinct Regions in Human Medial Frontal Cortex. *Proc. Natl. Acad. Sci. U.S.A.* **2004**, *101* (36), 13335–13340. <https://doi.org/10.1073/pnas.0403743101>.
 123. Lehericy, S. 3-D Diffusion Tensor Axonal Tracking Shows Distinct SMA and Pre-SMA Projections to the Human Striatum. *Cerebral Cortex* **2004**, *14* (12), 1302–1309. <https://doi.org/10.1093/cercor/bhh091>.
 124. Kaas, J. H.; Stepniewska, I. Motor Cortex. In *Encyclopedia of the Human Brain*; Elsevier Science Ltd, 2002; Vol. 3, pp 159–169.
 125. Gratton, C.; Neta, M.; Sun, H.; Ploran, E. J.; Schlaggar, B. L.; Wheeler, M. E.; Petersen, S. E.; Nelson, S. M. Distinct Stages of Moment-to-Moment Processing in the Cinguloopercular and Frontoparietal Networks. *Cereb Cortex* **2017**, *27* (3), 2403–2417. <https://doi.org/10.1093/cercor/bhw092>.
 126. Hawkins, J.; Ahmad, S.; Cui, Y. A Theory of How Columns in the Neocortex Enable Learning the Structure of the World. *Front. Neural Circuits* **2017**, *11*, 81. <https://doi.org/10.3389/fncir.2017.00081>.
 127. Utevsky, A. V.; Smith, D. V.; Huettel, S. A. Precuneus Is a Functional Core of the Default-Mode Network. *J. Neurosci.* **2014**, *34* (3), 932–940. <https://doi.org/10.1523/JNEUROSCI.4227-13.2014>.
 128. Allen, E. A.; Damaraju, E.; Plis, S. M.; Erhardt, E. B.; Eichele, T.; Calhoun, V. D. Tracking Whole-Brain Connectivity Dynamics in the Resting State. *Cerebral Cortex* **2014**, *24* (3), 663–676. <https://doi.org/10.1093/cercor/bhs352>.
 129. Van Den Heuvel, M. P.; Kahn, R. S.; Goñi, J.; Sporns, O. High-Cost, High-Capacity Backbone for Global Brain Communication. *Natl. Acad. Sci. U.S.A.* **2012**, *109* (28), 11372–11377. <https://doi.org/10.1073/pnas.1203593109>.
 130. Van Den Heuvel, M. P.; Sporns, O. Rich-Club Organization of the Human Connectome. *J. Neurosci.* **2011**, *31* (44), 15775–15786. <https://doi.org/10.1523/JNEUROSCI.3539-11.2011>.
 131. Cavanna, A. E.; Trimble, M. R. The Precuneus: A Review of Its Functional Anatomy and Behavioural Correlates. *Brain* **2006**, *129* (3), 564–583. <https://doi.org/10.1093/brain/awl004>.
 132. Fretton, M.; Lemogne, C.; Bergouignan, L.; Delaveau, P.; Lehericy, S.; Fossati, P. The Eye of the Self: Precuneus Volume and Visual Perspective during Autobiographical Memory Retrieval. *Brain Struct Funct* **2014**, *219* (3), 959–968. <https://doi.org/10.1007/s00429-013-0546-2>.
 133. Perfetti, B.; Saggino, A.; Ferretti, A.; Caulo, M.; Romani, G. L.; Onofri, M. Differential Patterns of Cortical Activation as a Function of Fluid Reasoning Complexity. *Hum Brain Mapp* **2009**, *30* (2), 497–510. <https://doi.org/10.1002/hbm.20519>.
 134. Graham, S.; Jiang, J.; Manning, V.; Nejad, A. B.; Zhisheng, K.; Saleh, S. R.; Golay, X.; Berne, Y. I.; McKenna, P. J. IQ-Related FMRI Differences during Cognitive Set Shifting. *Cerebral Cortex* **2011**, *20* (3), 641–649. <https://doi.org/10.1093/cercor/bhp130>.
 135. Seeley, W. W. The Salience Network: A Neural System for Perceiving and Responding to Homeostatic Demands. *J. Neurosci.* **2011**, *31* (50), 9878–9882. <https://doi.org/10.1523/JNEUROSCI.1138-17.2019>.
 136. Etkin, A.; Egner, T.; Peraza, D. M.; Kandel, E. R.; Hirsch, J. Resolving Emotional Conflict: A Role for the Rostral Anterior Cingulate Cortex in Modulating Activity in the Amygdala. *Neuron* **2006**, *51* (6), 871–882. <https://doi.org/10.1016/j.neuron.2006.07.029>.
 137. Pressman, P.; Rosen, H. J. Disorders of Frontal Lobe Function. In *Neurobiology of Brain Disorders*; Elsevier, 2015; pp 542–557. <https://doi.org/10.1016/B978-0-12-398270-4.00033-1>.
 138. Tschernegg, M.; Pletzer, B.; Schwartenbeck, P.; Ludersdorfer, P.; Hoffmann, U.; Kronbichler, M. Impulsivity Relates to Striatal Gray Matter Volumes in Humans: Evidence from a Delay Discounting Paradigm. *Front. Hum. Neurosci.* **2015**, *9*. <https://doi.org/10.3389/fnhum.2015.00384>.
 139. Korponay, C.; Koenigs, M. Gray Matter Correlates of Impulsivity in Psychopathy and in the General Population Differ by Kind, Not by Degree: A Comparison of Systematic Reviews. *Social Cognitive and Affective Neuroscience* **2021**, *16* (7), 683–695. <https://doi.org/10.1093/scan/nsab045>.

140. Ott, T.; Nieder, A. Dopamine and Cognitive Control in Prefrontal Cortex. *Trends in Cognitive Sciences* **2019**, *23* (3), 213–234. <https://doi.org/10.1016/j.tics.2018.12.006>.
141. Hilger, K.; Ekman, M.; Fiebach, C. J.; Basten, U. Intelligence Is Associated with the Modular Structure of Intrinsic Brain Networks. *Sci Rep* **2017**, *7* (1), 16088. <https://doi.org/10.1038/s41598-017-15795-7>.
142. Gratton, C.; Laumann, T. O.; Gordon, E. M.; Adeyemo, B.; Petersen, S. E. Evidence for Two Independent Factors That Modify Brain Networks to Meet Task Goals. *Cell Rep* **2016**, *17* (5), 1276–1288. <https://doi.org/10.1016/j.celrep.2016.10.002>.
143. Latora, V.; Marchiori, M. Efficient Behavior of Small-World Networks. *Phys. Rev. Lett.* **2001**, *87* (19), 198701. <https://doi.org/10.1103/PhysRevLett.87.198701>.
144. Brodmann, K. *Vergleichende Lokalisationslehre Der Großhirnrinde*; Barth: Leipzig (Germany), 1909.
145. Ben Shalom, D.; Poeppel, D. Functional Anatomic Models of Language: Assembling the Pieces. *Neuroscientist* **2008**, *14* (1), 119–127. <https://doi.org/10.1177/1073858407305726>.
146. Deschamps, I.; Baum, S. R.; Gracco, V. L. On the Role of the Supramarginal Gyrus in Phonological Processing and Verbal Working Memory: Evidence from RTMS Studies. *Neuropsychologia* **2014**, *53*, 39–46. <https://doi.org/10.1016/j.neuropsychologia.2013.10.015>.
147. Hilger, K.; Fukushima, M.; Sporns, O.; Fiebach, C. J. Temporal Stability of Functional Brain Modules Associated with Human Intelligence. *Hum Brain Mapp* **2020**, *41* (2), 362–372. <https://doi.org/10.1002/hbm.24807>.
148. Hilger, K.; Ekman, M.; Fiebach, C. J.; Basten, U. Efficient Hubs in the Intelligent Brain: Nodal Efficiency of Hub Regions in the Salience Network Is Associated with General Intelligence. *Intelligence* **2017**, *60*, 10–25. <https://doi.org/10.1016/j.intell.2016.11.001>.
149. Kruschwitz, J. D.; Waller, L.; Daedelow, L. S.; Walter, H.; Veer, I. M. General, Crystallized and Fluid Intelligence Are Not Associated with Functional Global Network Efficiency: A Replication Study with the Human Connectome Project 1200 Data Set. *NeuroImage* **2018**, *171*, 323–331. <https://doi.org/10.1016/j.neuroimage.2018.01.018>.
150. Pamplona, G. S. P.; Santos Neto, G. S.; Rosset, S. R. E.; Rogers, B. P.; Salmon, C. E. G. Analyzing the Association between Functional Connectivity of the Brain and Intellectual Performance. *Front Hum Neurosci* **2015**, *9*, 61. <https://doi.org/10.3389/fnhum.2015.00061>.
151. Schultz, D. H.; Cole, M. W. Higher Intelligence Is Associated with Less Task-Related Brain Network Reconfiguration. *J. Neurosci.* **2016**, *36* (33), 8551–8561. <https://doi.org/10.1523/JNEUROSCI.0358-16.2016>.
152. Hearne, L. J.; Mattingley, J. B.; Cocchi, L. Functional Brain Networks Related to Individual Differences in Human Intelligence at Rest. *Sci Rep* **2016**, *6* (1), 32328. <https://doi.org/10.1038/srep32328>.
153. Lindbergh, C. A.; Zhao, Y.; Lv, J.; Mewborn, C. M.; Puente, A. N.; Terry, D. P.; Renzi-Hammond, L. M.; Hammond, B. R.; Liu, T.; Miller, L. S. Intelligence Moderates the Relationship between Age and Inter-Connectivity of Resting State Networks in Older Adults. *Neurobiology of Aging* **2019**, *78*, 121–129. <https://doi.org/10.1016/j.neurobiolaging.2019.02.014>.
154. Thoma, R. J.; Yeo, R. A.; Gangestad, S.; Halgren, E.; Davis, J.; Paulson, K. M.; Lewine, J. D. Developmental Instability and the Neural Dynamics of the Speed-Intelligence Relationship. *NeuroImage* **2006**, *32* (3), 1456–1464. <https://doi.org/10.1016/j.neuroimage.2006.05.016>.
155. Li, Y.; Liu, Y.; Li, J.; Qin, W.; Li, K.; Yu, C.; Jiang, T. Brain Anatomical Network and Intelligence. *PLoS Comput Biol* **2009**, *5* (5), e1000395. <https://doi.org/10.1371/journal.pcbi.1000395>.
156. Penke, L.; Maniega, S. M.; Bastin, M. E.; Valdés Hernández, M. C.; Murray, C.; Royle, N. A.; Starr, J. M.; Wardlaw, J. M.; Deary, I. J. Brain White Matter Tract Integrity as a Neural Foundation for General Intelligence. *Mol Psychiatry* **2012**, *17* (10), 1026–1030. <https://doi.org/10.1038/mp.2012.66>.
157. Haász, J.; Westlye, E. T.; Fjær, S.; Espeseth, T.; Lundervold, A.; Lundervold, A. J. General Fluid-Type Intelligence Is Related to Indices of White Matter Structure in Middle-Aged and Old Adults. *NeuroImage* **2013**, *83*, 372–383. <https://doi.org/10.1016/j.neuroimage.2013.06.040>.
158. Schubert, A.-L.; Hagemann, D.; Frischkorn, G. T. Is General Intelligence Little More than the Speed of Higher-Order Processing? *Journal of Experimental Psychology: General* **2017**, *146* (10), 1498–1512. <https://doi.org/10.1037/xge0000325>.
159. Polich, J. Updating P300: An Integrative Theory of P3a and P3b. *Clin Neurophysiol* **2007**, *118* (10), 2128–2148. <https://doi.org/10.1016/j.clinph.2007.04.019>.
160. Funahashi, S. Working Memory in the Prefrontal Cortex. *Brain Sci* **2017**, *7* (5), 49. <https://doi.org/10.3390/brainsci7050049>.
161. Mesulam, M.-M.; Mufson, E. J. Insula of the Old World Monkey. III: Efferent Cortical Output and Comments on Function. *J. Comp. Neurol.* **1982**, *212* (1), 38–52. <https://doi.org/10.1002/cne.902120104>.
162. Mesulam, M.-M.; Mufson, E. J. Insula of the Old World Monkey. Architectonics in the Insulo-Orbito-Temporal Component of the Paralimbic Brain. *J. Comp. Neurol.* **1982**, *212* (1), 1–22. <https://doi.org/10.1002/cne.902120102>.
163. Mufson, E. J.; Mesulam, M.-M. Insula of the Old World Monkey. II: Afferent Cortical Input and Comments on the Claustrum. *J. Comp. Neurol.* **1982**, *212* (1), 23–37. <https://doi.org/10.1002/cne.902120103>.
164. Fornito, A.; Harrison, B. J.; Zalesky, A.; Simons, J. S. Competitive and Cooperative Dynamics of Large-Scale Brain Functional Networks Supporting Recollection. *Proc. Natl. Acad. Sci. U.S.A.* **2011**, *109* (31), 12788–12793. <https://doi.org/10.1073/pnas.1204185109>.
165. Betzel, R. F.; Satterthwaite, T. D.; Gold, J. I.; Bassett, D. S. A Positive Mood, a Flexible Brain. arXiv January 28, 2016. <https://doi.org/10.48550/arXiv.1601.07881>.
166. Mattar, M. G.; Betzel, R. F.; Bassett, D. S. The Flexible Brain. *Brain* **2016**, *139* (8), 2110–2112. <https://doi.org/10.1093/brain/aww151>.
167. Gu, S.; Pasqualetti, F.; Cieslak, M.; Telesford, Q. K.; Yu, A. B.; Kahn, A. E.; Medaglia, J. D.; Vettel, J. M.; Miller, M. B.; Grafton, S. T.; Bassett, D. S. Controllability of Structural Brain Networks. *Nat Commun* **2015**, *6* (1), 8414. <https://doi.org/10.1038/ncomms9414>.
168. Santarnecchi, E.; Galli, G.; Polizzotto, N. R.; Rossi, A.; Rossi, S. Efficiency of Weak Brain Connections Support General Cognitive Functioning: Efficiency of Weak and Strong Brain Connections and Intelligence. *Hum. Brain Mapp.* **2014**, *35* (9), 4566–4582. <https://doi.org/10.1002/hbm.22495>.
169. Gratton, C.; Dworetzky, A.; Adeyemo, B.; Seitzman, B. A.; Smith, D. M.; Petersen, S. E.; Neta, M. The Cingulo-Opercular Network Is Composed of Two Distinct Sub-Systems; preprint; *Neuroscience*, **2022**. <https://doi.org/10.1101/2022.09.16.508254>.
170. Barbas, H.; Pandya, D. Patterns of Connections of the Prefrontal Cortex in the Rhesus Monkey Associated with Cortical Architecture. In *Frontal Lobe Function and Dysfunction*; Levin, H. S., Eisenberg, H. M., Benton, A. L., Eds.; Oxford University Press, 1991

; pp 35–58.

171. Pandya, D. N.; Barnes, C. L. Architecture Connections of the Frontal Lobe. In *The frontal lobes revisited*; Perecman, Ed.; The I RBN Press, 1987; pp 41–72.
172. Spadone, S.; Della Penna, S.; Sestieri, C.; Betti, V.; Tosoni, A.; Perrucci, M. G.; Romani, G. L.; Corbetta, M. Dynamic Reorganization of Human Resting-State Networks during Visuospatial Attention. *Proc. Natl. Acad. Sci. U.S.A.* **2015**, *112* (26), 8112–8117. <https://doi.org/10.1073/pnas.1415439112>.
173. Machner, B.; Braun, L.; Imholz, J.; Koch, P. J.; Münte, T. F.; Helmchen, C.; Sprenger, A. Resting-State Functional Connectivity in the Dorsal Attention Network Relates to Behavioral Performance in Spatial Attention Tasks and May Show Task-Related Adaptation. *Front. Hum. Neurosci.* **2022**, *15*, 757128. <https://doi.org/10.3389/fnhum.2021.757128>.

■ Author

Quinn Smith is a passionate and hard-working student. Quinn has two loving parents, Stephanie Smith and Shawn Smith, and he has a twin brother, Nathan Smith. While Quinn attended South Western High School at the time of writing this paper, he is currently attending Bucknell University, majoring in neuroscience.

Effects of Caffeinated Beverages on Cardiac Dynamics Monitoring Data and Physically Subjective Perceptions of Adolescents in China

Xue Haowen

Beijing Royal School, Changping, Beijing, China; xuehaowen20060724@126.com

Mentor: ZhangYang

ABSTRACT: This study aimed to determine if drinking caffeine-containing beverages harms Chinese adolescents' hearts and poses a host of other risks if they rely solely on the stimulant to maintain their mental clarity. This study was planned as a double-blind, randomized control. Twenty participants participated in this experiment and were split into two groups with equal numbers of each gender. Volunteers were instructed to stay seated and abstain from food and water for two hours before consuming caffeinated beverages. Each participant in Group 1 had to consume 450 ml of caffeine-containing beverages containing 110 mg of caffeine. In contrast, each volunteer in group 2 had to consume 450 ml of caffeine-containing beverages containing 200 mg of caffeine. We took their blood pressure and heart rates at different time periods. This study revealed the results we didn't expect. We disproved the common misconception that consuming more caffeine can have a negative impact on adolescent heart health by concluding that there was no significant difference in systolic blood pressure, diastolic blood pressure, or heart rate over the same time period in carefully controlled experiments. The symptom of experiencing heart palpitations has become one of the key reflections of the vast majority of subjects in the subjective evaluation of subjects' personal experiences.

KEYWORDS: Biochemistry; General Biochemistry; Caffeinate Beverage; Cardiology; Chinese adolescents.

■ Introduction

Different caffeinated beverages have already established themselves as crucial study aids for Chinese high school students who study late at night. As a result, high school kids have begun to depend on caffeinated drinks like coffee, tea, and functional drinks daily. There has long been worry that caffeine may increase the risk of cancer and cardiovascular disease, even though these caffeinated beverages are effective for improving mental function and attentiveness due to enhanced alertness.^{1,2}

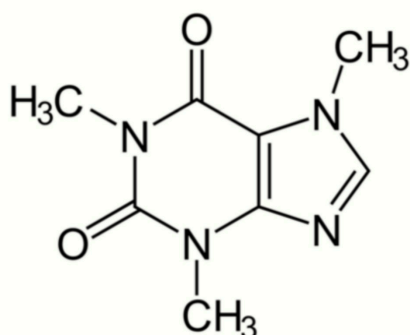


Figure 1: Chemical structure of Trimethyl xanthine 1,3,7(caffeine).

As shown in Figure 1., Trimethyl xanthine 1,3,7 is another name for caffeine.^{3, 4} There are two layers to its impact. First, caffeine is an antagonist of the adenosine receptor and an inhibitor of phosphodiesterase (PDE), shown in Figure 2., at the level of the physical cell.^{5, 6} Smooth muscle relaxation, slowed lipolysis, decreased release of adrenal hormones, and other

actions can be brought on by adenosine receptor activation (slowing down the work of cells).⁷ Caffeine thereby accelerates the work that cells do.⁸ Second, PDE is an enzyme that breaks down cyclic adenosine monophosphate (cAMP), which helps cells break down ATP.⁹ Thus, caffeine's inhibition of PDE is comparable to encouraging the breakdown of cellular ATP, which speeds up the work of cells.¹⁰



Figure 2: Protein structure of phosphodiesterase (PDE).

Additionally, due to the aforementioned actions, caffeine can support the adrenal gland's function (which includes other endocrine glands), increasing the release of glucocorticoids, aldosterone, and adrenaline (at least in advance).^{11, 12} The production of these hormones will rise, indirectly affecting energy and focus. Trimethyl groups are soluble in fat, can enter the brain, and are also present in caffeine. Caffeine also inhibits adenosine A receptors in the brain, primarily found in neurons

connected to the acetylcholinergic system. Caffeine, therefore, has a beneficial "refreshing" effect on work and learning because it is equivalent to stimulating acetylcholinergic neurons, primarily linked to memory, association, and learning.¹³ Some studies claim that very high concentrations of caffeine will cause GABA receptor antagonistic activity in the brain, although investigations have yet to be conclusive.¹⁴

Clinical studies have shown that caffeine increases blood pressure and heart rate, but no studies have been done on the physical characteristics of other ethnic groups, particularly Chinese teenage groups. Therefore, we will conduct this experiment to determine whether caffeine-containing beverages significantly affect Chinese teenagers' heart rates and blood pressure and indirectly contribute to associated risks.

■ Methods

Our study was planned as a double-blind, randomized control. Twenty teens (aged 17+–1), including ten boys and ten girls of Chinese heritage, participated in the experiment. Twenty participants participated in this experiment and were split into two groups with equal numbers of each gender. Volunteers were instructed to stay seated and abstain from food and water for two hours before consuming caffeinated beverages. To lessen the impact of participants' mental health on the study's outcomes, volunteers were also instructed to relax by listening to calming music twenty minutes before administering caffeine-containing beverages.

Each volunteer in Group 1 was required to consume 450 ml of beverages containing 110 mg of caffeine, whereas volunteers in Group 2 were instructed to consume 450 ml of beverages containing 200 mg of caffeine. We measured their blood pressure and heart rates 30 minutes, an hour, 1.5 hours, and two hours after drinking. First, the results were compared to those obtained before drinking caffeinated beverages to determine whether the change was statistically significant. Next, the p-value was calculated. Finally, we also calculated the difference between the two data groups to assess whether different caffeine doses will have other effects on Chinese teens' pressure and heart rates. We evaluated whether there were any significant changes.

We created the following questionnaire to examine how caffeine-containing beverages affect the subjective emotions of adolescent volunteers. There are seven questions in all on this survey: Are you anxious? Do you feel weak and easily exhausted? Can you feel your heart racing? Do you feel queasy and uneasy? Do you feel flustered and have heart palpitation? Does your breathing feel labored? Do you feel sweeter? The proportion of survey responses to the aforementioned questions allowed us to quantitatively assess the patients' subjective reactions to caffeine-containing beverages.

■ Results and Discussion

After statistical data, we obtained the following data:

Table 1: Data of the 110mg caffeine experimental group (The data in each column from left to right are systolic blood pressure, diastolic blood pressure, and heart rate). Statistically, the change in systolic blood pressure was greater in the 110 mg experimental group patients' with six patients experiencing varying degrees of increase in systolic blood pressure half an hour after caffeine intake.

110mg	Before drinking	Half an hour	An Hour	Two Hours
1	115/72/87	121/78/81	129/82/75	109/68/77
2	119/70/90	117/72/75	124/76/84	118/71/77
3	110/71/80	111/60/91	118/69/78	119/65/76
4	119/76/72	122/77/70	107/66/70	116/78/71
5	109/68/80	118/73/74	120/63/70	110/73/69
6	107/65/81	138/77/77	106/63/70	108/74/68
7	116/79/92	110/64/73	116/70/75	110/68/69
8	121/69/80	105/63/72	118/75/74	107/68/72
9	113/69/88	120/63/74	115/70/73	117/72/75
10	120/70/80	112/60/71	109/68/72	110/69/75

We started by setting the confidence threshold to a p-value of 0.05 or less. Then, by comparing the values of the three time periods with the values before the caffeine intake, we obtained the following findings in ten patients who consumed 110 mg of caffeine:

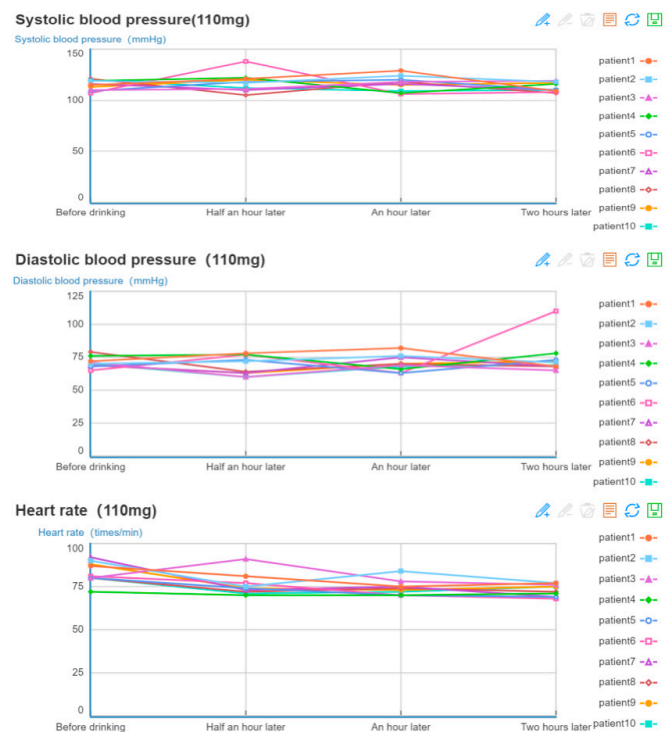


Figure 3: Trend chart of various data in the 110 mg caffeine experimental group. According to the image data, the diastolic blood pressure of patient 6 increased sharply two hours after caffeine intake, which was an exceptional case. In contrast, the heart rate images consistently maintained a steady downward trend.

As shown in Table 1. and Figure 3. above, regarding the change in vascular hypertension, the rising rate over three periods was not statistically significant (p-values = 0.229, 0.32, and 0.87). The diastolic pressure section showed the same outcome, and the data for the three time periods did not significantly rise (p-value = 0.789, 0.618, and 0.567). We made a startling discovery regarding the rate of change in heart rate when we discovered that the subjects' heart rates reversed after consuming caffeine. The value of the reverse growth is

statistically significant, demonstrating that it reversed (p-value=0.008605, 0.000821, 0.00021).

Table 2: Data of the 200 mg caffeine experimental group (The data in each column from left to right are systolic blood pressure, diastolic blood pressure, and heart rate.) The systolic blood pressure of all patients in the 200 mg experimental group increased to varying degrees half an hour after caffeine intake; this phenomenon was also confirmed in the statistical calculations (p-value).

200mg	Before drinking	Half an hour	An Hour	Two Hours
1	105/75/98	120/83/75	113/78/82.5	113/77.5/88
2	113/64/64	124/76/60	118/72/61	115/65/58
3	115/74/98	128/70/67	118/71/73	114/66/80.5
4	113/80/91	122/71/83	113/71/72	118/75/71
5	122/61/86	129/67/85	116/60/70	116/62/76
6	116/65/76	125/69/83	128/68/89	119/66/87
7	114/80/91	122/80/80	125/85/82	117/78/88
8	102/64/81	116/77/85	118/79/88	109/65/77
9	109/66/82	115/67/86	118/67/89	111/65/80
10	110/71/69	122/71/87	122/75/88	118/77/87

As shown in Table 2. and Figure 4., the 200 mg experimental group's hypertension growth rate in three periods showed a trend toward a statistically significant increase (p-values = 0.000152, 0.0043, and 0.078). The diastolic pressure growth rate did not fall inside the established confidence interval (p-value=0.417, 0.209, 0.546). Although there is still a subtle counter-growth trend in the heart rate data, it is not statistically significant (p-value=0.173, 0.199, 0.185).

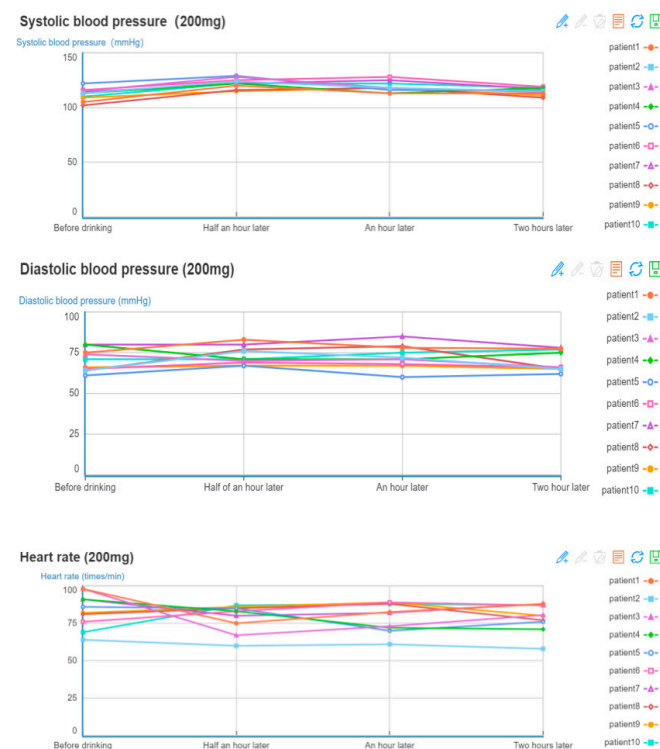


Figure 4: Trend chart of various data in the 200 mg caffeine experimental group. According to the image, all subjects in the 200 mg experimental group showed relatively similar trends in all data.

In evaluating data from two distinct dose test groups in a controlled experiment. After taking caffeine doses of 110 mg and 200 mg, we compared if there were any significant differences in the results throughout the course of the subsequent hour. We discovered no significant difference after comparing the three values of systolic blood pressure, diastol-

ic blood pressure, and heart rate between the two test groups (p-value=0.152, 0.271, 0.363).

Following data analysis, we discovered that 60% of the respondents who consumed 110 mg of caffeine reported, while this number rose to 80% for those who used 200 mg of caffeine.

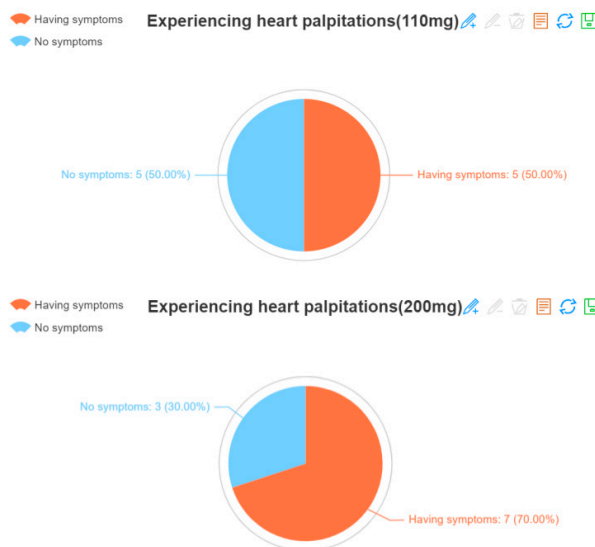


Figure 5: The proportion of palpitations in different test groups (110 and 200 mg). According to the data, 50% of the patients in the 110 mg group experienced heart palpitations. This ratio increased to 70% in the 200 mg group.

Additionally, as shown in Figure 5. above, patients who consumed 110 mg and 200 mg of caffeine generally responded (greater than 50%) to two side effects, including increased sweating at constant room temperature and some dizziness. The 110 mg caffeine intake values were correspondingly 50% and 70%. 200 mg of caffeine is consumed at rates of 60% and 70%, respectively. It also demonstrates that caffeine does cause the four reactions stated above in Chinese teenagers, even though the difference in the proportions of subjects in each data set between the two cases is not statistically significant (p-value>0.05).

Discussion

The first two results of the 110 mg experimental group are familiar because most Chinese teenagers only consume an average of 110 mg of caffeine daily. However, a considerable inverse heart rate growth must be more consistent with our earlier hypotheses. Because it makes sense that a stimulant like coffee would stimulate the heart to beat more frequently, this discovery challenges this theory. Because the caffeine intake of the 200 mg experimental group's coffee was higher than that of Chinese adolescents as a whole, the growth rate of the high-pressure data was statistically significant and did not exceed our expectations. Drinking more coffee stimulates the nervous system more, which raises systolic blood pressure. The higher caffeine dose did cause the subjects' heart rates to slightly reverse their growth trend, but this was not statistically significant, which perplexed us. In fact, this finding calls into doubt many of the prevalent hypotheses on a quick heartbeat.

Regarding the analysis of subjective experiences, coffee can interfere with the action of a chemical called adenosine, which is why most subjects experience panic and heart palpitations. Caffeine competes with adenosine's receptors, preventing the natural impact of adenosine on the heart that lowers heart rate. We discovered that most of the few subjects who did not experience this feeling had regularly consumed caffeinated beverages (more than two consecutive months). Although we do not yet have a scientific explanation, their bodies appear to have evolved a resistance to the interaction between coffee and adenosine.

No significant differences in the data were found in the controlled studies. This demonstrates that varying caffeine dosages did not affect Chinese teenagers' cardiac statistics. It also dispels the myth that caffeine consumption among Chinese teenagers may affect their heart health.

The following two conclusions can help to explain the experience of vertigo brought on by caffeine in subjects. First, because caffeine stimulates the brain's nerves, those susceptible to it may experience symptoms of lightheadedness after drinking coffee; Second, caffeine, which is frequently present in caffeinated beverages, can rapidly lower blood sugar levels. As a result, consuming coffee will result in a hypoglycemia reaction, which will create symptoms of dizziness. We hypothesize that the following theories can account for why caffeinated beverages increase sweating at constant temperatures: Because excitatory nerves will increase metabolism, which leads to increased sweating and disorders of sweat gland secretion, caffeine has the effect of stimulating excitatory nerves. However, precisely how caffeine stimulates nerves and affects sweat glands' secretion is still being determined.¹⁵

■ Acknowledgment

The author would like to thank Professor Xue Yajun from the School of Clinical Medicine, Tsinghua University, who provided suggestions on the research process and method. Thanks for the contribution made by all of the members of the scientific department of Beijing Royal School, which is guided by Zhang Yang.

■ References

1. van Dam, R.; Hu, F.; Willett, W., Coffee, Caffeine, and Health. *The New England journal of medicine* **2020**, *383* (4), 369-378.
2. De Giuseppe, R.; Di Napoli, I.; Granata, F.; Mottotese, A.; Cena, H., Caffeine and blood pressure: a critical review perspective. *Nutrition research reviews* **2019**, *32* (2), 169-175.
3. Fassina, G.; Gaion, R.; Caparrotta, L.; Carpenedo, F., A caffeine analogue (1,3,7-trimethyl-6-thioxo-2-oxopurine) with a negative inotropic and chronotropic effect. *Naunyn-Schmiedeberg's archives of pharmacology* **1985**, *330* (3), 222-6.
4. Pohanka, M., The perspective of caffeine and caffeine derived compounds in therapy. *Bratislavské lekárske listy* **2015**, *116* (9), 520-30.
5. Juhász, M.; Atanaskova Mesinkovska, N., The use of phosphodiesterase inhibitors for the treatment of alopecia. *The Journal of dermatological treatment* **2020**, *31* (3), 245-253.
6. Faudone, G.; Arifi, S.; Merk, D., The Medicinal Chemistry of Caffeine. *Journal of medicinal chemistry* **2021**, *64* (11), 7156-7178.
7. Fischer, T.; Bergmann, A.; Kruse, N.; Kleszczynski, K.; Skobowiat, C.; Slominski, A.; Paus, R., New effects of caffeine on corticotropin-releasing hormone (CRH)-induced stress along the intrafol-

licular classical hypothalamic-pituitary-adrenal (HPA) axis (CRH-R1/2, IP-R, ACTH, MC-R2) and the neurogenic non-HPA axis (substance P, p75 and TrkA) in ex vivo human male androgenetic scalp hair follicles. *The British journal of dermatology* **2021**, *184* (1), 96-110.

8. Yong, L.; Song, Y.; Xiao, X.; Sui, H.; Xu, H.; Tan, R.; Yang, X.; Song, J.; Li, J.; Wei, S., Quantitative probabilistic assessment of caffeine intake from tea in Chinese adult consumers based on nationwide caffeine content determination and tea consumption survey. *Food and chemical toxicology: an international journal published for the British Industrial Biological Research Association* **2022**, *165*, 113102.
9. Katsuragi, T.; Sato, C.; Usune, S.; Ueno, S.; Segawa, M.; Migita, K., Caffeine-inducible ATP release is mediated by Ca²⁺-signaling transducing system from the endoplasmic reticulum to mitochondria. *Naunyn-Schmiedeberg's archives of pharmacology* **2008**, *378* (1), 93-101.
10. Nehlig, A., Interindividual Differences in Caffeine Metabolism and Factors Driving Caffeine Consumption. *Pharmacological reviews* **2018**, *70* (2), 384-411.
11. Yamada, Y.; Nakazato, Y.; Ohga, A., The mode of action of caffeine on catecholamine release from perfused adrenal glands of cat. *British journal of pharmacology* **1989**, *98* (2), 351-6.
12. Xia, X.; Liu, Y.; Liu, L.; Chen, Y.; Wang, H., Selection and verification of the combination of reference genes for RT-qPCR analysis in rat adrenal gland development. *The Journal of steroid biochemistry and molecular biology* **2021**, *208*, 105821.
13. Oeltzschner, G.; Zöllner, H.; Jonuscheit, M.; Lanzman, R.; Schnitzler, A.; Wittsack, H., J-difference-edited MRS measures of γ -aminobutyric acid before and after acute caffeine administration. *Magnetic resonance in medicine* **2018**, *80* (6), 2356-2365.
14. Bishnoi, M.; Chopra, K.; Kulkarni, S., Involvement of adenosine receptor system in an animal model of tardive dyskinesia and associated behavioural, biochemical and neurochemical changes. *European journal of pharmacology* **2006**, *552*, 55-66.
15. Burke, L., Caffeine and sports performance. *Applied physiology, nutrition, and metabolism = Physiologie appliquée, nutrition et métabolisme* **2008**, *33* (6), 1319-34.

■ Author

Xue Haowen is a student at Beijing Royal School, Changping, Beijing, China student. He has a tremendous amount of enthusiasm for biochemistry and clinical medicine. Under the guidance of his biology teacher and his father, who is a professor from Tsinghua University, China, Xue Haowen is enjoying the trip of biology.



GENIUS OLYMPIAD

"Let's build a better future together"



www.geniusolympiad.org

International Environment Project Fair For Grades 9-12



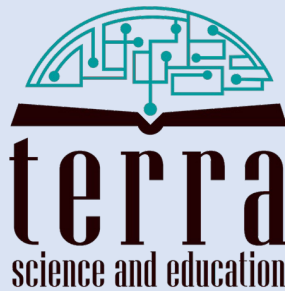
Rochester, New York
Hosted by Rochester Institute of Technology

@GeniusOlympiad



IJHSR International
Journal of
High School
Research

is a publication of



N.Y. based 501.c.3 non-profit organization
dedicated for improving K-16 education